

# IAEA TECDOC SERIES

---

TECDOC No. **1727**

## **Benchmarking Severe Accident Computer Codes for Heavy Water Reactor Applications**



**IAEA**

International Atomic Energy Agency

BENCHMARKING SEVERE ACCIDENT  
COMPUTER CODES FOR HEAVY WATER  
REACTOR APPLICATIONS

The following States are Members of the International Atomic Energy Agency:

AFGHANISTAN	GUATEMALA	PANAMA
ALBANIA	HAITI	PAPUA NEW GUINEA
ALGERIA	HOLY SEE	PARAGUAY
ANGOLA	HONDURAS	PERU
ARGENTINA	HUNGARY	PHILIPPINES
ARMENIA	ICELAND	POLAND
AUSTRALIA	INDIA	PORTUGAL
AUSTRIA	INDONESIA	QATAR
AZERBAIJAN	IRAN, ISLAMIC REPUBLIC OF	REPUBLIC OF MOLDOVA
BAHRAIN	IRAQ	ROMANIA
BANGLADESH	IRELAND	RUSSIAN FEDERATION
BELARUS	ISRAEL	RWANDA
BELGIUM	ITALY	SAUDI ARABIA
BELIZE	JAMAICA	SENEGAL
BENIN	JAPAN	SERBIA
BOLIVIA	JORDAN	SEYCHELLES
BOSNIA AND HERZEGOVINA	KAZAKHSTAN	SIERRA LEONE
BOTSWANA	KENYA	SINGAPORE
BRAZIL	KOREA, REPUBLIC OF	SLOVAKIA
BULGARIA	KUWAIT	SLOVENIA
BURKINA FASO	KYRGYZSTAN	SOUTH AFRICA
BURUNDI	LAO PEOPLE'S DEMOCRATIC REPUBLIC	SPAIN
CAMBODIA	LATVIA	SRI LANKA
CAMEROON	LEBANON	SUDAN
CANADA	LESOTHO	SWAZILAND
CENTRAL AFRICAN REPUBLIC	LIBERIA	SWEDEN
CHAD	LIBYA	SWITZERLAND
CHILE	LIECHTENSTEIN	SYRIAN ARAB REPUBLIC
CHINA	LITHUANIA	TAJIKISTAN
COLOMBIA	LUXEMBOURG	THAILAND
CONGO	MADAGASCAR	THE FORMER YUGOSLAV REPUBLIC OF MACEDONIA
COSTA RICA	MALAWI	TOGO
CÔTE D'IVOIRE	MALAYSIA	TRINIDAD AND TOBAGO
CROATIA	MALI	TUNISIA
CUBA	MALTA	TURKEY
CYPRUS	MARSHALL ISLANDS	UGANDA
CZECH REPUBLIC	MAURITANIA	UKRAINE
DEMOCRATIC REPUBLIC OF THE CONGO	MAURITIUS	UNITED ARAB EMIRATES
DENMARK	MEXICO	UNITED KINGDOM OF GREAT BRITAIN AND NORTHERN IRELAND
DOMINICA	MONACO	UNITED REPUBLIC OF TANZANIA
DOMINICAN REPUBLIC	MONGOLIA	UNITED STATES OF AMERICA
ECUADOR	MONTENEGRO	URUGUAY
EGYPT	MOROCCO	UZBEKISTAN
EL SALVADOR	MOZAMBIQUE	VENEZUELA
ERITREA	MYANMAR	VIETNAM
ESTONIA	NAMIBIA	YEMEN
ETHIOPIA	NEPAL	ZAMBIA
FIJI	NETHERLANDS	ZIMBABWE
FINLAND	NEW ZEALAND	
FRANCE	NICARAGUA	
GABON	NIGER	
GEORGIA	NIGERIA	
GERMANY	NORWAY	
GHANA	OMAN	
GREECE	PAKISTAN	
	PALAU	

The Agency's Statute was approved on 23 October 1956 by the Conference on the Statute of the IAEA held at United Nations Headquarters, New York; it entered into force on 29 July 1957. The Headquarters of the Agency are situated in Vienna. Its principal objective is "to accelerate and enlarge the contribution of atomic energy to peace, health and prosperity throughout the world".

IAEA-TECDOC-1727

**BENCHMARKING SEVERE ACCIDENT  
COMPUTER CODES FOR HEAVY WATER  
REACTOR APPLICATIONS**

INTERNATIONAL ATOMIC ENERGY AGENCY  
VIENNA, 2013

## COPYRIGHT NOTICE

All IAEA scientific and technical publications are protected by the terms of the Universal Copyright Convention as adopted in 1952 (Berne) and as revised in 1972 (Paris). The copyright has since been extended by the World Intellectual Property Organization (Geneva) to include electronic and virtual intellectual property. Permission to use whole or parts of texts contained in IAEA publications in printed or electronic form must be obtained and is usually subject to royalty agreements. Proposals for non-commercial reproductions and translations are welcomed and considered on a case-by-case basis. Enquiries should be addressed to the IAEA Publishing Section at:

Marketing and Sales Unit, Publishing Section  
International Atomic Energy Agency  
Vienna International Centre  
PO Box 100  
1400 Vienna, Austria  
fax: +43 1 2600 29302  
tel.: +43 1 2600 22417  
email: [sales.publications@iaea.org](mailto:sales.publications@iaea.org)  
<http://www.iaea.org/books>

For further information on this publication, please contact:

Nuclear Power Technology Development Section  
International Atomic Energy Agency  
Vienna International Centre  
PO Box 100  
1400 Vienna, Austria  
Email: [Official.Mail@iaea.org](mailto:Official.Mail@iaea.org)

© IAEA, 2013  
Printed by the IAEA in Austria  
December 2013

IAEA Library Cataloguing in Publication Data

Benchmarking severe accident computer codes for heavy water reactor applications. — Vienna : International Atomic Energy Agency, 2013.  
p. ; 30 cm. — (IAEA-TECDOC series,  
ISSN 1011-4289 ; no. 1727)  
ISBN 978-92-0-114413-3  
Includes bibliographical references.

1. Heavy water reactors — Safety measures. 2. Nuclear reactors — Safety measures — Computer programs. 3. Nuclear power plants — Accidents — Prevention. I. International Atomic Energy Agency. II. Series.

## FOREWORD

Requests for severe accident investigations and assurance of mitigation measures have increased for operating nuclear power plants and the design of advanced nuclear power plants. Severe accident analysis investigations necessitate the analysis of the very complex physical phenomena that occur sequentially during various stages of accident progression. Computer codes are essential tools for understanding how the reactor and its containment might respond under severe accident conditions.

The IAEA organizes coordinated research projects (CRPs) to facilitate technology development through international collaboration among Member States. The CRP on Benchmarking Severe Accident Computer Codes for HWR Applications was planned on the advice and with the support of the IAEA Nuclear Energy Department's Technical Working Group on Advanced Technologies for HWRs (the TWG-HWR).

This publication summarizes the results from the CRP participants. The CRP promoted international collaboration among Member States to improve the phenomenological understanding of severe core damage accidents and the capability to analyse them. The CRP scope included the identification and selection of a severe accident sequence, selection of appropriate geometrical and boundary conditions, conduct of benchmark analyses, comparison of the results of all code outputs, evaluation of the capabilities of computer codes to predict important severe accident phenomena, and the proposal of necessary code improvements and/or new experiments to reduce uncertainties. Seven institutes from five countries with HWRs participated in this CRP.

The IAEA expresses its appreciation to T. Nitheanandan (Canada) for leading this CRP as chairperson. The IAEA officer responsible for this publication was J.H. Choi of the Division of Nuclear Power.

#### *EDITORIAL NOTE*

*This publication has been prepared from the original material as submitted by the authors. The views expressed do not necessarily reflect those of the IAEA, the governments of the nominating Member States or the nominating organizations.*

*This publication has not been edited by the editorial staff of the IAEA. It does not address questions of responsibility, legal or otherwise, for acts or omissions on the part of any person.*

*The use of particular designations of countries or territories does not imply any judgement by the publisher, the IAEA, as to the legal status of such countries or territories, of their authorities and institutions or of the delimitation of their boundaries.*

*The mention of names of specific companies or products (whether or not indicated as registered) does not imply any intention to infringe proprietary rights, nor should it be construed as an endorsement or recommendation on the part of the IAEA.*

*The authors are responsible for having obtained the necessary permission for the IAEA to reproduce, translate or use material from sources already protected by copyrights.*

*The IAEA has no responsibility for the persistence or accuracy of URLs for external or third party Internet web sites referred to in this book and does not guarantee that any content on such web sites is, or will remain, accurate or appropriate.*

## CONTENTS

1.	INTRODUCTION .....	1
1.1.	BACKGROUND.....	1
1.2.	OBJECTIVES .....	2
1.3.	STRUCTURE OF REPORT.....	2
2.	REFERENCE SCENARIO AND ASSUMPTIONS .....	3
2.1.	REFERENCE PLANT AND SCENARIO .....	3
2.2.	FAILURE CRITERIA.....	4
2.2.1.	Fuel sheath failure .....	4
2.2.2.	Fuel channel failure.....	5
2.2.3.	Fuel channel disassembly .....	5
2.2.4.	Core collapse.....	5
2.2.5.	Calandria vessel failure .....	6
2.2.6.	Calandria vault (concrete) failure.....	6
2.2.7.	Containment failure.....	6
2.2.8.	Fission products release.....	7
2.3.	COMMON ASSUMPTIONS .....	7
2.4.	INITIAL CONDITIONS .....	8
3.	PARTICIPANT'S MODELS AND RESULTS .....	21
3.1.	AECL.....	21
3.1.1.	Computer codes.....	21
3.1.2.	Phenomena and system idealization.....	23
3.1.3.	Analysis results .....	30
3.2.	BARC-RED .....	66
3.2.1.	Computer codes.....	66
3.2.2.	Phenomena and system idealization.....	70
3.2.3.	Analysis results .....	74
3.3.	BARC-RSD.....	95
3.3.1.	Required systems models and software used.....	95
3.3.2.	Modelling details.....	98
3.3.3.	Analysis results .....	105
3.4.	KAERI.....	135
3.4.1.	Computer codes.....	135
3.4.2.	Phenomena and system idealization.....	137
3.4.3.	Analysis results .....	144

3.5.	NPCIL.....	175
3.5.1.	Computer codes.....	175
3.5.2.	Phenomena and system idealization.....	183
3.5.3.	Analysis results .....	184
3.6.	PUB .....	210
3.6.1.	Computer codes.....	210
3.6.2.	Phenomena and system idealization.....	213
3.6.3.	Analysis results .....	219
3.7.	SJTU .....	237
3.7.1.	Computer codes.....	237
3.7.2.	Phenomena and system idealization.....	237
3.7.3.	Analysis results .....	241
4.	COMPARISON OF KEY RESULTS.....	261
4.1.	PRIMARY HEAT TRANSPORT SYSTEM BEHAVIOUR.....	262
4.2.	STEAM GENERATOR SECONDARY SIDE BEHAVIOUR.....	268
4.3.	MODERATOR SYSTEM BEHAVIOUR.....	272
4.4.	CORE MELT RELOCATION BEHAVIOUR.....	280
4.5.	CONTAINMENT SYSTEM BEHAVIOUR.....	286
4.6.	FISSION PRODUCTS BEHAVIOUR.....	292
5.	LESSONS LEARNED.....	297
6.	CONCLUSIONS AND RECOMMENDATIONS.....	300
	REFERENCES.....	303
	GLOSSARY.....	307
	ABBREVIATIONS.....	309
	CONTRIBUTORS TO DRAFTING AND REVIEW.....	311

# 1. INTRODUCTION

## 1.1. BACKGROUND

Heavy Water Reactors (HWRs) possess a number of inherent and designed safety features that make them resistant to core damage accidents. The heavy water moderator in CANDU reactors provides a significant heat sink to prevent or delay the progression of an accident into the severe core damage realm. The fuel is surrounded by three water systems: heavy water primary coolant, heavy water moderator, and light water in the calandria vault and shield water system. The water inventories in the emergency core cooling system and the dousing system at the dome of the containment can also provide fuel cooling and water makeup to prevent severe core damage or mitigate the consequences of a severe core damage accident, should it occur.

A severe core damage accident is defined as a beyond design basis accident in which the reactor core is damaged significantly, irrespective of whether there are serious off-site consequences [1]. The term Severe Accident (SA) characterizes the transition of core geometry from an intact coolable state to a state that is more difficult to cool with the state of the core progressively deteriorating, starting from the fuel channels [2].

The severe accident phenomena in HWRs are complex and different than the severe accident phenomena in a Light Water Reactors (LWR). In a HWR, the core damage accidents are categorised into two accident classes [3]:

- The limited core damage accidents (LCDAs) where the core geometry is preserved, and;
- The severe core damage accidents (SCDAs) where the core geometry is lost.

The severe core damage accident progression is a step beyond the LCDAs that can be terminated at the moderator heat sink. The SCDAs in CANDU reactors begin with the depletion of liquid moderator, exposing the top row of internally voided fuel channels to steam cooling conditions on the outside. The uncovered fuel channels heat-up, deform and break-up into core debris. The large inventories of water passively reduce the rate of progression of the accident, prolonging the time for complete loss of engineered heat sinks. The calandria vessel and the containment are two engineered barriers that retain core debris (non-volatile radioactivity) and volatile fission products, respectively. These barriers ensure public safety against risk resulting from an inappropriate or uncontrolled release of radioactivity. Additional engineered features are provided to prevent phenomenological challenges, or mitigate consequences of challenge to these barriers.

The consequence analysis of severe core damage sequences are performed using a number of computational tools. For example, some of the computational codes used in severe accidents are MAAP-CANDU, ISAAC, SEVAX, RELAP/SCDAP, MELCOOL, and ASTEC. Plant specific severe core damage accident assessments rely on using best estimate codes, separate effects data, analytical solutions and failure criteria. The representative severe core damage sequence is performed using integral codes to quantify the:

- Changes to important variables with time and;
- Timing of major events.

These calculations are supported by sensitivity studies, expert opinion, single effect experiments, and mechanistic code calculations to estimate the overall uncertainties of the predicted behaviour in selected cases. The important variables include containment pressure, containment temperature, hydrogen generation, and activity release of Cs-137 and I-131. These plant specific consequence assessments are used to support the development and assessment of event trees in Level 2 Probabilistic Safety Assessment (PSA) and Severe Accident Management Guidelines (SAMG).

Despite significant progress in the understanding of severe accident phenomena, the application of the available knowledge for benchmarking integral codes remains limited because of the difficulties in incorporating realistic boundary conditions of experiments into integral codes. The extremely high temperatures impose additional challenges to realistic measurement of the phenomena, rendering the data itself to have significantly large uncertainties. As a result, the analysis results from integral severe accident codes can have significantly large uncertainties compared to the design basis accident analyses.

The Coordinated Research Project (CRP) described in this document is a benchmarking of severe accident analysis codes used for the analysis of severe core damage accidents in HWRs. The exercise promoted international collaboration among IAEA Member States to improve the phenomenological understanding and analysis capability of severe core damage accidents. The scope included the identification and selection of a severe accident sequence, selection of appropriate geometrical and boundary conditions, conducting benchmark analyses, and comparing the results of all code outputs, evaluating the capabilities of existing computer codes to predict important severe accident phenomena and suggesting necessary code improvements and/or new experiments to reduce uncertainties.

## 1.2. OBJECTIVES

The objective of the CRP is to conduct a benchmark exercise on severe accident computer codes used for consequence analysis of HWRs. The purpose is to compare the integrated effects of embedded models in the codes, gain an understanding of their limitations, assess the level of uncertainties, and thereby increase the confidence in severe accident code predictions. The code-to-code comparisons are likely to provide the justification required for model improvement and reduction of uncertainties.

The specific research objectives are:

- Identification of models and computer codes applicable to specific phenomena for in-vessel and ex-vessel phenomena of HWRs;
- Identification of database for specific phenomena during severe accident progression in HWRs;
- Standard Problem Exercise for specific sequence by different codes or models;
- Evaluate code capability and applicability, model applicability and limitations to specific phenomena of severe accident progression;
- Suggestions for code/model improvements and new tests for future.

## 1.3. STRUCTURE OF REPORT

Section 1 of the report provides a brief introduction of the CRP specifying its background and objectives. Section 2 discusses the scenario considered with major assumptions used in analysis, describing the details of reference plant, failure criteria, initial conditions of the plant and common assumptions used in the analysis by all participating organizations. Section 3 describes the models/computer codes used by each participant and describes the details of nodalization, assumptions made in the analysis and results of computations from phase 1 to 4. Comparison of results predicted by different participating organizations is discussed in Section 4. The lessons learnt from the exercise are discussed in Section 5. Major conclusions and recommendations from the exercise are provided in Section 6.

## 2. REFERENCE SCENARIO AND ASSUMPTIONS

### 2.1. REFERENCE PLANT AND SCENARIO

The Heavy Water Reactor plant considered for the benchmarking analysis is a generic CANDU-6 power plant with 2064 MW thermal output to the steam generators. Some of the design features of the CANDU reactor are: (1) the pressure boundary of the reactor core established by a number of small diameter fuel channels, (2) heavy water ( $D_2O$ ) for low pressure moderator and high pressure fuel cooling systems, (3) on-power refuelling, (4) reactivity devices located in the cool low pressure moderator not subjected to high temperatures or pressures, (5) natural uranium fuel, and (6) two fully capable safety shutdown systems, independent from each other and the reactor regulating system.

The CANDU 6 station consists of a reactor building, service building, turbine building, and other auxiliary structures. The reactor building (Fig. 2-1) contains all the equipment directly associated with the production of steam, e.g., Primary Heat Transport System (PHTS), steam generators, reactor assembly and other components.

The reactor assembly consists primarily of a calandria vessel, which is penetrated by 380 horizontal fuel channels and contains heavy water moderator (Fig. 2-2). Each fuel channel consists of a pressure tube, a calandria tube and 12 fuel bundles containing 37 fuel elements each. The calandria vessel is located inside a steel-lined concrete reactor vault. The reactor vault is filled with light water, which provides shielding and maintains the calandria vessel at nearly a constant temperature during normal operation. End-shields at both ends of the calandria vessel provide shielding at each end of the reactor.

The PHTS is designed to circulate pressurized heavy water through the fuel channels to remove the heat produced in the fuel (Fig. 2-2). The heat is carried by the reactor coolant to the steam generators, where it is transferred to light water to produce steam to drive the turbine generator. The coolant leaving the steam generators is returned to the inlet of the fuel channels. The low pressure steam exhausted by the low pressure turbine is condensed in the condensers by a flow of condenser cooling water. The feed water system processes condensed steam from the condensers and returns it to the steam generators via pumps and a series of heaters. The steam supply system's power production process functions like any other nuclear steam supply system, with controlled fission in the reactor core.

Neutrons produced by nuclear fission are moderated (slowed) by the  $D_2O$  in the calandria. The moderator  $D_2O$  is circulated through systems that cool and purify it, and control the concentrations of soluble neutron absorbers used for adjusting the reactivity.

Fuelling machines connect to each fuel channel as necessary to provide on-power refuelling; this eliminates the need for refuelling outages. The on-power refuelling system can also be used to remove a defective fuel bundle in the unlikely event that a fuel defect develops. CANDU 6 reactors have systems to identify and locate defective fuel.

The CANDU 6 pressure and inventory control (P&IC) system consists mainly of a pressurizer, degasser condenser,  $D_2O$  storage tank,  $D_2O$  feed pumps, bleed cooler, pressurizer relief valves and heat transport system liquid relief valves. Pressurizer relief valves, steam bleed valves and PHTS liquid relief valves (LRV) discharge into the degasser condenser. The degasser condenser has spring-loaded relief valves which discharge to a containment compartment. The LRVs are air-operated, with back-up instrument air, and are designed to fail open. Normally this back-up air supply should maintain the valves in operation for two hours following power loss (for example, in case of station blackout) and loss of normal instrument air. Pressurizer relief valves are designed to fail open. Further details of CANDU 6 power plant configuration can be found in References [4] and [5].

## **Station blackout scenario**

A station blackout is defined as an event initiated by a complete loss of off-site alternating current (AC) power concurrent with turbine trip and unavailability of the class IV and all back up power including loss of all on-site standby and emergency electric power supplies, i.e., the diesel generators. This may result in the loss of decay heat removal capability, if left unmitigated, leading to core damage.

The team of analysts participating in the Coordinated Research Project benchmarking analysis selected the Station Blackout (SBO) scenario as a postulated initiating event. The main reasons for selecting the SBO scenario are:

- The progression of the accident is slow and therefore it is reasonable to expect the analysis results to be less affected by numerical convergence issues;
- It is amenable to closed-form back-of-the-envelope numerical calculations for comparison with computer code outputs;
- A majority of the severe accident phenomena are captured in the sequence;
- The sequential events can be anticipated and tracked: moderator temperature increase secondary side boiloff, coolant inventory boiloff, primary side liquid relief valve opening, fuel channel heatup, calandria vessel rupture disk opening, core heatup and collapse.

If the high pressure, medium pressure and the low pressure emergency core cooling, crash-cooling function, shut-down cooling and shield cooling systems are not available, the loops not isolated from each other, the local air coolers and operator intervention are assumed unavailable, the SBO accident sequence can progress to a severe core damage accident.

## **2.2. FAILURE CRITERIA**

In a reactor the systems and components have limiting design conditions beyond which they cannot operate, but could restart if conditions allowed. For example a pump can restart provided the supply of electrical power, cooling water and the control system signals are restored. There are more extreme conditions beyond which the reactor systems and components are assumed to fail and cannot be reasonably expected to be restored. For example, in the case of the fuel sheath, its primary function as a barrier to fission products cannot be confidently restored if the sheath temperature exceeds the phase transformation temperature of Zircaloy-4. A severe accident analysis is required to identify the limiting conditions for each plant component that can potentially fail. These limiting conditions are called the failure criteria.

In addition to the analysis assumptions and models employed, the results of the analysis will depend on the failure criteria for components such as containment, calandria vessel, fuel channel, reactor vault, etc. Failure criteria may be identified as limiting temperatures, masses, pressures, fluid levels, and the status or geometry of plant systems or components, which specify the conditions that this component does not perform the initially prescribed function. The failure criteria may also be a combination of factors, and there may be multiple sets of criteria for the same final state of a particular plant component.

### **2.2.1. Fuel sheath failure**

A typical approach for fuel failure is to assume that the fuel cladding fails if the average fuel element temperature is higher than a specified value. A value of 1,073°K (800°C) for fuel sheath temperature was recommended and used as the fuel sheath failure criteria for present analysis. Sheath temperature of 2,123°K, the Zircaloy melting temperature, was used as the bundle slumping criteria for the present analysis.

The Politechnica University of Bucharest used a different model using RELAP5/SCADAP to calculate cladding ballooning and rupture using a mechanistic model to calculate the elastic-plastic deformation using the theory of Hill [6] and the Prandtl-Reuss equations [7].

### **2.2.2. Fuel channel failure**

Fuel channel failure is defined as a perforation in its pressure boundaries followed by mass transfer between the environment inside the pressure tube and the calandria vessel, which means that both the pressure tube and calandria tube are perforated.

The mechanism for fuel channel failure depends on the Primary Heat Transport System (PHTS) pressure. At high PHTS pressure, the non-uniform circumferential temperature distributions lead to pressure tube rupture. An approximation is to assume that the pressure tube fails when it reaches a temperature at which it starts to deform, i.e., balloon. Therefore, the channel is assumed to have failed under high pressures and temperatures when the ballooning criterion is satisfied. A value of 1,000°K at pressure tube inner surface was used for the present analyses.

At low PHTS pressure (< 1.0 MPa(a)), fuel channels may fail because of a local melt-through or sagging of pressure and calandria tubes. Fuel channel melt-through occurs if the local volume-weighted-average of the pressure-tube and the calandria-tube temperature is greater than the melting point of oxygenated zirconium, or if either tube is hotter than user input temperature currently used as 2,125°K. The fuel channel is assumed to fail by sagging when the fuel channel temperature exceeds 1,473°K.

The Reactor Engineering Division of Bhabha Atomic Research Centre and Nuclear Power Corporation of India Limited used a mechanistic model to predict the high temperature behaviour of the pressure tube based on accumulated strain. However, no failure occurs until the fuel channel disassembly when the average pressure tube and calandria tube temperatures reaches 1,473°K.

### **2.2.3. Fuel channel disassembly**

Disassembly is a process during which fuel and channel structural materials are separated from the original channel and relocate downward to either the suspended debris or to the terminal debris bed. The suspended debris bed will transfer to the calandria vessel bottom when the core collapses. An axial segment of the fuel channel is deemed to be disassembled if and when the average temperature of the pressure tube and calandria tube reach 1,473°K for the uncovered channel.

### **2.2.4. Core collapse**

The term core collapse refers to a massive relocation of suspended debris and some intact fuel channels to the bottom of the calandria vessel. When a large amount of core debris becomes lodged above the water level on top of the supporting channels (submerged channels) and the total debris mass exceeds the load-bearing capacity of the supporting channels, the supporting channels along with the debris bed can collapse. It is assumed that the suspended debris is supported by the calandria tubes rather than the pressure tubes since the latter could be hot and weak. Under those conditions two main calandria tube failure mechanisms are considered. The supporting calandria tubes can either pull out from the rolled joints or shear. When the suspended debris bed mass exceeds 25,000 kg per one PHTS loop, the core material in the suspended bed, plus some of the intact channels covered by the moderator relocate into the bottom of the calandria vessel. The 25,000 kg mass is equivalent to seventy channels [3], assuming seven consecutive channels above a submerged channel are able to support the accumulated mass. Under some conditions partial core relocation may also occur, as molten

core material relocates, depriving sufficient mass from accumulating in the suspended debris bed to reach core collapse criteria (25,000 kg).

The analysis by Shanghai Jiao Tong University assumed that core relocation to the bottom of the calandria vessel to start at a cladding oxide layer temperature of 2,500°K (2,227°C). The relocation process continues as individual channel segments reach the oxide layer temperature.

#### **2.2.5. Calandria vessel failure**

The calandria vessel can fail due to creep, over-pressurization or attack from molten corium. As a result, a number of failure criteria may be employed to determine the failure of calandria vessel:

- Failure by creep: this involves calculating the hoop-stress on the calandria vessel wall at a given temperature and pressure. It then uses the stress and Larson-Miller parameter to obtain the creep rupture time and the conditions to fail the calandria vessel by creep;
- Failure by high pressure: calandria vessel pressure of 2.25 MPa;
- Failure due to molten metal layer attack: this requires calculation of the erosion due to impingement of the jet, until the wall is breached;
- Failure due to reduced external cooling (prolonged film boiling/dryout).

The Reactor Engineering Division of Bhabha Atomic Research Centre used the calandria vessel creep and the calandria vessel steel reaching melting temperature as the failure criteria.

#### **2.2.6. Calandria vault (concrete) failure**

The calandria vault can fail in two different modes under severe accident conditions. The first failure mode is a pressure-induced failure mode that occurs due to internal pressurization. It normally involves a gradual pressure excursion, so no dynamic load needs to be examined. The second failure mode is a temperature-induced failure mode that can be defined as the loss of the structural integrity (normally because of the molten corium-concrete interaction) of the calandria vault concrete bottom or sidewall that facilitates a relocation of core debris out of the vault. Thus, the failure criteria for the calandria vault are as follows:

- Over pressurization – the calandria vault can be deemed to have failed if a preset pressure differential between outside and inside is achieved;
- Rupture disk failure – 70 kPa differential pressure across rupture disk;
- Corium-concrete interaction – the calandria vessel can be deemed to have failed either as the wall is breached, or when a certain thickness remains.

When the core debris/corium is relocated into the reactor vault after the calandria vessel failure, the reactor vault floor erodes as a result of core-concrete interaction. The thickness of the reactor vault concrete floor is 2.45 m. When the eroded concrete thickness reaches a user-specified value, the floor can no longer support the weight of concrete and corium and the reactor vault is considered failed. This eroded concrete depth is set to 2 m in the present work.

#### **2.2.7. Containment failure**

Two containment failure criteria are proposed:

- Containment equipment airlock seal failure at 334 kPa(a) with an failure cross sectional area of 0.027871 m<sup>2</sup>;
- Containment failure under pressure loads when containment pressure of 500 kPa(a) is reached with an failure surface area of 0.1 m<sup>2</sup>

The failure cross sectional area is normally taken up by the inflatable seals. In reality, the airlocks connect the reactor building (containment) with the service building. In this document, the term environment represents anything outside the containment boundary.

In the current analyses it was conservatively assumed that the seals on both the inner and outer airlock doors failed together, with no time delay to pressurize the airlock volume between the doors. Therefore, an airlock seal blowout, connecting the containment to the environment, was assumed to happen as soon as the containment pressure reached 334 kPa(a). This assumption also covered the possibility that an airlock door was open during the accident.

In addition to the airlock seal blow out model, the containment was assumed to leak at a maximum rate of 0.5% of containment volume in 24 hours, when pressurized to 224 kPa(a). The leakage rate was modelled to be proportional to the pressure differential between containment and the environment. No fission product retention mechanisms are credited through the containment leakage openings.

There was no other model or criterion employed, in the current study, for a large scale containment failure (i.e., concrete cracking), if there was a large pressure rise that could not be accommodated by the airlock seal blowout.

### **2.2.8. Fission products release**

The initial release of fission products from fuel sheath occurs when the combined fuel sheath/UO<sub>2</sub> temperature reaches a user defined value. At this value the noble gases in the gap are released from the fuel bundle. In the current analysis, fission product release from the sheath is assumed to occur as the sheath fails. The remaining fission products are released depending on the fuel temperature based on the fractional release models. During core disassembly process, when fuel bundles leave the original core boundary, fission products are released from the suspended debris bed in the calandria vessel. During core collapse and calandria vessel failure (leading to corium-concrete interaction), fission products are released from the terminal debris bed and containment, respectively.

A brief summary of the failure criteria used by various analysis codes in the benchmarking study are compared in Table 2-1.

## **2.3. COMMON ASSUMPTIONS**

A severe accident at a nuclear power plant would involve numerous physical and chemical processes, which are complex phenomena to model. Therefore, several assumptions were required for the analyses reported in this document. Where possible, best estimate assumptions were used for this study, including some conservative or bounding assumptions when information was limited. Several assumptions for plant systems, component and phenomena were made for SBO scenario analysis. These are summarized in Tables 2-2 and 2-3.

The purpose of the benchmarking is to compare code capabilities and therefore it is imperative that all code inputs used by the participating organizations are based on the same assumptions and initial conditions. The common assumptions which are shared among the participating organizations will be described in this section. They are discussed in detail in the report on CANDU 6 plant parameters [8]. The assumptions used in the benchmarking analysis of a SBO sequence are intended for a direct comparison of code outputs and the efficacy of embedded models in the analysis code. Therefore, the assumptions made in this analysis do not represent any real nuclear power plant design.

The assumptions used in the benchmarking analysis are:

- AC Power and all outside standby emergency power (Class III and IV) are unavailable;
- Reactor shutdown is initiated immediately after accident initiation;
- Moderator cooling and shield cooling are unavailable;
- Shut down cooling is not available;
- Main and auxiliary feed water are unavailable;
- Steam Generator (SG) main steam safety valves (MSSVs) are available, they open and close at set point to relieve pressure. Their set points are 5.11 MPa(a). The steam flow rate at that pressure is 99.1 kg/s per valve and they open/close within 1 second;
- Turbine main stop valves are closed after accident initiation. The valve closure time is assumed to be 20 s;
- Containment leakage is considered. Each participant used an appropriate opening area to satisfy the leakage rate of 0.5% of free space volume per 24 h at 124 kPa(g). The leak location is assumed to be at stack;
- Emergency Core Cooling System (high, medium, and low pressure) are unavailable;
- SG Crash cool-down not credited;
- Dousing is not credited;
- Local Air Coolers (LACs) are not available;
- Air-operated Atmosphere Steam Discharge Valves have no back-up air and springs. They are fail-closed and are not considered in the case of SBO;
- All operator Interventions are not credited;
- PHTS Liquid relief valves are assumed to be connected to the containment directly. They open and close based on the open set point of degasser condenser relief valve. The water flow rate of 26.7 kg/s (D<sub>2</sub>O) is used at the opening set point of 10.157 MPa(a);
- Under steady state conditions, the following heat balances are used: core power of 2155.9 MW, PHTS pump power of 17 MW, thermal power to SG 2064 MW, heat loss to containment 3 MW, and heat load to moderator of 105.9 MW;
- Pressurizer initial inventory of 30,600 kg is assumed for light water. This is approximately 27,567 kg of heavy water (according to the ratio of heavy water to light water density);
- The structural data are given by AECL and the data in the AECL report [8] are used;

In addition, the CANDU 6-specific PHTS configuration with elevation data is used for the PHTS modeling. Figure 2-3 shows the CANDU 6 PHTS dimensions used for the accident simulation and Table 2-3 gives the dimension list for the 23 items shown in Figure 2-3. Also Figure 2-4 shows the channel power distribution.

#### 2.4. INITIAL CONDITIONS

Although care was taken to apply consistent initial conditions in the codes used in the benchmarking study some variations were unavoidable due to how the codes interpret the supplied initial conditions. The variations in the input conditions are however documented so that they can be factored in the comparisons to make useful observations and conclusions. The major initial conditions are given by AECL and they are shown from Tables 2-4 to 2-7. Table 2-4 shows the core inventories and geometry. Table 2-5 shows the Calandria Vessel geometry data. The active and stable fission products in a generic CANDU 6 core are shown in Table 2-6. The steady state conditions used by each participant are given in Table 2-7. When the given information is not enough for the accident simulation, each participant used their own data along with the AECL information.

TABLE 2.1. APPLICATION OF PHENOMENA CONTROL CRITERIA

Phenomena	Criteria	AECL	BARC-RED	BARC-RSD	KAERI	NPCIL	PUB	SJTU
Fuel sheath failure	Sheath temperature 1073°K (800°C)	√	√	√	√	√		√
	Mechanistic model to calculate the elastic-plastic deformation in SCDAP						√	
Fuel bundle slumping	And combination:	√	-	-	-	-	-	-
	1. Clad temperature of 2123°K (1850°C) (Zircaloy melting temperature)							
	2. Fuel channel must be covered by moderator 3. Pressure tube temperature exceeds a predefined user-input value of 1273°K (1000°C)							
Fuel channel failure	High pressure fuel channel (PT & CT after contact) failure temperature of 1000°K (727°C) at PT inner surface	√	-	√	√	-	√	√
	Low pressure fuel channel failure temperature of 1473°K (1200°C)	√	-	-	-	-	-	-
	Local true stress exceeds ultimate stress at specified temperature		√	-	-	√	-	-
Fuel channel sagging to below channel	Pressure tube temperature of 1473°K (1200°C) - from longitudinal creep correlations.	√	-	-	√	-	-	-
Fuel channel disassembly	Average temperature (PT and CT) of 1473°K (1200°C) for uncovered channel	√	√	√	√	√	√	√
Core collapse	Channel mass of 25,000 kg per loop	√	√	√	√	√	√	-
	Cladding oxide layer temperature of 2500°K (2227°C)							√

TABLE 2.1. APPLICATION OF PHENOMENA CONTROL CRITERIA (CONTINUED)

Phenomena	Criteria	AECL	BARC-RED	BARC-RSD	KAERI	NPCIL	PUB	SJTU
Calandria vessel failure	Calandria vessel failure due to Larsen-Miller parameter	√	-	-	√	-	√	-
	Failure due to internal pressure exceeding 2.25 MPa(a)	√	-	-	-	-	-	-
	Failure due to coherent melt jet impinging on calandria vessel wall	√	-	-	-	-	-	-
	Water level falls below debris level	-	-	-	-	√	-	-
	10% local creep of CV	-	√	-	-	-	-	-
	Melting temperature of CV (1873°K, 1600°C)	-	√	√	-	-	-	√
Calandria vault failure	Failure by MCC1: remaining thickness of 0.45 m (2 m eroded from original thickness of 2.45 m)	√	-	√	√	-	√	-
	Ablation of total concrete slab due to dehydration	-	√	-	-	√	-	-
Containment failure	Containment equipment airlock seal failure at 334 kPa(a) – 0.027871 m <sup>2</sup>	√	√	√	√	√	√	√
	Containment pressure of 500 kPa(a) – 0.1 m <sup>2</sup>	√	√	√	√	√	√	√

TABLE 2.2. SBO ANALYSIS ASSUMPTIONS FOR SYSTEMS AND COMPONENTS

System	Assumption	
	Available	Not available
Class IV power		√
Class III power		√
Reactor shutdown	√	
PHTS loop isolation	NPCIL, KAERI	√
Emergency Power Supply		√
D <sub>2</sub> O supply system		√
D <sub>2</sub> O recovery system		√
D <sub>2</sub> O make up system		√
Turbine main stop valve closure	√	
Main feedwater system		√
Auxiliary feedwater system		√
Emergency water supply system		√
Main steam safety valves (MSSV)	√ (Use lowest setpoint of 5.11 MPa(a) only)	
Main steam isolation valves (MSIV)		√
Air-operated atmospheric steam discharge valves (ASDV)		√ (assume fail-closed)
Condenser steam discharge valves (CSDV)		√
Steam generator crash cool-down		√
Moderator cooling system		√
Shield cooling system		√
Shutdown cooling system		√
High pressure ECCS		√
Medium pressure ECCS		√
Low pressure ECCS		√
Dousing spray		√
Local air coolers in containment		√
Moderator rupture disk rupture	√	
Calandria bleed valve	√	NPCIL
H <sub>2</sub> recombiners (PARs)		√
Hydrogen igniters		√
Containment Isolation system		√
Containment ventilation system		√
Calandria (or Reactor) vault rupture disk rupture	√	
PHTS liquid relief valves (LRV) open	√ (Assume degasser condenser relief valve at LRV location)	
Degasser condenser tank and related pressure & inventory control components		√
Operator interventions		√

TABLE 2-3. CANDU PHTS DIMENSION LIST

Item #	Value (m)	Description
1	0	Elevation of calandria inside bottom (at zero elevation)
2	3.380	Elevation of calandria center line
3	0.863	Elevation of ROH bottom
4	0.534	Height of ROH
5	9.8814	Elevation of RIH bottom
6	0.483	Height of RIH
7	10.269	Elevation of bottom of SG inlet at ROH
8	4.974	Length of SG inlet
9	1.263	Height of SG bottom to tube sheet top
10	12.508	Elevation of SG tube sheet top
11	21.860	Elevation of SG U tube top
12	9.352	Height of SG U tubes
13	0.394	SG tube sheet thickness
14	4.776	Length of pump suction line
15	10.9775	Elevation of bottom of pump suction line
16	2.655	Height of pump discharge line
17	10.307	Elevation of RIH top
18	6.760	Elevation of calandria inside top
19	6.789	Elevation of calandria outside top
20	16.216	Elevation of pressurizer bottom
21	29.550	Length of pressurizer surge line (to SG inlet)
22	0.281	Pressurizer surge line ID
23	0.0214	Pressurizer surge line wall thickness

TABLE 2.4. CORE INVENTORY AND GEOMETRY DATA

Description	Value	Units	Comments
Initial mass of UO <sub>2</sub> in the whole core	98815.2	kg	21.67 * 12 * 380 (21.67 kg/bundle)
Fuel channel length (12 bundles)	5.944	m	
Fuel bundle length	0.495	m	
Outside diameter of a pressure tube	0.112064	m	PT inside diameter (ID) =0.103378
Wall thickness of the pressure tube	0.004343	m	
Outer diameter of calandria tubes	0.1317	m	
Calandria tube wall thickness	0.0014	m	
Calandria tube pitch	0.2860	m	

TABLE 2.5. CALANDRIA VESSEL (CV) GEOMETRY DATA

Description	Value	Units	Comments
Number of CV rupture disks	4	-	
CV Rupture disk opening	137.8	kPa	Difference of CV pressure with containment pressure.
Rupture flow area per disk	0.1642	m <sup>2</sup>	
Delta pressure for next disk rupture	4.594	kPa	
Flow area of all bleed and relief valves	0.008908	m <sup>2</sup>	
Gauge pressure for opening of CV bleed valves	29.7	kPa	

TABLE 2.6. INITIAL FISSION PRODUCT (ACTIVE AND STABLE) INVENTORY IN A GENERIC CANDU 6 CORE

FP Number	Fission product element group	Average atomic weight* used in MAAP4-CANDU (kmole/kg)	Initial mass (kg)
1	Xe	131	53.82
2	Kr	84	3.88
3	I	131	2.60
4	Rb	86	3.55
5	Cs	133	25.36
6	Sr	88	11.83
7	Ba	138	14.28
8	Y	89	5.89
9	La	139	12.28
10	Zr	91	35.01
11	Nb	109	1.73
12	Mo	96	27.4
13	Tc	99	8.46
14	Ru	101	23.72
15	Sb	122	0.184
16	Te	128	4.81
17	Ce	140	33.84
18	Pr	141	9.19
19	Nd	144	30.51
20	Sm	150	4.94
21	Np	237	7.94
22	Pu	239	206.5

TABLE 2.7. INITIAL CONDITIONS USED BY EACH PARTICIPANT

Parameters	Unit	Target value	AECL	BARC-RED	BARC-RSD	KAERI	NPCIL	PUB	SJTU
Core thermal power	MWt	2,155.9	2,155.9	2156.0	2155.9	2155.9	2154.9	2,155.9	2064.0
PHT pump power	MW	17.0		15.0	17.0	17.0	19.6		
Heat loss to containment	MW	3		3	3	3	3	3	3
Heat load to moderator	MW	105.9		116.0	105.9	105.9	100.0	2.131*	
Thermal power to SGs		2,064	2,082	2,052	2,064	2,064	2,169	2,065	2,064
RIH temperature	°C	266	289	264.5	267.0	289	266	267	262
ROH temperature	°C	310	289	310.5	309.6	289	312	310	310
RIH pressure	MPa(a)	11.85	10.69	11.26	11.8	10.0	11.43	11.26	10.4
ROH pressure	MPa(a)	10.1	10.69	10.01	10.1	10.0	10.0	9.98	9.99
Pressurizer pressure	MPa(a)	9.99	10.69	10.01	9.9	9.9	10.0	9.85	9.99
PHTS loop flow	kg/s	1925	1925	1840	1901	1925	2100.9	1780	1925
Loop inventory (one loop)	kg	47,545	47,545	45,200	46,565	40,919	46,598	42,100	46,600
Pressurizer inventory	kg	30,555	30,614	29,500	27,620	31,143	30,176	20,449**	27,899
Total primary inventory including pressurizer	kg	125,704	125,704	120,036	120,750	112,982	123,371	104,648**	121,099
SG pressure	MPa(a)	4.7	4.7	4.7	4.62	4.7	4.7	4.7	4.69
SG temperature	°C	260	260.2	260	259.02	260.1	260	260	260
SG inventory (per SG)	kg	38,000	38,000	37,400	37,500	38,000	37,167	38,215	38,000
Moderator cover gas pressure	kPa(a)	123	97	123	126.0	123	123	105.9***	122.97
Moderator temperature	°C	69	69	70	69	68.9	69	69	70.7
Moderator inventory	kg	227,000	227,000	226,350	226,079	214,800	214,500	226,915	226,136
End shield pressure	kPa(a)	101	101		101.3	111.6		101	
End shield temperature	°C	63	63		38 <sup>(1)</sup>	63.4		52	
End shield inventory	kg	14,508	14,508		14,604	14,272		14,544	
Reactor vault pressure	kPa(a)	101	101	101	101.3	111.6	101	101	101.3
Reactor vault temperature	°C	51.5	51.5	50.1	38 <sup>(1)</sup>	51.8	52.0	52.0	51.5
Reactor vault inventory	kg	499,687	499,687	520,000	518,600	512,300	518,000	520,270	521,627

TABLE 2.7. INITIAL CONDITIONS USED BY EACH PARTICIPANT (CONTINUED)

Parameters	Unit	Target value	AECL	BARC-RED	BARC-RSD	KAERI	NPCIL	PUB	SJTU
Containment pressure	kPa(a)	101	101	101	101.3	100.8	101	101	101
Containment temperature	°C	31.85	31.85	30	30	32	31.85	32	35
Total containment free volume	m <sup>3</sup>	51,325 (Assuming no water is in dousing tank and reactor vault)	51,325 (Assuming no water is in dousing tank and reactor vault)	51,321	51,321 (Assuming no water is in dousing tank and reactor vault)	51,325	51,325 (Assuming no water is in dousing tank and reactor vault)	51,325 (Assuming no water is in dousing tank and reactor vault)	53,000

**Special notes on Table 2.7:**

**AECL**

MAAP-CANDU, used by AECL, has one-node PHTS thermal hydraulic model and therefore ROH and RIH temperatures are the same in MAAP-CANDU input (562 K or 289°C).

**BARC-RED**

Initial inventories of PHTS and SG were smaller as compared to targeted values. This occurred due to initial adjustment by RELAP5 code during achieving steady state. This may be the reason for early SG dryout. End shield system has not been modelled.

**BARC-RSD**

- (1) The endshield water temperature is taken same as end shield gas temperature i.e. 38 °C (311°K)
- (2) The reactor vault water temperature is taken same as reactor vault gas temperature i.e. 38 °C (311°K)

**KAERI**

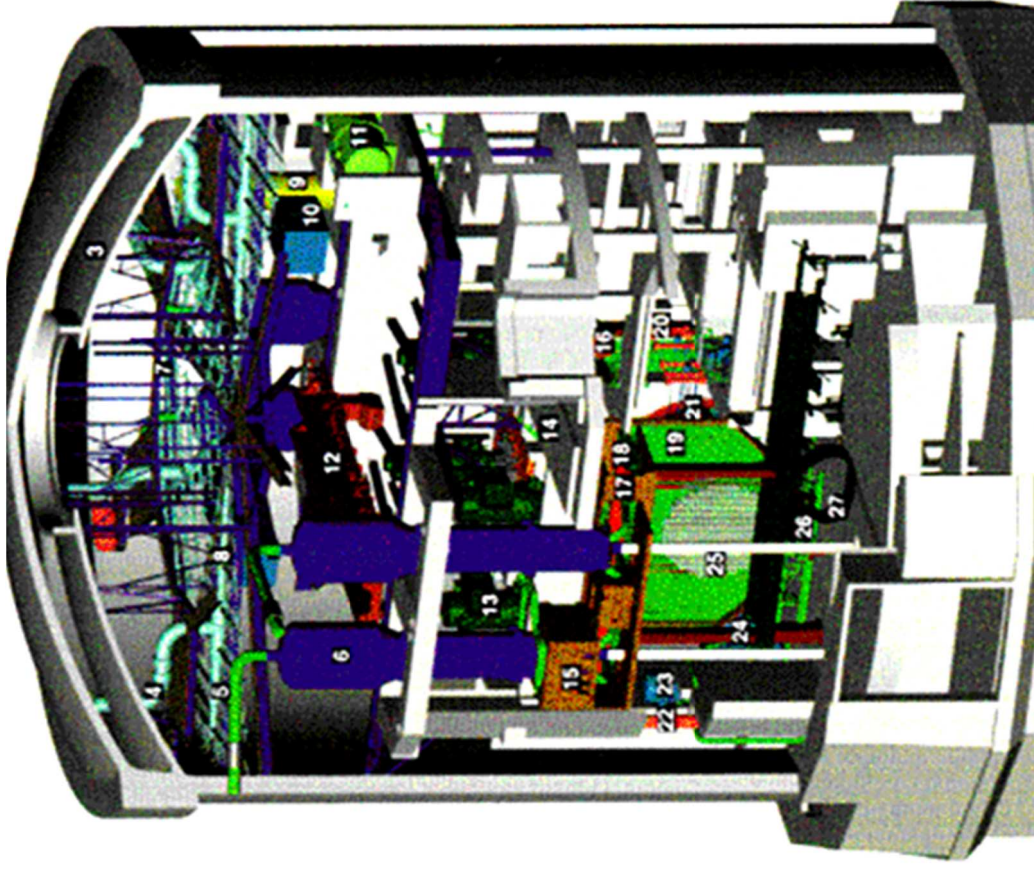
- Since ISAAC has a single PHTS volume, it has the same pressure and temperature around the loop initially.

**NPCIL**

Data which a not available are supplemented by Indian HWR.

**PUB**

- \* The amount of heat transferred to the moderator from the fuel channels
- \*\* Inventory from pipes connecting ROH and pressurizer not included
- \*\*\* Average value between top and bottom of the calandria vessel



### CANDU 6 CUTAWAY KEY

- 1 Reactor building
- 2 Turbine building (not shown)
- 3 Dousing tank
- 4 Dousing system supply pipe
- 5 Main steam line
- 6 Steam generator
- 7 Walkway
- 8 Dousing headers & nozzles
- 9 Pressurizer
- 10 Local air cooler
- 11 D<sub>2</sub>O Storage tank
- 12 Crane
- 13 Heat transport pump
- 14 Reactivity mechanism deck
- 15 Boiler enclosure
- 16 Helium supply tank
- 17 Feeder pipe insulation cabinet
- 18 Headers

FIG. 2.1. A cutaway view of CANDU reactor building.

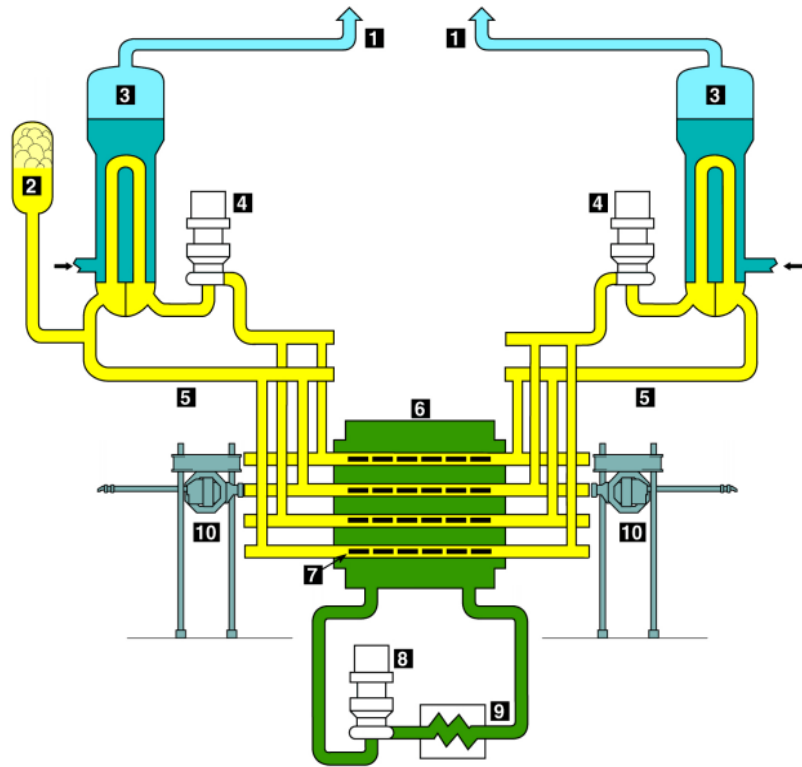


*FIG. 2.2. A schematic of a CANDU primary heat transport system (Legend: 1. steam line leading to turbines, 2. pressurizer, 3. steam generator, 4. pumps, 5. inlet headers, 6. calandria vessel, 7. fuel channel, 8. moderator circulation pump, 9. moderator heat exchanger, and 10. online refueling machines).*

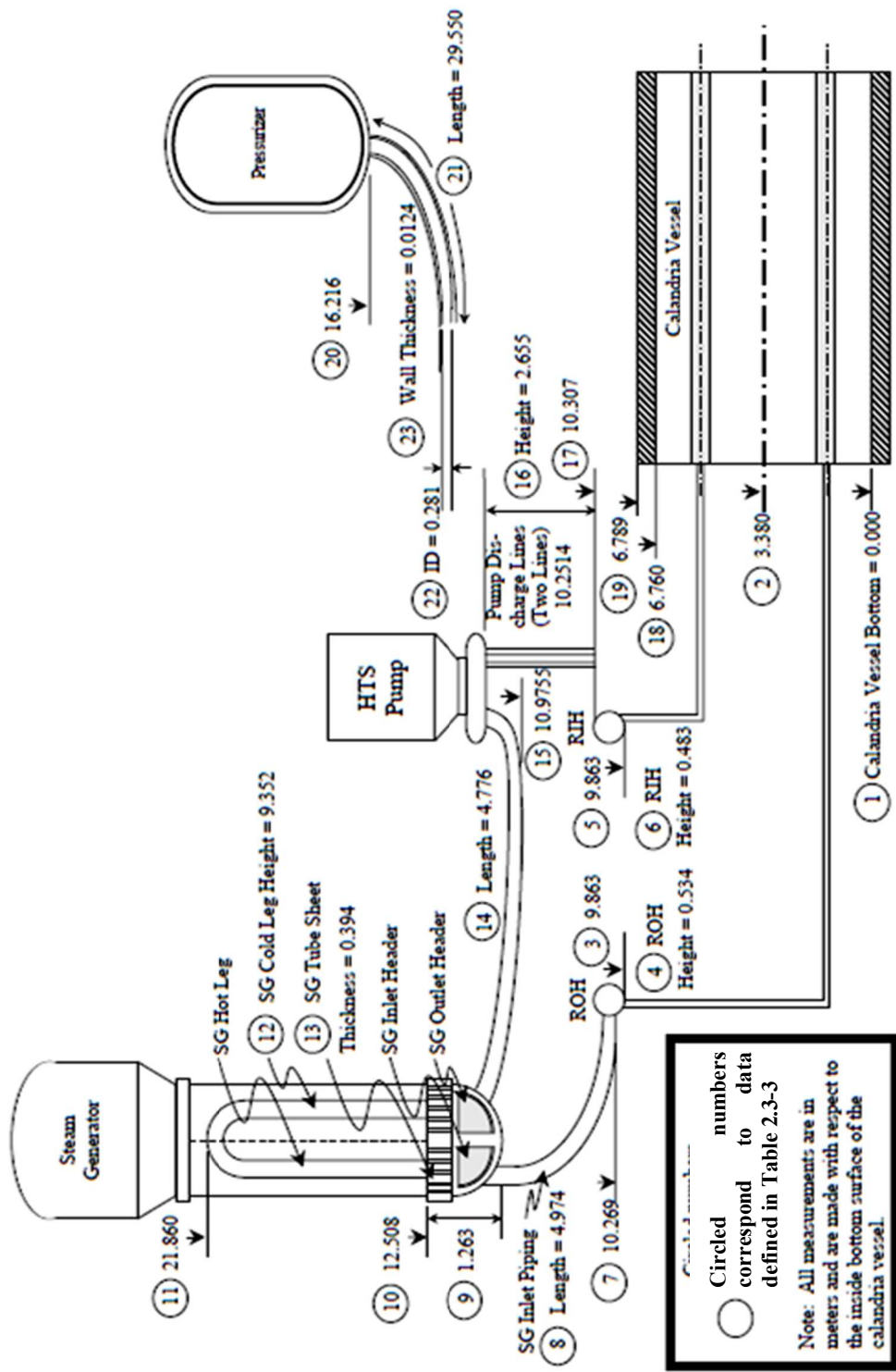


FIG. 2.3. Reference CANDU6 PHTS configuration with elevation information.

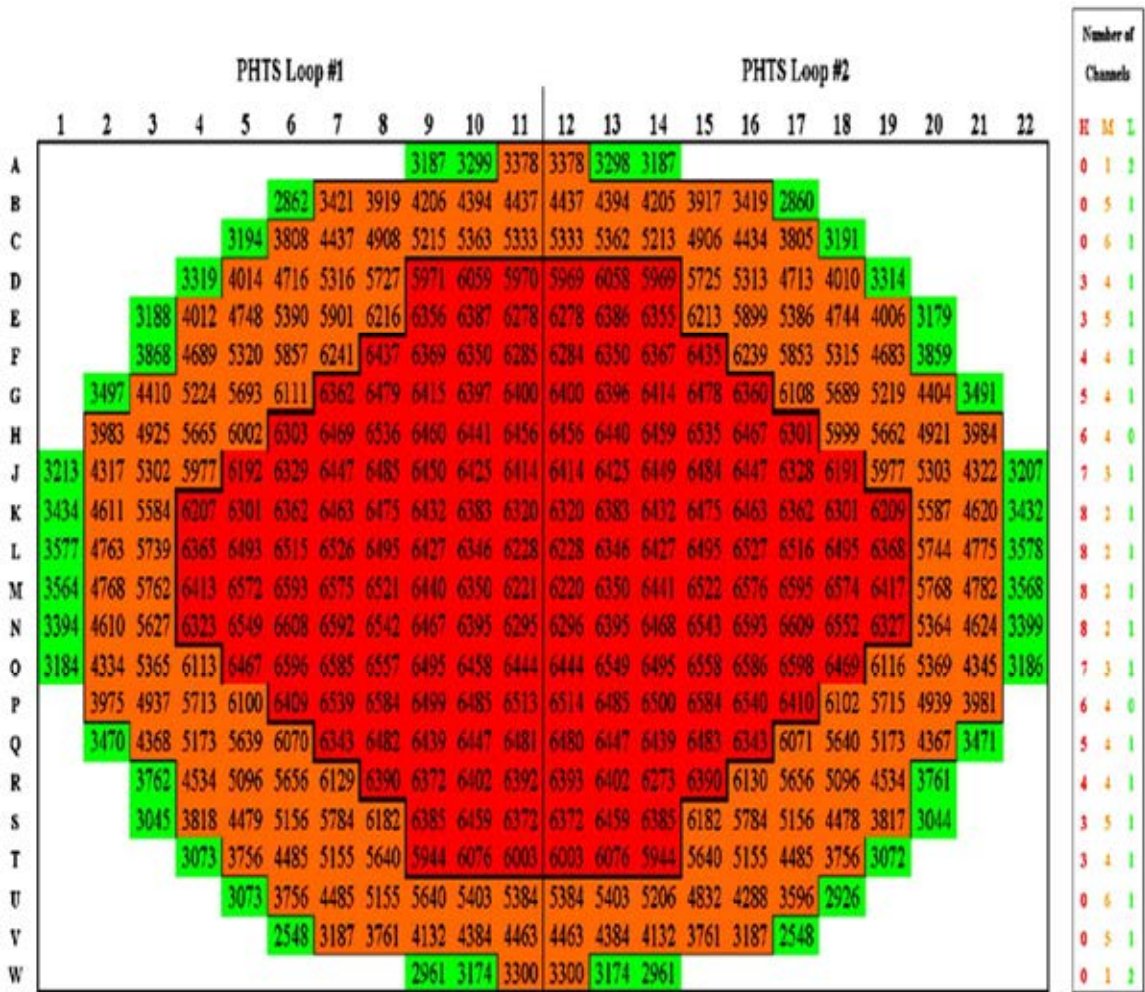


FIG. 2.4. Channel power distribution in CANDU6 reference plant.

### 3. PARTICIPANT'S MODELS AND RESULTS

#### 3.1. AECL

##### 3.1.1. Computer codes

AECL used the severe accident code MAAP (Modular Accident Analysis Program) for the Coordinated Research Project. The version MAAP4-CANDU v4.0.6A was executed on a PC Pentium IV 3.2 GHz computer. MAAP is an integral nuclear plant analysis code for modelling severe core damage accidents [9]. The code was developed for pressurized and boiling light water reactors by Fauske and Associates Incorporated (FAI), and is owned by the Electric Power Research Institute (EPRI). The MAAP4-CANDU Channels System is the portion of the MAAP4-CANDU code that models the thermal-hydraulic, thermal-chemical, and thermal-mechanical behaviour of the CANDU horizontal channels as they heat up and disassemble into debris.

The MAAP4-CANDU can simulate the response of the CANDU power plant during severe accident sequences, including actions taken as part of accident management. These predictions encompass the evolution of a severe accident starting from full power conditions, when provided with a set of system faults and initiating events, through events such as core melt, primary heat transport system failure, calandria tank failure, shield tank failure, and containment failure. Furthermore, models are included to represent the actions that could stop the accident by cooling the debris in the calandria tank or containment. The code can also model the thermal-hydraulics and fission product behaviour in the primary heat transport system, steam generator and pressurizer in loops 1 and 2, calandria tank, shield tank, containment, and vacuum building. Models are included for engineered safeguard system logic and performance. Operator actions can also be simulated by specifying intervention conditions and responses.

The MAAP4-CANDU Channels System is a segment of MAAP4-CANDU code that simulates the characteristic fuel channels and their contents after the channels are dry (i.e., empty of water) and during the channel heat up and subsequent processes (e.g., Zr-steam reaction, channel disassembly, suspended debris behaviour). Each characteristic channel represents a larger number of associated channels with similar power, elevations within the core, and feeder geometries. The core heat-up processes are modelled in the characteristic channels only after the channel is deemed dry (i.e., when the water remaining in the channel, attached feeders and end fittings is less than a user input value, which is typically 1.0 kg). The Channels System also models the disassembly of the fuel and fuel channel into suspended debris, but the processes after the debris (solid and molten) has moved to the terminal debris bed are modelled by a different system in the MAAP4-CANDU code.

The modelled processes and phenomena, which control the core behaviour in the MAAP4-CANDU Channels System, include:

- The fuel / fuel-channel heat up and temperature excursion, and fuel bundle / sheath melting;
- Heat transfer from dry channels to the calandria vessel steam and water;
- Pressure tube / calandria tube ballooning and rupture at high pressure;
- Steam / hydrogen flow in the channels and channel remnants;
- The zirconium-steam reaction in fuel channels and suspended debris;
- The thermal-mechanical failure (perforation) of calandria tubes;
- The disassembly of fuel channels to the suspended debris;

- Tracking fission products that remain within the in-channel fuel and within suspended fuel debris, plus the heat generation;
- The formation of suspended solid debris and molten debris, and;
- The motion of solid and molten suspended debris to the terminal debris bed.

The CANDU core is different from that of PWRs and BWRs. The disassembly of the horizontal channels and core relocation during a severe accident is more complex. Several phenomenological models [10, 11, and 12] specific to the CANDU core have been implemented by best-estimate calculations. The MAAP4-CANDU Channels System is computationally intensive. A modular code structure was used to provide code architecture that decouples the MAAP4-CANDU Channels System from other MAAP4-CANDU components and from MAAP4 generic routines, to allow better code maintainability, model improvements, and adjustments to other CANDU reactor configurations. Code improvements are thus performed in a more secure and independent manner. The basic architecture of the MAAP4 CANDU code is shown in Figure 3-1. The design of this architecture enables MAAP4 CANDU to be developed and maintained in a reasonably independent manner, minimally affected by generic MAAP4 updates. The MAAP4-CANDU Channels System architecture is shown in Figure 3-2. The “F” denotes a FORTRAN source file.

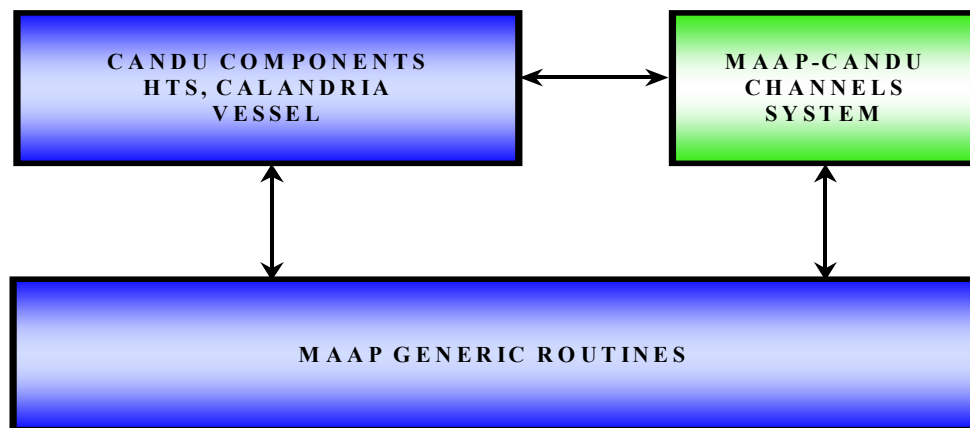


*FIG. 3.1. MAAP4-CANDU architecture.*

The MAAP4-CANDU parameter file for the CANDU 6 station consists of ~5,000 parameters, which describe the most important systems and components. It is not practical to list all input data here. The input data was provided separately in a document [13]. The concrete composition is an important parameter that will determine the erosion progression and gas release into containment during corium-concrete interaction. The concrete composition can vary from one station to another. Each fission product element group is composed of all the constituent isotopes (radioactive plus stable), and has an average atomic weight, as listed in Section 2.4.

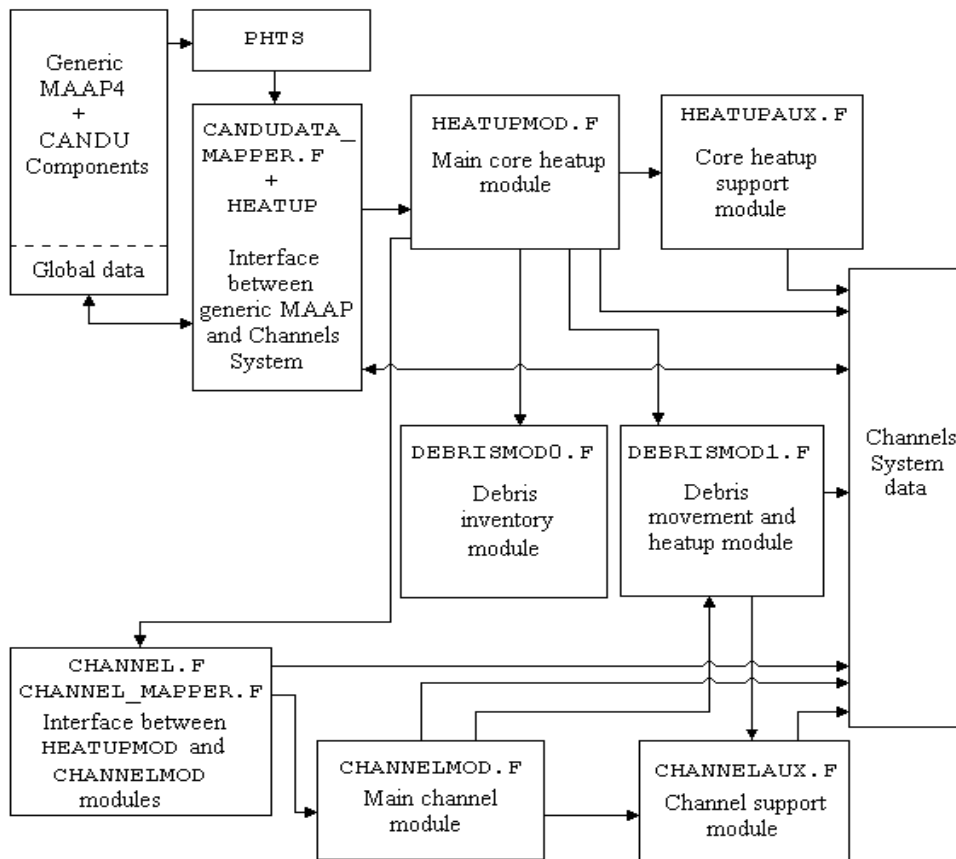


FIG. 3.2. MAAP4-CANDU Channels system modularization.

### 3.1.2. Phenomena and system idealization

In this section the system idealization, the major initial and boundary conditions used in the benchmark analysis will be described. The CANDU 6 station consists of a reactor building, service building, turbine building, and other auxiliary structures. The reactor building contains all the equipment directly associated with the production of steam, e.g., PHTS, steam generators, reactor and other components. The PHTS is designed to circulate pressurized heavy water through the fuel channels to remove the heat produced in the fuel. The heat is then transferred to ordinary light water in the steam generators, where the boiling produces the steam to drive the turbine generator.

The reactor assembly consists primarily of a calandria vessel, which is penetrated by 380 horizontal fuel channels and contains heavy water moderator. Each fuel channel consists of a pressure tube, a calandria tube and 12 fuel bundles containing 37 fuel elements. The calandria vessel is located inside a steel-lined concrete reactor vault. The reactor vault is filled with light water, which provides shielding and maintains the calandria vessel at nearly a constant temperature during normal operation. End-shields at both ends of the calandria vessel provide shielding at each end of the reactor.

#### 3.1.2.1. Containment model

The CANDU 6 containment is a very complex engineered enclosure consisting of many compartments and rooms. It is impractical to model each room as a single node. For example, if large openings connect several rooms, the gas pressure will be very similar in those rooms; therefore these rooms may be combined. In the present work, the containment has 13 nodes and 31 flow junctions (Fig. 3-3). Details of the containment rooms were obtained from the CANDU 6 containment design drawings.

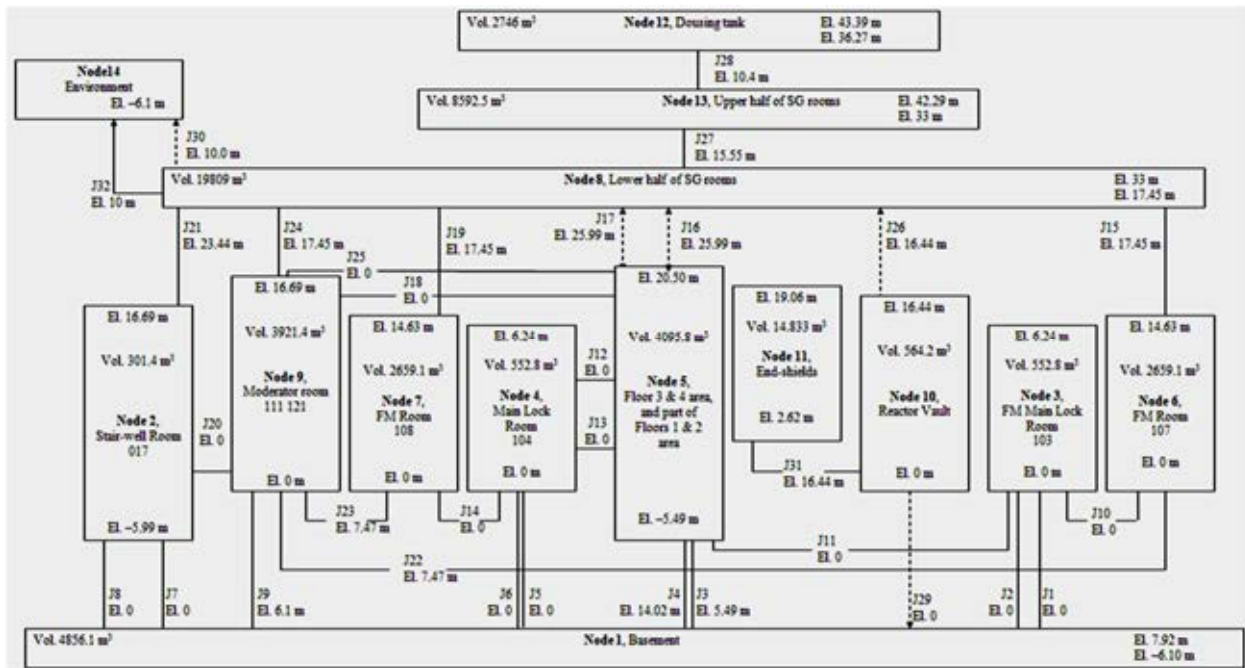


FIG. 3.3. Nodalization scheme for CANDU 6 containment.

Solid lines represent open junctions between nodes, and dotted lines represent failure junctions opened by pressure differences or (for J29) due to the molten corium – concrete interaction. J30 is containment failure junction open to the environment, and J26 represents the rupture disk between the reactor vault and containment. Junction 32 represents the containment leakage. Junction 17 is a hatchway, but it is kept sealed by imposing a very large pressure differential.

The containment nodalization used reactor vault and end shields as containment Nodes 10 and 11, respectively. The steam generator rooms are modelled as 2 nodes in MAAP4-CANDU. A total of 90 wall heat sinks (walls and floors) in containment are modelled in the present work. Structural steel in the containment (steel beams, columns, gratings, etc.) with a total mass of 820,000 kg is represented as a “two-sided” steel plate with a thickness of 2.54 cm and a total surface area of 8,200 m<sup>2</sup>. The structural steel mass is distributed within the containment compartments.

### 3.1.2.2. PHTS Nodalization

The CANDU 6 Primary Heat Transport System is comprised of two loops, each loop serving 190 of the 380 fuel channels. Each loop contains two steam generators, two pumps, two inlet headers, and two outlet headers. Feeders connect the inlet and outlet end of fuel channels to the reactor inlet and outlet headers, respectively. In CANDU 6, the flow through the fuel channels in one loop follows the shape of “figure of eight” with some channels carrying the flow inward and others outward from each reactor face. This “figure of eight” PHTS configuration is modeled in MAAP4-CANDU. The following PHTS components are modelled as 14 nodes in MAAP4-CANDU (Fig. 3-4):

1. Pump discharge line before inlet header 1
2. Reactor inlet header 1
3. Reactor outlet header 2
4. Inlet piping of steam generator 2
5. Hot leg tubes of steam generator 2
6. Cold leg tubes of steam generator 2

7. Pump suction line after cold leg tubes of steam generator 2
8. Pump discharge line before inlet header 2
9. Reactor inlet header 2
10. Reactor outlet header 1
11. Inlet piping of steam generator 1
12. Hot leg tubes of steam generator 1
13. Cold leg tubes of steam generator 1
14. Pump suction line after cold leg tubes of steam generator 1

Feeder pipes connecting headers and fuel channels are modeled as part of the fuel channel nodalization scheme. As discussed below, the 380 inlet feeder pipes are modelled as 18 nodes and the 380 outlet feeder pipes are modelled as an additional 18 nodes. MAAP4-CANDU has models of heat sinks of all the above-mentioned 14 PHTS components and all PHTS feeder pipes.

### 3.1.2.3. Core nodalization

The CANDU 6 core has 380 fuel channels arranged in 22 rows and 22 columns (Fig. 3-5). In MAAP4-CANDU not every fuel channel is modelled; rather, a simplified core model was used. The 22 rows were divided into 6 vertical nodes, with 4, 4, 3, 3, 4, 4 rows in each node. Within each vertical node, the fuel channels were divided into 3 fuel power groups; the highest power group within the given vertical node (high power channels), the medium power group within the given vertical node (medium power channels), and the lowest power group within the given vertical node (low power channels) (Fig. 3-6). The 22 columns of fuel channels were divided into 2 loops symmetric about the vertical axis. The left 11 columns are in one loop and the right 11 columns are in the other loop. Thus, we reduced 380 fuel channels to 2 loops, and each loop has 18 (= 6 x 3) representative channel groups.

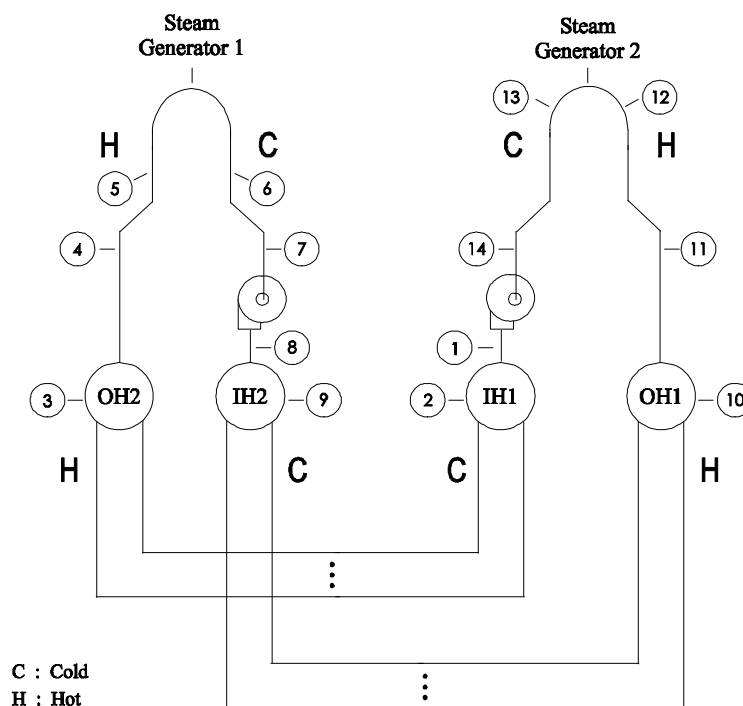


FIG. 3.4. Nodalization scheme for CANDU 6 Primary heat transport system heat sinks.

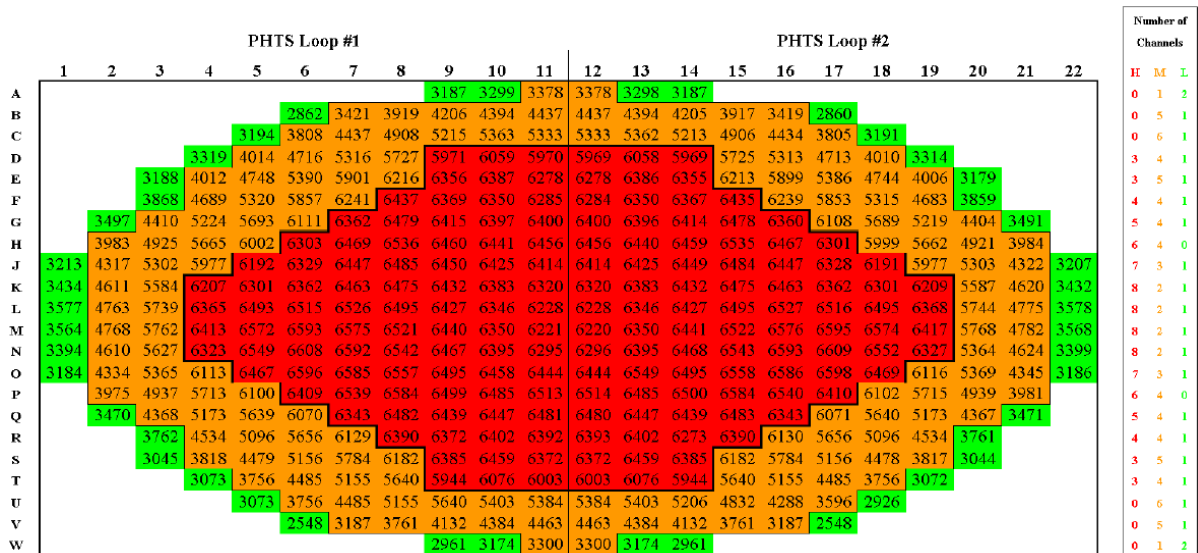


FIG. 3.5. Nodalization Scheme for CANDU 6 Core (time-averaged power for each channel is shown with four digits in [kW]). The notations H, M and L in the right hand box refer to high, medium and low power groupings per loop.

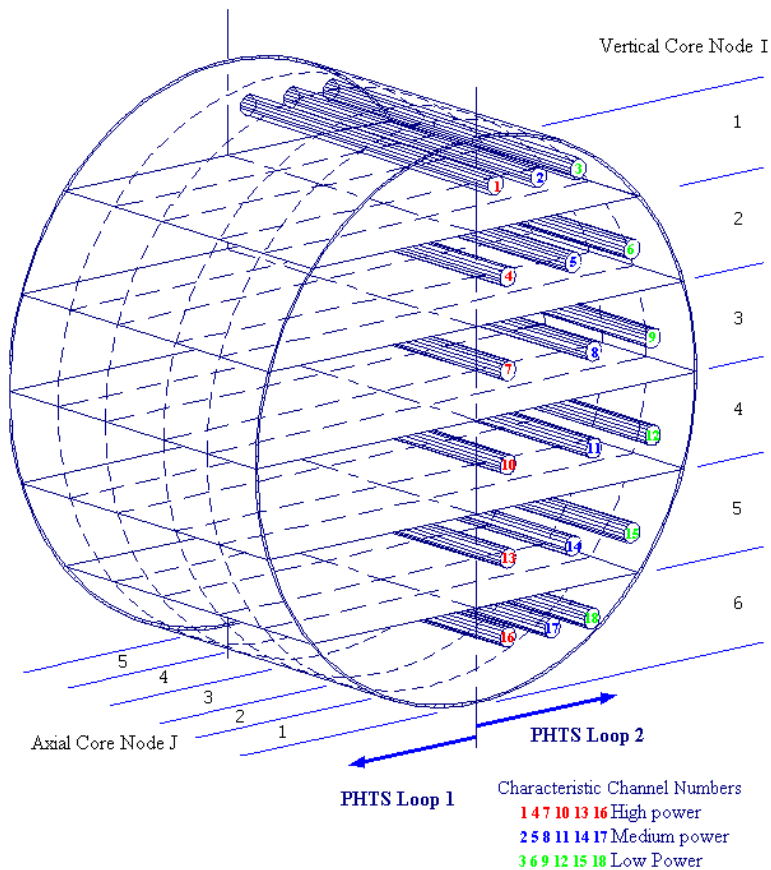


FIG. 3.6. Nodalization scheme for CANDU 6 Core.

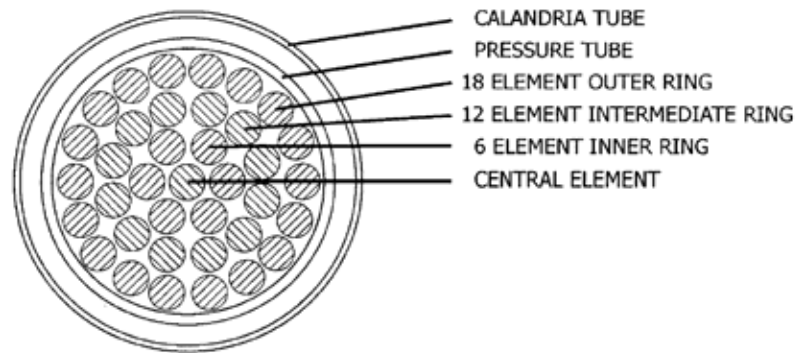


FIG. 3.7. CANDU 6 Fuel bundle consisting of a calandria tube, a pressure tube and 37 fuel elements.

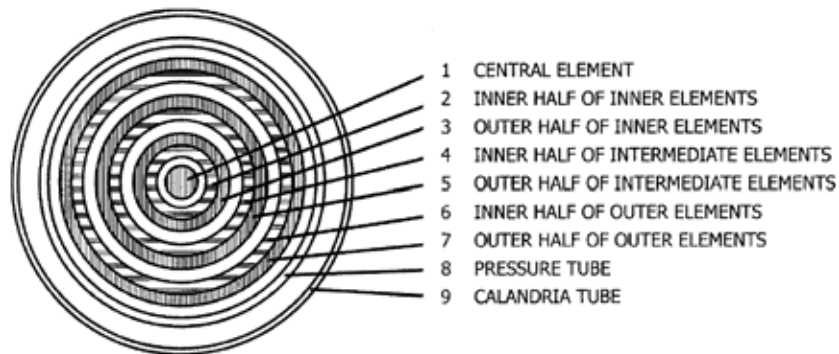


FIG. 3.8. CANDU 6 Fuel channel nodalization scheme used in MAAP4-CANDU.

In a CANDU 6, each fuel channel has 12 fuel bundles. In this study each fuel bundle is modelled as one axial node (see Fig. 3-6). Thus, the 380 channels, each containing 12 fuel bundles are modeled by a total of  $432 = 2 \times 6 \times 3 \times 12$  nodes (Fig. 3-6). Each fuel channel in a CANDU 6 consists of a calandria tube, a pressure tube, and 37 fuel elements arranged in 4 rings (central, inner, intermediate, and outer rings, see Fig. 3-7). We modelled each of the inner, intermediate, and outer fuel rings as 2 rings. Thus 9 rings represent a CANDU 6 fuel channel (Fig. 3-8).

#### 3.1.2.4. Calandria vessel wall nodalization

MAAP4-CANDU models a two-dimensional temperature distribution in the calandria vessel walls. Two types of the CV walls are considered: one wall-type (flat) represents the front and back face of the vessel and the other represents the cylindrical shell of the vessel. Both types of walls are sliced horizontally into 15 nodes from the vessel floor to the ceiling along the elevation levels (Fig. 3-9). The CV wall thickness is divided into radial nodes. The node thickness is determined by the code and is used for the CV wall internal heat conduction calculations. MAAP4-CANDU code assumes that the CV circumferential wall slice has the same temperature along the surface at a given time. The wall temperature of each slice of the front and back face of the calandria vessel is also uniform in the vertical direction.

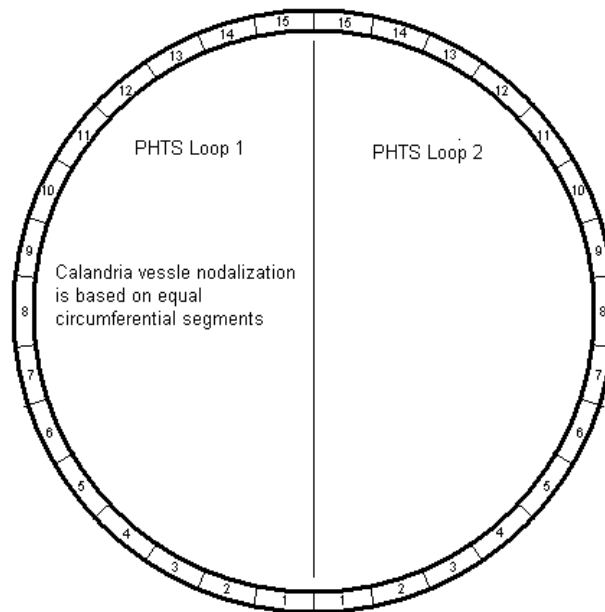


FIG. 3.9. Nodalization for CANDU 6 calandria vessel wall.

### 3.1.2.5. Steam generator model

The steam generator secondary side is represented as one node in MAAP4-CANDU. The primary side of the steam generator is represented as two nodes (cold legs and hot legs). A number of parameters for the primary and secondary sides of the steam generator are used in the MAAP4-CANDU input deck to describe the steam generator design. The parameters include the pressure set point for safety relief valves, the total volume of the primary side, the total number of U-tubes, the inside diameter of the U-tube, the diameter of tube sheet, the height of the shell above the tube sheet, a table of volume versus height in the secondary side, etc.

### 3.1.2.6. Pressure and inventory control system modeling

The CANDU 6 pressure and inventory control (P&IC) system consists mainly of a pressurizer, degasser condenser, D<sub>2</sub>O storage tank, D<sub>2</sub>O feed pumps, bleed cooler, pressurizer relief valves and HTS liquid relief valves. Pressurizer relief valves, steam bleed valves and PHTS liquid relief valves discharge into the degasser condenser. The Degasser condenser has spring-loaded relief valves which discharge to a containment compartment. The LRVs are air-operated, with back-up instrument air, and are designed to fail open. Normally this back-up air supply should maintain the valves in operation for two hours following power loss (for example, in case of SBO) and loss of normal instrument air. Pressurizer relief valves are designed to fail open.

The P&IC system is represented in MAAP4-CANDU by a pressurizer, which is connected to reactor outlet header. The line connecting the pressurizer with the reactor outlet header contains a motor operated pressurizer isolation valve, which is designed to be closed automatically in case of a LOCA. The closing pressure set point and valve closure time are user-specified in the parameter file.

All the basic thermal hydraulic processes such as boiling and condensation, flashing and rain out, behaviour of fission products as well as pressurizer heaters are modelled in MAAP4-CANDU. The degasser condenser, however, is not modelled in this analysis. MAAP4-CANDU models the PHTS LRVs which discharge directly to a user-specified containment compartment. The relief capacity of the HTS LRVs is assumed to be equal to the LRV design

value. Sensitivity analyses conducted for SBO shows that the relief capacity of HTS LRVs/degasser condenser relief valves has no significant contribution to the accident consequences and timing of events.

To model the P&IC system configuration in the current SBO analysis, the following assumptions are made:

- pressurizer steam bleed valves (PCV5 and PCV6) do not operate, because they are not spring-loaded; they are assumed closed all the time;
- pressurizer relief valves (PV47 and PV48), which have higher set points than the PHTS LRVs, are also considered closed all the time, and;
- opening and closing set-points for the LRVs are artificially assumed to be equal to the set-points of the degasser condenser spring-loaded relief valves RV-11 and RV-21 in the parameter file. We assumed no back-up instrument air to maintain LRV operation after SBO initiation available.

In addition to the analysis assumptions and models employed, the results of the analysis will depend on the failure criteria used to fail various CANDU 6 components, such as containment, calandria vessel, fuel channel, reactor vault and so on. Some of the criteria used in the analysis require user input values. Other criteria are calculated and applied by MAAP4-CANDU code. These failure criteria have been developed from experimental results, when available. If experimental data are not available, engineering judgment was used. A description of the failure criteria used in the present analysis is given in Section 2.2.

### 3.1.2.7. Phenomena important for station blackout scenario

The severe accident analysis is required for the determination of timing of events, containment integrity, and the level of fission product release. As opposed to design basis accidents, the timing of events in a severe accident occurs in hours rather than in seconds. As a result, only macroscopic behaviour of the core and other components is predicted. The phenomena required for the severe accident analysis have been identified as shown in TABLE 3.1.

TABLE 3.1. PHENOMENA RELEVANT TO CANDU SEVERE ACCIDENT ANALYSIS

Phenomenon Name	Phenomenon ID #	Phenomenon Name	Phenomenon ID #
Core Heat up	SA1	Debris Coolability	SA12
Clad Oxidation	SA2	Core-Concrete Interaction (CCI)	SA13
Fission Product Release	SA3	Reflective Insulation	SA14
Aerosol Transport and Deposition	SA4	Wall Ablation	SA15
Hydrogen Combustion – Complete	SA5	Fan Cooler	SA16
Hydrogen Combustion – Incomplete	SA6	Re-evaporation	SA17
In Vessel Cooling	SA7	Primary Heat Transport System(PHTS) Thermal-hydraulics	SA18
Vessel External Cooling	SA8	Containment Natural Circulation	SA19
Molten Debris Heat Transfer	SA9	Containment Strain	SA20
Debris Fragmentation	SA10	CANDU Fuel & Fuel Channels Thermal Response	SA21
Debris Dispersal	SA11		

### 3.1.3. Analysis results

#### 3.1.3.1. Phase I

The results of the Station Blackout consequence analyses performed using MAAP4-CANDU code are presented below. The station blackout scenario was considered to be a transient scenario initiated by a loss of off-site AC (Class IV) power with subsequent loss of all on-site standby (Class III) and emergency electric power supplies. The analysis assumptions for the SBO case are summarized in Section 2. The SBO sequence was run up to 500,000 s. The execution time was ~61 min. Table 3-2 lists the sequence of significant events observed during this simulation.

TABLE 3-2. SIGNIFICANT EVENTS TIMING COMPARISON FOR SBO SCENARIO

Time (h)	Time (s)	Events
0.0	0	AC power loss (Class IV & III)
0.0	0	Reactor trip due to loss of power.
0.0	0	Turbine main stop valves (MSIVs) closed
0.0	0	Moderator and shield cooling systems off
0.0	0	Main and auxiliary feed water off
0.0	0	Containment dousing system forced off
0.01	55	First opening of main steam safety valves in the SGs to the atmosphere
1.62	5818	Calandria vessel bleed/relief valves open
2.31	8332	LRV first opening
2.65	9559	Steam generator secondary side is dry, Loops 1&2
2.85	10 245	Reactor vault rupture disk opens to Node 8 (lower SG room), end shield water starts to boil off
3.35	12 058	Water and steam phases are separated in Loops 1&2 (PHTS coolant stagnant)
3.63	13 082	Fuel bundles are uncovered inside fuel channels in Loops 1&2
4.04	14 567	Pressurizer is empty
4.92	17 708	At least one channel is dry Loops 1&2 – Channel 7
4.97	17 918	Pressure and calandria tubes are ruptured Loop 2 – Channel 7
5.02	18 088	Calandria vessel rupture disk 1 is open to Node 8 (lower SG room)
5.04	18 147	Moderator in calandria vessel reaches saturation temperature
5.51	19 833	Beginning of the core disassembly in Loop 1
5.51	19 849	Beginning of the core disassembly in Loop 2
9.18	33 054	Containment failed
14.62	52 614	Water is depleted in calandria vessel
14.63	52 695	Core collapse to bottom of calandria vessel, Loops 1&2
14.87	53 554	Reactor Vault water reaches saturation temperature
14.93	53 749	End of core relocation onto calandria vessel bottom, Loops 1&2
55.6	200 189	Calandria vessel bottom wall failed (due to creep), core debris relocates to Reactor Vault
55.63	200 250	Calandria vessel rupture disks 2&3 is open to Node 8 (lower SG room)
63.78	229 621	Water is depleted in Reactor Vault
68.47	246 481	Molten corium-concrete interaction begins in Reactor Vault
68.25	245 711	Hydrogen/Carbon monoxide burning predicted in containment Nodes 8&11
68.53	246 711	Hydrogen/Carbon monoxide burning stopped in containment Node 11
N/A	N/A	Reactor Vault floor failed because of the molten core-concrete interaction.

## Primary heat transport system and steam generators response

The postulated initiating events for the SBO accident scenario are imposed at the start of the run. Figure 3-10 shows the pressure in the PHTS Loops 1 and 2. The pressure in the pressurizer is shown in Figure 3-11. As expected the pressure in both loops show similar behaviour. Initially the pressures in both loops decrease slightly with time. Such a decrease in pressure is mainly due to the following reasons: (1) the loss of fission power in the reactor core, (2) the core decay heat is transferred through the PHTS (no break in the PHTS yet) to the steam generators, and (3) the secondary side of the steam generators has sufficient heat sink capacity to absorb the decay heat. The heat transfer from the PHTS to the steam generators causes the water in the steam generator secondary side to boil off. As a result, the pressure in the secondary side of the steam generators increases gradually (Fig. 3-12) and causes the MSSVs to open and to discharge steam from the secondary side to the environment outside the containment. The secondary side steam generator pressure then oscillates at the MSSV set point as the MSSVs open and close. Figure 3-12 shows that all four steam generators have similar behaviour since the curves almost overlap each other. The water level in the steam generators decreases as a result of boil-off (Fig. 3-13).

When the steam generator secondary side inventory is depleted (Figs 3-13 and 3-14) at  $\sim 9,559$  s ( $\sim 2.7$  h), the steam generators dry out and no longer act as heat sinks to remove heat from the PHTS. Note that Figure 3-13 shows the reduction of the water level in the SG; zero level corresponds to the bottom of the wetted SG surface. The pressure in the PHTS increases until it reaches the PHTS liquid relief valve set point, 10.24 MPa(a), which was assumed to be the same as the degasser condenser relief valves set-point. The pressure in the PHTS then oscillates at the relief valve set point (Fig. 3-10). The degasser condenser tank is not modelled in this simulation, thus the coolant is assumed to discharge through the liquid relief valves into the containment rather than the degasser condenser. Continuous loss of inventory through the LRVs results in fuel channel dryout. In parallel, the moderator level in the CV decreases gradually as a result of decay heat from the core leading eventually to the uncovering of some top fuel channels. Subsequently, heat up of the calandria tubes and pressure tubes at the PHTS pressure of 10 MPa results in the PT ballooning and the rupture of the both tubes, causing a rapid blow-down from the PHTS into the calandria vessel. The PHTS pressure drops drastically at  $\sim 18,000$  s ( $\sim 5.0$  h) (Fig. 3-10), because of a fuel channel rupture at high pressure in PHTS Loop 1. For the PHTS loop inventory blow-down into the CV, MAAP4-CANDU assumes the blow-down flow area is equivalent to the flow area of a single fuel channel and that the blow-down is from both ends of the ruptured fuel channel.

Loop isolation valves are not closed to isolate the pressurizer from the PHTS when the pressure in the PHTS drops to 5.5 MPa (pressurizer isolation set-point) because the function of the PHTS isolation valves was not credited in this analysis. Therefore, the pressure in the pressurizer behaves similarly to the PHTS as shown in Figures 3-10 and 3-11. After the fuel channels in both loops rupture, the steam generator secondary side pressure decreases gradually (Fig. 3-12) because heat is no longer transferred from the PHTS to the steam generators.

Figures 3-15 to 3-17 show heat to PHTS and Steam Generators, water level in the Pressurizer, and water masses in PHTS Loops 1 and 2 to illustrate the events during SBO scenario. Figure 3-18 shows the loop void fractions and LRV steam and water flows from Loops 1 and 2. The amount of heat transferred to the moderator from the fuel channels and the amount of heat transferred to reactor vault water and gas/steam are shown in Figures 3-19 and 3-20, respectively.

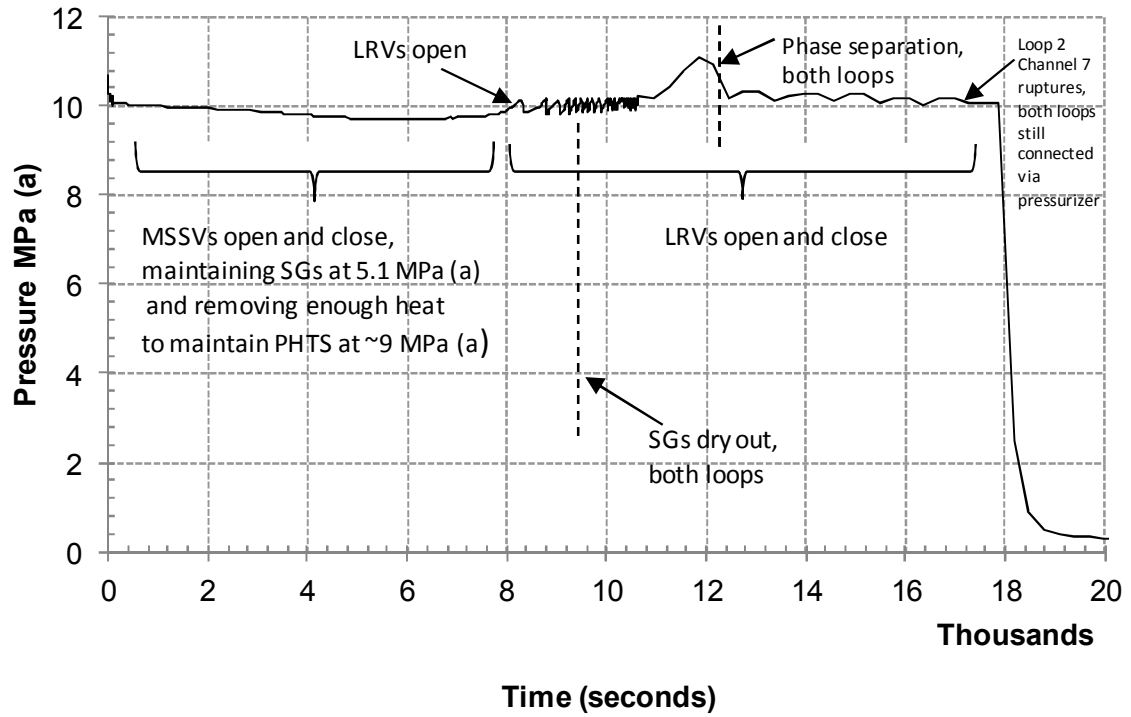


FIG. 3.10. Primary system loops 1 and 2 pressure (0 – 20,000 s).

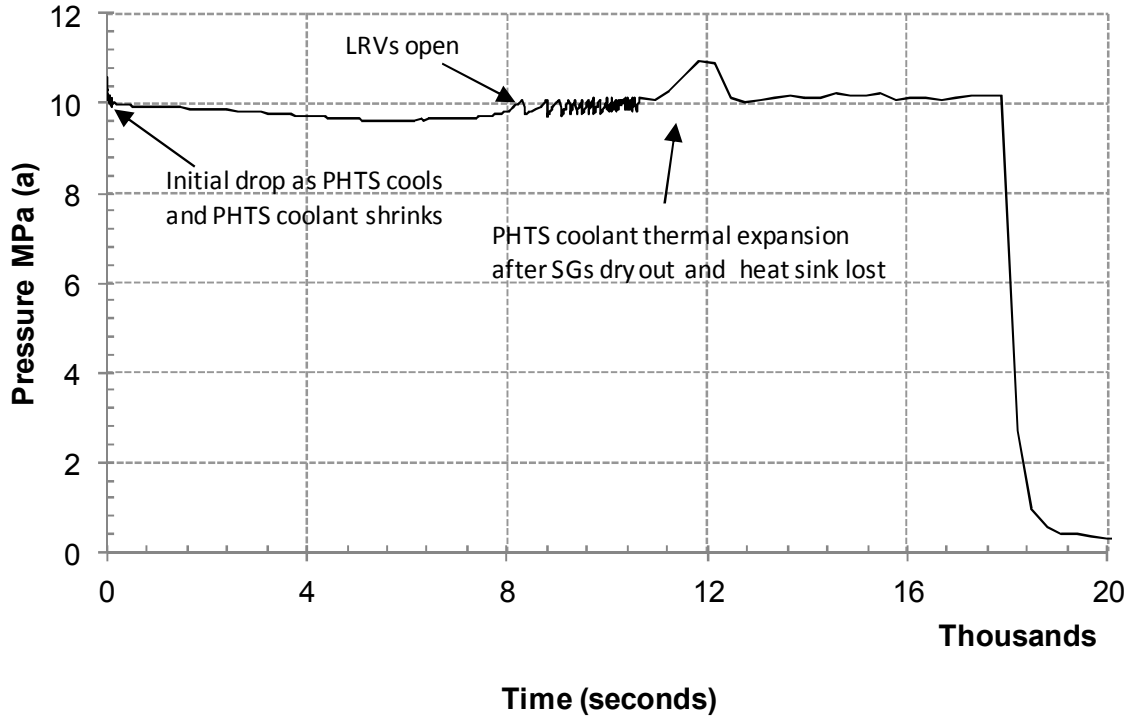


FIG. 3.11. Pressurizer pressure (0 – 20,000 s).

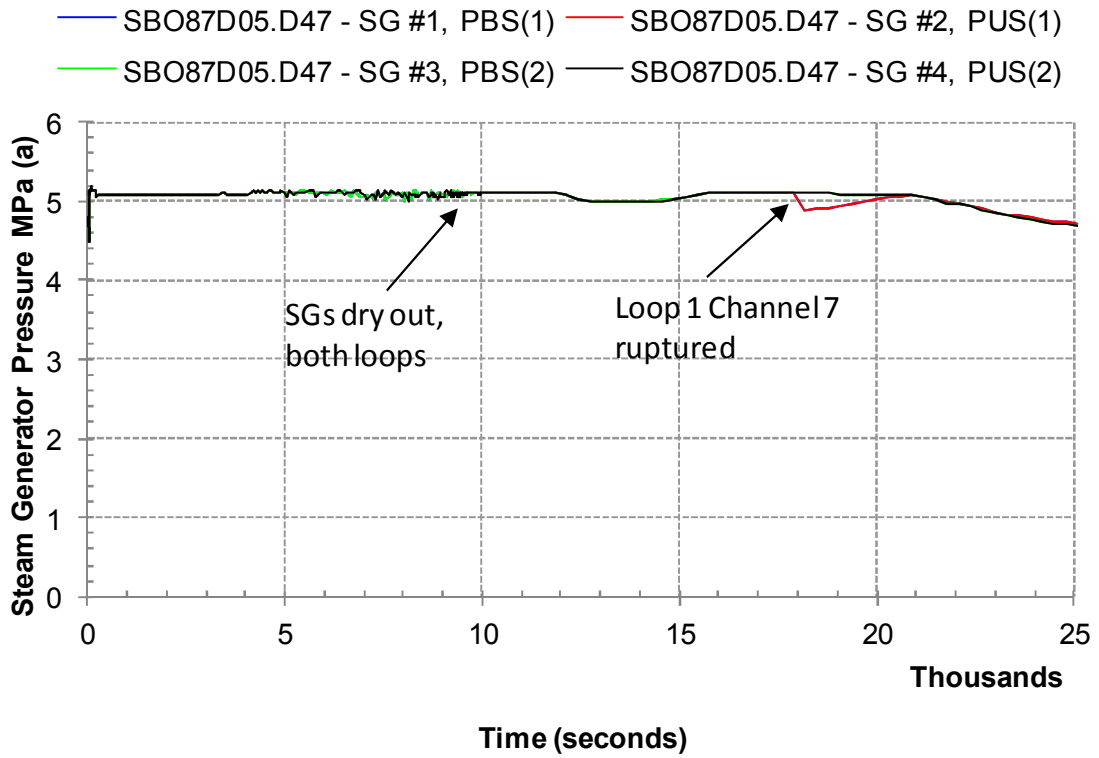


FIG. 3.12. Steam generator secondary side pressures for PHTS Loops 1 and 2 (0 – 25,000 s).

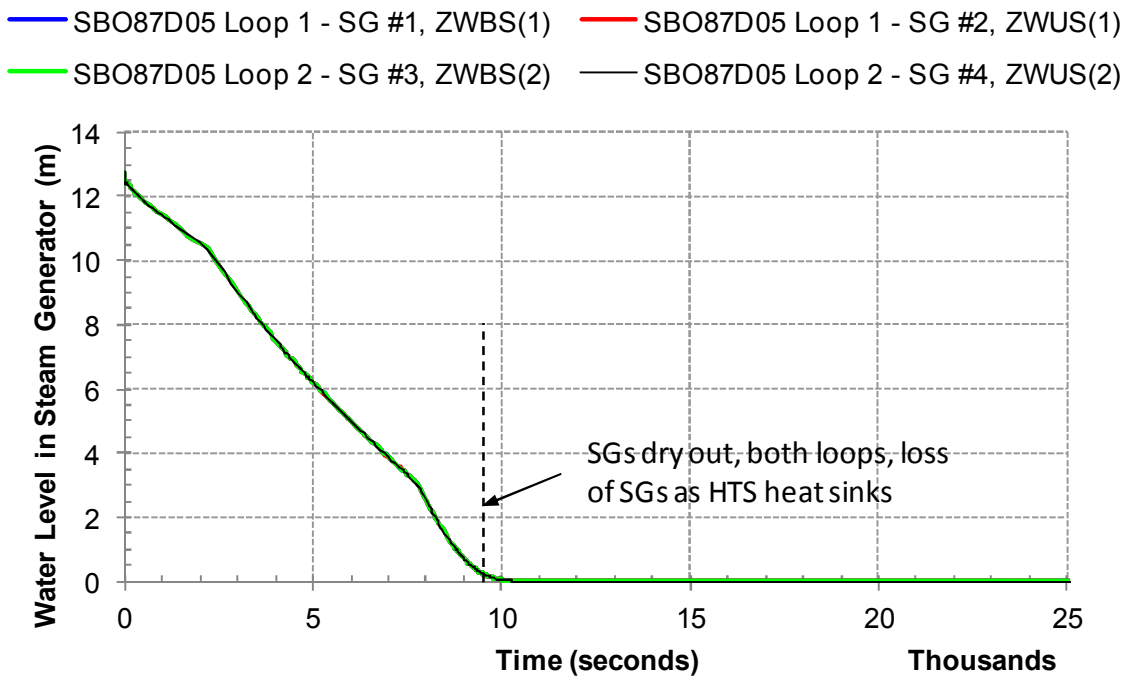


FIG. 3.13. Steam generator water levels for PHTS loops 1 and 2 (0 – 25,000 s).

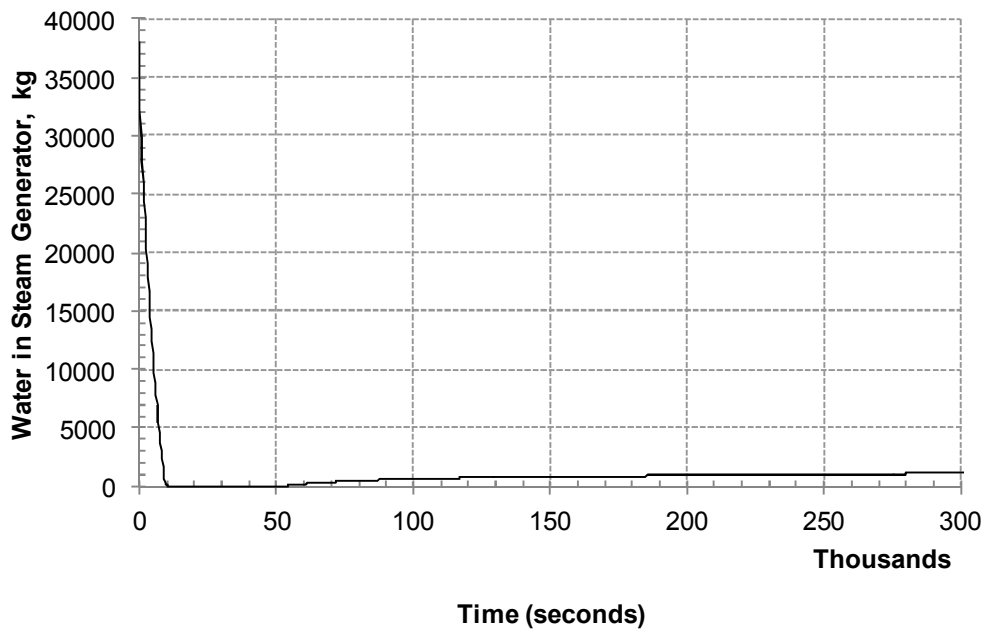


FIG. 3.14. Water mass in steam generator (0 – 300,000 s).

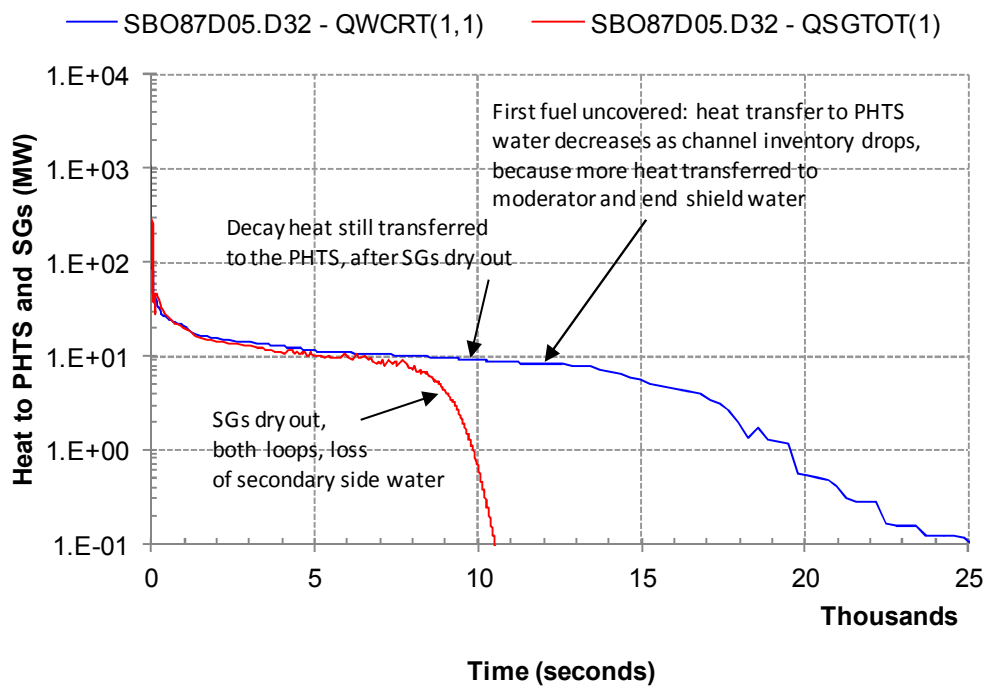


FIG. 3.15. Heat to PHTS and steam generators (0 – 25,000 s).

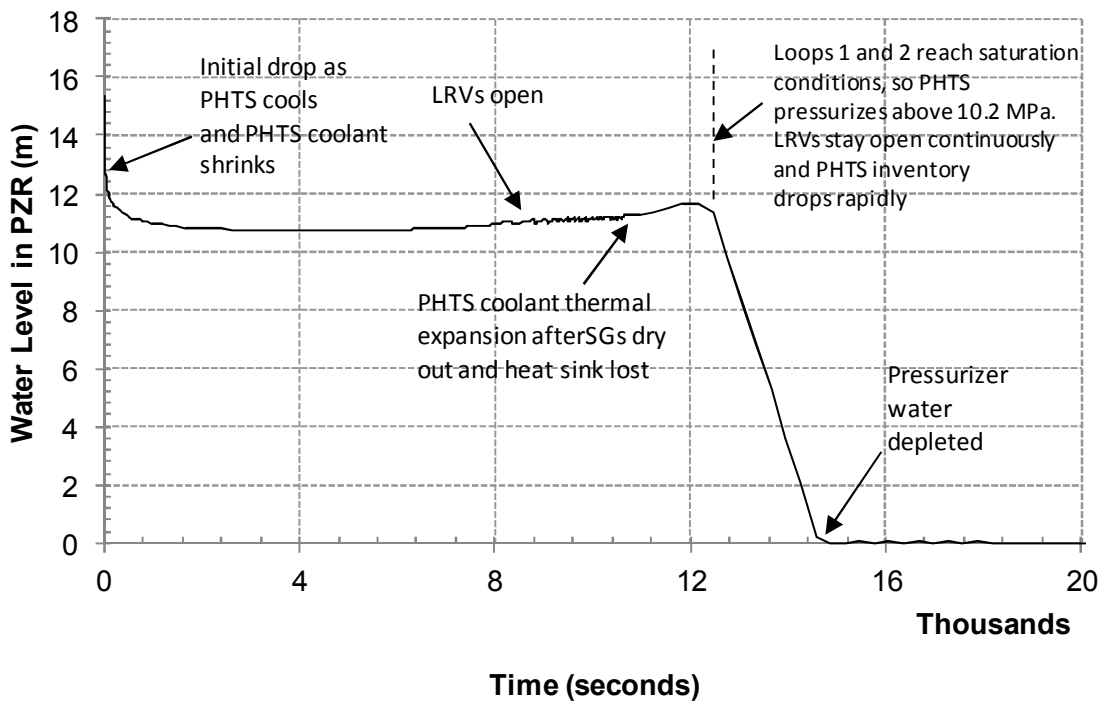


FIG. 3.16. Water level in the pressurizer (0 – 20,000 s).

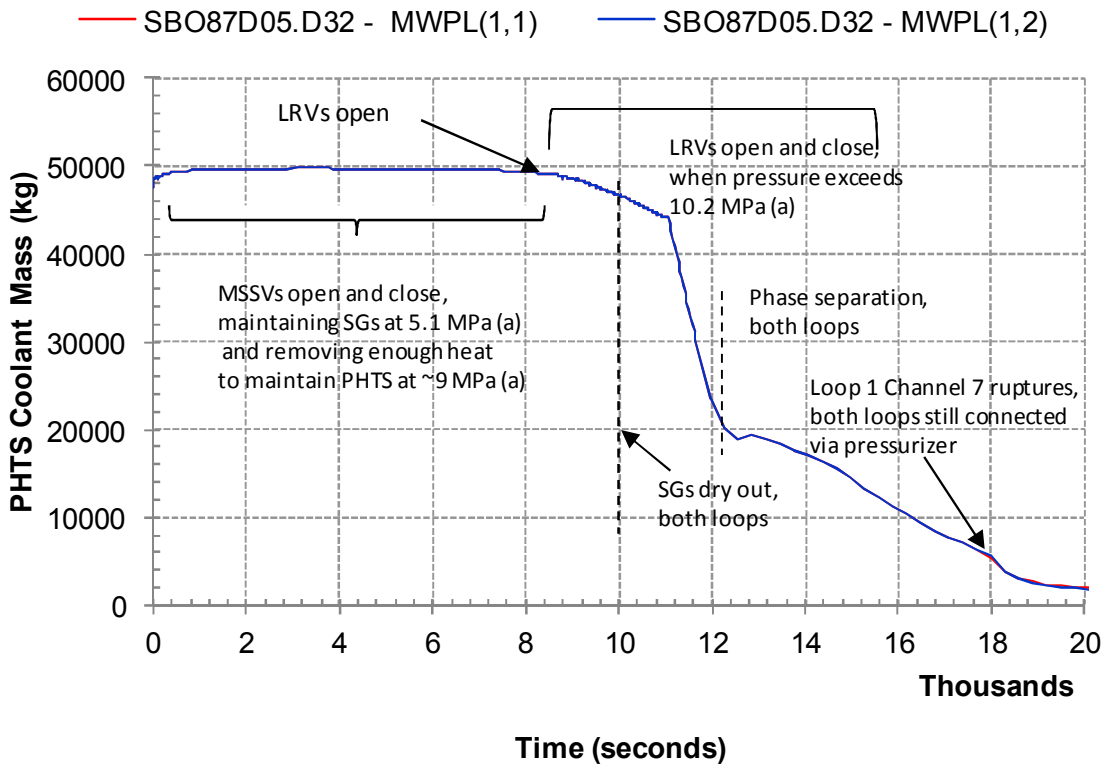


FIG. 3.17. PHTS Loops 1 and 2 water masses (0 – 20,000 s).

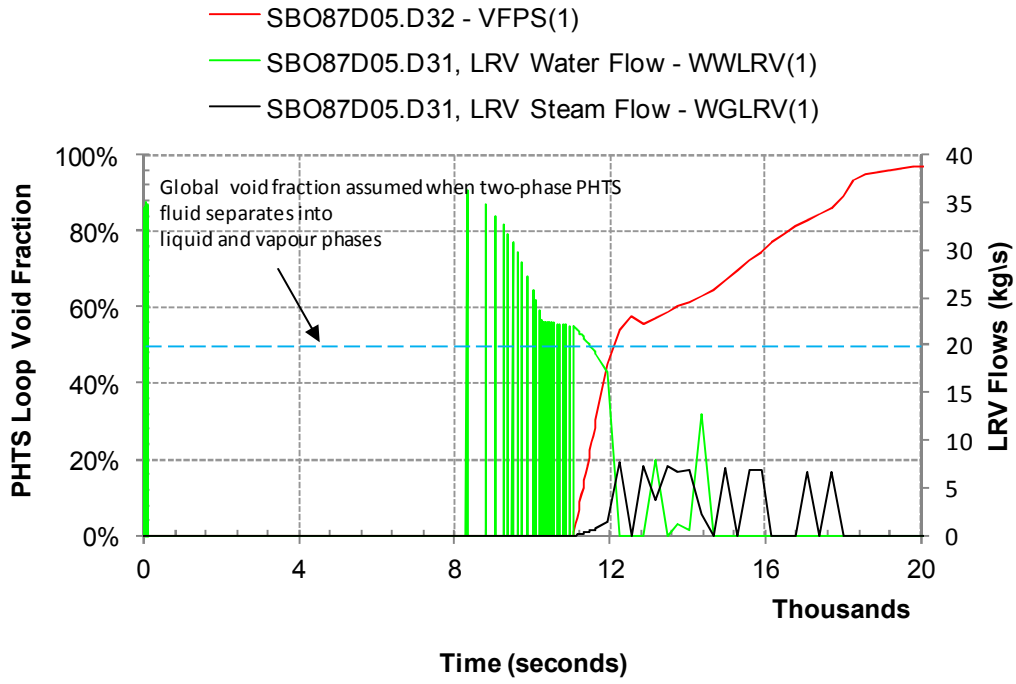


FIG. 3.18. Loop void fractions and LRV steam, and water flows for PHTS loops 1 and 2 (0 - 20,000 s).

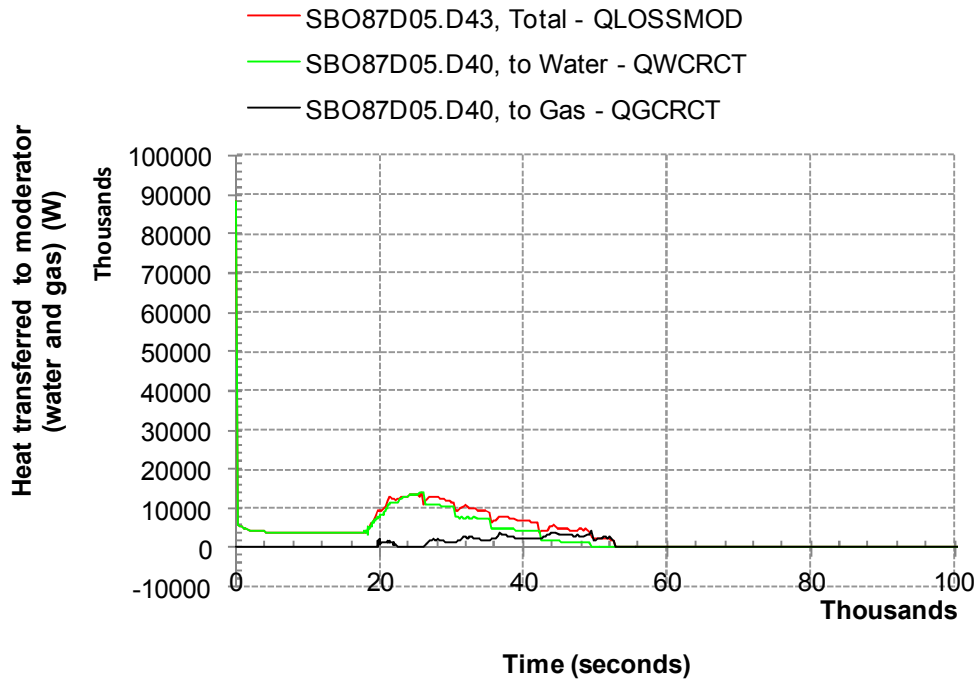


FIG. 3.19. The Amount of heat transferred to moderator from the fuel channels (0 - 100,000 s).

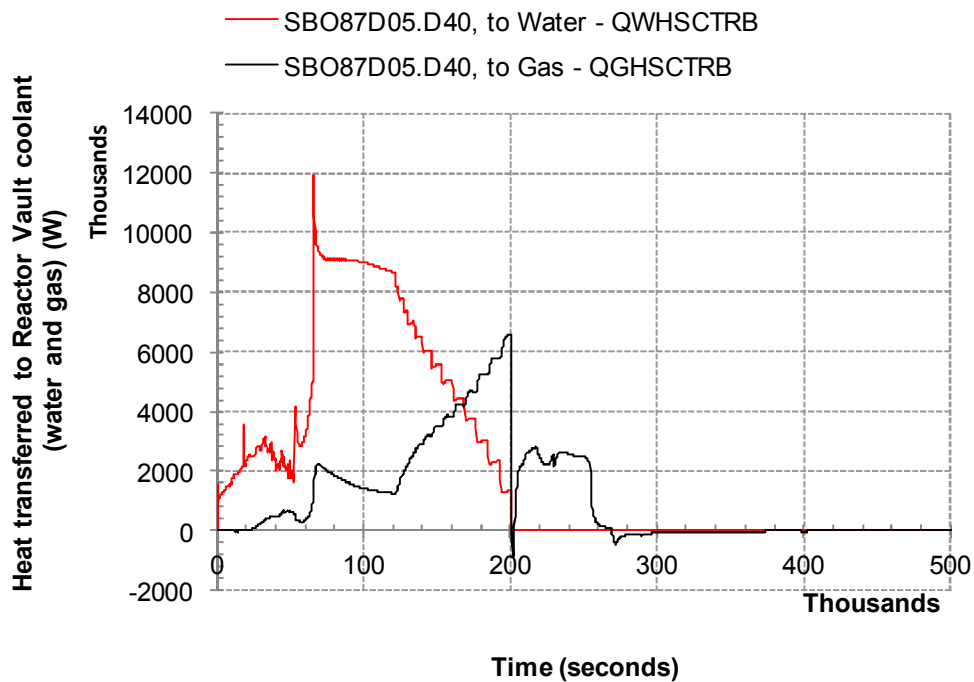


FIG. 3.20. The amount of heat transferred to reactor vault water and gas/steam (0 – 500,000 s).

### Fuel channel response

Table 3-2 shows that the first fuel bundles are uncovered inside fuel channels at ~13,082 s (~3.6 h) in both loops. Uncovering fuel elements is the result of one or more of the following phenomena: (1) the decay heat from core boils off coolant, (2) the loss of coolant through the PHTS liquid relief valves, and (3) the loss of a heat sink at the steam generators with the loss of water inventory from the secondary side. When sufficient PHTS coolant is lost from a fuel channel, the fuel elements inside the fuel channel start to uncover. When the temperature of the pressure and calandria tubes rises to approximately 900°K, the PT and CT rupture at ~17,918 s (~5.0 h) (Table 3-2) in Channel 7, Loop 2. The channel rupture is caused by ballooning at high temperature and high pressure. The temperatures of the pressure and calandria tubes, as well as fuel in Bundle 7 (Channel 1) are presented in Figures 3-21 to 3-23. Prior to the first fuel channel dryout, calculations of PT, CT and fuel temperatures are not performed in the current code; it is assumed that the core decay heat goes directly into PHTS coolant. Therefore, the PT, CT and fuel temperatures remain constant up to ~18,700 s (~5.2 h) (Fig. 3-21). When a fuel channel is dry at ~18,700 s (~5.2 h), the channel module of the code is initialized and the fuel channel conditions, PT, CT and fuel temperatures are analysed at every time step. After PT and CT rupture at ~17,918 s (~5 h), PHTS inventory is discharged through the break. Therefore, fuel and subsequently PT and CT temperatures increase at ~19,000 s (~5.3 h). This fuel temperature increase is assisted by a moderator level (and mass) decrease in the CV (Fig. 3-24) because of moderator discharge through the CV relief pipes into containment. More details about the CV response are given in the next section.

When the pressure and calandria tubes reach disassembly conditions, fragments of the fuel channel relocate to “holding bins” and stay temporarily there in the form of a suspended debris bed. The core material in the suspended debris bed heats up further from the decay heat. The Zircaloy/steam exothermic reaction provides additional heat resulting in partial melting of the debris. Eventually the molten material relocates from the suspended debris bed to the bottom of the calandria vessel and is quenched in the water. When the suspended debris bed

mass in the core exceeds a user- specified value (25,000 kg per PHTS loop is used in the present work), the core material in the suspended bed and most of the intact channels relocate to the bottom of the calandria vessel.

The dynamics of channel disassembly and relocation phenomena are represented in Figure 3-25 to 3-27. Figure 3-25 shows that the mass of UO<sub>2</sub> in the intact core-material in each loop decreases rapidly at ~20,000 s (~5.6 h). It is the result of material transfer to the holding bins and relocation of molten material to the calandria vessel bottom. In accordance with the above explanation, Figures 3-26 and 3-27 show that corium mass in suspended debris bed increases rapidly at ~20,000 s (~5.6 h) and becomes essentially zero at ~52,700 s (~14.63 h) as a result of core collapse. The temperature of the suspended debris bed in vertical core Nodes 1, 4, 5, and 6 are shown in Figure 3-28. Similarly, the debris temperatures in the vertical core Node 6 for axial Nodes 1 and 2 are shown in Figure 3-29.

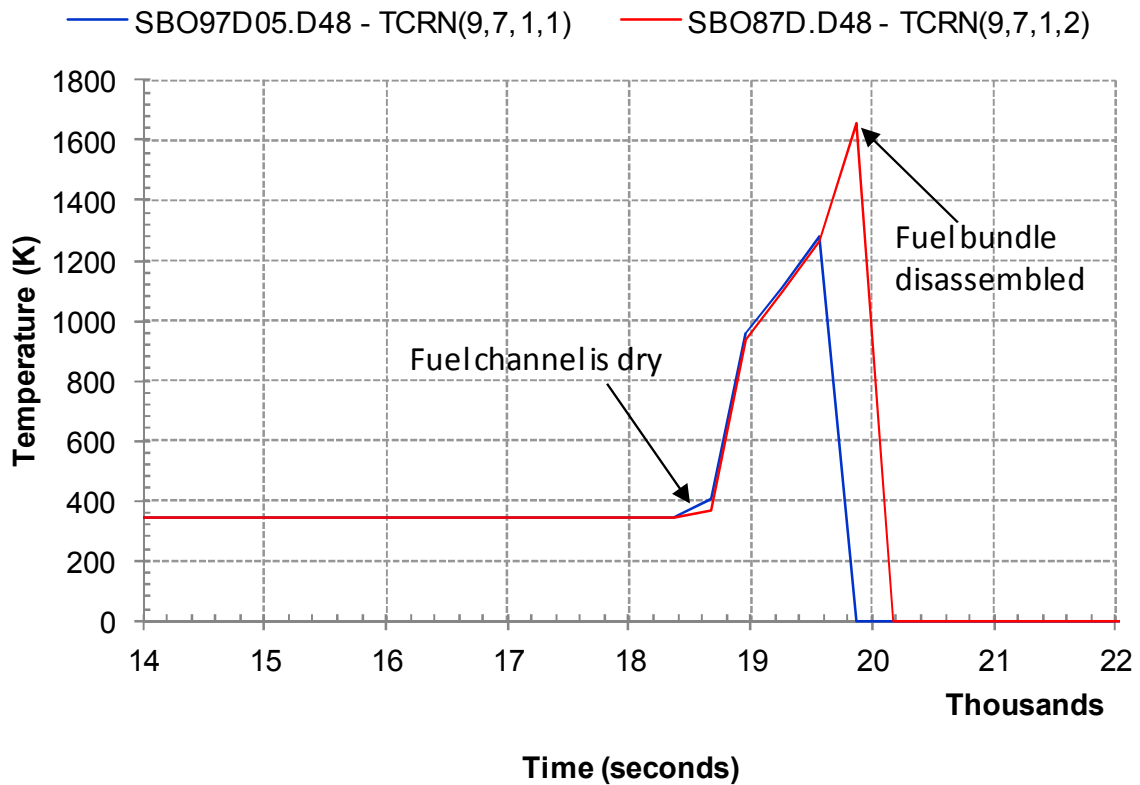


FIG. 3.21. Calandria tube temperatures bundle 7, channel 1, loops 1 and 2 (14,000 – 22,000 s).

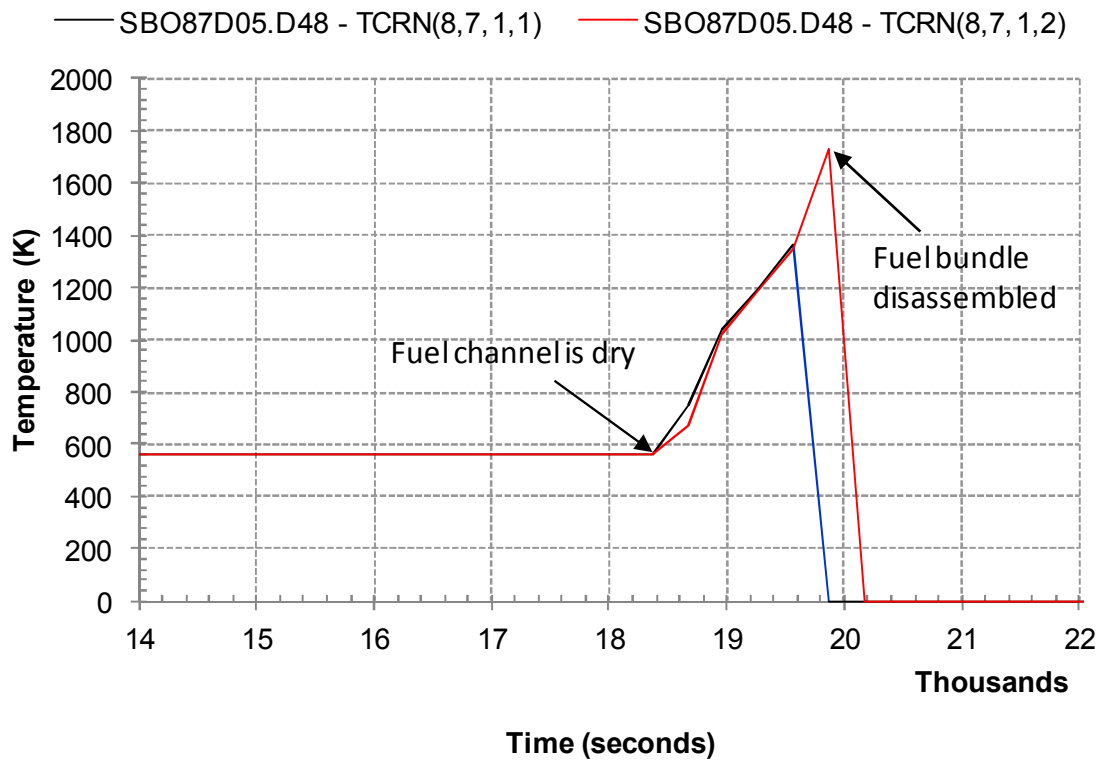


FIG. 3.22. Pressure tube temperatures bundle 7, channel 1, loops 1 and 2 (14,000 – 22,000 s).

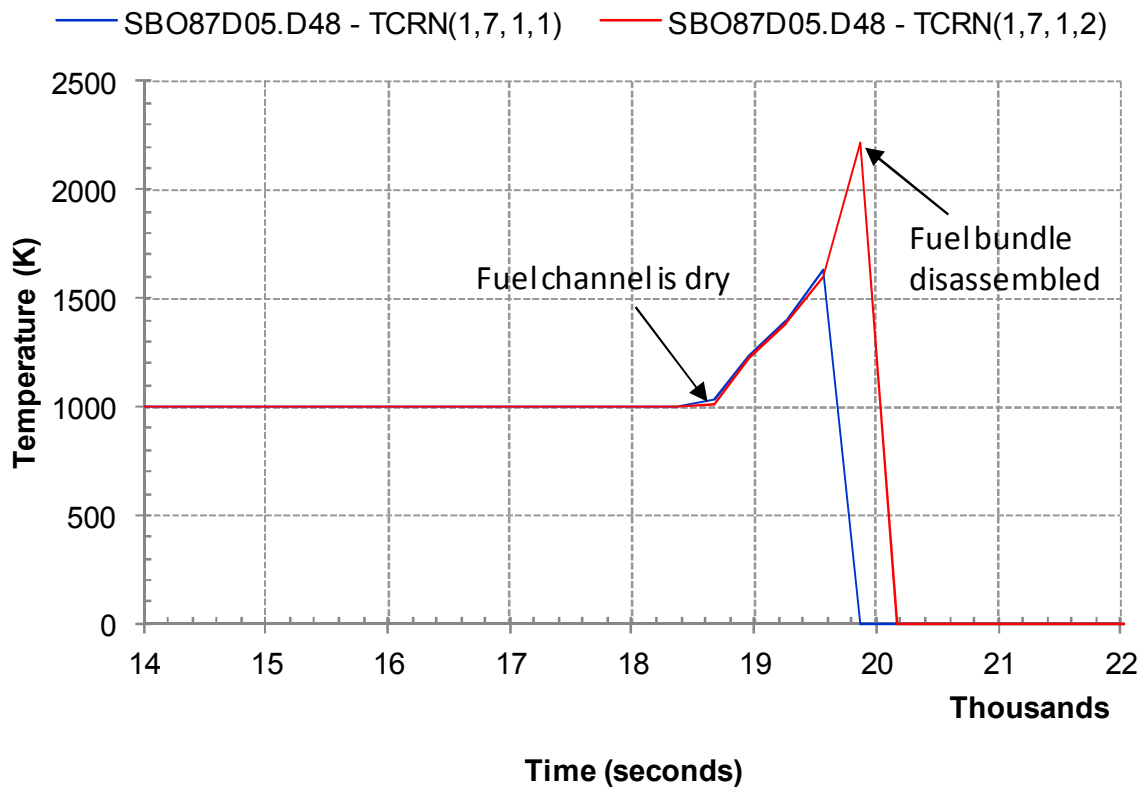


FIG. 3.23. Fuel temperatures bundle 7, channel 1, loops 1 and 2 (14,000 – 22,000 s).

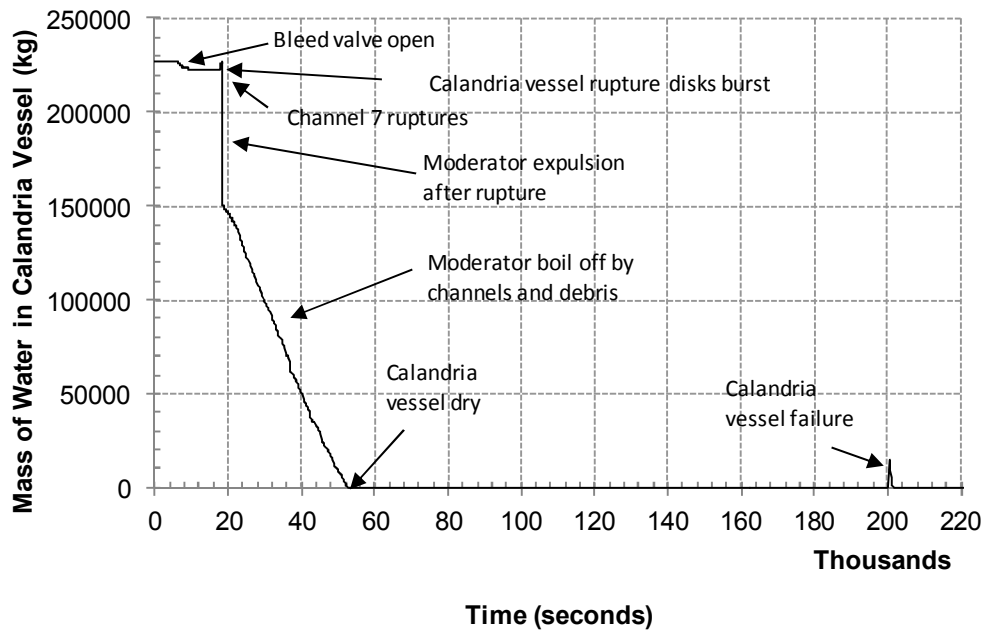


FIG. 3.24. Moderator mass (0 – 220,000 s).

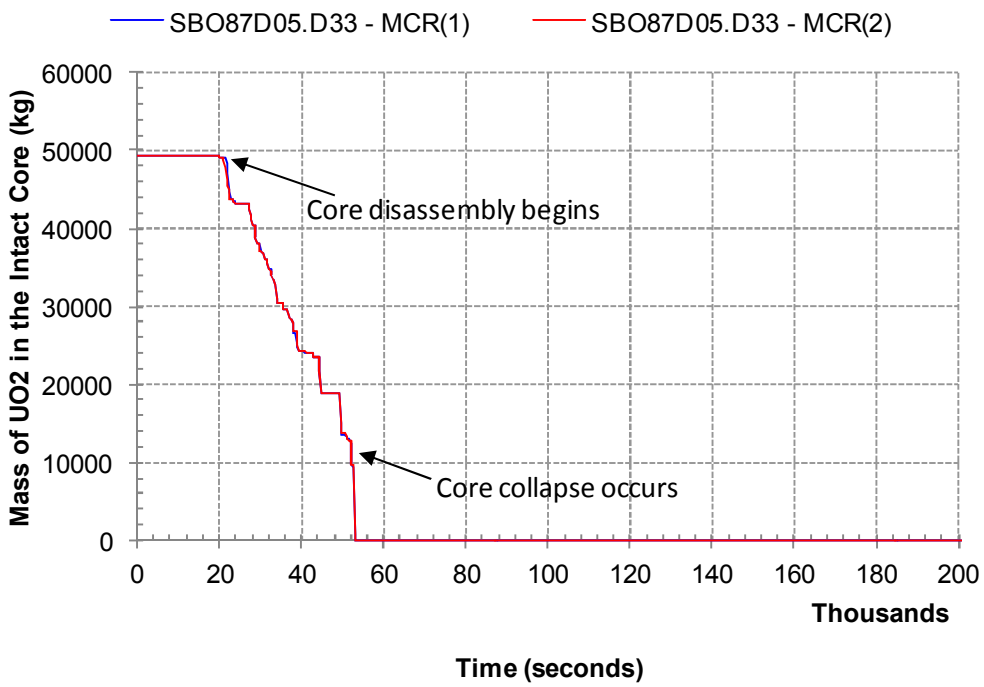


FIG. 3.25. UO<sub>2</sub> Mass remaining in the intact fuel channels, loops 1 and 2 (0 – 200,000 s).

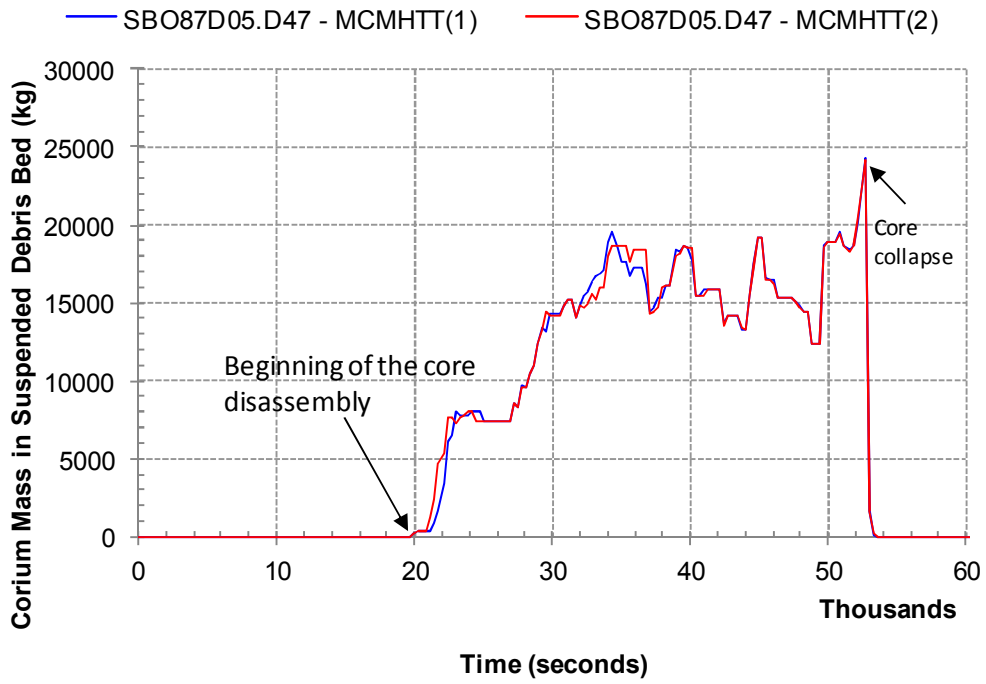


FIG. 3.26. Debris mass held up by intact core (0 – 60,000 s). Note: Blue and red lines show loop 1 and 2, respectively.

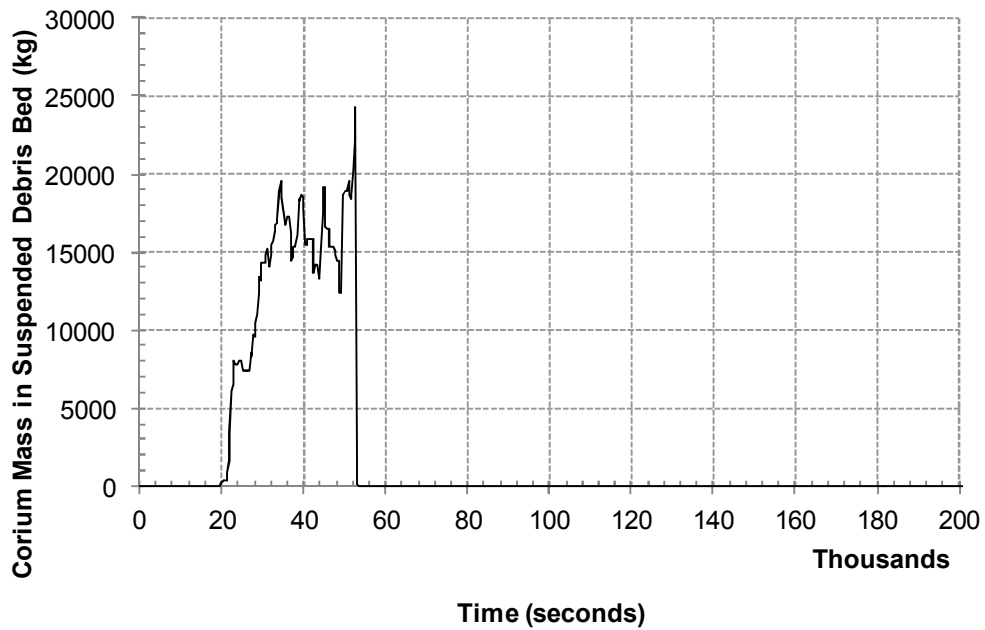


FIG. 3.27. Debris mass held up by intact core (Loop 1) (0 – 200,000 s).

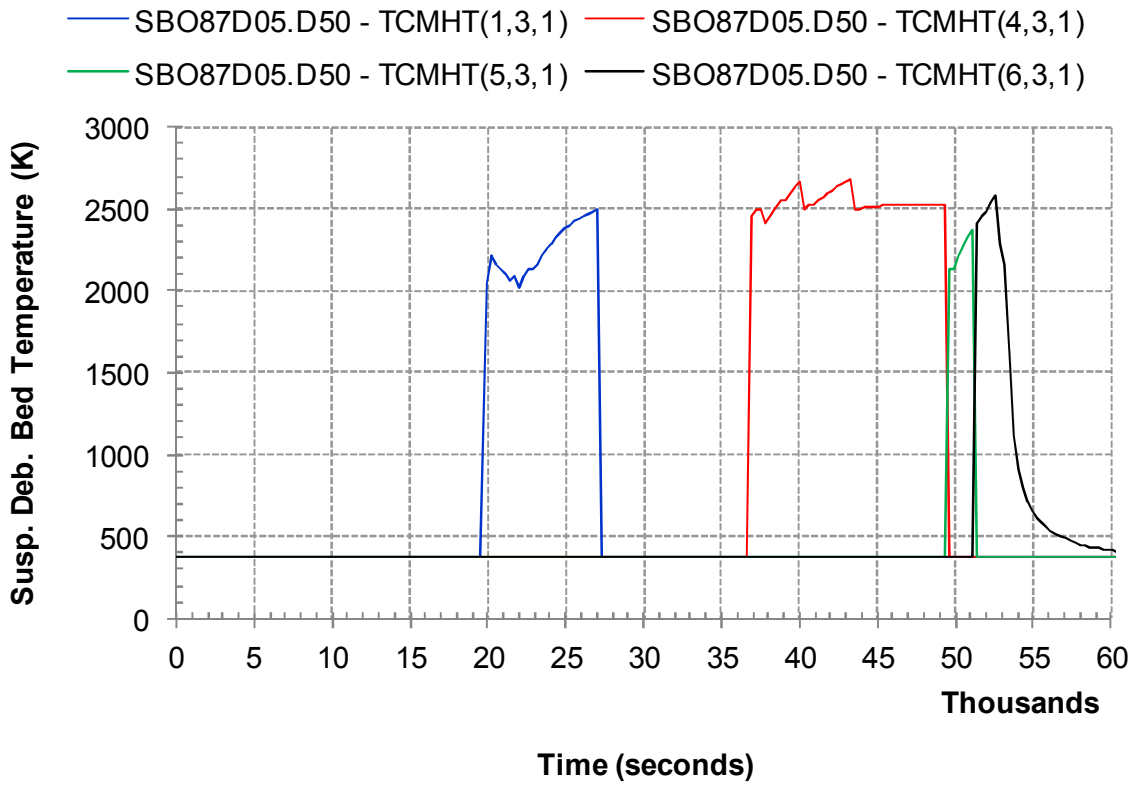


FIG. 3.28. Temperature of the suspended debris bed (vertical core nodes 1, 4, 5, and 6, axial Node 3, PHTS loop 1), (0 – 50,000 s).

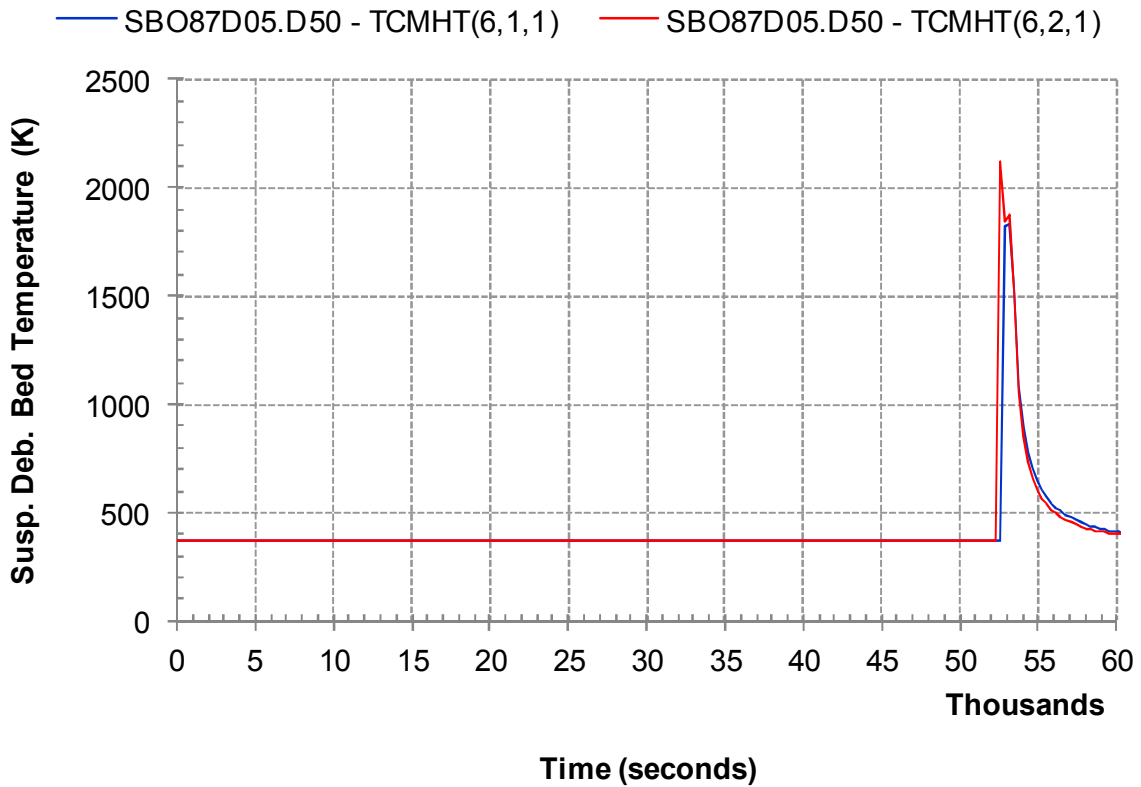


FIG. 3.29. Temperature of the suspended debris bed (vertical core Node 6, axial Nodes 1 and 2, PHTS Loop 1), (0 – 60,000 s).

### 3.1.3.2. Phase 2

#### Calandria vessel response

Figures 3-30 and 3-31 show the two-phase water level and pressure in the calandria vessel, respectively. The moderator temperature in the calandria vessel is assumed to be 342°K prior to the accident. As a result of the accident, the moderator temperature and pressure in calandria vessel increase because of the loss of moderator cooling and the heat transfer from the core. At 17,918 s (about 5.0 h), the PT and CT rupture and PHTS inventory is discharged into CV. Pressure inside the calandria vessel reaches the set point of the rupture disk, 238 kPa(a), and the CV rupture disk fails at 18,088 s (about 5.0 h) (Table 3-2). This phenomenon is associated with a rapid decrease in the calandria vessel water level (Fig. 3-30). After the initial rapid moderator expulsion, the moderator continues to discharge gradually into the containment as a result of continued moderator boil off due to the heat transfer from the core (Fig. 3-30).

The rapid increase of the calandria vessel pressure at about 20,000 s (5.1 h), up to 340 kPa (Fig. 3-31), is the result of a major relocation of core material from the suspended debris bed into the moderator inside the calandria vessel, as a result of core collapse. Also, at 52,600 s (14.6 h) the moderator inside the calandria vessel is depleted (see Fig. 3-24); therefore, no steaming source is available for pressure increase. The water in the reactor vault acts as a heat sink to cool the external calandria vessel wall. The calandria vessel pressure (Fig. 3-31) decreases after 33 000 s (9.2 h) due to containment failure.

At about 53,000 s (14.7 h), the calandria vessel pressure begins to increase because water inside the reactor vault, surrounding the calandria vessel, starts to boil off (see Fig. 3-31). Steam generated on the CV outer wall is released from the reactor vault into containment. The CV and containment are connected via the CV relief ducts; therefore, any increase/decrease in containment pressure results in pressure increase/decrease in the CV. At 200,189 s (55.6 h), the calandria vessel fails (Table 3-2 and Fig. 3-31). The failure of the CV was predicted by creep of the cylindrical shell at low elevation.

The calandria vessel pressure spike at 200,189 s (55.6 h) is the result of the calandria vessel failure and subsequent relocation of corium from the calandria vessel to the reactor vault floor (Fig. 3-32). The molten core concrete interaction begins in the reactor vault at 246,481 s (68.5 h) (Table 3-2).

Figure 3-32 shows the total mass of debris (including particulates, corium crust, and molten corium), the mass of the corium crusts (bottom, side, and top surfaces) and the mass of particulates in the calandria vessel. The mass of corium particulates and the mass of the corium crust in the calandria vessel are shown in Figures 3-33 and 3-34, respectively. A crust is formed on the CV walls soon after the core collapses onto the CV bottom.

After the water in the CV is depleted, the core debris in the calandria vessel starts to heat up and eventually the particulates melt to join the molten debris pool at 66,000 s (18.3 h) (Fig. 3-33). The corium and molten pool temperature are shown in Figures 3-35 and 3-36, respectively. When the calandria vessel fails, all corium falls into the reactor vault at 200,189 s (55.6 h).

Figure 3-37 shows the inside surface temperature of calandria vessel wall for the top node. The surface temperature of 10th node and the temperatures of four bottom nodes of the calandria vessel cylindrical shell are shown in Figures 3-38 to 3-39. As mentioned in Section 3.1.2, the calandria vessel wall is sliced horizontally to 15 nodes from the vessel floor to the ceiling along the elevation levels (see Fig. 3-9). Initially the temperature of all these nodes at different elevations is about the same because the CV shell is immersed in the water in the

reactor vault. At 50,000 s (13.9 h), the two bottom nodal temperatures show a spike. This temperature spike is caused by core collapse, the major relocation of hot core material from the suspended debris bed into the calandria vessel bottom. At 52,550 s (14.9 h) the water in the reactor vault starts to boil off (Fig. 3-40) and at 65,000 s (18.0 h) for the top node of calandria vessel is not immersed in the water. Therefore, the temperature of the top node and 10th Node sharply increase to 445°K (Figs 3-37 and 3-38). The temperatures of the top nodes are relatively low because heat is transferred from the top wall nodes by several mechanisms: i) to bottom nodes by circumferential conduction and eventually to the water in reactor vault, and ii) by convection/radiation to the RV steam and concrete walls. Therefore, the top nodes of calandria vessel wall do not fail even though they are not covered by reactor vault water. When the water level in the reactor vault decreases to 2.5 m at 195,600 s (54.3 h) (Fig. 3-40), the calandria vessel bottom heats up rapidly. As mentioned, the CV bottom fails due to creep at 200,189 s (55.6 h). When the calandria vessel fails, the debris relocates into the reactor vault and is cooled by the water in the reactor vault. As a result, the calandria vessel wall temperatures drop as shown in Figure 3-37. The molten fraction of the debris in the calandria vessel is shown in Figure 3-41.

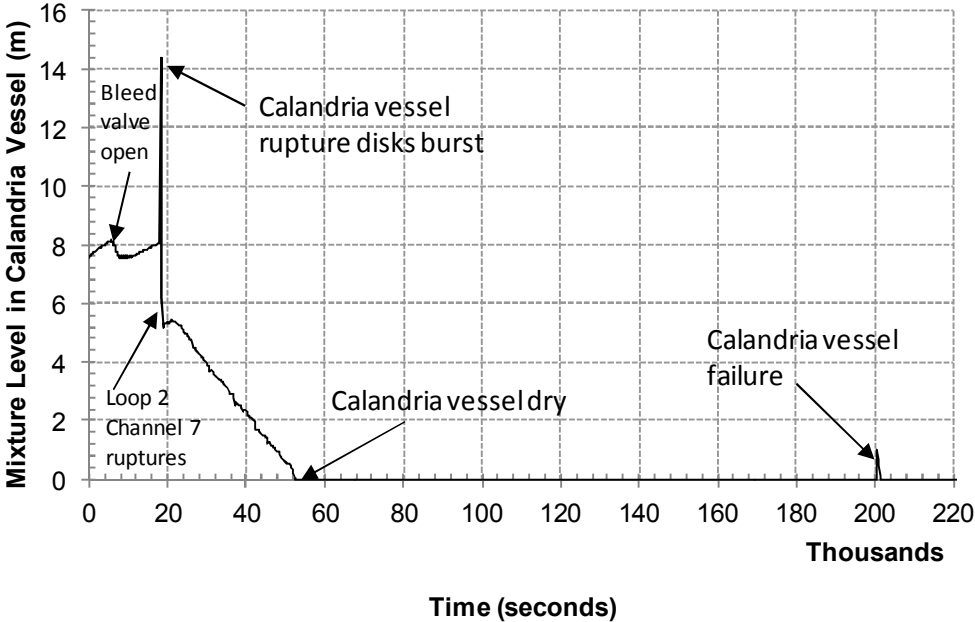


FIG. 3.30. Calandria vessel two-phase water level (0 – 220,000 s).

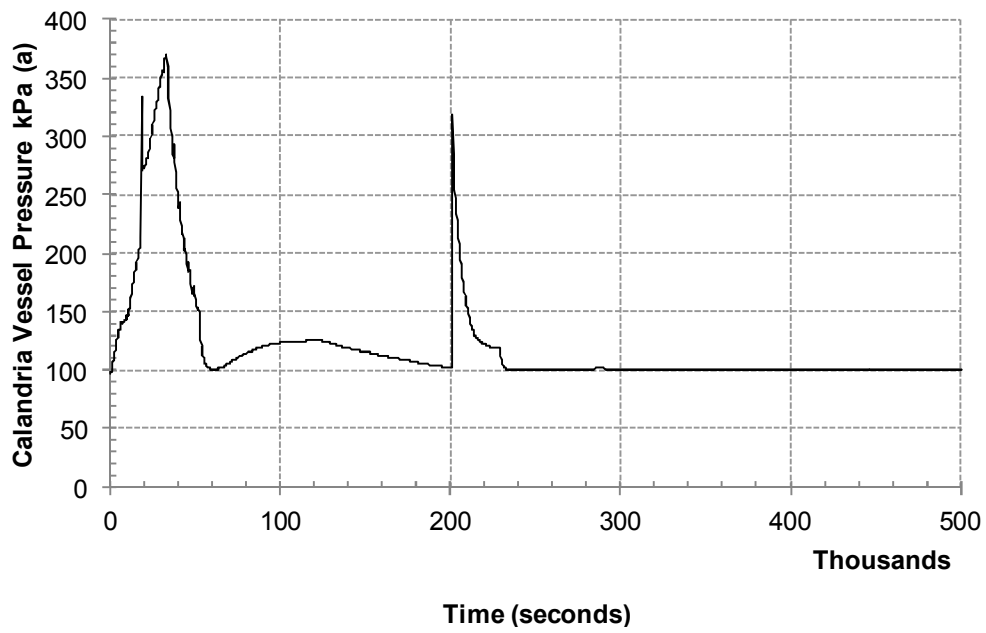


FIG. 3.31. Calandria vessel pressure (0 – 500,000 s).

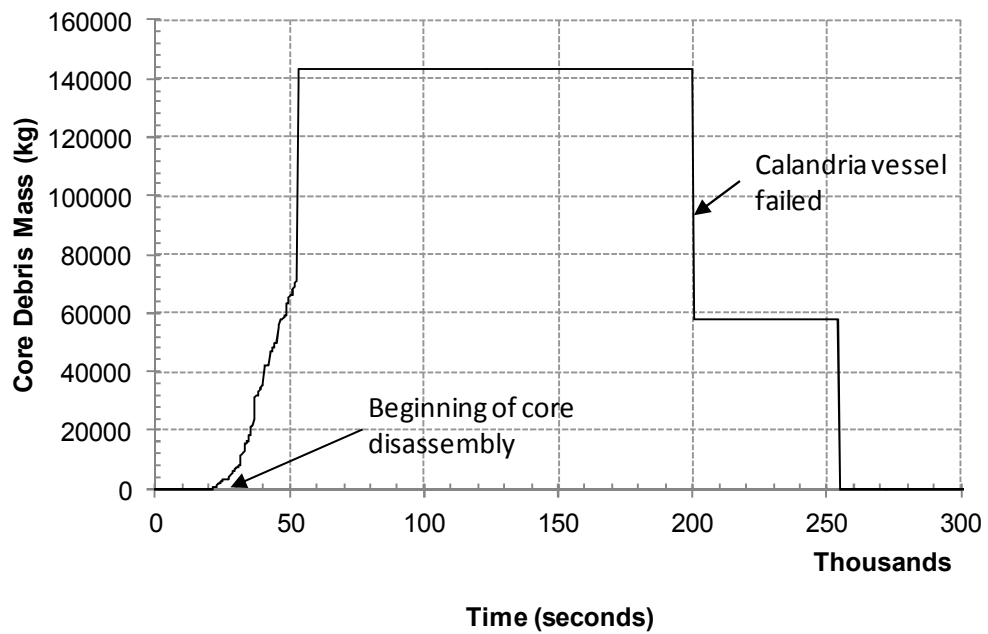


FIG. 3.32. Total mass of debris in calandria vessel terminal debris bed (0 – 300,000 s).

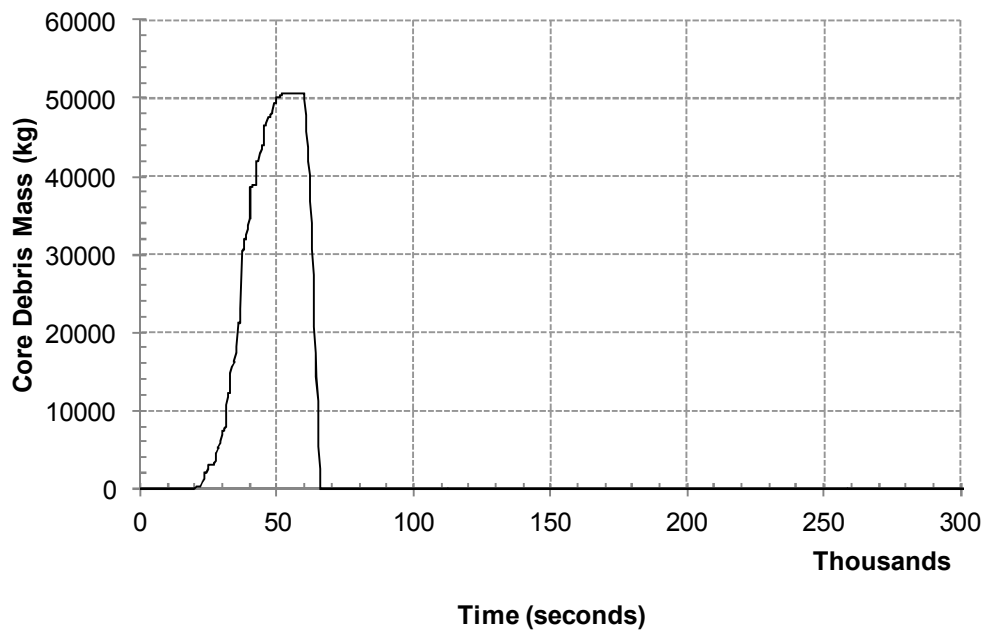


FIG. 3.33. Mass of corium particulates in calandria vessel (0 – 300,000 s).

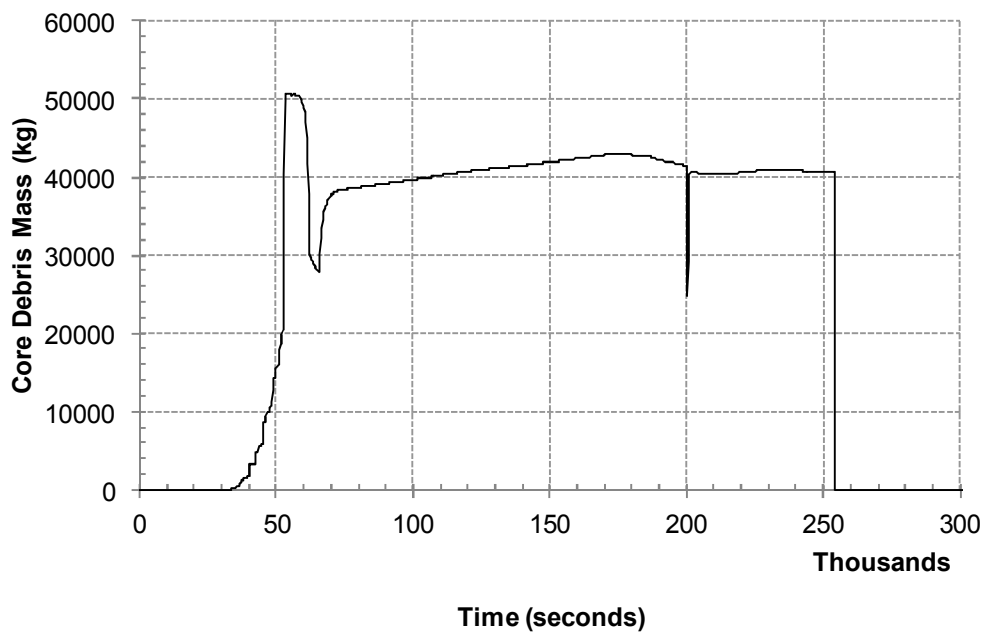


FIG. 3.34. Mass of corium crust in calandria vessel (0 – 300,000 s).

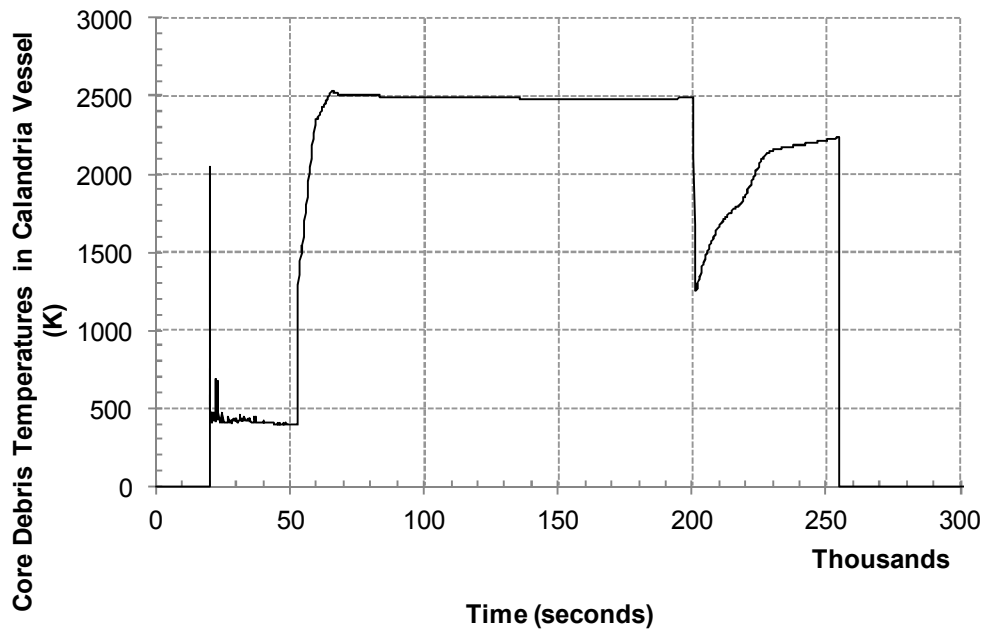


FIG. 3.35. Corium temperatures in calandria vessel (oxide-molten+crust, metal & particulates), (0 – 300,000 s).

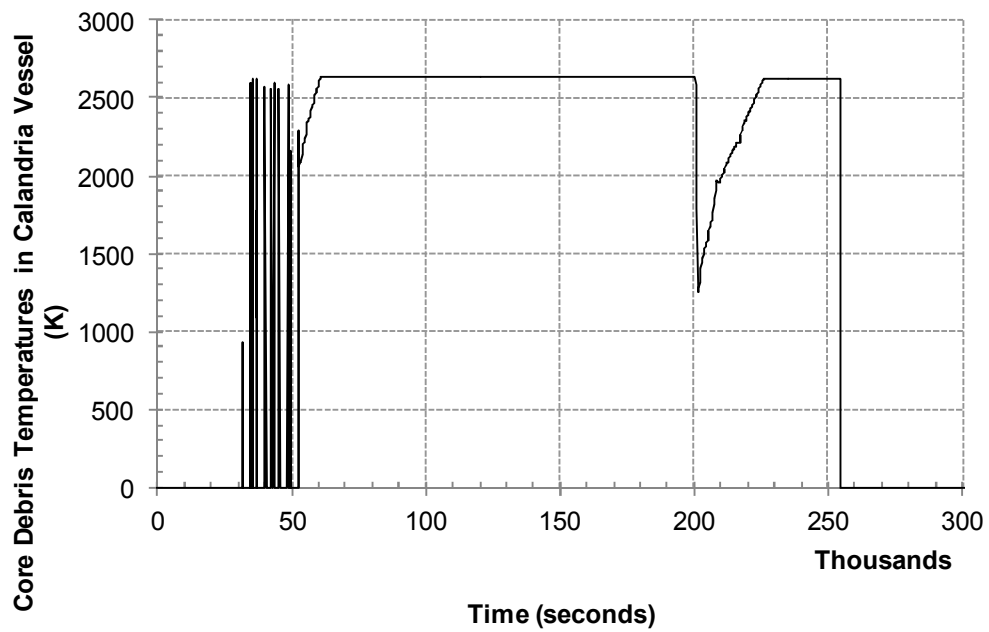


FIG. 3.36. Corium Temperatures (Molten Pool) in Calandria Vessel (0 – 300,000 s).

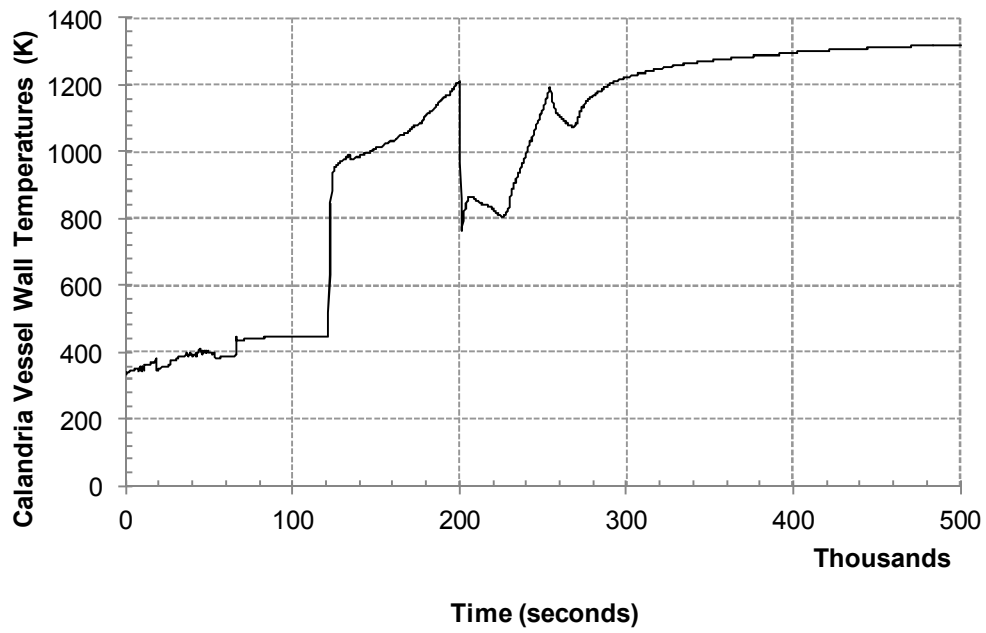


FIG. 3.37. Calandria vessel wall temperatures (top node) (0 – 500,000 s).

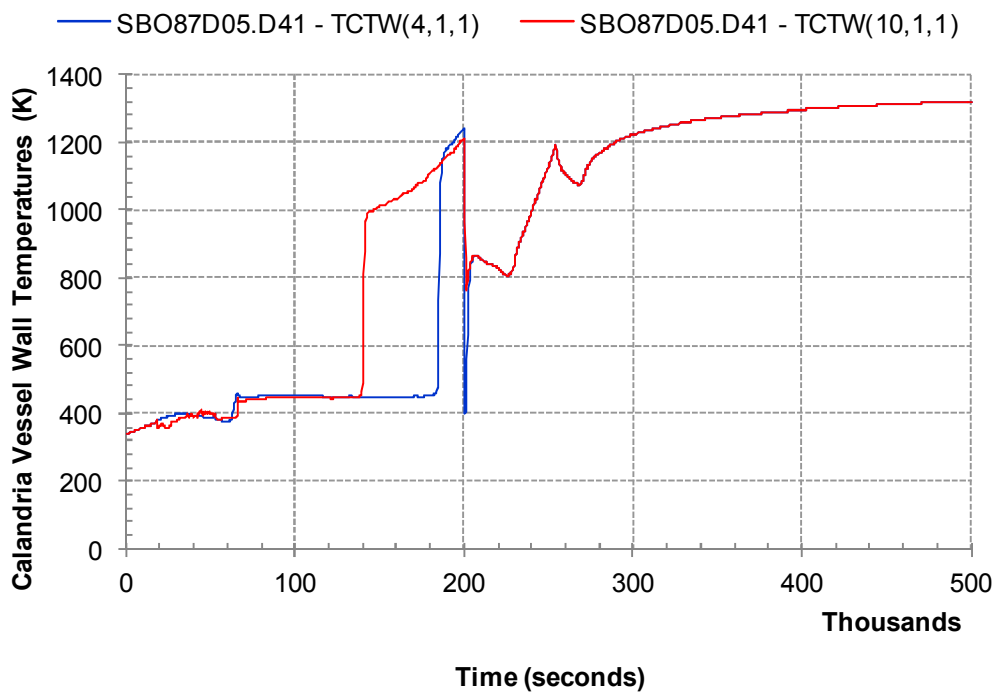


FIG. 3.38. Calandria vessel wall temperatures (nodes 4 and 10) (0 – 500,000 s).

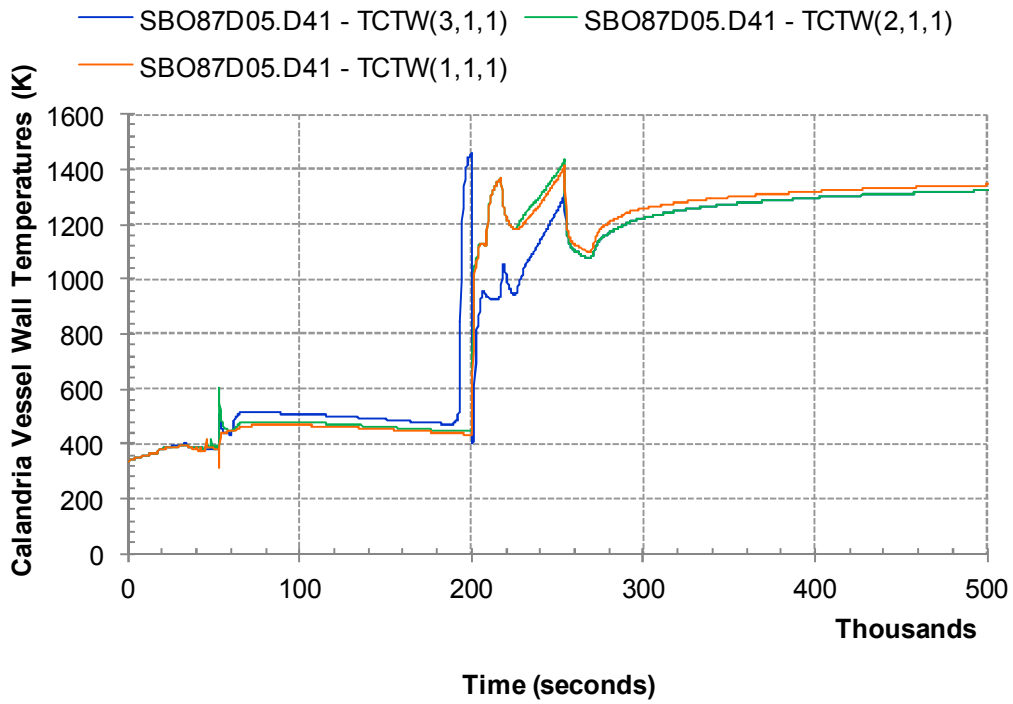


FIG. 3.39. Calandria vessel wall temperatures (nodes 2, 3, and bottom) (0 – 500,000 s).

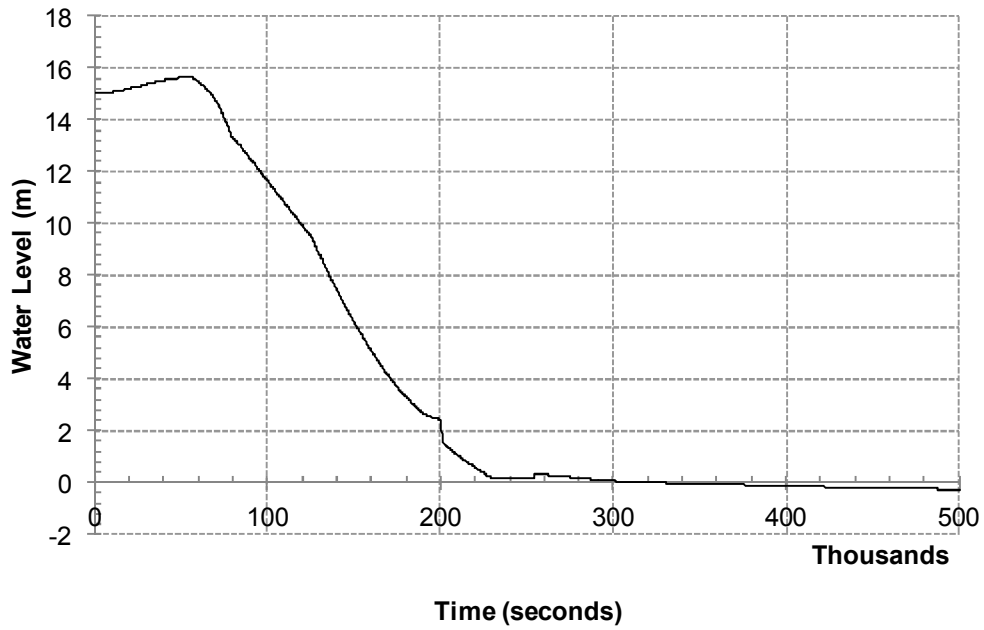


FIG. 3.40. Reactor vault water level (0 – 500,000 s).

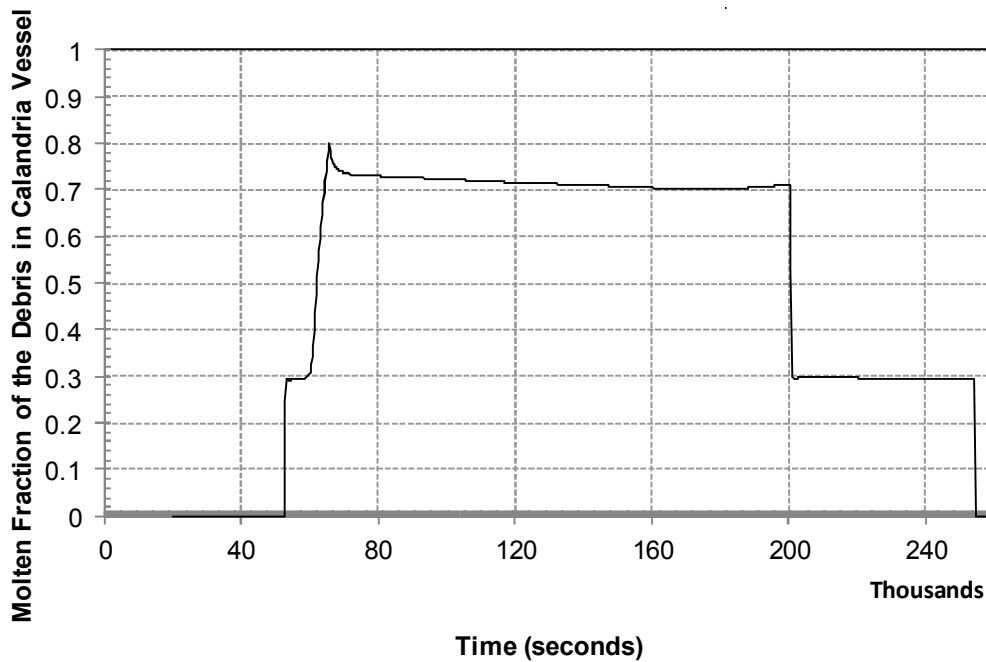


FIG. 3.41. Molten fraction of the debris in calandria vessel for run SBO87D05 (20,000 – 260,000 s).

### 3.1.3.3. Phase 3

#### Reactor vault and end-shield response

Figures 3-40, 3-42, and 3-43 show the water level and pressure in the reactor vault and end-shields. The pressure and water levels increase gradually after the initiating event. This behaviour is caused by the loss of shield and moderator cooling and heat transfer from the core to the moderator and end-shield. The reactor vault and end-shield have combined vent lines, and two rupture disks are connected to the combined vent lines to relieve the over-pressure caused by boiling the reactor vault and end-shield water. As mentioned in Reference [13], there are combined vent lines for RV/end shields for steam/water relief. Thus the pressure in the reactor vault and end-shield has the same behaviour (Figs 3-43 and 3-44). At 10,245 s (2.9 h) the shield cooling system rupture disks burst due to pressure build up resulting from water thermal expansion and subsequent RV water boiling (see Fig. 3-43). Steam is discharged from the end-shield into the containment. As a result, the water level in the end-shield decreases as shown in Figure 3-42.

Because of the larger water inventory in the reactor vault the boil off in the reactor vault takes longer. The reactor vault inventory starts to boil off at 53,550 s (14.9 h) resulting in a gradual water level decrease. At 200,189 s (55.6 h), the CV bottom fails and corium in the CV relocates onto the reactor vault floor. Eventually all the water in the reactor vault is evaporated at 230,000 s (63.8 h) (Fig. 3-40). Then corium reacts with the concrete floor. The amount of ablated concrete depth in reactor vault floor due to corium concrete interaction is shown in Figure 3-45. There was no failure of the reactor vault floor predicted. The containment pressure history is shown in Figure 3-46.

Figures 3-47 and 3-48 show the corium mass and corium temperature in the reactor vault. In these figures, “corium” represents a mixture of core debris and any other structural material including dissolved molten concrete. Initially the corium mass in the reactor vault is zero. At 200,189 s (55.6 h), the calandria vessel fails and the corium in the calandria vessel relocates into the reactor vault floor. As a result, the corium mass and corium temperature in the

reactor vault rapidly increase, as shown in Figures 3-47 and 3-48. The corium is then quenched by the water in the reactor vault and the corium temperature drops rapidly. At 246,500 s (~68.5 h), the corium is re-heated by the decay heat. At that time the corium temperature increases to 2,200°K (Fig. 3-48) and thus the corium-concrete interaction is initiated.

The capability of the code to model corium crust behaviour in the RV is shown in Figure 3-49. The initial crust thickness is high because of rapid solidification of corium on the cooler concrete surface. As a result of core-concrete interaction the concrete is dissolved by the corium, decreasing its melting point. At 268,000 s (74.4 h) the crusts disappear as a result of this process.

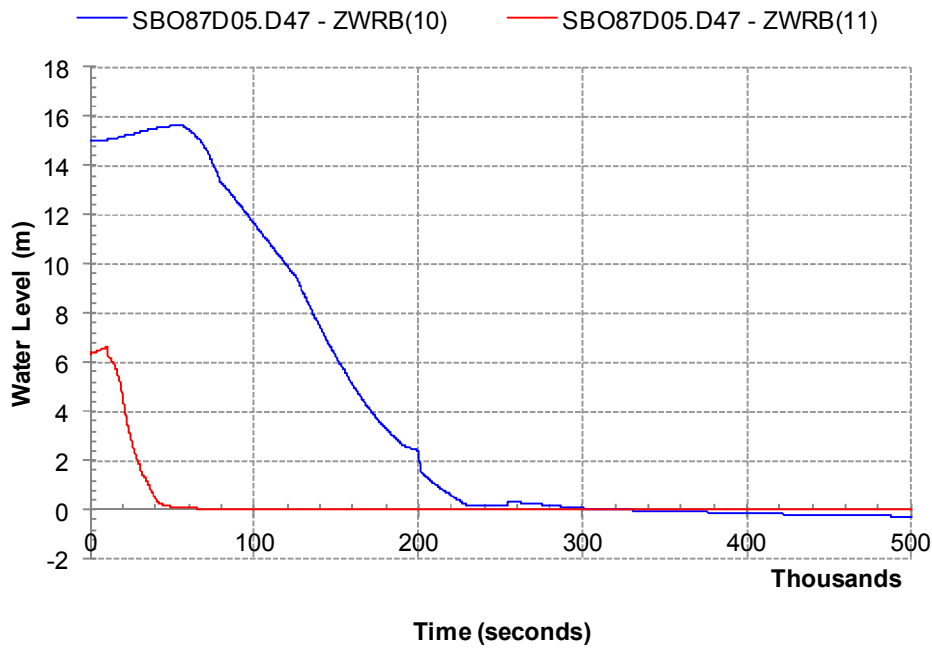


FIG. 3.42. Reactor vault (blue) and end shield (red) water level (0 – 500,000 s).

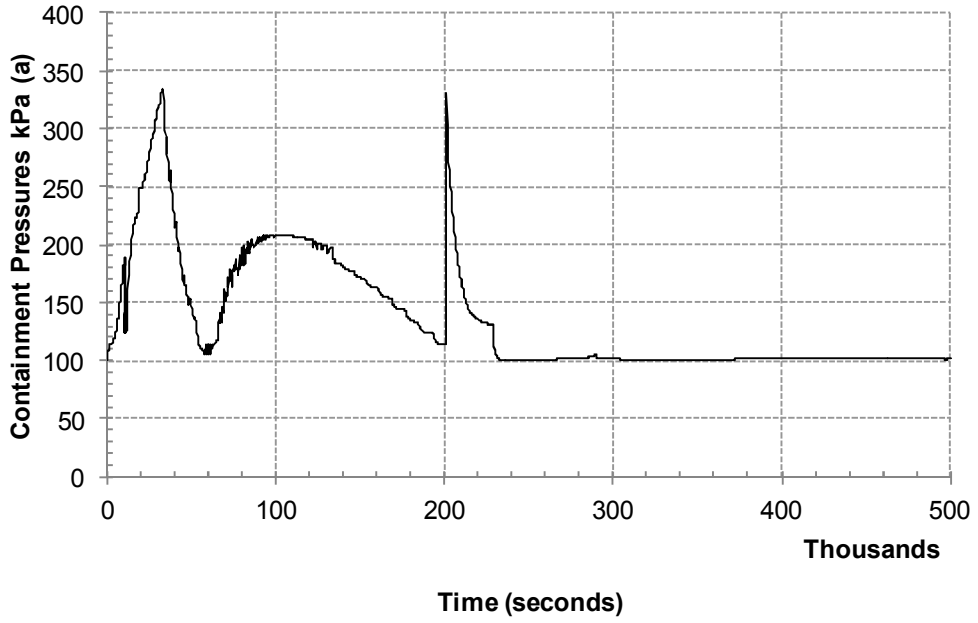


FIG. 3.43. Reactor vault pressure (0 – 500,000 s).

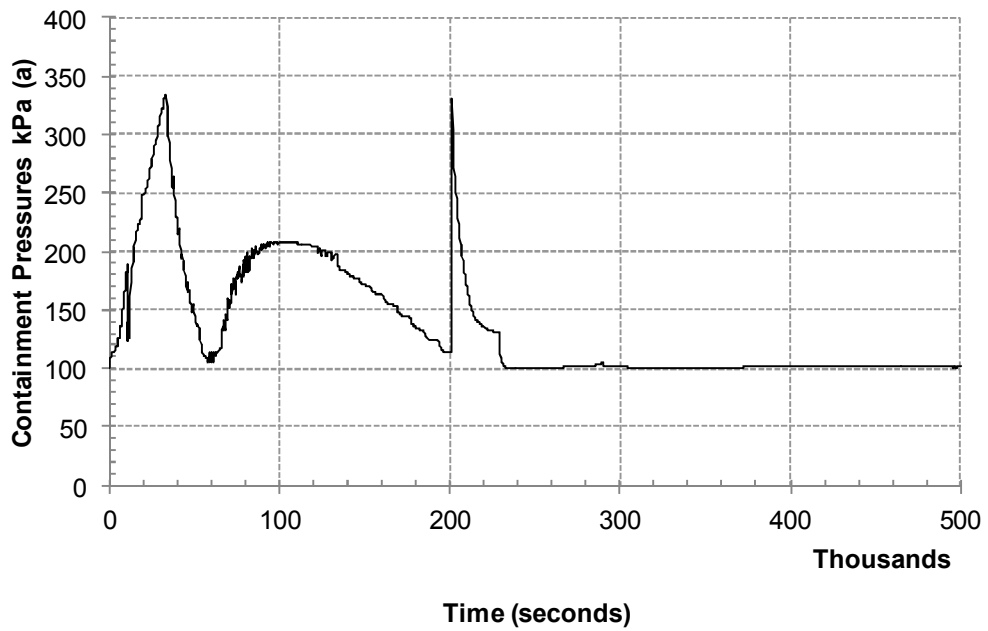


FIG. 3.44. End shield pressure (0 – 500,000 s).

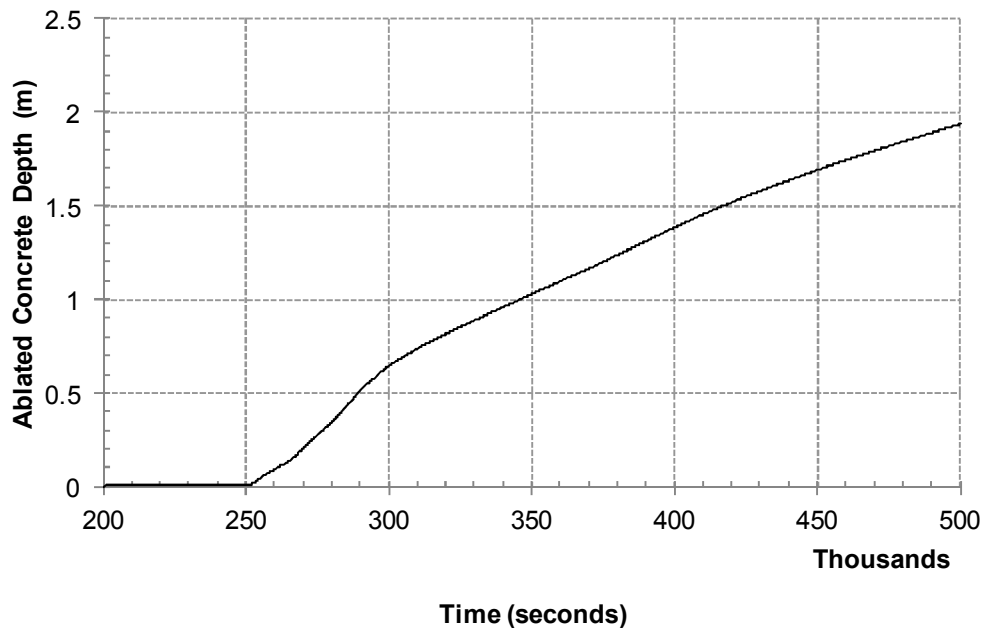


FIG. 3.45. Ablated concrete depth in reactor vault (200,000 – 500,000 s).

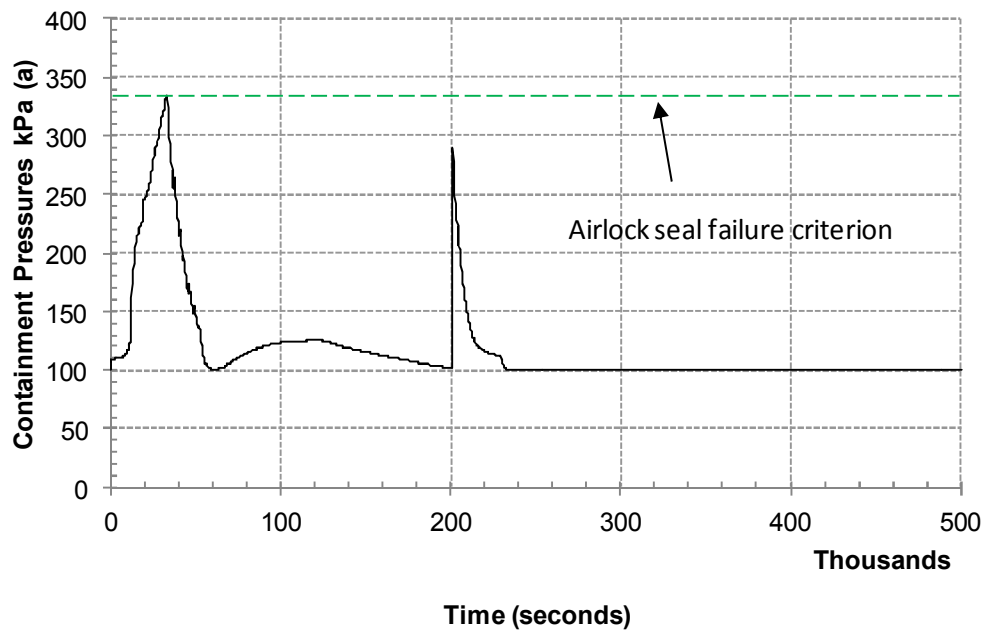


FIG. 3.46. Containment pressure (Node 8), (0 – 500,000 s).

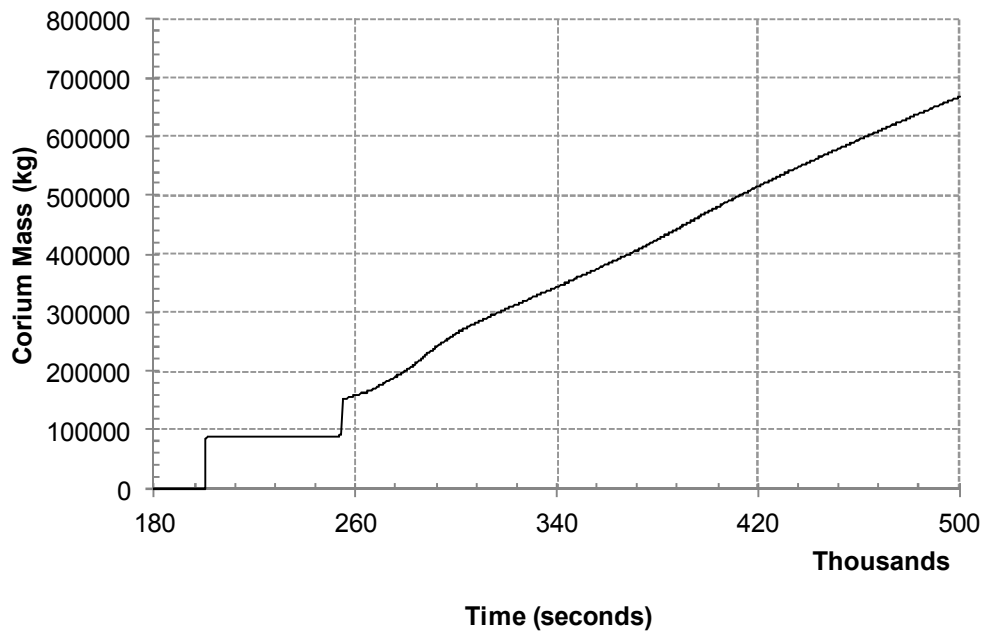


FIG. 3.47. Corium mass in reactor vault (180,000 – 500,000 s).

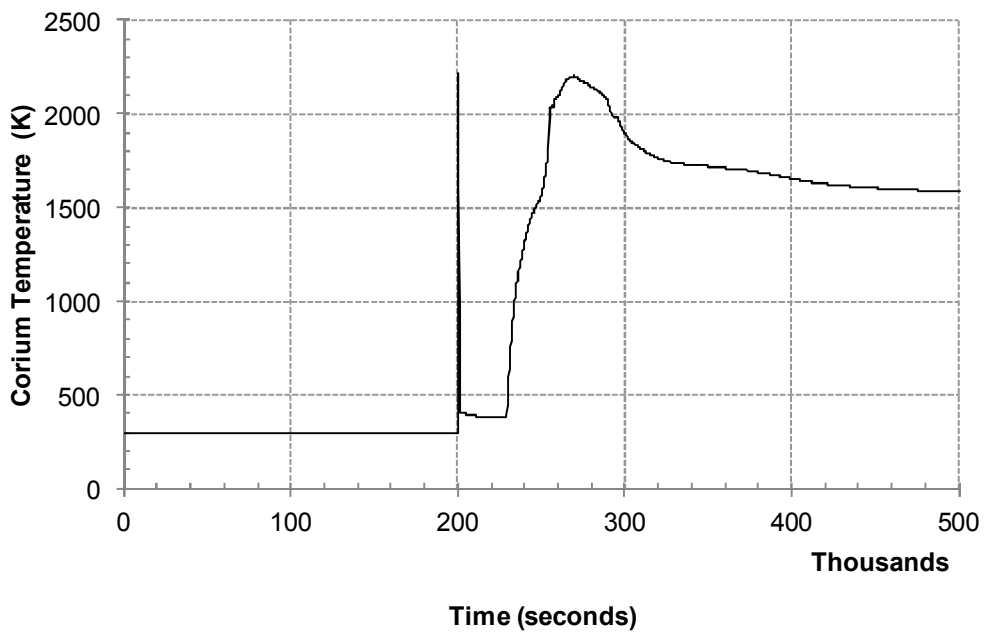


FIG. 3.48. Corium temperature in reactor Vault (0 – 500,000 s).

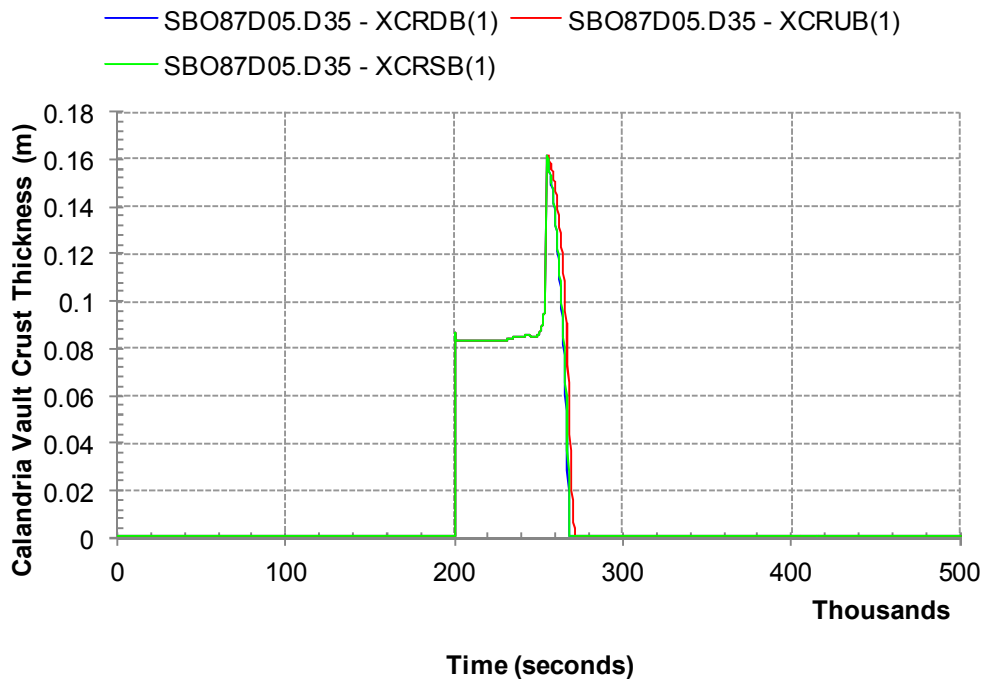


FIG. 3.49. Crust thicknesses (downward-blue, upward-red, sideward-green) in reactor vault (0 – 500,000 s).

#### 3.1.3.4. Phase 4

##### Containment response

Figure 3-46 shows the pressure in containment Node 8, i.e., lower half of steam generator enclosure. Initially, the containment pressure is 100 kPa(a). After the accident initiation, the containment pressure increases gradually because water is discharged into the containment through the PHTS liquid relief valves. Note that the dousing system is assumed to be unavailable in the present analysis. The rapid increase of containment pressure at 9,000 s (2.5 h) is due to PHTS coolant release via the LRVs. The increase of containment pressure at 25,000 s (6.9 h) is due to the rupture of pressure and calandria tubes and PHTS coolant release to and from the CV through the CV rupture disks in the containment. Containment pressure decreases after that (it is not clearly visible in the figure due to scale) because of the steam condensation on the containment walls and structures such as steel beams, columns, stairs, etc.; in the accident initial period these structures are relatively cool. The rapid increase of containment pressure at 200,200 s (55.6 h) is due to corium relocation into the basement after the calandria vessel failure following intensive steam generation.

Containment pressure gradually increases and at 33,054 s (9.18 h) reaches the failure set point of air lock seal 335 kPa(a) (Fig. 3-46). At this time the containment fails. At 53,554 s (14.87 h), water in reactor vault reaches the saturation temperature and starts to boil off (Table 3-2). The RV water gradually evaporates and steam is released in the containment. The containment gas temperature in the lower steam generator room is shown in Figure 3-50. The mass of water in the containment basement and the volume fraction of steam in the lower steam generator room are shown in Figures 3-51 and 3-52, respectively.

##### Fission product release and distribution

The initial inventory of fission products (radioactive plus stable) in a generic CANDU 6 station core is summarized in Table 2-6 of the current document.

Figure 3-53 shows the mass of noble gases released in the calandria vessel (“in-vessel”) and to the environment. As shown in Figure 3-53 the major portion of the noble gases is released into the CV from the fuel and the suspended debris bed during core disassembly and core collapse, starting from 19,833 s (5,51 h) until 53,749 s (14.93 h). In the present analysis, containment leakage is modelled at 0.5% free volume per day. Eventually all the noble gases are released to the environment after the containment fails at 33,054 s (9.18 h).

Figure 3-54 to 3-59 show the mass of CsI and RbI released in-vessel (inside the CV), ex-vessel (outside the CV) and to the environment along with the mass in the PHTS, calandria vessel, and containment. At 17,918 s (5.0 h), pressure and calandria tubes rupture and the fuel element temperatures exceed 1,000°K. Because the calandria vessel rupture disks opened at 18,088 s (5.0 h), the fission products are released through the calandria vessel relief ducts into the containment (Fig. 3-59). Figure 3-59 shows that the mass of CsI and RbI in the containment (including airborne and deposited) remains at 4.59 kg until 500,000 s (138.9 h).

The water in reactor vault is almost depleted at 229,621 s (63.78 h). After that, the corium reacts with the concrete and fission products are released ex-vessel (outside calandria vessel, Fig. 3-54). Because almost all of the CsI and RbI are retained in the containment by various fission product retention mechanisms, only a very small amount (9.36%) is released to the environment when the containment fails.

### **Hydrogen release and concentration**

Figure 3-60 shows the hydrogen released from PHTS Loops 1 and 2, respectively. The releases include all the hydrogen generated in fuel channels and in the suspended debris beds prior to corium relocation to the reactor vault. At 17,708 s (4.9 h), some fuel channels dry out; steam inside the channel reacts with the fuel cladding and inner surface of the pressure tube. Such reactions at high temperature produce hydrogen, but the mass of hydrogen produced is relatively small during this period, which is not clearly seen in Figure 3-60 because of scaling of the figure. The hydrogen production, however, increases rapidly after pressure and calandria tube failure (at 17,918 s or 5.0 h) as shown in Figure 3-60 because most of the coolant from the channel is lost through the break, and fuel/Zr heat up. At 52,695 s (14.6 h), the core collapse was predicted and core debris relocates into the calandria vessel bottom followed by the depletion of moderator in the calandria vessel. The code assumes no hydrogen generation from the debris located at the calandria vessel bottom after core collapse, because of crust formation on top of the debris bed. Therefore, hydrogen generation reaches almost a plateau.

It should be noted that Figure 3-60 represents the hydrogen generated in one PHTS loop only. The behaviour of the other PHTS loop is similar as shown in Figure 3-60, so the total amount of hydrogen generated in PHTS is twice as much as indicated in Figure 3-61. Figure 3-61 shows the total amount of hydrogen generated in the reactor vault. Major quantities of hydrogen are generated in the reactor vault due to the jet break-up of molten debris in the water pool and the molten core - concrete interaction. At 200,189 s (55.6 h), the calandria vessel was predicted to fail and corium relocates into the reactor vault. At 229,621 s (63.8 h) the water inside reactor vault is almost depleted, and at 246,711 s (68.5 h) molten corium starts to interact with the reactor vault concrete floor, which results in an increase of hydrogen release (Fig. 3-61). In addition to the oxidation of Zircaloy, iron from rebar in the concrete is also oxidized to produce hydrogen.

Figure 3-62 shows the hydrogen volume fraction in containment Node 8, the lower half of the steam generator rooms. It should be noted that hydrogen igniters are not credited in this sequence. Figure 3-62 is consistent with Figure 3-61. Note that Fig 3-61 represents hydrogen generated from both PHTS loops as well as from the reactor vault. After pressure and

calandria tubes fail at 17,918 s (5.0 h), the hydrogen released within the calandria vessel enters containment through the calandria vessel rupture disk openings. As a result, the hydrogen concentration increases rapidly as shown in Figure 3-62. At 52,695 s (14.6 h), core collapse was predicted and core debris relocates to the calandria vessel bottom. The moderator inside the calandria vessel is subsequently depleted and no more hydrogen is produced. Thus the hydrogen concentration in containment shows a rapid decrease (see Fig. 3-62). Subsequently, the hydrogen concentration starts to increase at 250,000 s (69.4 h) as a result of MCCI in RV.

At 53,554 s (14.9 h), the water in the reactor vault reaches saturation temperature (Fig. 3-63) and begins to boil off. Steam from the reactor vault starts to discharge into containment (Figures 3-64 and 3-65). As a result, steam concentration in the containment increases rapidly. On the other hand, the mass of hydrogen remains approximately constant. Thus the increase of the steam mass in the atmosphere results in a decrease in the hydrogen concentration (Fig. 3-62). When containment fails at 33,054 s (9.18 h), hydrogen is released into the environment resulting in a rapid decrease in the hydrogen concentration in containment.

At 200,189 s (55.6 h), the calandria vessel fails and corium relocates into the reactor vault causing a small spike in hydrogen concentration (Fig. 3-62). At 229,621 s (63.8 h), the water inside the reactor vault is depleted, and molten corium eventually reacts with the concrete of the reactor vault floor. When the corium temperature gradually increases (Fig. 3-48) molten corium/concrete interaction begins at 246,481 s (68.5 h) and hydrogen is produced. This results in a rapid increase in the hydrogen concentration after 250,000 s (69.4 h). After 296,000 s (82.2 h), the CO<sub>2</sub> volume fraction inside compartment #8 increases rapidly as a result of MCCI (Fig. 3-66). The CO<sub>2</sub> is produced in the RV as a result of CaCO<sub>3</sub> decomposition during corium-concrete interaction. The CO<sub>2</sub> reacts with the metallic components in the corium (Zr and steel) and therefore is not released from the melt to the containment until all the Zr and steel are oxidized, which occurs at 290,000 s (80.5 h). On the other hand, the mass of hydrogen remains more or less at a constant value. Therefore, the CO<sub>2</sub> mass increase in containment causes the hydrogen concentration decrease. The behaviour of O<sub>2</sub>, N<sub>2</sub>, and CO gases are shown in Figure 3-66.

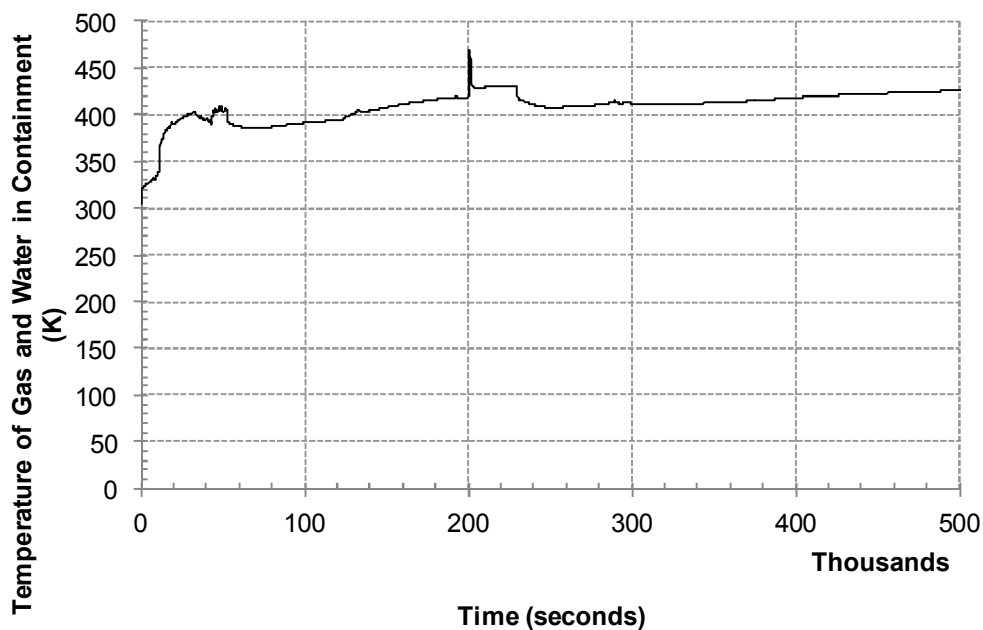


FIG. 3.50. Containment gas temperatures in lower SG room (Node 8), (0 – 500,000 s).

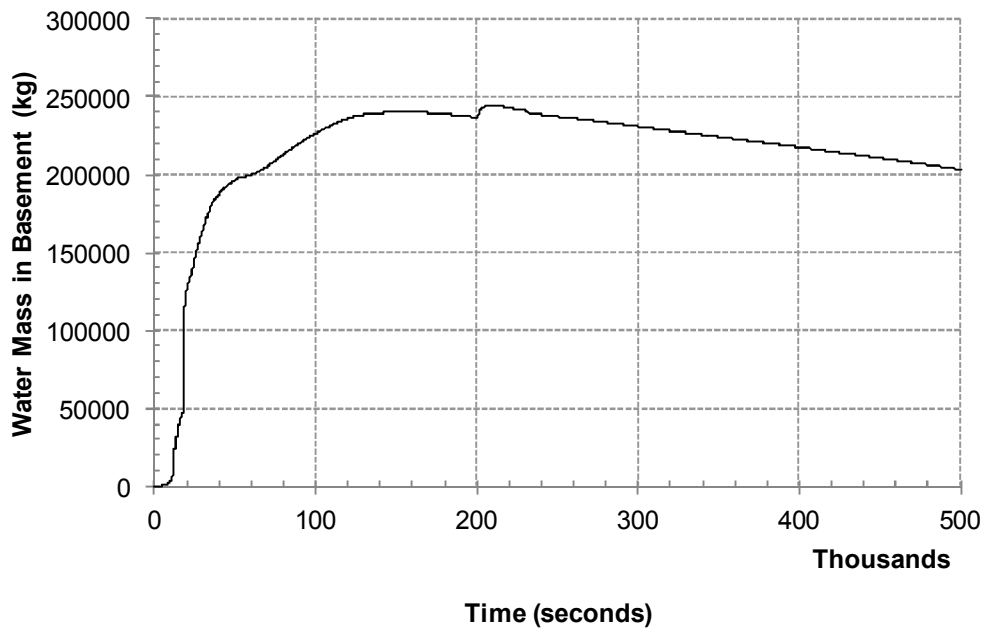


FIG. 3.51. Mass of water in the containment basement (0 – 500,000 s).

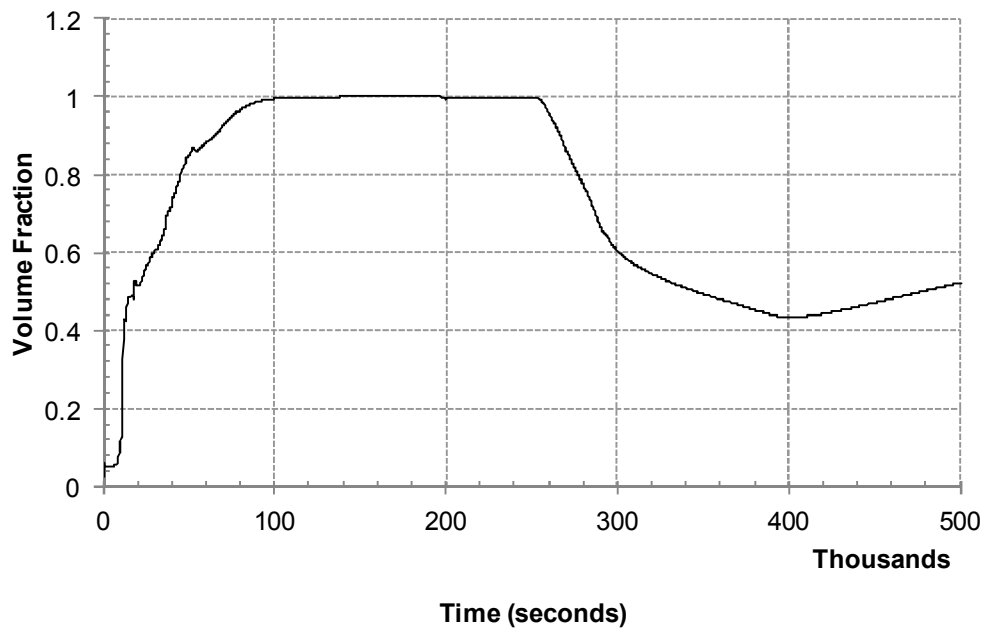


FIG. 3.52. Volume fraction of steam in lower SG room (Node 8), (0 – 500,000 s).

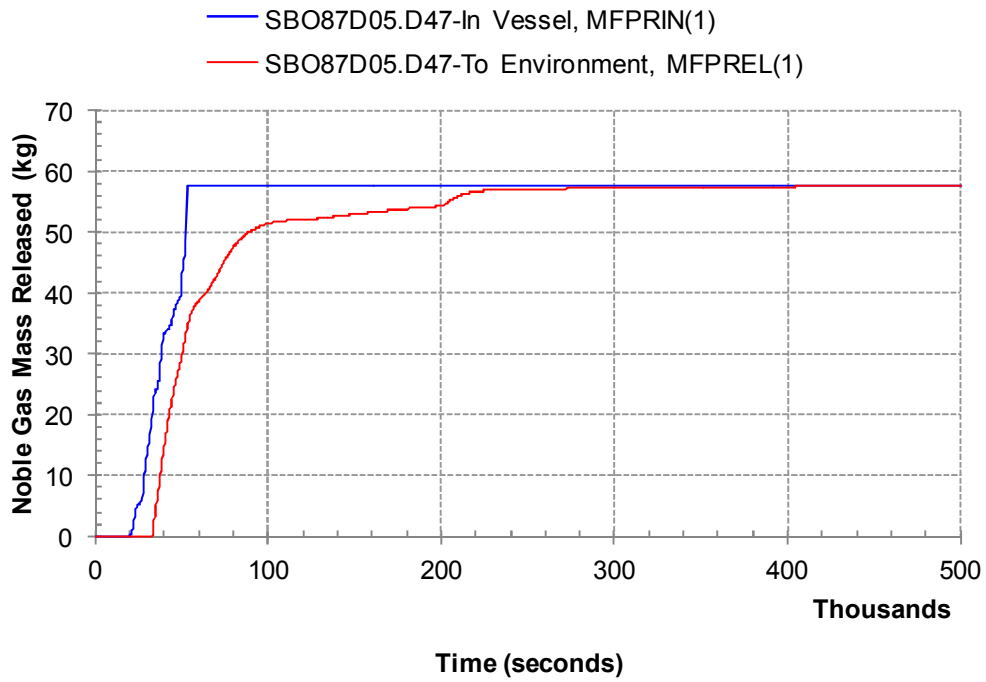


FIG. 3.53. Mass and location of noble gas (both active and stable components included) (0 – 500,000 s).

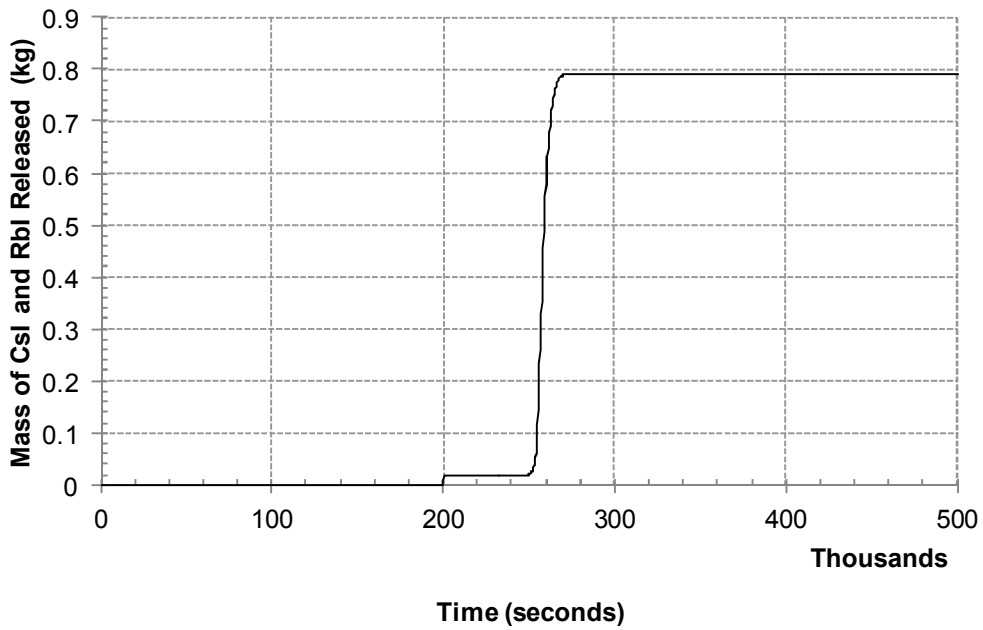


FIG. 3.54. Mass of CsI and RbI Released “ex-vessel” (both active and stable components included) (0 – 500,000 s).

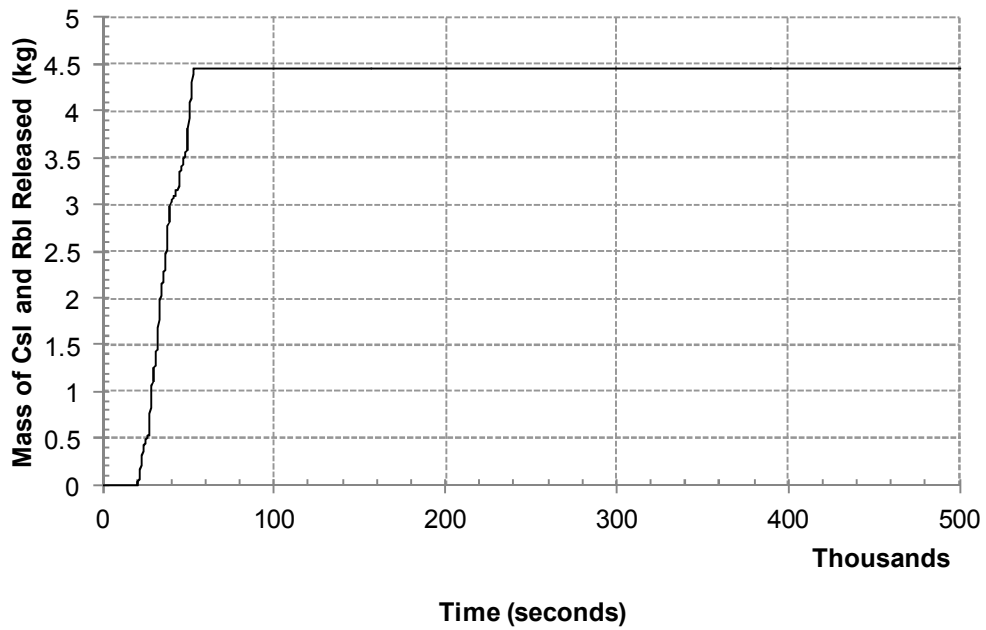


FIG. 3.55. Mass of CsI and RbI released “in-vessel” (both active and stable components included) (0 – 500,000 s).

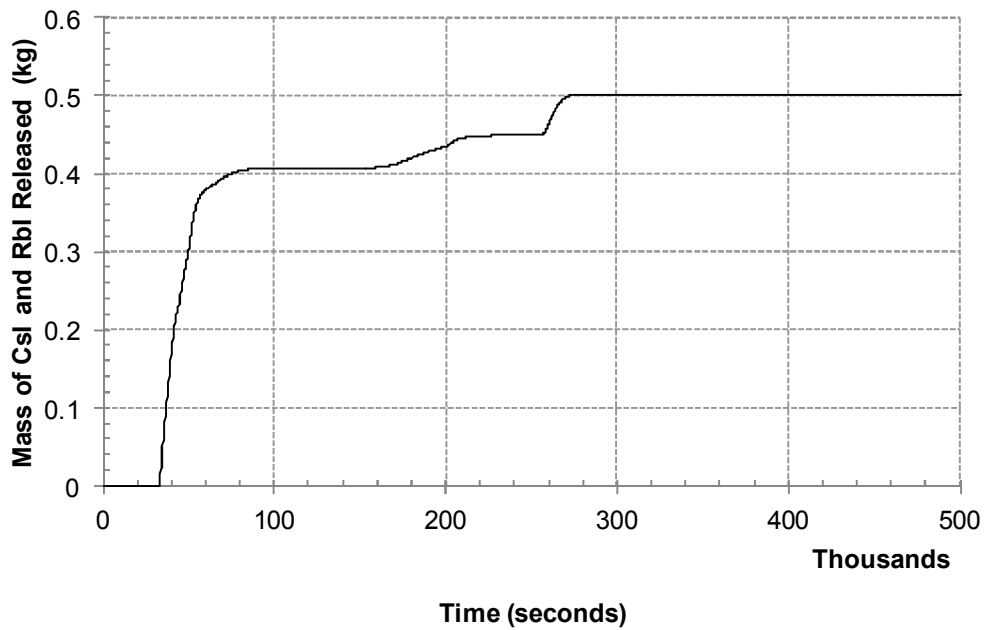


FIG. 3.56. Mass of CsI and RbI released to the environment (both active and stable components included) (0 – 500,000 s).

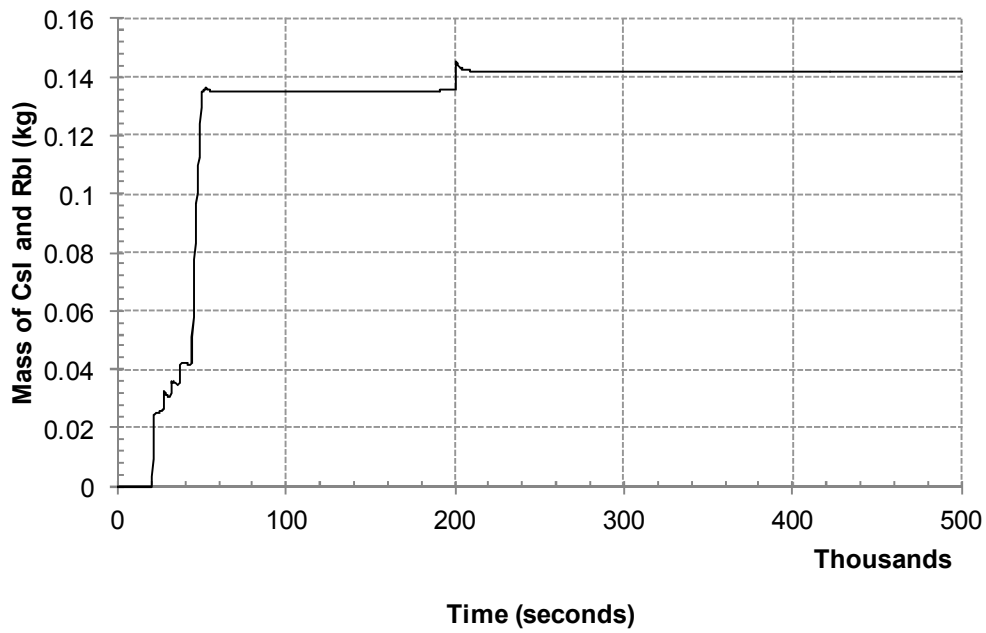


FIG. 3.57. Mass of CsI and RbI in PHTS (both active and stable components included) (0 – 500,000 s).

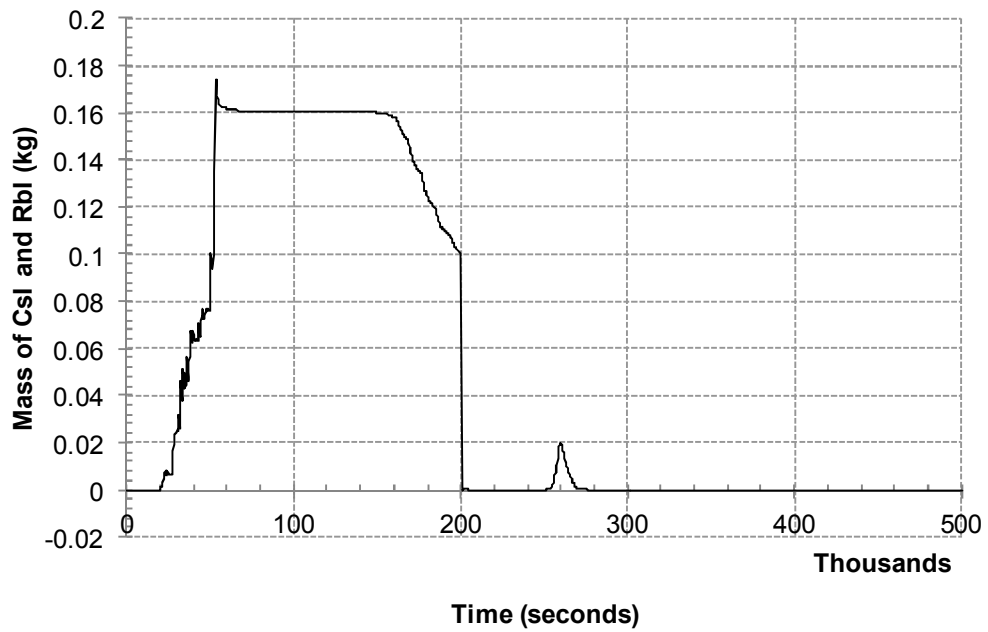


FIG. 3.58. Mass of CsI and RbI in Calandria Vessel (both active and stable components included) (0 – 500,000 s).

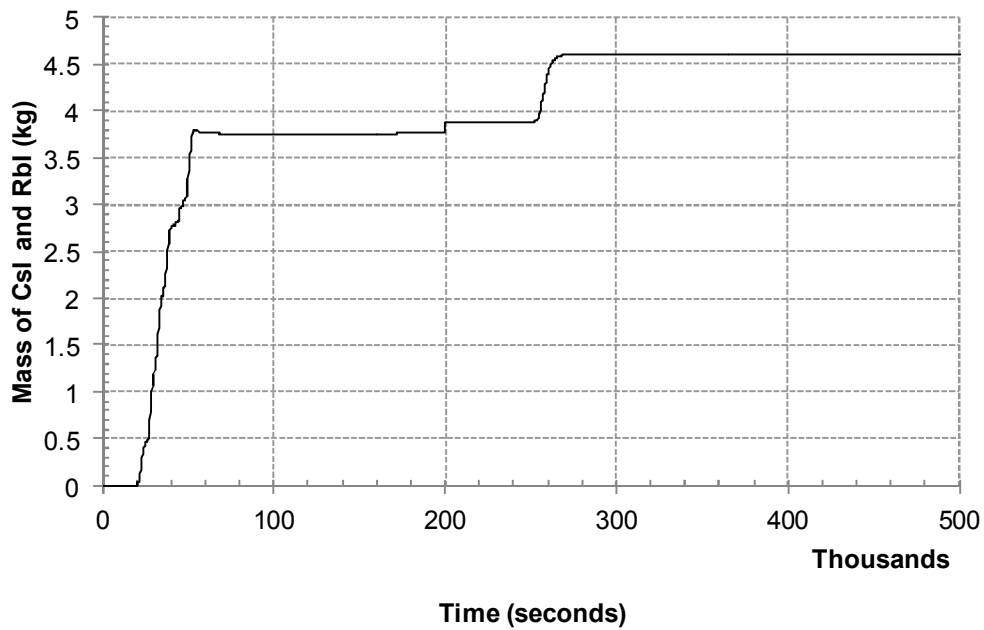


FIG. 3.59. Mass of CsI and RbI in containment (both active and stable components included) (0 – 500,000 s).

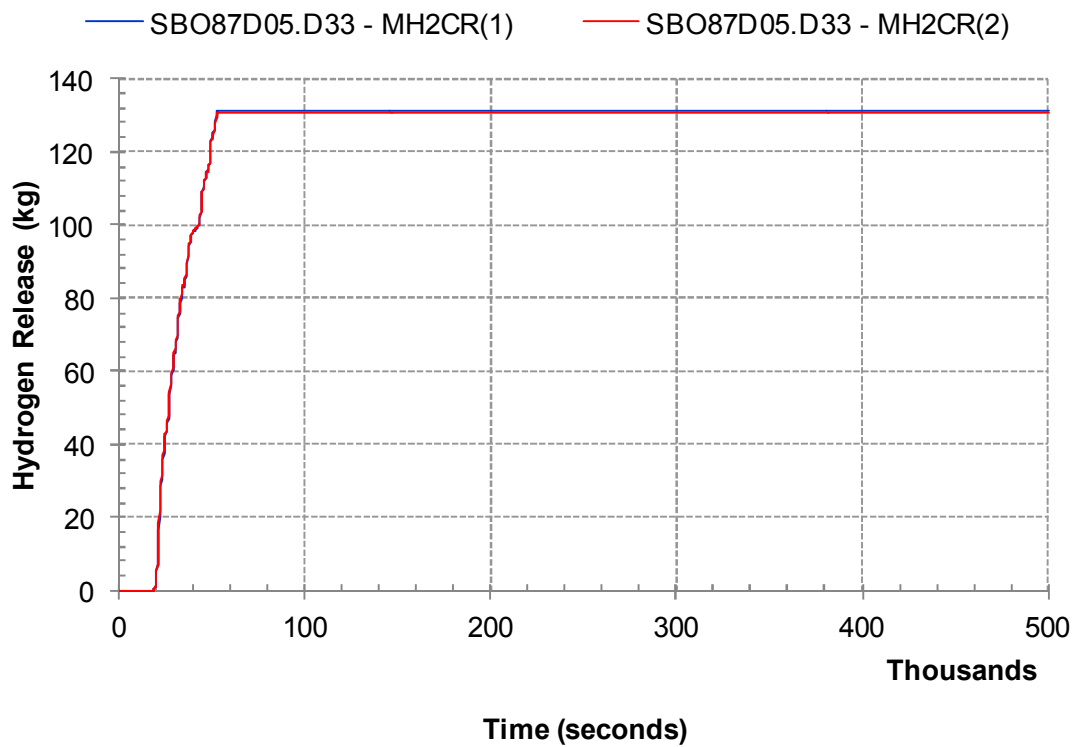


FIG. 3.60. Hydrogen release histories “in-vessel”, Loop 1 and 2 (0 – 500,000 s).

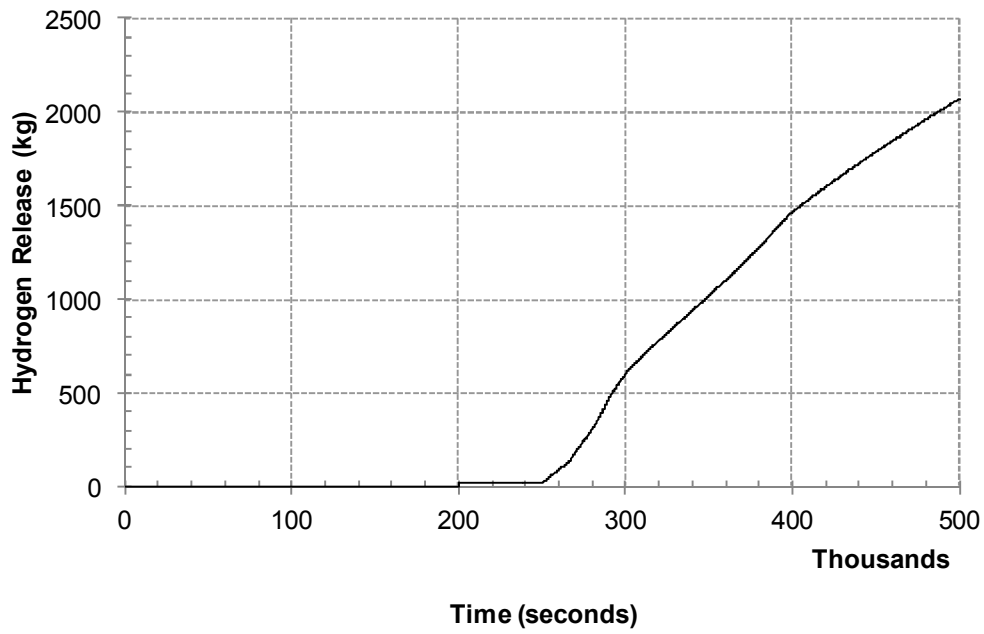


FIG. 3.61. Hydrogen release histories in reactor vault (0 – 500,000 s).

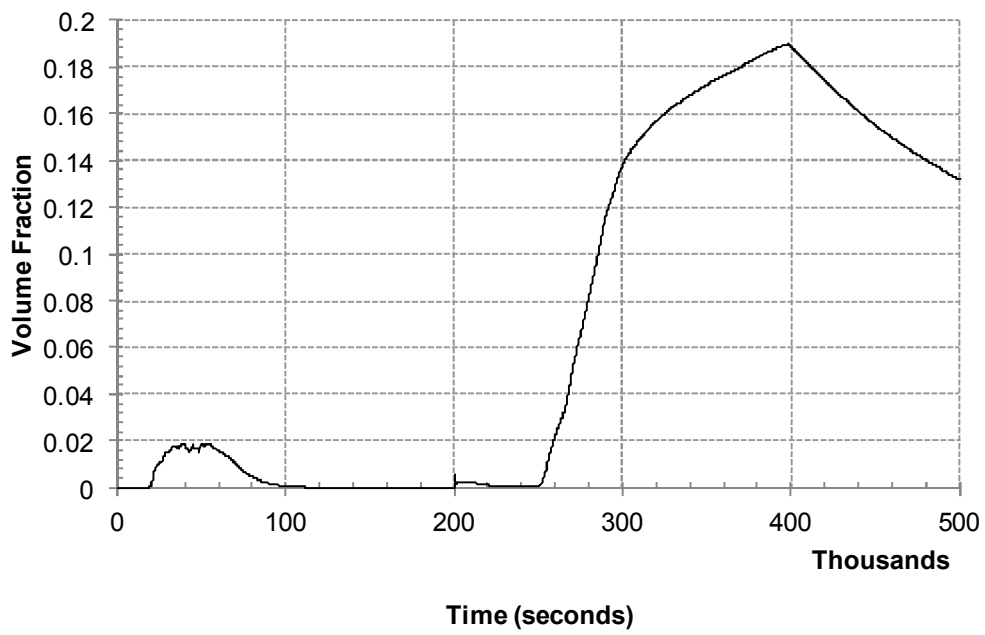


FIG. 3.62. Volume fraction of hydrogen in containment (Node 8), (0 – 500,000 s).

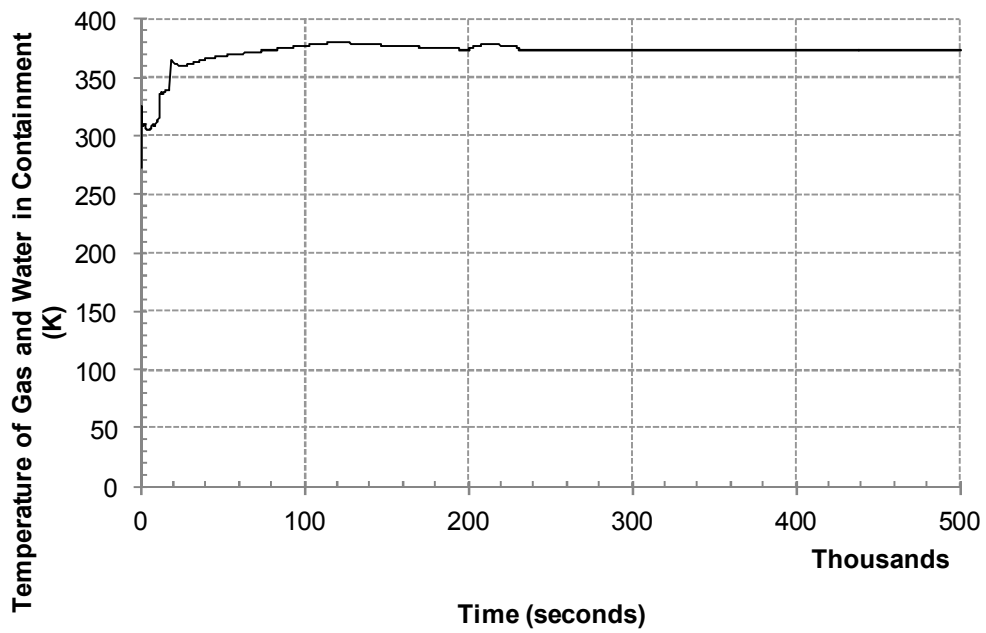


FIG. 3.63. Containment water temperatures in the containment basement (0 – 500,000 s).

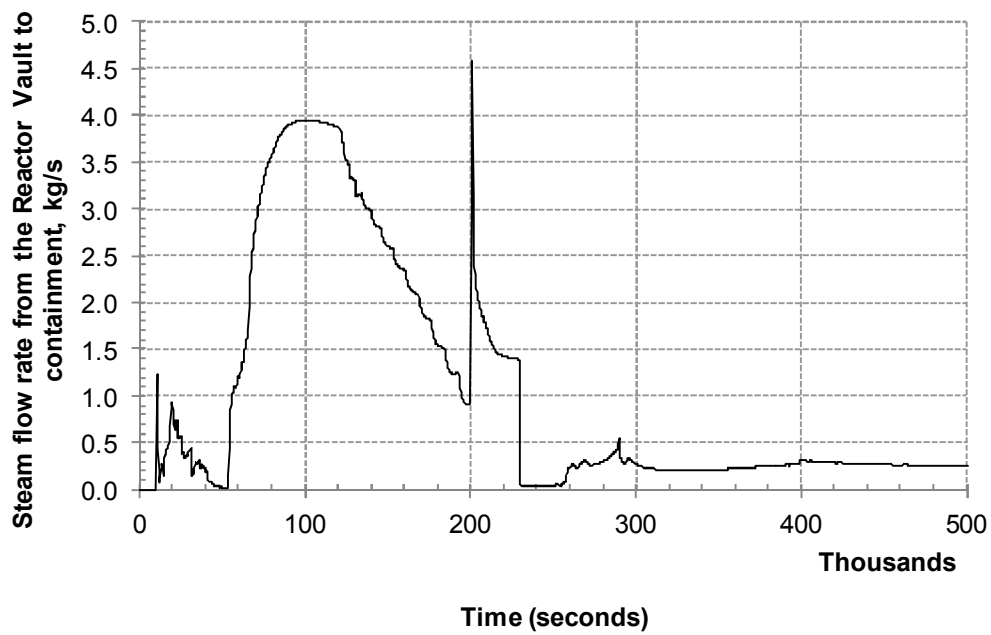


FIG. 3.64. Gas flow rate from the reactor vault to containment (0 – 500,000 s).

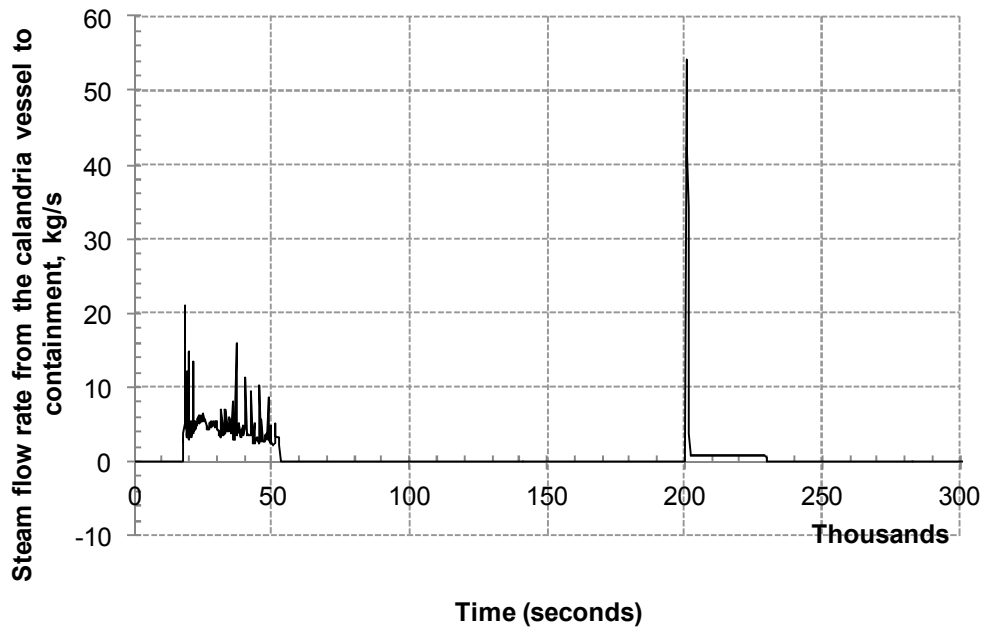


FIG. 3.65. Steam flow rate from the calandria vessel to containment (0 – 300,000 s).

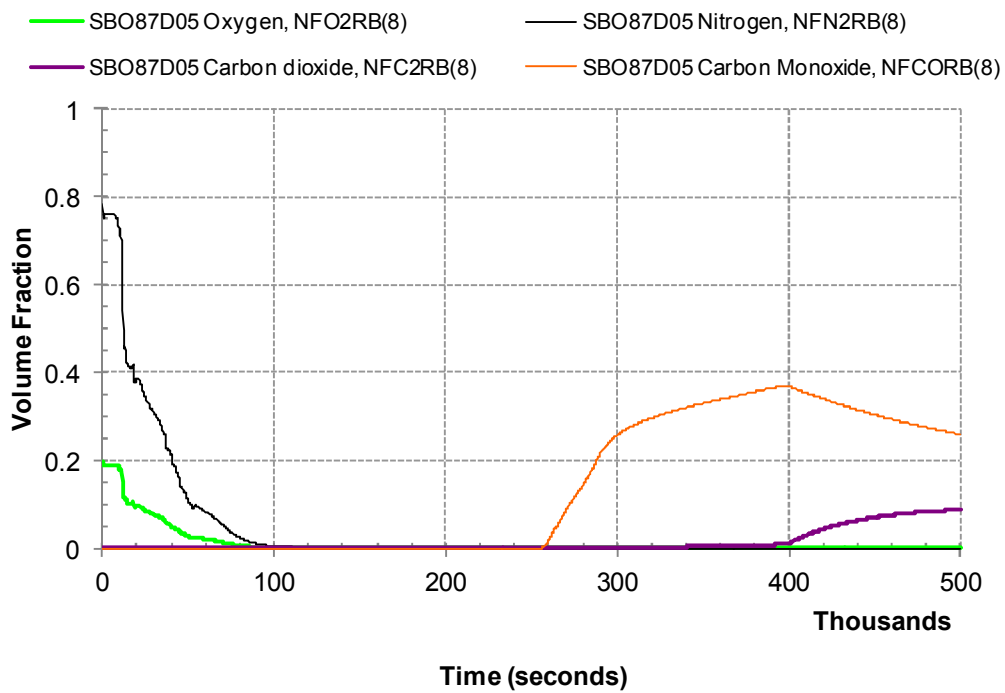


FIG. 3.66. Volume fraction of carbon dioxide, oxygen, nitrogen, and carbon monoxide in containment (Node 8), (0 – 500,000 s).

## 3.2. BARC-RED

### 3.2.1. Computer codes

The entire accident progression has been divided into four phases:

- Phase 1: Accident Initiation to start of fuel channel uncover;
- Phase 2: Start of fuel channel uncover to core collapse;
- Phase 3: Core collapse to calandria vessel failure;
- Phase 4: Calandria vessel failure to containment failure.

The modelling strategy for each phase is given in Table 3-3.

Phase 1 and 2 are simulated using the code RELAP5 [14]. In Phase 3, after the core collapse and relocation into calandria, the heat transfer behaviour for debris bed has been simulated using the model by Sinha et al [15]. After the calandria water gets evaporated, the heat transfer in dry debris and its melting has been simulated using the code ANSWER. Stresses in the calandria are predicted by the code CAST3M. In Phase 4, after the molten corium is relocated into the reactor vault, the corium concrete interaction is modelled with the code MELCOOL-CCI. The details of the codes are as given below.

TABLE 3.3. MAJOR PHENOMENA AND MODELING STRATEGY

Phase	Phenomena	Modelling strategy
1	<ul style="list-style-type: none"> <li>– Steady state loop thermal hydraulic behaviour</li> <li>– Accident initiation</li> <li>– PHT thermal hydraulic response</li> <li>– Fuel and fuel channel thermal response</li> <li>– Containment heat transfer</li> </ul>	RELAP5/Mod3.2
2	<ul style="list-style-type: none"> <li>– PT Thermo-mechanical behaviour</li> <li>– PT-CT contact</li> <li>– Ballooning</li> </ul>	Thermo-mechanical Modelling
	<ul style="list-style-type: none"> <li>– Moderator Boil-off</li> <li>– Core uncover</li> </ul>	RELAP5/Mod3.2
	<ul style="list-style-type: none"> <li>– Core collapse</li> </ul>	Mass based criteria
3	<ul style="list-style-type: none"> <li>– Debris coolability</li> </ul>	Heat transfer correlation
	<ul style="list-style-type: none"> <li>– Debris heat-up and melt pool formation</li> </ul>	ANSWER
	<ul style="list-style-type: none"> <li>– Calandria thermo-mechanical behaviour</li> </ul>	CAST3M
4	<ul style="list-style-type: none"> <li>– Core-concrete interaction</li> </ul>	MELCOOL-CCI

#### 3.2.1.1. Computer code ANSWER

The **ANSWER**<sup>TM</sup> software package is a comprehensive mathematical model for simulation of fluid flow, heat and mass transport processes in laminar or turbulent, compressible or incompressible, flows at any speed can be used to simulate transient or steady state problems in Cartesian or cylindrical geometry. It provides a unified theoretical treatment of concepts relevant to fluid flow and transport. The physical processes incorporated in the software are shown in Figure 3-67. As can be seen from this figure, various levels of interaction and coupling exist between the different components of the flow system. In the **ANSWER**<sup>TM</sup> software package, these components may be employed either in a coupled or uncoupled mode.

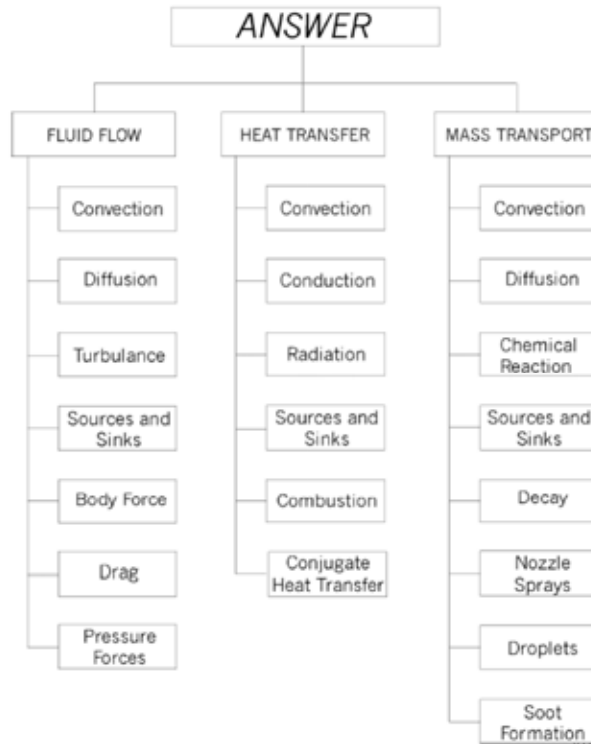


FIG. 3.67. Models in ANSWER.

For ANSWER™ the governing equation for momentum is modified to account for porosity of the medium as shown below.

$$\frac{\partial}{\partial t}(\rho\theta V_j) + \frac{\partial}{\partial X_i}(\rho\theta V_i V_j) = \frac{\partial}{\partial X_i}(\mu\theta \frac{\partial V_j}{\partial X_i}) - \theta \frac{\partial P}{\partial X_j} + \rho\theta g_j - S_{BF} + S_j$$

$$S_{BF} = \theta^2(1 + C_F Re_K) \frac{\mu}{K} V_j$$

$$Re_K = \frac{\rho\theta|V|\sqrt{K}}{\mu}$$

Where:

- t is the time
- $X_i$  is the coordinate in  $i^{\text{th}}$  direction
- $\rho$  is the mass density
- $\theta$  is the porosity of the medium
- $V_j$  is the  $j^{\text{th}}$  component of the fluid velocity
- $\mu$  is the viscosity
- p is the fluid thermodynamic pressure
- $g_j$  is the gravitational acceleration in  $j^{\text{th}}$  direction
- $S_{BF}$  is the Brinkmann Forchheimer drag term
- $S_j$  is the source term
- $C_F$  is the Forchheimer-Ergun drag coefficient
- $Re_K$  is the Reynolds number based on permeability length scale
- K is the permeability of the medium

Similarly, the energy equation is modified using the porosity of the medium to calculate the average thermal conductivity of the bed.

### 3.2.1.2. Computer code CAST3M

CAST3M is a computer code for the analysis of structures by finite element method (FEM). The development of CAST3M enters within the framework of an activity of research in the field of mechanics; the goal being to build a high level instrument, being able to be used as a valid support for the design, dimensioning, and the analysis of structures and components, in the nuclear field as in the more traditional industrial sector.

Accordingly, CAST3M presents a complete system, integrating not only the functions of calculation themselves, but also of the functions of construction of the model (pre-processor) and of processing of the results (post-processor). CAST3M is a powerful, flexible analysis and optimization program for mechanical linear elastic problem in statics and dynamics (vibration, extraction of eigenvalue), thermal and heat transfer problem, nonlinear problem (elastic, plastic, creep materials), step by step dynamic problem.

In CAST3M, different types of analyses (strains or stresses plane, axisymmetry, etc.) can be done. Also, different types of elements (beams, hulls, etc.), properties of material, and geometrical characteristics which cannot be deduced from the meshes and the boundary conditions can be modelled. Different types of material behaviour models like elastic, plastic, elasto-plastic, viscoelastic, viscoplastic etc. can be used in the code. In present problem, elasto-viscoplastic analysis with Chaboche model has been carried out.

### 3.2.1.3. Computer code MELCOOL-CCI

A code MELCOOL-CCI has been developed for predicting the ablation of concrete and evolution of gases due to thermal decomposition of concrete under heat load.

#### (a) Governing equations of MELCOOL-CCI

2-D transient conduction equation in melt pool:

$$\rho C_p \frac{\partial T}{\partial t} = \frac{\partial}{\partial x} \left( k \frac{\partial T}{\partial x} \right) + \frac{\partial}{\partial y} \left( k \frac{\partial T}{\partial y} \right) + q''$$

2-D transient conduction equation in Concrete layer:

$$\rho_{con} C_{p_{con}} \frac{\partial T_{con}}{\partial t} = \frac{\partial}{\partial x} \left( k \frac{\partial T_{con}}{\partial x} \right) + \frac{\partial}{\partial y} \left( k \frac{\partial T_{con}}{\partial y} \right)$$

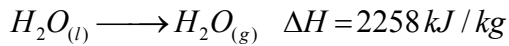
Boundary conditions:

$$T_{i_{pool}} = T_{i_{concrete}} \quad \text{Temperature continuity}$$

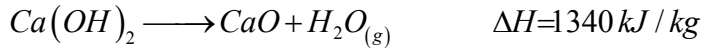
$$k_p \left. \frac{\partial T}{\partial z} \right|_{pool} = k_{cn} \left. \frac{\partial T}{\partial z} \right|_{concrete} \quad \text{Flux continuity}$$

(b) Phenomena taking place during MCCI

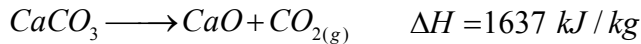
For  $T > 100^\circ\text{C}$ , loss of evaporable water



For  $T \sim 500 - 600^\circ\text{C}$ , dehydration of  $\text{Ca}(\text{OH})_2$



For  $T > 750^\circ\text{C}$ , decomposition of lime



Melting of Concrete at about  $1400^\circ\text{C}$ .

(c) Solution Strategy: Enthalpy Temperature hybrid method

The equations can be written in form of enthalpy-temperature hybrid form as follows

$$\rho_{con} \frac{\partial(h_{con})}{\partial t} = \frac{\partial}{\partial x} \left( k \frac{\partial T_{con}}{\partial x} \right) + \frac{\partial}{\partial y} \left( k \frac{\partial T_{con}}{\partial y} \right)$$

This method allows us to:

- 1) Take into account the  $C_p$  of concrete as a strong function of temperature as shown in Figure 3-68 which is converted into  $h = f(T) = \int C_p dT$  (Fig. 3-69) to take into account all the chemical reactions

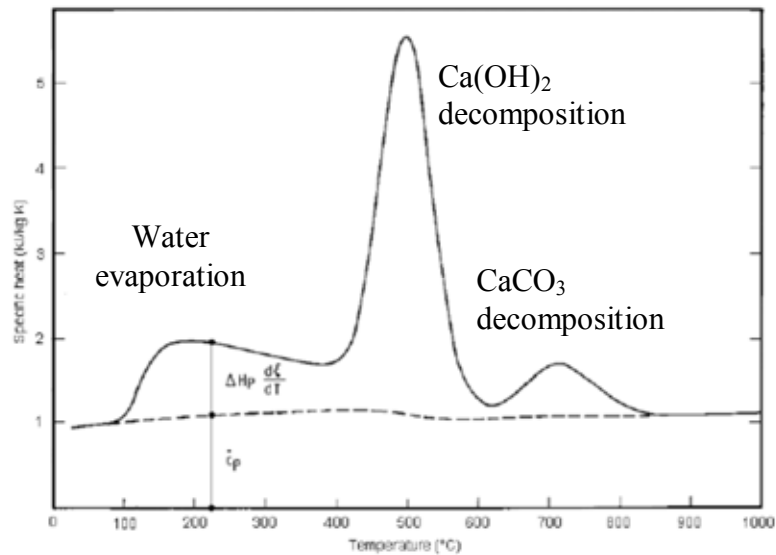


FIG. 3.68.  $C_p$  vs Temperature of concrete.

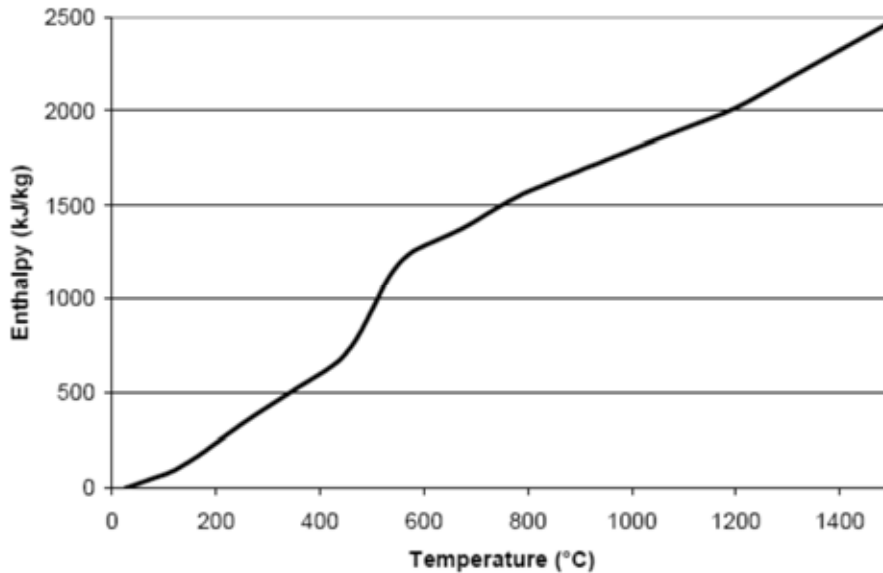


FIG. 3.69. Enthalpy vs temperature for concrete.

- 2) Ease in tracking the melt front in the concrete as enthalpy is continuous even though concrete may melt at different temperature.

The interface is tracked as follows:

$$\text{If } h_{i,j}^n > h_{T_{\text{solidus}}} + \frac{h_{\text{fusion}}}{2} \text{ and } h_{i,j}^{n+1} < h_{T_{\text{solidus}}} + \frac{h_{\text{fusion}}}{2}$$

$$x = \frac{\frac{h_{\text{fusion}}}{2} + h_{\text{solidus}}}{h_{i,j}^{n+1} - h_{i,j}^n} \text{ which will give the contour position.}$$

The equations are solved by simple explicit method. Since the time frame involved in melting phenomena is quite large, we can have a sufficient stability by using explicit method.

These enthalpy-temperature relationships are specific for each type of concrete. In the present code, there are three main types of concrete which can be taken into account:

- Haematitic aggregates
- Basaltic aggregates
- Limestone and Common Sand (LCS)

The libraries contain the information regarding enthalpy – temperature data, density, thermal conductivity and mole fraction of main components of the concrete.

### 3.2.2. Phenomena and system idealization

#### 3.2.2.1. Primary and secondary system modelling

The CANDU 6 Heat Transport System (HTS) has been modelled in RELAP5/Mod3.2 as shown in Figure 3-70. It represents both the loops of the HTS system. The 380 channels of CANDU 6 reactor have been represented by 20 channels, 10 in each loop of which five are forward and five backward as shown in Figure 3-71. The 12 bundles in a CANDU 6 fuel channel are modelled as 12 axial nodes with individual peaking factors. The rest of the system includes inlet headers, feeders, outlet headers, feeders, steam generators primary side tubing and reactor coolant pumps. The two loops are connected by pressurizer. The secondary

system consists of steam generator (SG) downcomer, riser, steam separator and steam dome as shown in Figure 3-72. The turbine has been simulated with a Time Dependent Volume (TDV) so as feed water pumps. Moderator system has also been modelled consisting of Calandria as a pipe component and considering heat loss through PT and CT to the moderator (Fig. 3-73).

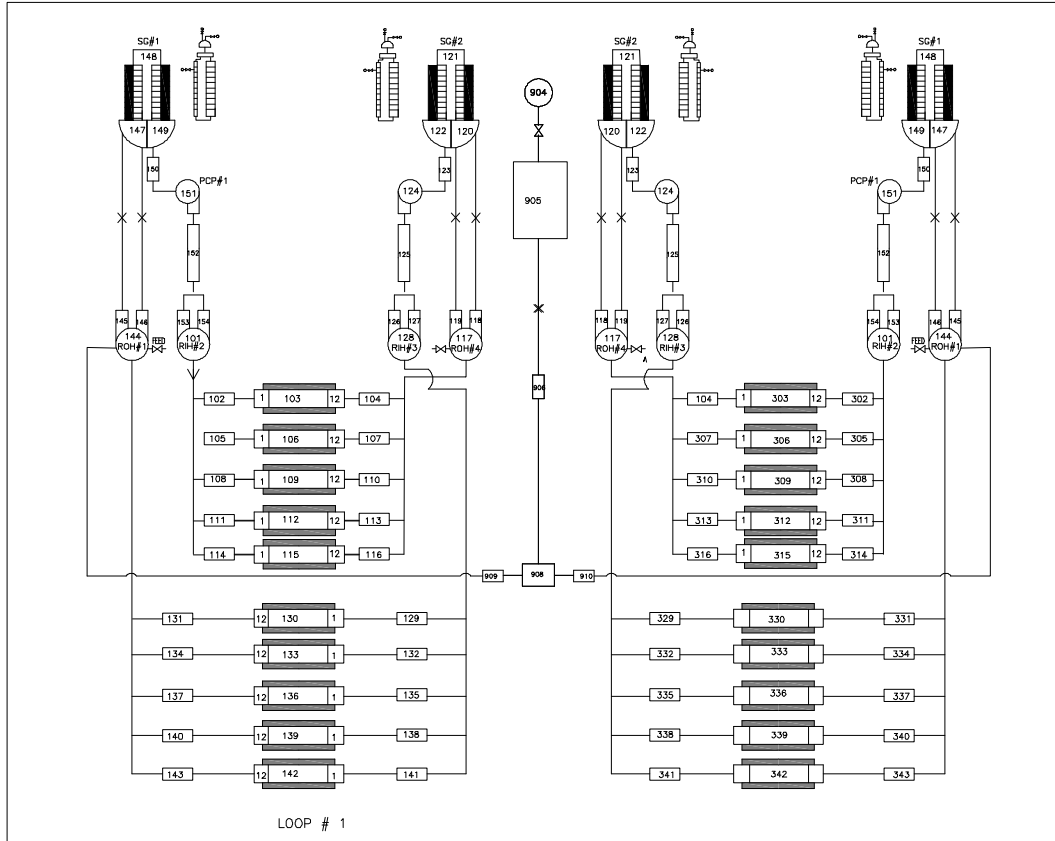


FIG. 3.70. CANDU nodalization in RELAP5/MOD3.2.

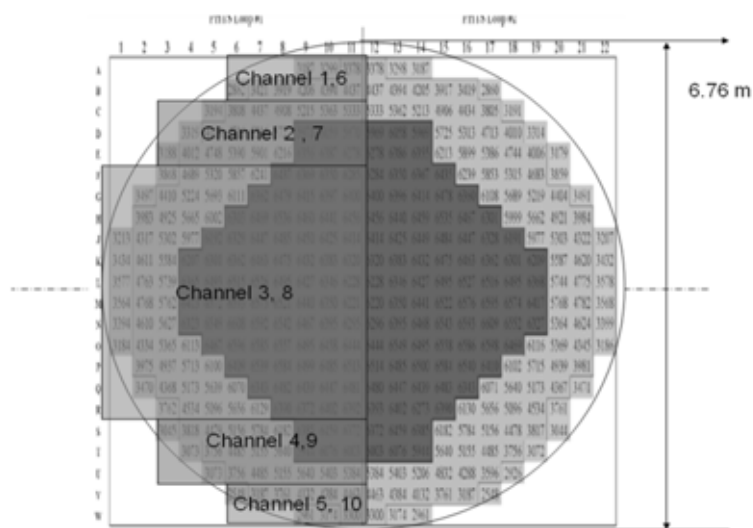


FIG. 3.71. Division of half core into 10 channels.

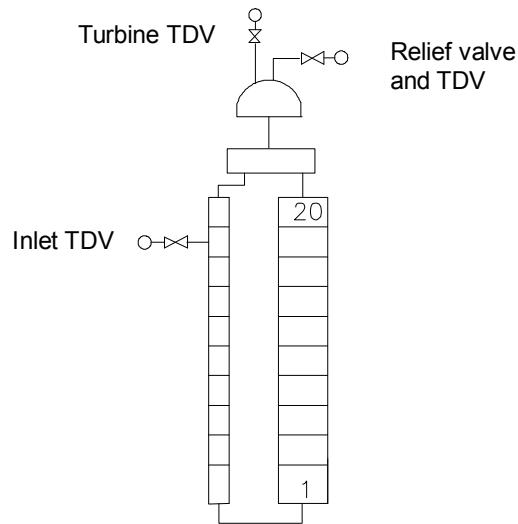


FIG. 3.72. RELAP5 Nodalization of secondary side.

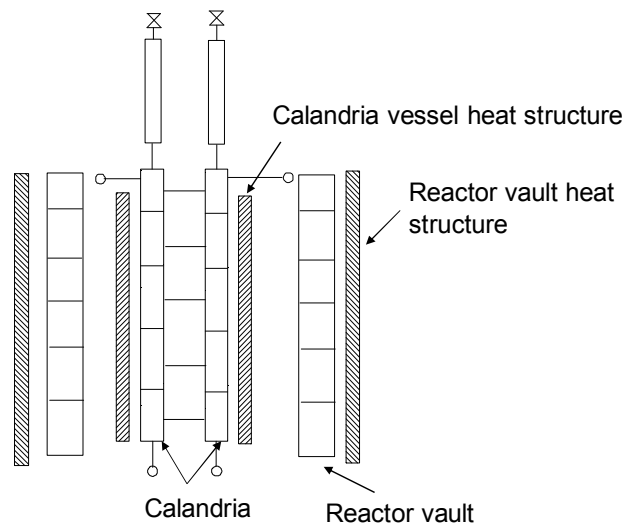


FIG. 3.73. Moderator system nodalization.

### 3.2.2.2. Modelling of heat transfer in Debris bed:

Figure 3-74 shows the modelling strategy and boundary conditions for heat transfer from the flooded debris bed to the moderator. The heat transfer is calculated by Sinha-Nayak correlation [15] for film boiling in heat generating debris.

Once the debris is dry, the heat transfer from debris to calandria and to the vault water is calculated by the code ANSWER. Calandria vessel nodalization for debris bed heat transfer in ANSWER is shown in Figure 3-75.

An analysis of the thermal stresses inside calandria wall was carried out using the computer code CAST3M. Half cylindrical geometry has been modelled in 3D as shown in Figure 3-76.

The molten core concrete interaction has been simulated using the code MELCOOL-CCI. The nodalization scheme and boundary conditions have been given in Figure 3-77.

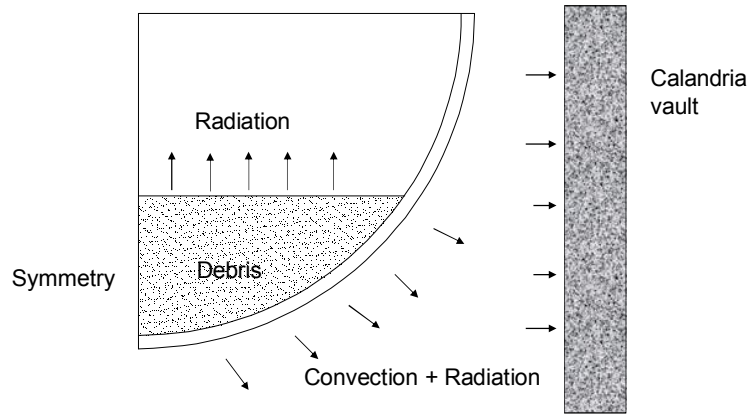


FIG. 3.74. Modelling of heat transfer in debris bed inside calandria.

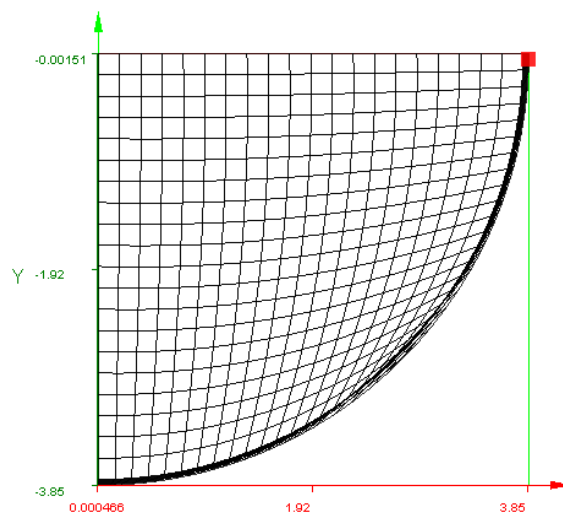


FIG. 3.75. Calandria vessel nodalization for debris bed heat transfer in ANSWER

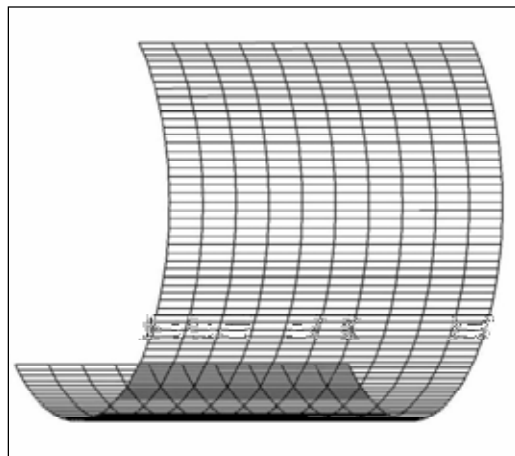


FIG. 3.76. Calandria vessel nodalization scheme for structural analysis

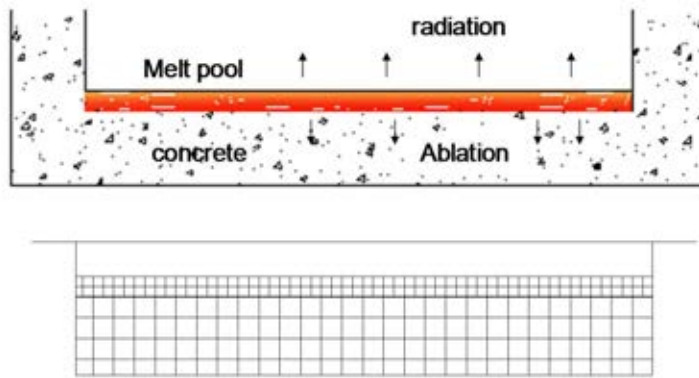


FIG. 3.77. Nodalization scheme for MCCI.

### 3.2.2.3. Containment modelling

The containment has been modelled in RELAP5. The nodalization given by AECL has been adopted. The horizontally cross connected volumes are grouped together. The cross section areas, volumes and heat transfer areas of each node provided by AECL have been preserved. The RELAP5 nodalization scheme is as shown in Figure 3-78. Number 1 to 5 in Figure 3-78 are RELAP nodes used in calculation.

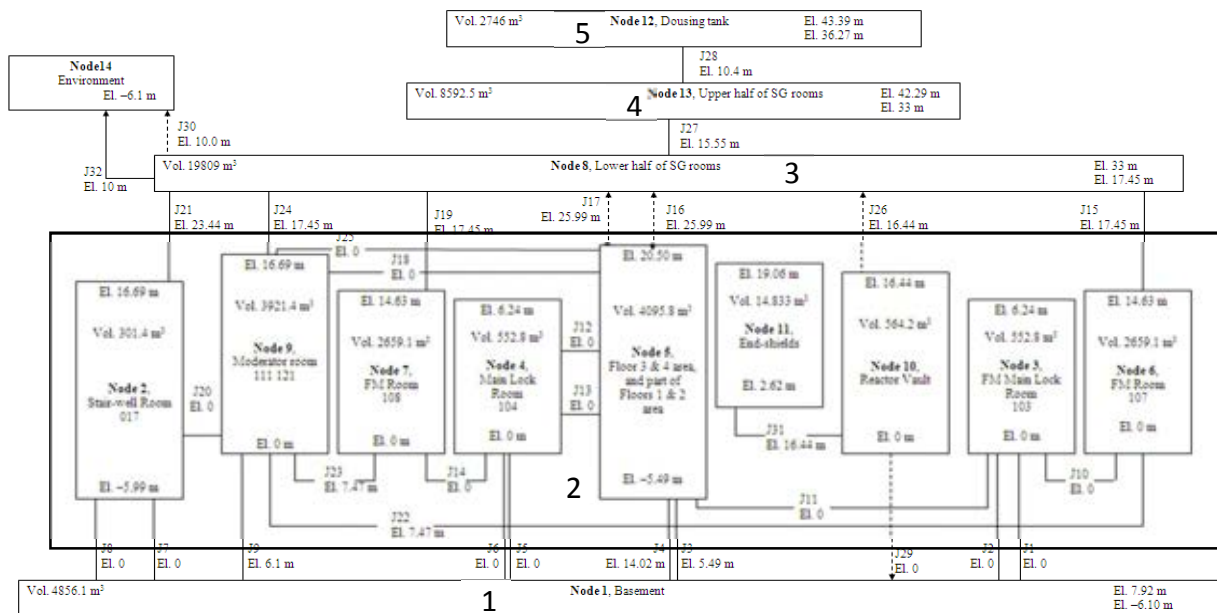


FIG. 3.78. Containment nodalization.

### 3.2.3. Analysis results

Table 3-4 shows the timing of events taking place during the progression of accident.

#### 3.2.3.1. Phase 1 and 2 of accident progression

After initiation of the SBO, the pumps coast down. Immediately the reactor is also tripped. This leads to slight depressurization of primary system. The pressure in the ROH and RIH are shown in Figure 3-79. The corresponding pressures in SG are shown in Figure 3-80. Due to the box-up of secondary side, the secondary side pressure rises and is relieved by opening of

MSSVs (Fig. 3-85). As a result of which, the inventory in the SG continuously depletes (Fig. 3-81). Also, as level depletes, the heat transferred to secondary side reduces (Fig. 3-82). At around 6,000 s, the inventory in all the four SG's is completely boiled off. As a result, the primary side pressure starts rising to the set point of the LRVs at around 6,198 s (Fig. 3-79). When the pressure increases above the LRV set point, it opens and discharges the inventory into the containment. During this time, the inventory in primary side depletes. As shown in Figure 3-83, the pressurizer becomes empty in 7,500 s and at around 10,000 s, the primary inventory completely depletes (Fig. 3-84).

The mass flow rate in the primary side is shown in Figure 3-86. After tripping of the pumps, the mass flow rate reduces due to combined action of the pump coastdown and built up of thermosyphon. However, after nearly 6,700 s, the thermosyphon flow rate is very small because of no heat removal from secondary side. Due to this, channels get completely voided as shown in the Figure 3-87.

TABLE 3.4. SUMMARY OF THE EVENTS

Events	Time (s)
Class IV and Class III Power loss	0
Turbine stop valves closed	20
Reactor trips	0
First opening of MSSV	28
LRVs open for the first time, PHTS Loop 1	6198
LRVs open for the first time, PHTS Loop 2	6198
SG secondary sides are dry, Loop 1	6100
SG secondary sides are dry, Loop 2	6100
Calandria vault rupture disk open	13 647
Pressurizer empty	7500
At least one channel is dry Loop 1 (complete boil-off)	7880
At least one channel is dry Loop 2 (complete boil-off)	7880
Fuel sheath failed in fuel channel 3, bundle 7,	11 000
Calandria vessel rupture disks #1-4 open	13 647
Moderator reaches saturation temperature	14 010
Beginning of the core disassembly, Loop 1	17 040
Beginning of the core disassembly, Loop 2	17 040
Core collapse (loop 1) to calandria vessel bottom	17 691
Core collapse (loop 2) to calandria vessel bottom	17 691
Water is depleted inside calandria vessel	36 000
Water in calandria vault reaches saturation temperature	62 000
Calandria vessel failed	204 000
Water is depleted inside calandria vault	200 000
Molten corium-concrete interaction begins in calandria vault	205 000

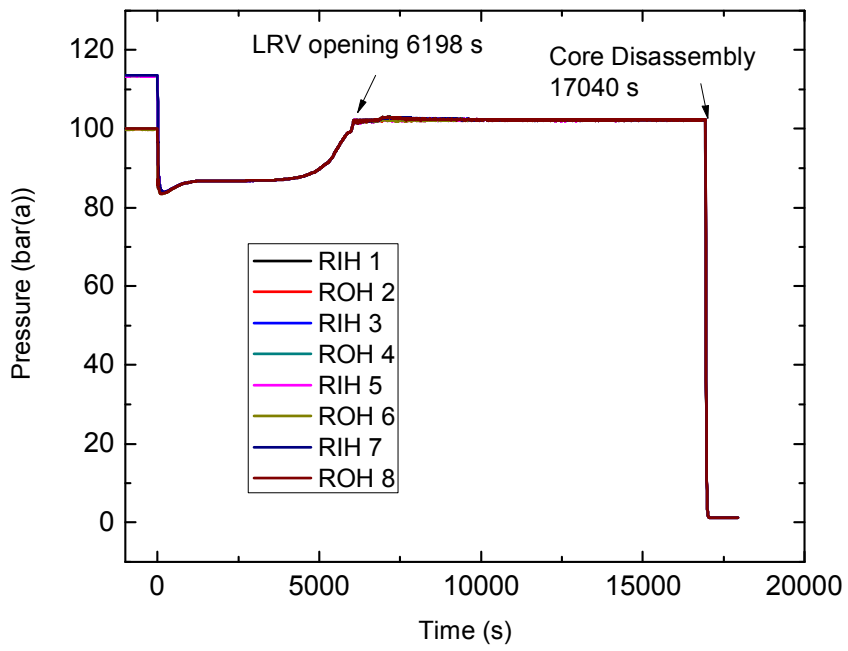


FIG. 3.79. PHTS pressures.

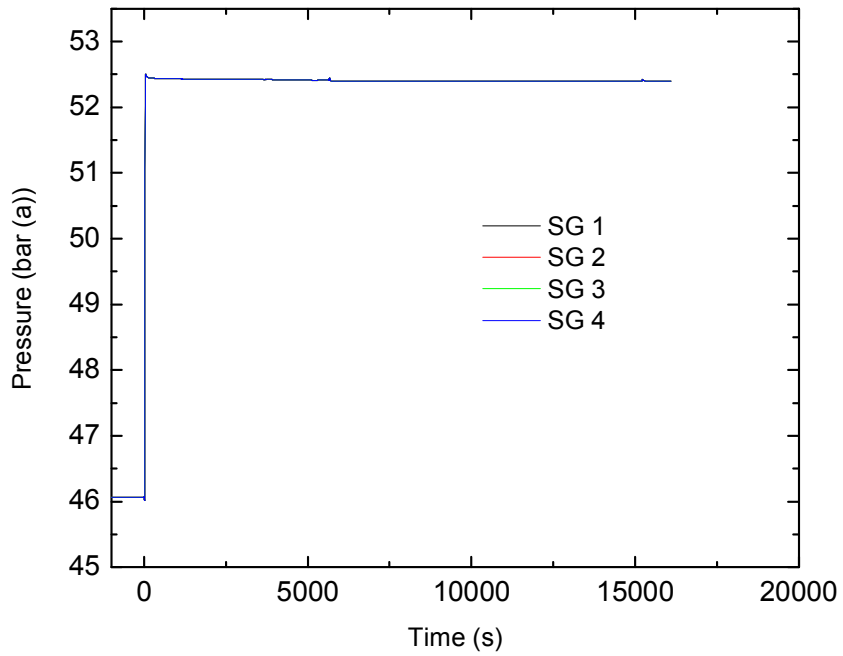


FIG. 3.80. SG pressures.

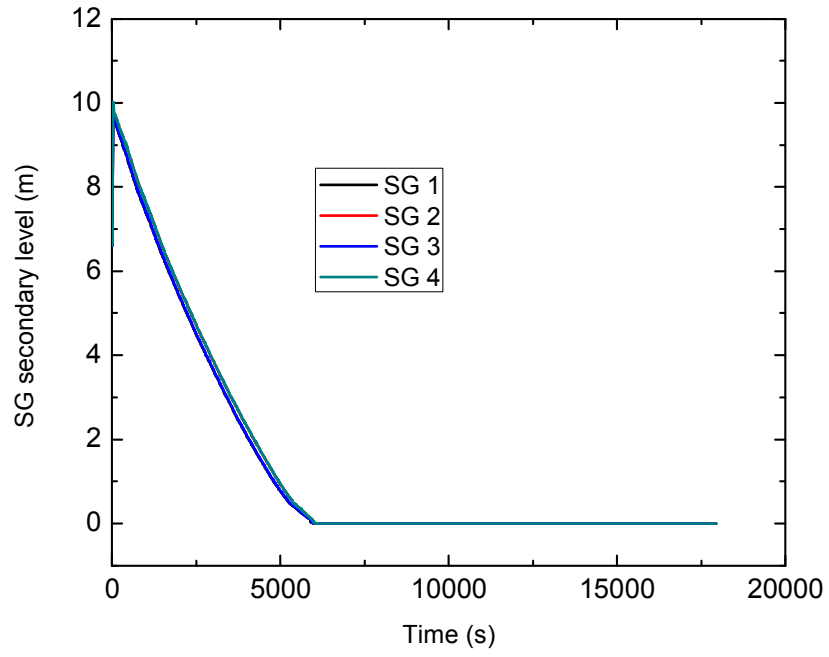


FIG. 3.81. SG water level.

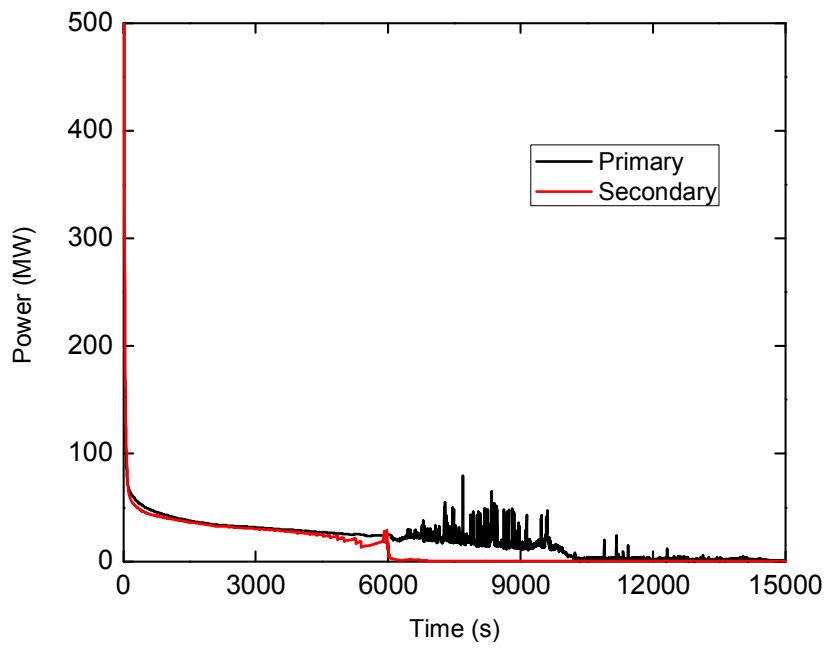


FIG. 3.82. Heat transfer at SG.

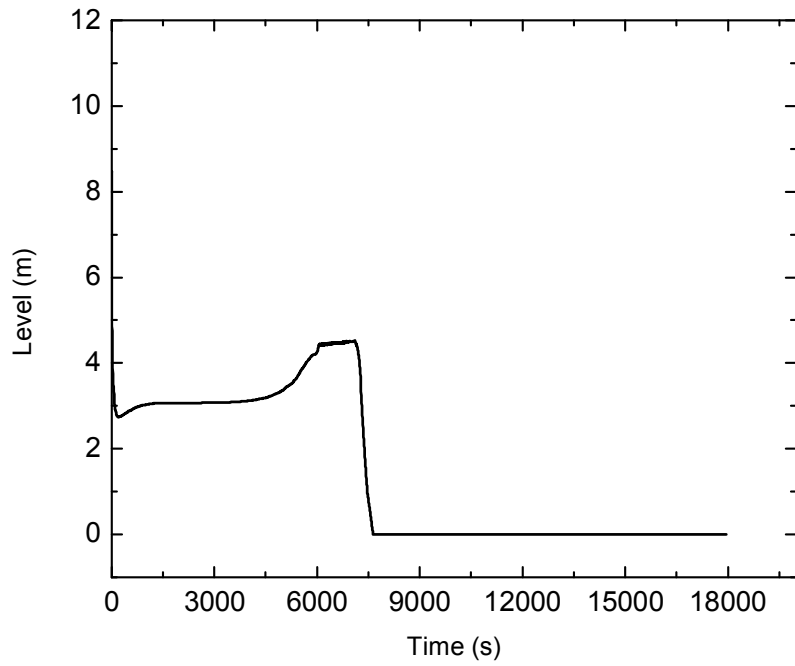


FIG. 3.83. Pressurizer water level.

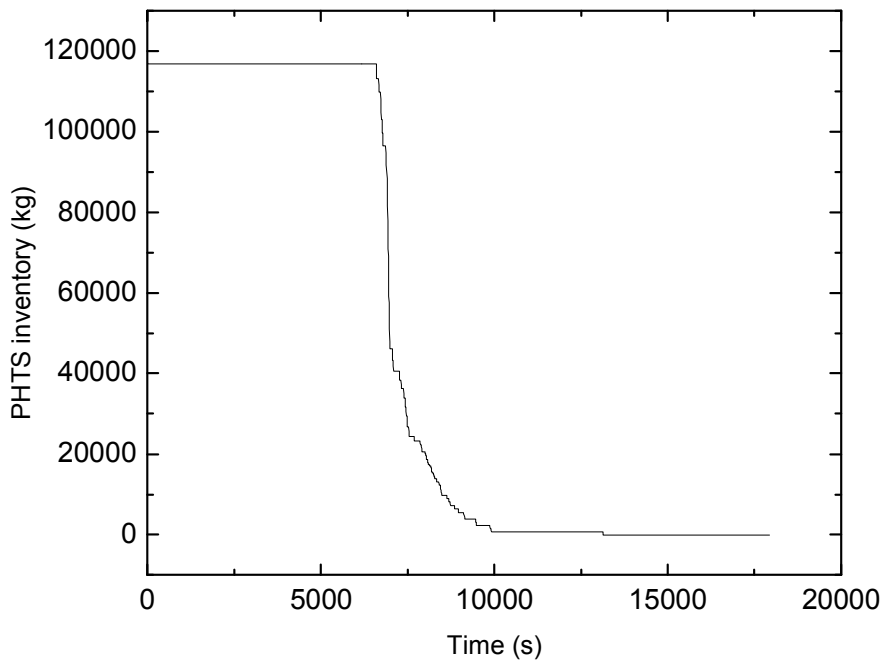


FIG. 3.84. PHTS inventory.

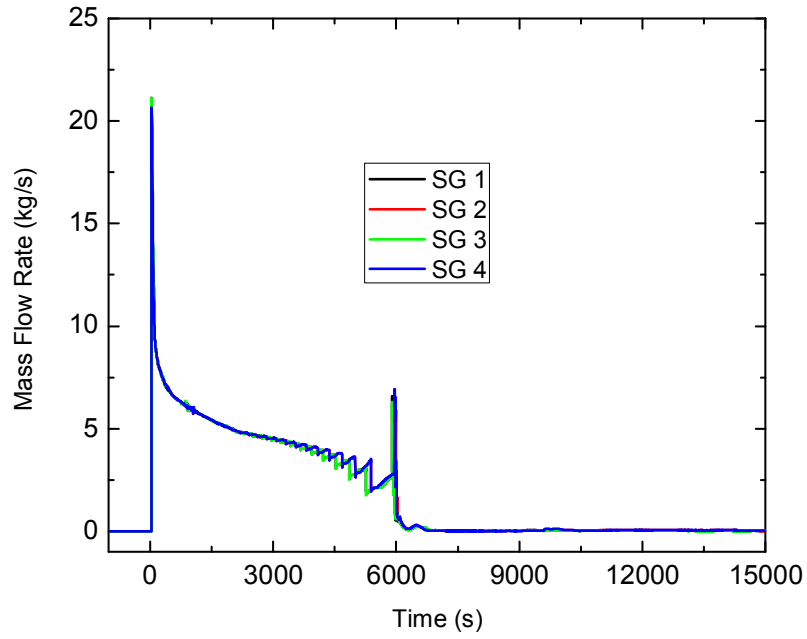


FIG. 3.85. SG relief valve (MSSV) mass flow rates.

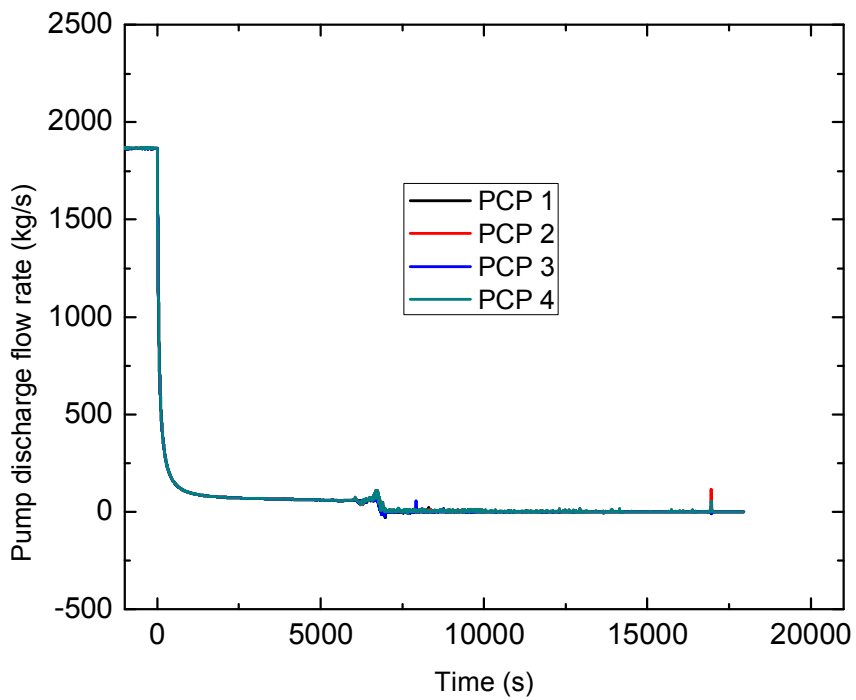


FIG. 3.86. PHT pump discharge mass flow rates.

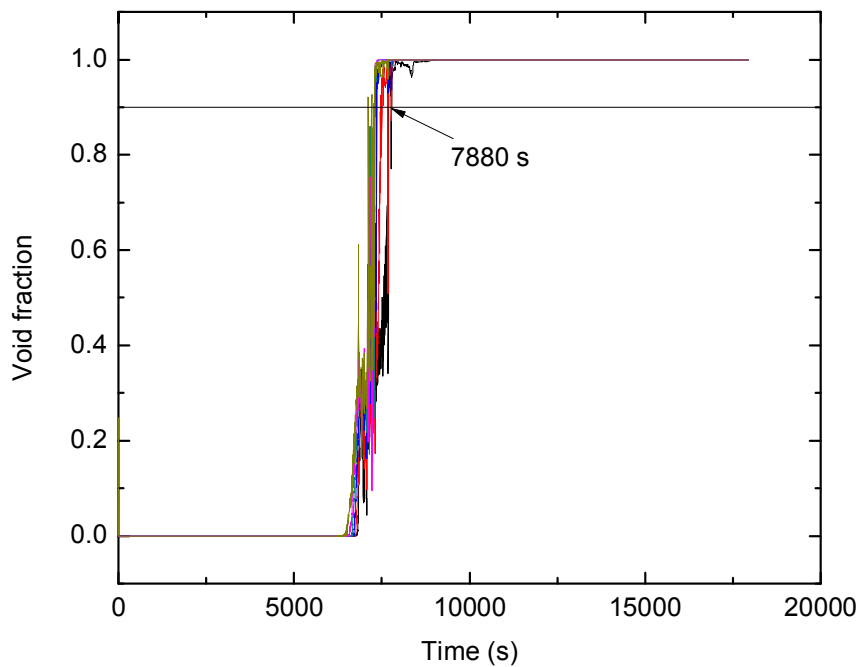


FIG. 3.87. Channel void fractions.

The corresponding temperatures of Fuel, clad, PT and CT are shown in Figures 3-88 to 3-92 for channels 1-5 (Fig. 3-70). Since the channels are completely voided and there is no flow, the clad surface temperature is found to start rising after 6,000 s. After around 7,500 s, the clad temperature starts rising significantly in the hottest channel (Channel 3, Fig. 3-90) whereas, for low power channels, it starts rising after 10,000 s. At around 10,000 s, the temperature of PT rise to about 900°K for channel 3. At such a high temperature, Zircaloy behaves as a superplastic material as shown in Figure 3-93. Due to this condition [16], PT-CT balloons at such high pressure and temperature and touches the CT.

However, for low power channels the contact occurs at nearly 11,000 s. Subsequent to contact, PT temperature does not rise further. At the same time, heat transfer to calandria increases as a result of PT-CT contact (Fig. 3-94). It leads to rise in pressure inside calandria (Fig. 3-95). At around 13,647 s, the calandria rupture disc bursts. It leads to flashing of liquid inside calandria causing the calandria level dropping to about 6 m (Fig. 3-96). As a result, the top two channels (1 & 2) become uncovered. This leads to increase in CT temperature of channel 1 and 2 (Figs 3-88 and 3-89) whereas channel 3-5 remain submerged and their CT temperature is lower. When CT average temperature reaches 1,400°K, channel disassembly takes place at 17,000 s for channel 1 and at 17,040 s for channel 2. Whereas the other channels (3-5) are still submerged. Due to disassembly of uncovered channels, the primary pressure reduces to atmospheric pressure (Fig. 3-79) at around 17,200 s.

During this time, the calandria boiloff takes place and the level continuously decreases. At approximately 17,691 s the level falls to 5 m which corresponds to uncovering of 7 rows. After 7 rows are exposed, the core is considered to be collapsed at around 17,691 s. The total steam discharged to containment which includes release from LRV and calandria rupture disc is shown in Figure 3-97 and corresponding variation in the containment pressure variation is shown in Figure 3-98.

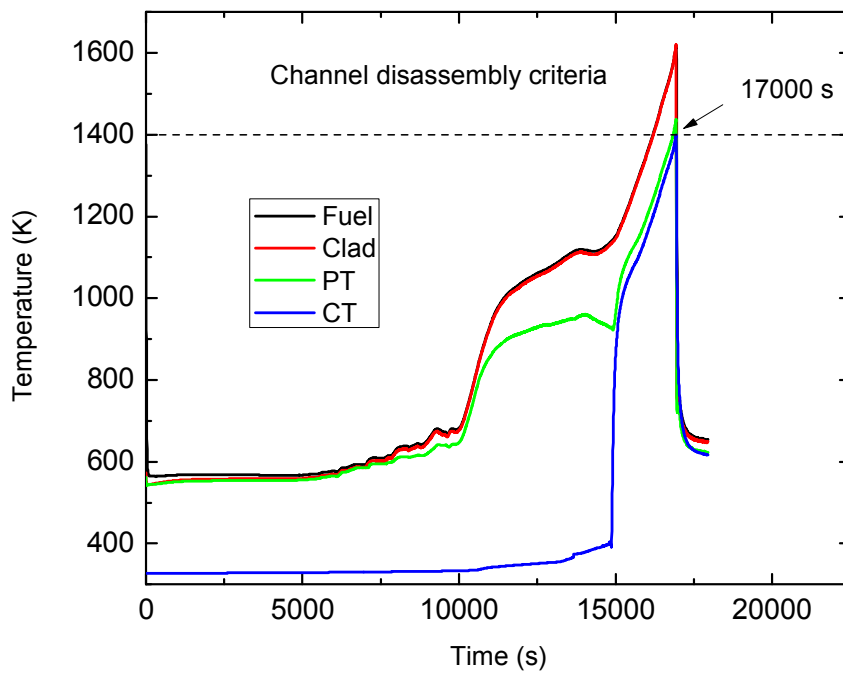


FIG. 3.88. Channel 1 temperatures.

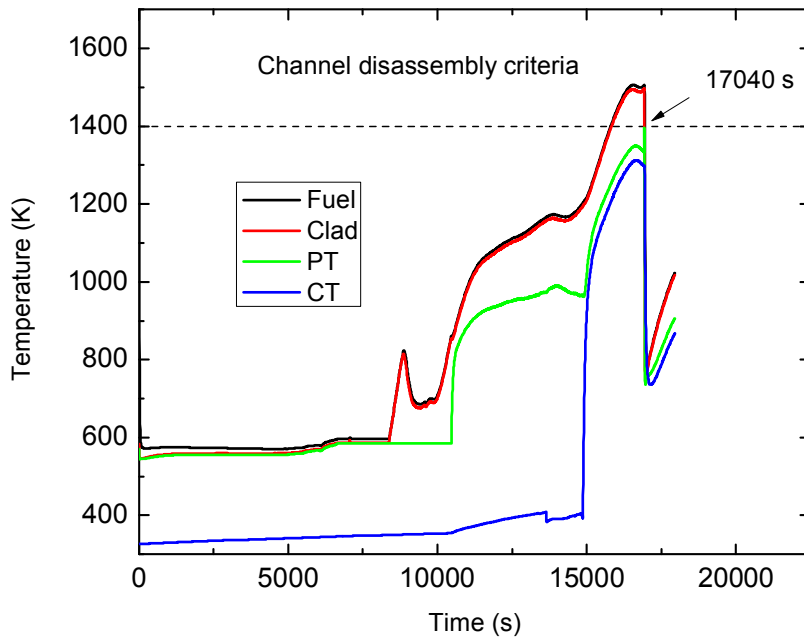


FIG. 3.89. Channel 2 temperatures.

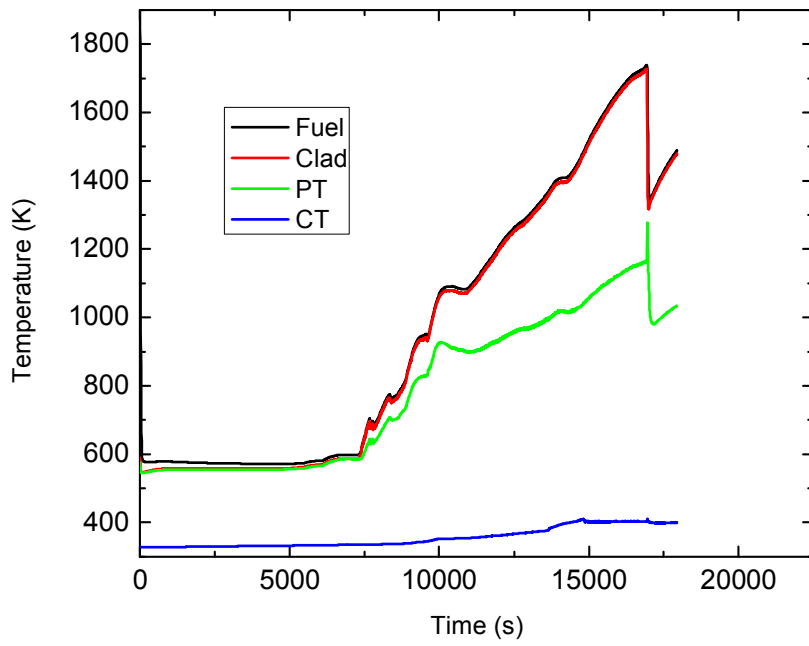


FIG. 3.90. Channel 3 temperatures.

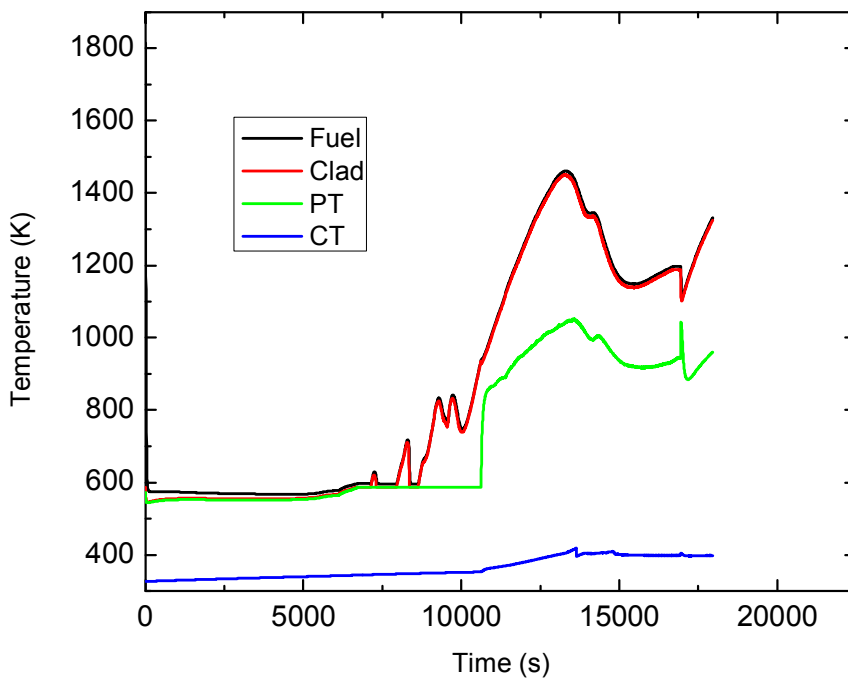


FIG. 3.91. Channel 4 temperatures.

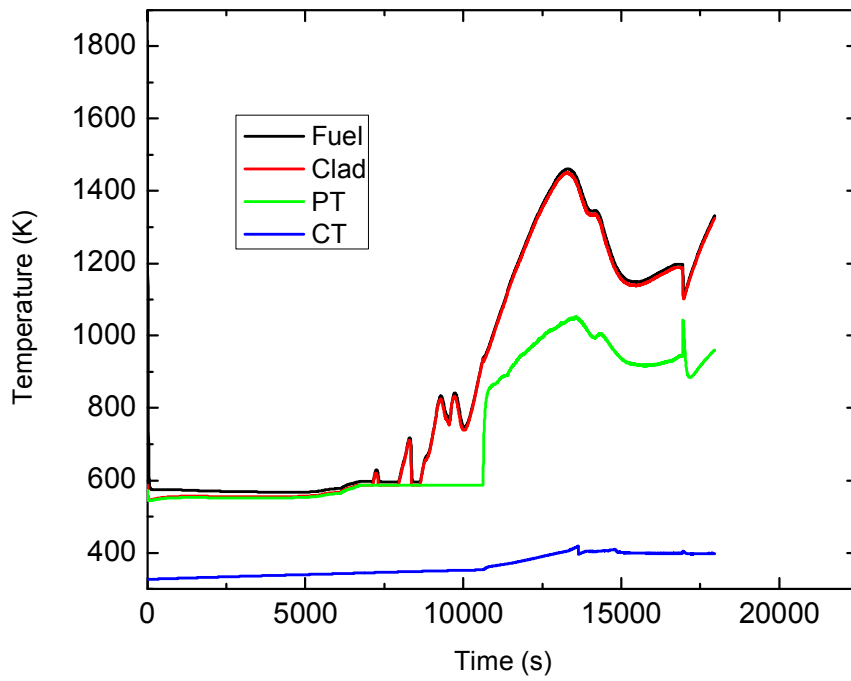


FIG. 3.92. Channel 5 temperatures.

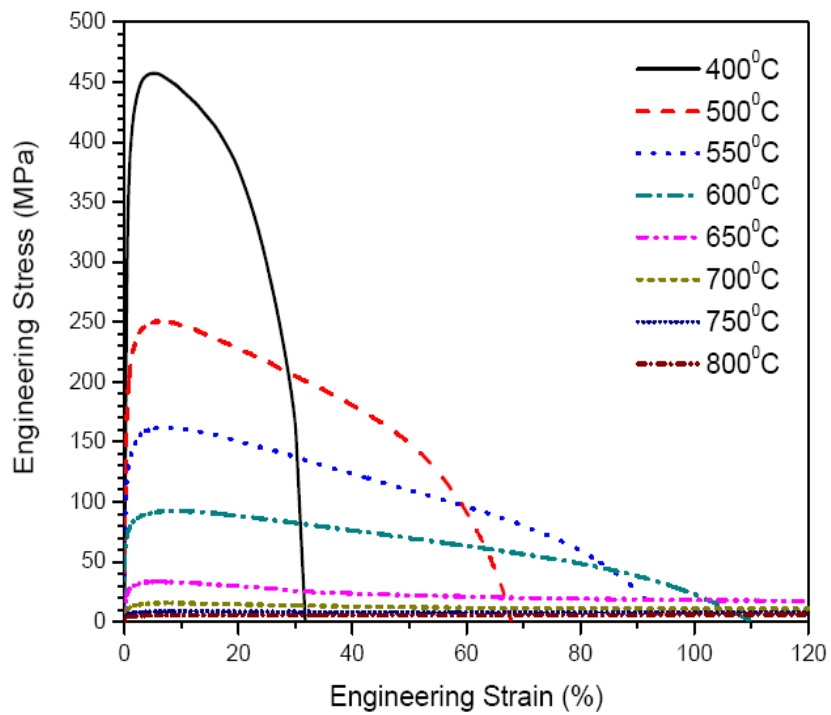


FIG. 3.93. Stress – strain relationship of Zircaloy at high temperature.

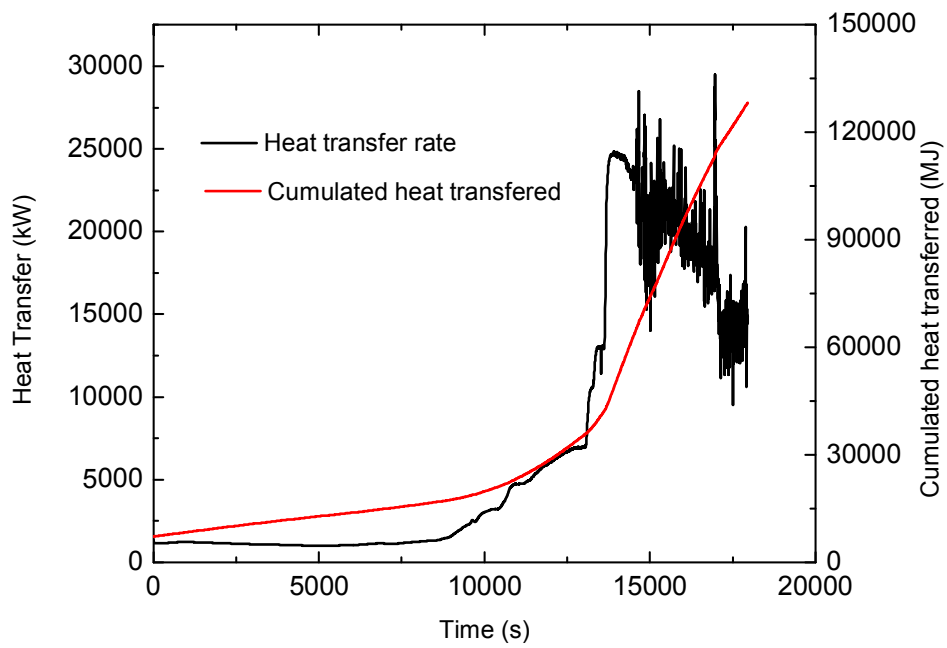


FIG. 3.94. Heat transfer to moderator.

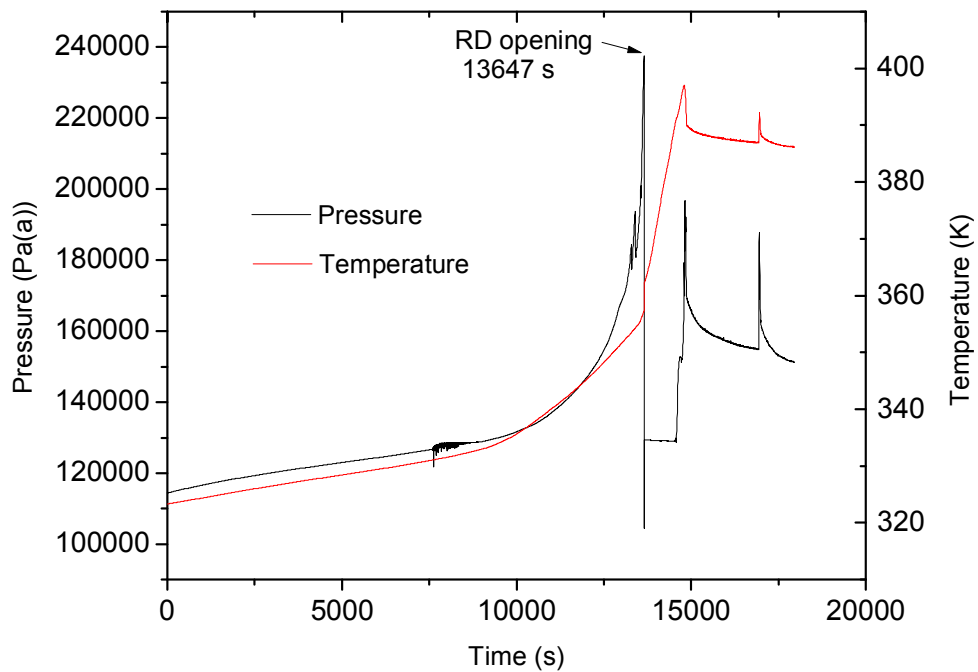


FIG. 3.95. Moderator pressure and temperature inside Calandria.

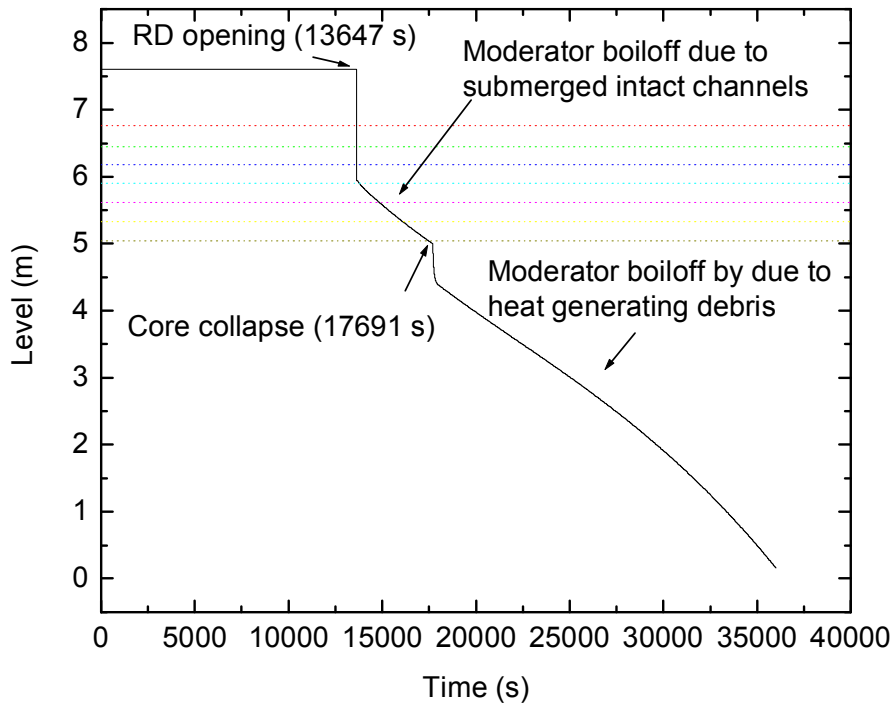


FIG. 3.96. Calandria water level.

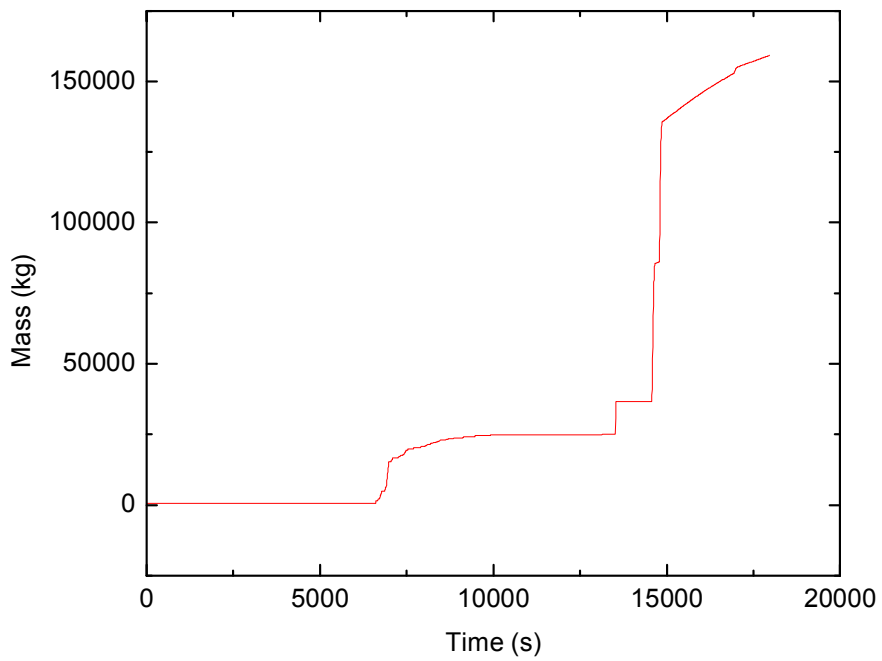


FIG. 3.97. Total steam discharge to containment.

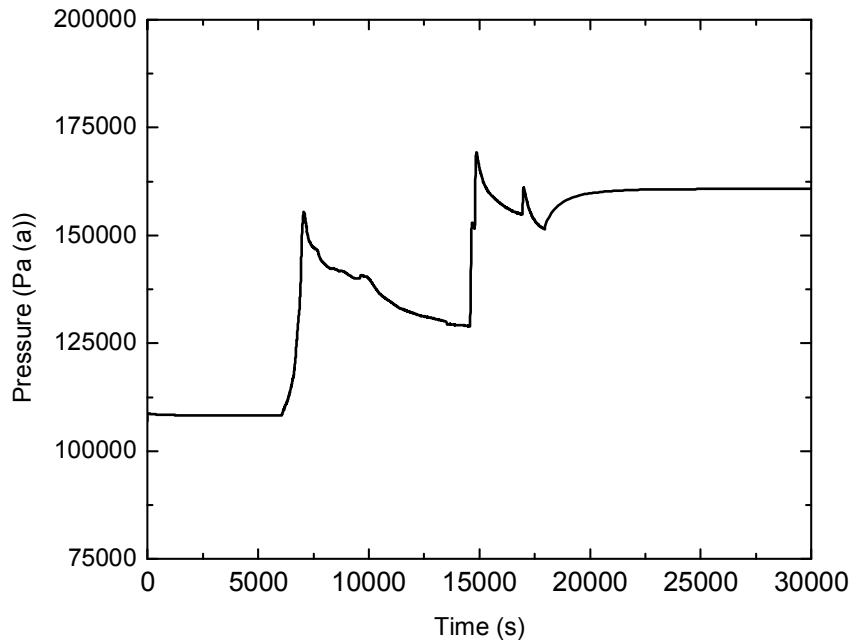


FIG. 3.98. Containment pressure.

### 3.2.3.3. Phase 3 of accident progression

After the core collapse, the uncovered hot channels as well as submerged channels fall into the calandria forming a debris bed. The debris so formed continuously gets cooled by boil-off of moderator. Figure 3-99 shows the temperatures in various regions of debris. The top region includes the low power uncovered channels (channel 1 and 2 in Fig. 3-71). The middle region corresponds to high power channels (channel 3 in Fig. 3-71) and the bottom region consists of the low power submerged channels (channel 4 and 5 in Fig.3-71).

After boil-off of the moderator at around 36,000 s (Fig. 3-96), the temperature of the debris continuously increases (Fig. 3-100). The heat transfer from debris to calandria wall is considered by combination of conduction and radiation from calandria wall to vault water by nucleate boiling. The debris at the central region is found to be at very high temperature as compared to bottom and top. This is due to poor thermal conductivity of debris bed. At the bottom part, due to large heat sink, the temperatures are near saturation temperature of water. The vault water continuously gets heated and evaporated. The temperature and inventory of the vault water is shown in Figure 3-101. It can be seen that, it takes up to 200,000 s from start of SBO to evaporate the vault water. The total heat transferred to calandria vault water is given in Figure 3-102.

After the water from vault boils off, the calandria wall temperature starts rising (after 200,000 s in Fig. 3-100). The corresponding debris temperature also rises. The temperature distribution inside calandria vessel as predicted by ANSWER is given in Figure 3-103. It can be seen that most of the debris in the central region is in molten state.

With the boundary conditions obtained from this, analysis of stresses in the calandria vessel walls have been carried out using the code CAST3M. The elasto-viscoplastic Chaboche [17] material model was used for analysis. Plastic strain accumulation in calandria under thermal and structural loading was calculated. Figure 3-104 shows maximum plastic strain

accumulation in calandria wall and Figure 3-105 shows the deformed geometry of the calandria vessel. It can be seen that, as temperature difference across the vessel is less due to small thickness, high thermal conductivity and also the internal pressure being low, the plastic strain accumulation is insufficient to cause failure ( $\sim 9.5\%$ ). Hence, it can be said that, calandria does not undergo creep failure because of temperature and structural loading. Hence, it is considered to be failed due to melting only.

The total hydrogen generated at the end of phase 3 is given in Figure 3-106. At the start of Phase 3, because of core collapse, there is lot of hydrogen generation as hot debris falls into the moderator. At the end of phase 3, around 478 kg of hydrogen is generated. The variation of containment pressure during the phase 3 is given in Figure 3-107. It can be seen that, initially, the vault water evaporation causes containment pressurization from around 225 kPa to 325 kPa. At 113,950 s, containment RD opens as the differential pressure between atmosphere and containment exceeds 224 kPa which causes the containment depressurization which indicates containment failure at this time. Containment wall heat load and internal energy change in containment is given in Figure 3-108.

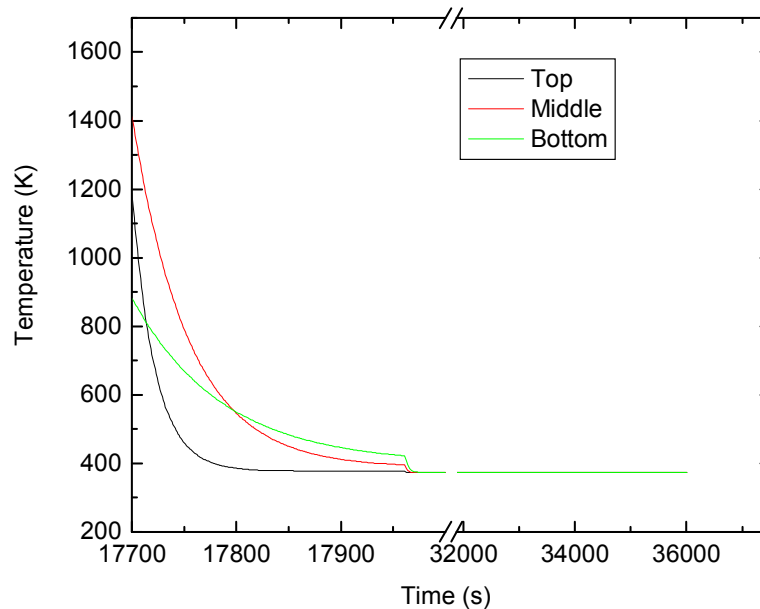


FIG. 3.99. Temperature of fallen debris channels in calandria.

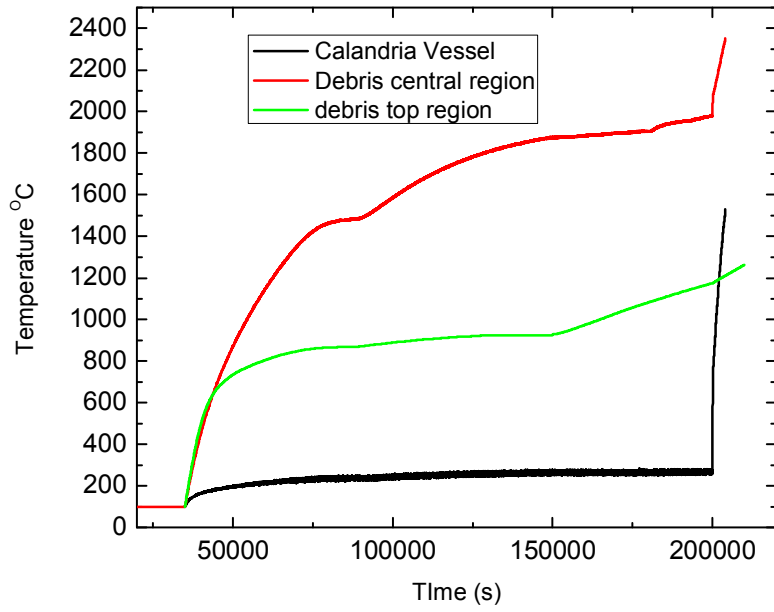


FIG. 3.100. Temperature history in debris.

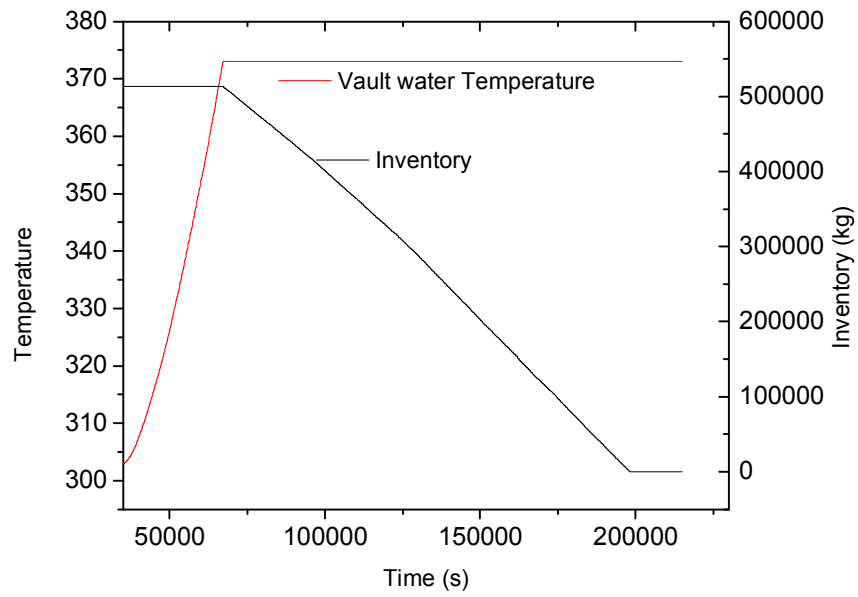


FIG. 3.101. Temperature and mass of calandria vault water.

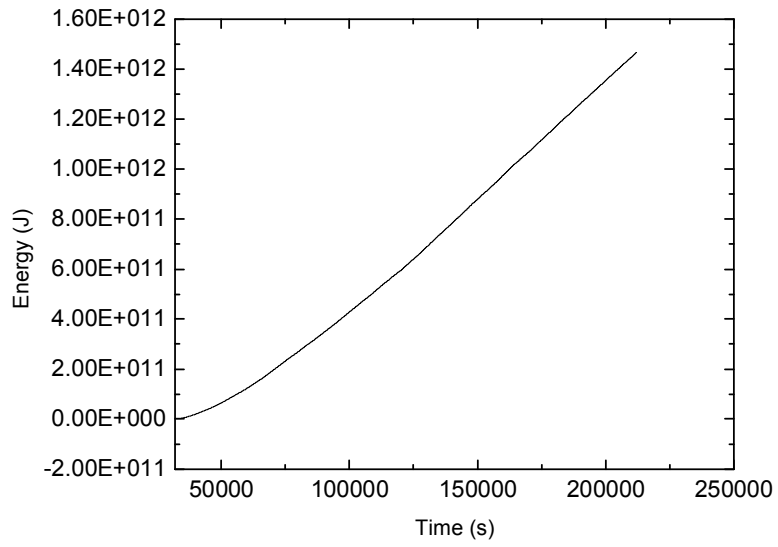


FIG. 3.102. Total heat transferred to reactor vault.

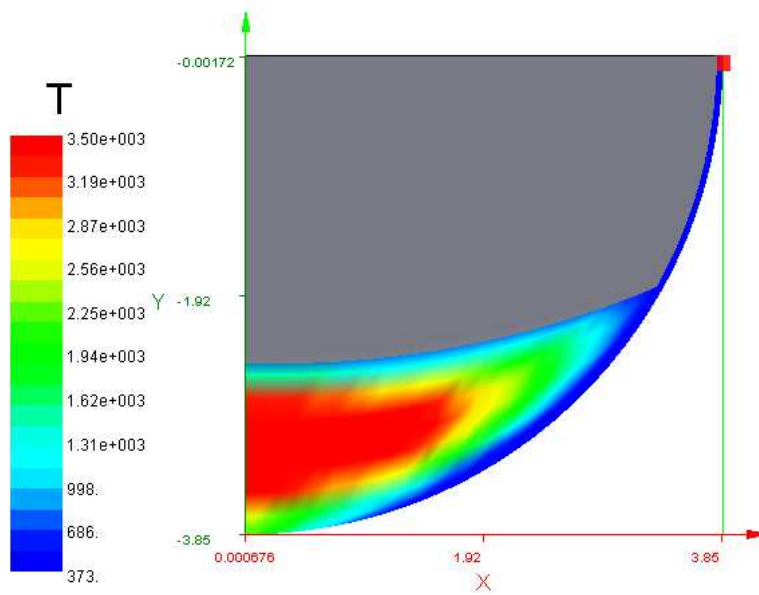


FIG. 3.103. Debris temperatures in calandria just after vault water exhausts (200,000 s).

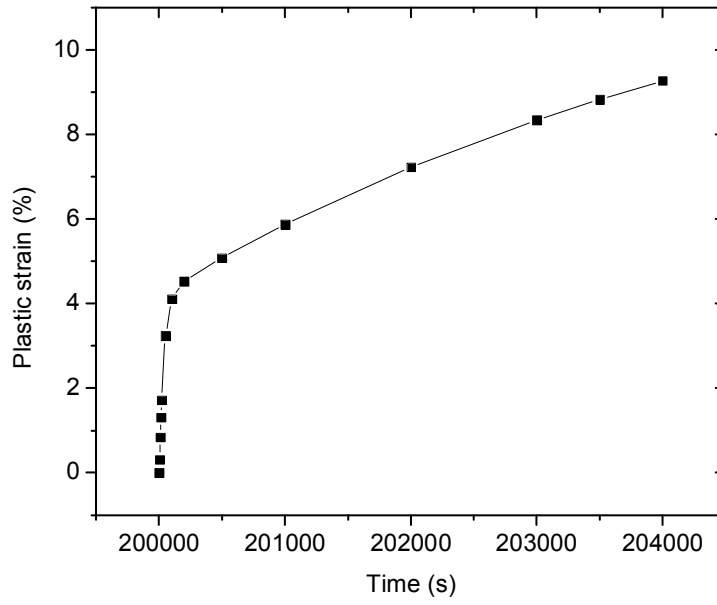


FIG. 3.104. Plastic strain accumulation with time.

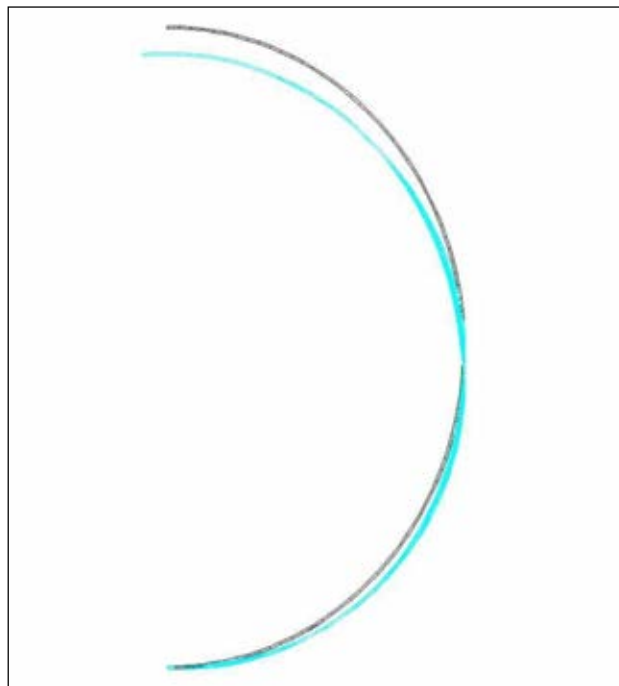


FIG. 3.105. Deformation of calandria vessel.

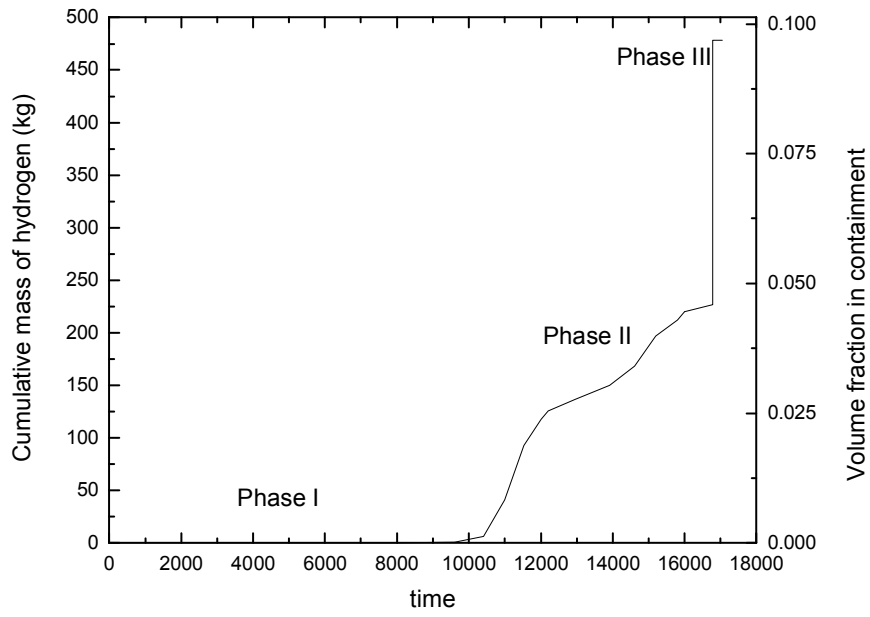


FIG. 3.106. Hydrogen generation

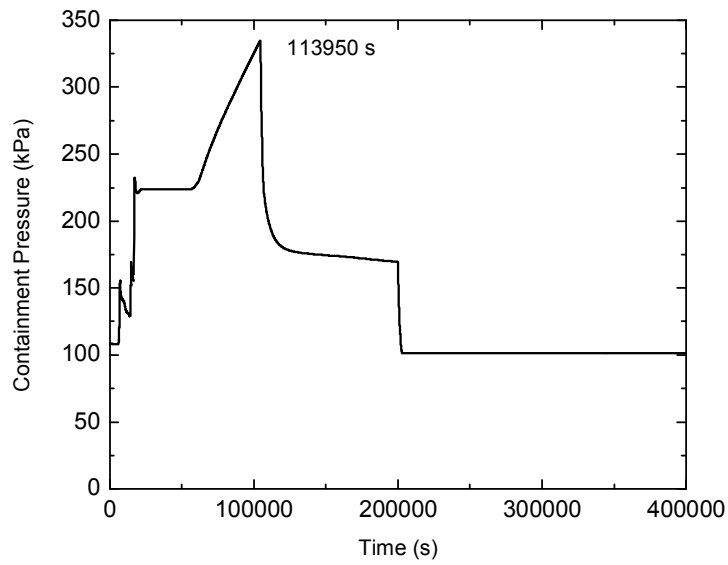


FIG. 3.107. Containment pressure transient

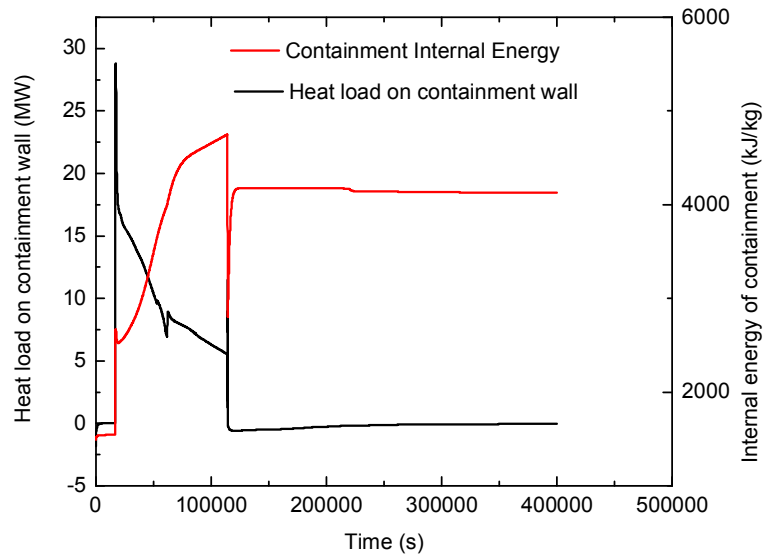


FIG. 3.108. Heat transfer inside containment.

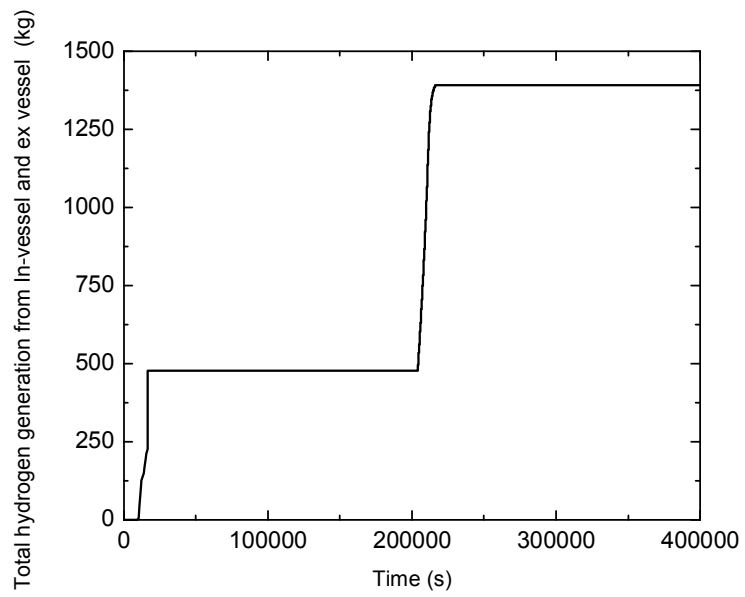
#### 3.2.3.4. Phase 4 of accident

After the calandria failure at 204,000 s, it is assumed that, all the molten corium is relocated onto the reactor vault basement. The basemat still contains large amount of water below the calandria level. The molten mass falls in the water and quickly vaporizes it. During this time, the molten mass reacts with water and causes lot of hydrogen is generated as shown in Figure 3-109. A total of 1,340 kg of hydrogen is generated.

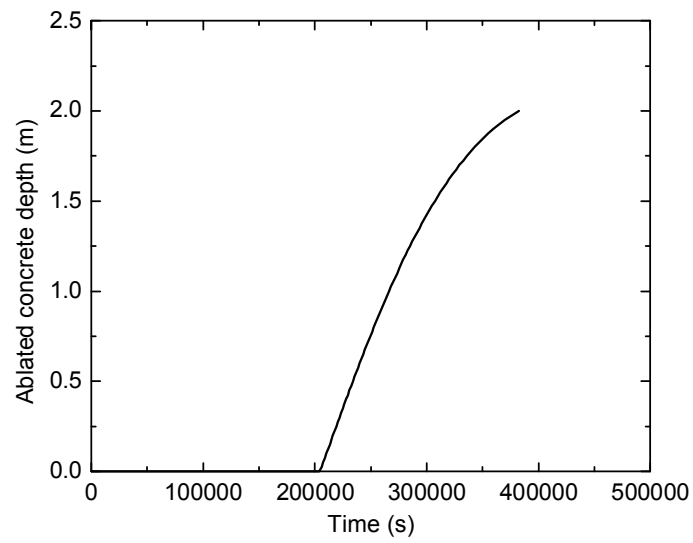
After all the water is evaporated, the molten core- concrete interaction starts. Considering the vault floor area, the molten mass will form a height of 0.3 m on the vault floor. The Molten core – concrete interaction has been modelled using the code MELCOOL-CCI.

Figure 3-110 shows the ablation of the concrete floor of reactor vault. Initially, the rate of ablation is higher but later on it decreases. It was observed that, up to 40,000 s, the complete concrete ablation observed. When the melt falls on the concrete, the bottom part of the corium cools initially, but later on, due to heat generation, its temperature rises again. The corium loses heat from top surface due to radiation; hence the top surface gets cooled faster.

Figure 3-111 shows the temperature history in MCCI region. It can be seen that, the concrete temperatures start rising after the melt falls on the concrete. As more and more concrete gets mixed with corium, its solidus temperature starts decreasing and melting occurs at lower temperature. During the MCCI, the amount of CO<sub>2</sub> released is shown in Figure 3-112. Total of 20,000 kg of CO<sub>2</sub> is released during the interaction.



*FIG. 3.109. Hydrogen generation in phase 4.*



*FIG. 3.110. Ablation of the vault basemat.*

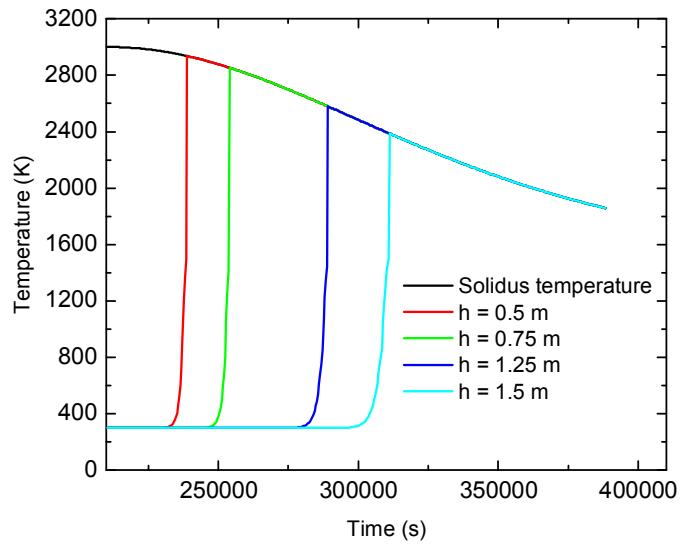


FIG. 3.111. Temperature history in corium- concrete mixture.

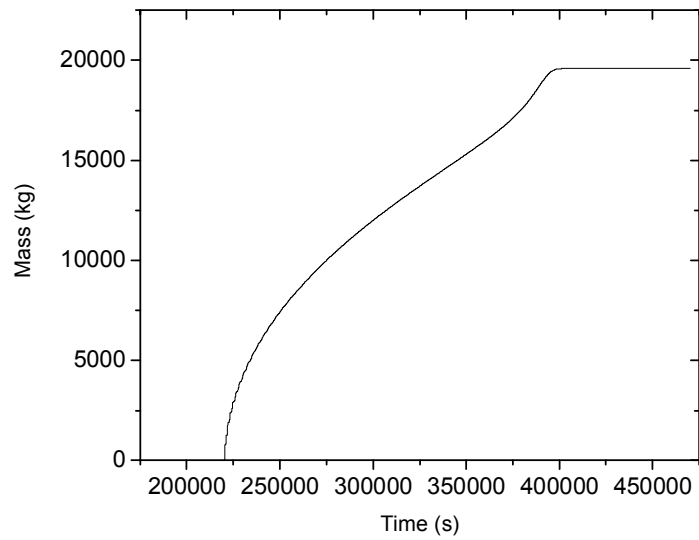


FIG. 3.112. Cumulative amount of carbon dioxide generated during the MCCI.

### 3.3. BARC-RSD

#### 3.3.1. Required systems models and software used

The CRP included analysis of progression of severe accident with Station Black out as the initiating event. Since different types of thermal hydraulic and heat transfer mechanisms dominate at different stages of the accidents, various computer codes, modules and combinations were used to analyse accident evolution through different phases. The categorization of the codes/modules used for each phase along with the components and phenomena modelled using the specific code is tabulated in Table 3-5.

The evolution of each stage of the accident depends to a large extent on the initial condition for that stage of the accident as well as on the evolution of previous stage of accident. Keeping in mind the relative importance of the mechanisms in consecutive stages of the accident, a particular sequence of calculations was adopted. Figure 3-113 shows the schematic of the sequence of codes used and the parameters obtained during each stage of evaluation. The above mentioned methodology to estimate source term has been established and applied to estimate the source term for LOCA with Loss of ECCS event for 220 MWe PHWR [18].

TABLE 3.5. COMPONENTS AND PHENOMENA MODELED AND CODES/MODULES USED

Phase	Components & phenomena modelled	Codes Used
Phase 1: From SBO Initiation to First Channel Uncovery	Plant thermal hydraulic systems	RELAP5/SCDAP
	Fuel, pressure tube and calandria tubes heat up	
	Pressure tube deformation (sagging and ballooning)	PTCREEP
Phase 2: First Channel Uncovery to Core Disassembly	Plant thermal hydraulic systems and heat structures	RELAP5/SCDAP
	Fuel, pressure tube and calandria tubes heat up	
	Fission product release from fuel	PHTACT
	Fission product transport in PHT system	ASTEC
Phase 3 : Core Disassembly to Calandria Vessel Failure	Relevant thermal hydraulic systems	RELAP5/SCDAP
	Debris bed heat up	
	Fission product release from fuel	PHTACT
	Fission product transport in PHT and calandria vessel	ASTEC
Phase 4 : Calandria Vessel Failure to Calandria Vault Failure	Relevant thermal hydraulic systems and fission product dispersion in containment	ASTEC
	Molten core concrete interaction	
	Containment iodine chemistry	
	Fission products release from corium	PHTACT

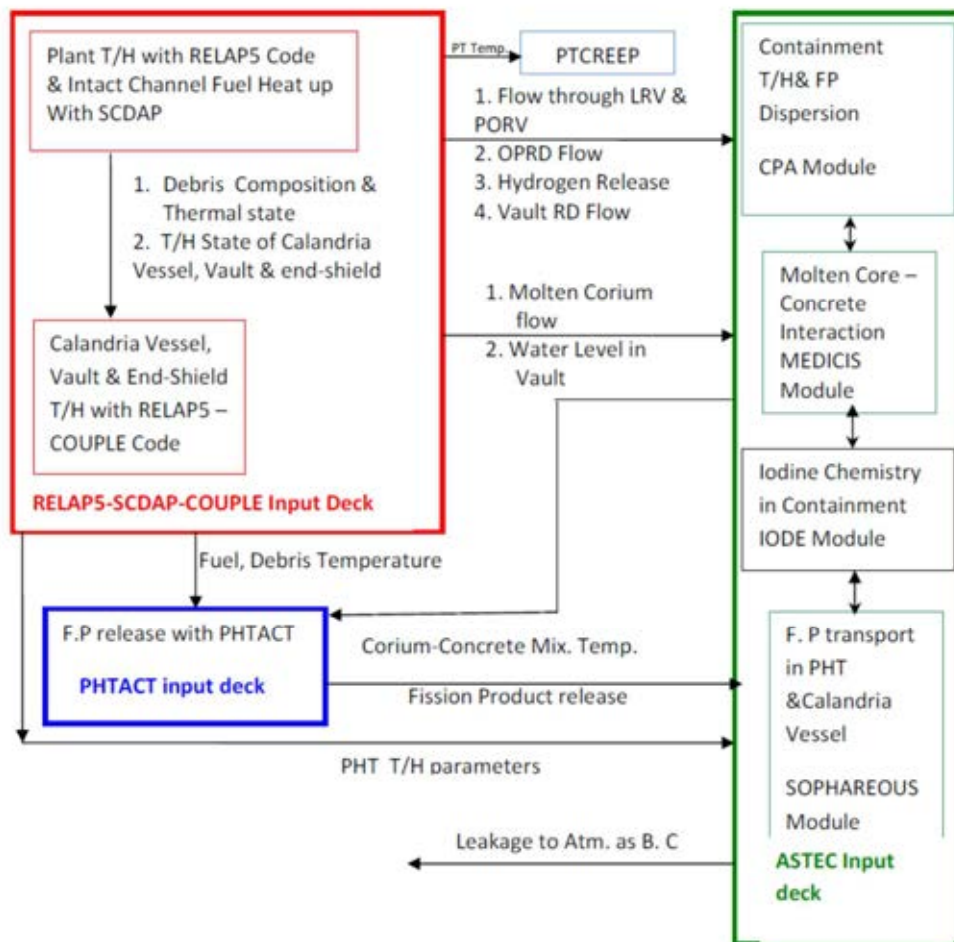


FIG. 3.113. Multiple physics multi step calculation methodology.

### 3.3.1.1. RELAP5/SCDAP code

Thermal Hydraulic models of RELAP5/SCDAP code [14, 19] is being used for simulation of PHT and steam generator, moderator simulation etc. The RELAP5/SCDAP code has been developed for best-estimate transient simulation of light water reactor coolant systems during an accident. The code is based on a non-homogeneous and non-equilibrium model for the two-phase system that is solved by a partially implicit numerical scheme for economical calculation of system transients. Light water and heavy water properties are available in this code. The code includes many generic component models from which general systems can be simulated. The SCDAP Module solves integral form of the heat conduction equation for an isotropic solid continuum in a two dimensional cylindrical coordinate system. Radiation heat exchange between various solid, liquid and gases as participating media are also considered. RELAP5/SCDAP models have been validated through the Independent Code Assessment and Code Assessment and Maintenance Programs. These programs were organized by the US NRC and have involved between 20-30 organizations around the world over period spanning more than 2 decades. This code has been used in international standard problem exercises conducted by the Organization for Economic Cooperation and Development. Applicability of RELAP5 thermal hydraulic models and the core degradation models present in SCDAP have been compared with various experiments related to LWRs such as FLCHT-5, PBF SFD 1-1, PBF SFD 1-4, PBF SFD ST, KFK CORA-13, PHEBUS etc. The code has been used extensively for HWR and validated against experimental data from RD-14M test facility for

scenarios like large and small break LOCA as well as natural circulation under depleted inventory conditions [20].

The thermal hydraulic behaviour of systems post core collapse has been modelled using COUPLE Module of code RELAP5/SCDAP. This module uses a 2-dimensional heat conduction model for calculating temperature distribution in the debris. Effect of radiation heat transfer at high void fraction ( $>0.8$ ) is incorporated into the conductivity of the material calculated as effective conductivity. This model is developed for PWR debris configuration in lower plenum which is having a porosity of around 0.5 and particle diameter as 10 mm. Special heat transfer and the pressure drop models are developed and validated for this configuration for void fraction over 80%. Below 80% of void fraction the heat transfer and pressure drop model are similar to the pipe flow system. The model is adopted for HWR debris heat up calculation. Considering a unit cell with four slumped reactor channels with fuel bundle, PT and CT, the porosity is calculated to be 0.6. It is assumed that the pressure drop and heat transfer characteristics are similar over 80% of void fraction and applicable to HWR debris configuration. However, experimental program to study HWR debris bed is in progress to find the applicability of heat transfer and pressure drop models developed for PWR debris bed.

### 3.3.1.2. *ASTEC Code*

The code ASTEC [21] is capable to simulate core degradation, fission product release and transportation, and containment behaviour under severe accident conditions of PWRs. Different modules of this code are being used to simulate some of the phenomena for HWR severe accident. Different modules like CPA, SOPHAREOS, and MEDICIS are being used.

The CPA module of the code is used for containment thermal hydraulics and fission product dispersion and is composed of two main sub-modules, respectively in-charge of the computation of thermal-hydraulics and aerosol behaviour in the reactor containment. The containment discretization uses a lumped-parameter approach in which volumes represented by nodes connected by junctions simulate simple or multi-compartment containments such as tunnels, pits, dome etc., with possible leakage to the environment or to other buildings. For a realistic description of nuclear power plant accidents, a number of specific models representing the main phenomena involved in engineered safety systems (e.g., the Containment Spray System, hydrogen re-combiners, pressure suppression systems) are models in the CPA module. The module is well validated against series of experiment like BNWL, DEMONA, PHEBUS-FPD, PANDA etc.

The SOPHAEROS module of code ASTEC has been used to assess and analyse the transport of fission products in the PHT system of HWRs in the event of a postulated accident scenario. The module considers 60 elements (oxygen, hydrogen, caesium etc.) and 150 compounds ( $O_2$ , CsI, and  $I_2$  etc.) in gaseous phase which includes volatile elements and compounds. In the condensed phase (aerosols or condensates), volatile and non-volatile species can be found. The number of non-volatile groups is limited to 20. The module is validated against PHEBUS-SFD experiments.

The MEDICIS module of code is used for Molten Core Concrete Interaction (MCCI). It simulates MCCI using a lumped parameter approach with averaged melt/crust layers. Corium remaining in the cavity interacts with concrete walls. This module assumes either a well-mixed oxide/metal pool configuration or pool stratification into separate oxide and metal layers. It describes concrete ablation, corium oxidation and release of non-condensable gases ( $H_2$ , CO,  $CO_2$ ) into the containment. Most convective heat transfer correlations from the literature are implemented in the MEDICIS module. MEDICIS consist of models of corium coolability in case of water injection upon the corium pool surface, including water ingress

through the upper crust and corium eruption through the upper crust towards the overlying water pool. Different models of evolution of corium pool configurations with homogeneous and stratified pools are available. Shapiro diagrams are used to indicate the hydrogen and CO concentrations in various compartments of the containment and the possibility of hydrogen or CO burning and hydrogen detonation.

#### 3.3.1.3. *PTCREEP code*

In HWRs LOCA or SBO can lead to significant temperature rise in the Pressure Tube (PT). This high temperature can cause metallurgical and geometrical changes in the PT. PT would deform plastically due to internal pressure and fuel weight and eventually burst. An indigenous code PTCREEP [22] was developed to model the pressure tube ballooning and burst. Ballooning creep model in 'PTCREEP' is based on the transverse strain rate equations developed by Shewfelt et al. These correlations were developed based on uni-axial creep tests on Zr-2.5 wt% Nb test specimen. Creep tests under biaxial stress condition indicated that the axial stress had little effect on the transverse creep rate. PTCREEP does not simulate the heat transfer process and hence the PT temperature is needed to be imposed as boundary condition. The code is validated against BARC experiments [23].

#### 3.3.1.4. *PHTACT code*

PHTACT Code [24] is used to calculate the release rate for each species at each node in the different channel. Following two methods of computing the release is given in the code.

##### (a) Method 1

The following temperature dependent relation as below gives fractional release coefficient in this method:

$$FRC = A(I,J)*EXP(B(I,J)*T)$$

Where T is temperature in °C, A and B are constants dependent upon I<sup>th</sup> species and J<sup>th</sup> temperature range. The three temperature ranges for which constant is defined are 900 – 1,400°C, 1,400 – 2,200°C, and 2,200 – 2,760°C. Maximum temperature for any node is 2,760 °C. The values of these constants are taken from NUREG-0772 (U.S. Nuclear, 1981), in which attempt is made to reduce experimental data into single usable data set through consideration of experimental condition and informed engineering judgment of data points available. For the case of Te, the value of FRC calculated using A and B value in the temperature range of interest is reduced by a factor of 40 if nodal extent of Zr oxidation is less than 70%. This method of calculation is recognized as being non mechanistic and no attempt is made to account for any scaling effects to which release coefficient may be subject in transition from the experiment to accident situation.

##### (b) Method 2

This method makes use of a more physical description of release process. In this method release rate coefficients are given by Arrhenius type equation of the form:

$$FRC = KO(I)*EXP(-Q(I)/(1.987E-3*T))$$

Where T is the nodal temperature in Kelvin, KO and Q are species dependent constants.

### 3.3.2. **Modelling details**

The plant specific model is based on the CANDU6 Plant data provided by IAEA [25]. The CANDU 6 plant model for severe accident has been built with RELAP5/SCDAP code

coupled with several other codes namely ASTEC, PTCREEP, and PHTACT to address different stages of accident progression. The model simulates the following systems:

- Primary Heat Transport system: Two loops including Fuel Channels, Inlet & Outlet Headers, inlet and outlet feeders, Primary Circulation Pumps (PCP), Steam Generators, Pressurizer, Liquid Relief Valves (LRVs) etc.;
- Secondary Heat Transport System: Steam Generator Secondary side which includes Steam Separator, down comer, riser, and steam drum. Governors, Main Steam Safety Valves (MSSVs) and Atmospheric Steam Discharge Valves (ASDVs) are also modelled;
- Moderator System: Calandria Vessel with moderator and Over Pressure Rupture Disks (OPRD), the connecting relief lines and bleed valves;
- Calandria Vault and End Shield: Calandria Vault and End shield with water and structural material along with common rupture disk;
- Containment System: Containment with 12 compartments, leakage provision, and rupture disk.

Details of the different models have been given below.

### 3.3.2.1. Reactor core model

The CANDU reactor core is symmetric by geometry about vertical axis. The core was divided into 8 zones for each loops depending upon the elevation of fuel channels. Division of 8 zones for one of the loops has been shown in Figure 3-114. Number of channels is clubbed in a zone. Elevation of the clubbed channels from Calandria vessel bottom and the average power for the representative zones are given in Table 3-6.

The convective heat transfer characteristic is conserved in the clubbed channel by providing equivalent fuel pins with internal heat generation, PT and CT with their corresponding surface areas. Equivalent flow rate has been provided in the clubbed channel to conserve the energy balance and the dimensionless numbers like Nusselt number, Reynolds number. The radiative heat transfer characteristics is conserved for a single channel and applied to the entire clubbed channel. SCDAP “fuel” and “shroud” components are used for fuel elements and PT-CT elements respectively. Shield plugs at the end of each fuel channel are also modelled with “fuel” component in the SCDAP structure with zero power generation.

TABLE 3.6. CLUBBED CHANNEL DISTRIBUTION IN EACH LOOP

Zone/clubbed channel No	No. of channels clubbed	Elevation from calandria bottom(m)	Average power per channel (MW)
1	16	1.085	4.03
2	36	2.081	5.42
3	18	3.225	6.46
4	25	3.225	5.57
5	13	4.369	6.56
6	30	4.369	5.66
7	36	5.513	5.42
8	16	6.508	4.05

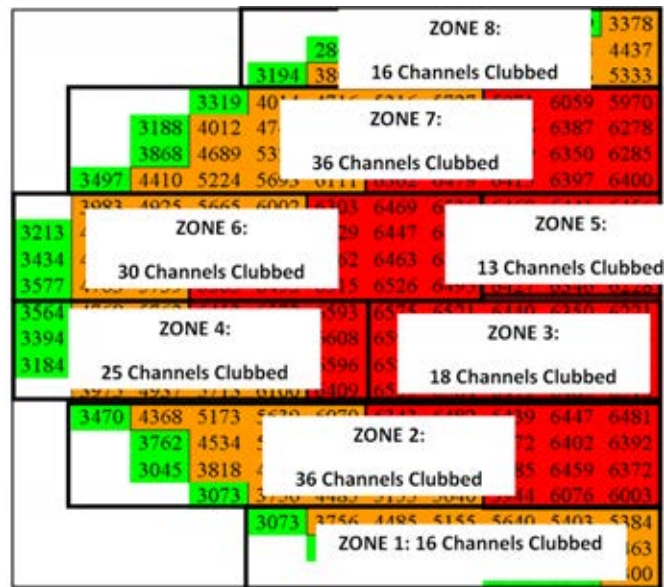


FIG. 3.114. Division of half core into eight zones

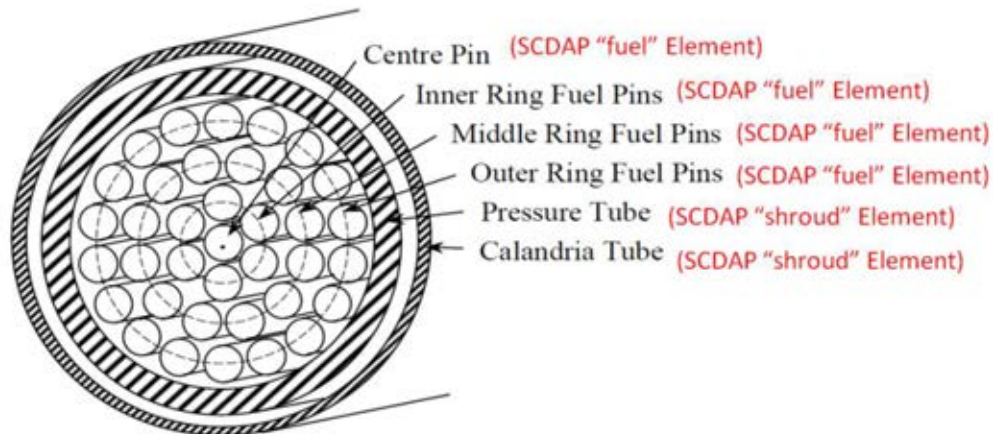


FIG. 3.115. SCDAP Specific Reactor Channel Model

### 3.3.2.2. Primary heat transport system model

RELAP5 specific CANDU 6 PHT system model has been developed based on the data provided by IAEA [13]. The PHT system consists of 2 loops, each loop contains 190 reactor channels. These channels are modelled with eight representative channels. Each channel is sub divided into 10 control volumes. The 190 inlet feeders and outlet feeders of a single loop are clubbed into eight equivalent flow paths. Individual inlet and outlet headers are modelled. The flow path between the headers and the steam generators are modelled individually as well as the steam generators. Each steam generator consists of 3530 number of tubes. All tubes are clubbed and represented by a single tube with equivalent flow area. The hydraulic diameter and heated equivalent diameter of this clubbed single tube is conserved for a proper thermal hydraulic calculation. PHT circulation pumps are modelled individually with RELAP “pump” component model. The pump coast down is modelled with coast down data as communicated by IAEA. Two pump down-stream flow paths are clubbed to represent a single flow path. Two LRVs mounted on outlet headers of both loops are modelled with “motorized valve” component. Flow areas of these valves are adjusted to get the desired flow at desired pressure. The Nodalization of one loop has been shown in Figure 3-116. The Pressurizer is modelled

with RELAP5 hydraulic and heat structure components. The stored heat of the pipe walls for all the systems are modelled with RELAP heat structures with convective heat transfer as boundary condition.

### 3.3.2.3. Secondary heat transport system model

The secondary heat transport system consists of steam generator secondary side, governor valves, main steam line stop valves and steam generator feed system. Figure 3-117 shows the Nodalization of one of the four steam generators along with the corresponding steam drum, separator, feed line etc. Heat structures have been used to model the structural part of steam generator that simulates heat transfer from the primary circuit to the secondary circuit.

The steam obtained from all the steam generators is fed to a common header and the Main Steam Safety Valves (MSSV), Atmospheric Steam Discharge Valves (ASDV), governor etc. are connected to this common header as shown in Figure 3-118.

### 3.3.2.4. Moderator calandria vault (CV) & end shield system model for phase 1-2 analysis

Moderator, calandria vault and end shield model includes hydraulic volumes for the Moderator, End Shield Water, Calandria Vault Water, Calandria OPRDs, and Calandria Vault RDs. Figure 3-119 shows the Nodalization for this system. RELAP5 heat structure component is used to simulate all the heat structures like Calandria vessel walls, Calandria Vault SS liner and concrete, Calandria tube sheet, end shield CS balls.

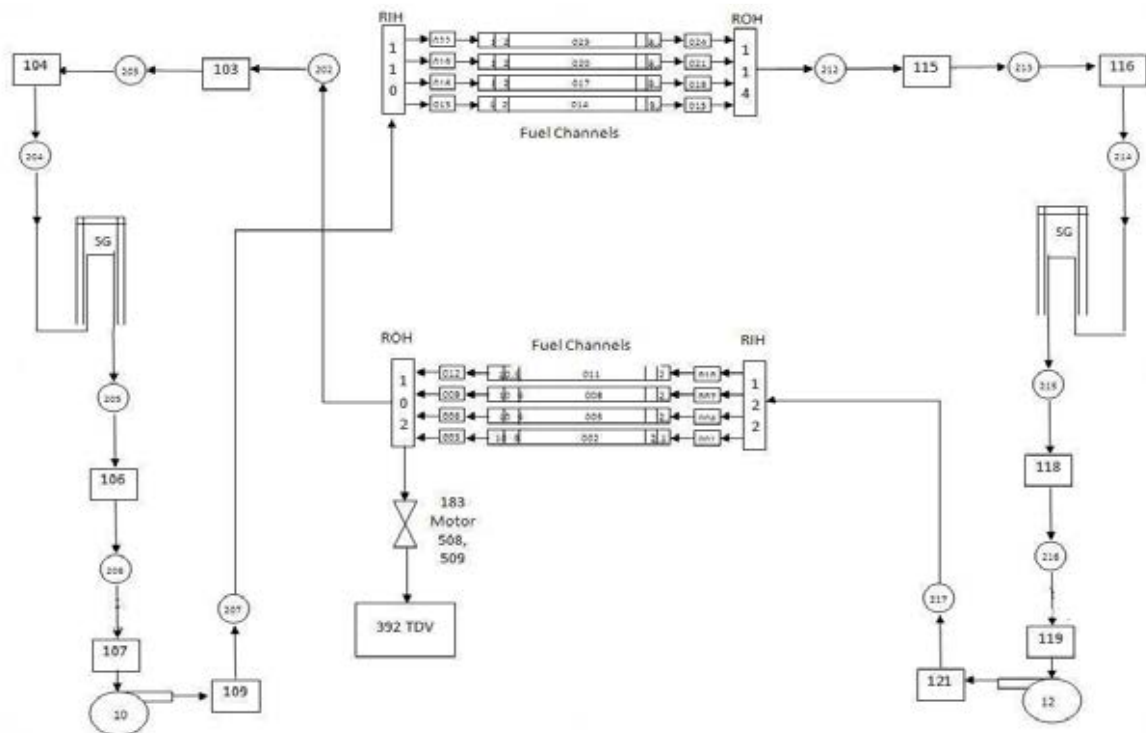


FIG. 3.116. Nodalization of One Loop of PHTSystem

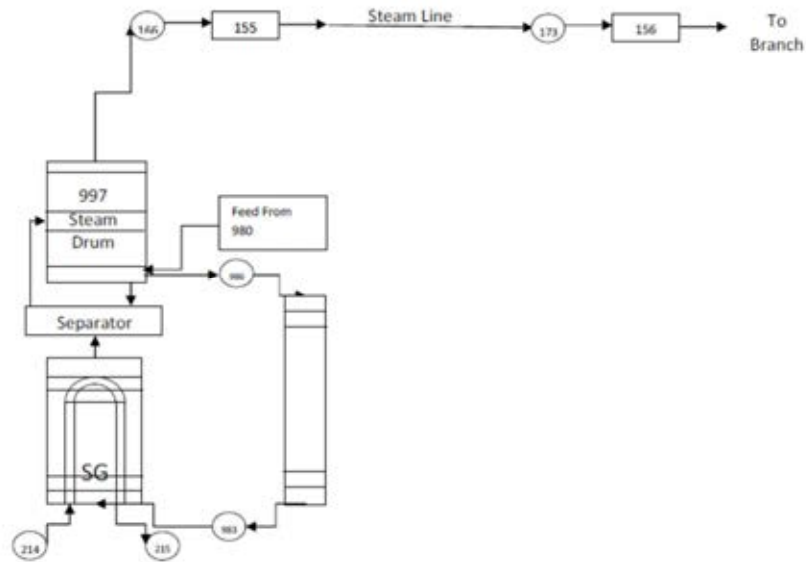


FIG. 3.117. Nodalization of Steam Generator Secondary Side

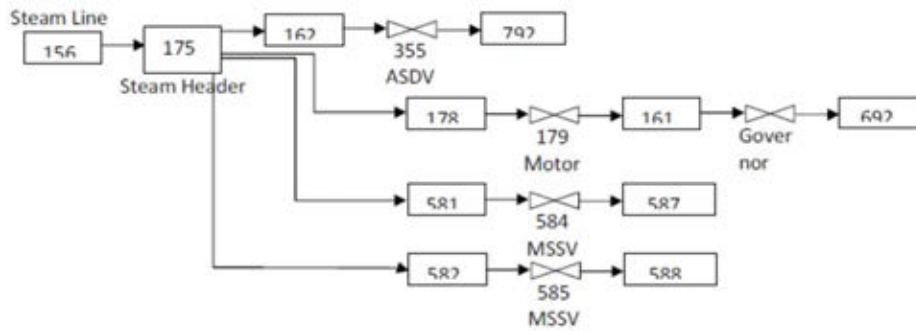


FIG. 3.118. Nodalization of ASDV, Governor, MSSV

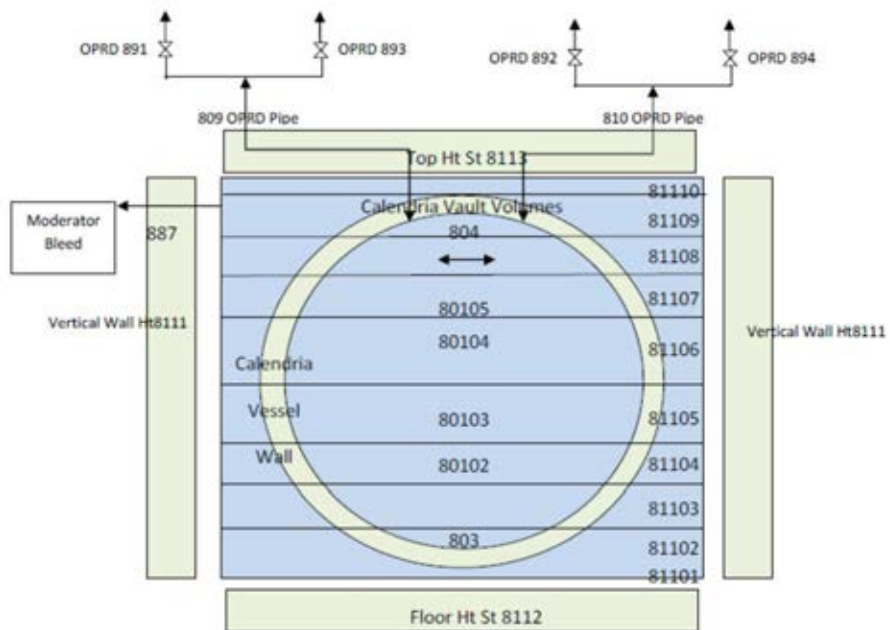


FIG. 3.119. Nodalization for moderator, CV & End shield for Phase 1-2.

### 3.3.2.5. Moderator, calandria vault (CV) & end shield system model for phase 3 analysis

During the Phase 3 of the accident, entire core is assumed to have slumped at the initial condition in the form of debris. The COUPLE mesh used for the lower part of the Calandria Vessel has been shown in Figure 3-120. This COUPLE model along with RELAP5 hydraulic and heat structure components for Calandria Vessel, CV and End Shield are model and represented in Figure3-121.

Inventories and thermal-hydraulic conditions like pressure, fluid and structure temperatures, and void fraction of Calandria Vessel, Calandria Vault, and End Shield at the time of core collapse as obtained at the end of phase 2 calculation are assigned as initial conditions for 3 phase calculation.

The Calandria Vessel failure is considered from failure from “creep” or from vessel temperature exceeding the “melting” temperature of the Calandria Vessel material. The stainless steel “creep” model is being used for the analysis. A melting temperature of 1873°K is considered for the failure.

In the COUPLE model, initial debris porosity of 0.5 and particle radius of 10 mm are used for the analysis. Mass of UO<sub>2</sub>, ZrO<sub>2</sub>, and Zr are considered as a debris material. Shield plug is not considered in the composition of debris.

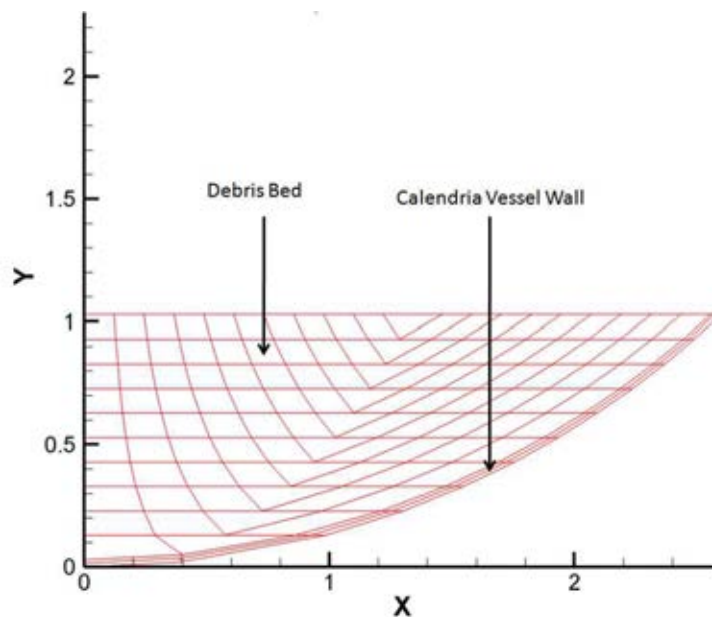


FIG. 3.120. COUPLE Mesh for Calandria Vessel Bottom.

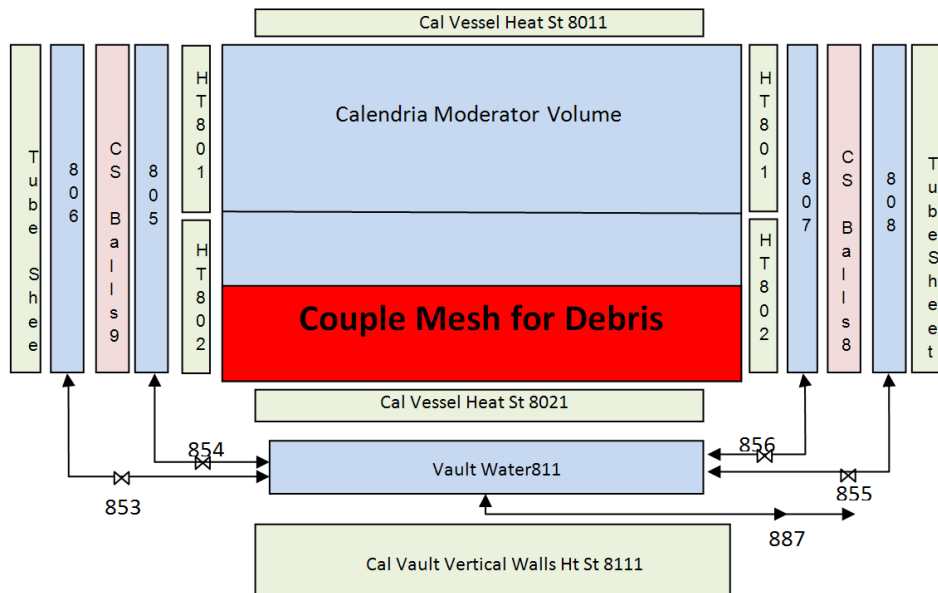


FIG. 3.121. Nodalization for moderator, CV & End shield for Phase 3

### 3.3.2.6. Containment model

The containment model consists of modelling of several compartments of containment, exhibiting thermal hydraulic volumes, heat structures representing walls, various rupture disks. The model calculates thermal hydraulic behaviour of volumes, fission gas release and deposition on the Calandria Vault wall. It also takes care of the Molten Core Concrete Interaction (MCCI). The Nodalization used for the containment modelling is the same as that of AECL. The model is built on the information available in reference 2 and later received communication from IAEA. Different boundary conditions like steam flow rate, hydrogen flow rate, fission product flow rates and molten corium flow rate are given in this model at different phases of the accident. Leakage area is calculated based on the leakage condition given as 5% volume per day at 224 kPa. This calculated area has been used throughout the transient.

For performing the Molten Corium Concrete Interaction (MCCI) analysis it is assumed that molten corium, which consists of  $UO_2$ ,  $ZrO_2$ , Fe, Cr, Ni, spreads uniformly in the Calandria vault after vessel rupture. The Calandria vault is lined with a 6 mm steel liner on the inner surface. It is assumed that after corium pouring in the Calandria vault, this liner will melt and instantaneously mix homogeneously with the corium. Analysis has been carried out for homogenous corium configuration considering the water level in the Calandria vault above the corium surface. A water inventory of 112.5 tons (water inventory in the Calandria vault based on water level just below the Calandria) is used above the molten corium at the beginning of MCCI. The initial corium temperature has been taken as 2,273°K. The concrete Calandria vault is assumed to be limestone common sand concrete. Mixtures of different species do not have single melting points. Instead, they change from solid to liquid over a range of temperatures, between so-called solidus and Liquidus temperatures. Figure 3-122 shows the Solidus and Liquidus Temperatures of  $UO_2$ - $ZrO_2$  mixtures for limestone common sand concrete [25] and is being used for the analysis.

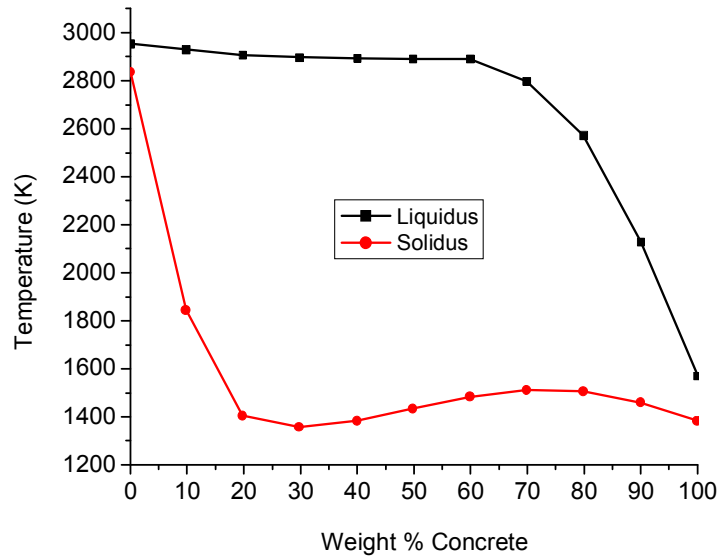


FIG. 3.122. Solidus and Liquidus for  $UO_2 - ZrO_2$  Mixture

### 3.3.2.7. Fission product release and transport model

FP release has been calculated with the PHTACT code specific model. The code needs plant specific information like initial species inventory and their distribution in different channels at different nodes along with the temperature history. The transport has been modelled with the SOPHAREOUS module of the ASTEC code. This module requires accident specific information like the time history for fluid mass inventories and flow rates in different control volumes, junctions and inter connection of different control volumes as obtained from PHTS calculations. The code computes release rates versus time for different species groups in different core volumes, distribution of each species in PHT and releases into containment.

### 3.3.3. Analysis results

Table 3-7 shows the major sequence of events.

TABLE 3.7. SUMMARY OF IMPORTANT EVENTS

	Scenario	Time (s)	Time (hr)
Phase 1	Class 3 and class 4 power loss	0.0	0.0
	Turbine stop valves closed	0.0	0.0
	PHT pump trip	0.0	0.0
	Feed isolation	0.0	0.0
	Reactor trip	0.001	0.0
	Steam isolation	20.0	0.0
	MSSV opens for the first time	100.0	0.027
	Calandria vessel bleed opens	200.0	0.054
	SG Dryout in loop 1	6000.0	1.81
	SG Dryout in loop 2	6000.0	1.81
	LRV Opening in loop 1	6900.0	1.91
	LRV Opening in loop 2	6900.0	1.91
	Fuel Failure	7000.0	1.94
	Pressurizer PORV opens	7400.0	2.05
	At least 1 channel dry in loop 1	8000.0	2.222
	At least 1 channel dry in loop 2	8050.0	2.236
	OPRD rupture	10 885.0	3.023
	First Channel uncover	10 900.0	3.027
Phase 2	PT-CT Rupture in loop 1	11 500.0	3.194
	PT-CT Rupture in loop 2	11 550.0	3.208
	Moderator reaches saturation temperature	11 500.0	3.194
	First clubbed channel disassembly in both loops	13 607.0	3.77
	Second clubbed channel disassembly in both loops	15 666.3	4.35
	Third clubbed channel disassembly in both loops	17 936.0	4.98
	Core collapse to calandria vessel bottom for both loops	17 936.0	4.98
Phase 3	Calandria vault and end shield RD opens	18 000.0	5.0
	Vault water reaches saturation temperature	23 200.0	6.44
	Water depletion inside calandria vessel	40 060.0	11.13
	Containment failure	51 800.0	14.38
	Calandria vessel failure	95 710.0	26.58
Phase 4	MCCI begins in calandria vault	95 710.0	26.58
	Pressurizer empty	Never	Never
	Calandria vault water depletion	177 539.0	49.31
	Calandria vault structure failure by ablation	205 228.0	57.00

3.3.3.1. Phase 1 (0 – 10,900 s)

Phase 1 of the analysis begins with initiation of Station Black Out at time  $t = 0.0$  s, and ends at uncover of first fuel channel. In the present analysis the uncover of first fuel channel occurs at 10,900 s. Following figures show the transients for various parameters with respect to time, post SBO initiation: The outlet header temperature and pressure is shown in Figure 3-123.

As the SBO is initiated at  $t = 0$  s, the PHT pressure drops owing to coasting down of primary circulation pumps. This results in decrease in the PHTS mass flow rate as shown in Figure 3-

124. Steam Generator Secondary side pressure rises to the relief valve set point as Steam Generator inventory starts acting as heat sink for the natural circulation through the primary loops and removes heat by boil-off through Steam Relief Valves (Main Steam Safety Valves) till Steam Generator dryout occurs at 6,000 s. Figures 3-125 and 3-126 show the steam generator pressure and steam generator level respectively.

The maximum fuel sheath temperature starts rising post SG dryout as shown in Figure 3-127. The primary side relief valves (LRVs) open leading to loss of inventory on the primary side. The flow rates through the LRVs have been shown in Figure 3-128. Loss of Primary Inventory and pressure also leads to voiding of the primary channels as shown in Figure 3-129.

Figure 3-130 shows the average temperature for the topmost channel, PT-CT. This temperature is the highest among all the modelled channels.

Continuous addition of heat to the moderator causes pressurization in the Calandria Vessel and subsequent depressurization due to OPRD rupture which has been shown in Figure 3-131. There is initial drop in moderator temperature due to reduction in heat load from channels as reactor trips. Subsequently the temperature rises due to continuous addition of heat to the moderator (Fig. 3-132). Loss of moderator inventory through the OPRD also causes decrease in the moderator level as shown in the Figure 3-133. The top most of the channels thus gets un-covered and the CT temperature of that channel goes high as shown in Figure 3-134.

Ballooning of PT due to a rise in temperature is shown in Figure 3-135 for the channel experiencing the highest temperature. Contact of PT-CT is observed for the maximum temperature channel till phase 1, thus modelling of heat transfer due to contact conductance between PT and CT is not essential. In this analysis channel rupture occurs at 11,500 s and 11,550 s for Loop 1 and Loop 2 respectively. This is based on the thermal criteria of 1000°K and high pressure of 9.9 MPa(a).

Since the fuel temperature does not rise beyond 980°C during this phase of the accident the hydrogen generation due to Zr oxidation is negligible small and is shown in Figure 3-136. However the containment pressure varies because of the steam released from LRVs and OPRDs. The variation in the containment pressure has been shown in Figure 3-137.

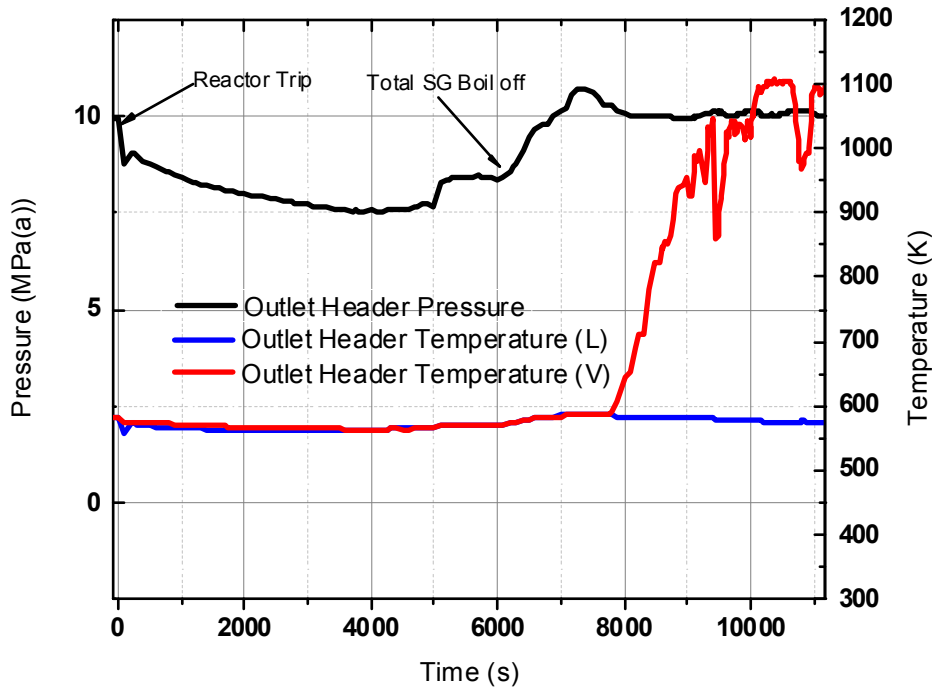


FIG. 3.123. Outlet header pressure and temperature

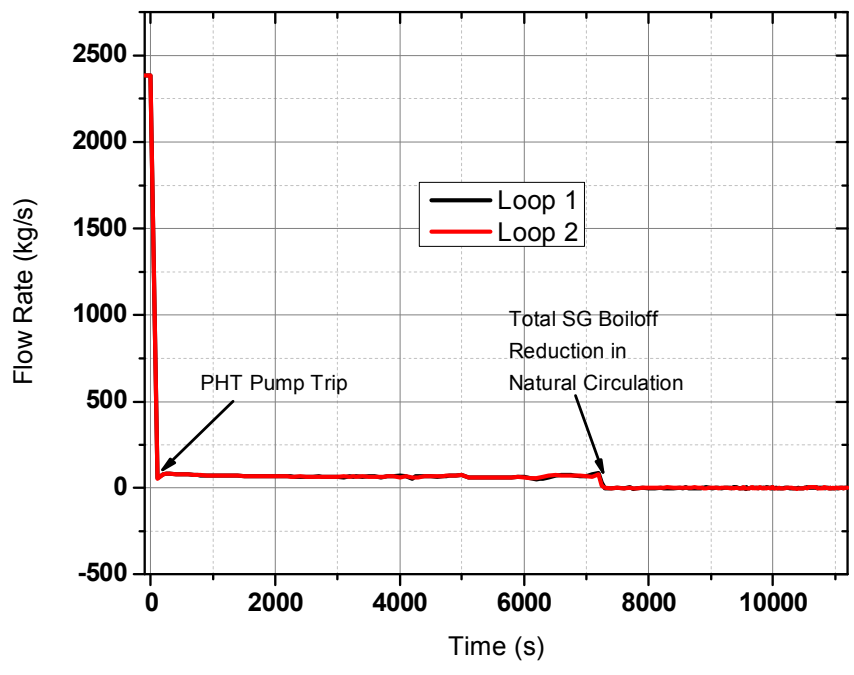


FIG. 3.124. PHTS Flow rate transient.

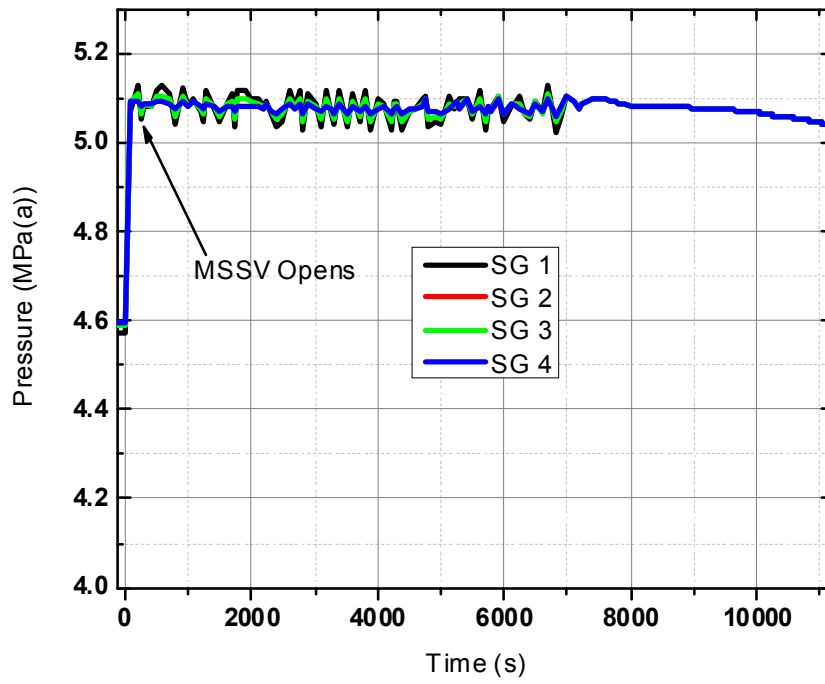


FIG. 3.125. Steam generator pressure transient.

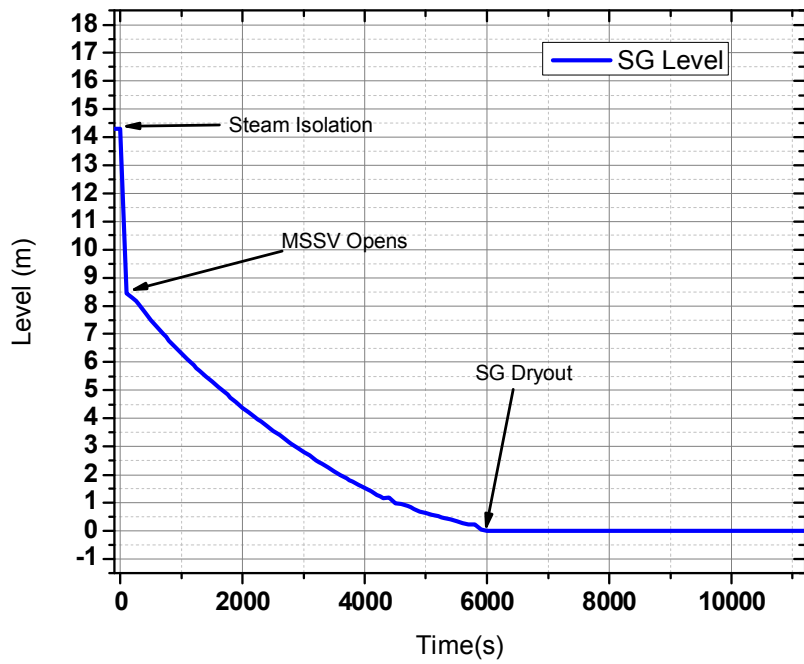


FIG. 3.126. Steam generator level transient.

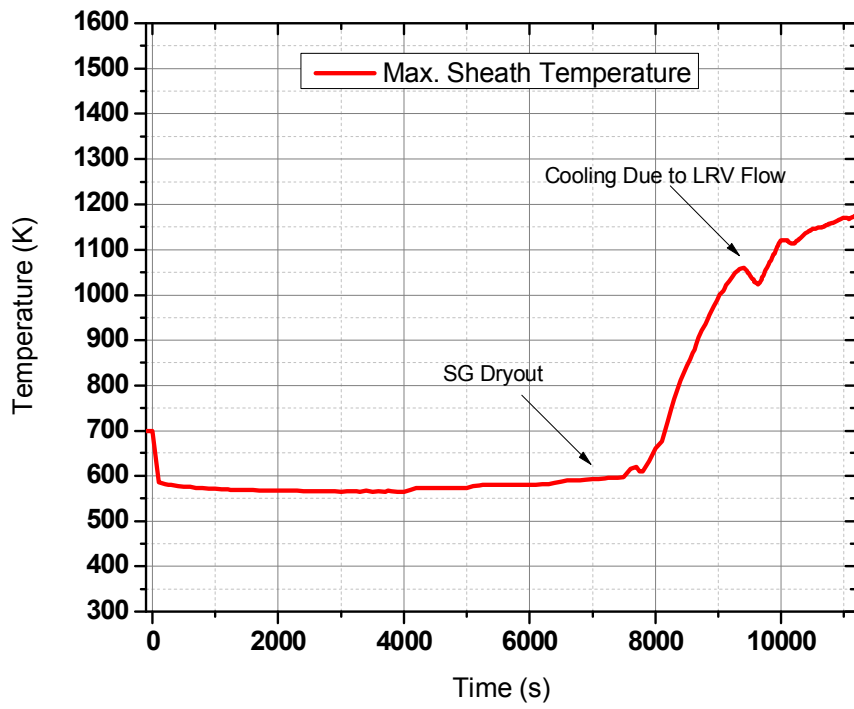


FIG. 3.127. Maximum fuel sheath temperature transient.

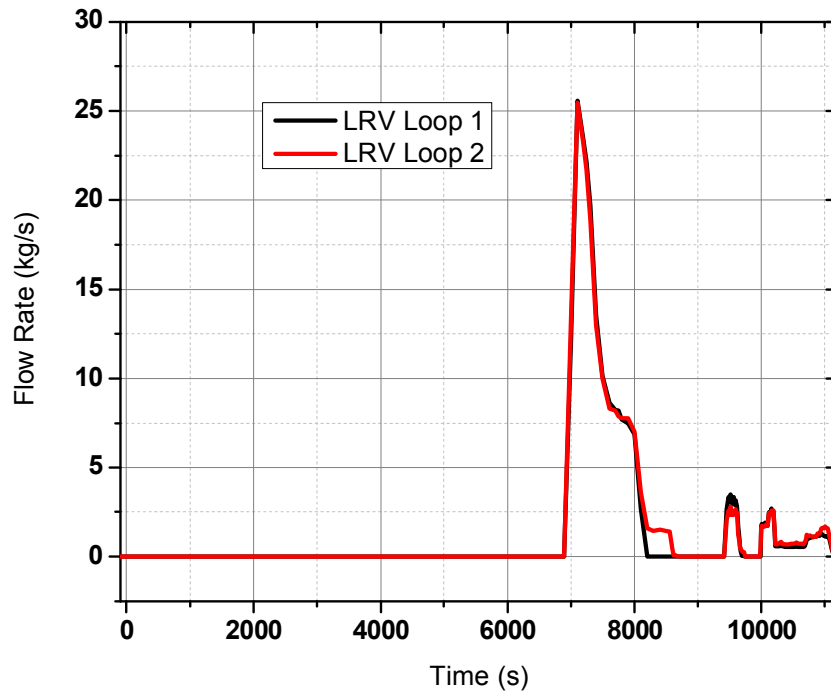


FIG. 3.128. LRV Flow rate transient.

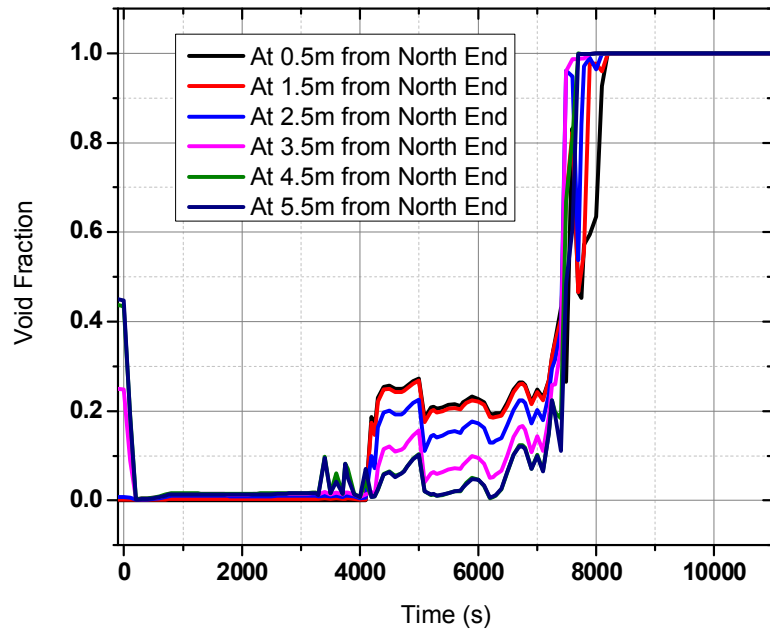


FIG. 3.129. Fuel channel void fraction transient for top most channel.

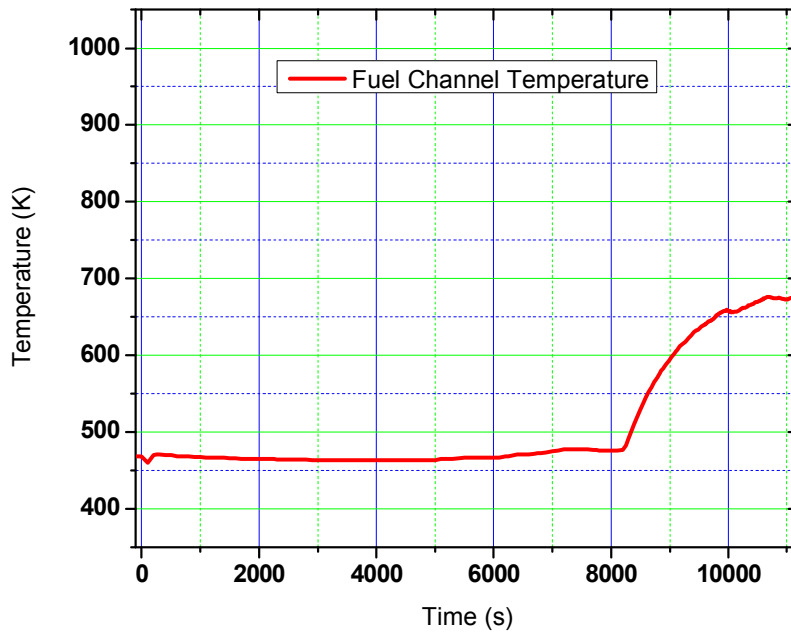


FIG. 3.130. Fuel channel(PT-CT) temperature transient.

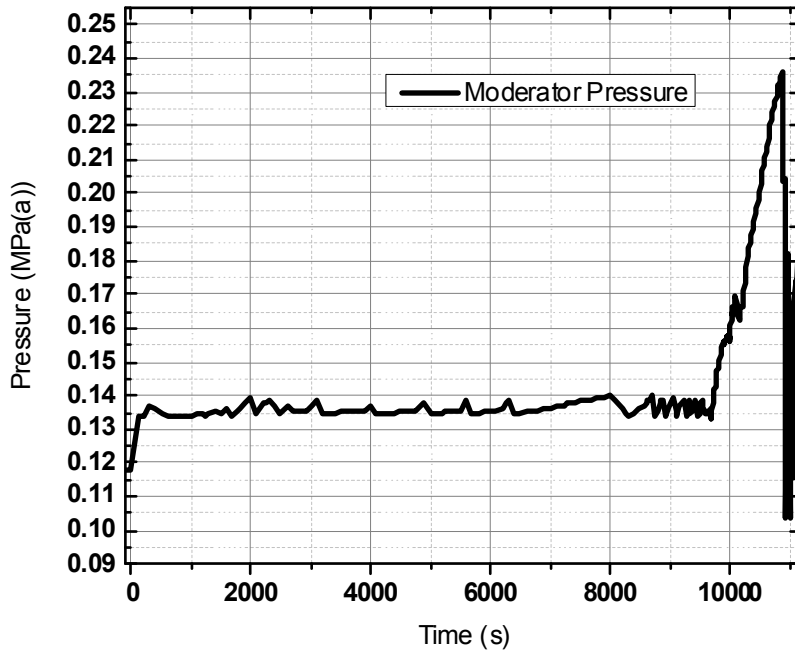


FIG. 3.131. Moderator pressure transient.

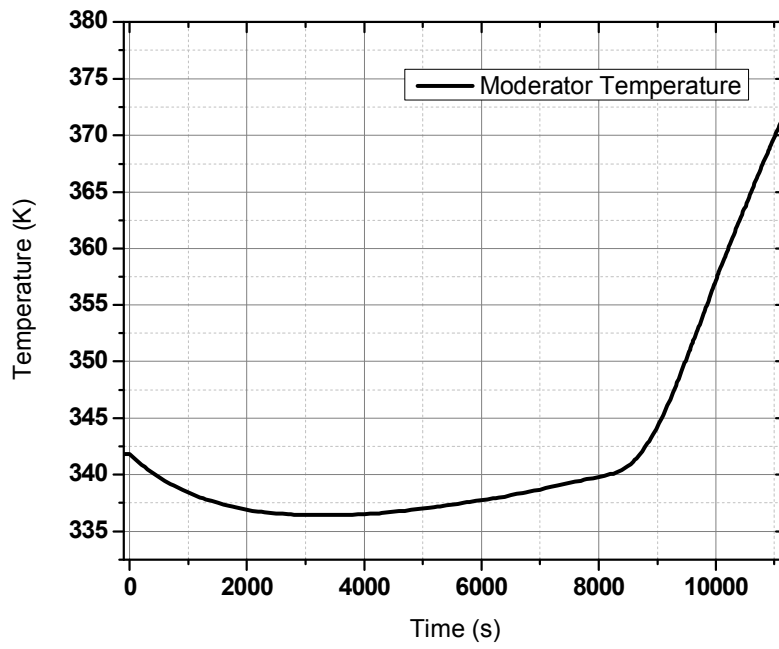


FIG. 3.132. Moderator temperature transient.

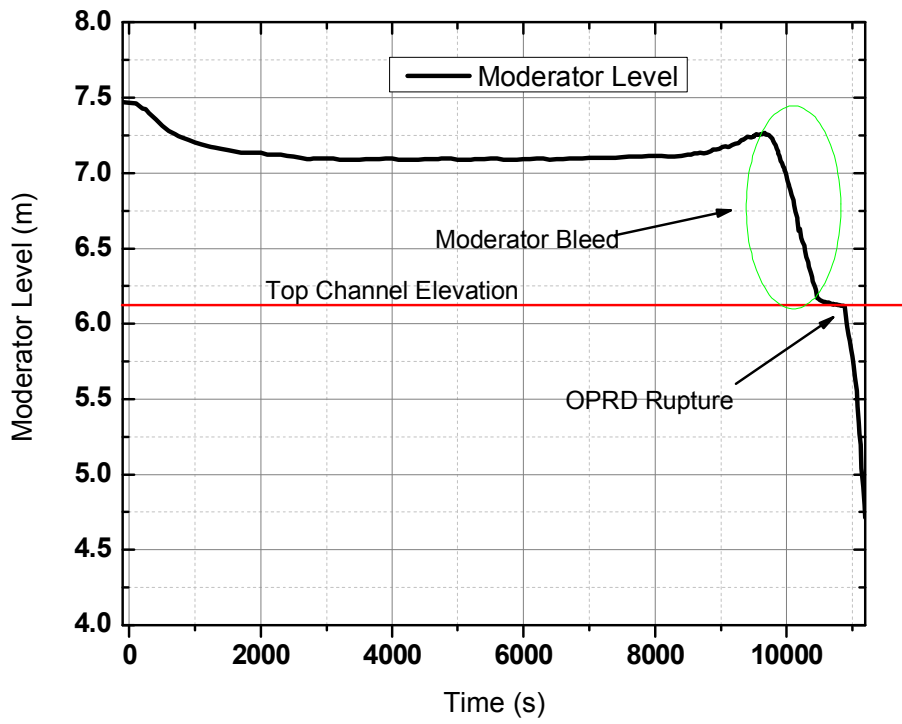


FIG. 3.133. Moderator level transient.

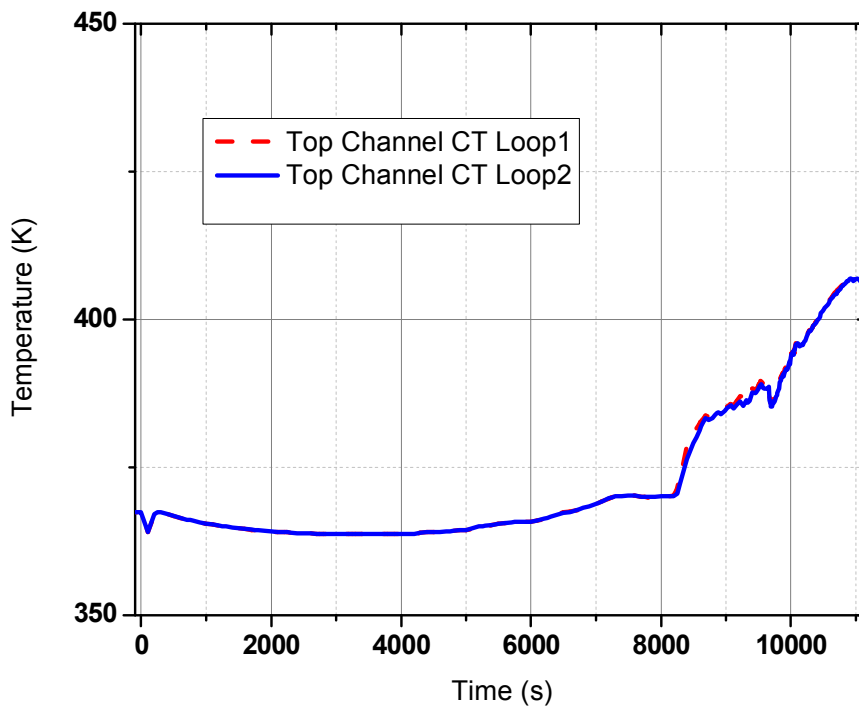


FIG. 3.134. CT Temperature transient for top most channels.

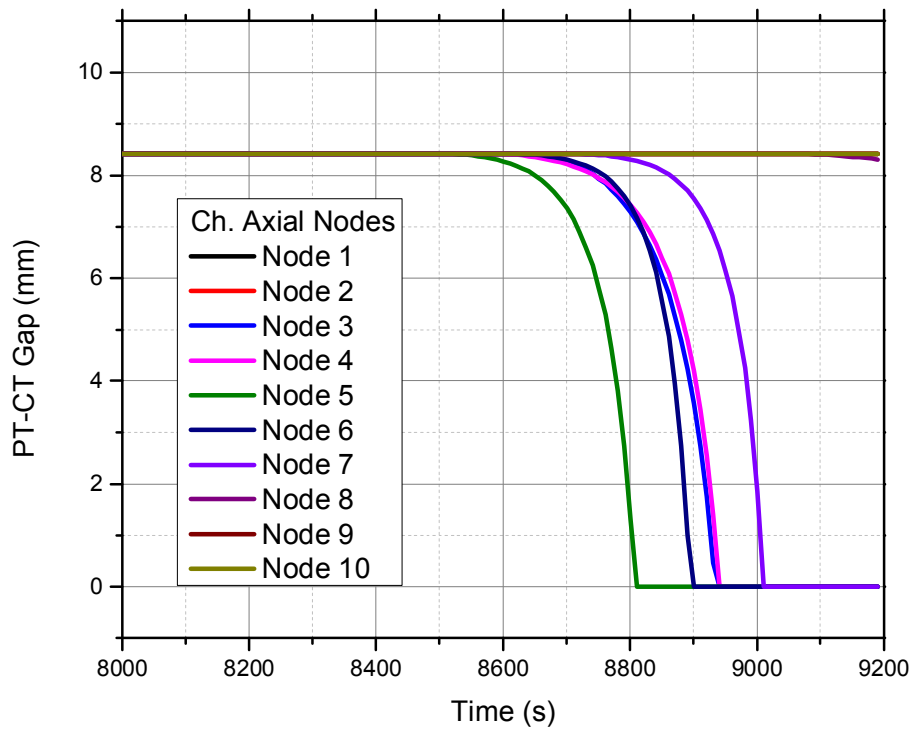


FIG. 3.135. PT CT Gap Transient.

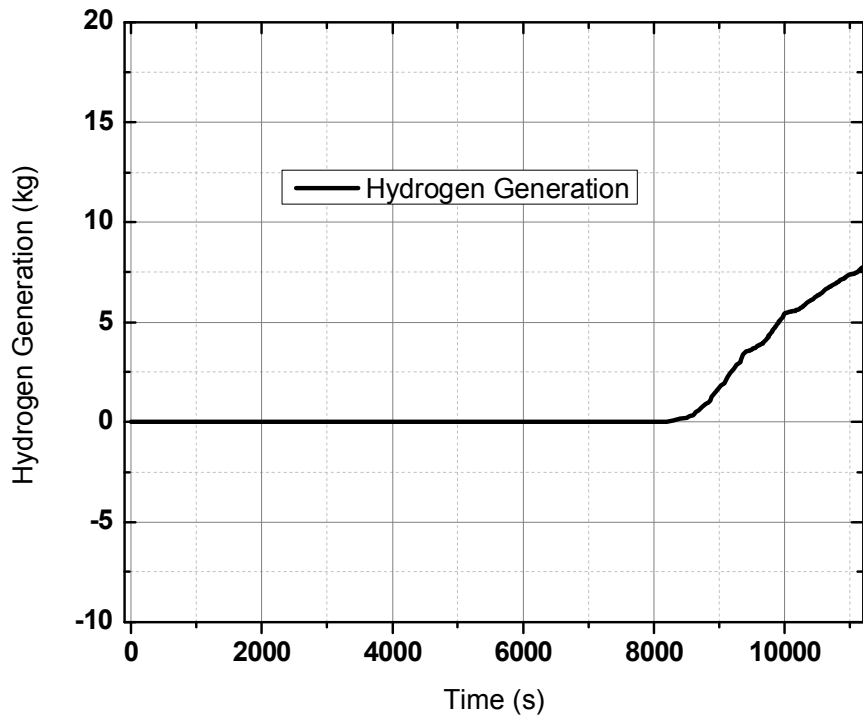


FIG. 3.136. Total cumulative hydrogen generation.

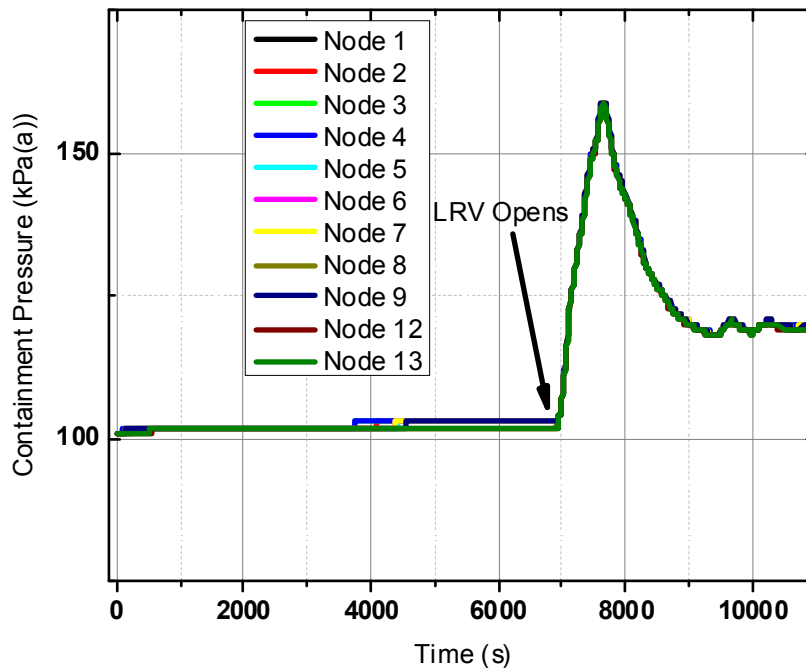


FIG. 3.137. Containment pressure transient.

### 3.3.3.2. Phase 2 (10,900 – 17,936 s)

Phase 2 begins from the uncovering of first reactor channel ( $t = 10,900$  s) to the disassembly of the entire reactor core ( $t = 17,936$  s). As the temperature in the top most channels increases due to decrease in the moderator level, the channels reach disassembly temperature. Disassembly of 70 channels per loop, in such a manner, amounts to a weight of 25,000 kg on the intact channels below. These channels thus collapse under core collapse criteria leading to total core collapse. The following figures show the transients of various parameters during this phase of accident.

Continuous addition of heat to the moderator causes increase in the moderator temperature to boiling point. This also results in increase in Calandria vessel temperature. The vessel temperature follows the moderator fluid temperature as shown in Figure 3-138.

Further addition of heat to the moderator causes boil off of the moderator. Figure 3-139 shows the flow rate through the OPRD and the drop in level in the moderator is shown in Figure 3-140. Due to a drop in the moderator level the channels start getting exposed one by one. Lack of external cooling for the exposed channel results in an increase in the Calandria tube and pressure tube average temperature and subsequently reaches the disassembly criteria of  $1,473^{\circ}\text{K}$  for channel disassembly as shown in Figure 3-141.

Figures 3-142 and 3-143 show a corresponding increase in the fuel channel temperature and sheath temperature respectively.

A rise in fuel temperature triggers oxidation of the fuel clad Zr material. Figure 3-144 shows the corresponding release of hydrogen due to clad oxidation reaction.

Since the core collapse criteria is 25 tons of weight for one loop, disassembly of top three clubbed channels is required. The time required for the top three clubbed channels to reach the channel disassembly temperature is 17,936 s. Instantaneous core collapse can be assumed to occur at 17,936 s.

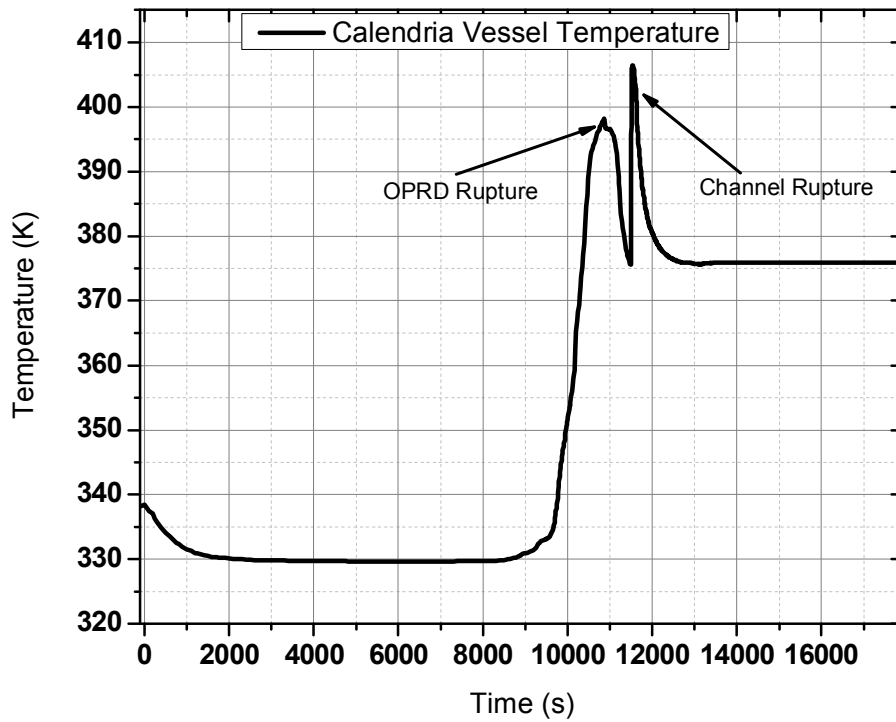


FIG. 3.138. Calandria vessel temperature transient.

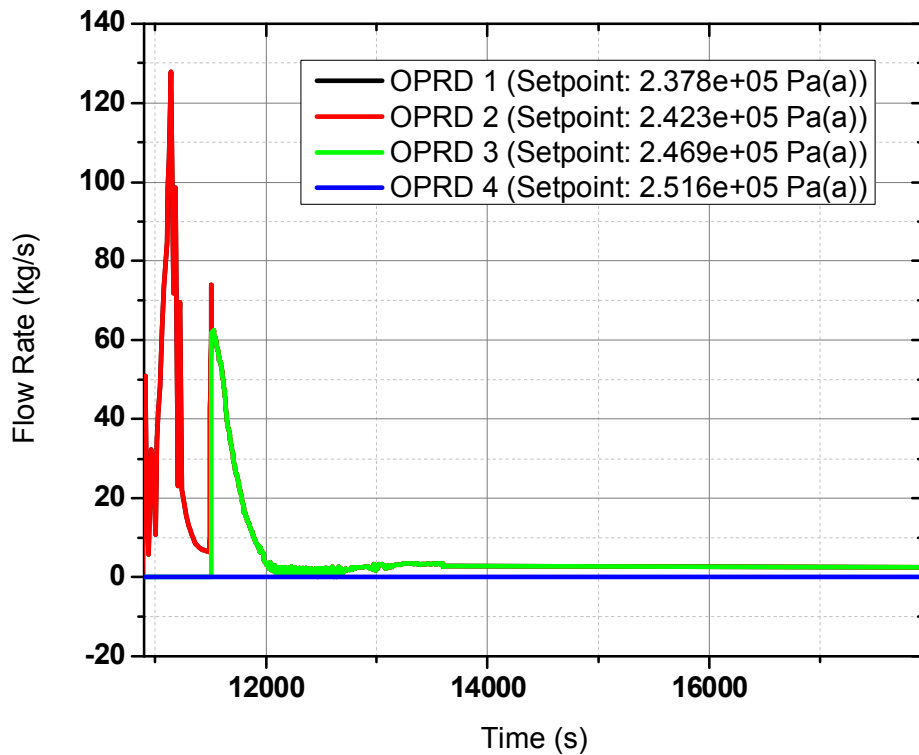


FIG. 3.139. OPRD flow rate transients.

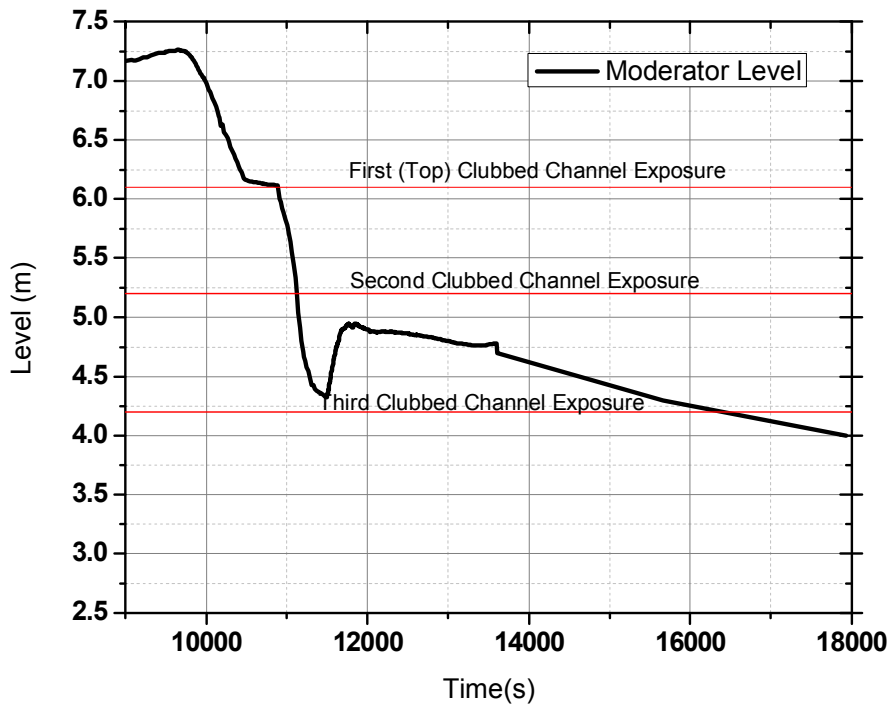


FIG. 3.140. Moderator level transients.

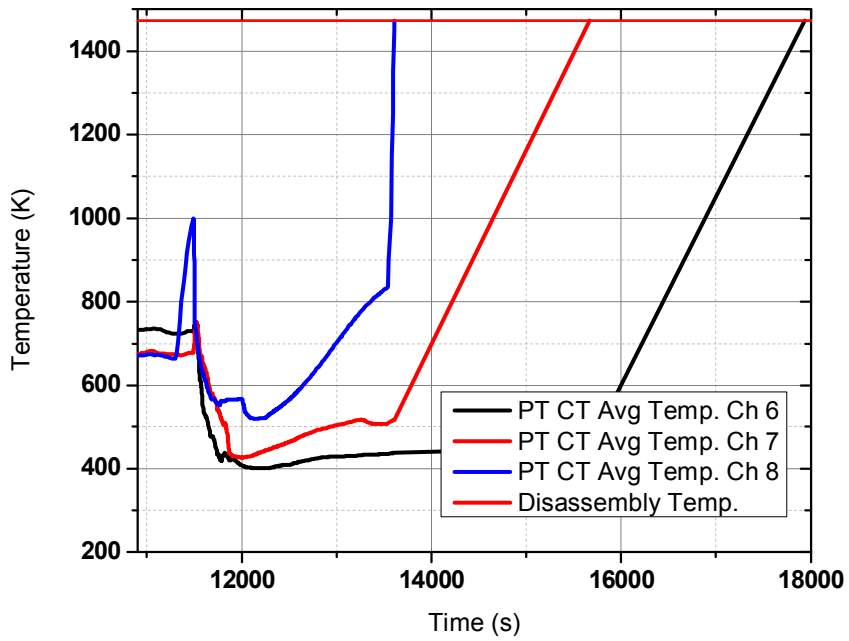


FIG. 3.141. PT-CT Average temperature transients.

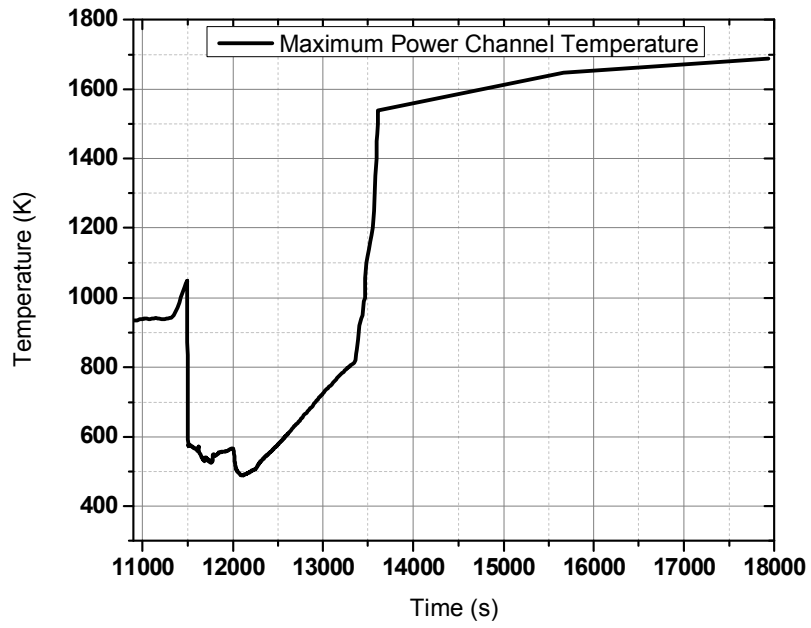


FIG. 3.142. Top most channel (PT) temperature transient.

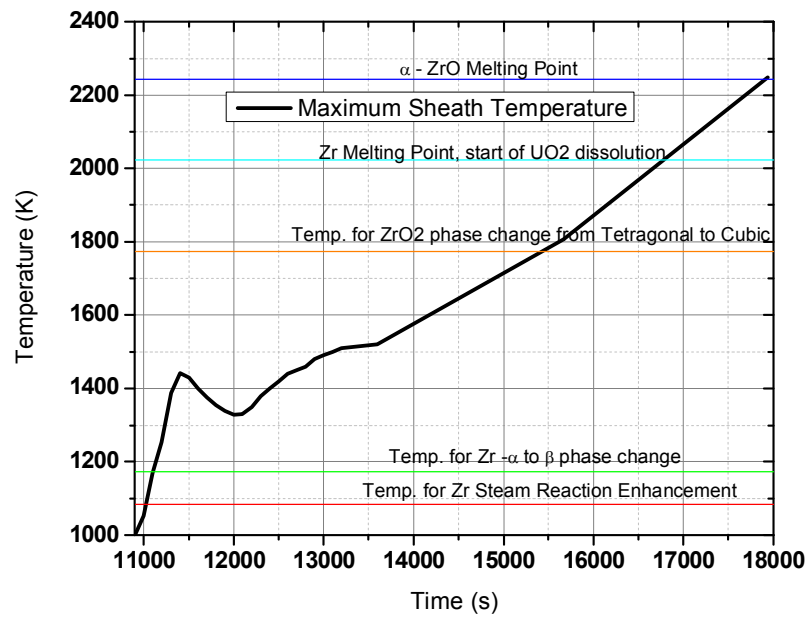


FIG. 3.143. Maximum sheath temperature(top channel) transient.

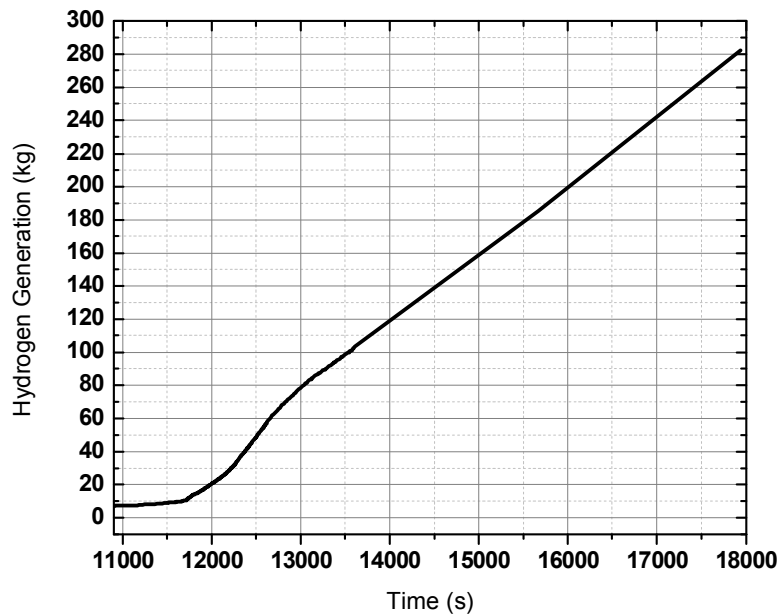


FIG. 3.144. Total hydrogen generation.

### 3.3.3.3. Phase 3 (17,936 – 95,710 s)

Phase 3 of the calculations begins from core collapse at 17,936 s and extends up to Calandria vessel failure. The moderator present in the collapse channels inside the Calandria vessel boils off due to decay heat. Further the collapsed channels degrade to form a mixture of solid debris and molten corium mass. As the only heat sink available is the Calandria Vault water, it boils off up to a level below the Calandria vessel level. Loss of cooling of the Calandria vessel from the outside causes an increase in its temperature up to its failure temperature (assumed as its melting point here). Failure of the Calandria vessel results in discharge of the corium mass into the Calandria vault. As the initial condition all the channels were assumed to have collapsed to the Calandria vessel bottom half. The water inventory present in the Calandria vessel at the time of collapse is such that the moderator in the Calandria vessel post core collapse attains a level of 2.6 m. The corresponding Calandria vault water level is also considered. Variation of some of the parameters with respect to time has been shown in following Figures:

As the channels get collapsed into the Calandria vessel bottom, they are assumed to have formed debris which continues to generate heat as per the decay heat. This causes heat up of debris and the maximum debris temperature is shown in Figure 3-145. Decay heat is being removed by the moderator boil off in the form of latent heat of vaporization which is reflected in the fall in the moderator level as shown in Figure 3-146.

The maximum debris temperature rises with total boil-off and stabilizes at 2,273°K. At this temperature part of the debris has formed a U-Zr-O eutectic mixture. With depletion of moderator, the Calandria vault water is the only heat sink available. The Calandria vault water reaches its boiling temperature at 23,340 s. Boiling of the Calandria vault water causes pressurization of the Calandria vault beyond the RD set point and the RD opens. This has been shown in Figure 3-144. The depletion in the Calandria Vault water level has been shown in Figure 3-148.

The Calandria vessel attains a temperature of 700°K during the moderator boil off period. It rises to 800°K after the moderator dries out. A sharp increase in temperature is observed when the Calandria vault water drops to a level below the Calandria vessel as shown in Figure 3-

149. The Calandria vessel is found to fail as the vessel wall has reached the melting temperature of 1,772°K. Extremely low creep of the vessel is being found. As a large section of the vessel attains the melting temperature, a large section of the vessel failure is assumed. This leads to the end of phase 3 at 95,710 s. Hydrogen generated due to the Zr oxidation reaction has been shown in Figure 3-150. As debris oxidation progresses from internal to external, the total hydrogen generation rate also changes.

Figures 3-151 and 3-152 show the progress of debris heating. The temperature distributions in the debris bed as calculated by the COUPLE module for four time instants are furnished. The temperature contours show that almost half of the fallen debris is melted. Figure 3-152 shows that the Calandria vessel wall has undergone melting during this instant to large extent. Hence instant release of the molten material is assumed for the next phase calculation. The molten material discharge content and thermal state has been provided for the next stage calculation.

Significant release of fission products occurs in this phase of the accident due to very high fuel temperatures close to the clad melting temperature. The rise in containment pressure is shown in Figure 3-153. The pressure in the containment (SG room) rises steadily. The containment follows the atmospheric pressure after containment airlock seal failure (334 kPa(a) at 51,800 s). The rise in pressure is attributed to a large hydrogen generation (659.8 kg) during the debris bed heat up.

Figures 3-154 and 3-155 show the Shapiro diagrams for various compartments of the containment indicating possibility of hydrogen and CO burning at a time close to the end of Phase 3. The concentrations in the Basement and Floor Area reach the hydrogen burning concentrations for some period of time during the transient. The pressure variation in the Vault and the End Shield is shown in Figure 3-156.

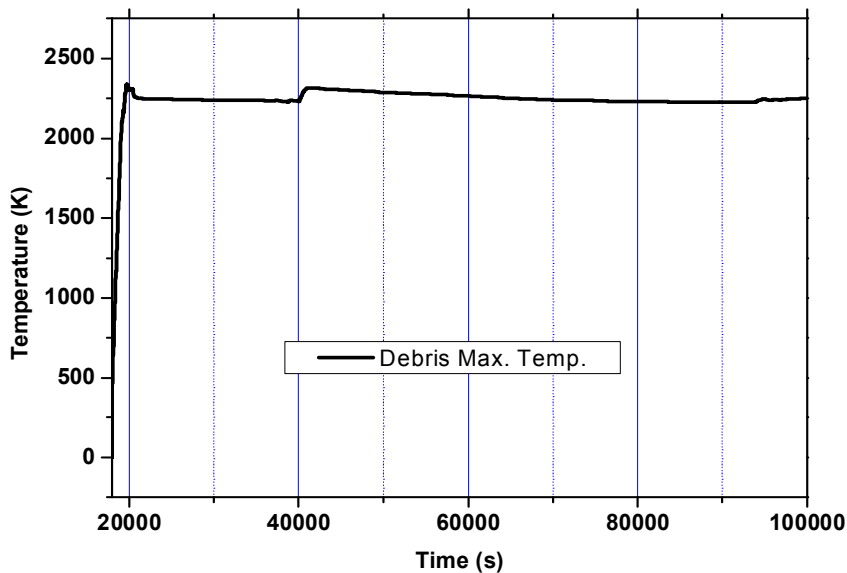


FIG. 3.145. Maximum debris temperature transient.

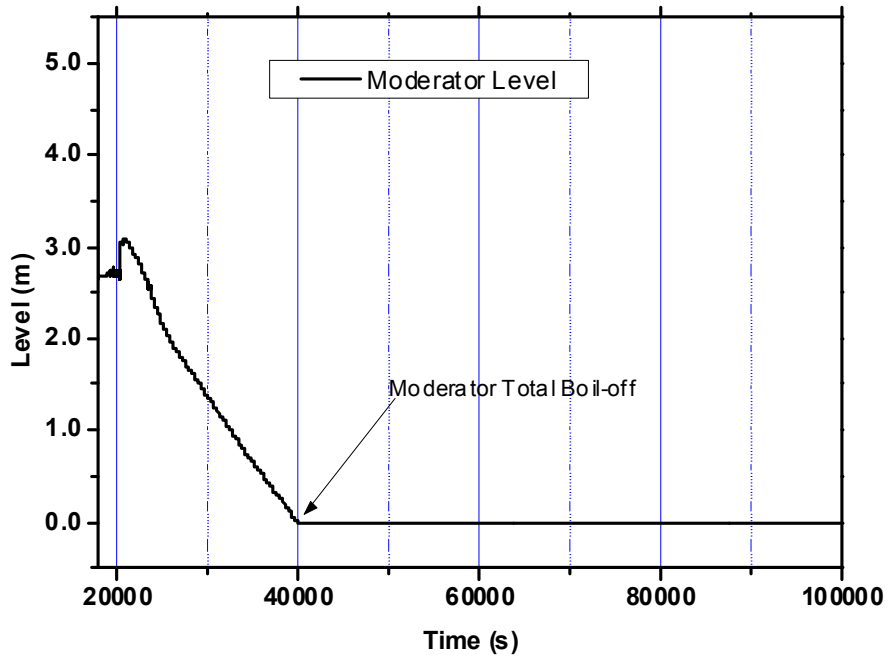


FIG. 3.146. Moderator level transient.

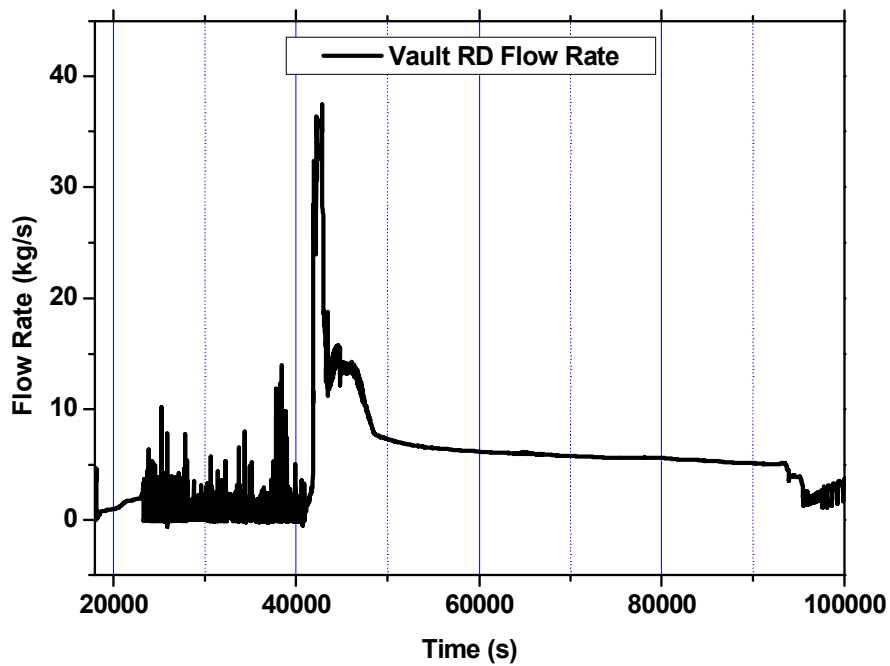


FIG. 3.147. Calandria vault RD flow rate transient.

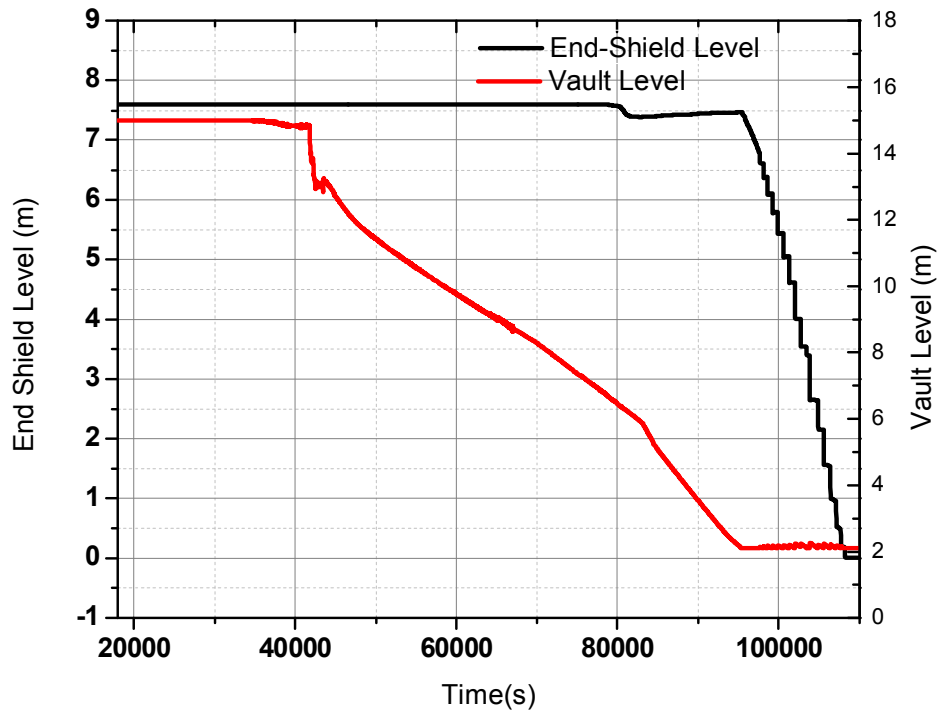


FIG. 3.148. Calandria vault and end-shield water level transient.

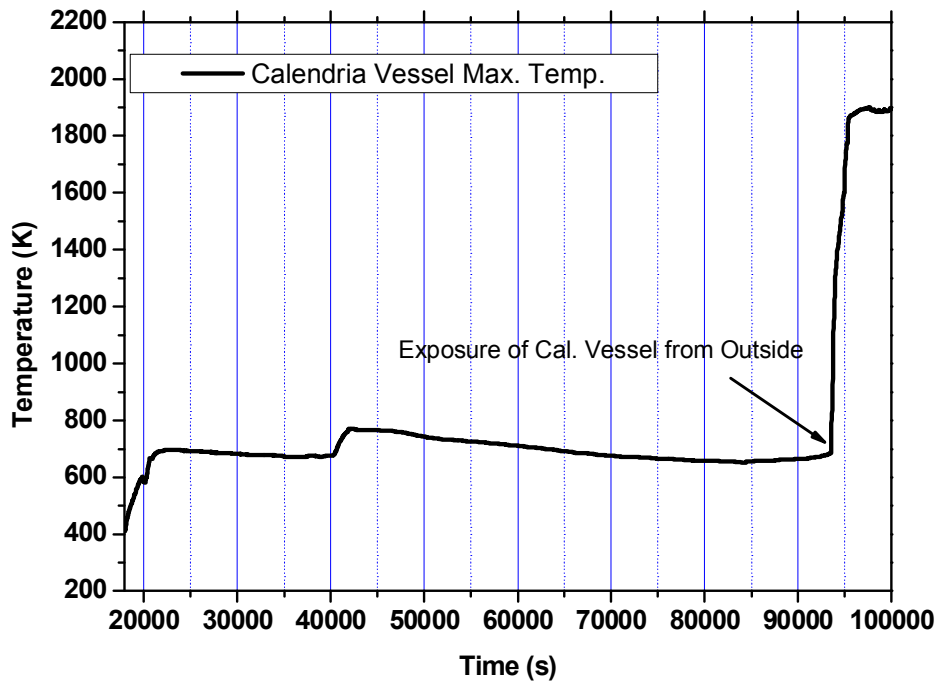


FIG. 3.149. Calandria vessel maximum temperature transient.

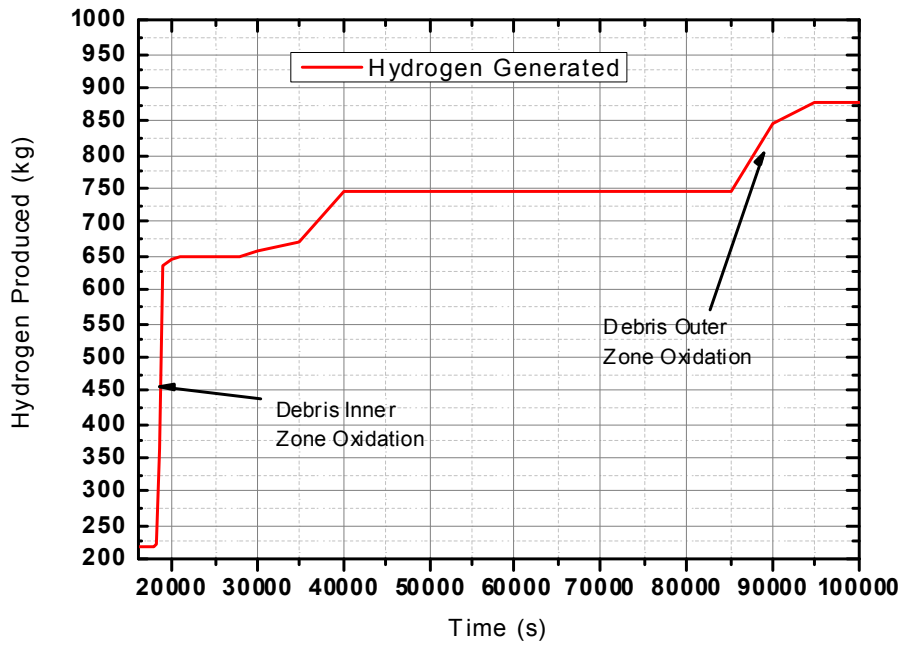


FIG. 3.150. Total cumulative hydrogen generation.

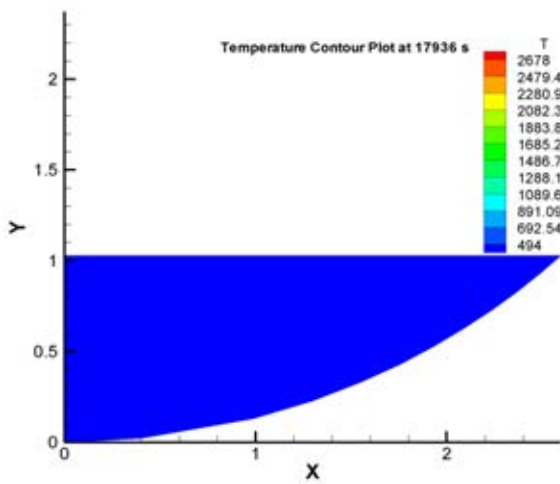


FIG. 3.151. Debris temperature contour at  $t=17,936$  s.

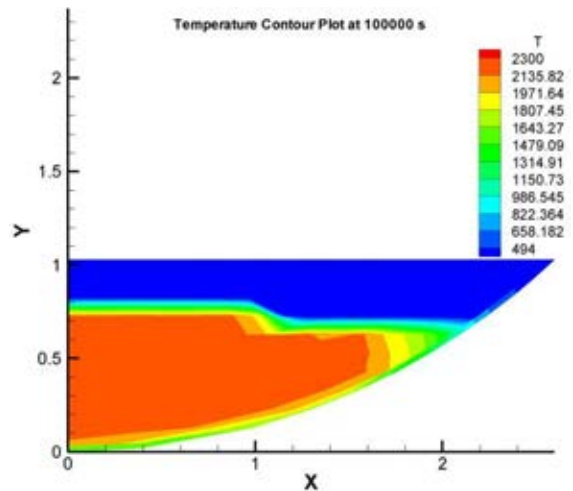


FIG. 3.152. Debris temperature contour at  $t=95,710$  s.

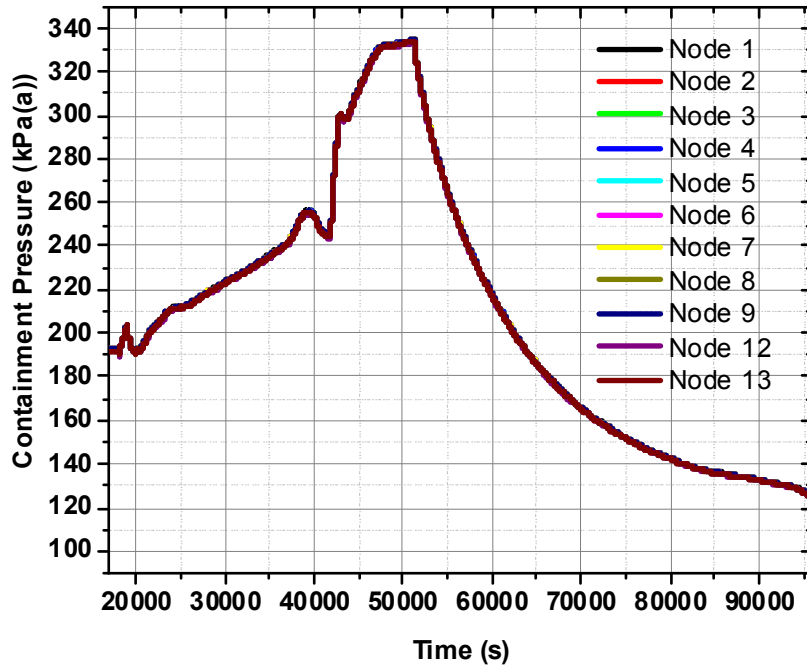


FIG. 3.153. Containment pressure transient.

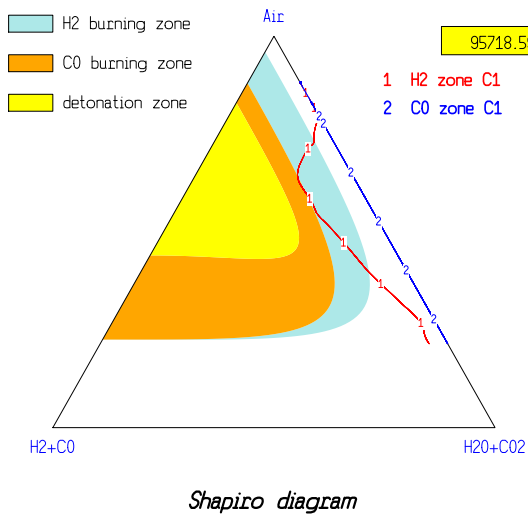


FIG. 3.154. Shapiro diag. for basement.

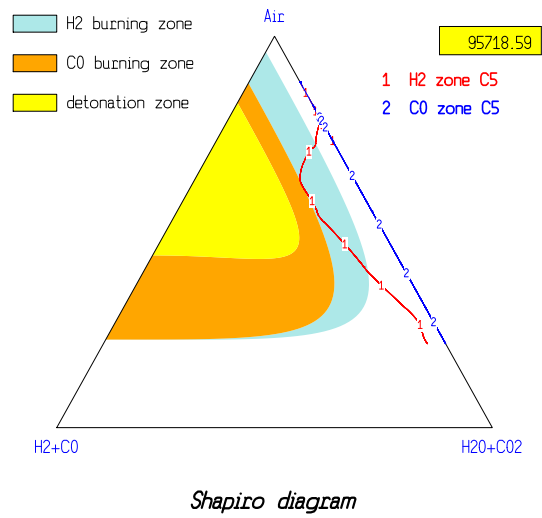


FIG. 3.155. Shapiro diag. for floor area.

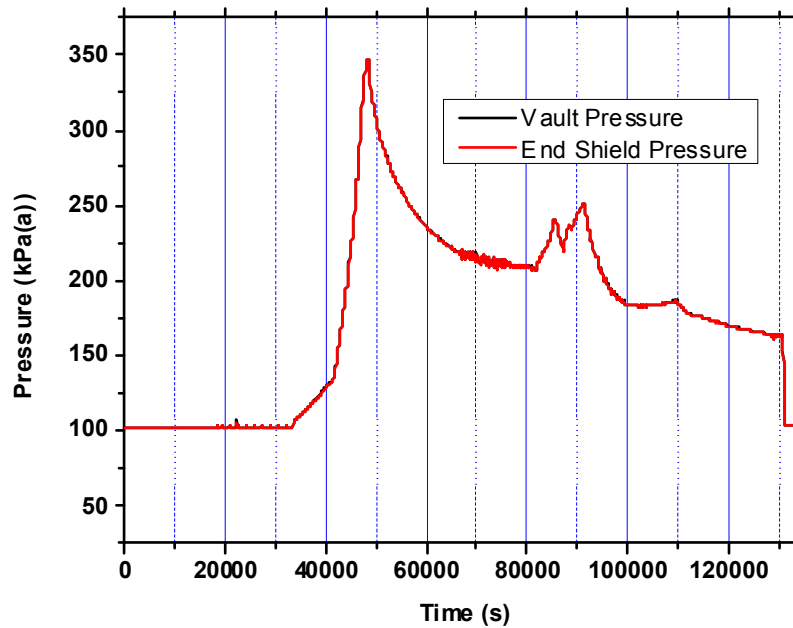


FIG. 3.156. Vault and end-shield pressure transient.

#### 3.3.3.4. Phase 4 (95,710 – 205,228 s)

Phase 4 of the accident begins from the Calandria vessel failure at 95,710 s and runs up to the failure of the Calandria vault floor due to ablation. With the discharge of corium into the Calandria vault the molten core concrete interaction begins. Ablation of concrete is accompanied by large release of hydrogen in the containment. The analysis is carried out up to complete ablation of the Calandria vault floor takes place. Due to failure of the Calandria vessel, the molten and solid parts of the debris present in the vessels get relocated to the Calandria vault. In presence of the Calandria vault water, the Zr-oxidation reaction continues. At the same time the, due to the molten core concrete interaction, concrete ablation begins. Figures 3-157 and 3-158 show the variation of containment atmosphere temperature and pressure respectively.

From the analysis it is observed that hydrogen present in the SG volume is significantly higher than other compartments as shown in Figure 3-159. The total mass of hydrogen generated is 2,208.0 kg of which 1,329.0 kg of hydrogen is produced due to MCCI. Since the containment is open to atmosphere after the RD rupture at 51,800 s, some part of the hydrogen generated gets released to the atmosphere. Around 1,515.0 kg of hydrogen is released to the atmosphere until 205,228 s and the remaining 693 kg of hydrogen is retained in the various compartments of the containment as shown in Figure 3-160.

As the molten core interacts with concrete, the concrete ablation begins. About 254,274 kg of concrete gets ablated till 205,228 s. This has been depicted in Figure 3-161.

Figure 3-162 shows the carbon monoxide concentration transient in the containment nodes. Variation of Calandria vault wall temperature and the corium-concrete mixture temperature has been shown in Figures 3-163 and 3-164 respectively.

Ablation of concrete takes place in the vault walls as well as in the floor of the Calandria vault. The ablated thickness in the vertical direction (ablation of floor) and in the radial direction (ablation of vault walls) has been shown in Figure 3-165.

Figures 3-166 and 3-167 show transient behaviour of the molten pool on concrete.

Figures 3-168 through 3-170 show the concentrations of steam, hydrogen and carbon monoxide in various containment compartments respectively.

Figures 3-171 and 3-172 show the Shapiro diagrams for the hydrogen-carbon monoxide mixture. The mixture in the end shields enters the burning zones for hydrogen and carbon monoxide. The mixtures in all the remaining compartments enter the hydrogen burning zone for some period of time.

The variation of upper crust thickness with time has been shown in Figure 3-173.

Table 3-8 shows the fission product released during Phase 4 of the accident. Entire inventory of the noble gases and volatiles gets released from the fuel up to the Phase 4 of the accident. However some amounts of semi volatiles and almost entire mass of refractory are retained within the molten corium owing to very high temperatures of melting and boiling for this class of elements.

Evolutions of the degradation parameters with respect to each phase have been tabulated in Table 3-9. A summary on fission product inventory and release is provided in Table 3-10.

TABLE 3.8. FISSION PRODUCT RELEASE DURING PHASE 4

Type	Element	Initial inventory (kg)	Release up to phase 4 (kg)	Release in phase 4 (kg)	% Release up to phase 4	% Release to containment in phase 4
Noble gases	Kr	3.88	3.88	6.20E-01	1.00E+02	1.60E+01
	Xe	53.8	53.82	8.50E+00	1.00E+02	1.58E+01
Volatiles	Cs	26.36	25.36	4.86E+00	1.00E+02	1.84E+01
	I	2.6	2.6	4.30E-01	1.00E+02	1.65E+01
	Rb	3.55	3.55	1.84E+00	1.00E+02	5.18E+01
	Te	4.81	4.81	8.10E-01	1.00E+02	1.68E+01
Semi volatiles	Ba	14.28	14.28	1.22E+01	1.00E+02	8.53E+01
	Sr	11.83	0.931	9.29E-01	7.87E+00	7.85E+00
Refractories	Ru	23.73	6.55E-01	6.55E-01	2.76E+00	2.76E+00
	Tc	8.46	2.30E-03	2.30E-03	2.72E-02	2.72E-02
	Zr	35.01	6.70E-03	6.69E-03	1.91E-02	1.91E-02

TABLE 3.9. EVOLUTION OF DEGRADATION PARAMETERS

Parameter	Units	Phase 1	Phase 2	Phase 3	Phase 4	
Maximum fuel sheath temperature	°K	1442.4	1688.0	--	--	
Fuel channel (PT-CT) average temperature	°K	1037.3	1611.0	--	--	
Maximum calandria tube temperature	°K	407.3	1490.0	--	--	
Maximum debris temperature	°K	--	--	2325.0	--	
Maximum calandria vessel temperature	°K	373.0	373.0	1873	--	
Maximum corium-concrete temperature	°K	--	--	--	2500.0	
CO produced per phase	kg	--	--	--	23,600.0	
H <sub>2</sub> produced per phase	kg	20.23	198.97	659.8	1329.9	
Zr material oxidized per phase	%	1.14	11.23	37.52	52.37	
Concrete ablation per phase	kg	0.0	0.0	0.0	254,274.0	
Noble gases released per phase from core	Kr	%	2.52E+00	5.21E+01	2.94E+01	1.60E+01
	Xe		2.52E-01	5.20E+01	2.94E+01	1.58E+01
Volatiles released per phase from core	Cs	%	4.00E+00	4.93E+01	2.81E+01	1.84E+01
	I		1.45E+00	5.27E+01	2.93E+01	1.65E+01
	Rb		1.68E-06	2.12E+01	2.69E+01	5.18E+01
	Te		6.56E-02	5.32E+01	2.99E+01	1.68E+01
Semi-volatiles released per phase from core	Ba	%	8.86E-05	1.27E+01	1.94E+00	8.53E+01
	Sr		8.24E-05	1.28E+00	6.93E-02	7.85E+00
Refractory released per phase from core	Ru	%	5.98E-11	8.93E-03	3.37E-05	2.76E+00
	Tc		5.54E-11	4.59E-07	1.56E-05	2.72E-02
	Zr		8.96E-11	4.87E-03	6.86E-05	1.91E-02
Noble gas fission product released to atmosphere per phase	Kr		--	--	27.06	60.8260.96
	Xe		--	--	26.95	

TABLE 3.10. SUMMARY OF IMPORTANT PARAMETERS

Total hydrogen release In-vessel	879 kg	
Total hydrogen release Ex-vessel	1329.9 kg	
Total noble Gas, Cs and iodine released from core	Kr	3.88 kg
	Xe	53.82 kg
	Cs	25.36 kg
	I	2.6 kg
Total noble Gas, Cs and iodine retained in PHT	Kr	0.0 kg
	Xe	0.0 kg
	Cs	10.0 kg
	I	1.15 kg
Total noble gas, Cs and iodine retained in containment	Kr	0.30 kg
	Xe	4.07 kg
	Cs	9.86 kg
	I	0.85 kg
Total noble gas, Cs and iodine release to environment	Kr	3.58 kg
	Xe	49.75 kg
	Cs	5.5 kg
	I	0.56 kg

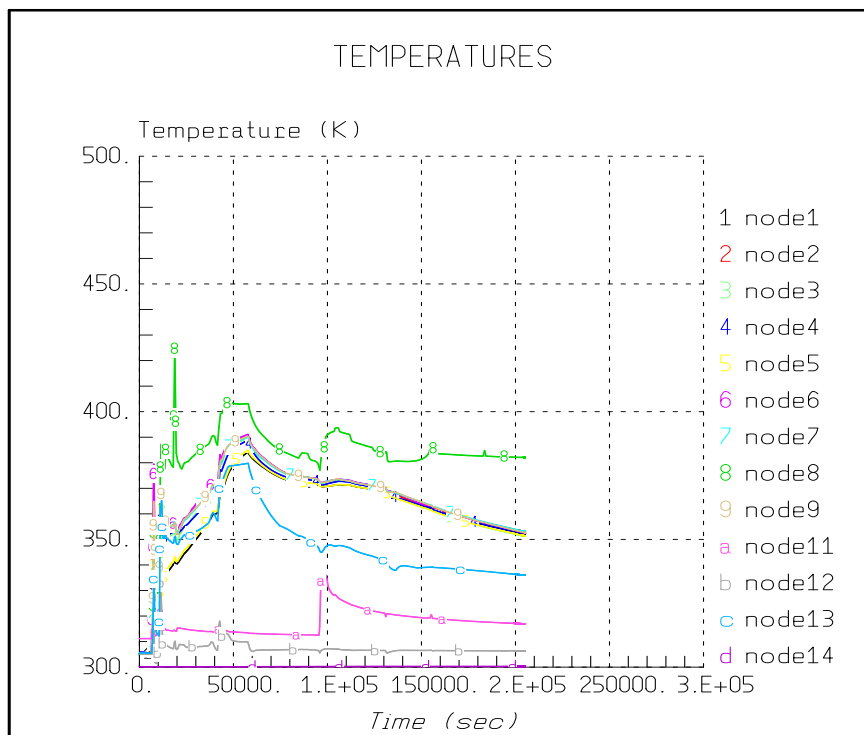


FIG. 3.157. Containment atmosphere temperature.

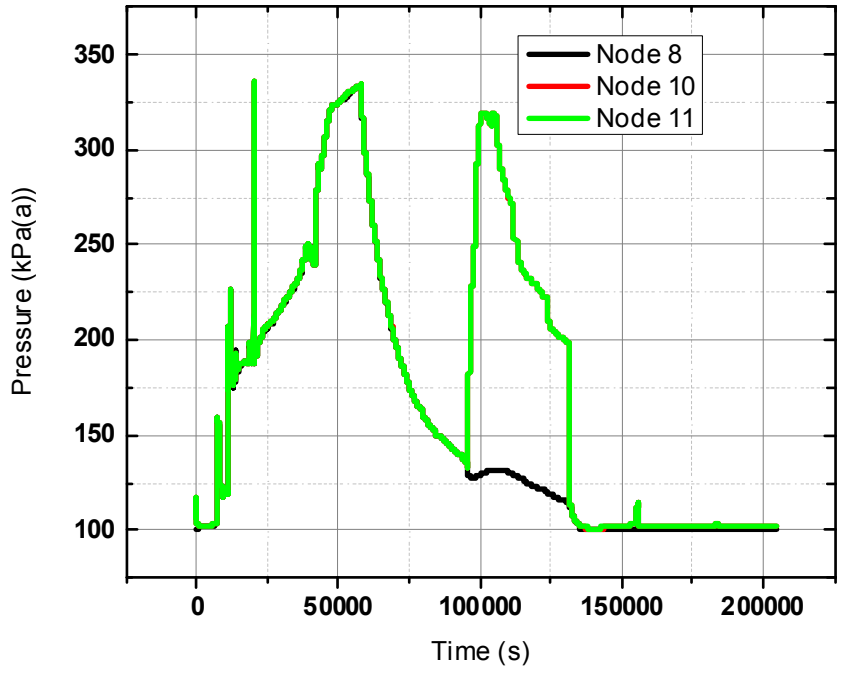


FIG. 3.158. Calandria vault and SG room pressure transient.

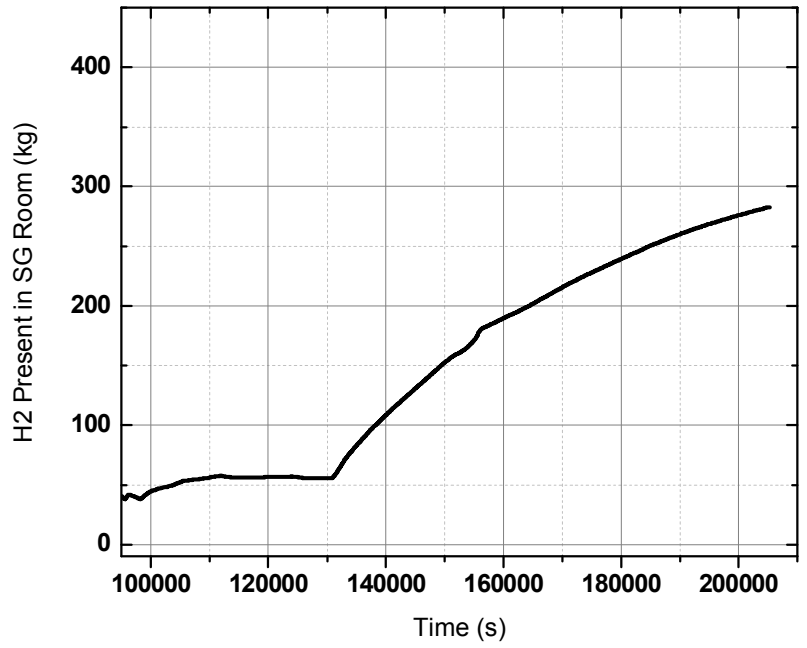


FIG. 3.159. Hydrogen present in SG Room

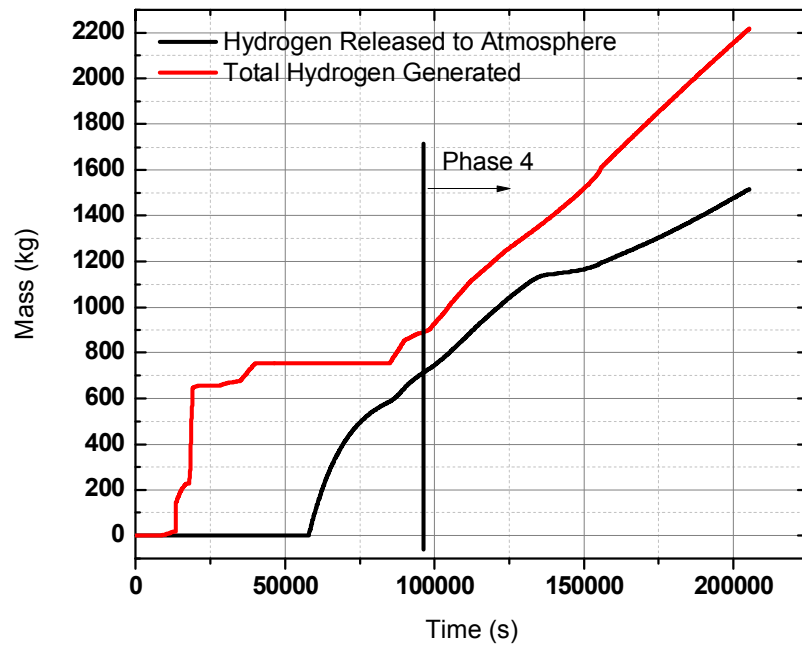


FIG. 3.160. Total hydrogen generation & release to atmosphere.

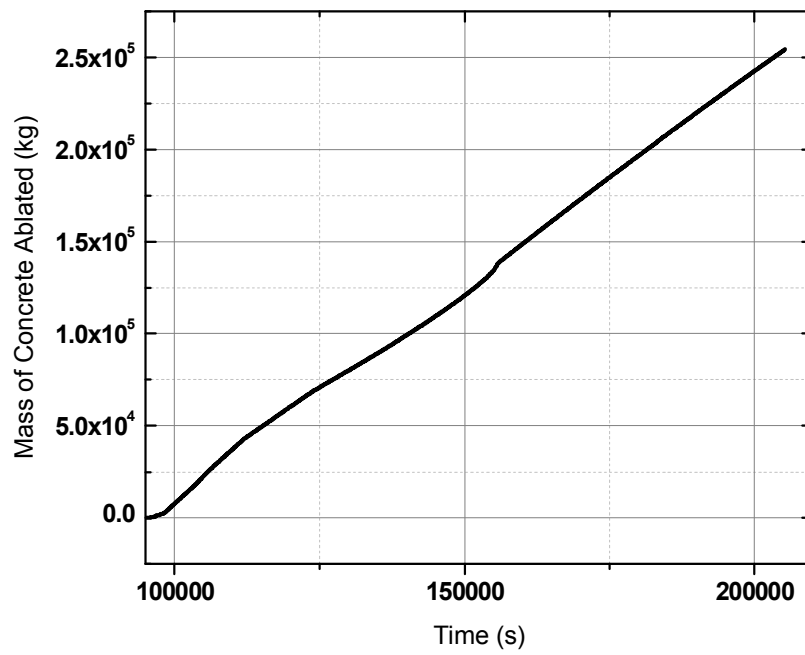


FIG. 3.161. Concrete ablation transient.

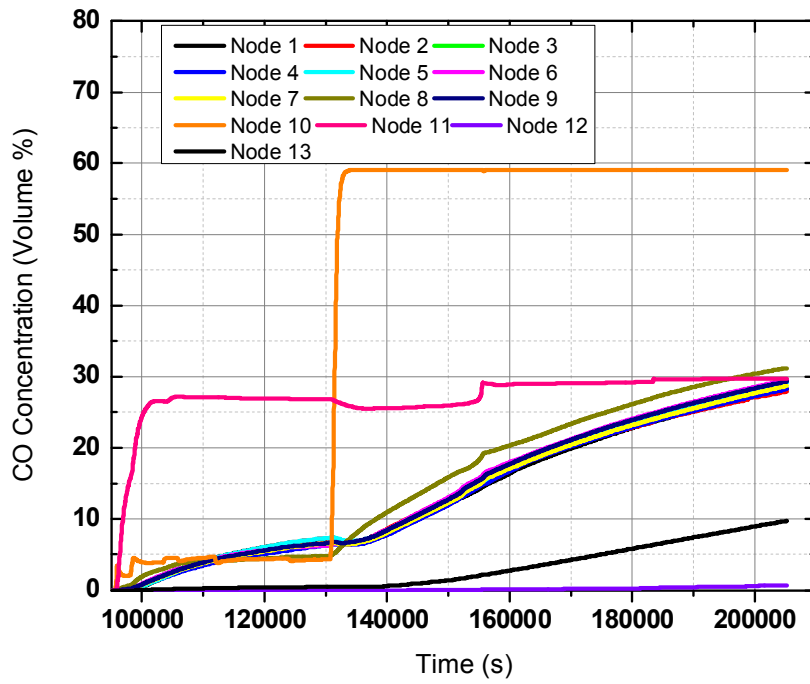


FIG. 3.162. CO Generation transient.

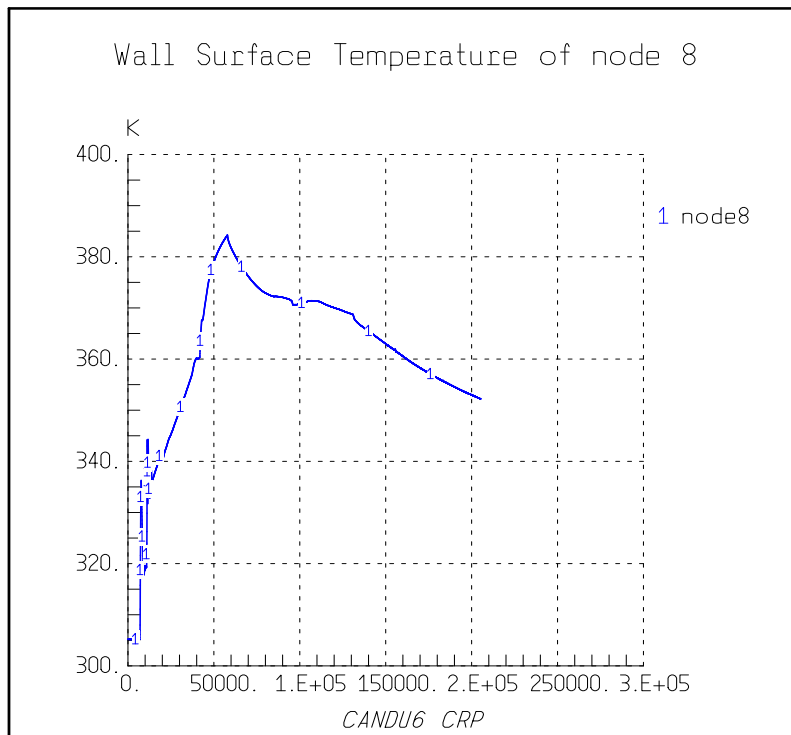


FIG. 3.163. Calandria vault wall temperature transient.

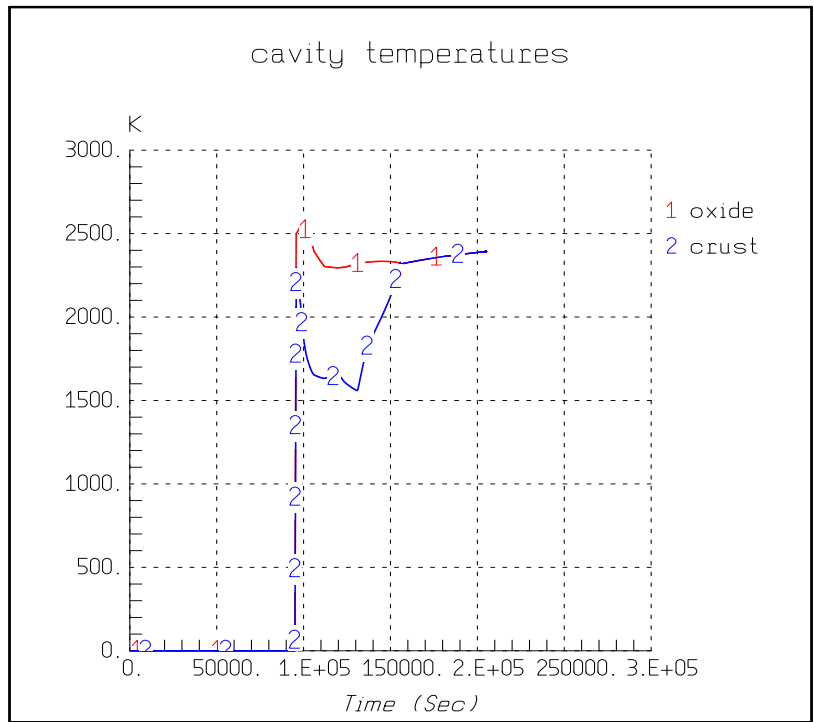


FIG. 3.164. Corium-concrete mixture Temperature Transient.

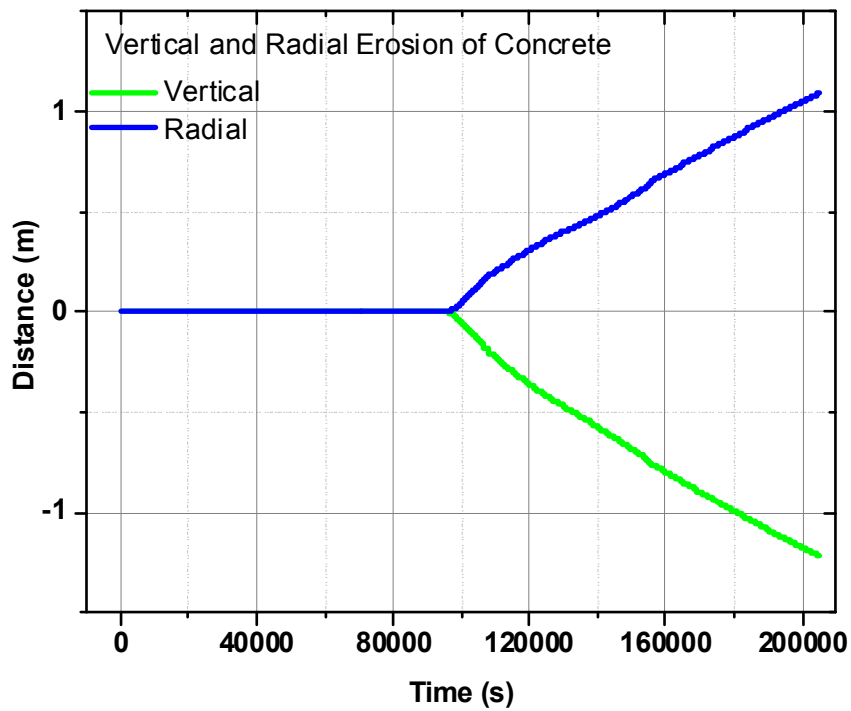


FIG. 3.165. Ablation of concrete transient.

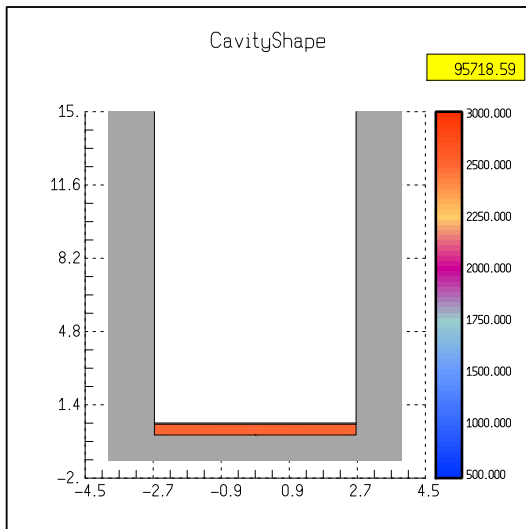


FIG. 3.166. Ablation of concrete at 95,710 s.

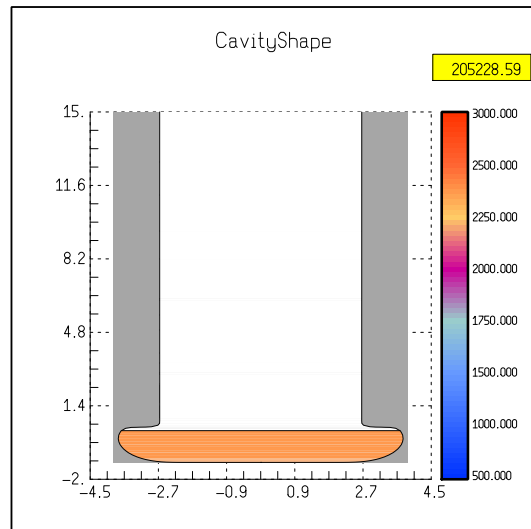


FIG. 3.167. Ablation of concrete at 205,228 s.

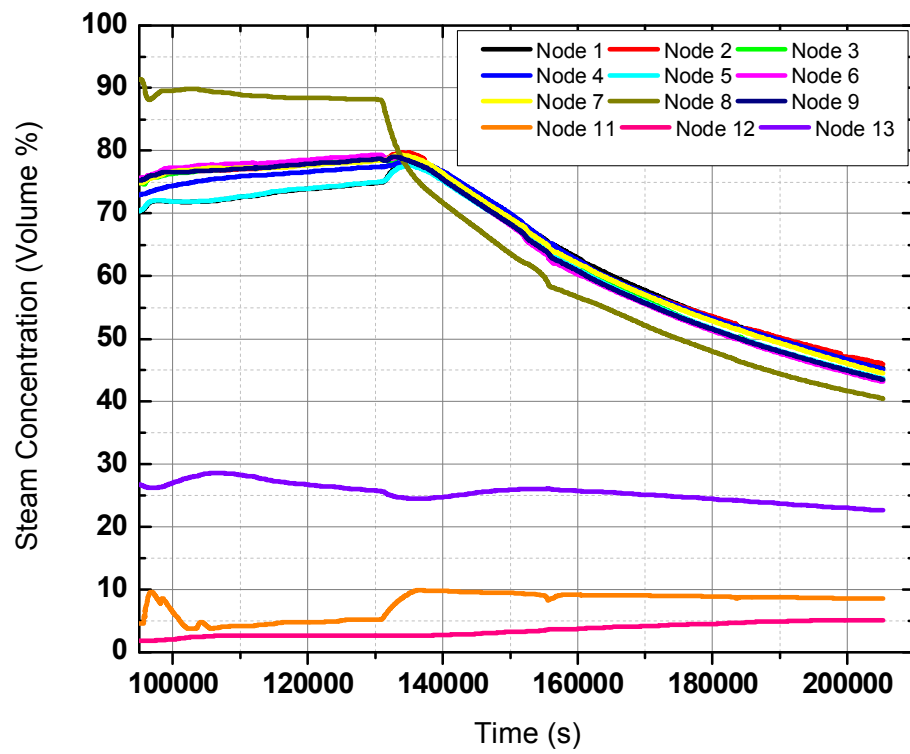


FIG. 3.168. Steam concentration transient.

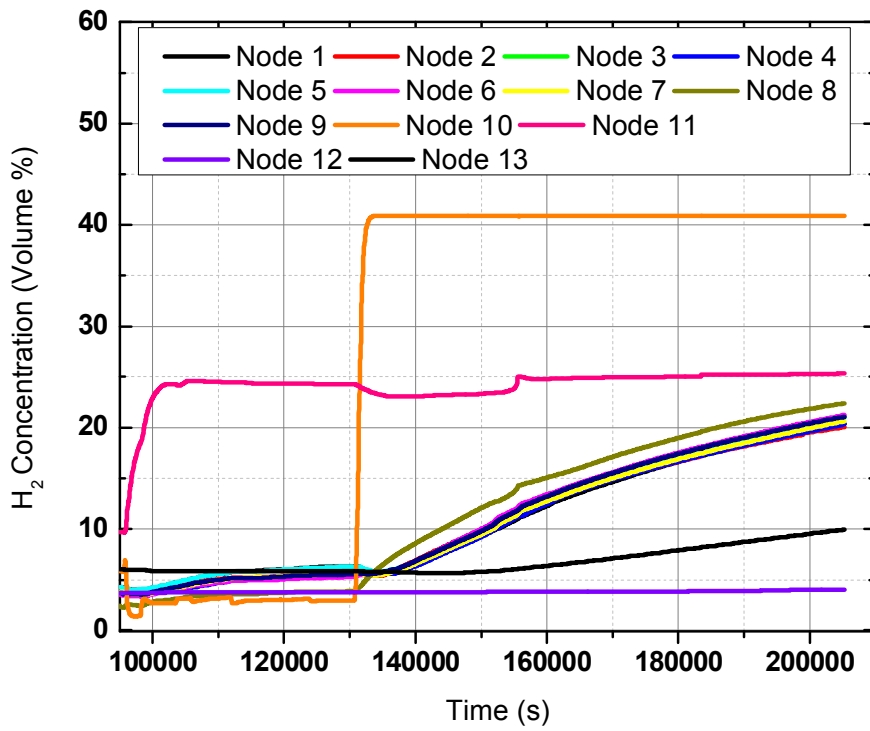


FIG. 3.169. Hydrogen concentration transient.

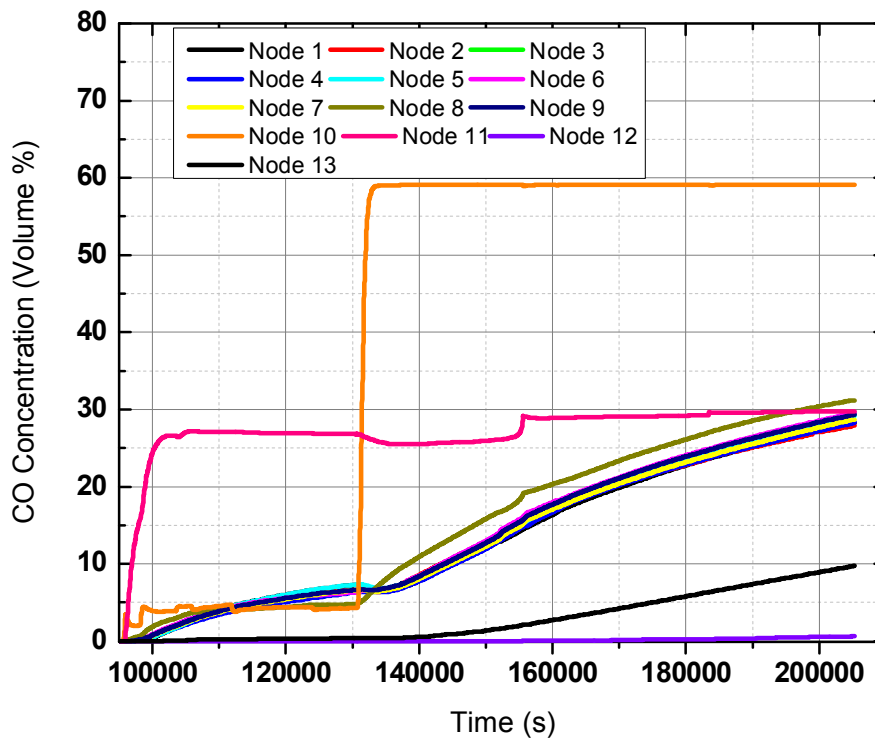


FIG. 3.170. Carbon monoxide concentration transient.

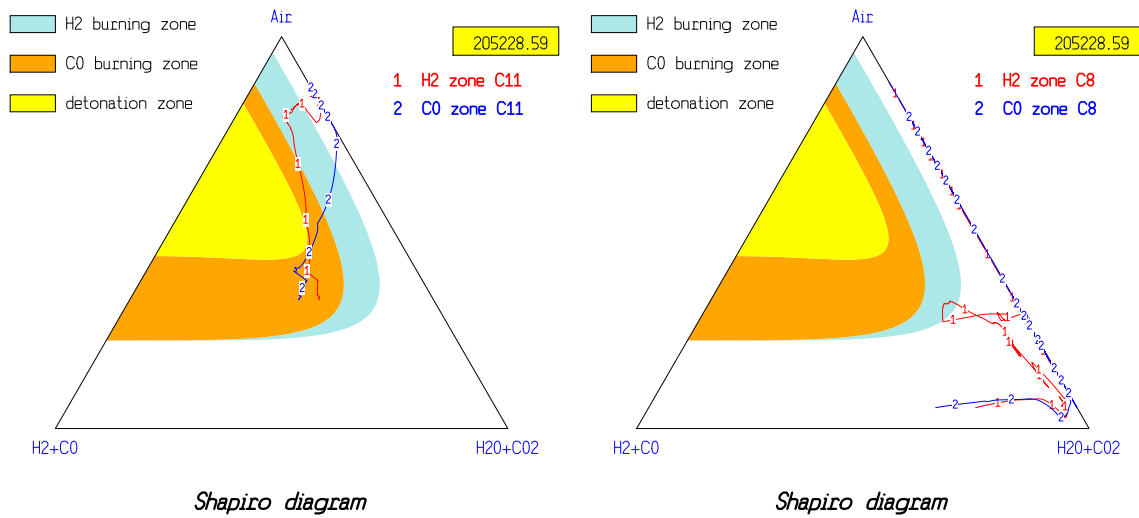


FIG. 3.171. Shapiro diag. for end shields. FIG. 3.172. Shapiro diag. for SG LH room.

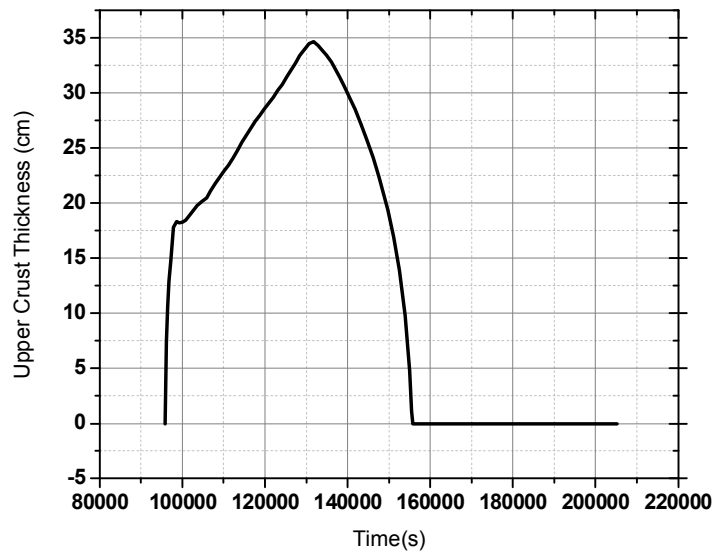


FIG. 3.173. Upper crust thickness variation.

### 3.4. KAERI

#### 3.4.1. Computer codes

Current study uses a computer code of ISAAC (Integrated Severe Accident Analysis code for CANDU plants) [26]. The ISAAC computer code provides a flexible, efficient, integrated tool for evaluating the in-plant effects of a wide range of postulated accidents and for examining the impact of operator actions on accident progressions. The code can predict the progression of hypothetical accident sequences from a set of initiating events to either a safe, stable, and coolable state or to an impaired reactor building (RB) and depressurization.

The ISAAC code is constructed in modules covering individual regions in the plant: primary heat transport system, pressurizer, steam generators, calandria, reactor vault, end-shields, degasser condenser tank, and RB. Every major engineered safety features are represented in

the code: shutdown cooling system, emergency core cooling system, moderator and shield cooling system, RB local air coolers, igniters, passive autocatalytic recombiner (PAR), and dousing spray system.

The code evaluates a wide spectrum of phenomena including steam formation, core heat-up, cladding oxidation and hydrogen generation, vessel failure, corium-concrete interactions, ignition of combustible gases, fluid entrainment by high-velocity gases and fission-product release, transport, and deposition. The code also addresses important engineered safety systems and allows a user to model operator interventions. Moreover, mathematical solution techniques are implemented to maintain a quick-running code suitable for extensive accident screening and parameter sensitivity analysis applications.

The generic models of ISAAC are evolved from the MAAP4 code developed by Fauske and Associates, LLC (FAI), for pressurized light water reactors [27]. Some of these models required minor modifications to adapt them to CANDU6 design features and to be integrated with the rest of the code, but these models were fundamentally unchanged from the generic MAAP4 models. As the CANDU6 type reactor differs from typical PWRs, the CANDU6-specific features are newly modeled and added to the ISAAC code. The CANDU6-specific models include the primary heat transport system (PHTS), calandria vessel, end shields, reactor vault, pressure and inventory control, and engineered safety systems (e.g., dousing, emergency core cooling).

One of the most important distinguishing features between ISAAC and other MAAP4 versions is the CANDU reactor core with fuel bundles situated inside horizontal pressure and calandria tubes. In addition, the large quantities of relatively cool water (moderator and reactor vault water) provide significant heat sinks, distinguishing the CANDU models from LWR models. The ISAAC models a broad spectrum of physical processes in the core that might occur during an accident, such as the:

- Fuel and fuel channel temperature excursions, deformation of fuel and fuel channels, and interactions with the moderator system;
- Zirconium-steam exothermic reaction;
- Thermal mechanical failures of fuel channels;
- Disassembly of fuel channels;
- Formation of suspended debris beds;
- Motion of solid and molten debris;
- Interaction of the core debris with steam.

In particular, ISAAC models the CANDU feeders, end-fittings, fuel channels and fuel. The models concentrate on the behaviour of these core components within the calandria vessel as the fuel channels disassemble, form suspended debris supported by intact channels, and relocate to the debris bed within the calandria vessel. Each characteristic channel represents a larger number of channels with similar powers, elevations and feeder geometries.

The ISAAC PHTS thermal hydraulic models are simplified by using assumptions such as coarse nodalization, equilibrium within a fluid phase, a uniform loop pressure and a single global void fraction at which phase separation occurs. The ISAAC PHTS thermal hydraulics results cannot be expected to be as accurate as those from more detailed PHTS models associated with a thermal hydraulic code such as CATHENA. Most importantly, however, ISAAC is an integrated code that models the interactions amongst many systems that are modelled in an integrated fashion. Thus, ISAAC calculates the effects of the interplay between the RB, calandria vessel, PHTS, reactor vault, core, etc. In addition, ISAAC has the

ability to input operator actions by enabling, disabling or modifying a system when the user requests.

The ISAAC code uses two files containing input data. The input data used to execute the code are entered in the plant-specific parameter file and the sequence-specific input deck. The user initially defines the reactor plant, e.g., primary system and RB, in the parameter file. The parameter file contains specific nuclear generating plant data such as component geometries and main operating parameters: pressures, temperatures, equipment volumes, water inventories, etc. The input deck file contains characteristics of the sequence to be analyzed (whether it is a station blackout, a small LOCA, etc.). The input deck provides run-specific information such as the run title, start and end times, whether it is an initial run or a restart run, and sequence-specific parameter changes. The input deck, through parameter changes, operator intervention and actions, and user-defined event codes, can be used to override or supplement data, which are initialized in the parameter file.

The separation of these files allows the ISAAC user to make desired changes in a flexible manner. The analyst uses an input file to apply specific analysis values or select certain options to model a particular accident scenario. This technique can be used to study the effect of different parameters or system availability on severe accident consequences, while using the same basic plant-specific information that is usually specified in the parameter file. The user implements a single large parameter file, in conjunction with different input files, to model series of different accident scenarios for the same reactor design, or to perform a parametric study of different model controls using the same plant data.

For this analysis, the parameter file is being prepared, using plant-specific information obtained from drawings, design manuals and analysis reports specific to the plant. The parameter file incorporates the following types of data:

- Station-specific data representing physical systems and system models,
- such as volumes representing the RB geometry;
- Phenomenological data, such as control flags;
- Component and system failure criteria, such as temperatures and pressures;
- Reactor initial conditions, including system pressures and temperatures;
- Program control parameters (e.g., data output, calculation time steps).

### **3.4.2. Phenomena and system idealization**

#### *3.4.2.1. Phenomena*

When the severe core damage occurs, four phases of accident progression are expected. Phase 1 covers the accident initiation to fuel channel dryout and Phase 2 from the fuel channel dryout to core collapse. The fuel channel heatup, failure and collapse, moderator boil-off, suspended debris bed formation and fission product/hydrogen behavior are treated in Phase 2. After core collapse to the calandria vessel failure and to the containment failure, Phases 3 and 4 include the phenomena regarding the debris melting and molten pool formation in the calandria vessel, calandria vessel cooling by reactor vault water, calandria vessel failure, ex-calandria vessel fuel-coolant interaction, molten corium-concrete interaction on the reactor vault bottom floor and containment pressurization. In this section, these phenomena are described briefly in order.

#### **(a) Phase 1**

ISAAC models each fuel channel with fuel rods, a pressure tube, a calandria tube, coolant, and moderator, and Figure 3-174 shows the channel configuration. Though there are thirty

seven fuel rods inside the pressure tube, a single representative fuel rod is modeled in ISAAC. Each channel has a maximum of twelve nodes, having equal length and configuration. In each node, temperatures of the fuel, cladding, pressure tube and calandria tube are calculated separately. A parabolic temperature profile within the fuel element is assumed to calculate the heat conducted out to the cladding. The core power after scram can be either given by the user or calculated by the code using the ANSI decay power correlations.

Each core node contains six components: fuel, cladding, pressure tube, calandria tube, coolant, and moderator. The fuel contains  $\text{UO}_2$ , the cladding contains Zr,  $\text{ZrO}_2$ , and a U-Zr-O mixture, the pressure tube and calandria tube contain Zr and  $\text{ZrO}_2$ , the coolant and moderator contain  $\text{H}_2$ , steam, and water. Light water properties are used for heavy water. Since the uranium may dissolve into the cladding to form the U-Zr-O mixture, decay heat may also be generated in the cladding material under accident conditions.

The energy equations for the heat transfer are written for each core node components. In this heat transfer model, a computational cell is comprised of four core material components plus coolant (water or steam) and moderator (water or steam) in the calandria vessel: 1) one ring of fuel pellets, 2) one ring of cladding, 3) pressure tube, 4) calandria tube, 5) water coolant, and 6) water moderator and gas in the calandria tank.

At high temperatures, Zr can react with water to produce  $\text{H}_2$ . These exothermic reactions can produce significant chemical power to accelerate the fuel cladding temperature and hence progression of a severe accident. This oxidation is assumed to take place at the Zr/ $\text{ZrO}_2$  interface leading to an increase in the oxide layer thickness. The oxidation calculation is employed for cladding, pressure tube, and calandria tube. After the fuel cladding ruptures, the code can model oxidation on either side of the cladding (a user option). It is assumed that in metal-water reaction, the heavy water steam behaves identically to the light water steam including the reaction energy. The kinetic rate law uses the Baker-Just model above  $1,875^\circ\text{K}$  and the Cathcart model below  $1,850^\circ\text{K}$ , and an interpolated rate between  $1,850^\circ\text{K}$  and  $1,875^\circ\text{K}$ .

#### (b) Phase 2

The fuel cladding may balloon due to pressurization as a result of the heating up the internal gases and fission products. When the fuel rod internal pressure exceeds the primary system pressure, the cladding forms a small leak. A typical approach for fuel failure is to assume that the fuel cladding fails if the average fuel element temperature is higher than a specified value. For example, a value of  $1,000^\circ\text{K}$  is used for LWR fuel, based on PHEBUS-FPT0 experimental results. This value is conservative for CANDU fuel, as it has a lower internal gas pressure. A more realistic value would be  $1,273^\circ\text{K}$ . Currently ISAAC uses the more conservative value of  $1000\text{K}$  (TCLRUP=1000.), though  $1,073^\circ\text{K}$  was the reference value in this benchmarking exercise. However this difference shows a negligible difference in the accident progression. The other way to find out whether the clad fails is to calculate the clad damage fraction based on Larson-Miller parameter first and then compare the clad oxide thickness against the minimum oxide thickness which needs to keep the clad intact. In ISAAC, 50% of Zr oxidation is assumed to keep the clad intact (*FZORUP*). After the cladding failure, cladding ballooning stops and fission products start to be released into PHTS.

Fuel channel failure is defined as a perforation of both the pressure tube (PT) and the calandria tube (CT), resulting in mass transfer between the pressure tube and the calandria vessel. This means by definition that both the pressure tube and the calandria tube have to be perforated for the fuel channel to fail. The mechanism for fuel channel failure depends on the PHTS pressures, some mechanisms being applicable at low PHTS pressure and others at high

PHTS pressure. At high pressure scenarios, high temperature fuel channel experiments have shown that non-uniform circumferential temperature distributions lead to pressure tube rupture. The calandria tube then fails due to pressurization and impingement of hot steam, etc. from the pressure-tube break. ISAAC models fuel channel failure with two options. The first option defines the channel failure when the pressure tube starts to balloon, considering the non-uniform deformation process (IPTRUP=1). The other determines the failure based on Larson-Miller calculation based on PT/CT average temperature assuming the uniform deformation of the pressure tube (IPTRUP=0). In the current calculation, the first option is used. When the fuel channel fails at high pressure, the perforated channel may whip and affect the adjacent intact channels. However, this dynamic effect is not considered in the current model. At low PHTS pressure, the fuel channels may fail because of a local melt-through or sagging of pressure and calandria tubes. For melt-through, the channel can be assumed to fail when a portion of the fuel channel exceeds the melting temperature for Zircaloy. Sagging is more complex. Again, a simplified approach is assumed that the fuel channel fails when the average temperature of the pressure tube and the calandria tube exceeds the Zircaloy melting temperature.

Fuel channel disassembly is another complex process, during which fuel and channel structural materials separate from the original fuel channel position and relocate downward, forming a suspended debris bed in the holding bin defined inside the calandria vessel. The corium in the suspended debris bed will be transferred to the calandria vessel bottom when either the molten corium formed in the suspended debris bed overflows to the calandria bottom or the core collapses. In ISAAC fuel channel disassembly starts with the channel sagging. When the average temperature of the pressure tube and the calandria tube exceeds a user specified value ( $TSAGKT=1,473^{\circ}\text{K}$ ), the corresponding channel sags. These sagging process of the heated channels causes less heat transfer to the moderator due to the piling up the sagged calandria tubes on the underneath channels.

ISAAC, hence, moves the sagged core material, as well as the fission products associated with, to holding bins or suspended debris bed and lets them heatup adiabatically by their own decay heat or allow heat transfer to the surrounding environment. ISAAC assumes the fuel material relocation by bundles. That is, when the channel fails, the integrity of each bundle is checked based on the average temperature of the pressure tube and the calandria tube using the Larson-Miller approach. ISAAC uses TPTMAX to control channel disassembly process and  $2,200^{\circ}\text{K}$  is currently used in this simulation. As the recommended value was  $1,473^{\circ}\text{K}$ , however, it may cause discrepancies with other benchmarking results. According to the new calculation with  $1,473^{\circ}\text{K}$ , the channel disassembly occurs about 1,200 s earlier than the current results. Though containment fails about 970 s later, calandria vessel fails about 10,000 s earlier in the new calculation. When more than 10 bundles are relocated, then the rest are assumed to relocate too. In addition, the bundles whose two adjacent bundles have been moved, will relocate to the holding bins, and the two end bundles will also relocate to the holding bins when all other bundles in the channel have been moved. The molten mass in the holding bin will subsequently relocate to the calandria vessel bottom.

In ISAAC, users define the number of holding bins for the suspended debris bed using *INVHDB* for the vertical (radial) locations (max. of 6) and *INHDB* for the horizontal (axial) locations (max. of 4) each loop. Hence maximum of 24 suspended debris bed locations can be defined per loop. Inside the suspended debris bed, heat transfer and oxidation process are modeled for the hydrogen generation and core collapse. The core materials,  $\text{UO}_2$ ,  $\text{ZrO}_2$ , Zr and U-Zr-O are assumed to be mixed as a new U-Zr-O mixture in the holding bins.

(c) Phase 3 & 4

Core collapse is a massive relocation of core material and some intact fuel channels within the moderator onto the bottom of the calandria vessel. When a large amount of core debris becomes lodged above the water level on top of the supporting channels (submerged channels) and the total debris mass exceeds the load-bearing capacity of the supporting channels, the supporting channels along with the debris bed can collapse. It is assumed that the suspended debris is carried by calandria tube rather than pressure tube since the latter could be hot and weak. Two main calandria tube failure mechanisms can be considered: pullout from the rolled joint and shearing of the calandria tube. The former failure mechanism, however, is the most dominant failure mechanism since it requires significantly less load. The suspended debris bed mass per PHTS loop, which will trigger core collapse, can be estimated from the load required to cause calandria tube pullout from the rolled joint. Currently 25 tons of corium in each loop is used as the critical mass [3]. Once the corium mass exceeds this critical mass of the supporting submerged channels, ISAAC assumes the total corium in the suspended debris bed to be relocated to the bottom of the calandria.

The corium bed formed in the bottom of the vessel interacts with water and the calandria vessel wall and the following phenomena are considered:

- Quenching of corium as it drops into water;
- Jet break-up and particle entrainment as corium drops into water pool;
- Oxidation ( $H_2$  generation) of entrained particles;
- The particulated and non-particulated (continuous) debris regions;
- The crust and the molten pool for the continuous region;
- The steel layer on top of the crust;
- Radiation from the corium bed to the calandria vessel walls;
- Possible steam explosion.

The heat transfer between the wall and the water outside the vessel, so called ex-calandria vessel cooling, is modeled in ISAAC. It considers forced and natural convection heat transfer and nucleate boiling heat transfer. For the natural convection, the correlation recommended by McAdams is used. When there is a forced convection flow, the heat transfer coefficient is calculated by the Dittus-Boelter correlation. If the forced water flow is low and the heat sink temperature is higher than the saturation temperature, the nucleate boiling heat transfer coefficient is calculated using the Rohsenow correlation. The calandria vessel can fail due to creep, over-pressurization or attack from molten corium. At present four failure criteria are modeled in ISAAC: 1) Failure of the calandria vessel wall by creep based on the Larson-Miller parameter, 2) Failure by high pressure through the rupture disks, 3) Failure of the vessel bottom wall due to debris impingement, and 4) Failure due to molten metal layer attack.

During a severe accident with core disassembly, water in the reactor vault can play an important role as an inherent heat sink outside the calandria vessel and impact core debris behavior within calandria vessel. However a boil-off of reactor vault water below the core debris bed level could eventually cause the failure of calandria vessel wall, causing the corium to relocate into the reactor vault bottom floor. While the reactor vault pressure increases due to the steaming of the vault water, the overpressure protection rupture disks open and a path is formed between the reactor vault and the RB. Currently, ISAAC defines the failure junction between the reactor vault and the boiler room and the junction opens when the pressure difference exceeds 68.9 kPa(d). The other failure mode is related with the ablation of the reactor vault concrete bottom or sidewall that facilitates a relocation of core debris out of the vault. Corium relocated onto the bottom concrete interacts with the concrete itself (molten corium-concrete interaction) and the concrete ablation process depends on water inventory as

well as the corium pool state. Currently ISAAC defines a corium failure junction between the reactor vault and the basement, and the junction opens when the downward ablation thickness exceeds the bottom floor thickness. Currently 2.0 m of ablation thickness is used as a criterion for concrete melt-through.

The failure to isolate the RB can lead to a direct release of radioactivity. A leak in the RB by failure to close the normally open lines (including airlocks) in contact with the environment opens a significant release pathway. The isolation failure also can be simulated with ISAAC by defining the junction between the RB and the environment with the opening area. Currently a leakage junction is defined in the input file for the source term evaluation during the intact RB sequences. According to the accident analysis approach for the source term assessment, 0.5% of reactor building volume in 24 h at a constant 124 kPa(g) reactor building pressure was considered to define the leakage area. The most dominant RB failure mode will be caused by the steam over-pressurization. Once the PHTS has voided (via break or boil-off), steam in the calandria vessel (as the first stage) and the reactor vault (as the second stage) gradually pressurizes the RB. Also non-condensable gases from the interaction of molten core material with the concrete basemat of the reactor vault (as the third stage) increase RB pressure. This pressurization process could last from hour to several days, depending upon stages and the effectiveness of engineered safety features. The local air coolers (LACs) are effective in condensing steam produced by decay heat emanating from the debris. Also the availability of the shield cooling system removes decay heat from the debris to avoid the RB pressurization (second stage). At the current analysis, two failure modes are taken into account. One is the containment equipment airlock seal failure at the pressure of 334 kPa(a) with 0.027871 m<sup>2</sup> area. Then the global failure is assumed to occur at 500 kPa(a) with the area of 0.1 m<sup>2</sup>.

#### 3.4.2.2. System idealization

##### (a) PHTS nodalization

The CANDU 6 PHTS comprises two loops and each loop has 190 fuel channels. The normal coolant flow passing the fuel channels in one loop follows a “figure-of-eight”, with adjacent channels having flow in opposite directions. Each PHTS loop, containing two steam generators, two PHTS pumps, two reactor inlet headers, and two reactor outlet headers, is modeled in ISAAC. Figure 3-175 shows the schematic of the ISAAC PHTS modeling. Though ISAAC handles each loop as a single control volume for a gas flow and pressure distribution, 14 nodes are defined for the PHTS components for the wall temperature and water level calculation. According to the PHTS information for the reference plant, shown in Figure 2-3, PHTS input data are prepared. Inlet and outlet feeders are also modeled in ISAAC. Because numbers, vertical lengths and the elevations of feeders depend on the definition of representative fuel channels in the core, these information is generated automatically in the code based on channel configurations defined by the user. Though the code identifies the feeder configuration from the channel information, users need to provide the inside diameter and the thickness of the inlet and outlet feeders, respectively. As a single variable is assigned for both loops, the channel configuration in both loops should be the same.

Circulation of two-phase mixture persists even after the primary pumps trip because of the buoyancy driven natural circulation. As the void fraction increases in the system, the phases eventually separate; the water settles on the bottom and the gas rises to the top. This results in formation of two separate water pools in each leg. From here on, two sets of mass and energy are tracked. After the phases separate, water pools are considered to be collapsed; boiled-up water levels are not considered. The water pool in each leg will split again when the water level falls below the bottom of the primary pump; the water in the pump bowl becomes

isolated, and its mass and energy will be tracked separately from now on. Lastly, when the water level in each leg falls below the headers, the water is split into multiple channels. From here on, the mass and energy of water in an individual channel are tracked. The process may reverse when the emergency core cooling injection fills up the primary system; multiple water pools merge into fewer pools until a single contiguous two-phase mixture circulates in the system.

#### (b) Core nodalization

In order to simulate 190 fuel channels in each loop, users may define representative fuel channels vertically (representing for 22 columns) and horizontally (for 22 rows of channels). In this report, 6 vertical and 3 horizontal core channels are defined in the ISAAC input for each loop. The 3 horizontal channels consider the channel power distributions of high, medium and low at the same elevation. The channel power distribution is shown in Figure 3-176, where four digits indicate the power in kW. High power channels are assigned to channels #1, #10, #4, #13, #7, and #16, and medium power to channels #2, #11, #5, #14, #8 and #17, and finally low power to #3, #12, #6, #15, #9, and #18. Table 3-11 shows the information of each representative channel including actual channel locations, numbers, average powers and peaking factors.

Figure 3-177 shows the core configuration of 9+9 type fuel channels. While the representative channels #1 to #9 are connected between RIH2 and ROH3, channels #10 to #18 are between RIH4 and ROH1. Three channels are defined at the same elevation with different power distributions (e.g., #1, #2, and #3). The same core configuration is defined in the other loop. Each fuel channel has 12 fuel bundles, and each fuel bundle is assigned to one axial channel node in the ISAAC input. As ISAAC tracks the channel behavior bundle-wise, 216 channel nodes (18 channels with 12 bundles) have their own characteristics of severe core damage progression. Once the fuel channel fails and starts to disassemble, the damaged bundles relocate into the holding bins (suspended debris beds). ISAAC could define up to 6 vertical bins and up to 4 axial bins, resulting in maximum of 24 suspended debris beds per loop. Figure 3-178 shows the location of 24 holding bins in the 9+9 type fuel channels. The relocation scheme can be controlled by the user with the ISAAC input parameters. In this report, vertically 6 and axially 4 holding bins are defined for the fuel material relocation after core damage.

Each fuel channel consists of 37 fuel elements arranged in four fuel-element rings (central fuel element, inner, intermediate, and outer rings), pressure tube, calandria tube, coolant and moderator. Inside the pressure tube, for each axial node, 37 fuel rods are represented by a single fuel pellet with clad, as shown in Figure 3-174.

#### (c) Calandria modeling

The calandria vessel module calculates the thermodynamic properties and the rates-of-change of dynamic variables in the calandria vessel. The module calculates a number of key quantities:

- Thermal-hydraulic variables in the calandria such as the pressure, gas and water temperatures, water level, steaming from the heavy water, flows in and out of the calandria vessel, and heat losses from the calandria to the shield tank;
- Modeling of corium, water, and calandria vessel wall heat transfer such as the quenching of corium dropping into the calandria water pool and oxidation of entrained particles, modeling of corium debris bed in the bottom of the vessel, and modeling of several calandria vessel failure mechanisms;
- Fission product transport in the calandria such as the source of fission products flows from ruptured calandria tubes and removal due to flows from the calandria vessel through

either the rupture valve or failed calandria vessel, the transport of fission product within a compartment such as depositing on heat sinks or water pools.

ISAAC also models a two-dimensional temperature distribution in the calandria vessel walls. Two types of calandria vessel walls are considered: a flat wall type represents the front and back face of the vessel (the tube sheets), and the other wall type represents the cylindrical shell of the vessel. Both types of walls are sliced circumferentially into 15 nodes from the vessel bottom to the top along the elevation levels. ISAAC represents the calandria vessel wall thickness with three radial nodes, and calculates the inner and outer surface temperatures for the heat transfer inside and outside the calandria vessel. The vessel wall failure is modeled based on temperatures and pressure differences.

(d) Steam generators modeling

Though ISAAC can model the steam generator secondary with two-region nodalization scheme, the current analysis uses typical one control volume model with a collapsed downcomer water level and a boiled-up level in the tube bundle region. Also four steam generators are connected through the main steam common header, resulting in the same pressure behavior among the steam generators.

A number of parameters for the primary and secondary sides of the steam generator are used in the ISAAC parameter file to describe the steam generator design. The parameters include: the pressure set points for the main steam safety valves (MSSVs), total volume of the primary side, total number of U-tubes, inside diameter of the U-tube, diameter of tube sheet, height of the shell above the tube sheet, and a table of volume versus height in the secondary side.

(e) Reactor building (containment) nodalization

As ISAAC adopts the general containment model, users may define the RB compartments for their analysis purposes. Based on the CANDU 6 reference plant containment elevation (refer to Fig. 3-179), Figure 3-180 shows the containment nodalization with elevation data: basement (compartment 1), reactor vault (2), front fueling machine room (3), rear fueling machine room (4), moderator room (5), access area (6), boiler room (7), upper dome (8), dousing tank (9), degasser condenser tank (10), two end-shields (11 & 12) and the environment (13). Flows of water, steam, non-condensable gases and molten corium between the compartments, are defined through a junction connecting two compartments. 19 junctions are defined, most of which are normally connected except for the failure junctions that open when a certain condition such as a RB failure (J18) or concrete floor melt-through (J14) is satisfied.

The RB surface area and the compartment volume are important to evaluate the RB pressure behavior. In ISAAC, distributed heat sinks for the RB walls and floors, and the lumped heat sinks for the steel structures are defined. As shown in Figure 3-181, 25 distributed heat sinks and 12 lumped heat sinks are used in this analysis. Total surface area of the concrete used in current study is 22,797 m<sup>2</sup>, and the total surface area of the structural steel is 8,648 m<sup>2</sup>. The total “free” volume of the RB compartments was 51,325 m<sup>3</sup>. And the steel ball mass in each end shield is around 88 tons and the total of 820,000 kg of steel is located in the containment building [13].

(f) Pressure and inventory control system modeling

The major equipment in the CANDU6 pressure and inventory control (P&IC) system to achieve the pressure and inventory control of the PHTS system are a pressurizer, liquid relief valves (LRVs), a degasser condenser tank (DCT), feed pumps, feed and bleed valves. The pressurizer is connected to one of the reactor outlet headers in each loop. The line connecting the pressurizer with each reactor outlet header contains a motor-operated isolation valve,

which is closed automatically upon receipt of the loop isolation signal in case of a LOCA. Loop isolation is initiated on a pressure set point of 5.516 MPa(a) (PLOCA) with a valve closure time (TDPSIS, 20 s is used), which are ISAAC inputs.

For the high pressure scenarios like a station blackout, the PHTS pressure is mainly controlled by LRVs and degasser condenser tank (DCT). The LRVs are air-operated with backup instrument air, and are designed to fail open. Normally, this back-up air supply should maintain the valves in operation for two hours following power loss (for example, in the case of a station blackout) and loss of normal instrument air. During the station blackout sequence, the LRVs fail open and the steam and water flow into DCT. In this analysis, however, LRVs are assumed to open at their set point of 10.16 MPa(a) with the area of  $7 \times 10^{-4} \text{ m}^2$  to allow the flow rate of 26.7 kg/s to the containment. The DCT is not considered here.

### 3.4.3. Analysis results

The station blackout (SBO) sequence is chosen for the benchmarking analysis. As there is no electric power available for the safety systems, all the cooling systems like a shutdown cooling, moderator cooling, shield cooling and an emergency core cooling fail initially. Also the main and auxiliary feedwater systems are unavailable and a crash cooldown operation is not credited. Main steam safety valves open at their set points to relieve the pressure from the secondary side. Though the liquid relief valves in the PHTS are designed to fail-open, they are assumed to open when the PHTS pressure reaches their set points, as no degasser condenser tank is modeled in this analysis. The passive containment dousing sprays are not credited during a station blackout accident. Local air coolers are assumed to be unavailable and all the operator interventions are not credited. The accident was simulated with ISAAC 4.02 and the major event timings are summarized in Table 3-12.

#### 3.4.3.1. Phase I

The loss of all electrical power causes an immediate reactor shutdown and only decay power is generated from the fuel. The PHTS pressure, which is shown in Figure 3-182, drops from the beginning after reactor scram and later increases due to less heat transfer to the steam generators as the feedwater stops. The peak pressure is controlled at the set point of LRV (10.16 MPa(a)) and the LRVs are first open around 6,200 s (1.7 h). As the LRVs were assumed to remain open, the pressure stays below the LRV set point. The fuel channel fails at around 10,178 s (2.8 h) into the accident when the pressure tube starts to balloon, and the PHTS pressure drops suddenly at this time. After a large blow down from the PHTS to the calandria tank through the failed tube, the pressure in the PHTS decreases to the calandria pressure. Pressurizer is isolated at 10,202 s (2.8 h) due to the LOCA signal generated when the PHTS system pressure drops below 5.516 MPa(a) and it shows the independent pressure behavior from the PHTS. The PHTS water (or steam when there is no water) temperature is given in Figure 3-183.

The pressure, water levels and water inventories in the steam generator are shown in Figs 3-184, 3-185, and 3-186, respectively. As a result of the heat transfer from the PHTS, the steam generator pressure increases and stays at the set point of MSSVs (5.11MPa(a)) until the fuel channel failure occurs at around 10,178 s (2.8 h). The steam generators lose water inventory through the MSSVs and they are depleted around 7,446 s (2.1 h). Figure 3-187 shows the amount of heat transferred to the steam generators. The jump around 85 s is caused by a different calculation path in the code after there is no coast-down flow into the steam generators following a RCP trip. It will be fixed in the next version of ISAAC.

As the steam generator water level goes down (refer to Figure 3-185), the primary heat transport system fluid heats up and the pressure of PHTS increases to the LRVs relief set

point (10.16 MPa(a)) after 6,217 s (refer to Fig. 3-182) and PHTS subsequently loses water inventory through the LRVs to the containment. Figure 3-188 shows the PHTS water masses. Initial water inventory in the PHTS including pressurizer water mass is about 113 tons and the inventory starts to decrease following the LRVs opening at 6,217 s. The loops are isolated around 10,202 s just after pressurizer is empty following the channel failure. The water levels in each fuel channel are shown in Figure 3-189. Initially homogeneous two-phase flow is circulating around the PHTS. When the void fraction becomes larger than 0.5 (around 7,500 s), the PHTS phases become separated and non-equilibrium thermodynamic model is turned on. The sudden drop of the fuel channel water levels around 7,500 s is caused by this modeling assumption in ISAAC. The channel depletion timings in each fuel channel depend on water masses left in the feeders which are connected to the corresponding fuel channels. Figure 3-190 shows average void fractions in each loop. The steam and water flow rates through the LRVs are given in Figure 3-191. Mostly water flows out at the beginning and then steam goes out after phase separation. In this simulation, LRVs are assumed to remain open once they open at their set point.

Figures 3-192 and 3-193 show the central fuel bundle (6th) temperatures in channel 1 (top-most) of both loops (refer to Fig. 3-177), respectively, as a function of time. The pressure tube temperature follows the fuel/cladding temperature behavior. The coolant of channel #1 in both loops is completely boiled off around 11,496 s and 10,584 s, respectively (refer to Table 3-12). Hence the accident progression up to around 11,000 s can be categorized as Phase 1, which covers the accident to the channel dryout. The fuel temperatures drops down after 16,000 s, and it means fuel material at that channel is completely relocated.

#### 3.4.3.2. Phase 2 & 3

Phases 2 and 3 cover the accident progression from fuel channel dryout to core collapse, and to the calandria vessel failure, respectively. The channel dryout will cause channel heatup and temperature increase of the fuel elements. Figure 3-192 and 3-193 shows the temperature increase in the fuel, sheath, and pressure tube after 11,000 s. The sudden drop of PHTS pressure around 10,000 s in Figure 3-182 is also related with channel dryout, causing the fuel channel failure due to non-uniform ballooning of the pressure tube.

The severe core damage and the subsequent core material relocation are closely related with the moderator behavior in the calandria vessel. The moderator temperature and the pressure in the calandria vessel initially increase due to both the lack of moderator cooling and the heat transfer from the core (PHTS) to the water through the calandria tubes and gamma-ray heating from the core. Figures 3-194 and 3-195 show the moderator/steam temperatures and calandria pressure, respectively. Calandria vessel pressure is controlled initially with the bleed valves and then after 6,000 s it keeps increasing until rupture valves open at 10,178 s following the fuel channel failure. Initially, the moderator water in the calandria was subcooled, and the moderator gets saturated at about 12,000 s. The moderator level and inventory are indicated in Figures 3-196 and 3-197, respectively. Though moderator gets depleted around 38,271 s, the moderator level remains around 1m because of corium pool volume in the calandria vessel. When the fuel channel fails at 10,178 s, the calandria vessel rupture disks also fail and moderator starts to be discharged to the containment boiler room. Figure 3-198 shows the water and steam flow rates through the rupture disks. The heat transfer rates from the fuel channel to the moderator and to the steam in the calandria are shown in Figure 3-199 and the total heat transferred to the moderator in Figure 3-200.

When the moderator level goes down, the uncovered fuel channel starts heating and relocation process begins. As Figure 3-201 indicates the maximum fuel temperature regardless the location, the temperature peaks mean the relocation timing with time. Figures 3-202 and 3-203 show the corium mass behavior in the core and in the calandria vessel, respectively. The

relocation of molten material from the core to the suspended debris bed starts from around 15,840 s in both loops. The mass difference between the leaving mass from the channel and the staying mass in the suspended debris bed goes to the calandria vessel bottom and Figure 3-203 shows the summation of collected mass from both loops. In this case most of corium is relocated to the calandria vessel by 50,000 s gradually without collapsing, because the corium mass collected in the suspended debris bed is less than the global collapsing failure criteria of 25 tons. Finally about 134 tons of corium is delivered to the calandria vessel bottom before calandria vessel fails at 160,794 s (44.7 h). Figure 3-204 shows the corium temperature in the vessel. As the vessel fails at 160,794 s, the corium temperature after failure is meaningless.

The calandria vessel wall temperatures at lower nodes (3rd & 4th) and upper nodes (12th & 15th) are shown in Figure 3-205. The wall temperatures changes along with corium relocation into the vessel and the water levels inside and outside the calandria. The 3rd node fails at 160,794 s.

#### 3.4.3.3. Phase 4

Phase 4 covers the accident progression after calandria vessel failure. The calandria vessel failure is closely related with the shield water inventory in the reactor vault. The water masses in the reactor vault and in the calandria are shown in Figure 3-206. Though moderator is depleted at 38,271 s, the calandria is still intact thanks to the heat transfer to the shield water surrounding the vessel. However, the shield water also evaporates after moderator depletion. When the bottom of the vessel is uncovered, then no more ex-calandria cooling is available and vessel fails at 160,794 s.

The containment pressure, which is shown in Figure 3-207, depends on the accident progression inside and outside the calandria vessel. When the moderator provides steam to the containment due to fuel channel failure and moderator evaporation, the containment pressure increases. After the calandria tank moderator was depleted at 38,271 s, the containment pressure decreases for a short period until steam is produced from the reactor vault after 52,200 s, causing containment pressure to rise again. The containment fails at 80,697 s (22.4 h) when the pressure reaches at 324 kPa(a). The containment pressure shows another peak at 160,794 s following calandria vessel failure. .

The corium masses in the reactor vault and in the basement are shown in Figure 3-208. After calandria vessel failure, corium mass of about 134 tons is relocated into the reactor vault floor and about 700 tons of corium and concrete slags are delivered to the basement around 378,904 s (105.3 h). Figures 3-209 and 3-210 show the corium temperature and the concrete ablation thickness, respectively. Though the reactor vault floor thickness is 2.45 m, it is assumed that 2 m ablation causes concrete melt-through.

The compositions of containment atmosphere in the steam generator boiler room are shown in Figure 3-211. The hydrogen mole fraction reaches about 16.1% around 287,500 s. The containment gas and wall temperatures at the boiler room are shown in Figure 3-212. The temperature peaks are related with the calandria vessel failure and reactor vault melt-through.

In-core hydrogen can be generated from the oxidation of fuel sheath (clad), pressure tube, calandria tube, and from the suspended debris bed. Figure 3-213 shows the mass of hydrogen generated from the core in Loop 1. The similar mass of hydrogen is generated from Loop 2. It can be noted that about 58% of the hydrogen comes from the suspended debris bed in this scenario. That is, the unoxidized Zircaloy relocated into the suspended debris bed is exposed to the steam and generates hydrogen. Hydrogen also can be generated from the unoxidized metal in the corium relocated onto the reactor vault. Figure 3-214 shows the amount of hydrogen coming from molten corium-concrete interaction (MCCI) as well as inside the

calandria vessel. About 1,960 kg of hydrogen is generated from the reactor vault, while about 504 kg is coming inside the calandria vessel.

Regarding the fission product release, Figure 3-215 shows the release fraction of the noble gas to the environment. When the containment failed around 80,697 s, most of the noble gas is released outside the containment. In the meantime, about 1.2% of the initial inventories of CsI and CsOH are released to the environment. The released mass fractions of MoO<sub>2</sub>, SrO and TeO<sub>2</sub> to the environment are given in Figure 3-216. The distribution of CsI at both loops, calandria and containment, which is shown in Figure 3-217, indicates that about 27% is deposited in the PHTS loops and the rest kept inside the containment.

TABLE 3.11. CHARACTERISTICS OF REPRESENTATIVE FUEL CHANNELS BASED ON CORE POWER DISTRIBUTION FROM FIGURE 3-176

Channel No	Rows included	Columns included	No of channels	Power distribution	Avg. power (kW)	Peaking factor
1	D-F	12-15	10	High	6245.1	1.277
2	A-F	12-19	25	Medium	4836.1	0.989
3	A-F	13-14, 17-20	7	Low	3269.7	0.668
4	J-L	12-19	23	H	6395	1.307
5	J-L	19-21	7	M	5190	1.061
6	J-L	22	3	L	3406	0.696
7	P-S	12-17	18	H	6439	1.316
8	P-S	15-21	17	M	5225	1.068
9	Q-S	21-21	3	L	3425	0.700
10	G-H	12-17	11	H	6427.8	1.314
11	G-H	15-21	8	M	5248.3	1.073
12	G	21	1	L	3491	0.714
13	M-O	12-19	23	H	6486	1.326
14	M-O	19-21	7	M	5195	1.062
15	M-O	22	3	L	3384	0.692
16	T	12-14	3	H	6008	1.228
17	T-W	12-18	16	M	4436	0.907
18	T-W	13-14, 17-18	5	L	2936	0.602
			Sum: 190		Avg: 4891.3 Sum: 88043	Avg: 1.0

TABLE 3.12. LIST OF SIGNIFICANT TIMING OF EVENTS/OTHER SIGNIFICANT RESULTS FOR SBO SCENARIO

Time (hr)	Time (s)	Events
	0	Class IV and Class III Power loss
	20	Turbine stop valves closed
	0	Reactor trips
	46	First opening of MSSV
0.23	817	Calandria vessel bleed valve opens (delta P=29.7kPa(d))
1.73	6217	LRVs open for the first time, PHTS Loop 1
1.73	6217	LRVs open for the first time, PHTS Loop 2
2.07	7446	SG secondary sides are dry, Loop 1
2.07	7446	SG secondary sides are dry, Loop 2
2.83	10178	Pressure and calandria tubes are ruptured Loop 1 Calandria vessel rupture disks #1-4 open
2.83	10186	Pressurizer empty
2.83	10202	Pressurizer isolated
2.84	10205	Reactor vault rupture disk open
2.85	10248	Pressure and calandria tubes are ruptured Loop 2
2.94	10584	At least one channel is dry, Loop 2 (complete boil-off)
2.95	10615	Fuel sheath failed in fuel channel 1, bundle 6, Loop 2
3.19	11496	At least one channel is dry, Loop 1 (complete boil-off)
3.33	12000	Moderator reaches saturation temperature
4.40	15837	Beginning of the core disassembly, Loop 1
4.40	15841	Beginning of the core disassembly, Loop 2
10.6	38271	Water is depleted inside calandria vessel
14.5	52215	Water in calandria vault reaches saturation temperature
16.1	57904	Hydrogen/CO burning predicted in containment node #1
22.4	80697	Containment failed
42.0	151254	Core mass all gone (loop 1) to calandria vessel bottom
42.0	151319	Core mass all gone (loop 2) to calandria vessel bottom
44.7	160794	Calandria vessel failed
-	Not occurred	Quenching of debris occurred in calandria vault
49.3	177630	Water is depleted inside calandria vault
52.8	190130	Molten corium-concrete interaction begins in calandria vault
105.3	378904	Calandria vault floor failed because of concrete ablation (2.4m ablation)
Total amount of Hydrogen release “in-vessel” (in PHTS and in Calandria Vessel”) in PHTS loop 1		252 kg
Total amount of Hydrogen release “in-vessel” (in PHTS and in Calandria Vessel”) in PHTS loop 2		252 kg
Total amount of Hydrogen release “ex-vessel” (outside of the Calandria Vessel”)		1960 kg
Total amount of noble gases released to environment (initial mass of 57.7 kg)		57.7 kg
Total amount of Cs and I released to environment (initial CsI mass of 5.24 kg)		0.063 kg

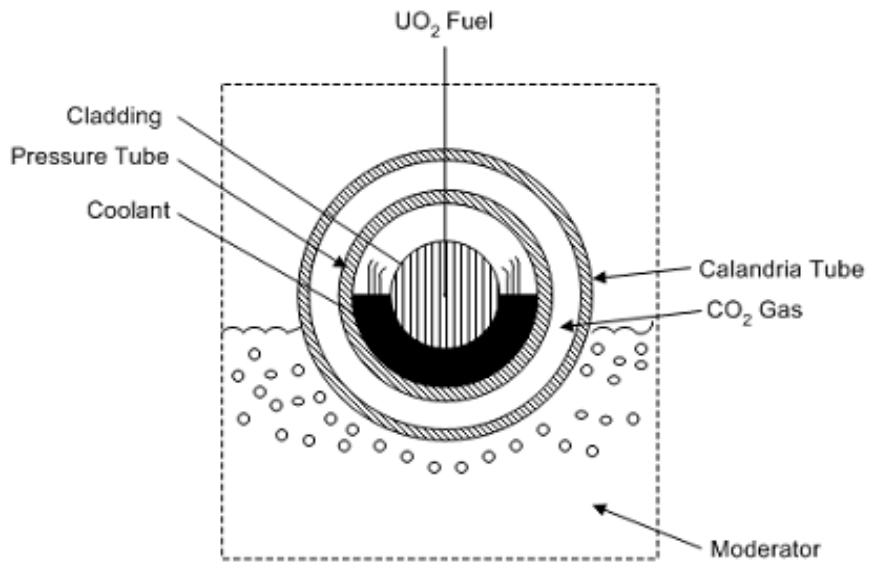
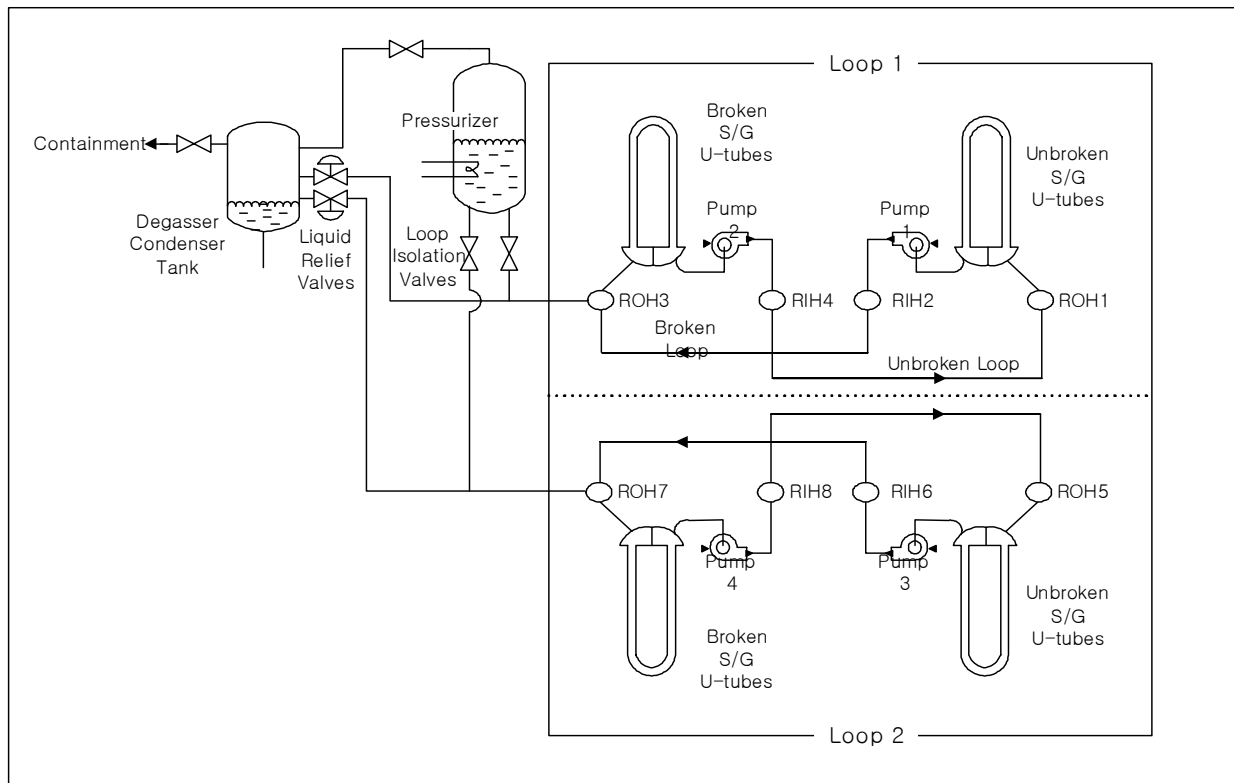


FIG. 3.174 Representative fuel channel configuration in ISAAC.



WS970211.VSD 97-02-20

FIG. 3.175. Schematic diagram of ISAAC modeling for primary heat transport system

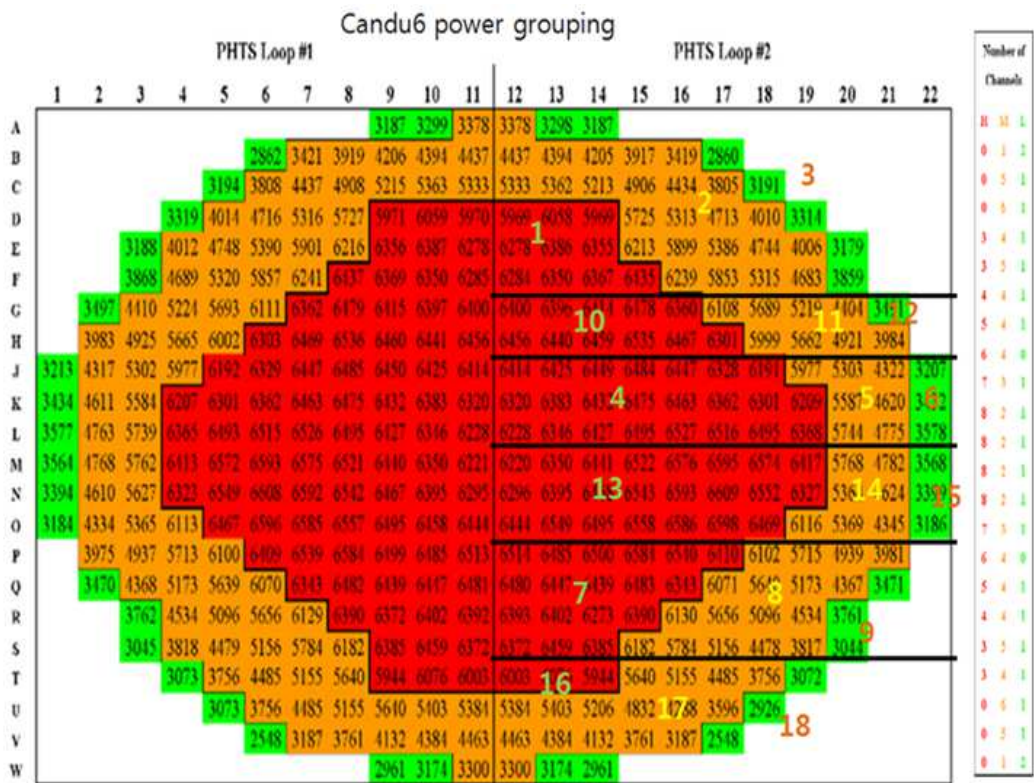
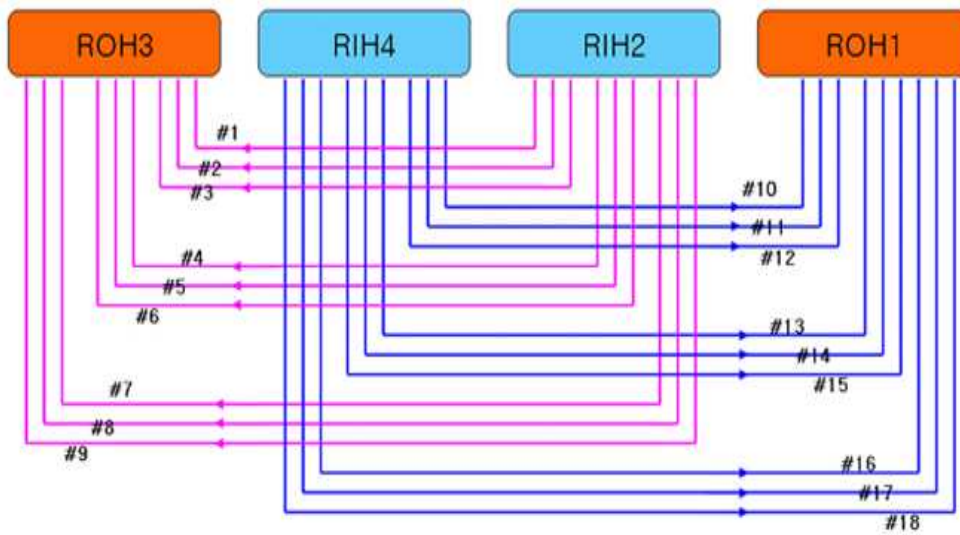
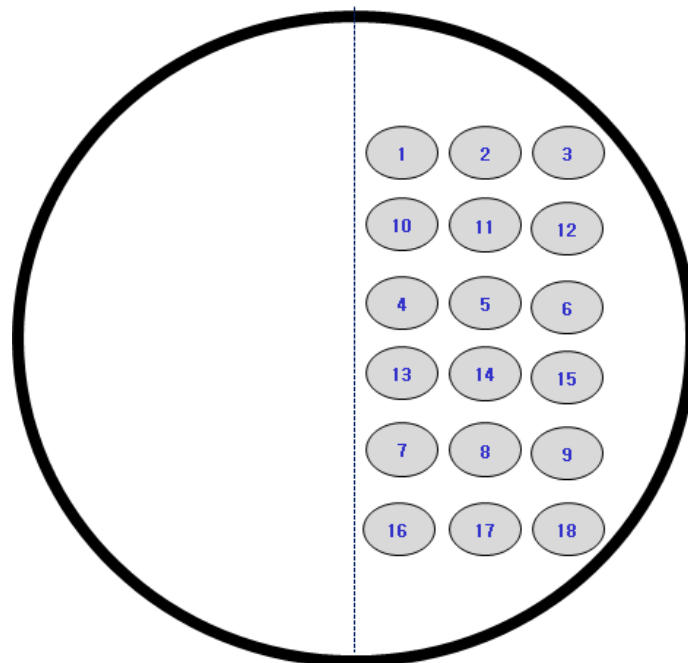


FIG. 3.176. Channel power distribution and grouping in the CANDU reference plant.



(a) Configuration of representative fuel channels (side view).



(b) Configuration of representative fuel channels (from F/M room)

FIG. 3.177. Core configuration of 9+9 fuel channels per loop.

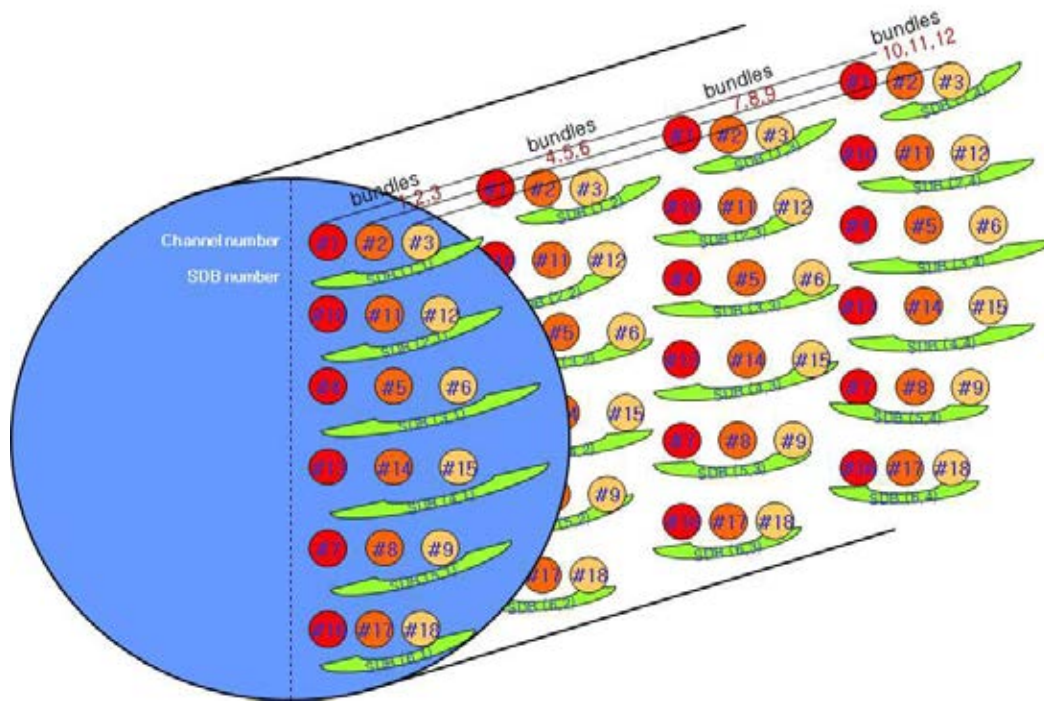


FIG. 3.178. Suspended debris bed locations defined for 9+9 type fuel channels in ISAAC.

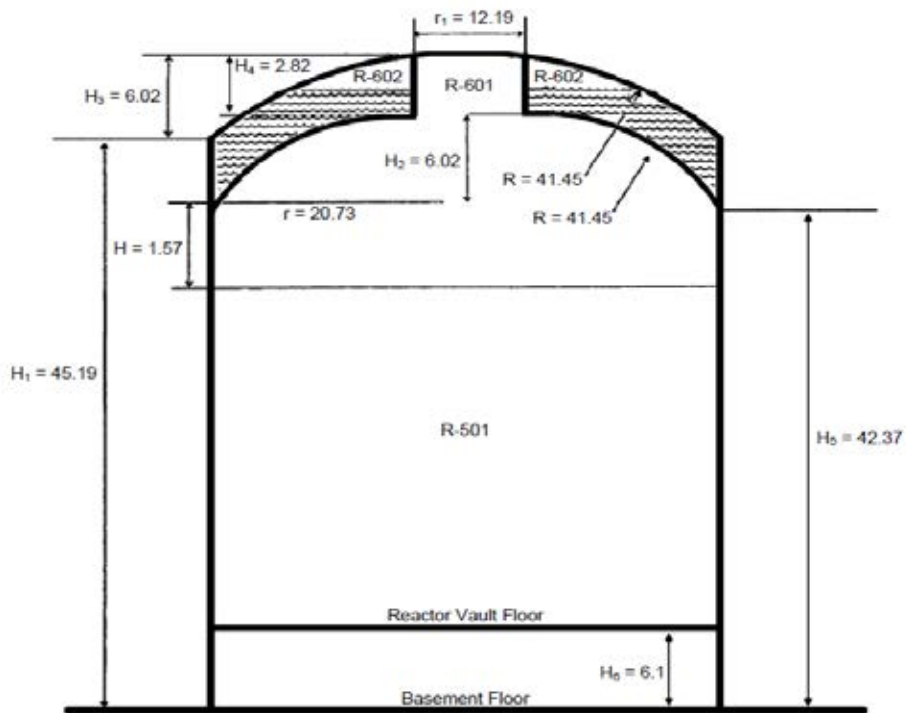


FIG. 3.179. CANDU6 Reference plant containment elevations.

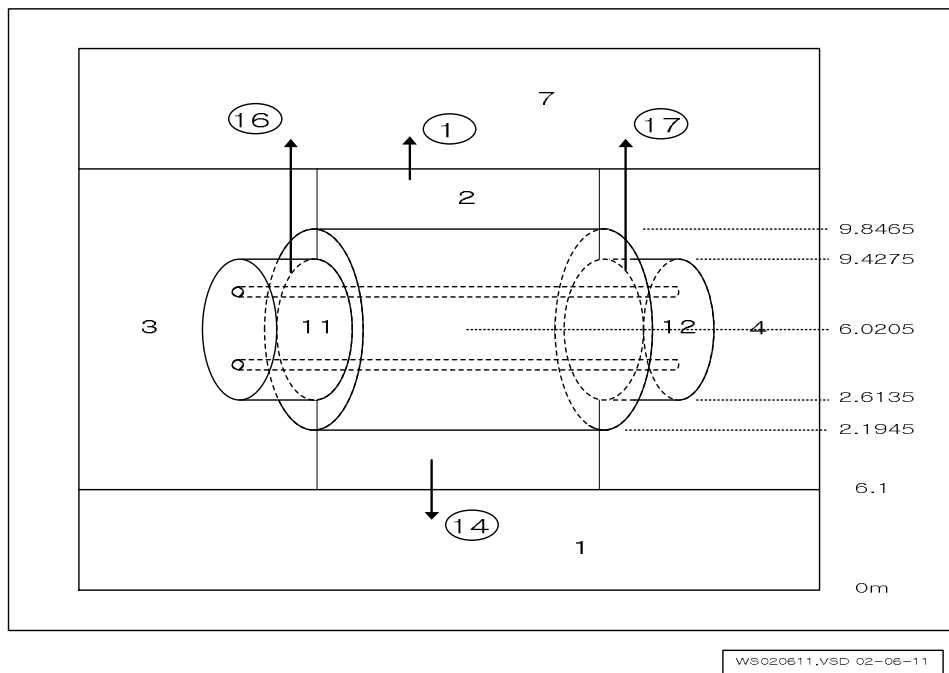
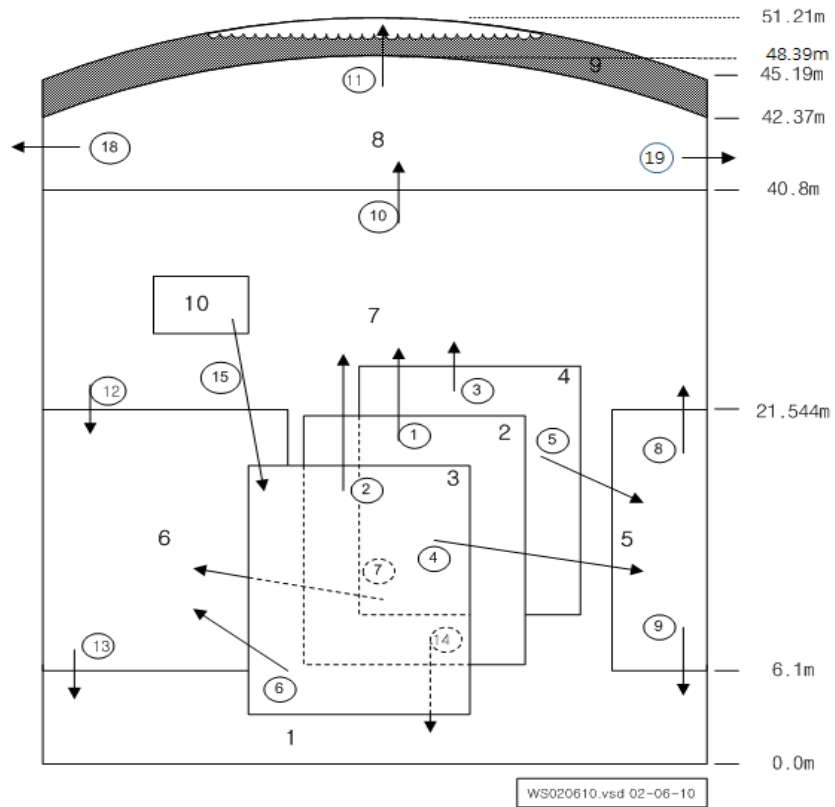


FIG. 3.180. Containment nodalization for reference CANDU6 in ISAAC.

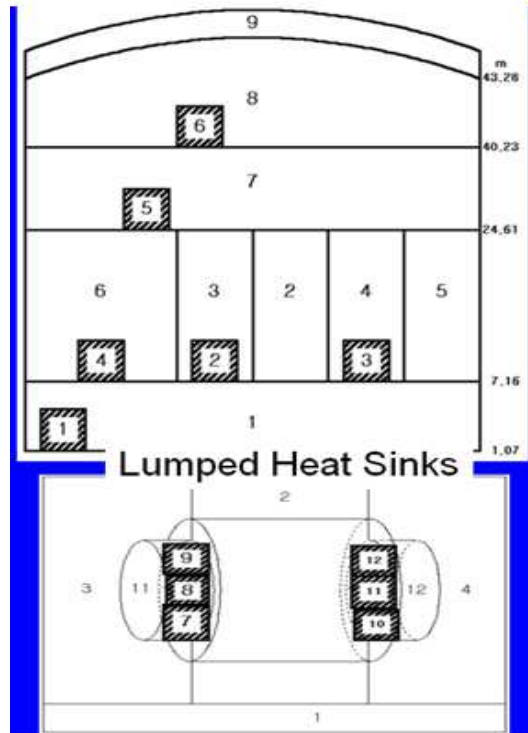
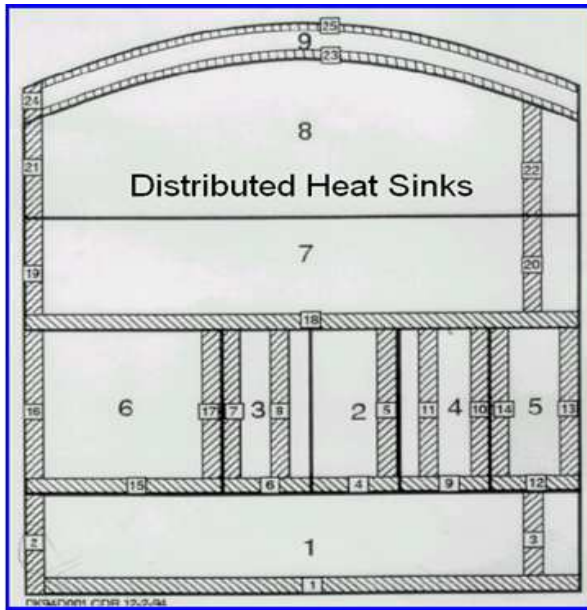


FIG. 3.181. Definition of containment heat sinks.

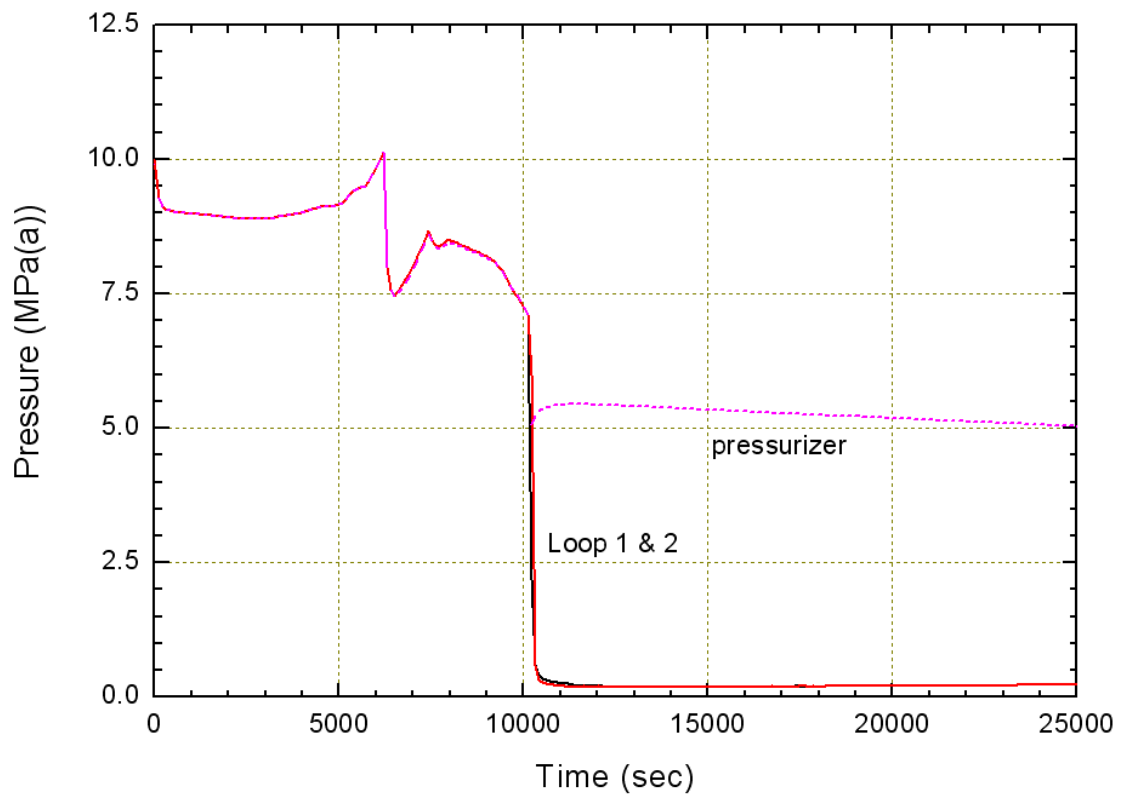


FIG. 3.182. Primary system and pressurizer pressures (0 - 25,000 s).

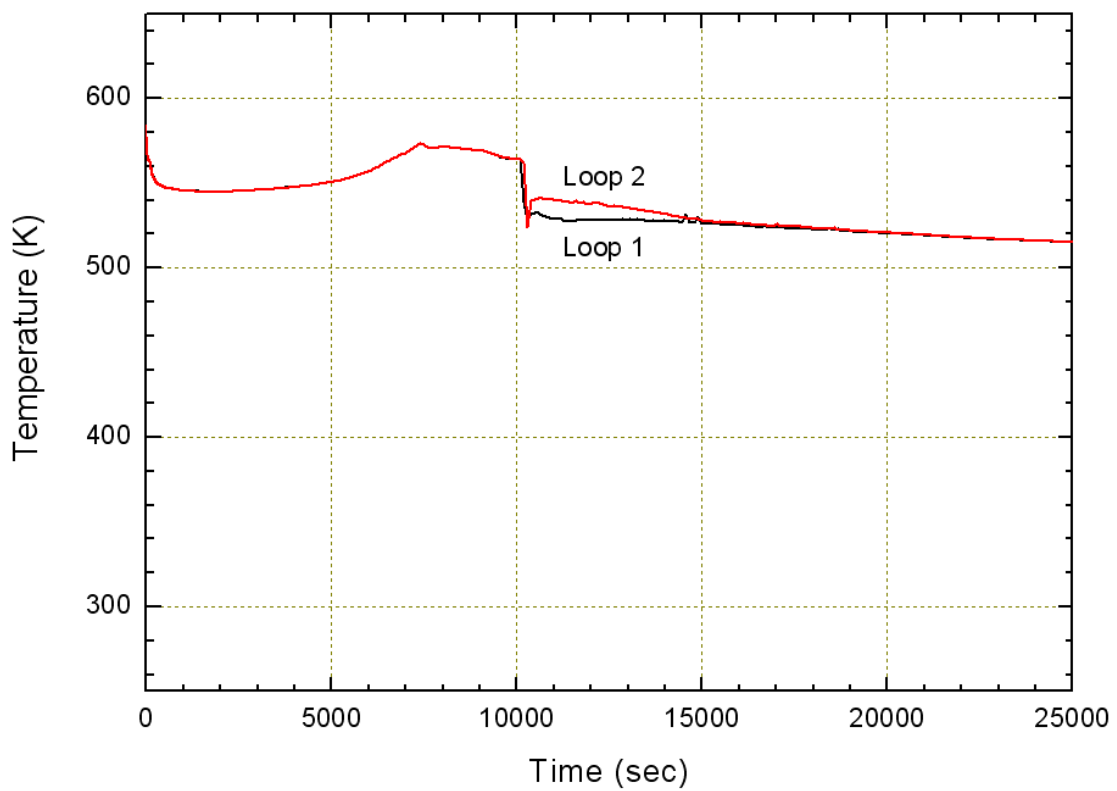


FIG. 3.183. Primary system average temperature (0 - 25,000 s).

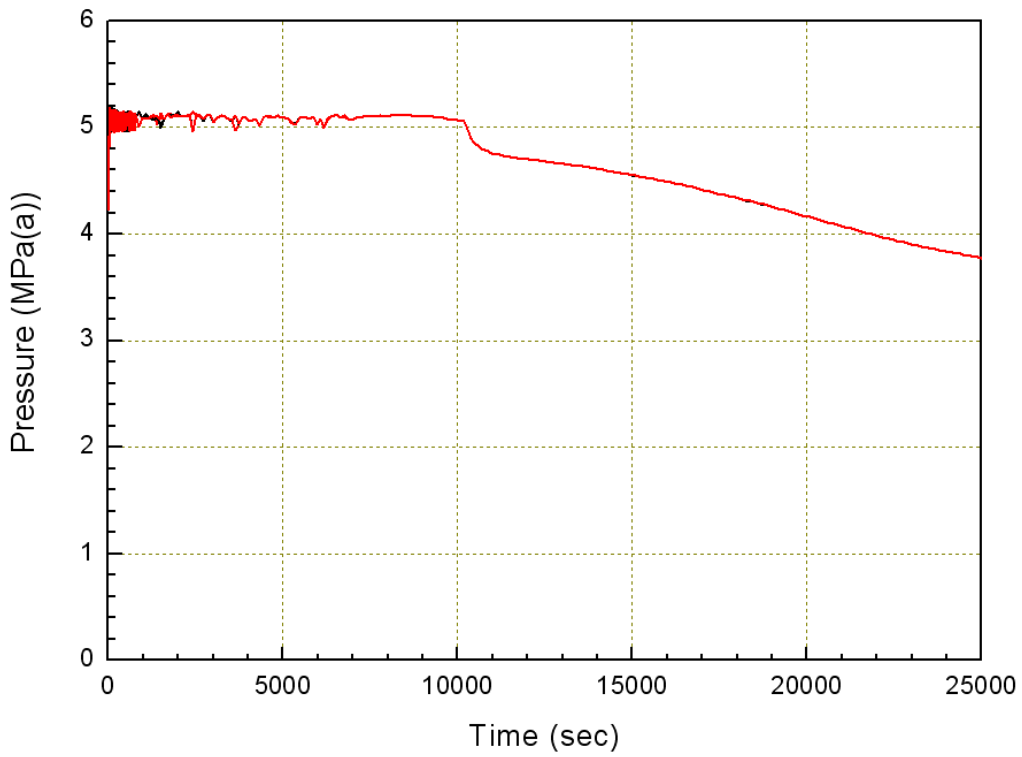


FIG. 3.184. S/G Secondary side pressure for PHTS loops 1 & 2 (0 - 25,000 s).

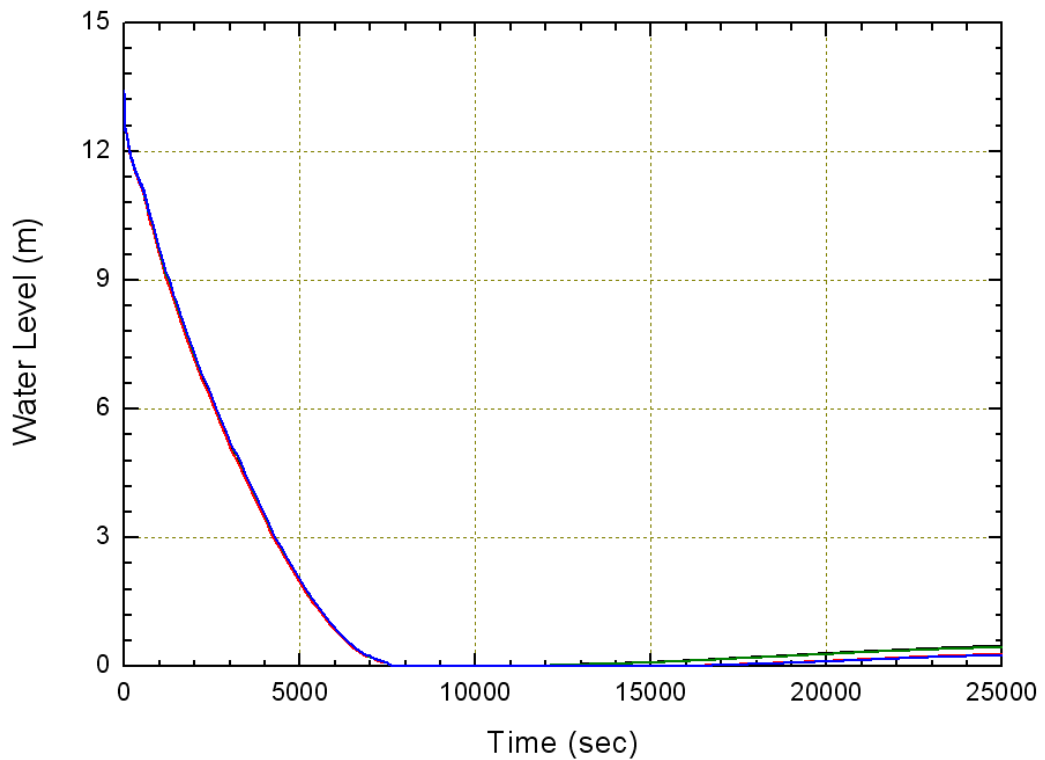


FIG. 3.185. S/G Water levels for PHTS loops 1 & 2 (0 - 25,000 s).

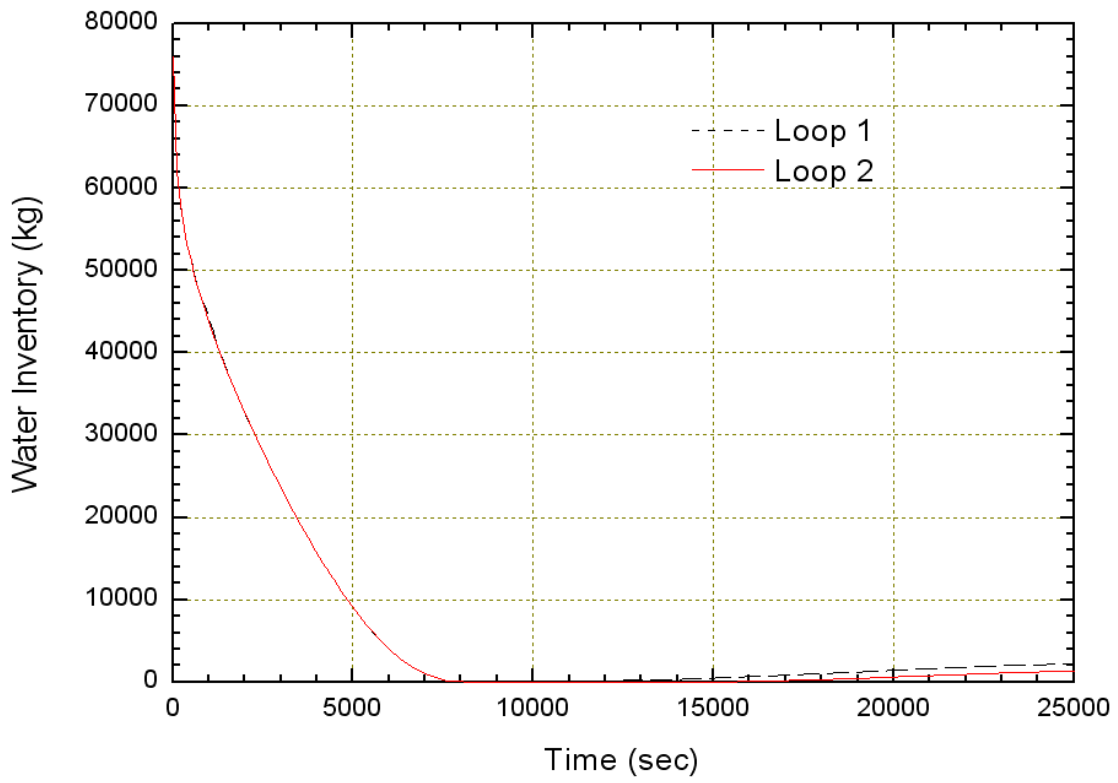


FIG. 3.186. S/G Water inventory (0 - 25,000 s).

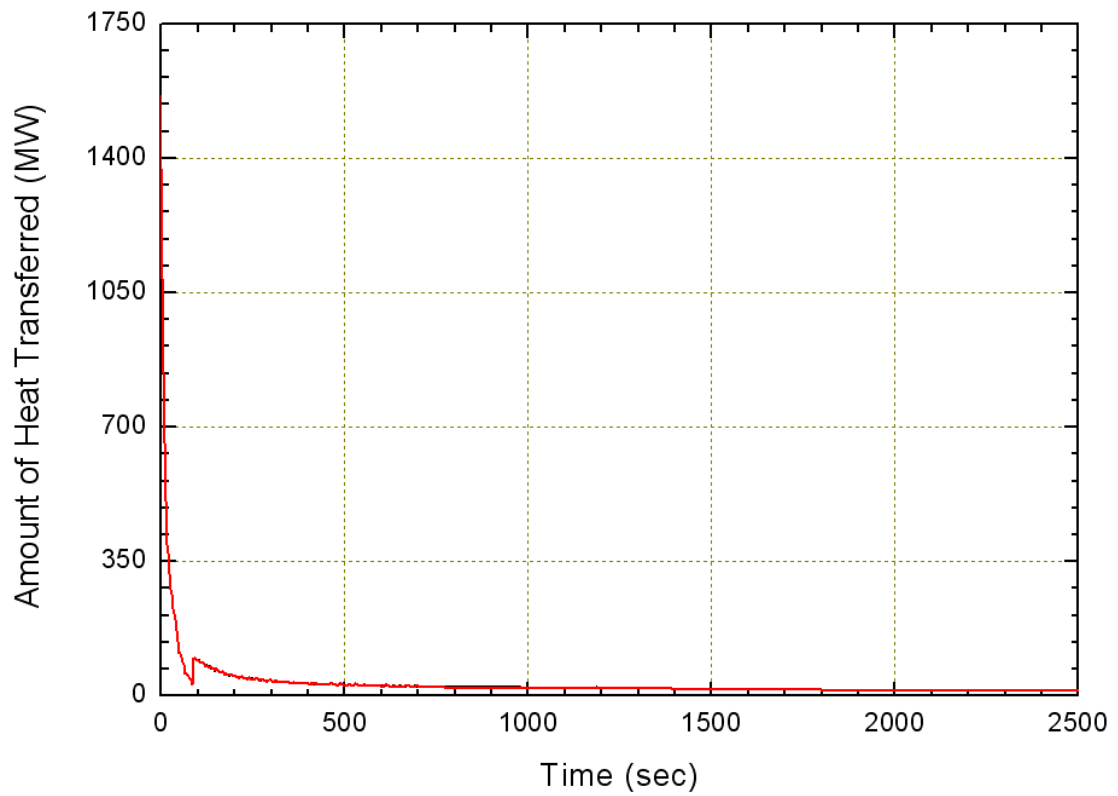


FIG. 3.187. Heat to steam generators (0 - 2,500 s).

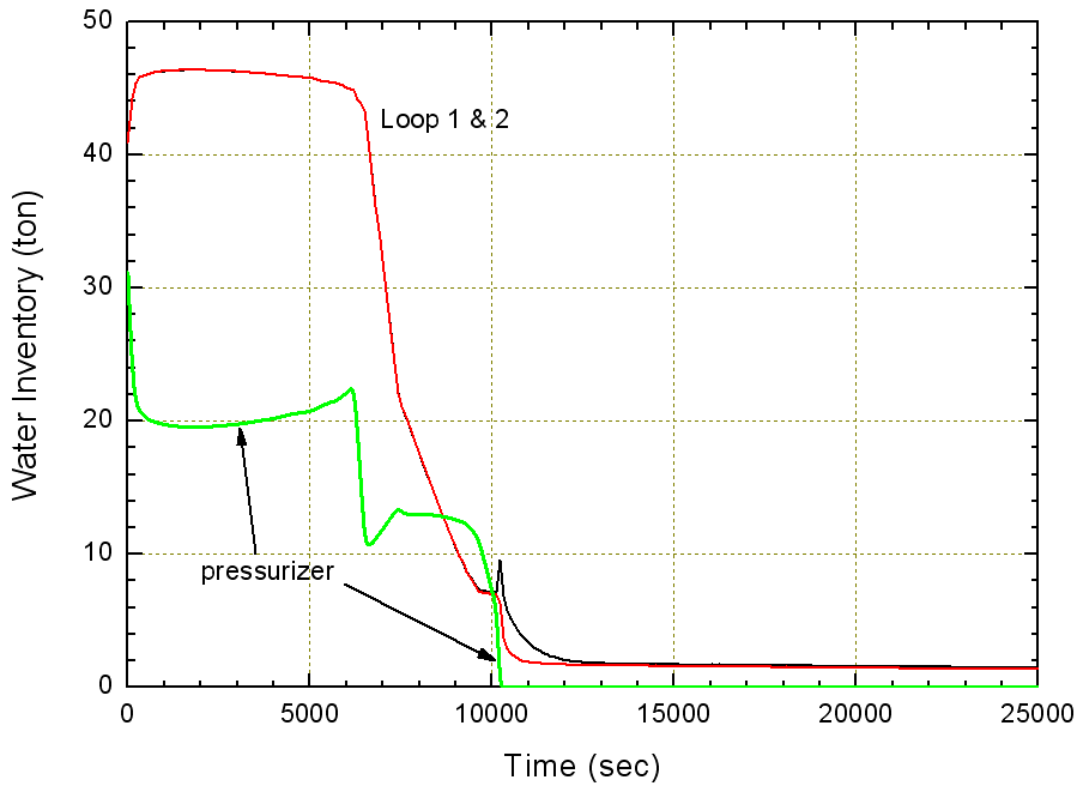


FIG. 3.188. PHTS Water inventories in loop 1, 2 and pressurizer (0 - 25,000 s).

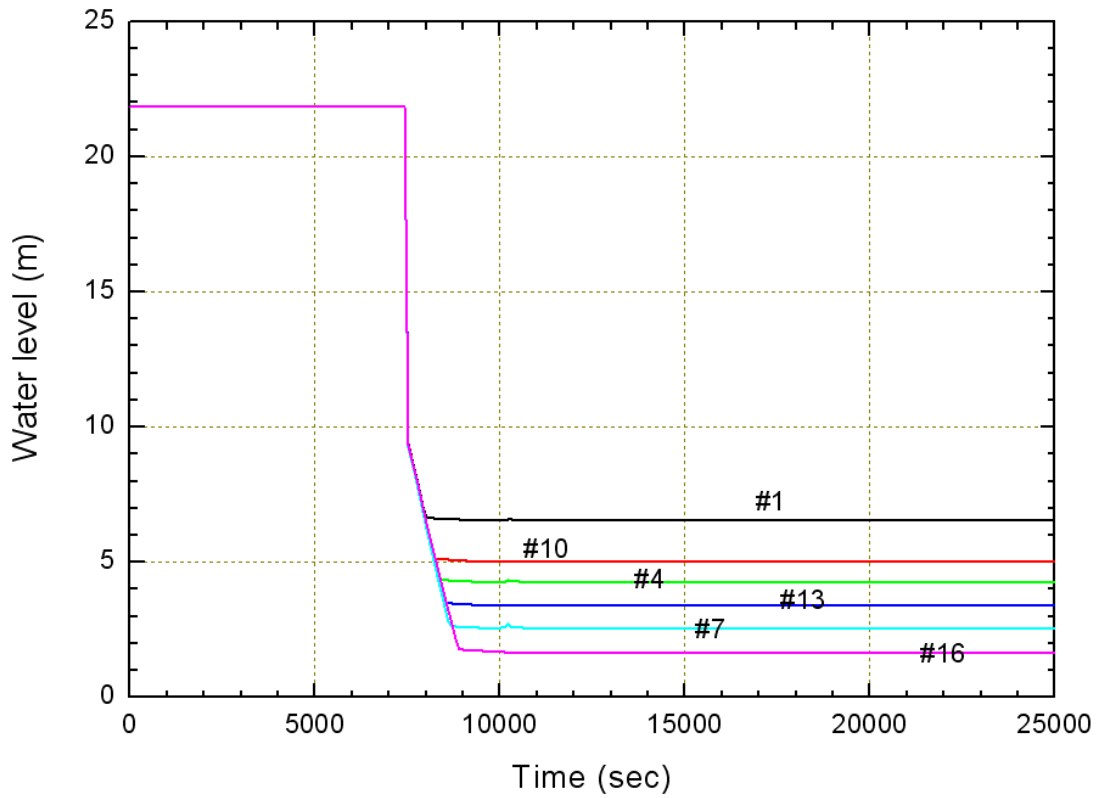


FIG. 3.189. PHTS Water levels in fuel channels, Loop 1 (0 - 25,000 s).

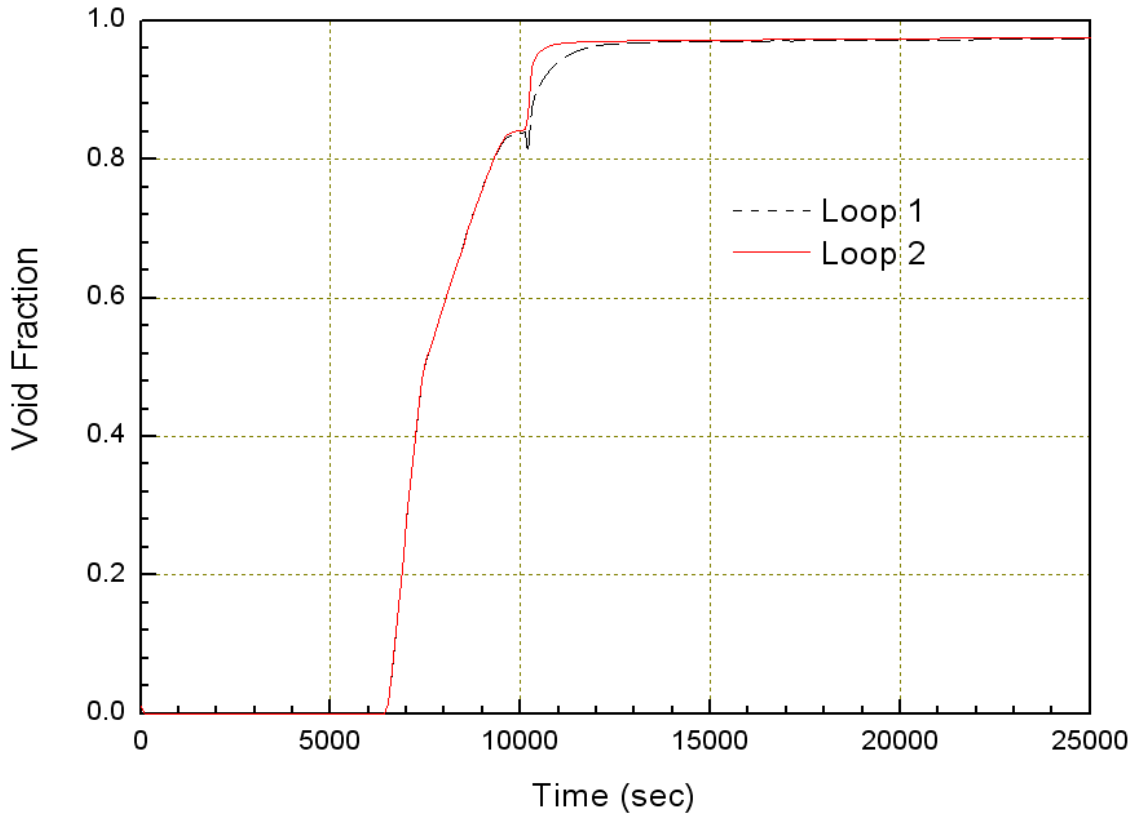


FIG. 3.190. Loop void fractions (0 - 25,000 s).

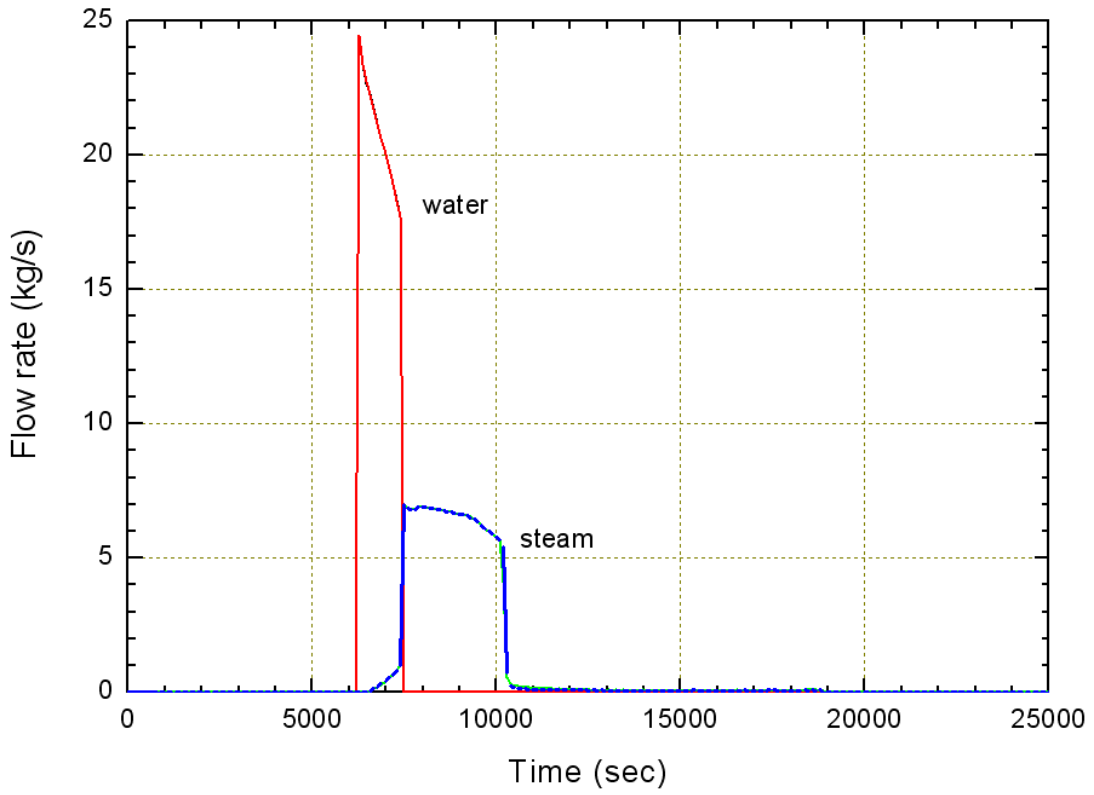


FIG. 3.191. LRV Steam and water flows for both loops (0 - 25,000 s).

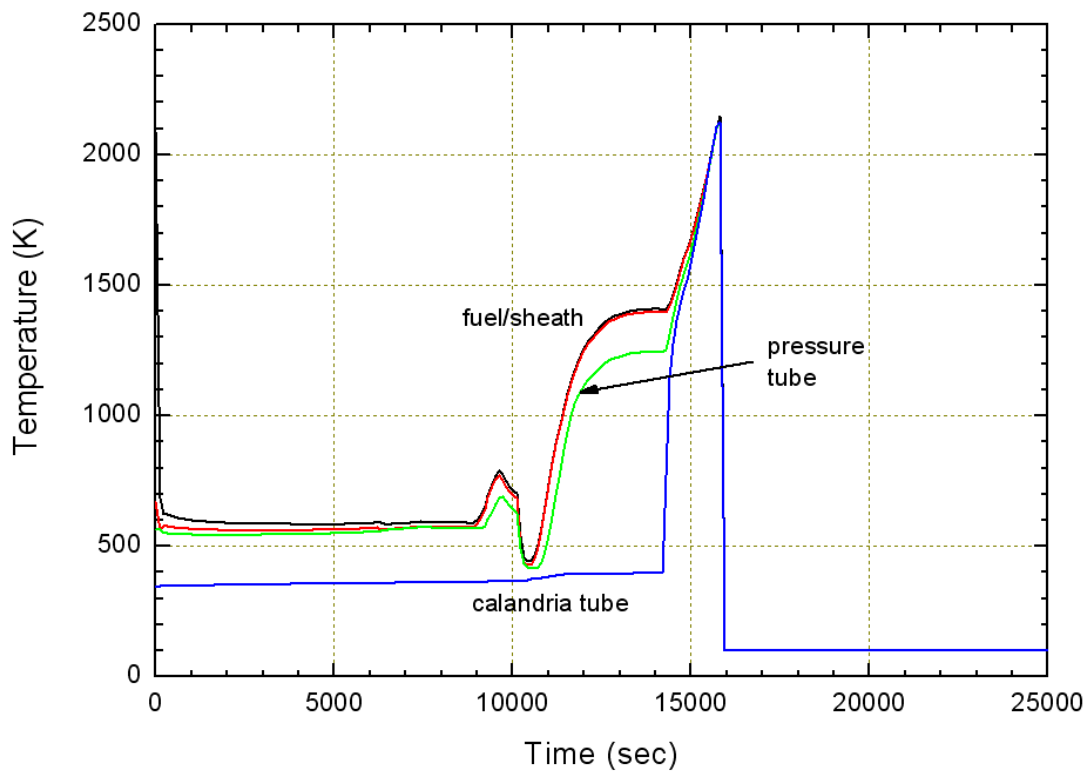


FIG. 3.192. Fuel, sheath, pressure tube and calandria tube temperatures at bundle 6, channel 1, loop 1 (0 - 25,000 s).

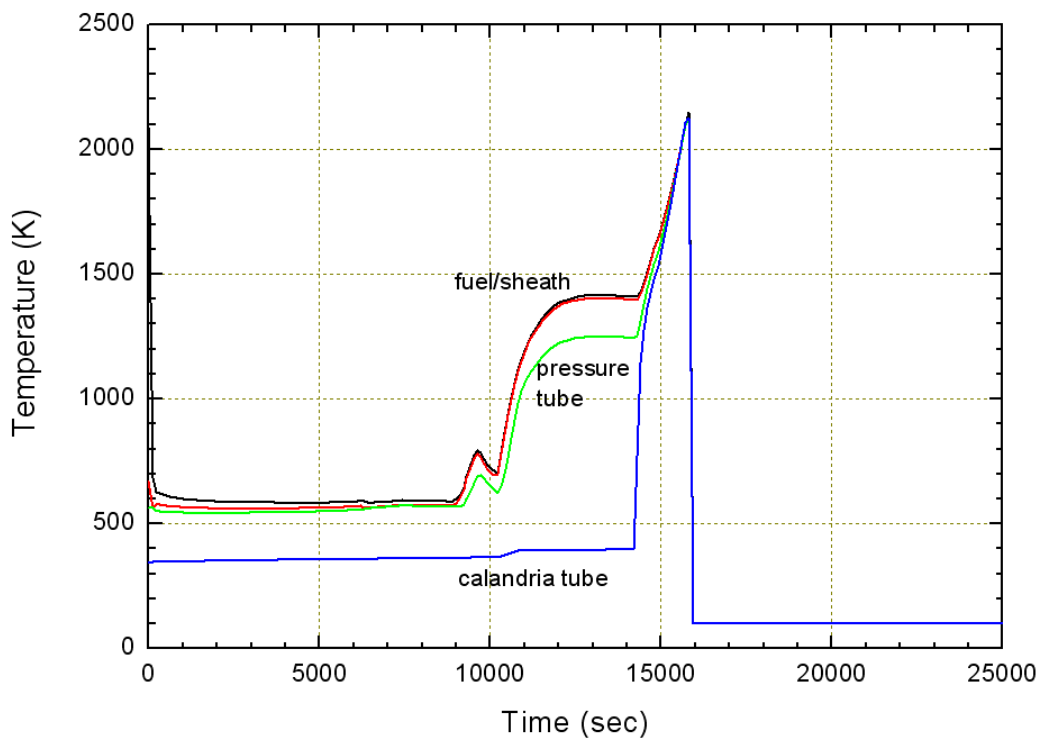


FIG. 3.193. Fuel, cladding, pressure tube and calandria tube temperatures at Bundle 6, channel 1, loop 2 (0 - 25,000 s).

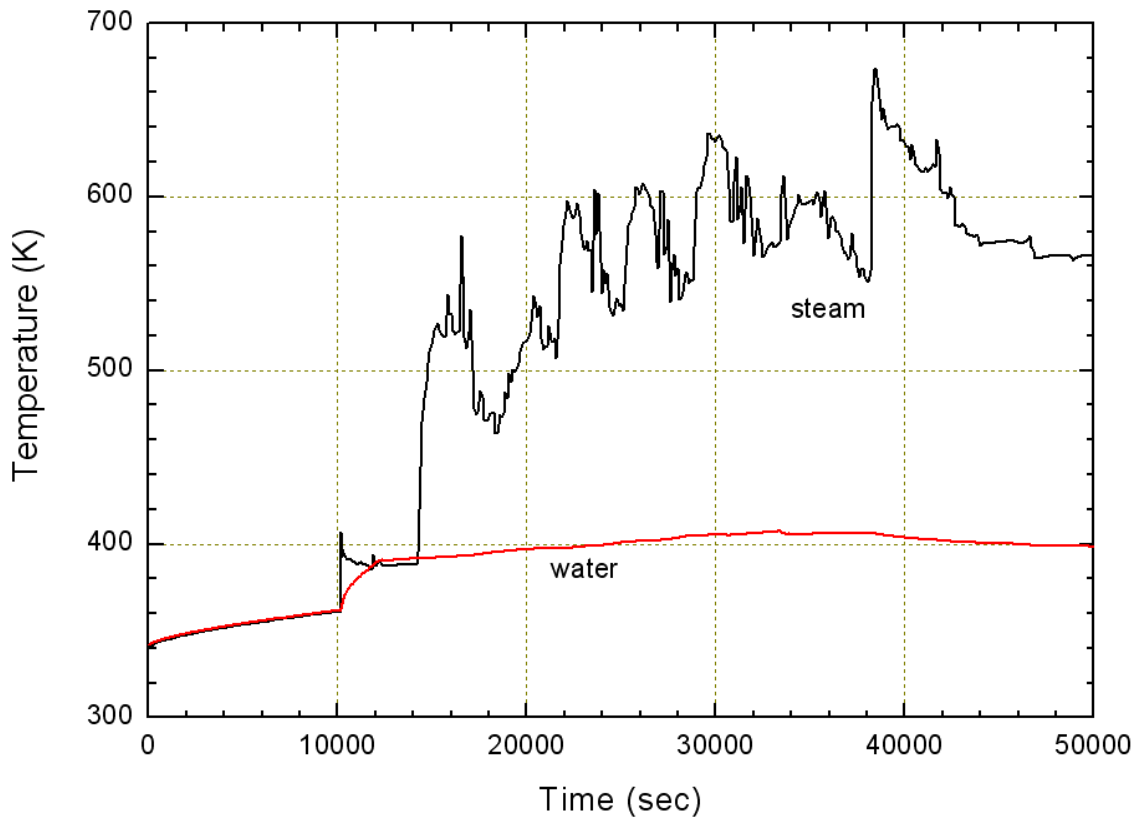


FIG. 3.194. Temperatures of moderator/steam in the calandria (0 - 50,000 s).

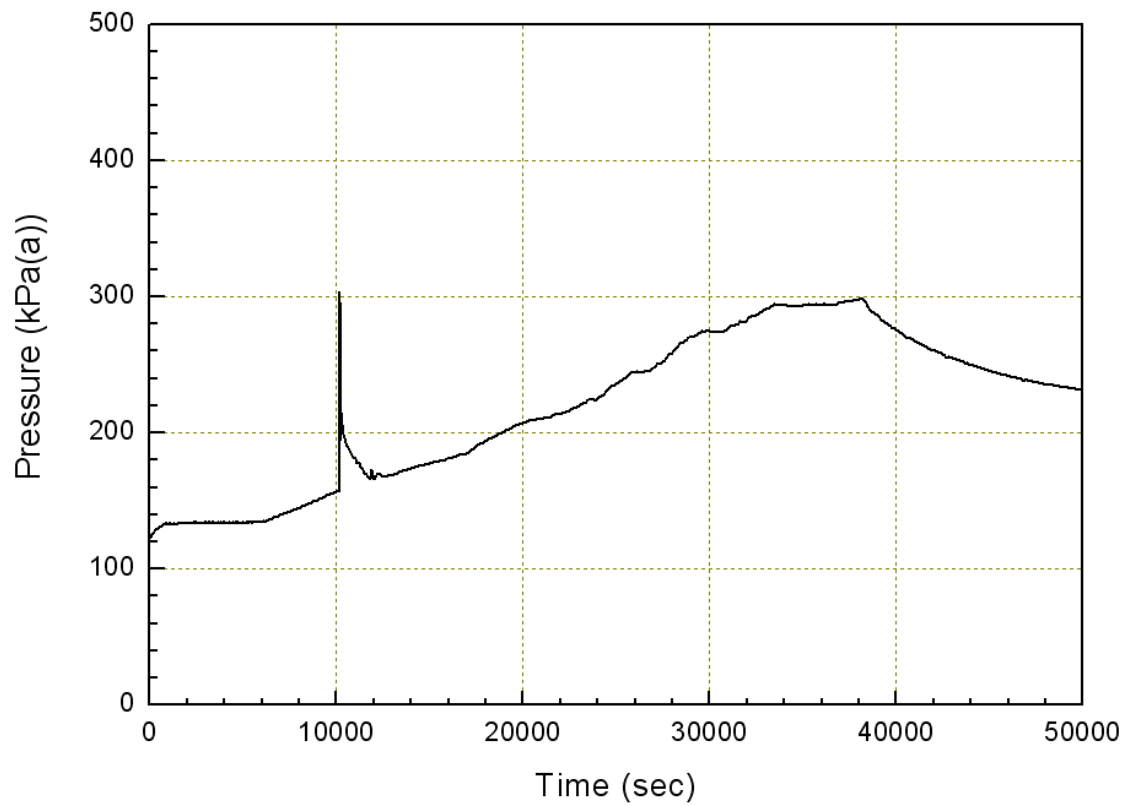


FIG. 3.195. Calandria vessel pressure (0 - 50,000 s).

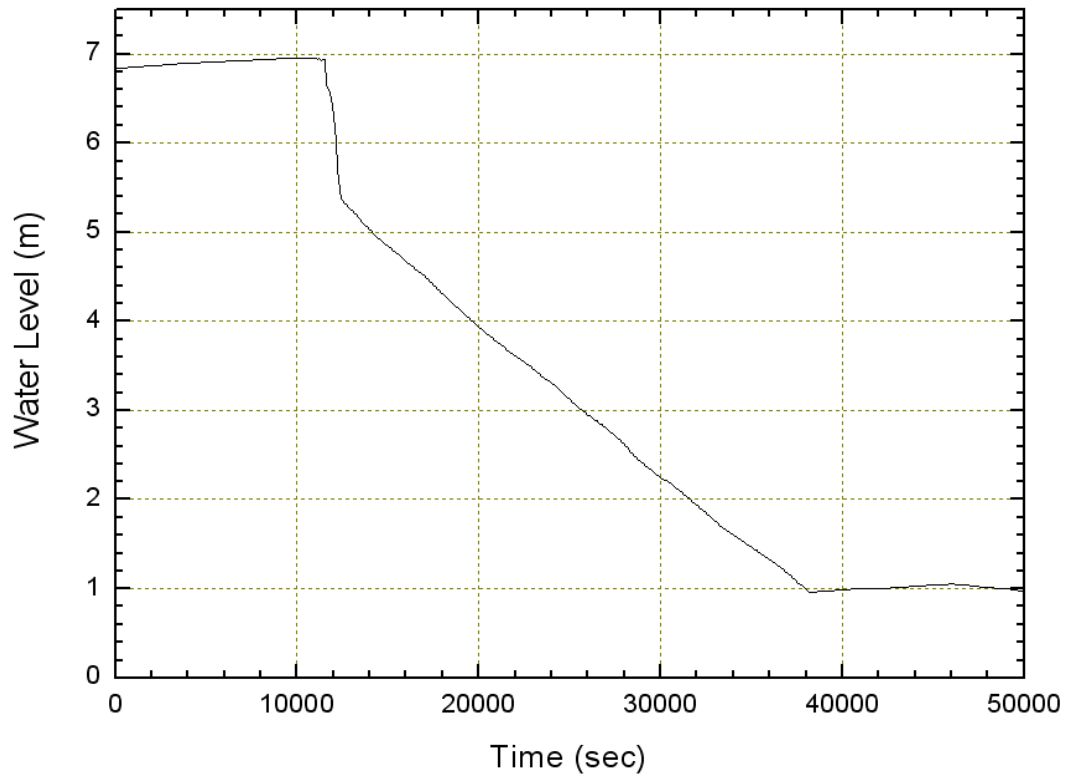


FIG. 3.196. Calandria vessel water level including corium volume (0 - 25,000 s).

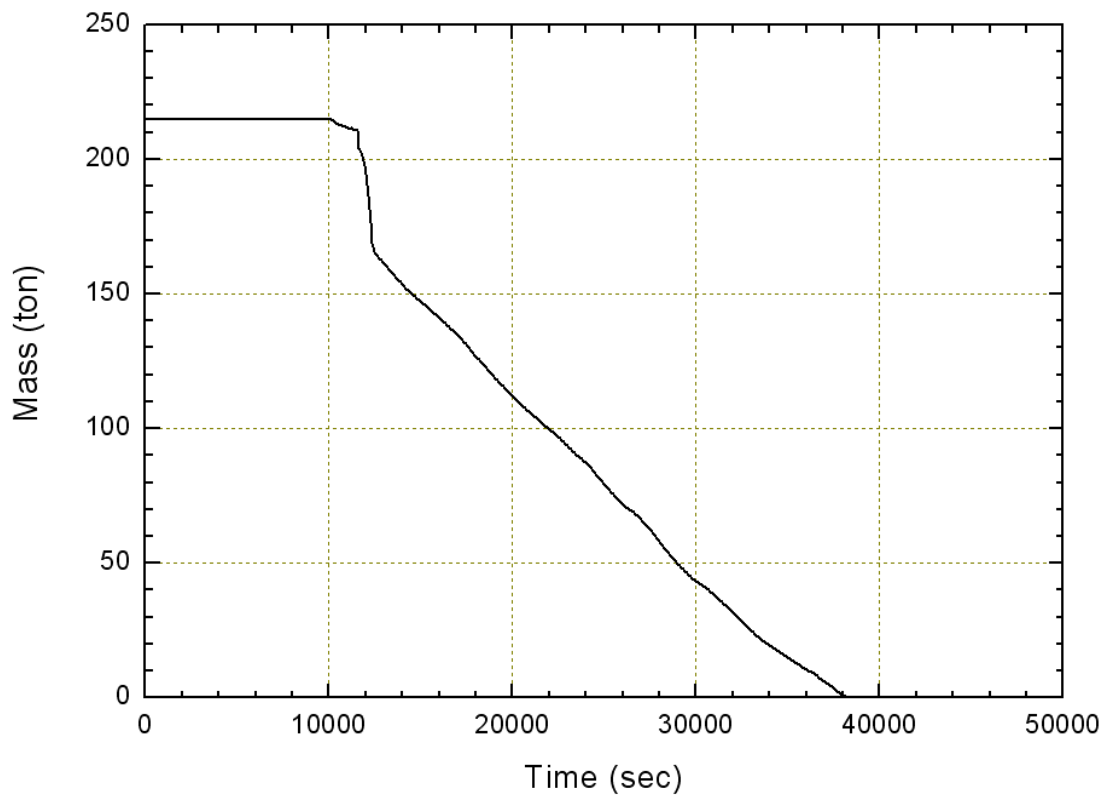


FIG. 3.197. Moderator mass (0 - 50,000 s).

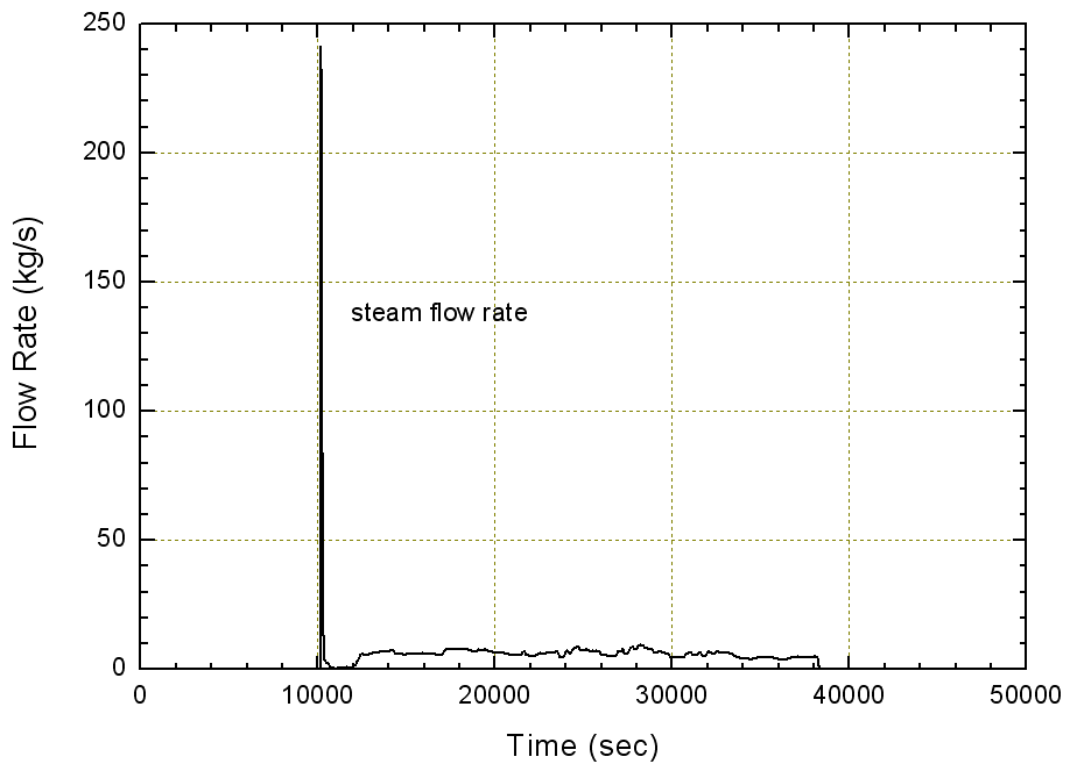
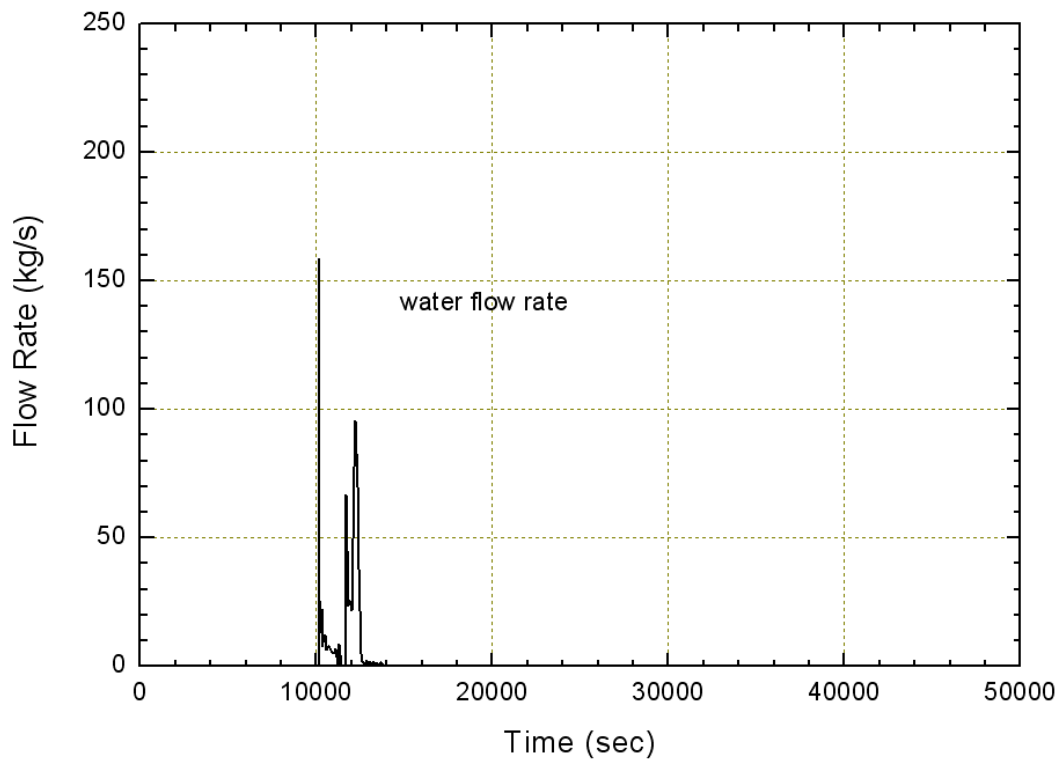


FIG. 3.198. Water and steam flow rates through the calandria rupture disks to the containment (0 - 50,000 s)

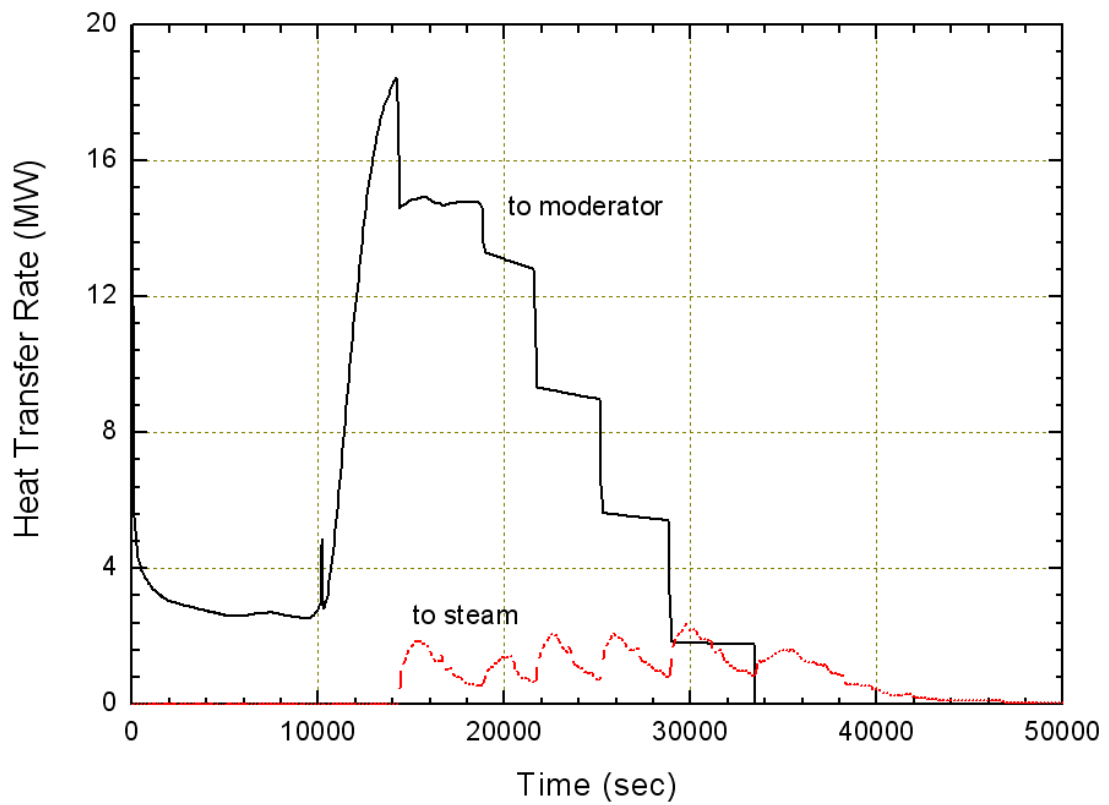


FIG. 3.199. Heat transfer rates from the channel to the moderator and to the steam (0 - 50,000 s).

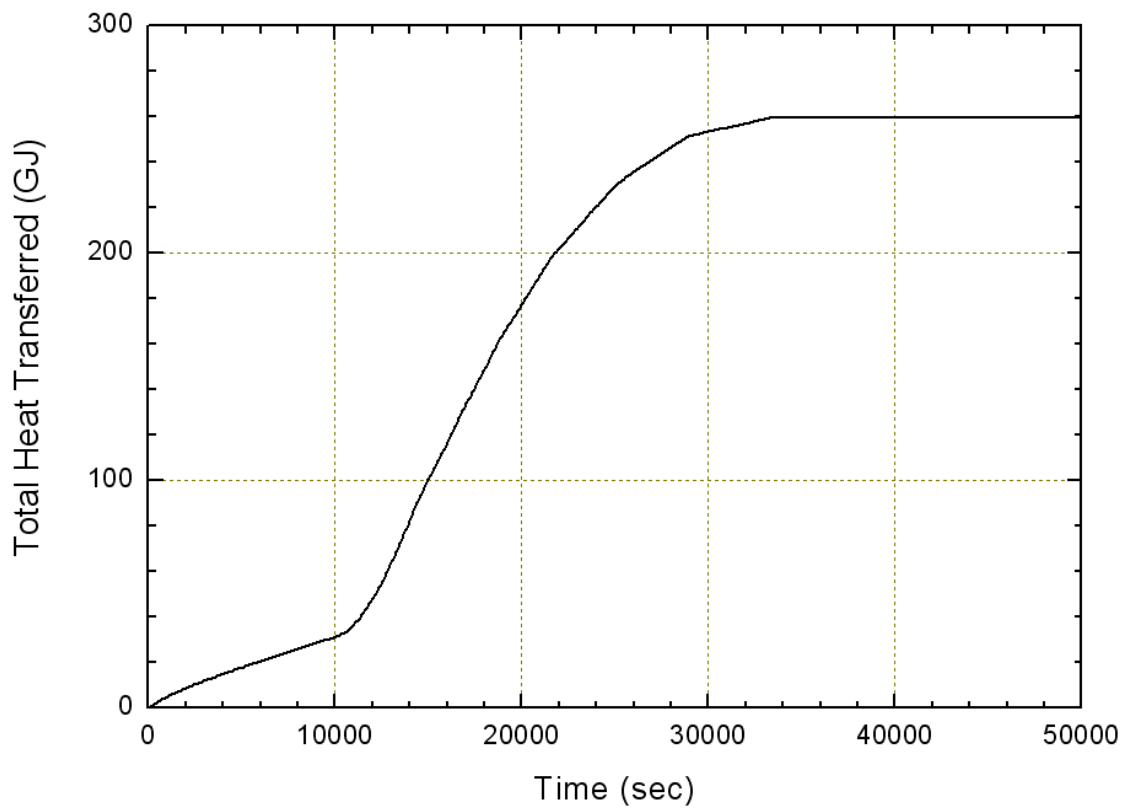


FIG. 3.200. Total heat transferred from the channel to the moderator (0 - 50,000 s).

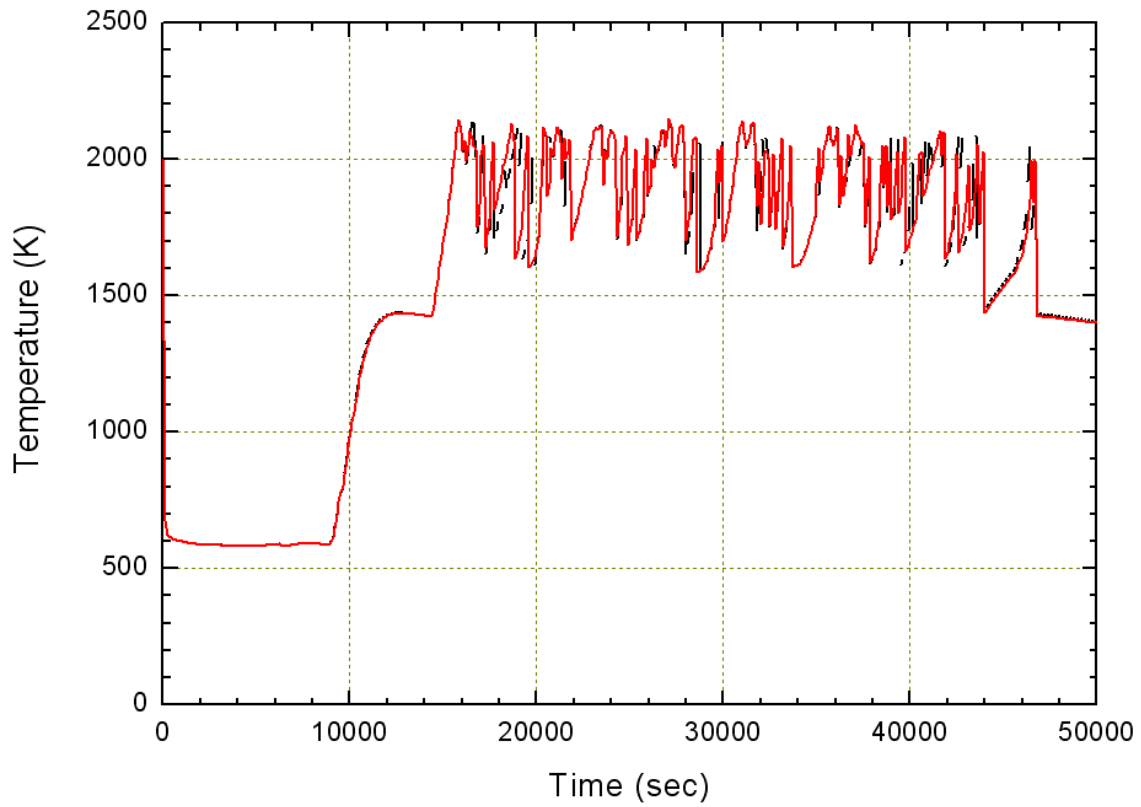


FIG. 3.201. Maximum fuel temperature behavior (0 - 50,000 s).

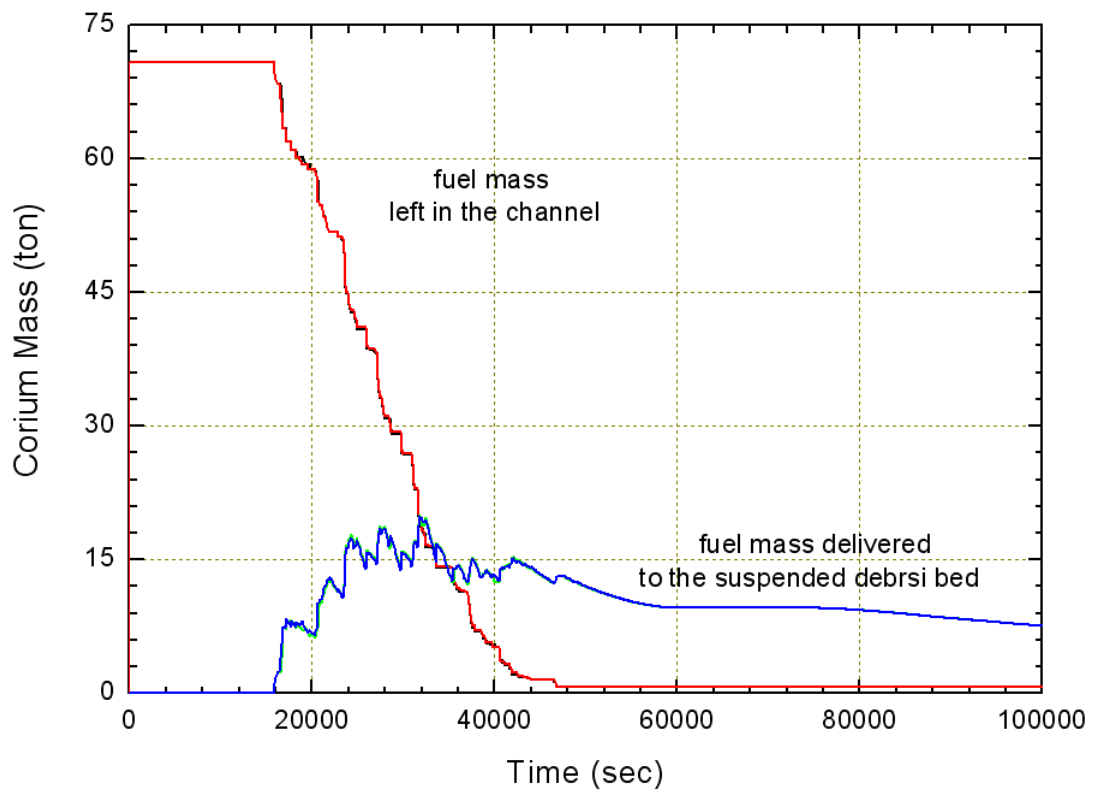


FIG. 3.202. Corium masses behavior in each loop and in the suspended debris bed (0 - 100,000 s).

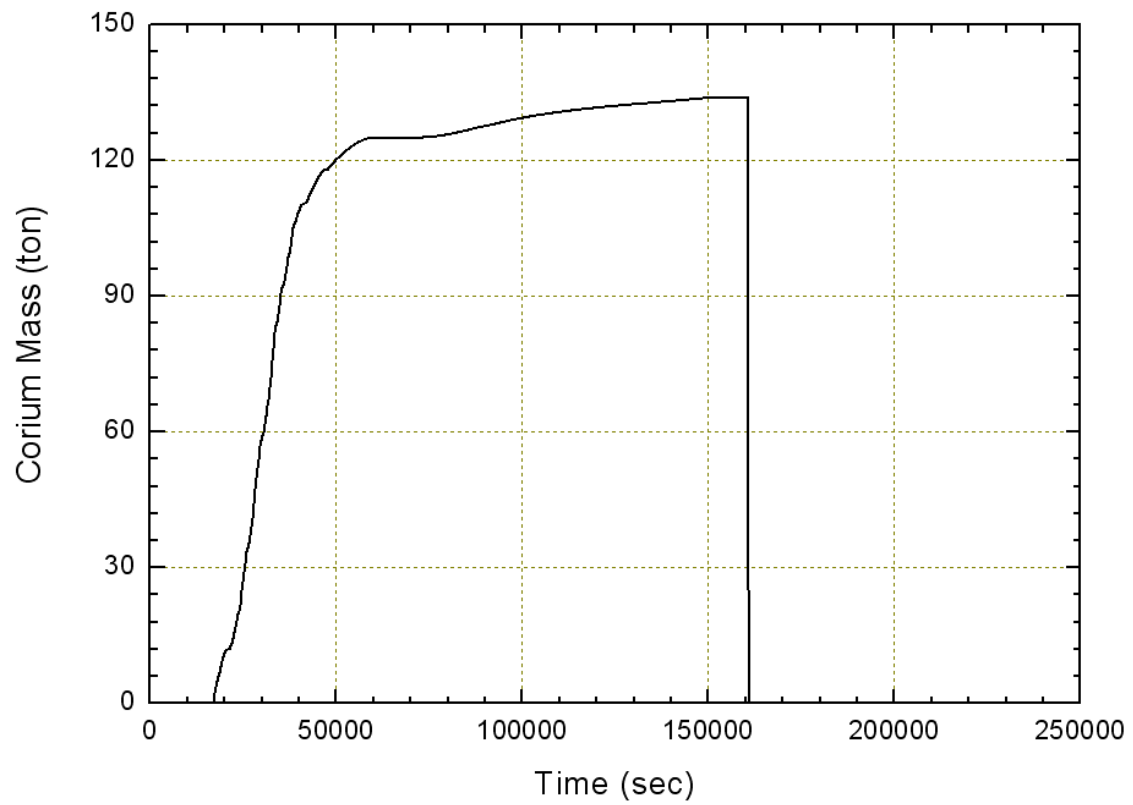


FIG. 3.203. Corium mass relocated into the calandria vessel (0 - 250,000 s).

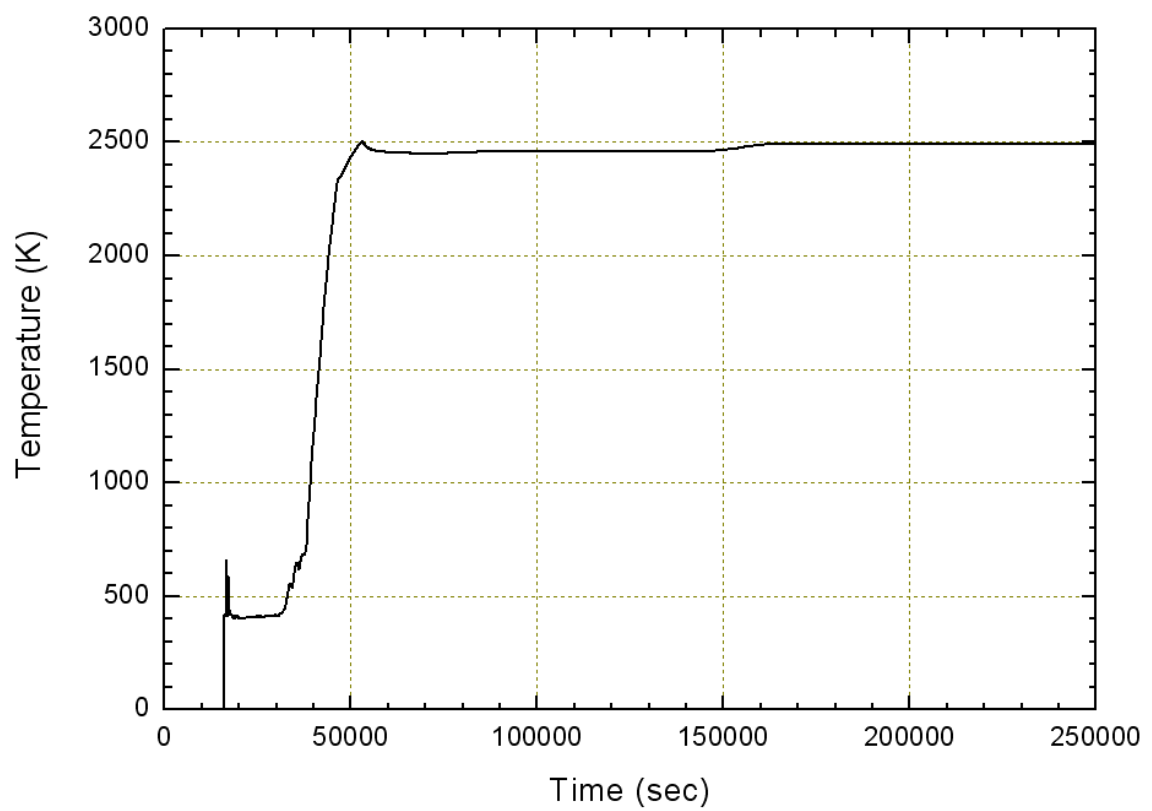


FIG. 3.204. Corium temperatures in calandria vessel (0 - 250,000 s).

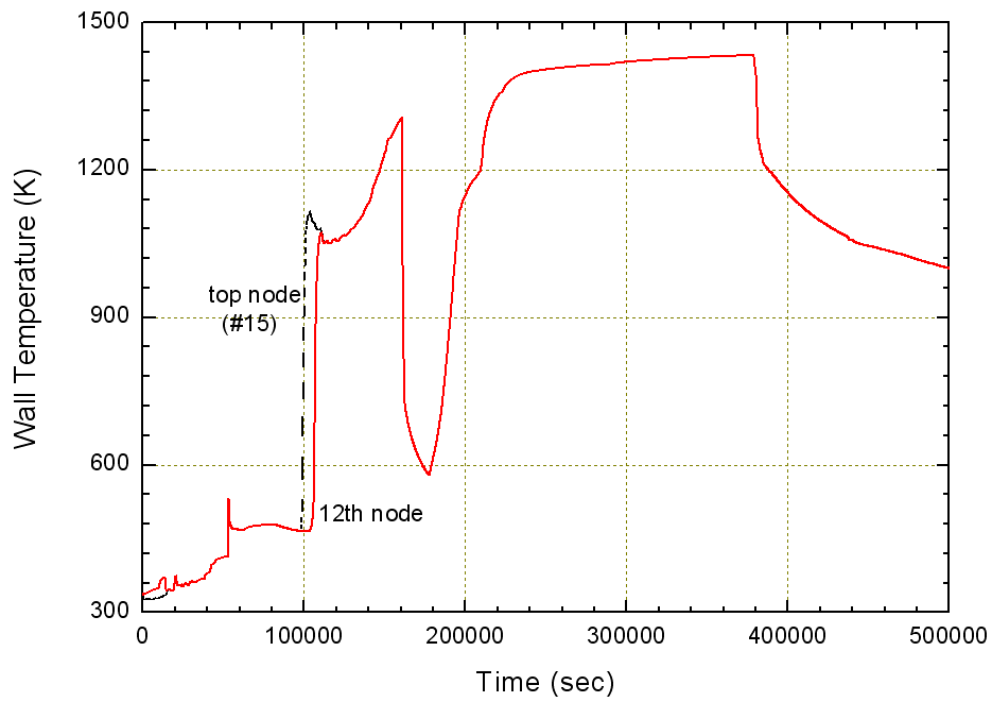
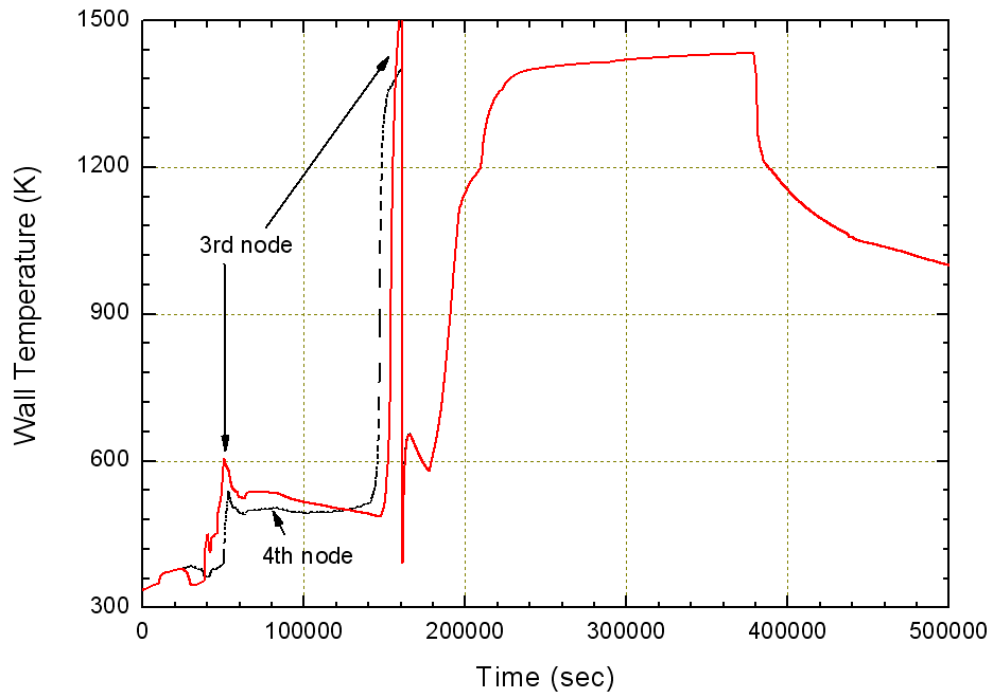


FIG. 3.205. Calandria vessel inside wall temperatures (0 - 500,000 s) (temperatures at the 3rd node from the bottom, at the 4th node, at the 12th node, and at the top 15th node).

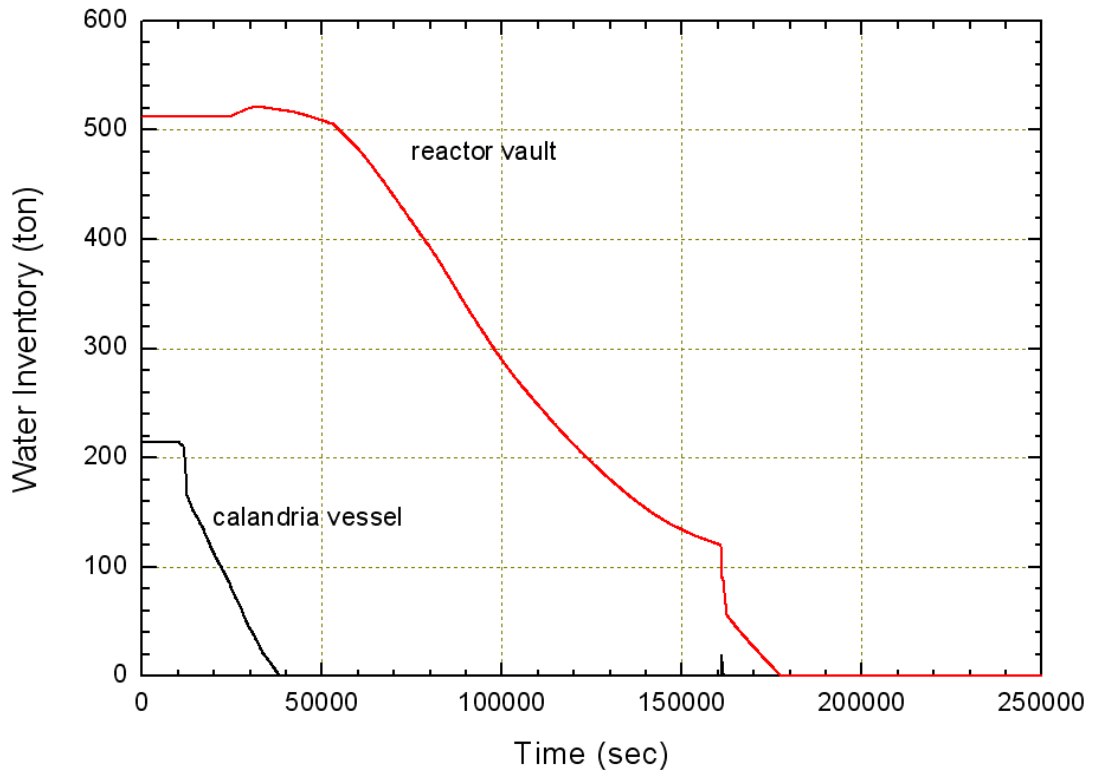


FIG. 3.206. Reactor vault and calandria vessel water mass (0 - 250,000 s).

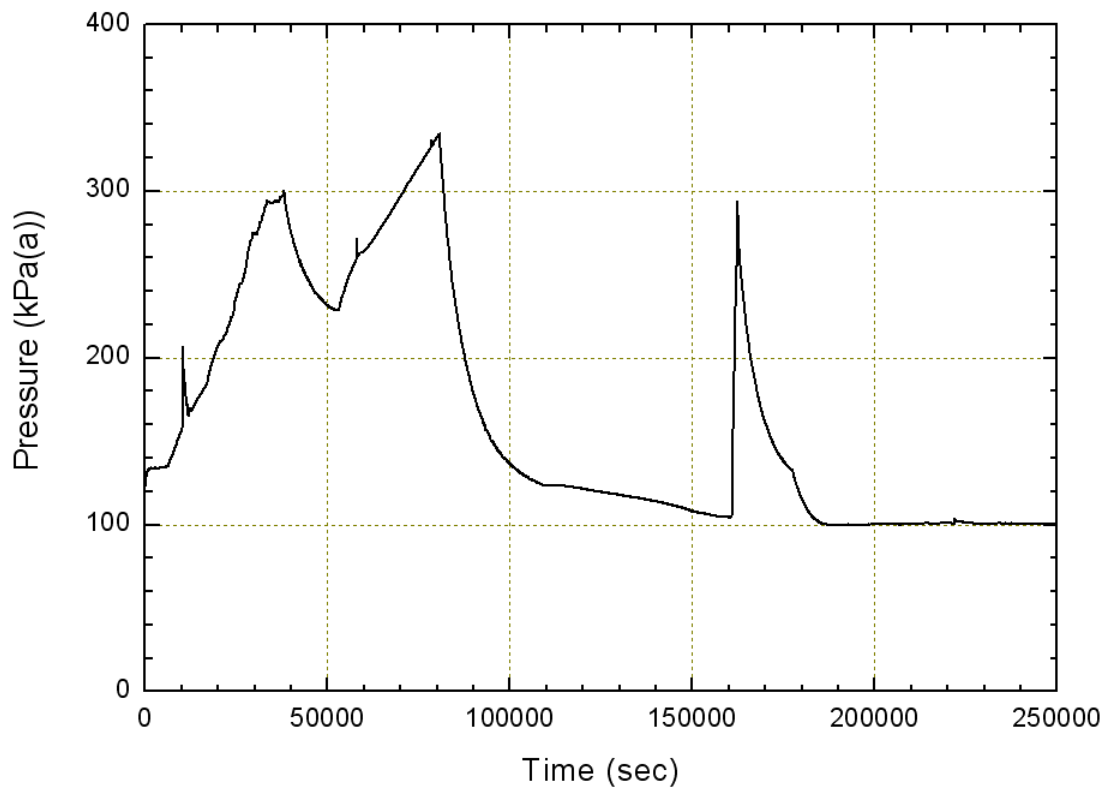


FIG. 3.207. Containment pressure (0 - 250,000 s).

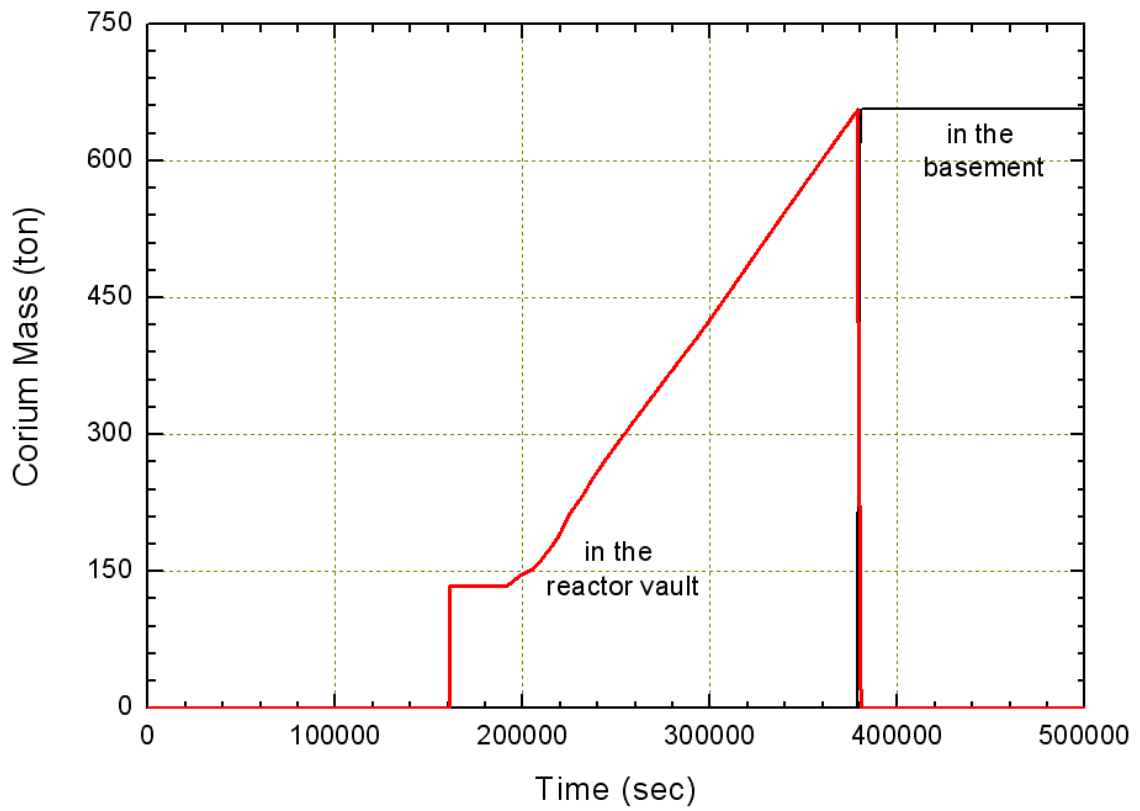


FIG. 3.208. Corium mass in the reactor vault and in the basement (0 - 500,000 s).

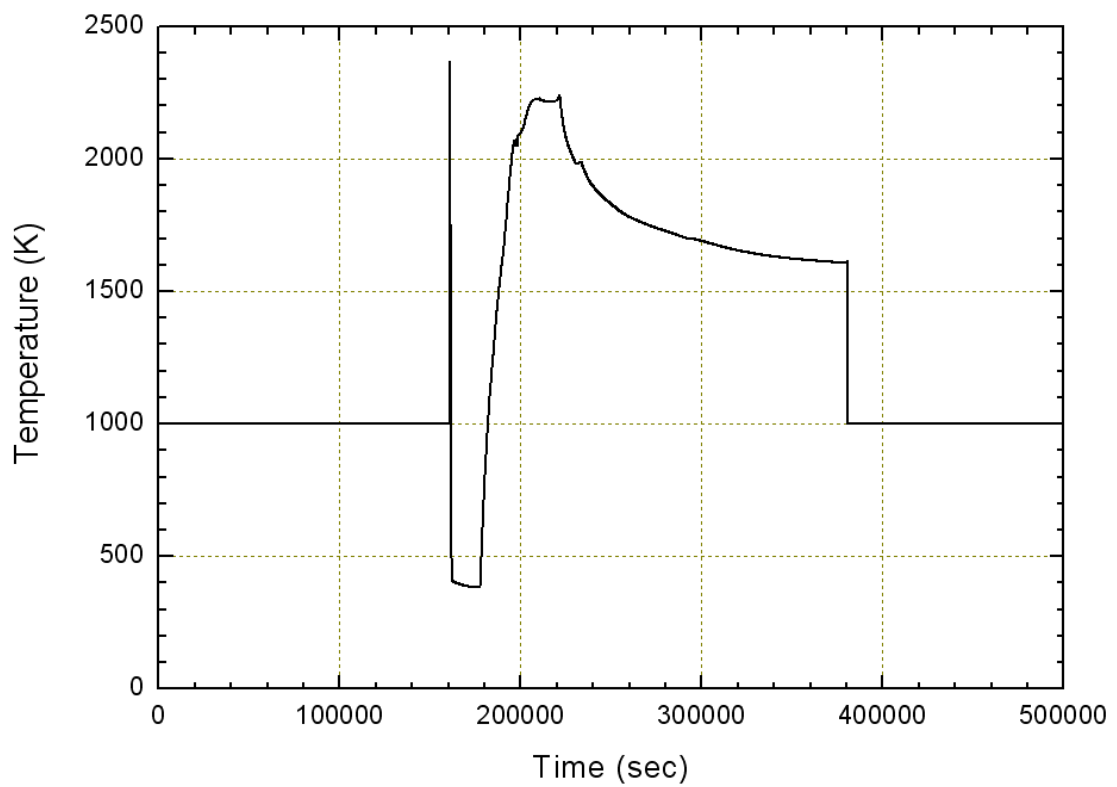


FIG. 3.209. Corium temperature in the reactor vault (0 - 500,000 s).

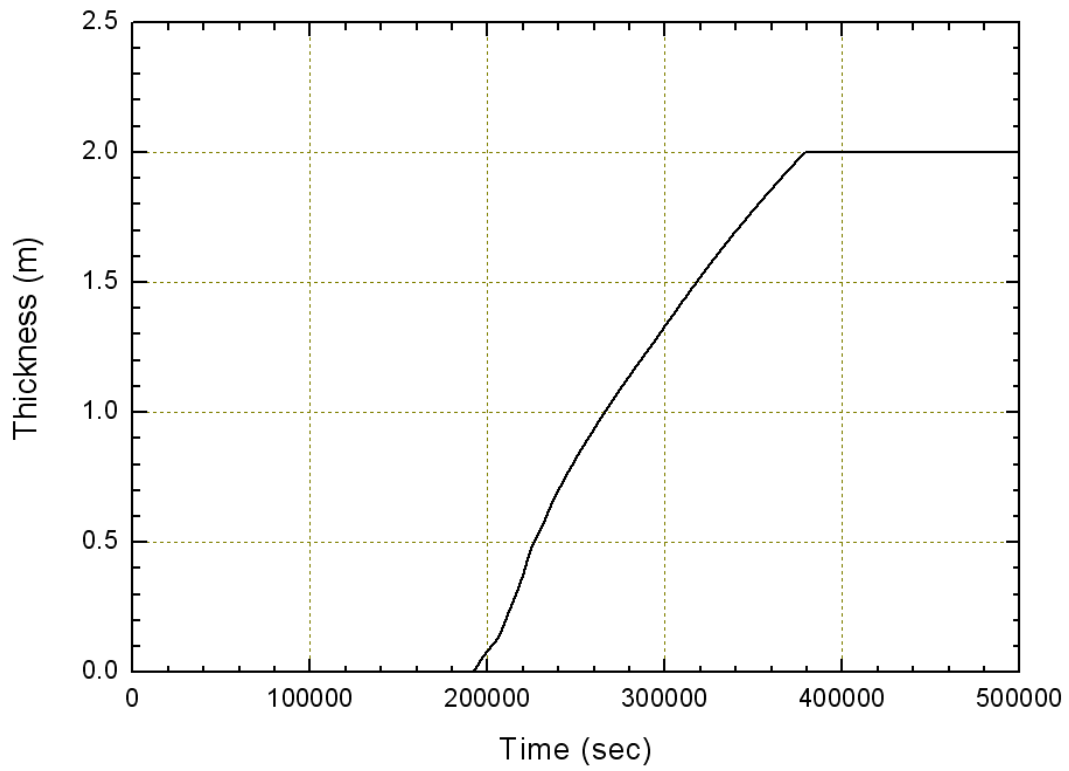


FIG. 3.210. Ablated concrete depth in reactor vault (0 - 500,000 s).

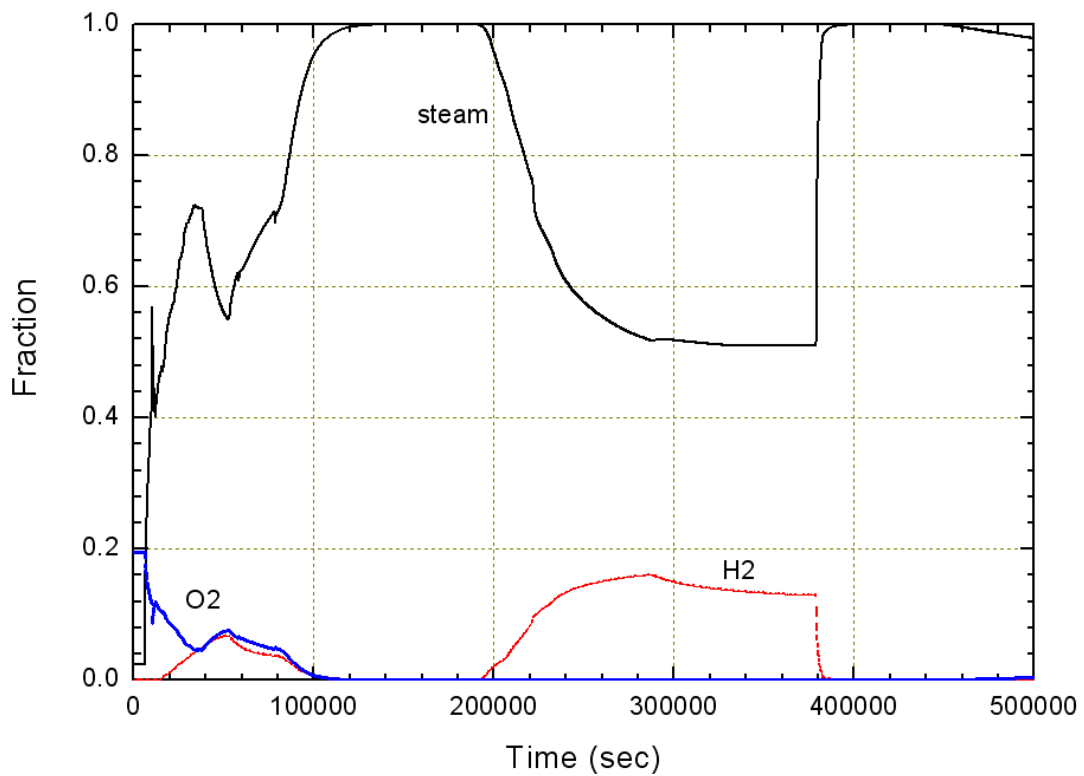


FIG. 3.211. Containment atmosphere compositions of steam,  $H_2$  and  $O_2$  in S/G boiler room (mole fraction) (0 - 500,000 s).

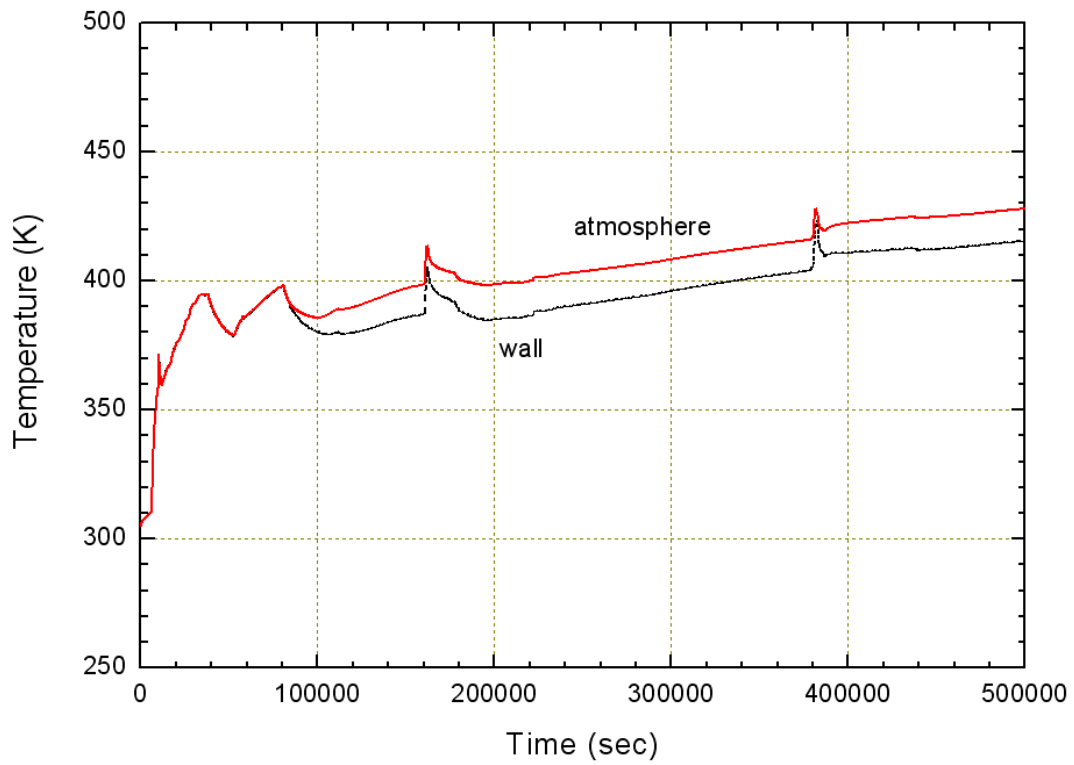


FIG. 3.212. Containment atmosphere and wall temperatures at the boiler room (0 - 500,000 s).

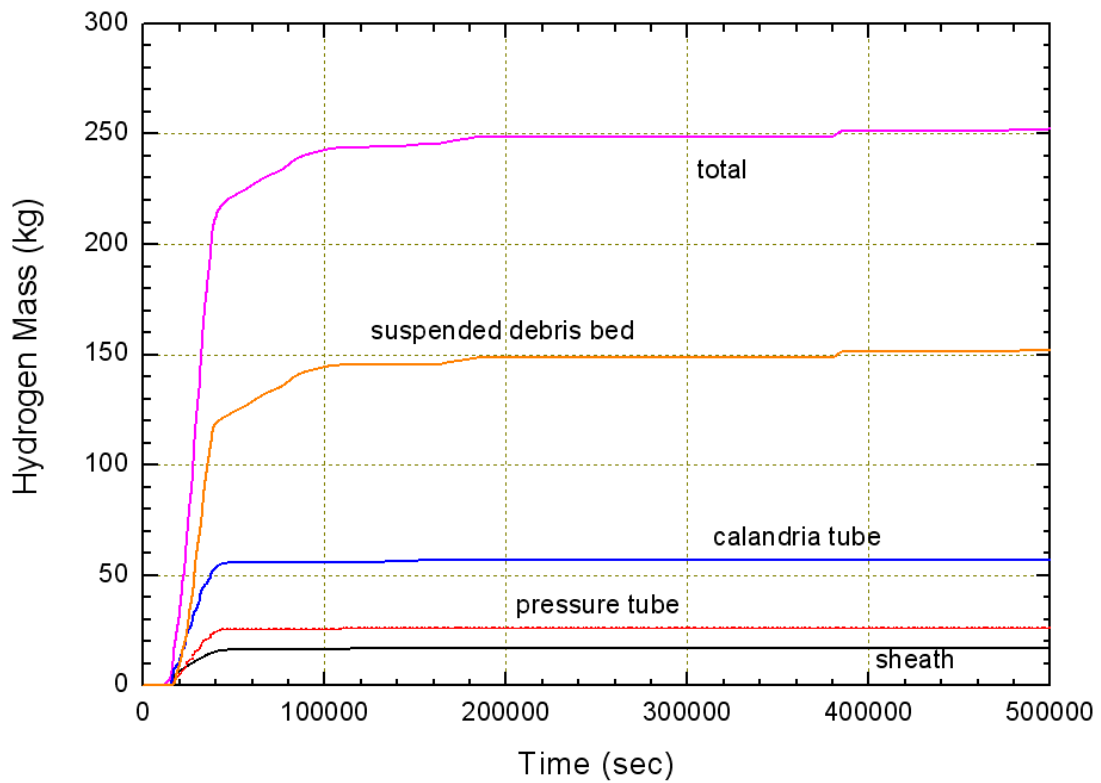


FIG. 3.213. Hydrogen release histories in various locations in loop 1 (core) (0 - 500,000 s).

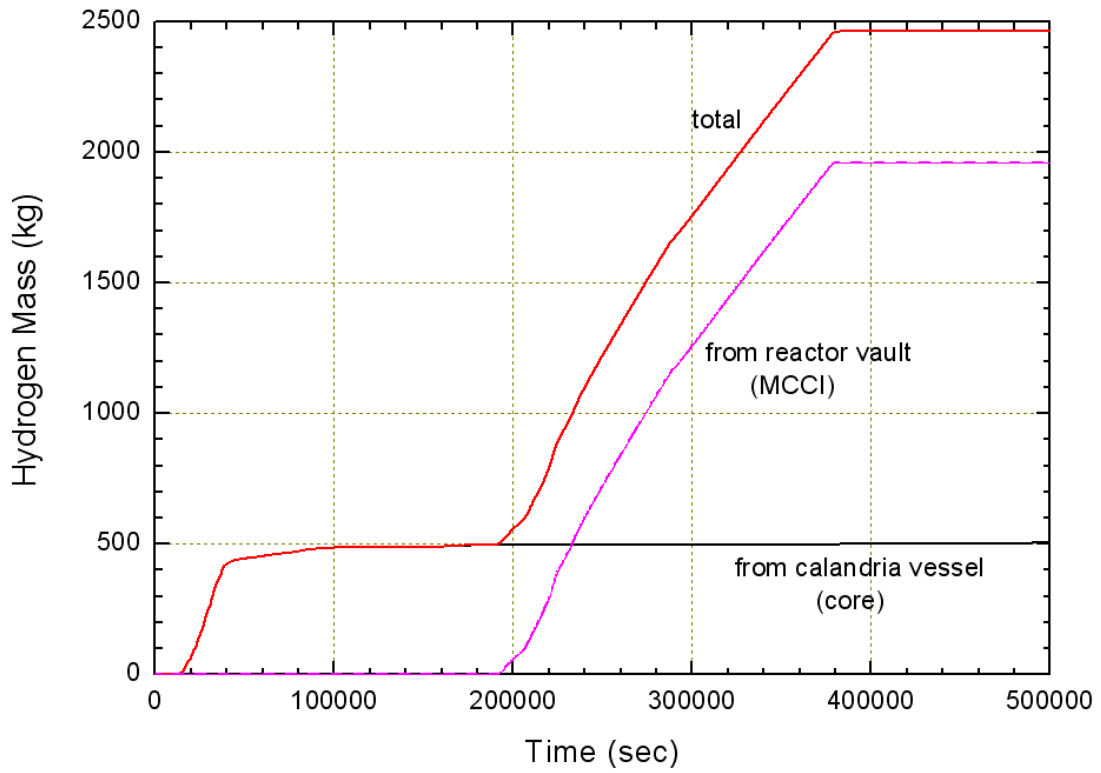


FIG 3.214. Amount of hydrogen generated from core and reactor vault (0 - 500,000 s).

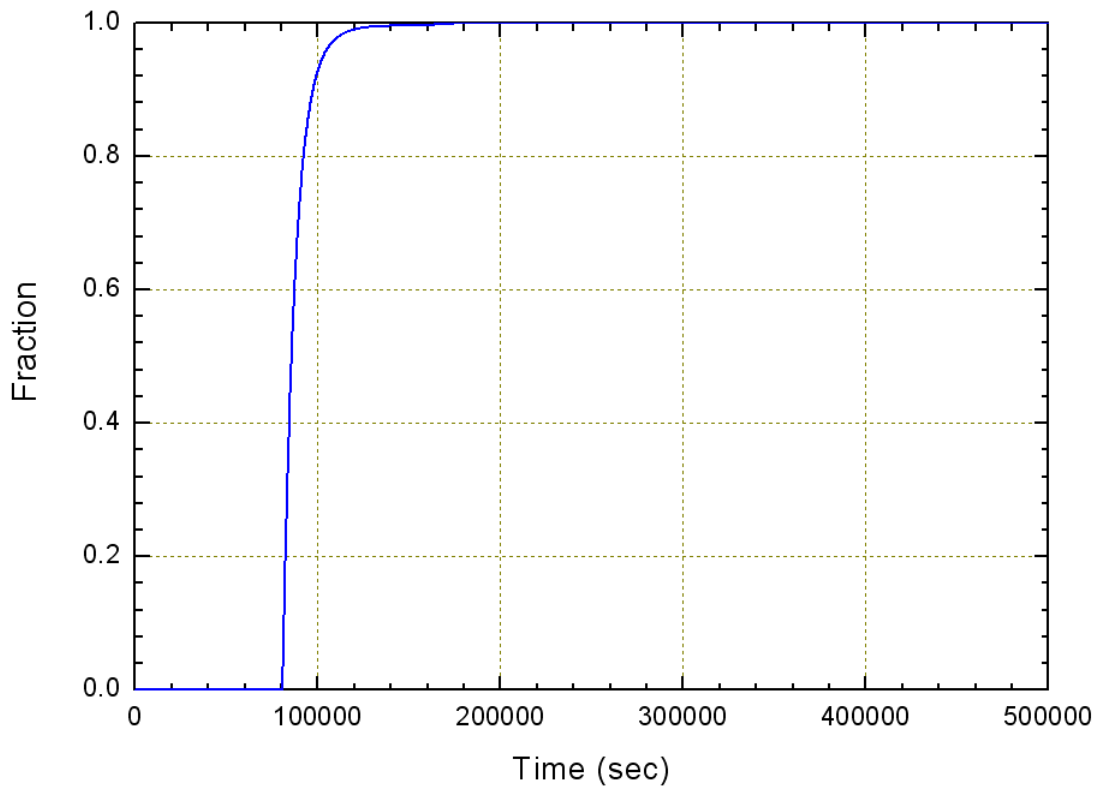


FIG. 3.215. Noble gas release fraction (0 - 500,000 s).

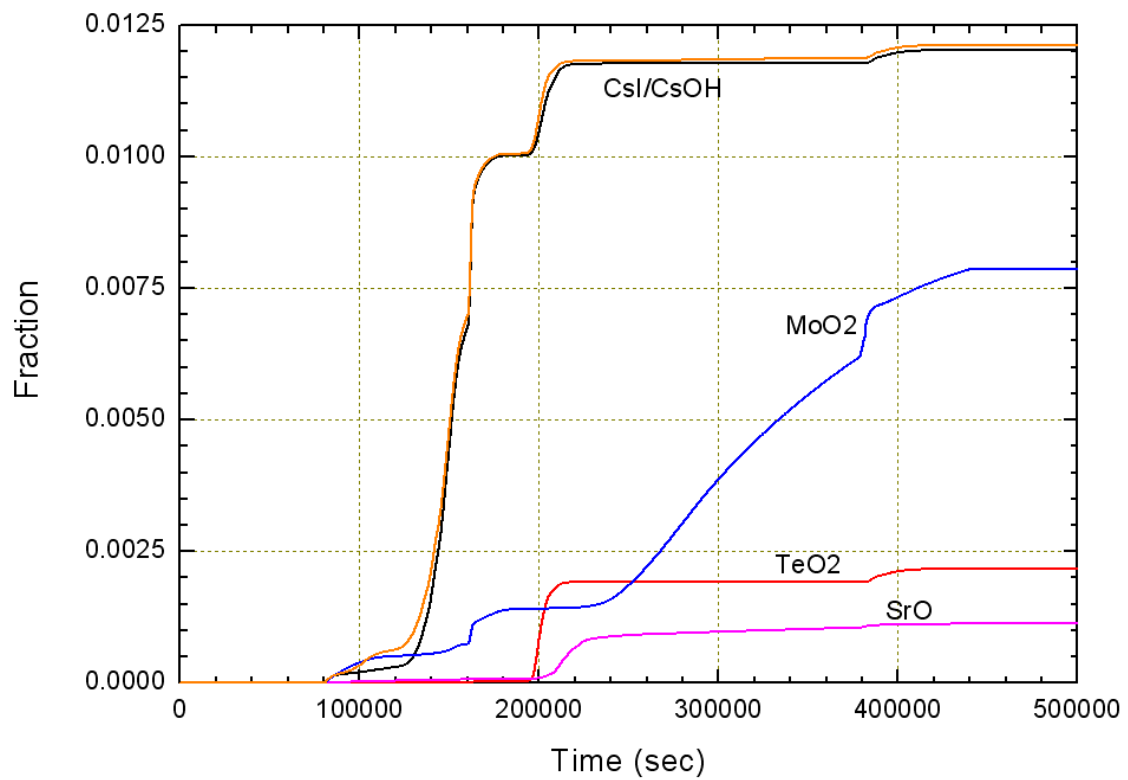


FIG. 3.216. Released mass fraction of CsI, CsOH, MoO<sub>2</sub>, SrO & TeO<sub>2</sub> to the environment (0 - 500,000 s).

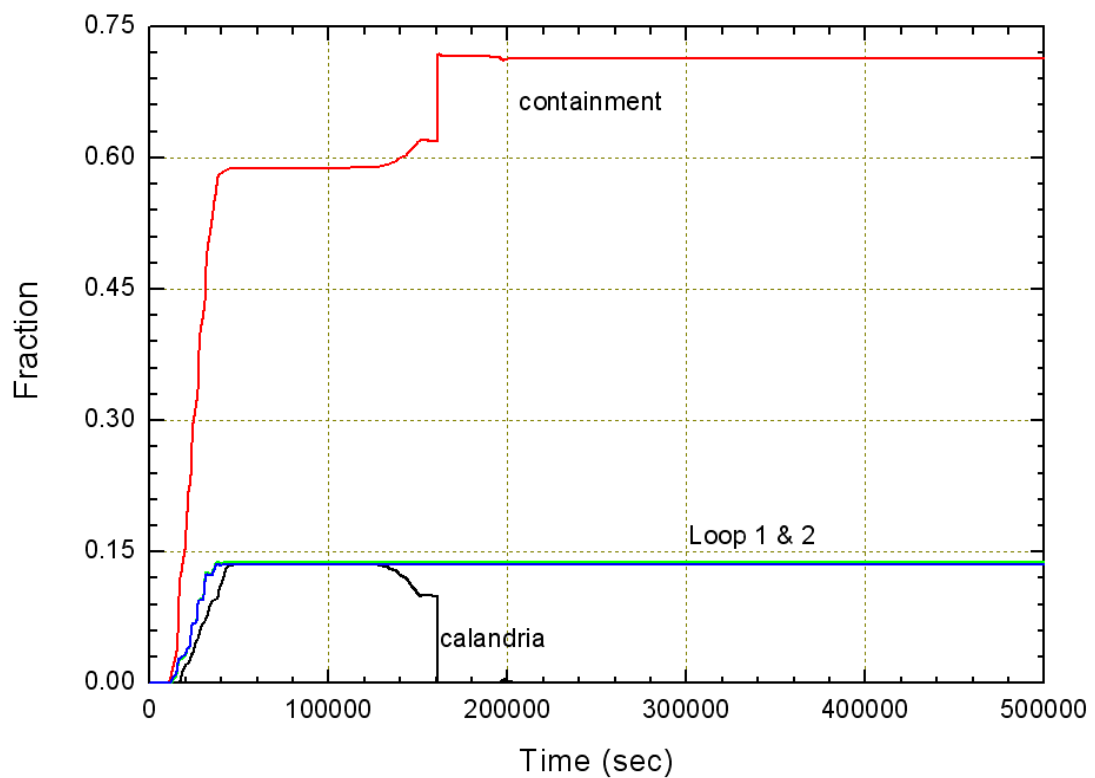


FIG. 3.217. Mass fractions of CsI at various location (0 - 500,000 s).

### 3.5. NPCIL

#### 3.5.1. Computer codes

For modeling of complete accident progression, different computer codes are used at various stages of accident progression. Computer codes used for different phases of the accident progression are summarized in Table 3-13.

A brief description of the codes used in the analyses is given below and their coupling is given in section 3.5.1.8.

TABLE 3.13. PHENOMENA AND COMPUTER CODES USED

Phase	Phenomena	Core thermal hydraulics and mechanical behavior	Containment response	Activity release
1	Accident initiation to start of fuel channel uncover, i.e. the calandria rupture disk blowing		PACSR	STAR & ACTREL
	– Core thermal hydraulics upto channel dryout	ATMIKA-T		
	– Fuel channel heatup, thermo mechanical behaviour and OPRD rupture	CONTACT, SEVAX		
2	Start of fuel channel uncover (i.e. the rupture disk blowing) to core collapse	SEVAX		
3	Core collapse to calandria vessel failure	SEVAX		
4	Calandria vessel failure to containment failure	MCCI		

##### 3.5.1.1. ATMIKA-T

The initial phase of SBO is modelled by using the code “ATMIKA-T”, which is a system thermal-hydraulic neutronic computer code for simulation of transients and LOCA. The entire system (primary and secondary) is divided into a number of control volumes, called nodes. Nodes are connected by means of flow paths. A flow path is defined along with a valve or a pump or both. Nodalization is done keeping in view the requirement of analysis and physical configuration of piping network. Usually control volume is chosen such that its boundaries coincide with the junctions of the flow paths, where there is a change in the geometry of the pipe or a valve/pump exists. In some cases a piping of same geometry throughout may have to be divided into two or more control volumes as per the requirement of the analysis. A multiple connection or a network of piping is modelled by considering the junction of two or more pipes as a nodal point. Following Figure 3-218 shows a sample network used.

To simulate the thermal-hydraulic transients of entire system, following models are used:

##### (a) Fluid dynamic model

Thermal-hydraulic part of ATMIKA is based on unequal velocity equal temperature (UVET) model. Governing equations of UVET model consist of 3 conservation equations of mass, energy and momentum. Unequal velocities between two phases are derived from drift flux correlation. A staggered mesh arrangement where pressure, density and enthalpy are defined at the node and flow is defined along the flow path at the junction of two control volumes is used. Mass and energy conservation equations are applied on lumped control volume and momentum equation is applied on flow paths.

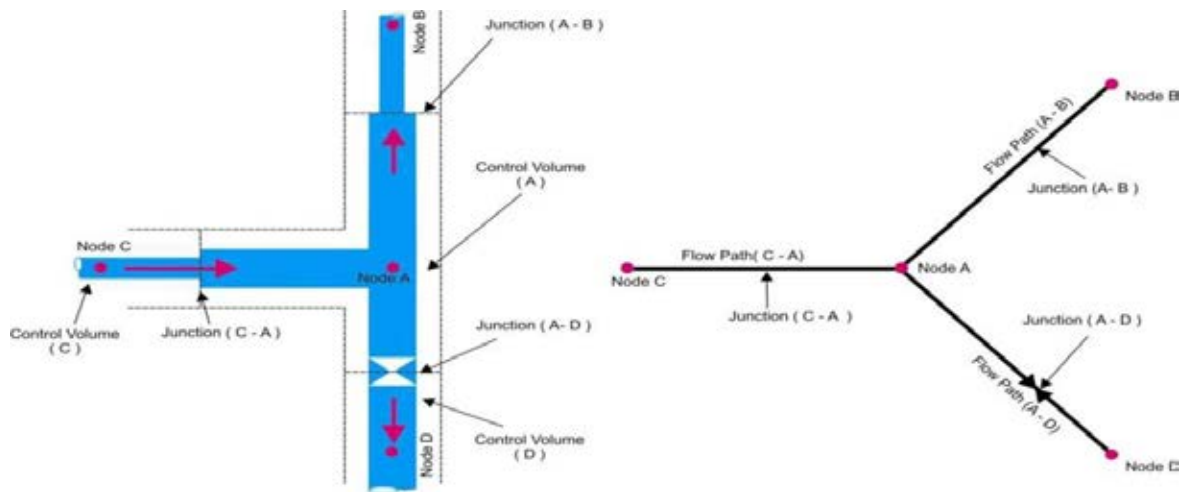


FIG. 3.218: A sample network.

(b) Heat transfer model

Heat Transfer Model consists of empirical correlations applicable in different heat transfer regimes. The correlations are chosen considering their applicability over wide range. All the correlations are made to have correct parametric and asymptotic trend in the region of consideration.

(c) Heat conduction in fuel

The maximum rated fuel pin at each node of core is taken as a representative fuel element. Heat conduction is assumed to dominate along radial direction of fuel pin. The fuel pin is divided radially into N number of zones with two fixed on sheath.

(d) Heat source in fuel

An accurate prediction of power and temperatures in a nuclear reactor in an accidental condition is very important. This requires the solution of space-time kinetics equation. There are two options in the code for solving these equations:

- I. By point neutron kinetics model it is assumed that the heat generation is uniform throughout a fuel element and neutron flux shape remains same.
- II. By 3-D neutron kinetics model using computer code IQS 3D based on flux factorization technique.

At elevated sheath temperature, zirconium in sheath reacts with water leading to the generation of hydrogen. This metal water reaction is an exothermic one and can be represented in simple terms by the equation



(e) Heat loss

The heat loss is heat transfer from fluid to outside system through piping wall (conduction wall). Conduction wall is lumped as single mass and energy balance is applied.

(f) Stratification

Two phase flow at low velocity and high void in a horizontal pipe can be stratified. Stratification is identified by Froude's number. Non equilibrium during stratification is defined by a correlation. Appropriate fuel model is used to calculate fuel temperature during stratification.

(g) Pressurizer model

Pressurizer is considered as two separate volumes of liquid-vapour mixture phase and vapour phase. Mass and energy balance are applied to both the volumes assuming pressure is same for both. The steam flow from the interface is calculated as a function of the voids in the liquid-vapour mixture zone, surface area, etc. using a correlation derived from the experimental data. In this calculation, total volume of the pressurizer is maintained constant. Level tracking is done using the liquid-vapour mixture zone volume and its cross section. This gives the swell level. As far as instrumentation is considered, it is the collapsed level in the range of the instrument.

Nodalization scheme of ATMIKA.T used for the analysis is shown in Figure 3-219. Four channels (representing highest, higher, intermediate and low power) per pass are modeled. Each channel is having three nodes in the core, one in end fitting and one in feeders. Model includes all headers, primary circulating pumps, steam generators, and pressurizer. On secondary side atmospheric steam discharge valves and steam relief valves are modeled (however as per analysis assumptions atmospheric steam discharge valves are considered unavailable).

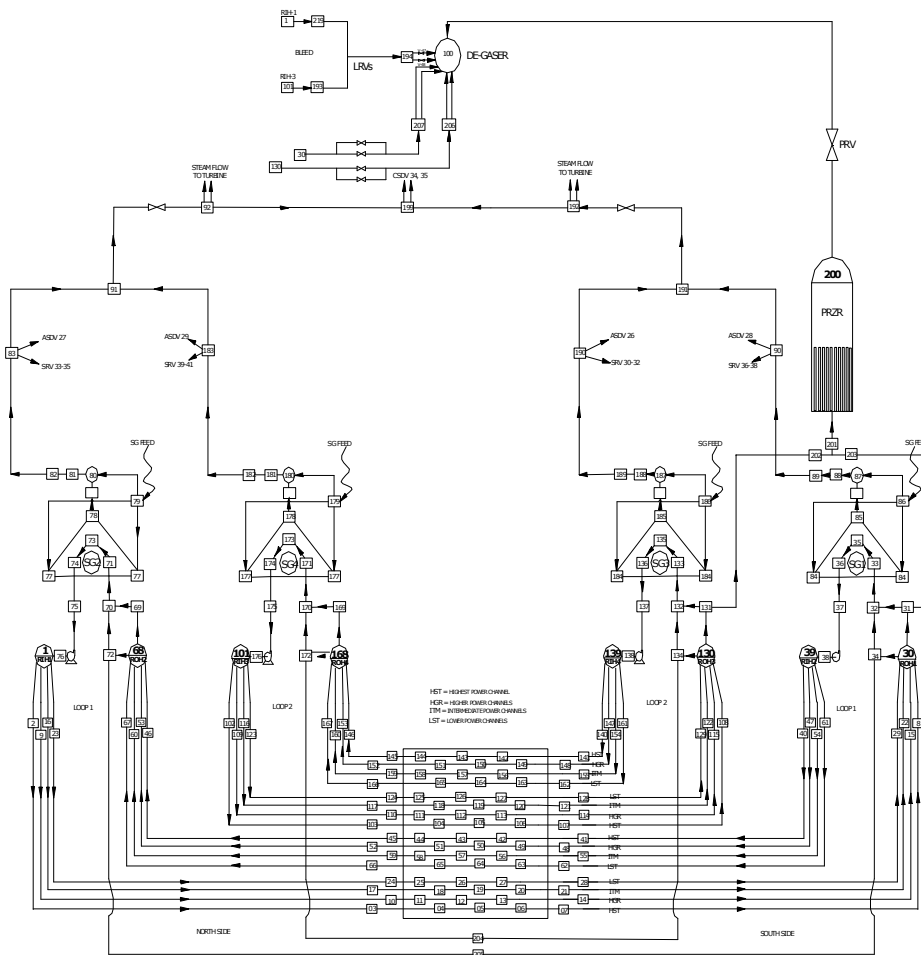


FIG. 3.219. ATMIKA.T Nodalization diagram.

### 3.5.1.2. CONTACT

“CONTACT” is thermal hydraulic computer code used for simulation of thermo mechanical behaviour of coolant channels. The channels are grouped depending on their power. Analysis is carried out on a representative channel of each group with maximum channel power in the group assigned to the representative channel of the group. The channel grouping used for the analysis is shown in Table 3-14.

TABLE 3.14. CHANNEL GROUPING IN CONTACT

Group	Channel power range in kW	Representative channel power in kW	Number of channels
1	2548 - 3500	3500	44
2	3500 – 4500	4500	56
3	4500 – 5500	5500	58
4	5500 – 6100	6100	44
5	6100 – 6380	6380	60
6	6380 – 6465	6465	56
7	6465 – 6609	6609	62

The representative channel is divided into axial elements corresponding to fuel bundles in the channel. In the cross section of the channel the fuel elements, pressure tube and calandria tube are modeled by a system of annular rings for calculation of heat transfer.

The pressure tube deforms under high temperature creep and contacts with calandria tube. If the internal pressure within the channel is high ( $> 1$  MPa) the principal deformation of the pressure tube is radially outwards (ballooning) and contact with calandria tube occurs completely around the circumference. If the channel pressure is low ( $< 1$  MPa) then the principal deflection is downwards(sags) and contact occurs in elliptically shaped patch at the bottom of pressure tube [28, 29].

A representative fuel channel model is shown in Figure 3-220. A representative fuel element in each segment of the ring is chosen for fuel thermal behaviour studies. Convective heat transfer on each fuel node has been coupled with “ATMKA-T” fuel element. Following voiding in the channels heat generated in fuel bundles is transferred by radiation to the pressure tube and calandria tube and then convective heat transfer to the moderator. Code uses internationally accepted validated correlations and is validated against experiments.

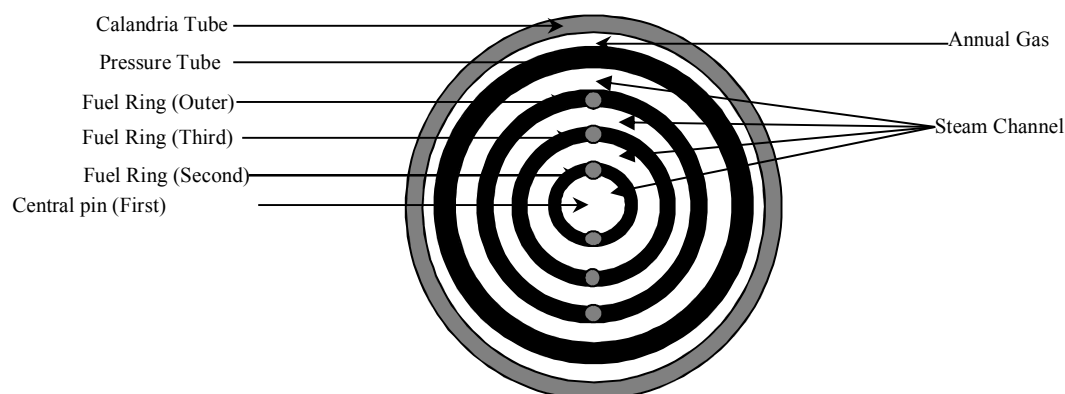


FIG. 3.220. Fuel channel model.

### 3.5.1.3. SEVAX

Computer code “SEVAX” is capable of modeling the complex sequence of severe accidents like channel heat up, metal-water reaction, moderator expulsion, slumping of the channels, core melt down and cooling of the corium at the bottom of calandria with calandria vault water cooling. The channel grouping of “CONTACT” described in Section 3.5.1.2 is used in “SEVAX”. However for the purpose of analysis all channels are modeled and the highest power in the group is assigned to each channel of the respective group. This way all 380 channels in the core are modeled at their respective physical location. Following Figure 3-221 shows grouping of channels in core.

	1	2	3	4	5	6	7	8	9	10	11	12	13	14	15	16	17	18	19	20	21	22
1									1	1	1	1	1	1								
2						1	1	2	2	2	2	2	2	2	2	1	1					
3					1	2	2	3	3	3	3	3	3	3	3	2	2	1				
4				1	2	3	3	4	4	4	4	4	4	4	4	3	3	2	1			
5			1	2	3	3	4	5	5	6	5	5	6	5	5	4	3	3	2	1		
6			2	3	3	4	5	6	5	5	5	5	5	5	6	5	4	3	3	2		
7		1	2	3	4	5	5	7	6	6	6	6	6	6	7	5	5	4	3	2	1	
8		2	3	4	4	5	7	7	6	6	6	6	6	6	7	7	5	4	4	3	2	
9	1	2	3	4	5	5	6	7	6	6	6	6	6	6	7	6	5	5	4	3	2	1
10	1	3	4	5	5	5	6	7	6	6	5	5	6	6	7	6	5	5	5	4	3	1
11	2	3	4	5	7	7	7	7	6	5	5	5	5	6	7	7	7	7	5	4	3	2
12	2	3	4	6	7	7	7	7	6	5	5	5	5	6	7	7	7	7	6	4	3	2
13	1	3	3	5	7	7	7	7	7	6	5	5	6	7	7	7	7	7	5	3	3	1
14	1	2	3	5	7	7	7	7	7	7	6	6	7	7	7	7	7	7	5	3	2	1
15		2	3	4	5	6	7	7	7	7	7	7	7	7	7	7	6	5	4	3	2	
16		1	2	3	4	4	5	7	6	6	7	7	6	6	7	5	4	4	3	2	1	
17			2	3	3	4	5	6	5	6	6	6	6	5	6	5	4	3	3	2		
18			1	2	2	3	4	5	6	6	5	5	6	6	5	4	3	2	2	1		
19				1	2	2	3	4	4	4	4	4	4	4	4	3	2	2	1			
20					1	2	2	3	3	3	3	3	3	3	3	2	2	1				
21						1	1	2	2	2	2	2	2	2	2	1	1					
22									1	1	1	1	1	1								

FIG. 3.221. Group wise distribution of channels.

Till the time average temperature of PT and CT is below 1,200°C, analysis is carried out by using “CONTACT” code. Once average temperature of PT and CT reaches 1,200°C, analysis is shifted to “SEVAX” code and the entire fuel channel is considered as lumped. As PT and CT average temperature of 1,200°C is considered as fuel channel dislocation criteria, it is assumed in the analysis that the lumped mass of the dislocated fuel channel will be relocated on the underneath intact channel. No inventory transfer from PHT to moderator is considered upon failure of channel. In accident progression the underneath fuel channel also dislocates, when it meets the dislocation criteria and it is assumed that it gets lumped with dislocated fuel channels supported by it. This process continues till core collapse criteria is met (which is, a single fuel channel can withstand maximum of seven fuel channels load). After reaching the core collapse criteria, all channels (dislocated as well as intact in that particular column) are relocated to calandria bottom. The core collapse is modeled column wise and calculations are done for all columns of fuel channels in the core. At the time of complete core collapse (i.e. all columns of fuel channels falling to the calandria bottom), there may still be moderator inventory left in calandria, which will eventually be boiled off. It is assumed that channel

columns take a rectangular cask shape upon falling in the calandria and rest on calandria shell. As the moderator continues to evaporate, fallen channels get re-exposed and reheat due to the decay heat and oxidation.

After boiloff of entire moderator inventory, due to complete loss of heat sink, the debris reaches their melting point. It is assumed that oxidation of exposed channels is limited up to the calandria tube thickness. As the debris continues to heat up and reaches to 70% of its melting (i.e., Energy stored is equal to 70% of latent heat of melting), debris redistributes uniformly in the calandria. Debris upon redistribution forms a uniform porous structure, composed of  $UO_2$ ,  $ZrO_2$  and Zr in their actual proportions. The dimensions of the debris bed are defined by mass and densities of debris material and assumed porosity (considered as 50%). The shape of debris is considered as calandria shape at the bottom and a flat surface at the top.

Body fitting co-ordinates have been used for discretization of debris (Fig. 3-222). The heat transfer within the debris bed is modeled with an equivalent conductivity including the effect of the conduction in the solid and gas phases, as well as the radiation between solid particles.

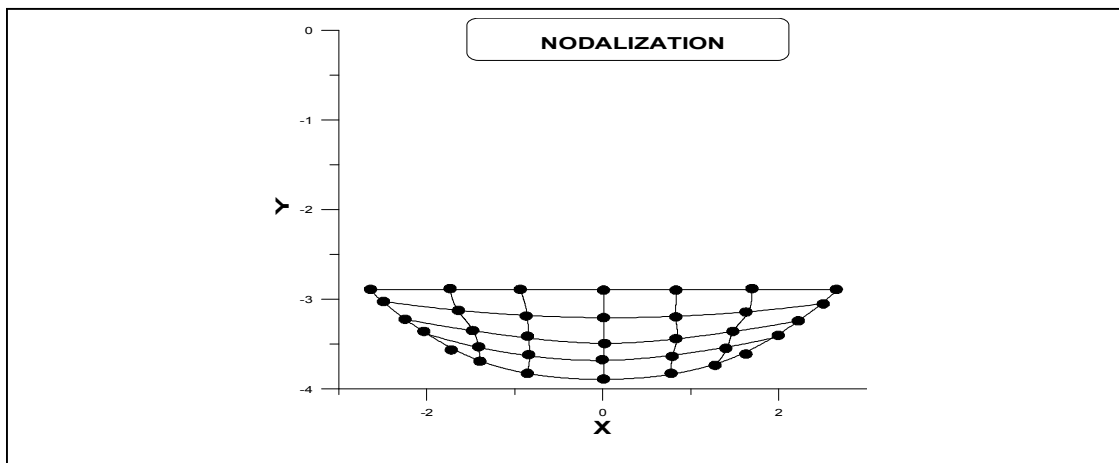


FIG. 3.222. Grid model used for debris in calandria vessel.

After calandria vessel failure, whole of the lumped mass is considered to be instantaneously transferred to calandria vault basement and it is assumed that corium takes the shape of half cylinder above the calandria vault floor (See Fig. 3-223).

#### 3.5.1.4. MCCI

Two-dimensional heat conduction equation is solved for the temperature distribution throughout the corium and concrete basement.

Concrete ablation at each node is in proportion to percentage evaporation of water content in the node [30]. Linear proportionality is considered between ablation rate and the evaporation rate [31]. It is assumed that ablated concrete will be uniformly mixed in the corium. Weighted average is considered for estimation of the change in the thermal conductivity of the node.

For modeling MCCI, body fitting co-ordinates are used [32]. Finer grid is considered at the interface of corium and the concrete. Corium debris on the calandria vault floor and grid used for mathematical model is shown in Figure 3-223.

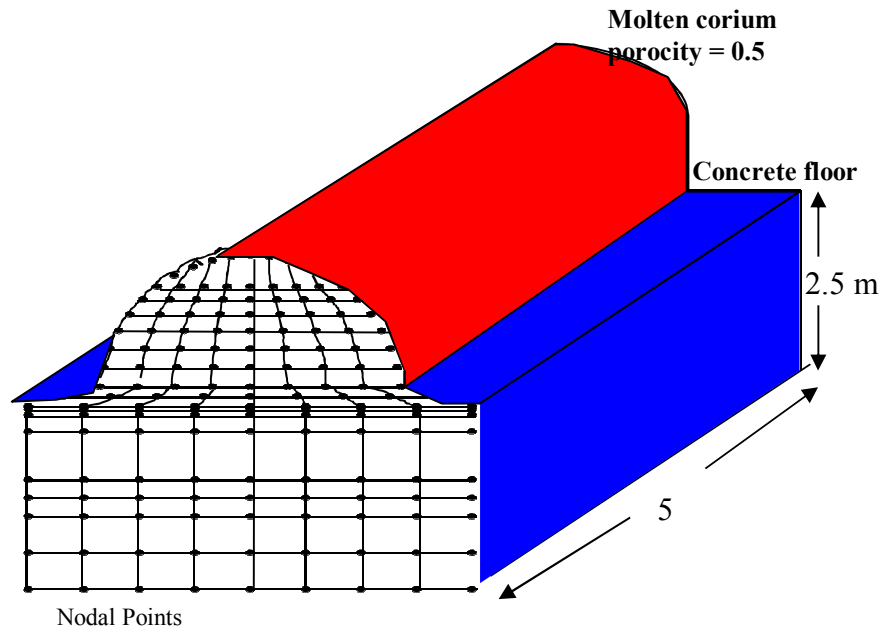


FIG. 3.223. Corium debris on the calandria vault floor and grid used for MCCI.

#### 3.5.1.5. PACSR

Analysis of containment pressure and temperature is carried out by computer code PACSR (Post Accident Containment System Response). The method involves breaking up the whole duration of the event into small time steps and then considering the effect of energy and mass addition in the small time interval for arriving at the pressure/temperature at the end of the time step using the applicable thermodynamic laws.

This code can simulate any number of compartments. In the analysis reported here, the containment has been simulated by total 15 volumes. Each compartment is divided into two regions: a liquid region containing water, and a vapors region containing uniform mixture of air, water vapor and liquid droplets. Vapor region is assumed to be in thermodynamic equilibrium, and have uniform temperature and density throughout the region. The flashed coolant (steam) is assumed to mix instantaneously and uniformly in the vapour region of high enthalpy area (F/M Vaults, Pump room, Dome area etc.). The separation of the two regions in each volume allows a more realistic assessment of the pressure and temperature in the containment atmosphere by removing the liquid droplets from vapour region and adding them to liquid region. It also allows consideration of transient super-heating condition in the event of a direct energy input.

The code can also simulate the containment walls and structures for their heat absorption and conduction calculation. It can generate the temperature profile across the wall thickness at any instant of time.

The mass and energy flow entering or leaving any compartment are based on lumped parameter approach. That means that an atmospheric flow leaving a zone will be of the average composition and temperature of this zone. The equation for calculation of transient flow through junctions is based on conservation of momentum.

The diffusion of steam, air and other non-condensibles (hydrogen) from high concentration compartment to low concentration compartment through the cross-section of junction is modeled by using Fick's 1st law.

#### 3.5.1.6. *STAR*

Computer code STAR (Source Term Analysis and Release) is used to calculate release fraction of fission products from overheated fuel. The verification of the code “STAR” is carried out with bench mark problems given in open literature. Initial core inventories, fraction gap inventories, geometry data related to core, temperature transient, percent oxidation of Zirconium, channel power and fractional contribution of pins within a bundle, and axial power factors are input to the code. The code calculates transient release of specified fission products. The equilibrium core inventory and fractional gap inventories are calculated by ORIGIN-2 and in-house developed code GAPin respectively.

The code contains various release models like CORSOR, CORSOR-M, KRESS/BOOTH relative volatility, CORSOR-BOOTH, ORNL-BOOTH and ORNL-BOOTH modified to estimate the release of the fission products from the fuel. The code can estimate the release of about 23 important radio nuclides; these are selected based on their health effects upon release. There is zirconium trapping effect consideration for the species like tellurium. For present estimation, ‘CORSOR-M’ which is the first order release rate model, is used.

#### 3.5.1.7. *ACTREL*

Computer code “ACTREL” (ACTivity RELease) is used for Radiological Impact Assessment (RIA) of an accident scenario in NPP. It estimates radio nuclides released to the environment from containment, the concentration in air and ground contamination, and the doses imparted to a hypothetical individual of general public. ACTREL models primary containment as a single compartment. It incorporates radioactivity removal by radioactive decay, plate out and other engineered safety features. ACTREL uses Gaussian Plume Model, for dispersion calculation of radio nuclides. The Time Integrated Concentration (TIC) is corrected for reactor building wake effect and sampling time. ICRP dose conversion factors are used to estimate the dose.

#### 3.5.1.8. *Coupling of all codes*

Since different codes are used at various stage of accident progression, coupling of codes and their interaction is shown in the flow diagram (Fig. 3-224).

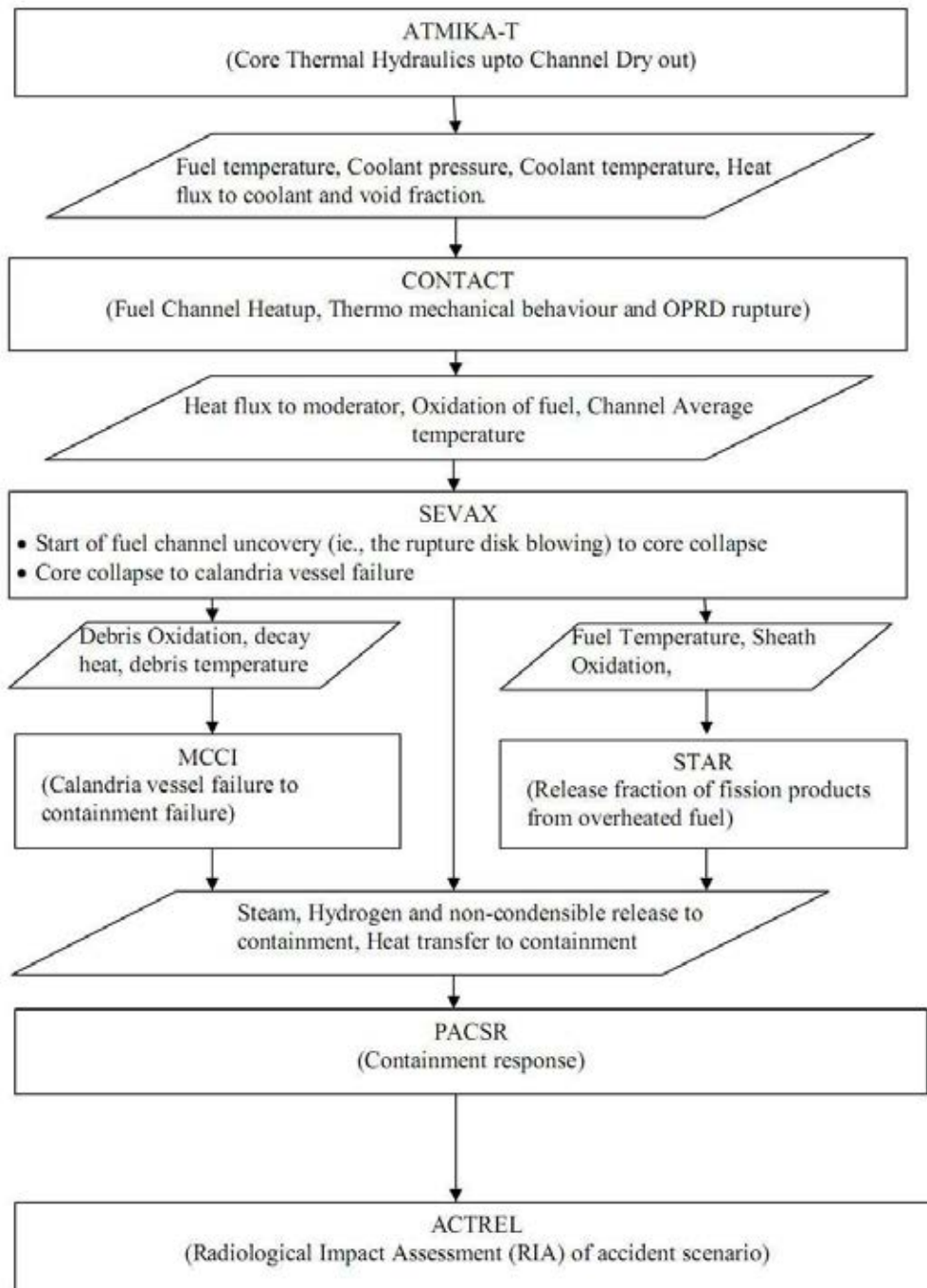


FIG. 3.224. Flow diagram of the analysis.

### 3.5.2. Phenomena and system idealization

An extended and unmitigated Station Black Out (SBO) could lead to severe accident. At time  $t=0$  s, SBO is initiated and reactor is also tripped. Due to sudden loss of SG feed water supply, SG pressure increases and leads to opening of the SRVs, which open and close as per their set point (atmospheric steam discharge valves are considered to be unavailable). Opening of SRVs lead to loss of inventory and ultimately SGs dry out.

After SG inventory is completely boiled off (i.e. SG dryout), PHT system starts swelling due to loss of heat sink. Pressuriser level, PHT pressure and sheath temperature starts increasing. PHT pressure increases at a faster rate once pressuriser is completely filled up. The pressure

reaches to LRV set pressure and after LRV opening PHT inventory starts getting lost to degasser condenser.

Decrease in PHT inventory leads to voiding of coolant channels. As the channels completely void, sheath temperature starts rising. Due to loss of moderator cooling, moderator temperature and calandria pressure starts rising as it continues to get heat from the coolant channels. After the SGs inventory boil off, rate of calandria pressure rise increases due to more heat load coming from PHT. When calandria cover gas pressure reaches to rupture disk bursting set pressure, rupture disks rupture and moderator spills out of calandria. After rupture disks rupture, calandria is at atmospheric pressure and the already heated moderator starts boiling and is lost from the calandria. It leads to reduction of moderator inventory.

As the moderator evaporates, rows get uncovered progressively. Respective uncovered row channels get heated up due the decay heat, metal water reaction heat and no heat sink available. Each channel gets heated up and at high temperature, pressure tube and calandria tubes lose their strength, get deformed and dislocates by creep-rupture under the imposed gravity loads. PT and CT are expected to fail within a few minutes after channel uncover and relocates on the underneath intact channel. No inventory transfer from PHT to moderator is considered upon channel failure. After the underneath fuel channel also dislocates, it gets lumped with already dislocated fuel channels supported by it. As the moderator evaporates lower row channels also start uncovering and channels slumping progresses.

It is estimated that a submerged channel can support upto seven additional channels before its pullout from rolled joint occurs. Therefore, it is assumed that after seven channels get lumped together, all the remaining channels in the column fail and fall to the calandria bottom and get lumped together. It is assumed that fallen channels take a rectangular cask shape resting on calandria shell. As the moderator continuous to evaporate fallen channels will re-expose after some time and reheat due to the decay heat and oxidation. After complete moderator boil off, due to complete loss of heat sink debris reaches to their melting point. During this heat up there is no heat transfer from debris to calandria vault due to line contact between solid debris and calandria shell. Channel oxidation is assumed to be limited up to the calandria tube thickness

As the debris continues to heat up and reaches to 70% of its melting (i.e., Energy stored is equal to 70% of latent heat of melting), debris redistributes uniformly in the calandria and heat transfer to calandria vault establishes. Because of the heat removal from the debris to the calandria vault water debris get cooled. It is also assumed radiation heat transfer from debris to calandria shell will be effective only after debris re-distribution. During the period of heat removal from debris by calandria vault water, temperature of calandria vault water rises and reaches its boiling point. Upon reaching boiling, calandria vault water also starts escaping and its level starts falling.

As the calandria vault water level falls below debris level in calandria, the heat transfer from debris to calandria vault water gets degraded. Due to degradation in heat transfer, calandria shell temperature increases. The calandria bottom heats up rapidly by the heat from the core debris inside the calandria and calandria fails due to creep and the partial molten debris material falls down in the calandria vault water which quenches the debris. The remaining calandria vault water starts boiling off into containment. Corium also starts reacting with concrete floor and resulting into failure of the concrete floor. Molten corium concrete interaction leads to calandria vault basement failure.

### **3.5.3. Analysis results**

The major sequence of events is summarized in Tables 3-15 and 3-16.

### 3.5.3.1. Phase 1 (Accident initiation to calandria rupture disk blowing – 20,251 s)

#### (a) Steam generator dryout (9,080 s)

At time  $t=0$  s, SBO is initiated. The loss of off-site power causes reactor trip. Due to reactor trip, there is a dip in PHT pressure for initial few seconds (Fig. 3-225) and also reduction in flow of PHT (Fig. 3-258). Further flow in core is governed by natural circulation and heat removal through SGs. As there is no feed water supply to SGs, their pressure increases. As atmospheric steam discharge valves are considered unavailable, SG pressure continues to rise till SRV set point is reached (Fig. 3-226). SRVs open to relieve pressure but continued heat up causes them to open again. This cyclic opening and closing of SRVs cause loss of inventory from SGs (Fig. 3-227). Due to loss of inventory, SGs level also decreases (Fig. 3-228) and SGs dry out occurs at 9,080 s. Till the time SGs dry out, they provide heat sink to PHT (Fig. 3-229) and as such PHT pressure decreases (Fig. 3-225). During the time when PHT pressure was reducing, there is inventory transfer from pressurizer to PHT main circuit and as such there is fall in pressurizer level (Fig. 3-230). As heat from PHT is getting removed through SGs, PHT temperature (Fig. 3-257) and fuel sheath temperature (Fig. 3-237) also remain low.

#### (b) LRV opening (10,980 s)

After SGs dry out (9,080 s), PHT starts to swell due to loss of heat sink and PHT pressure starts increasing (Fig. 3-225). The rise in PHT pressure causes inventory transfer to pressurizer and as such pressurizer starts getting filled up (Fig. 3-230). As cooling to PHT is lost, there is gradual rise in fuel sheath temperature (Fig. 3-237) and PHT temperature (Fig. 3-257). After SG heat sink is lost, heat transfer from PHT to moderator increases (Fig. 3-259) causing rise in moderator temperature (Fig. 3-260) and cover gas pressure (Fig. 3-236). PHT pressure continues to rise till it reaches LRV set pressure at 10,980 s (Fig. 3-225). Thereafter, it is maintained at LRV set pressure till channels failure.

#### (c) Calandria rupture disk blowing (20,251 s)

Due to LRV opening there is a net loss of PHT inventory (Fig. 3-231). Opening of LRVs causes a momentary dip in PHT pressure, which increases again due to continued heat up leading to opening of LRVs and such cycles continue (Figs 3-225 and 3-234). Due to loss of PHT inventory (Fig. 3-231) channel voiding increases (Fig. 3-233). After the channels get completely voided fuel sheath temperature (Fig. 3-237) shoots up.

Loss of moderator cooling and continued heat transfer from coolant channels causes continuous heat up (Fig. 3-259) of moderator in the calandria. This causes calandria cover gas pressure (Fig. 3-236) to rise, which reaches calandria over pressure relief disk burst pressure and rupture disks rupture at 20,251 s.

#### (d) Containment response:

Due to LRV opening, steam is released into the containment and a rise in containment pressure is noted (Fig. 3-241). Subsequently, due to condensation of this steam on the concrete structure, containment pressure reduces and mass of water in the containment basement increases (Fig. 3-249).

### 3.5.3.2. Phase 2 (Calandria rupture disk blowing to core collapse – 44,946 s)

#### (a) Fuel channel failure (23,791 s)

Due to calandria rupture disk opening, a sudden dip in calandria cover gas pressure (Fig. 3-236) and loss of moderator inventory (Fig. 3-235) due to flashing is noted. As calandria cover gas pressure is reduced to atmospheric pressure, moderator in the calandria starts boiling and

the resulting steam gets into the containment (See Figure 3-262 for steam release to containment). The opening of relief path provides an escape path for moderator and moderator inventory and its level in calandria fall continuously (Fig. 3-235).

With moderator getting lost from calandria, coolant channel rows progressively get exposed (i.e. they are no longer submerged in moderator). First row uncover occurs at 20,711 s. The exposed channels get heated up due to decay heat and heat generated due to metal water reaction. Due to metal water reaction, hydrogen is generated (Fig. 3-261). As there is no heat sink for the channels they continue to heat up and their temperature reaches up to 1,200°C. At this temperature it is considered that the channel fails and dislocates from its position and rests on the channel underneath. The first fuel channel failure occurs at 23,791 s.

(b) Core collapse (44,946 s):

This kind of disassembly of fuel channels in a channel column continues as fuel channels are progressively getting exposed (due to loss of moderator inventory) and reaching the dislocation criteria. As more channels get dislocated, the UO<sub>2</sub> mass in the intact channels get reduced (Fig. 3-238).

When seven channels in a channel column get lumped with each other, the core collapse criteria is satisfied and that particular channel column (i.e. dislocated channels and intact bottom channels) falls to the bottom of calandria and upon collapse of columns, all channels in the column are considered to be lumped together. Figure 3-239 shows the number of channels falling with time at calandria bottom. Figure 3-242 shows weight of these channels on calandria.

The starting of core collapse is at 32,976 s and complete core collapse at 44,946 s.

(c) Containment response:

Due to calandria rupture disk opening, containment pressure shows a spike (Fig. 3-241), which gets arrested due to condensation of steam on concrete structure. Subsequently during boiling of calandria inventory, containment pressure shows an increasing trend. During collapse of first column of coolant channels (32,976 s), more heat is transferred to calandria resulting in more steam generation and therefore containment pressure rises faster. During this phase mass of water in sump continues to rise as steam from calandria is getting condensed on concrete walls (Fig. 3-249).

Hydrogen & steam concentration (%v/v) are shown in Figure 3-250. Hydrogen, steam & air concentration (%v/v) are shown in Figure 3-251 on the ternary diagram. During this phase hydrogen concentration will be out of deflagration and detonations zones. Figure 3-252 shows Containment temperatures in lower SG room and basement room. The temperature and pressure rises during boiling of moderator.

### 3.5.3.3. Phase 3 (Core collapse to calandria vessel failure – 117,111 s)

(a) Moderator boil off (53,086 s):

After complete core collapse (i.e. falling of all columns of channels), all channels are at bottom of the calandria and submerged in moderator. Boiling of moderator continues and this keeps debris temperature low (Fig. 3-243). In this period due to debris temperature being less than 800°C, there is no oxidation of debris. It is assumed that fallen channels take a rectangular cask shape at the bottom of the calandria. As the moderator continues to evaporate, fallen channels re-expose after some time and reheat due to the decay heat and oxidation. Moderator will be completely boiled off by 53,086 s. Figure 3-235 shows the variation of inventory of moderator and level of moderator. In this figure, level in calandria at

the time of complete boil off indicates debris height. Heat transfer from moderator to calandria vault is neglected till redistribution of debris in calandria vessel.

(b) Calandria vessel failure (117,111 s)

Debris temperature (Fig. 3-243) starts rising after complete boil off of moderator inventory. During this heat up of debris there is no heat removal from debris to calandria vault water due to line contact between solid debris and calandria shell. Channel oxidation is limited up to the calandria tube thickness

As the debris continuous to heat up and reaches to 70% of their melting, debris redistributes uniformly in the calandria. Redistribution of debris takes place at 53,536 s. At this point heat transfer from debris to calandria vault water increases (Fig. 3-244 shows the solidification of debris due to heat removal from calandria vault) and as such calandria vault water temperature shoots up (Fig. 3-240) and reaches saturation at about 56,976 s. With calandria vault water boiling off steam release to containment starts again (Fig. 3-262). The level in the calandria vault keeps on falling and the calandria vault water falls below debris level in the calandria at about 117,061 s. The calandria vessel gets devoid of cooling and calandria vessel temperature shoots up (Fig. 3-245). Calandria vessel failure is considered when calandria vessel temperature reaches 800°C at 117,111 s. With failure of calandria vessel, corium from the calandria relocates to calandria vault (Fig. 3-246).

(c) Containment response:

After complete boil off of moderator inventory, there is no steam generation and as such containment pressure reduces (Fig. 3-241). After steam generation from calandria vault water starts, rise in containment pressure is noted again. Containment pressure reaches 334 kPa(a) at which equipment airlock seals fail and containment pressure drops. Mass of water in the containment basement is shown in Figure 3-249. It is seen that mass continues to rise due to condensation of steam on the concrete structure.

Hydrogen & steam concentration (%v/v) are shown in Figure 3-250. Hydrogen, steam & air concentration (%v/v) are shown in Figure 3-251 on the ternary diagram. Figure 3-252 shows Containment temperatures in lower SG room and basement room. The temperature and pressure rises during boiling calandria vault water and containment equipment airlock seal opens at 334 kPa(a) around 97,000 s . Pressure and temperatures starts falling due to opening of containment equipment airlock seal at 334 kPa(a) and transfer of heat from Inner Containment Wall (ICW) to outside environment. Figure 3-253 shows Hydrogen concentration in different compartments of containment. It is also seen from the analysis that hydrogen concentration reaches to deflagration zone and then comes out of this zone. Hydrogen concentration never reaches to detonation zone.

*3.5.3.4. Phase 4 (Calandria vessel failure to containment failure due to ablation of containment basement floor – 191,171 s)*

(a) Molten core concrete interaction (MCCI):

The remaining calandria vault water continues to boil off and corium at the calandria vault bottom heats up further and generates hydrogen (Fig. 3-261) due to metal water reaction. Due to MCCI, calandria vault basement concrete temperature increases and corium penetrates (Fig. 3-247) into the calandria vault basement concrete thickness. Figure 3-248 shows ablated concrete depth. Failure of calandria vault basement concrete due to ablation of calandria vault basement is predicted at 191,171 s. Due to MCCI Oxygen and CO<sub>2</sub> is generated (Figs 3-263 and 264).

(b) Release to environment:

Initial release from the containment is due to leakages from the containment due to high pressure in the containment. It is seen that all release from containment is from the ground level. In the analysis radioactive decay of active fission product is not considered. A sudden release from the containment is due to opening of containment rupture disk at 334 kPa around 97,000 s.

Figure 3-254 shows mass of noble gas release to environment. Figure 3-255 shows mass Cesium release to environment and Figure 3-256 shows mass Iodine release to environment.

TABLE 3.15. CHRONOLOGICAL ORDER OF ACCIDENT PROGRESSION

Event	Timing (Sec)
Phase – 1	
Class IV and Class III power loss	0
Reactor shutdown	0
First opening of MSSV	27.5
SG complete dry out	9080
LRV 's first opening	10 980
Channel void reaches 0.9 for the entire length of channel for the first time in a channel	15 400
Calandria rupture disk rupture.	20 251
Phase -2	
First channel uncover occurs	20 711
First fuel channel failure	23 791
Starting core collapse	32 976
Complete core collapse	44 946
Phase-3	
Complete moderator boil off	53 086
Calandria vessel failure	117 111
Calandria vault water below debris level	117 061
Phase-4	
Containment failure due to failure of equipment airlock seals	97 000
Calandria vault basement concrete failure due to ablation	191 171

TABLE 3.16. LIST OF SIGNIFICANT TIMING OF EVENTS/OTHER SIGNIFICANT RESULTS FOR STATION BLACKOUT SCENARIO

Time (hr)	Time (s)	Events
	0	Class IV and Class III Power loss
	0	Turbine stop valves closed
	0	Reactor trips
	27.5	First opening of MSSV
2.52	9080	SG secondary sides are dry, Loop 1
2.52	9080	SG secondary sides are dry, Loop 2
3.05	10 980	LRVs open for the first time, PHTS Loop 1
3.05	10 980	LRVs open for the first time, PHTS Loop 2
4.27	15 400	At least one channel is dry Loop 1 (complete boil off)
4.27	15 400	At least one channel is dry Loop 2 (complete boil off)
5.62	20 251	Calandria vessel rupture disks #1-4 open
5.62	20 251	Moderator reaches saturation temperature
6.60	23 791	Pressure and calandria tubes are ruptured Loop 1
6.60	23 791	Pressure and calandria tubes are ruptured Loop 2
9.16	32 976	Beginning of the core disassembly, Loop 1
9.16	32 976	Beginning of the core disassembly, Loop 2
12.48	44 946	Core collapse (loop 1) to calandria vessel bottom
12.48	44 946	Core collapse (loop 2) to calandria vessel bottom
26.94	97 000	Containment failed due to equipment air lock seals failure
14.74	53 086	Water is depleted inside calandria vessel
15.82	56 976	Water in calandria vault reaches saturation temperature
32.51	117 061	Calandria vessel failed
32.53	117 111	Quenching of debris occurred in calandria vault
53.10	191 171	Water is depleted inside calandria vault
32.53	117 111	Molten corium concrete interaction begins in calandria vault
53.10	191 171	Calandria vault floor failed because of concrete ablation
Total amount of Hydrogen release “in-vessel” (in PHTS and in Calandria Vessel”) in PHTS loop 1 = 245 kg		
Total amount of Hydrogen release “in-vessel” (in PHTS and in Calandria Vessel”) in PHTS loop 2 = 245 kg		
Total amount of Hydrogen release “ex-vessel” (outside of the Calandria Vessel”) = 214 kg		
Total amount of noble gases released to environment = 57.7 kg		
Total amount of Cs and I released to environment = 1.02 kg (Cs) and 0.105 kg (I)		

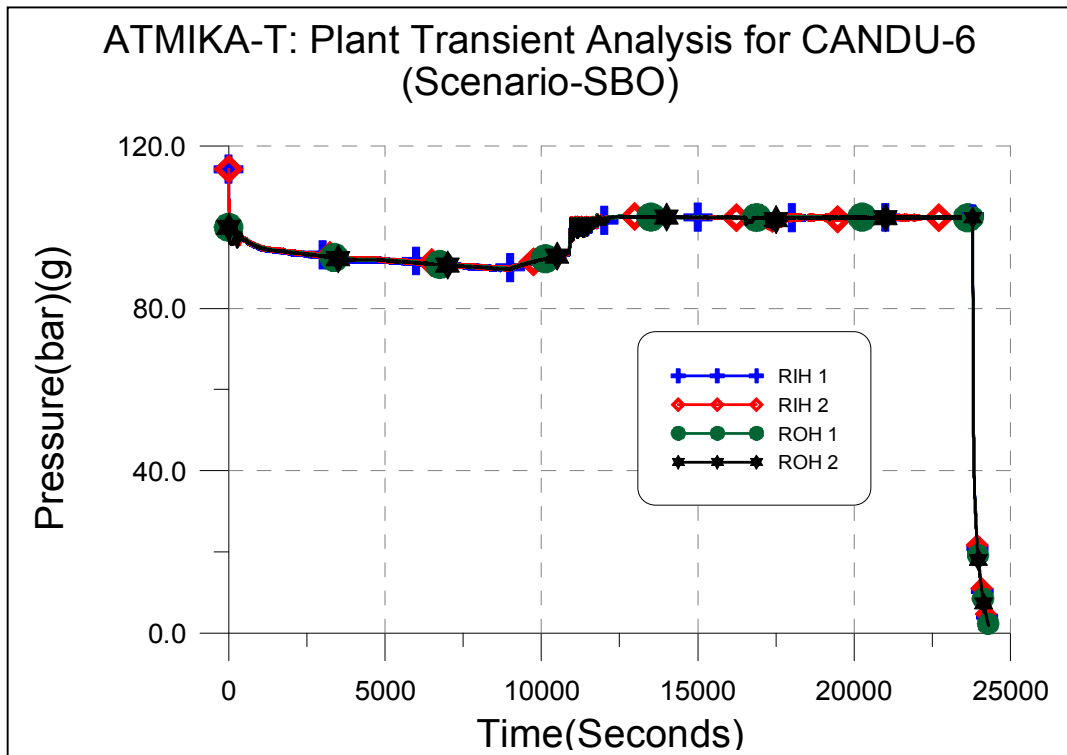


FIG. 3.225. PHT Pressure variation in Loop-1.

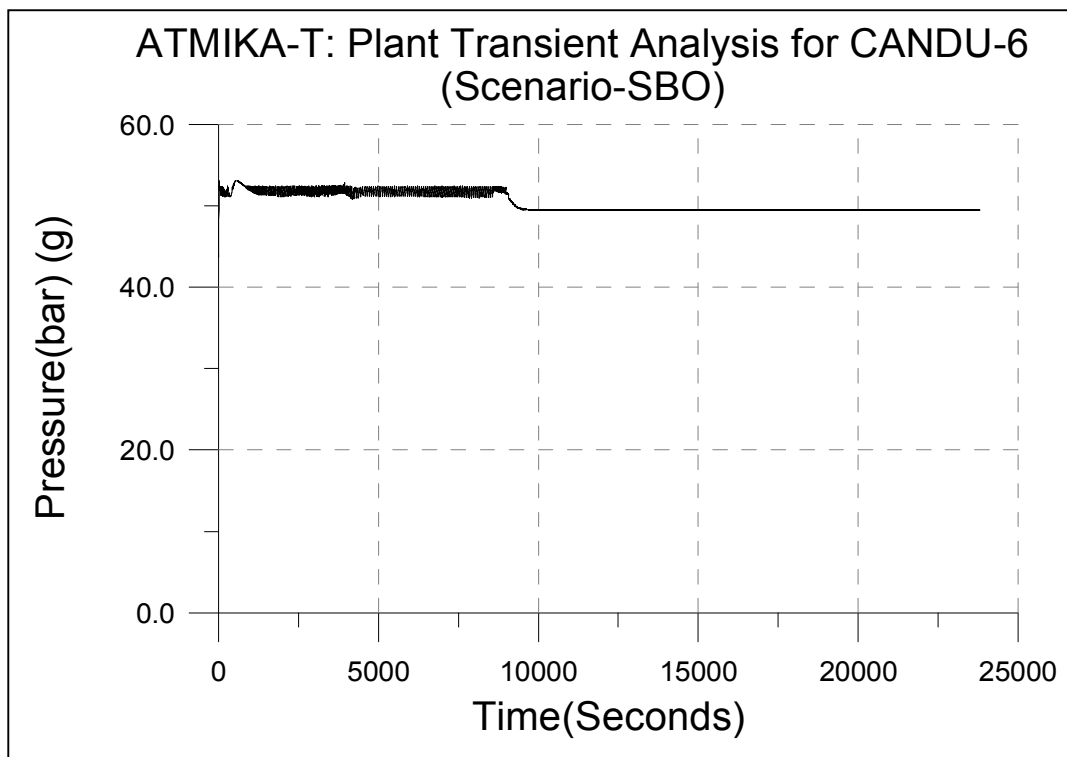


FIG. 3.226. Steam generators pressure variation.

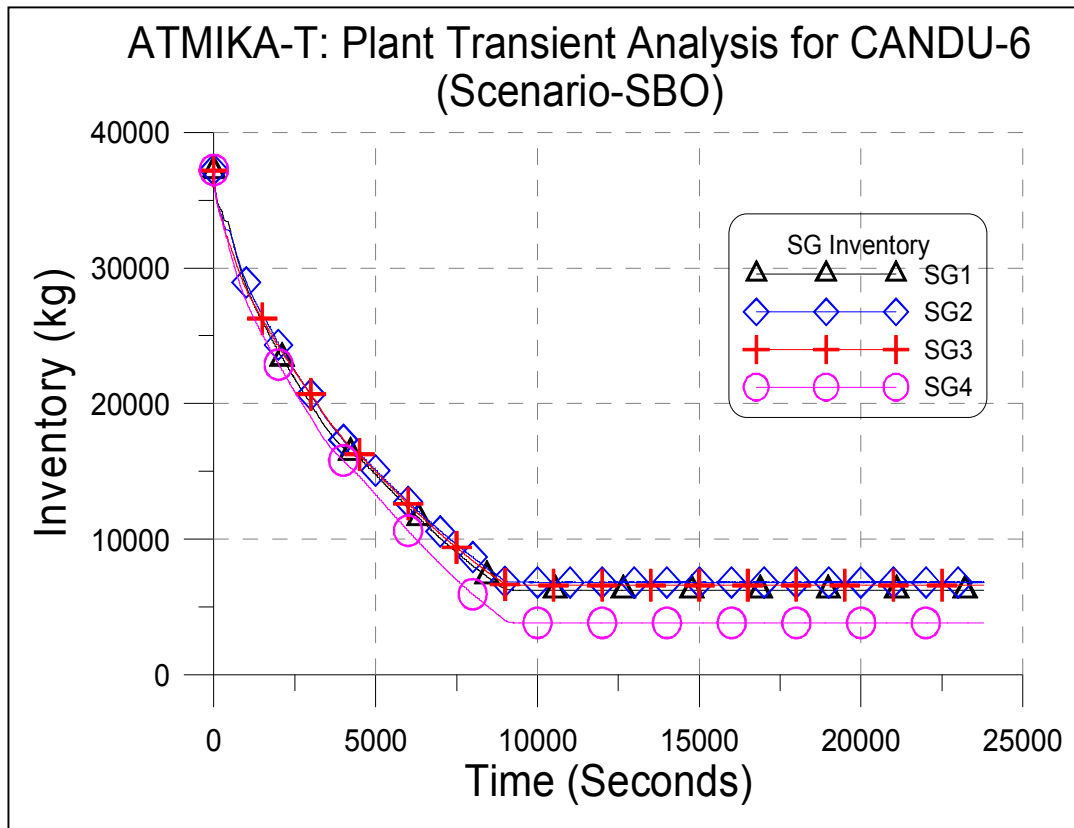


FIG. 3.227. Steam generators inventory variation.

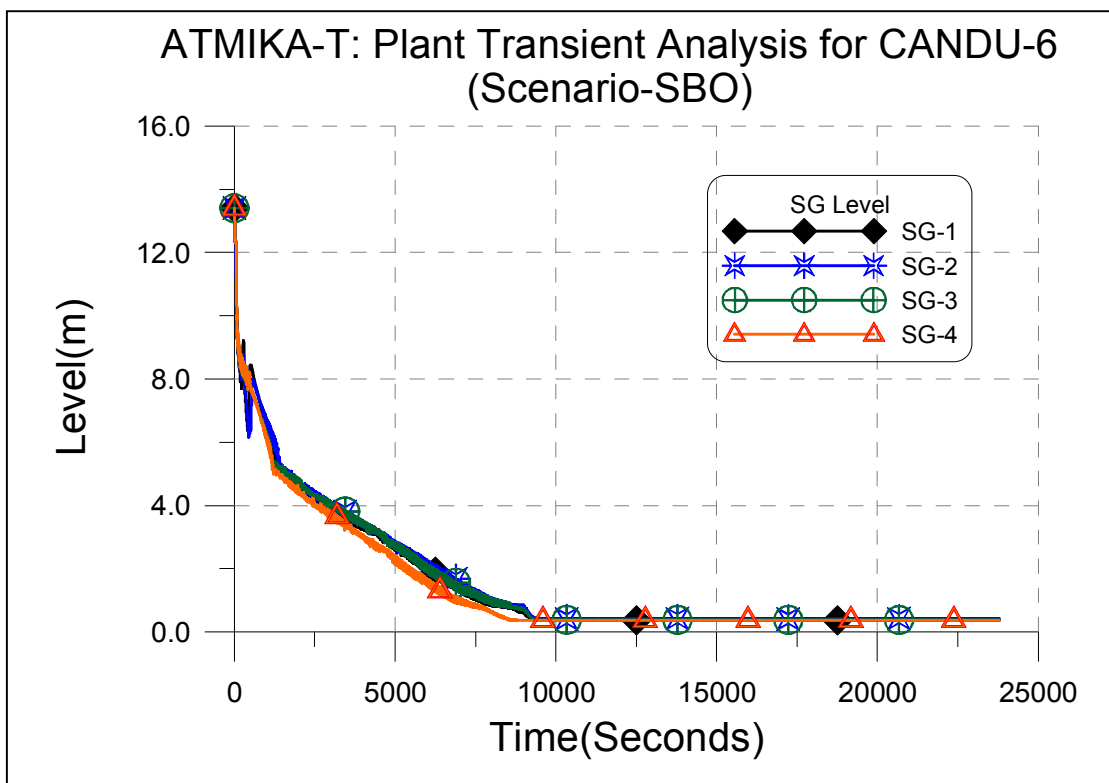


FIG. 3.228. Steam generators water level variation.

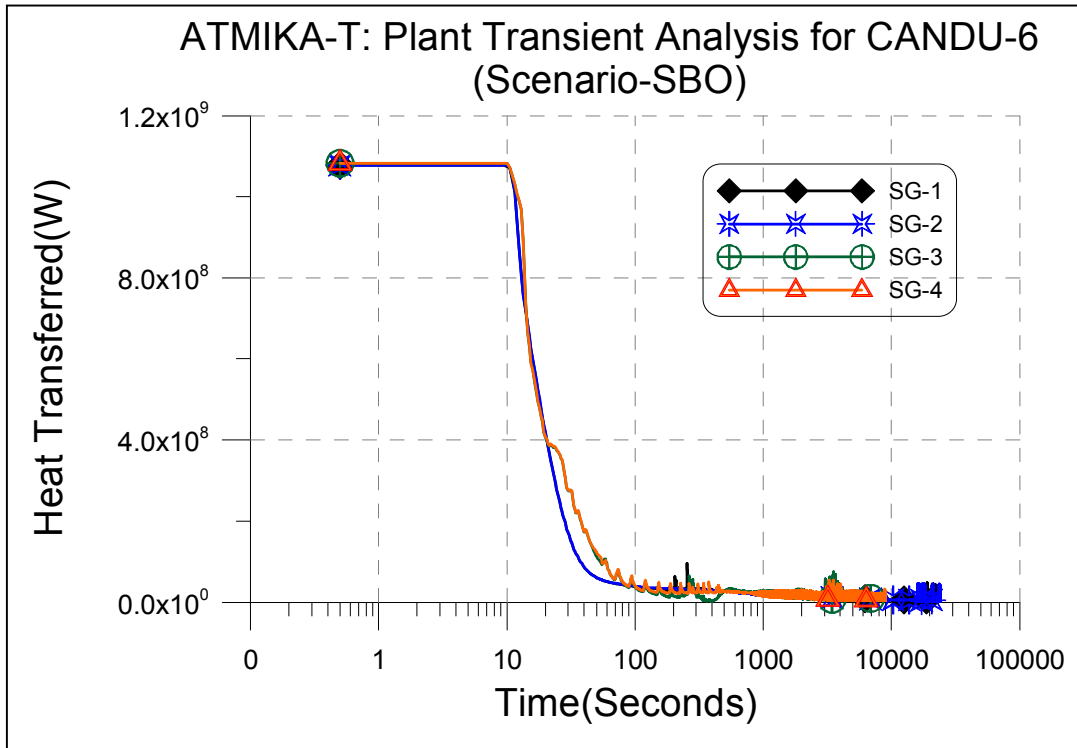


FIG. 3.229. Heat transfer from PHT to steam generators.

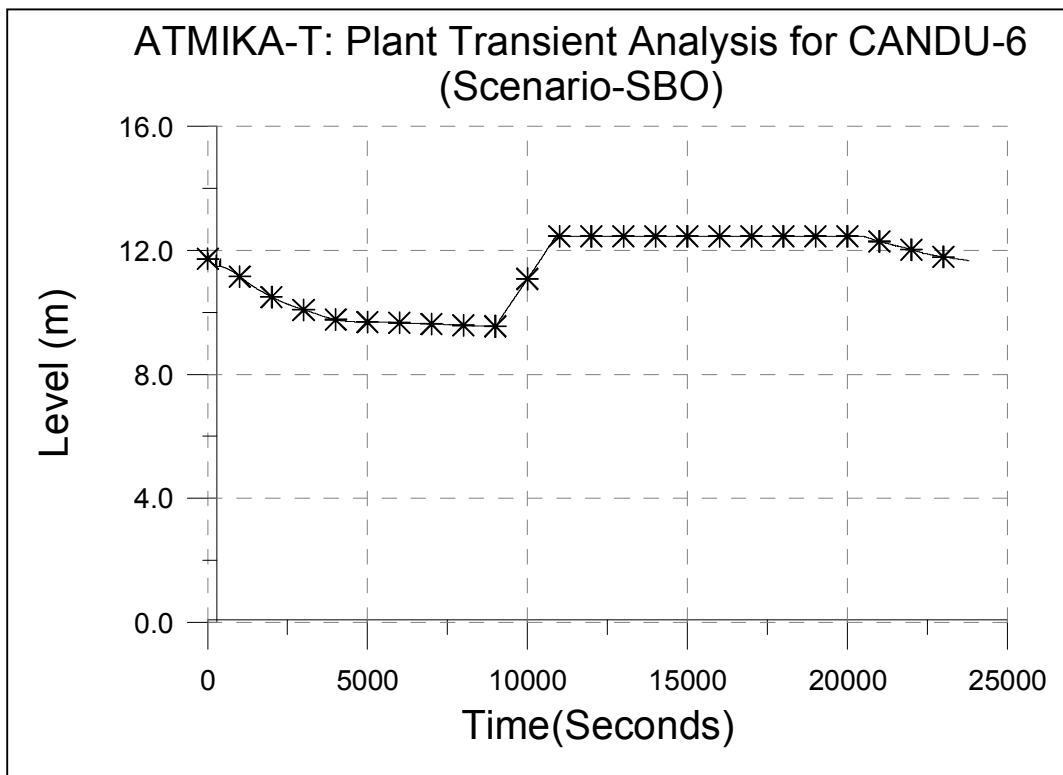


FIG. 3.230. Pressuriser level variation.

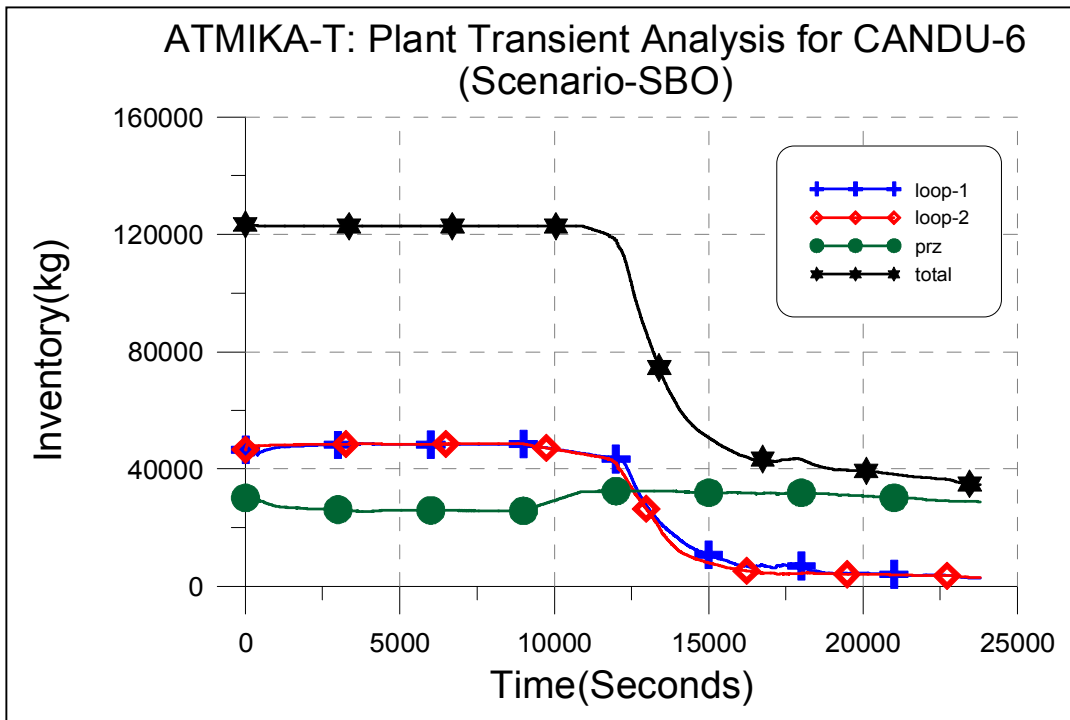


FIG. 3.231. PHT Inventory variation.

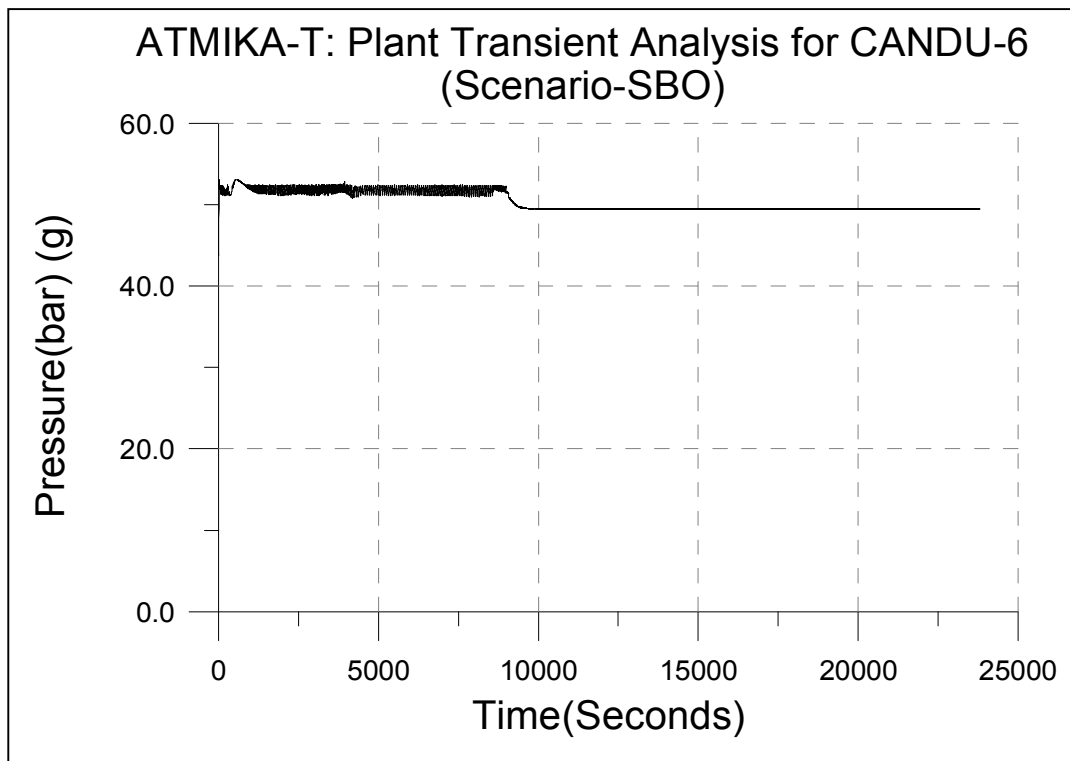


FIG. 3.232. Steam generators pressure variation.

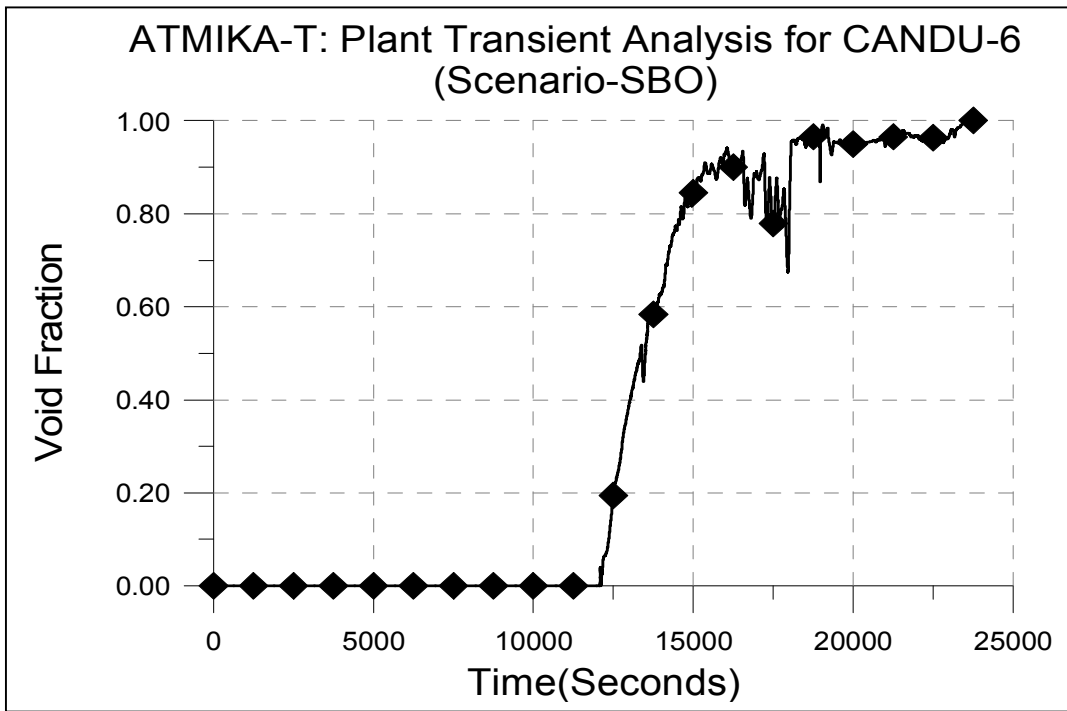


FIG. 3.233. PHT loop void fraction.

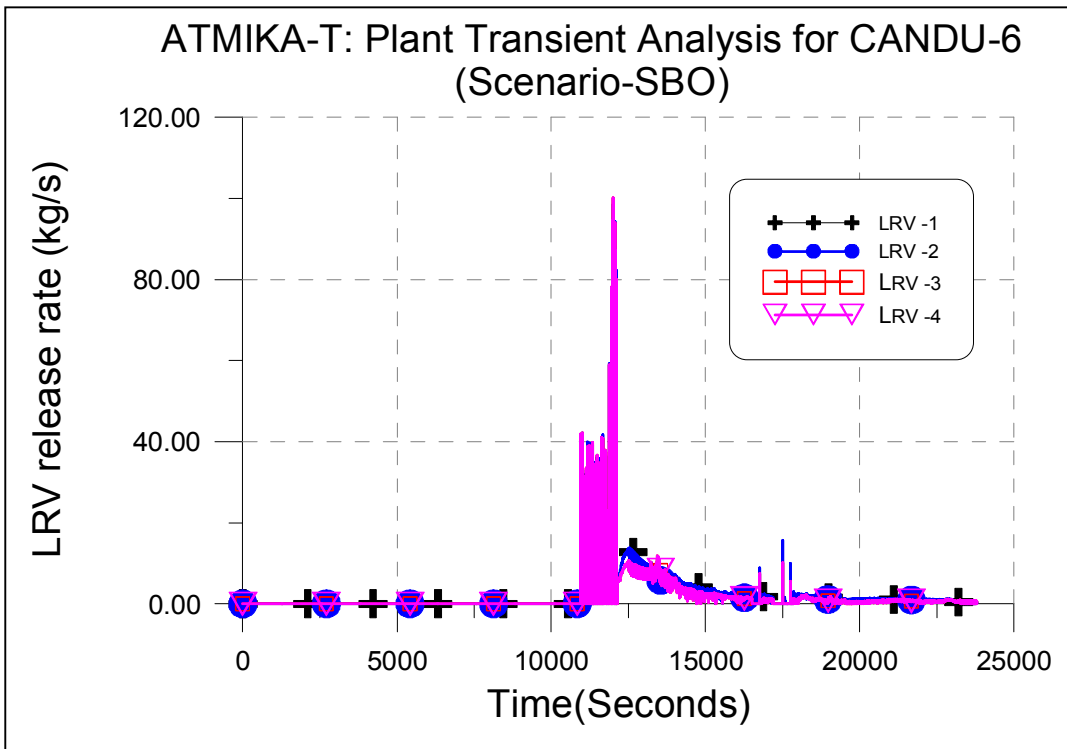


FIG. 3.234. LRV release rate variation.

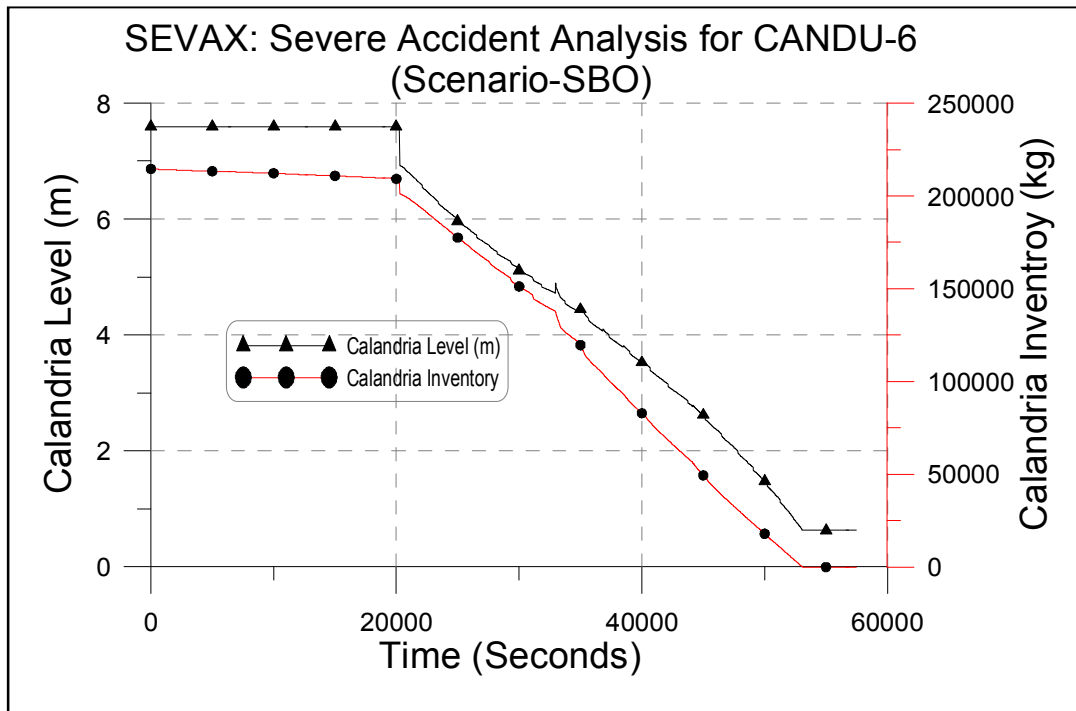


FIG. 3.235. Calandria level and inventory variation

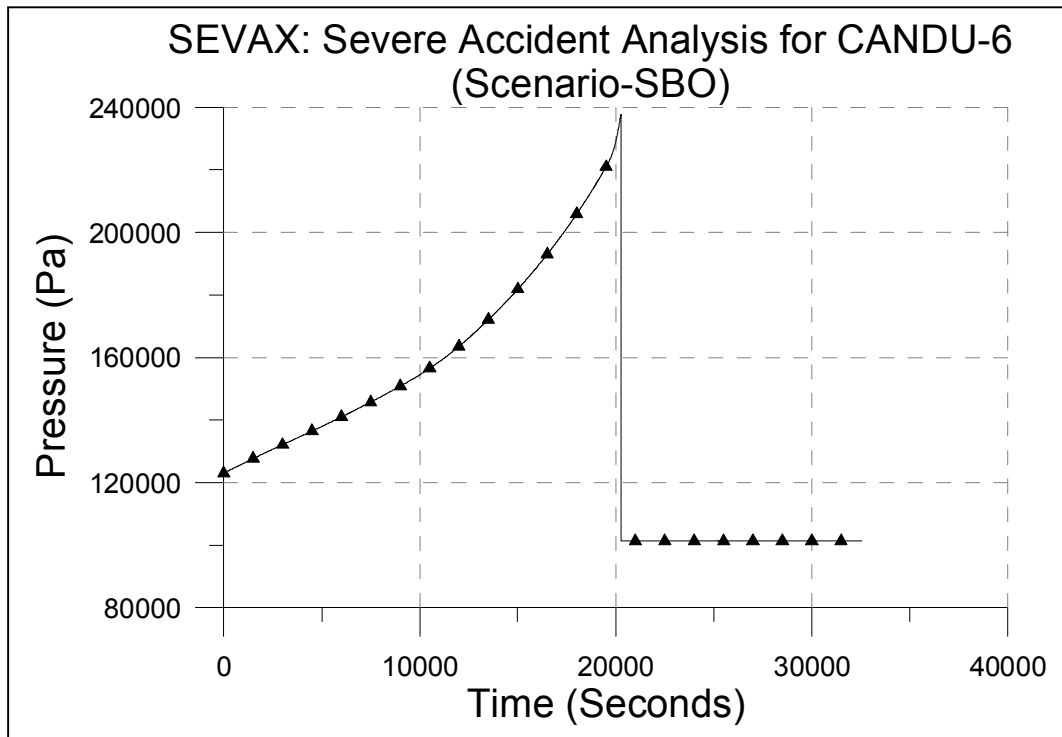


FIG. 3.236. Calandria cover gas pressure variation.

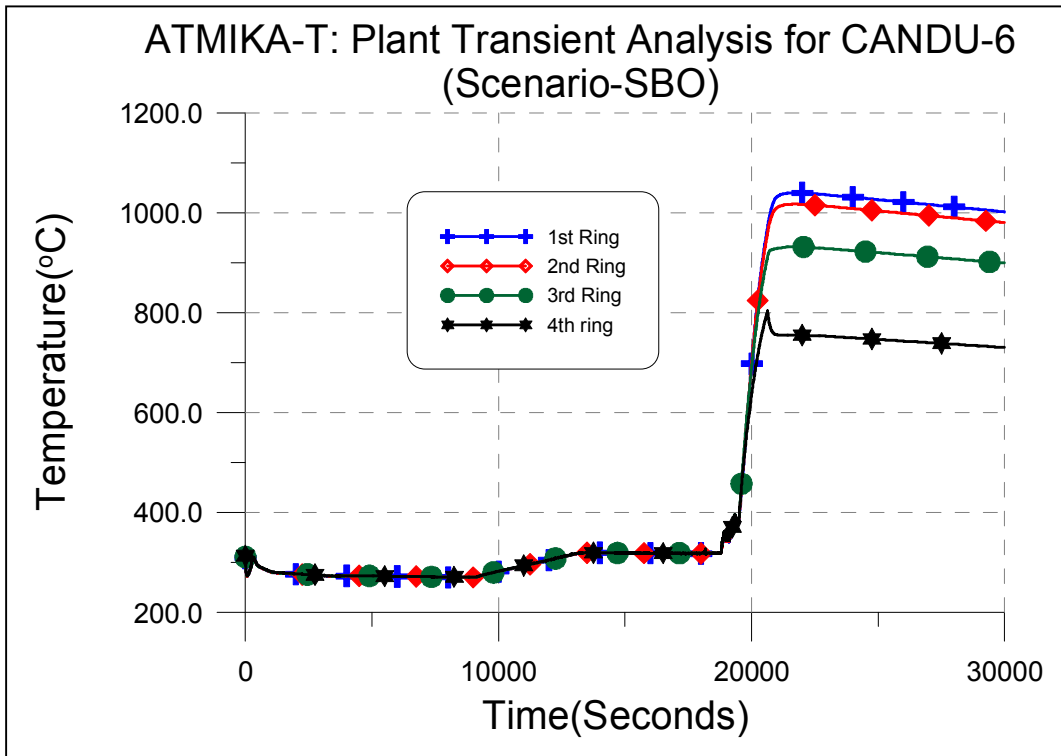


FIG. 3.237. Fuel Sheath temperature variation in submerged channels.

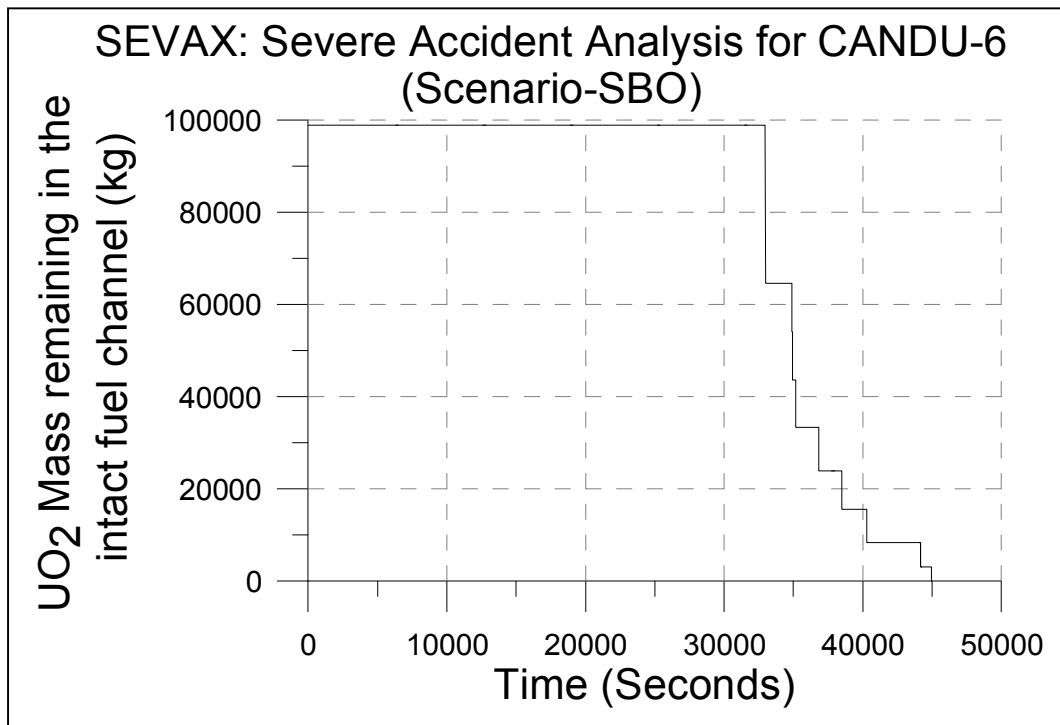


FIG. 3.238. UO<sub>2</sub> mass remaining in the intact fuel channel.

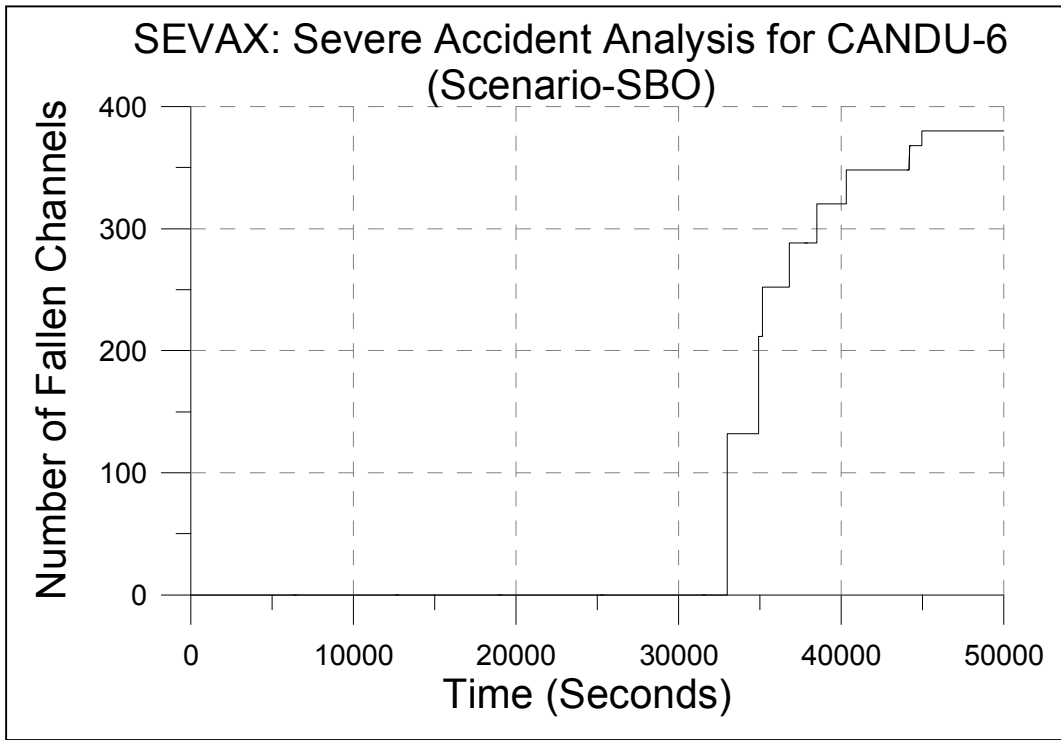


FIG. 3.239. Number of fallen channels.

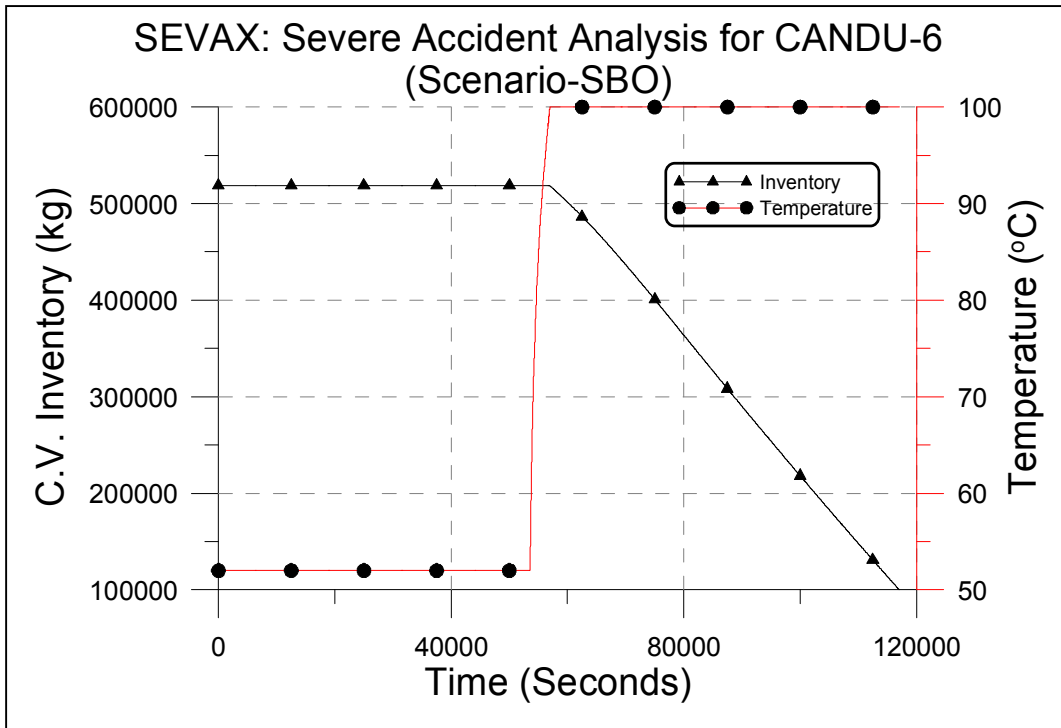


FIG. 3.240. Calandria vault water temperature and inventory variation.

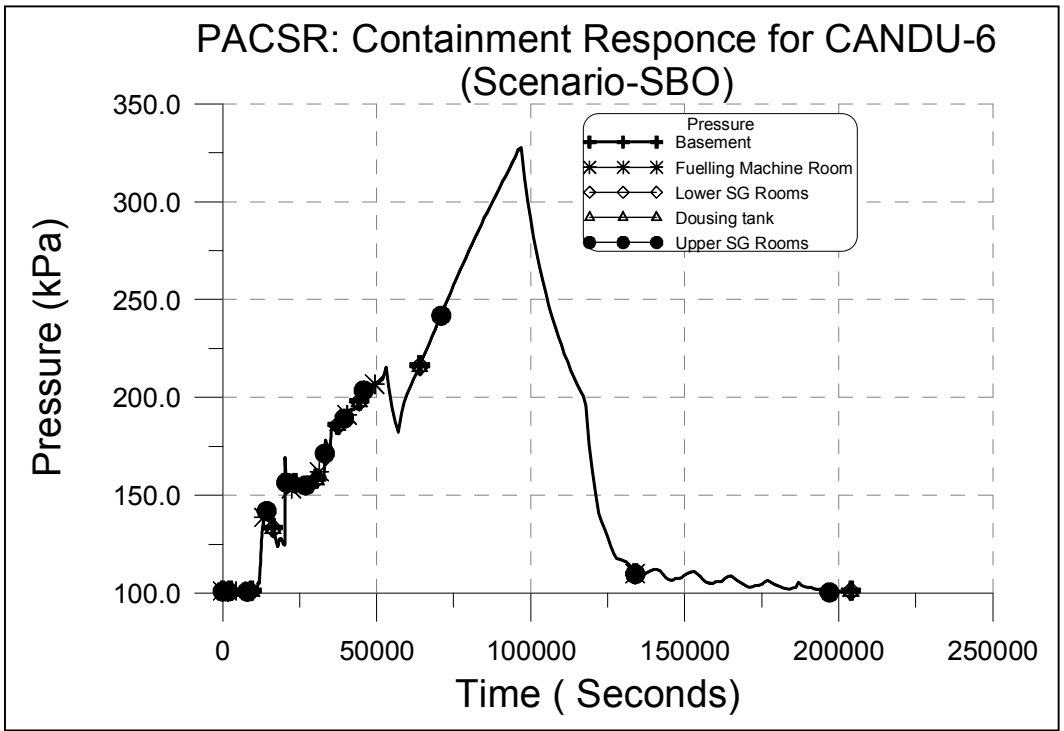


FIG. 3.241. Containment pressure variation at different locations.

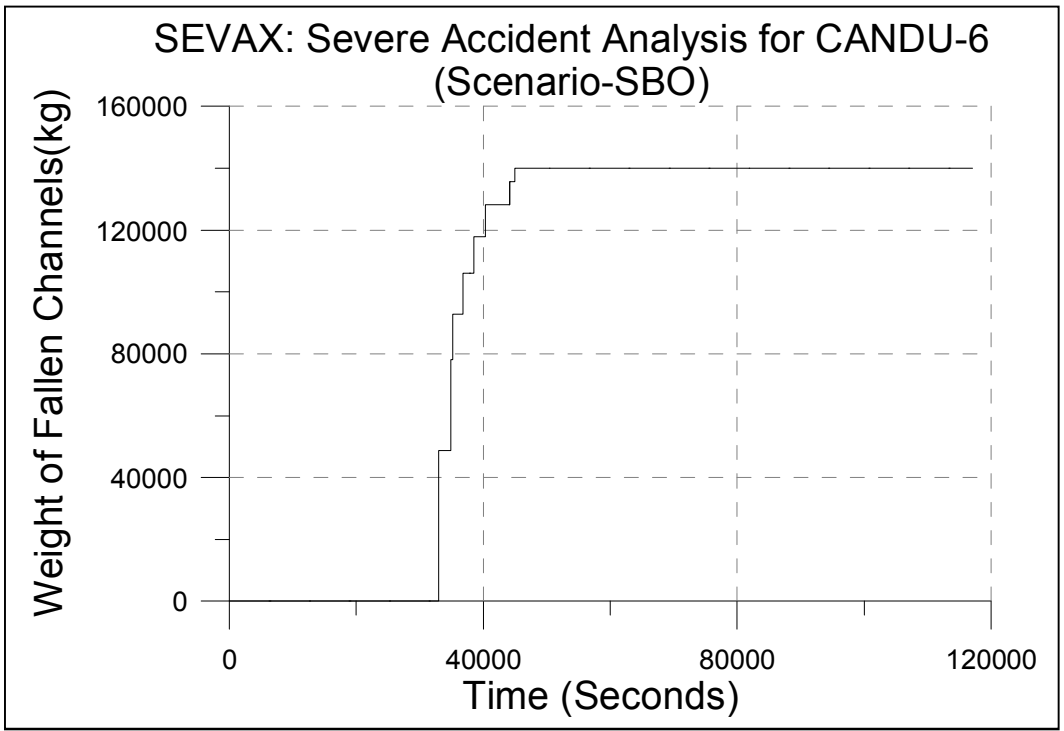
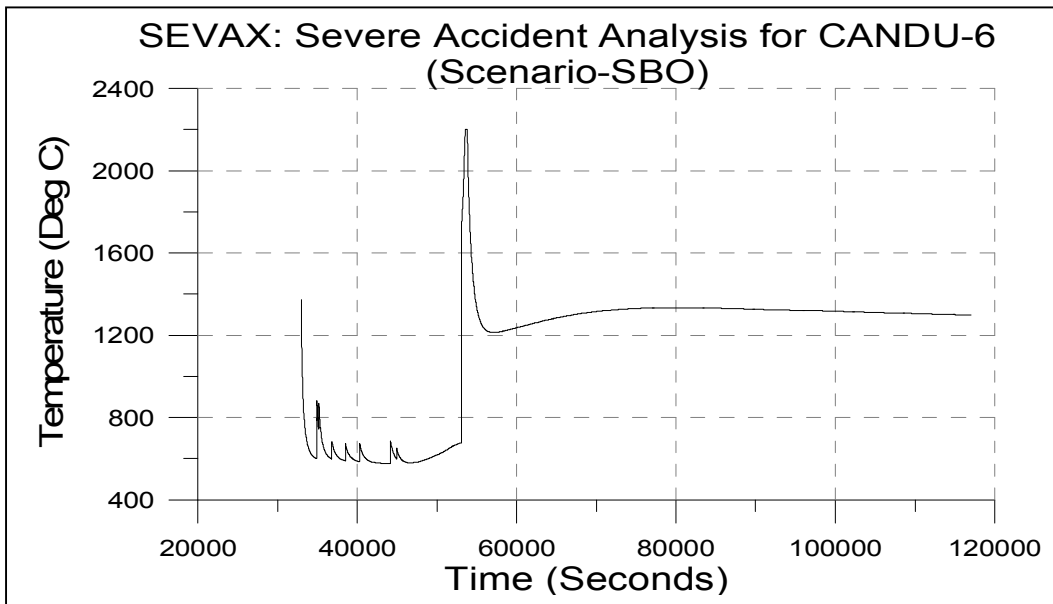
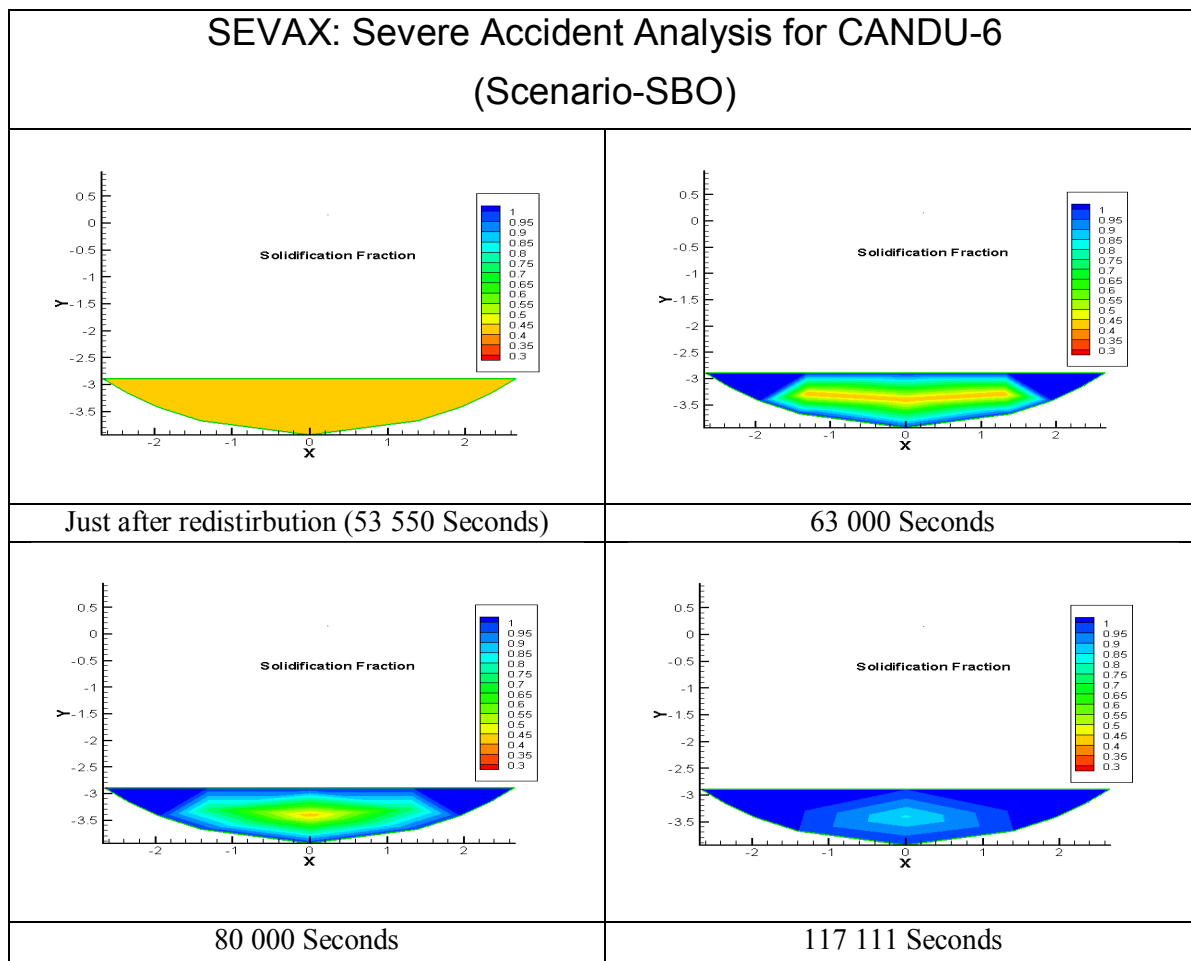


FIG. 3.242. Weight of fallen channels.



*FIG. 3.243. Debris temperature in calandria vessel.*



*FIG. 3.244. Debris solidification fraction at different time instant.*

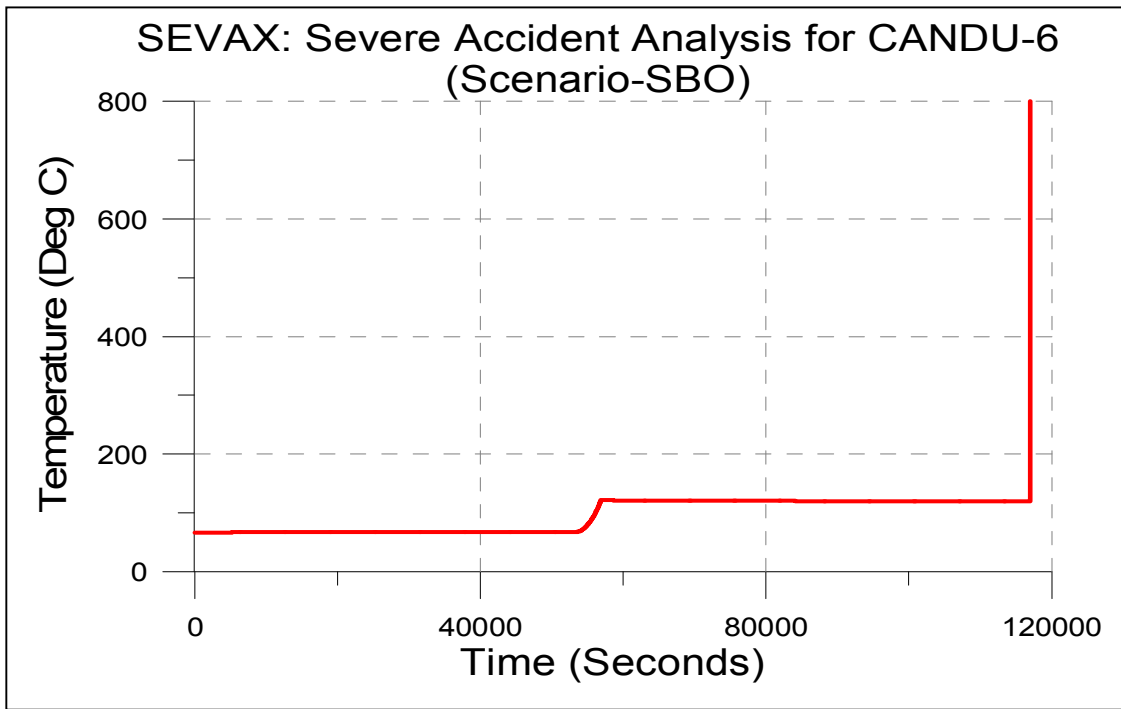


FIG. 3.245. Calandria vessel wall temperature variation.

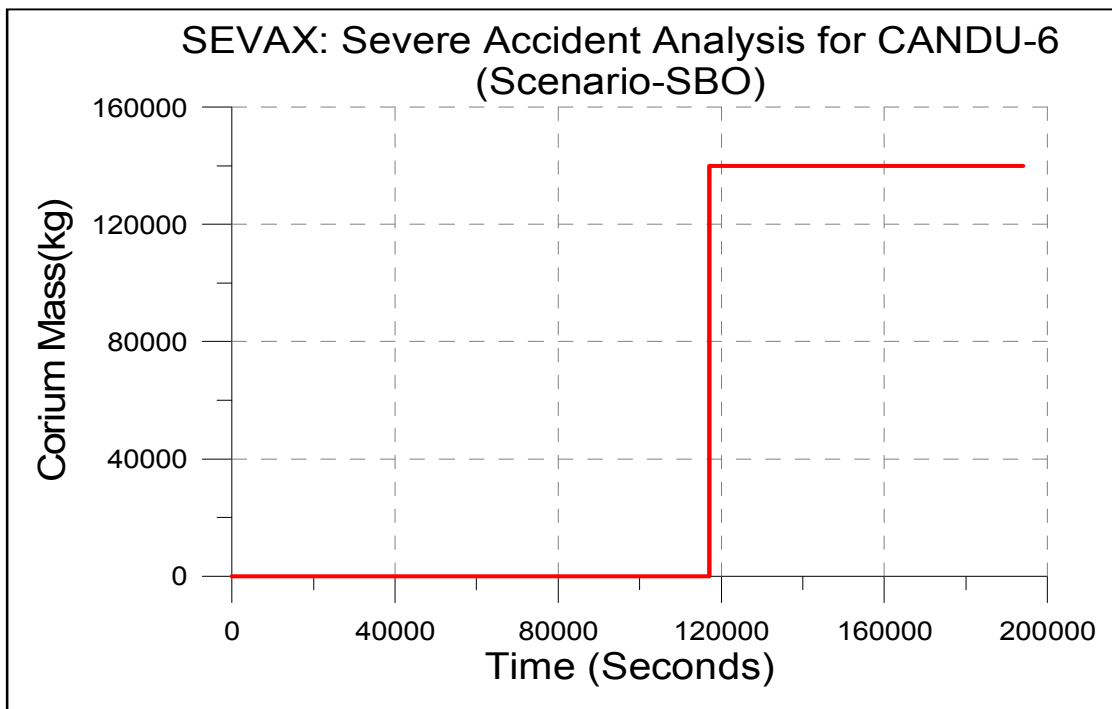


FIG. 3.246. Corium mass in Calandria vault basement.

# SEVAX: Severe Accident Analysis for CANDU-6

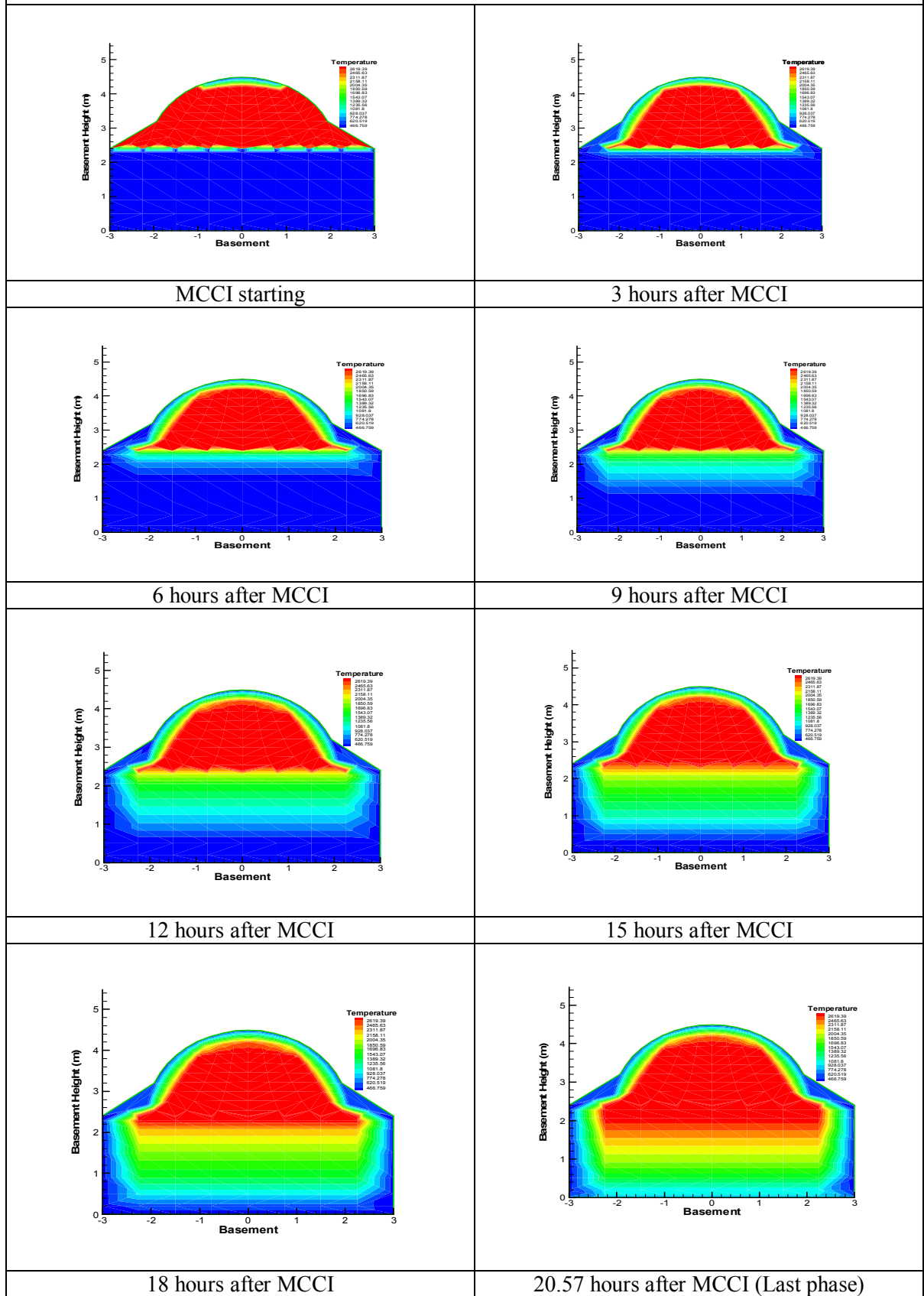


FIG. 3.247. Corium temperature variation in calandria vault during MCCI.

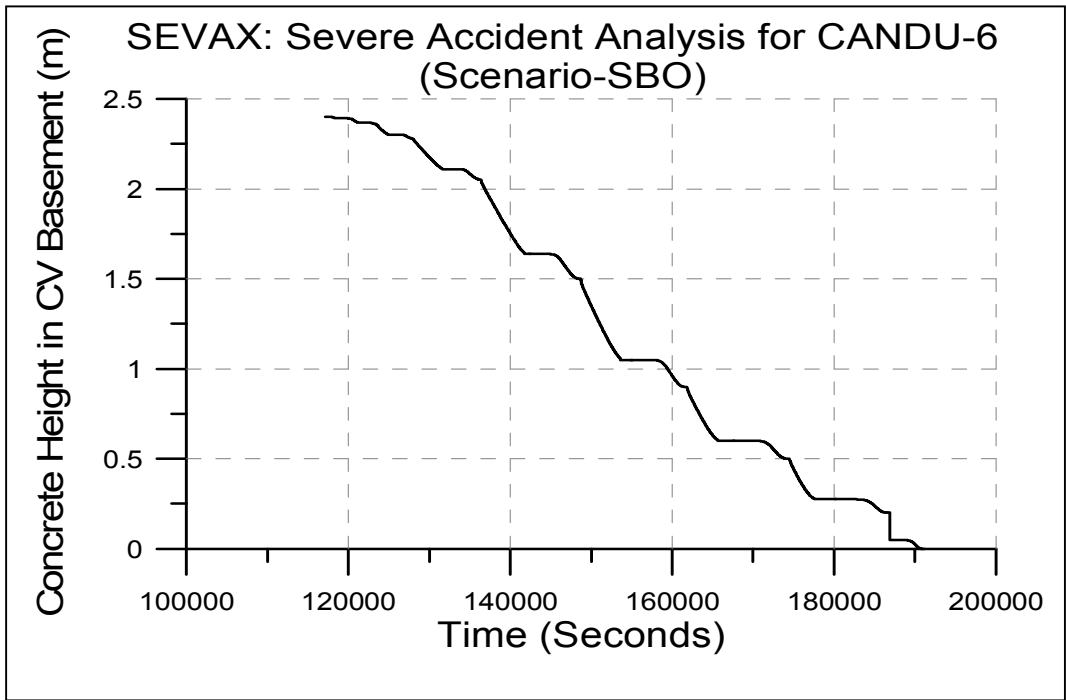


FIG. 3.248. Ablated concrete depth in calandria vault.

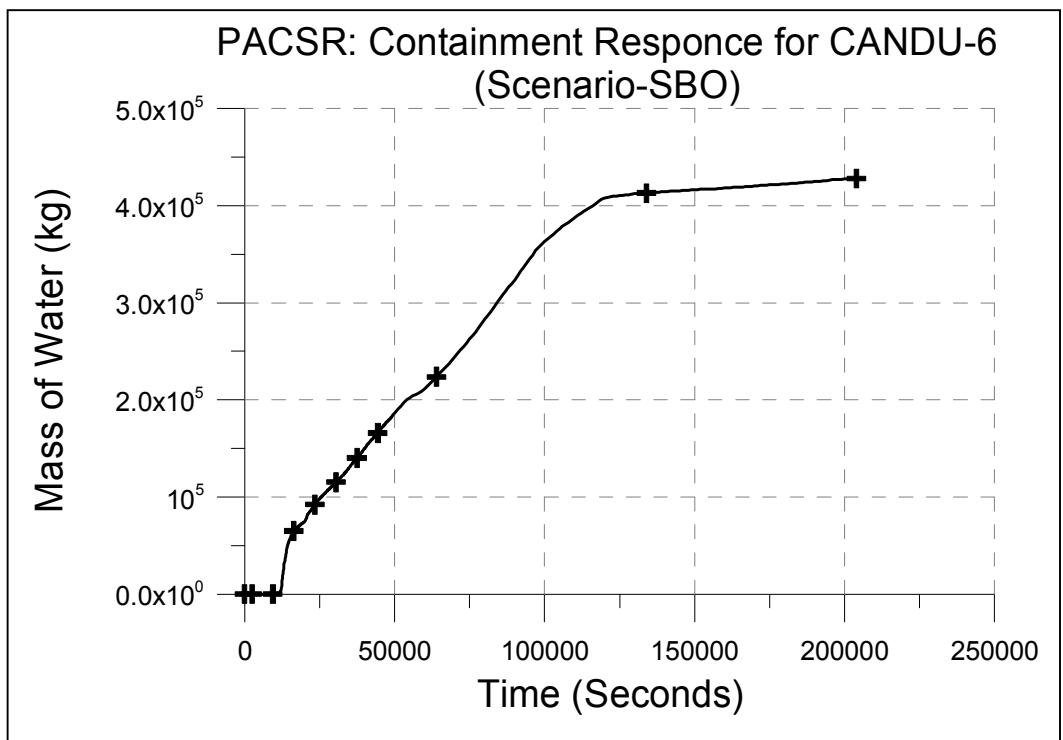


FIG. 3.249. Mass of water in containment basement.

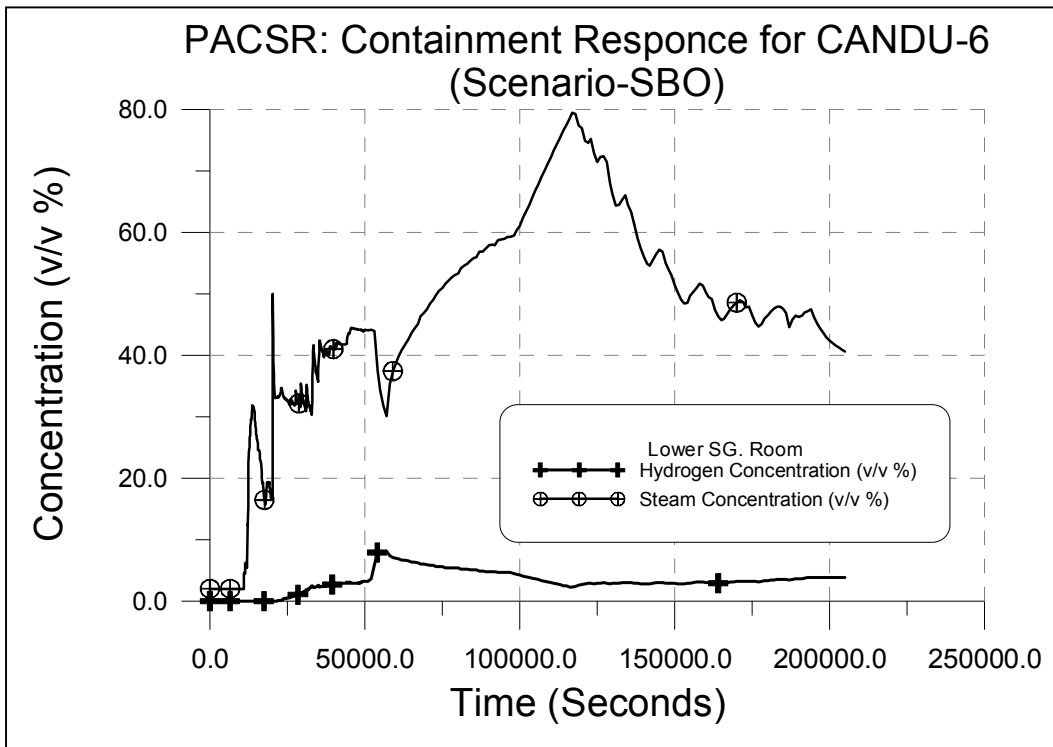


FIG. 3.250. Containment atmosphere composition in lower SG room.

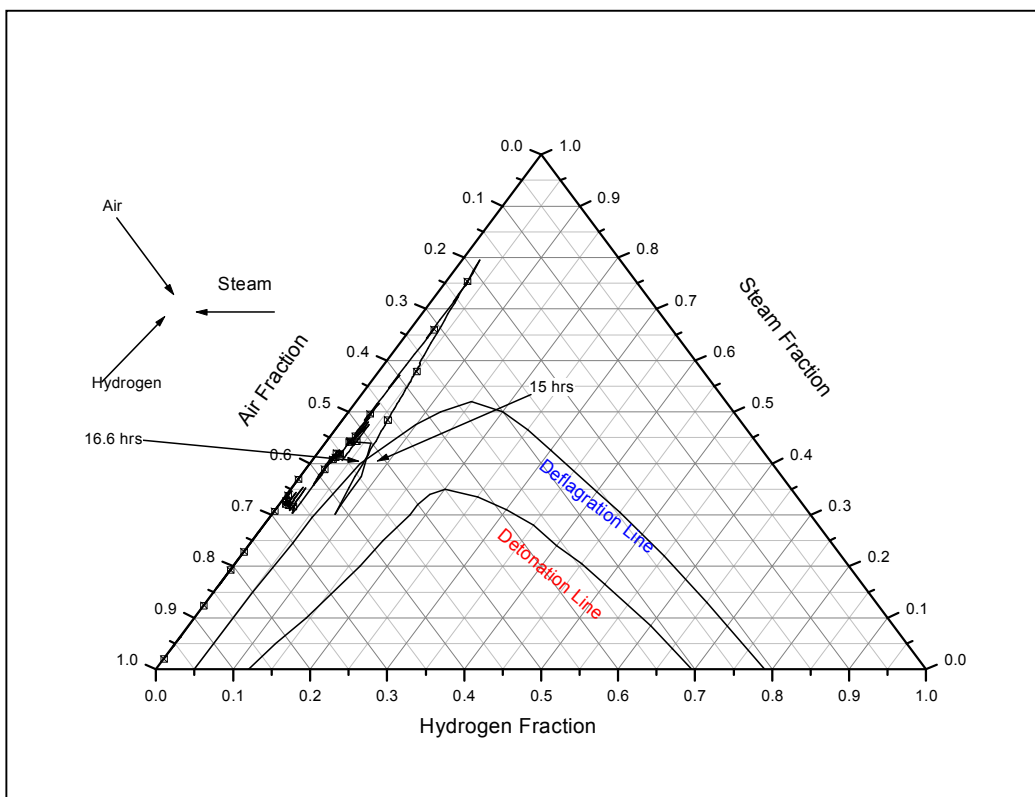


FIG. 3.251. Containment atmosphere composition in lower SG room.

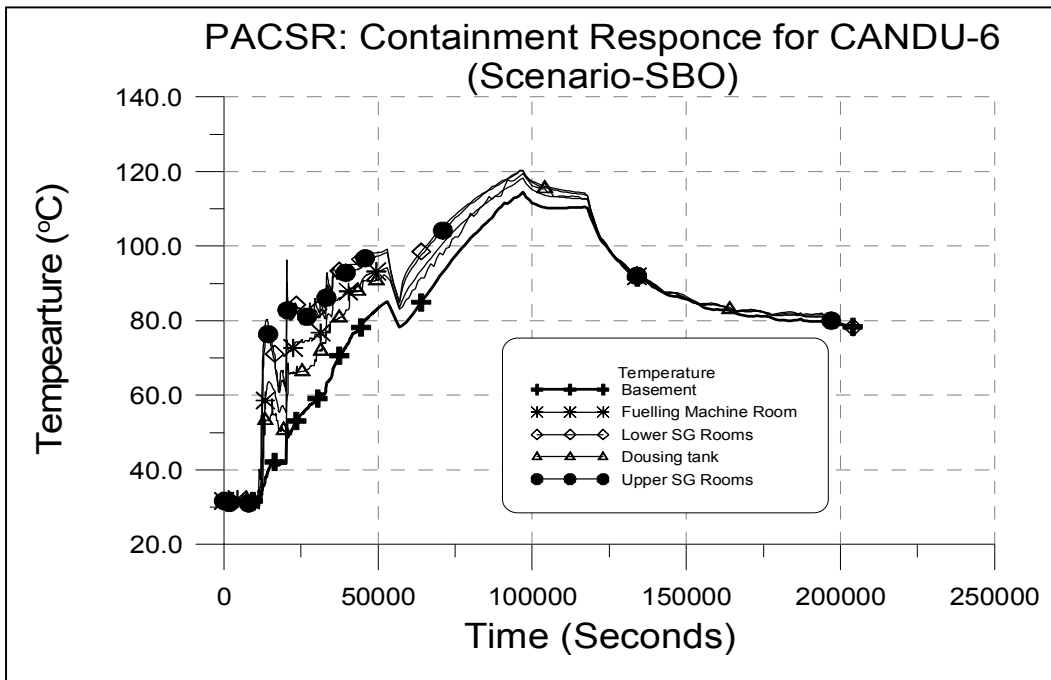


FIG. 3.252. Containment temperatures in different compartments.

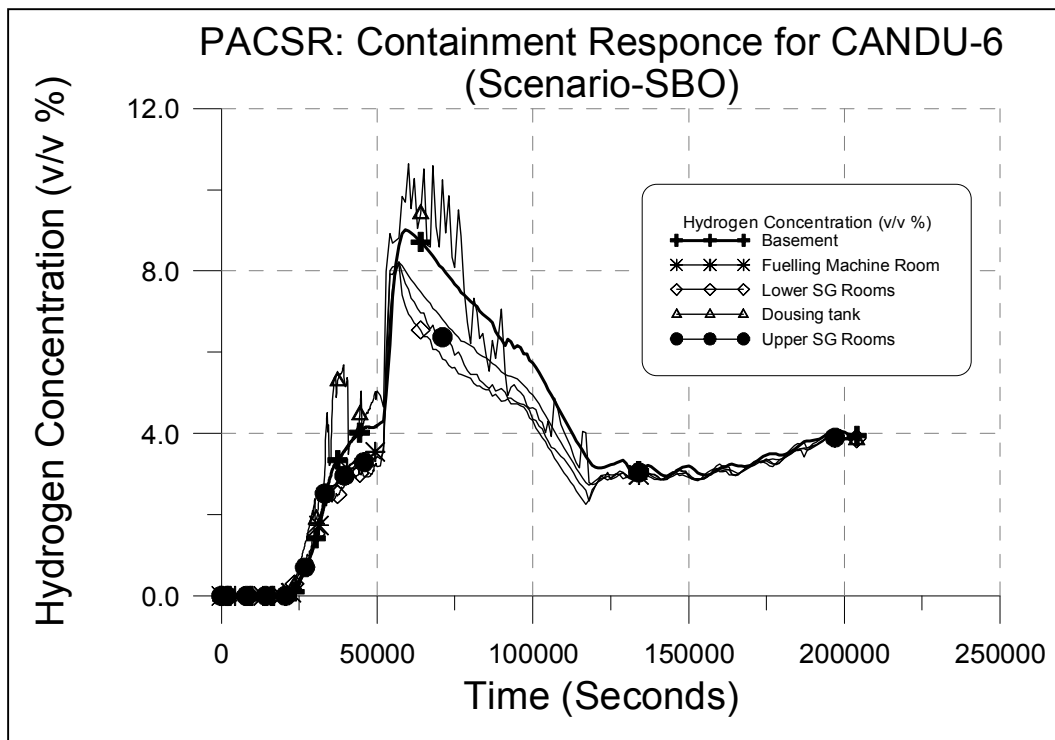


FIG. 3.253. Hydrogen concentrations in various locations.

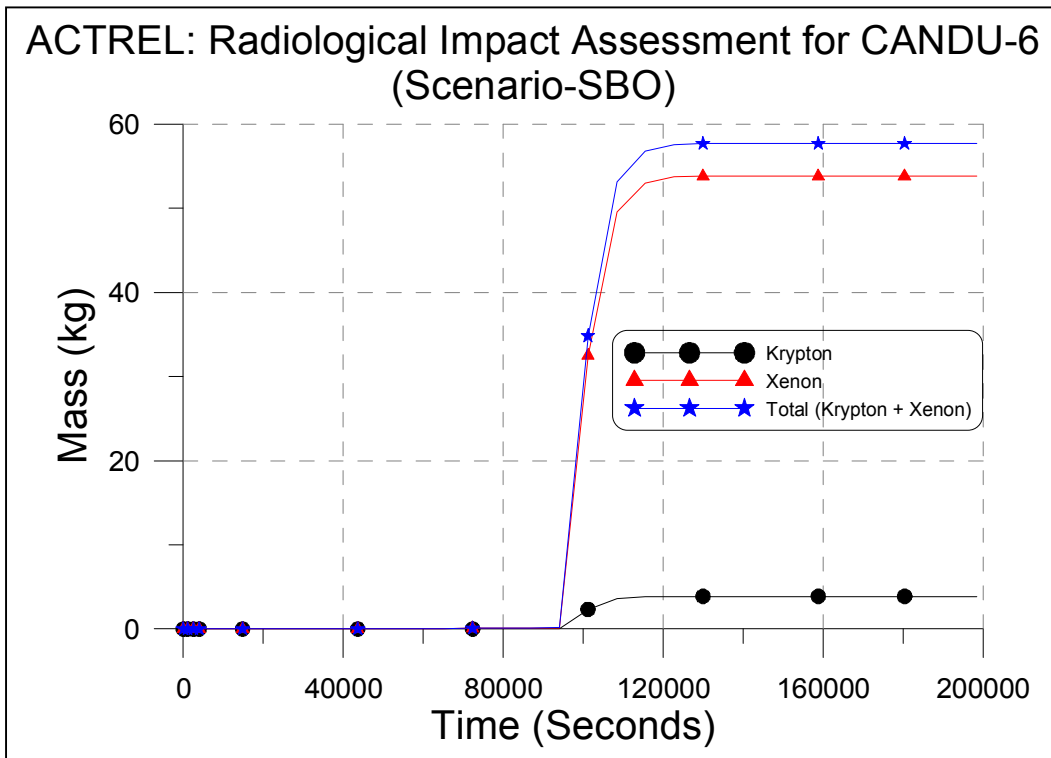


FIG. 3.254. Mass of noble gases released from containment.

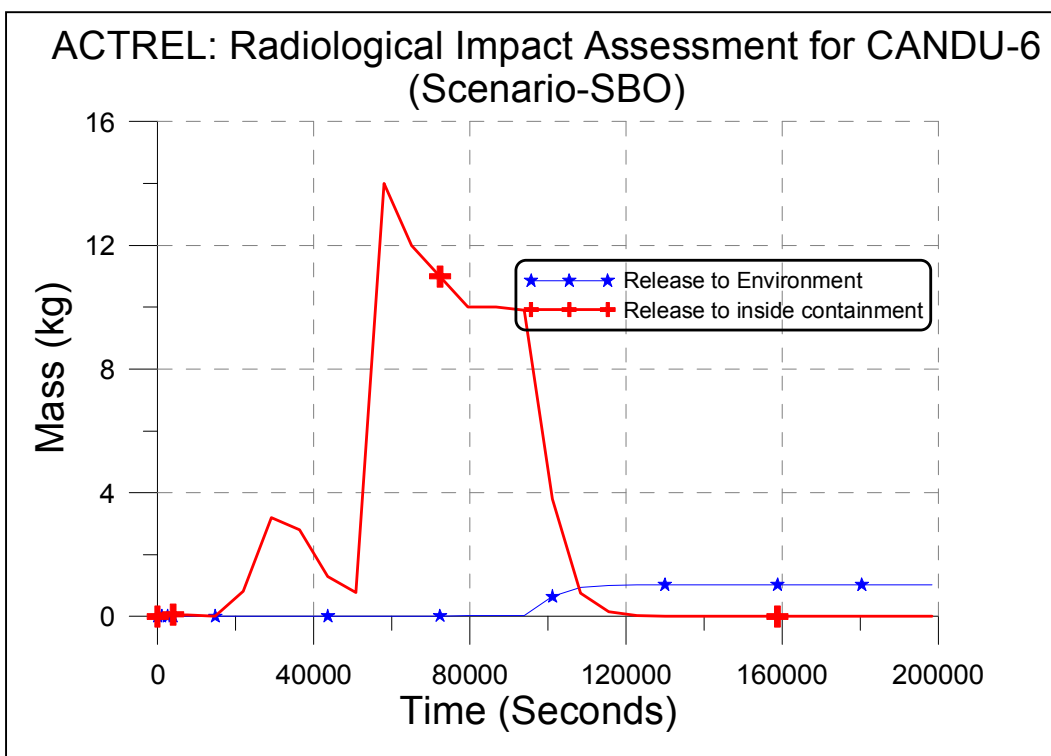


FIG. 3.255. Mass of Cesium released.

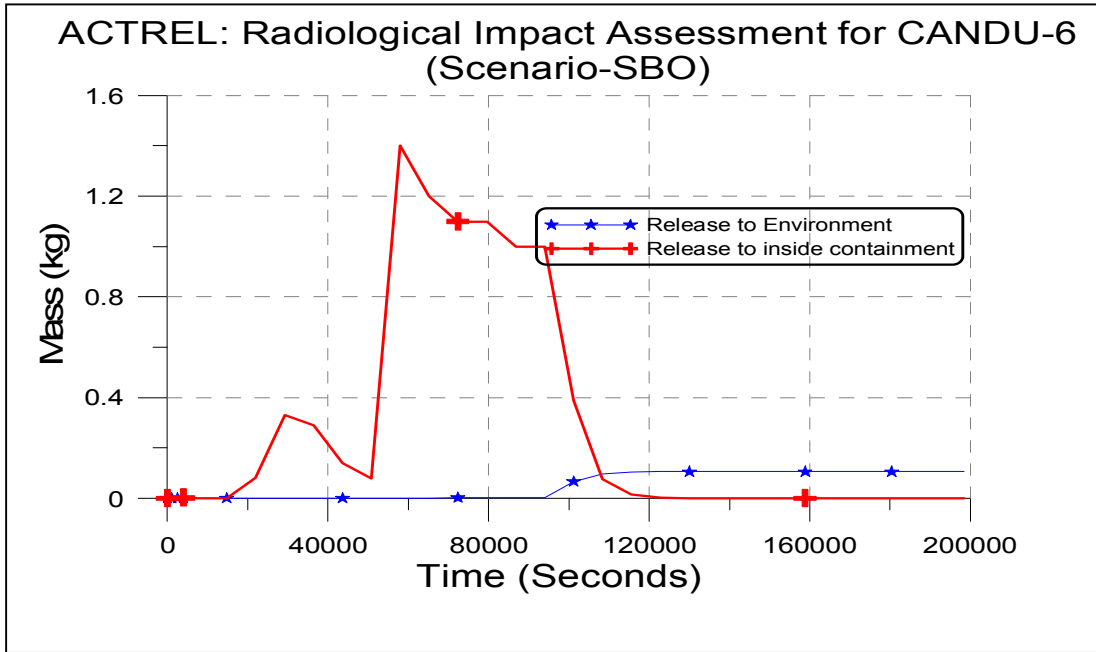


FIG. 3.256. Mass of iodine released.

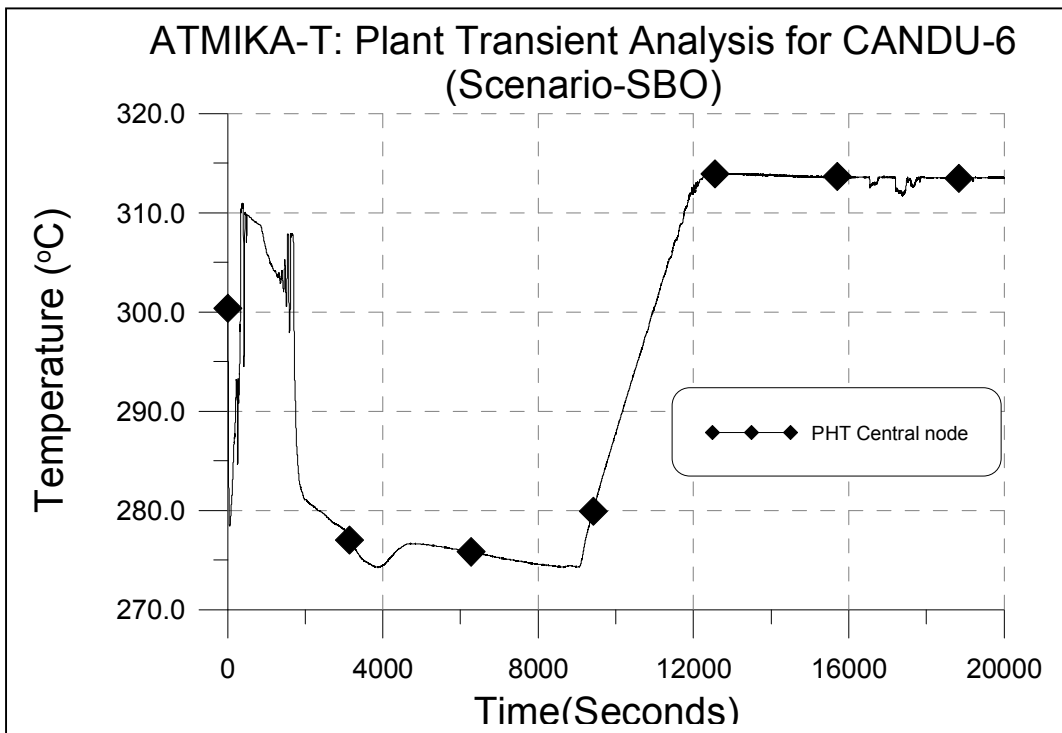


FIG. 3.257. PHT temperature variation in highest power channel.

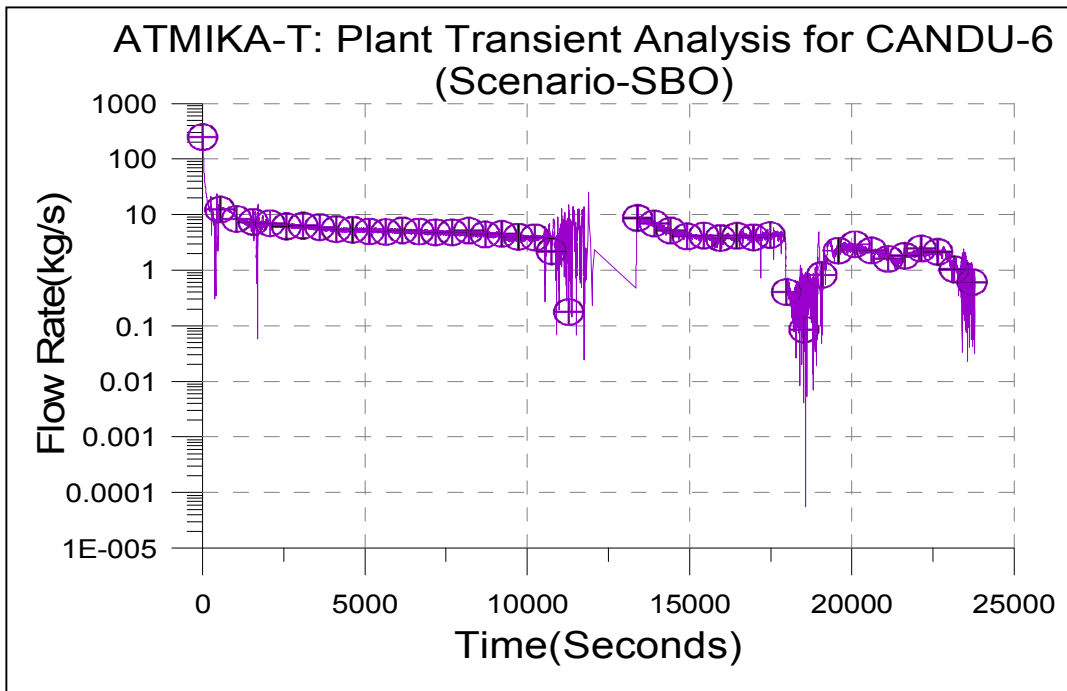


FIG. 3.258. PHT flow rate variation.

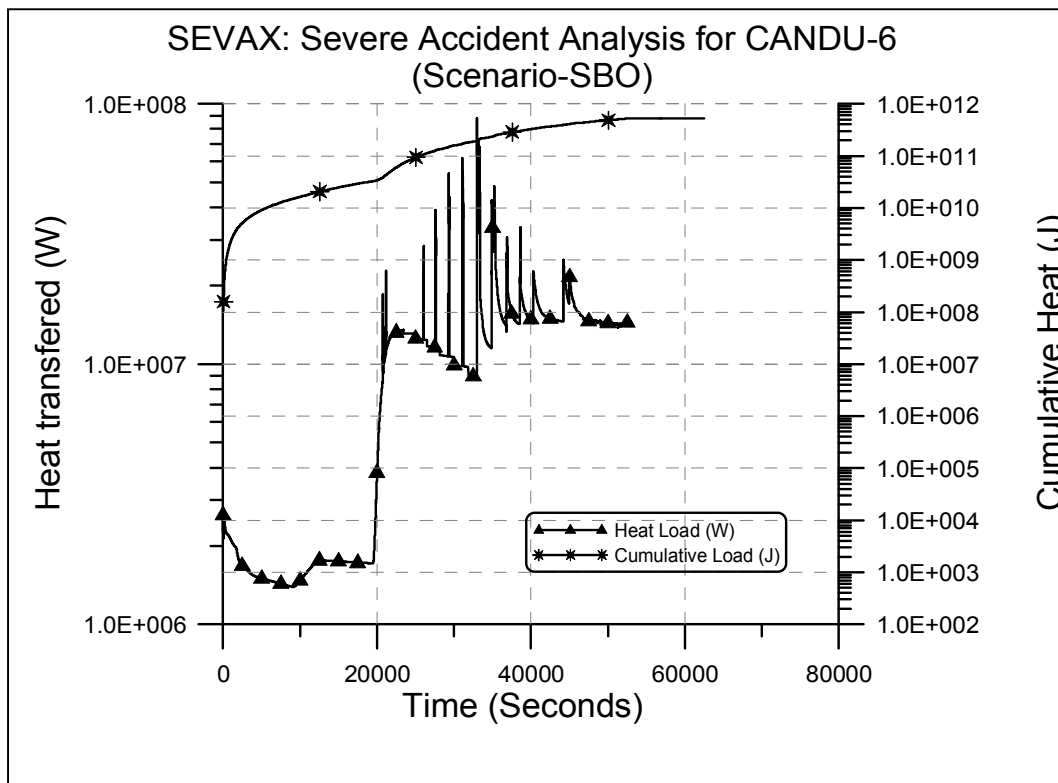


FIG. 3.259. Heat load to moderator

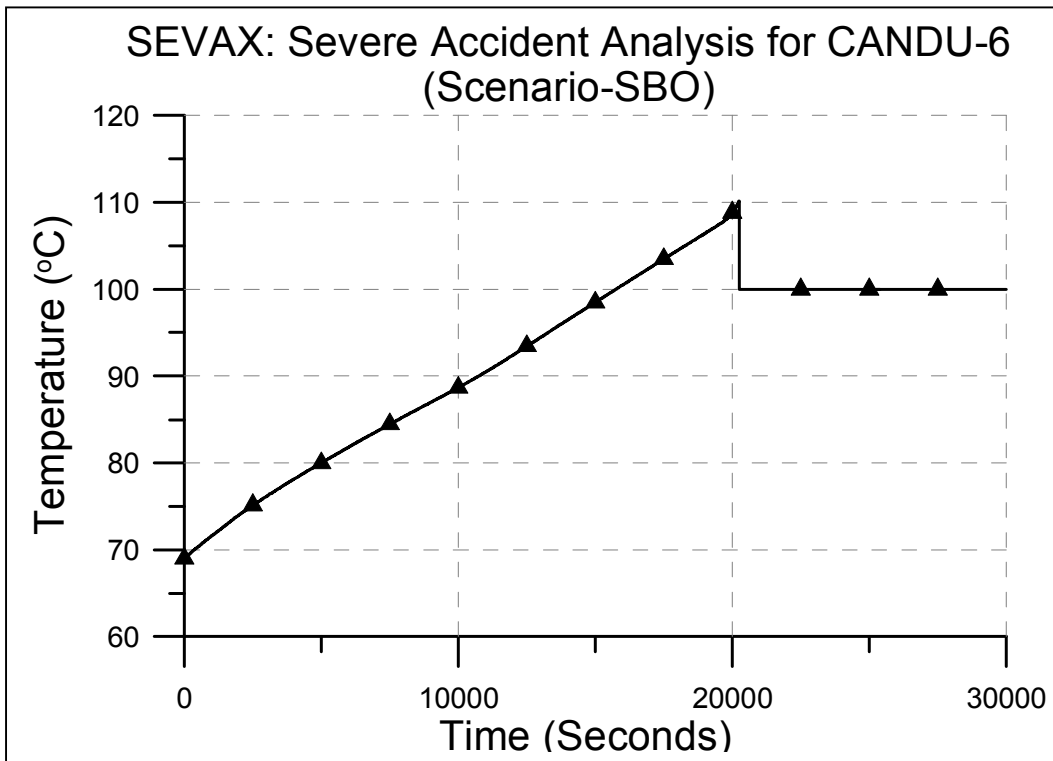


FIG. 3.260. Moderator temperature variation.

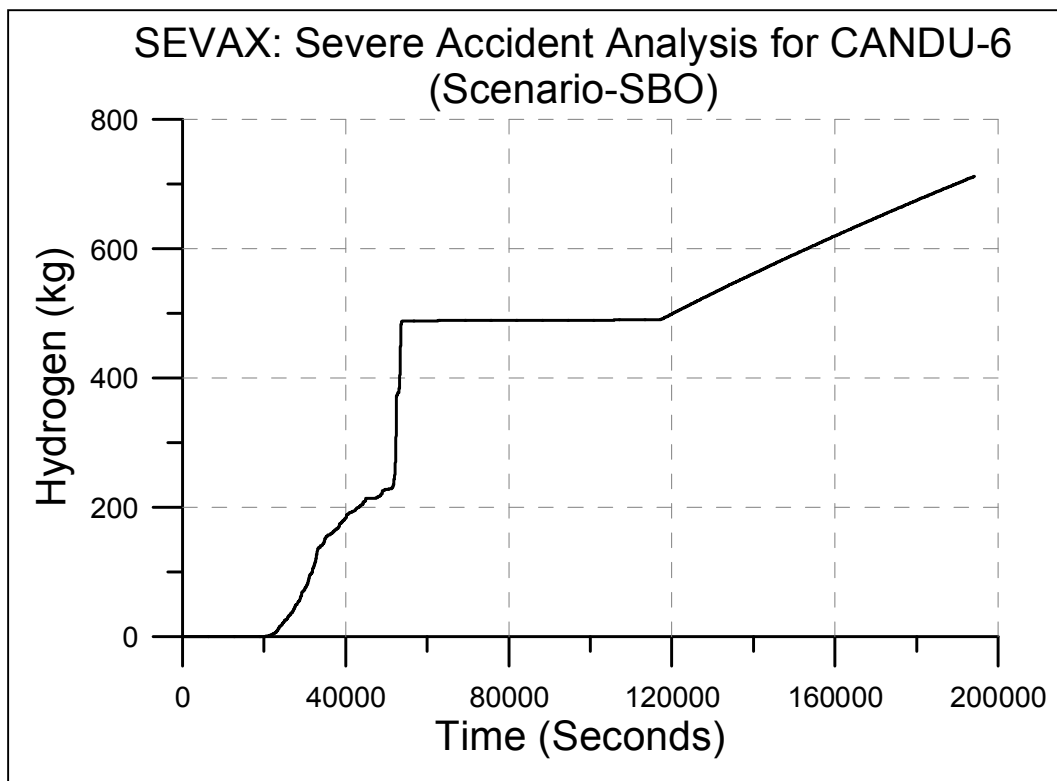


FIG. 3.261. Hydrogen generation during accident.

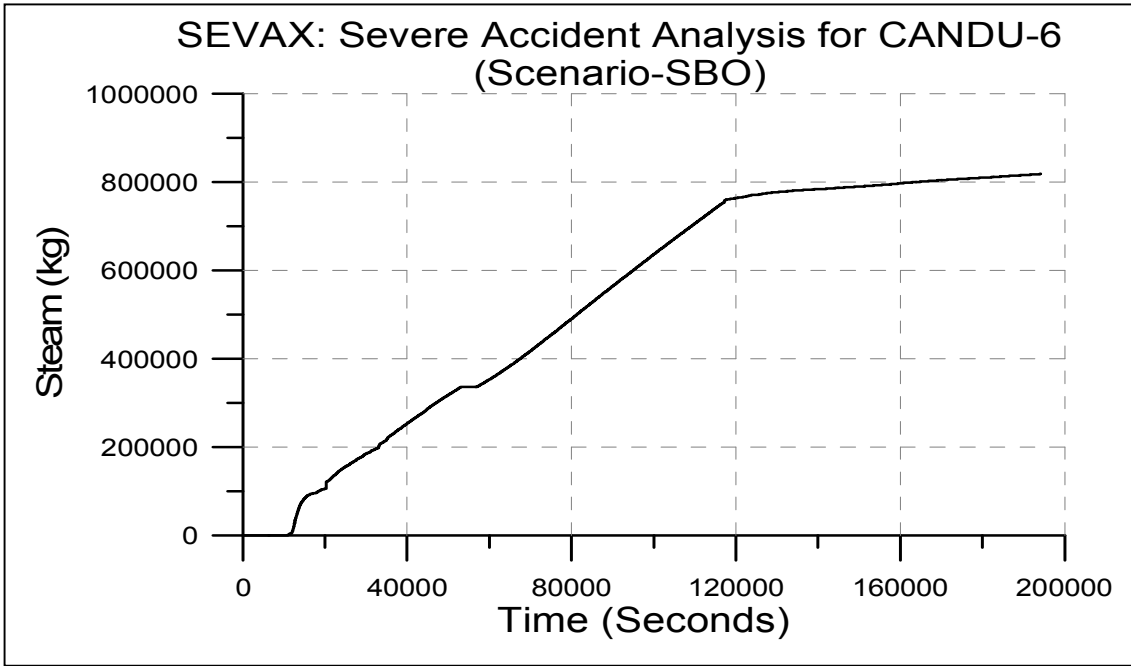


FIG. 3.262. Steam released to containment during accident.

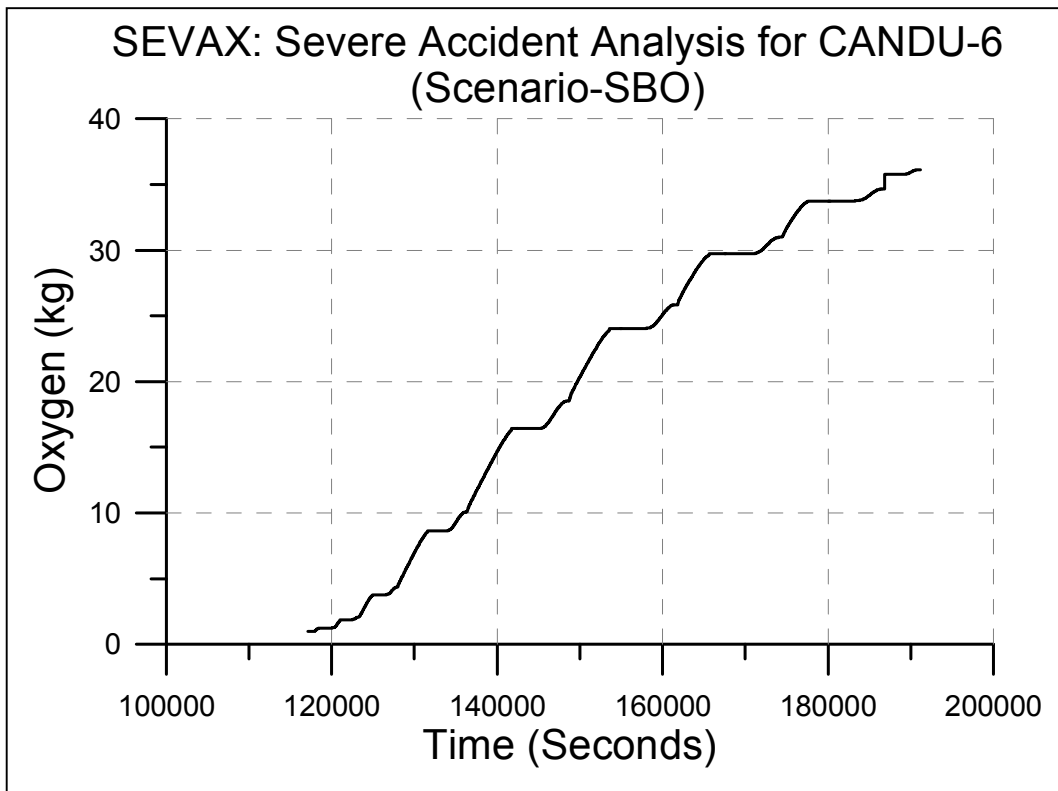


FIG. 3.263. Oxygen production during MCCI.

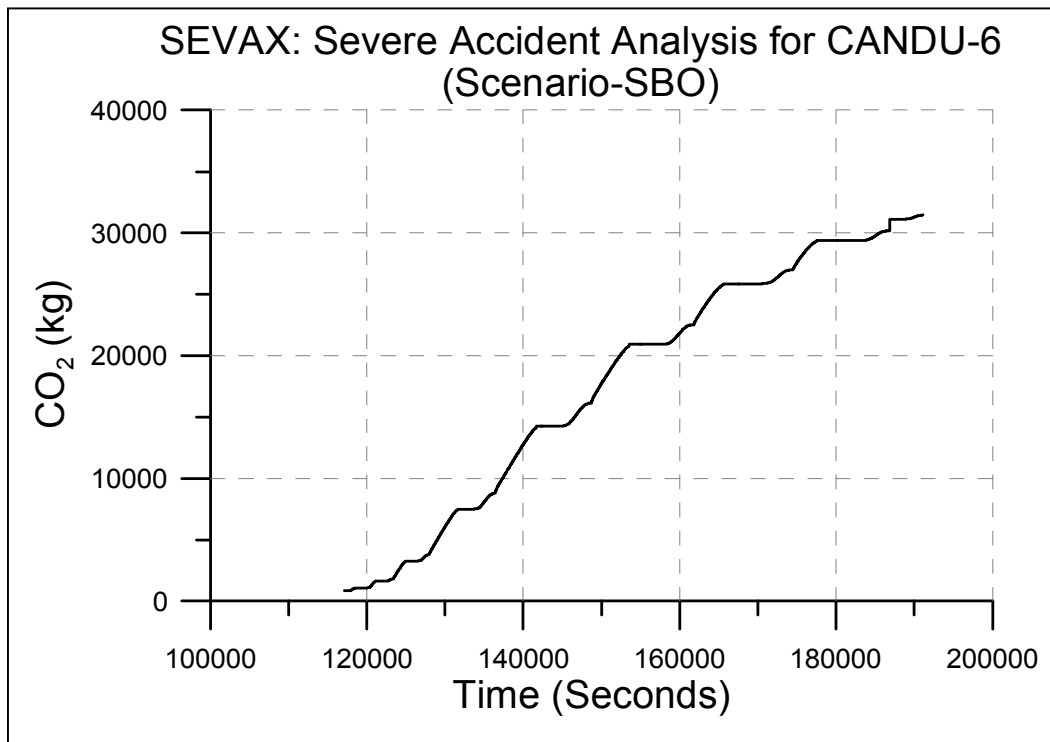


FIG. 3.264. CO<sub>2</sub> production during MCCI.

### 3.6. PUB

#### 3.6.1. Computer codes

The SCDAPSIM/RELAP5 code was used to analyse the progression of the severe accident and CATHARE2 code was used for containment analysis. SCDAPSIM/RELAP5 [19] code has been developed in US for best-estimate simulation of light water reactors (LWR) transients during nuclear power plant accidents. It uses publicly available RELAP5/MOD3.3 and SCDAP/RELAP5/MOD3.2 models, developed by the US Nuclear Regulatory Commission in combination with advanced numerics, advanced programming, and SCDAP Development and Training Program (SDTP) member-developed models and user options. The code models the coupled behaviour of the cooling system, reactor core and fission products release during the accident. It is the result of the coupling between RELAP5, modelling thermal hydraulic, control system, reactor kinetics and the transport of noncondensable gases, and SCDAP code modelling the behaviour of the reactor core during severe accidents.

The thermal hydraulic models for the hydrodynamic systems are integrated in the RELAP5 part of the code. The code is based on a non-homogeneous and non-equilibrium model for the two-phase system that is solved by a fast, partially implicit numerical scheme. RELAP5 solves the conservation equations for each phase within a control volume. The variables in these equations are time and volume averaged and time and one space dimension are the independent variables. A control volume is characterized by one single pressure and two temperatures for the liquid and gas phase. Control volumes are connected by junctions through whom transport of hydrodynamic materials takes place.

The constitutive relations are formulated using empirical correlations. Those constitutive relations, needed to solve the two-fluid equations, include models for defining flow regimes

and flow regime related models for interphase drag, wall friction, heat transfer and interphase heat and mass transfer. The applied two-phase flow regime maps are defined by a simplified mapping technique which controls the use of the constitutive relations. A generic modelling approach is used that permits simulating a variety of thermal hydraulic systems.

Heat structures provided in RELAP5 permit calculation of the heat transferred across solid boundaries of hydrodynamic volumes. Modelling capabilities of heat structures are general and are assumed to be represented by one-dimensional heat conduction in rectangular, cylindrical, or spherical geometry. Surface multipliers are used to convert the unit surface of the one-dimensional calculation to the actual surface of the heat structure. Temperature dependent thermal conductivities and volumetric heat capacities are provided in tabular or functional form either from built-in or user-supplied data. The heat transfer model in RELAP5 is based on the boiling curve which is used to govern the selection of the heat transfer correlation.

The RELAP5 code was used to simulate all hydrodynamic systems of CANDU plant and heat transfer surfaces except fuel channel and calandria vessel wall during late phase of severe accident.

The SCDAP code is modular, a series of components being defined in the input deck in a similar manner as RELAP5 components (the latter can be volumes, pipes, junctions, pumps, heat structures etc.). Besides the general input options (general core input or severe accident core behaviour input), the user has the possibility to introduce in his model the some generic SCDAP core components.

Each of these SCDAP components has a series of associated physical models which are invoked by the code whenever the corresponding component is used. Obviously, many models are dedicated to PWR or BWR to such an extent that makes them inapplicable to CANDU. Nevertheless, some models are sufficiently general to make their use to CANDU severe accidents possible.

SCDAP code is used to describe the core components. Treatment of the core includes fuel rod heat-up, ballooning and rupture, fission product release, rapid oxidation, Zircaloy melting,  $\text{UO}_2$  dissolution,  $\text{ZrO}_2$  breach, flow and freezing of molten fuel and cladding, and debris formation and behaviour. The code also models control rod and flow shroud behaviour.

A two-dimensional, finite element model based upon the COUPLE code is used to calculate the heat-up of debris and/or surrounding structures.

The two-dimensional debris and surrounding structures model takes into account the decay heat and initial internal energy of slumped debris and then calculates the transport by conduction of this heat in the radial and axial directions to the wall structures and water surrounding the debris. Perhaps the most important use of this model is to calculate the heat-up of the vessel wall so that the time at which the vessel may rupture can be determined. Notable capabilities include the modeling of the following phenomena and conditions: (a) spatially varying porosity, (b) thermal conductivity of porous material, (c) a debris bed whose height grows sporadically with time, (d) radiation heat transfer in a porous material, and (e) natural circulation of melted debris. The limitations of this model are: (a) molten material does not flow into an adjacent porous region, (b) oxidation does not occur in the debris bed, and (c) fission product release does not occur in the debris bed.

The rate of heat transfer from a debris region into a structure in contact with the debris is a strong function of the conditions at the interface between the debris and structure. The modelling of this heat transfer is performed using the concept of a null element, which is an element with zero volume and whose nodes overlay the interface between the debris and the

structure. Null elements are defined by the code user along possible interfaces between debris and structure.

The COUPLE model has been employed for PWR/BWR situations, with vertical core and hemispherical lower head. Although the actual hemispherical geometry was used to model this phase of CANDU severe accident [33], improvements in COUPLE was made which allow properly modelling of an horizontal cylinder (calandria vessel) [34].

The CATHARE2 code (Code for Analysis of Thermal-Hydraulics during an Accident of Reactor and Safety Evaluation) is developed to perform best-estimate calculations of pressurized water reactor accidents: PWR loss of coolant (large or small break, primary and secondary circuit), reactivity insertion, steam generator tube rupture, etc. [35]. It is developed in Grenoble by the French Atomic Energy Commission (CEA) and it is owned by four partners: CEA, EDF, FRAMATOME-ANP, and IRSN.

CATHARE2 includes several independent modules that take into account any two-phase flow behaviour:

- Mechanical non-equilibrium:
  - Vertical: co- or counter-current flow, flooding counter-current flow limitation (CCFL), etc.;
  - Horizontal: stratified flow, critical or not critical flow co- or counter-current flow, etc.;
- Thermal non-equilibrium: critical flow, cold water injection, super-heated steam, reflooding (vertical fuel only), etc.;
- All flow regimes and all heat transfer regimes.

In order to take into account these phenomena the CATHARE2 code is based on a two-fluid and six equation model with a unique set of constitutive laws. Various modules offer space discretization adapted to volumes (0D), pipes (1D) or vertical vessels (3D). CATHARE2 is limited to transients during which no severe damage occurs to fuel rods; more precisely, fuel ballooning and clad rupture are assumed to have no major effect on water flow in the primary circuit. Includes oxidation model but only for vertical rods defined by means of FUEL operator. Time discretization is fully implicit (semi-implicit for 3D).

Related to capability of CATHARE2 to simulate the fission products transport, radio-chemical components can be specified and associated to the circuit. There are 13 predefined radio-chemical components, out of which 4 fission products: Kr-87, Xe-133, I-131, Cs-137, treated separately, i.e. without chemical interactions of the released species. The relationship between mass and radioactivity is governed by the weight of one GBq:

- Kr-87, 9.52E-13 kg;
- Xe-133, 1.44E-10 kg;
- I-131, 2.18E-10 kg;
- Cs-137, 3.10E-7 kg.

One possibility, besides using predefined activity functions for fission products to be released when clad rupture is calculated by the code (for PWR), is to externally define fission products activity in a gas or liquid source placed inside the circuit at user's choice.

Related to containment analysis capabilities, CATHARE2 is limited to maximum 4 noncondensable gases from the list: hydrogen, helium, oxygen, nitrogen, argon, air. The reactor containment may be modelled using a VOLUME module or a set of VOLUME modules. Special models have been developed to take into account containment components (circuits, exchangers related to safety systems), a break between the primary coolant system

and the containment, or specific physical phenomena occurring in the containment such as film condensation on the containment walls. Several available correlations exist for heat transfer from walls to fluid in case of film condensation. The recent versions of the code include also specially designed water properties tables for low pressure applications.

### **3.6.2. Phenomena and system idealization**

The plant model includes the representation for the two loops, fuel channels, inlet headers, feeders and end fittings, outlet headers, feeders and end fittings, associated reactor coolant pumps, pressurizer, steam generators and a simplified model for balance of plant systems. Generally, all plant components are modelled using RELAP5 components, except for the fuel and fuel channel thermal response which are modelled using SCDAP components and the debris bed modelled by the COUPLE module. Containment is modelled using both RELAP5 and CATHARE2 code.

#### *3.6.2.1. Primary heat transport system modelling*

The nodalization scheme used for the Primary Heat Transport System (PHTS) is shown in Figure 3-265. In this approach, two hydrodynamic characteristic channels per pass, eight in total, are considered. Each representative channel is subdivided into 12 control volumes. These two hydrodynamic characteristic channels per pass represent the average channels for each pass located in the upper, respectively the lower half of the calandria vessel (CV). This representation was considered adequate to represent the fuel channels behaviour after the rupture of the calandria vessel rupture disk. However, a sensitivity analysis considering up to four representative channels per pass has shown that no major hydrodynamic behaviour differences was observed for SBO accident scenario when only one representative channel per pass was used instead of two or more representative channels per pass.

The heat losses from the PHTS to the containment environment are modelled with RELAP heat structures with convective heat transfer as boundary condition.

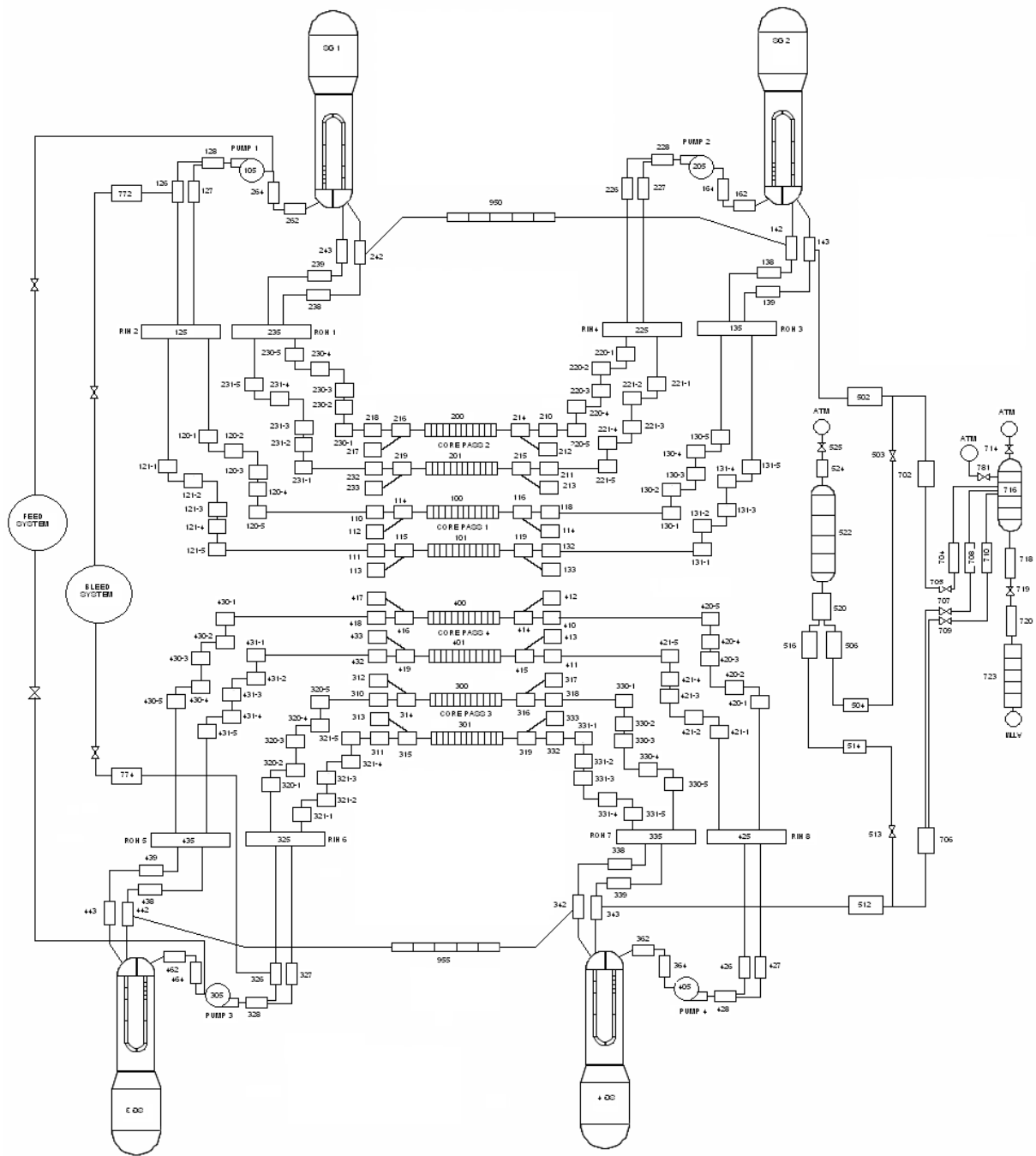


FIG. 3.265. Primary heat transport system nodalization.

### 3.6.2.2. Steam generators modelling

Figure 3-266 shows the nodalization scheme for the steam generator (SG) and main steam lines. The U-Tubes are discretized in 8 nodes and separate nodes for the inlet and outlet plenum are provided. The secondary side consists of the preheater, riser, separator, drum and downcomer volumes discretized in different number of nodes to properly model the steam generator performances. The turbine and condenser are represented by time-dependent volumes. The feed water is injected in the preheater, a time-dependent volume gives the temperature and a time-dependent junction is used as a boundary condition for the feed water flow rate.

### 3.6.2.3. Fuel channels modelling

In a fuel channel, the 37 fuel elements of the fuel bundle, the pressure tube (PT) and the calandria tube (CT) are modelled using SCDAP core components, Figure 3-267. All fuel elements which belong to the same fuel bundle are considered to have the same power. The pressure tube, the CO<sub>2</sub> filling the annular space between PT and CT, and the calandria tube are modelled using shroud components. The 12 bundles in a CANDU fuel channel were modelled as 12 axial nodes.

The fuel rod component include models for UO<sub>2</sub> pellets, gap, and Zircaloy sheath behaviour. Together with the heat conduction model, this component has a series of associated physical models which are invoked by the code whenever the corresponding component is used. These models are: material oxidation model, fission product release models, fuel rod cladding deformation model and fuel rod internal gas pressure model.

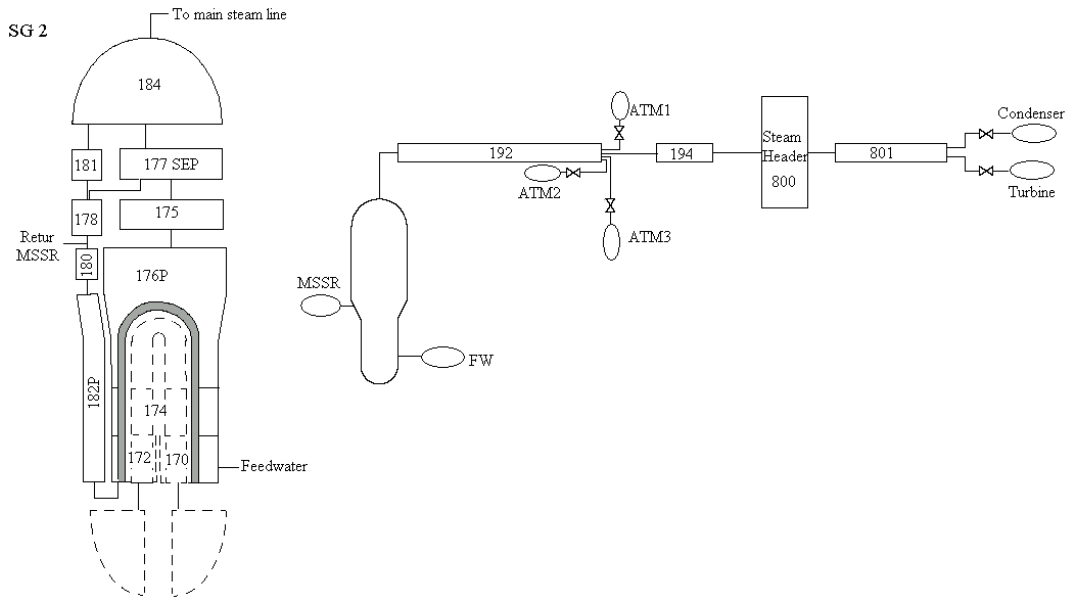


FIG. 3.266. Nodalization scheme for the SG secondary-side and main steam lines.

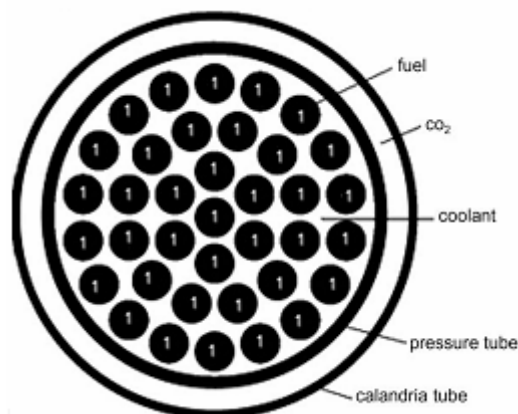


FIG. 3.267. SCDAP model for the fuel channel.

The shroud component represents cylindrical structures with a wall thickness much smaller than the radius of the cylinder. The temperature distribution in the structure is calculated using the basic heat conduction equation. An internal heat generation term can also be specified by the user. The structures can be defined by multiple layers of materials, at least three materials, with the possibility to input a user defined material layer. Modelling the heat transfer in the

internal gas layer of the shroud component to take into account for the pressure tube sagging was realized by altering the thermal conductivity of the input declared material, which simulates the carbon dioxide inside the annular gap. First, it was calculated an effective conductivity of the annulus material, incorporating the radiation heat transfer between the pressure tube and the calandria tube. Second, enhanced heat transfer due to sagging is calculated by multiplying with a constant the value of the gas thermal conductivity in the above expression of the effective conductivity.

Four representative channels per core pass were considered to simulate the thermal response of fuel channels. The core power map and the division into representative channels are shown in Figure 3-268. Two representative channels, modelled as SCDAP components, are linked to one hydrodynamic characteristic channel modelled with RELAP5 components. Thus, channels 1 and 2 shown in Figure 3-268 are linked to the hydrodynamic channel located on the lower half of calandria vessel whereas channels 3 and 4 are linked to the hydrodynamic channel located on the upper half of calandria vessel for each core pass. For each core pass the fuel channel were grouped according to their elevation irrespective to their power. Related to the time scale of the severe accident events, single channel analysis illustrates that more important is the channels elevations that the channels power for the timing at which core collapse occur [36]. This happen because as once the fuel channel uncover occurs, the calandria tube temperature increase rapidly leading to the core disassembly. Thus, when the number of the modelling fuel channels is restricted as present SCDAPSIM/RELAP5 mod 3.4 code version does, the consideration of a larger number of channels with different elevation would be more significant that consideration of many fuel channels with different power but same elevation. Moreover, as loop behaviour channels of one loop are modelled using RELAP5 heat structures whereas the channels of the other loop are modelled using SCDAP components, as analysis had shown that the thermal response of fuel and fuel channel for the two PHTS loops are similar when compare to the severe accident time scale. Two separate runs were done using this nodalization, each loop being modelled alternatively by SCDAP component.

This modelling approach was required as the actual SCDAPSIM/RELAP5 mod 3.4 code allow only 16 SCDAP core components as input.

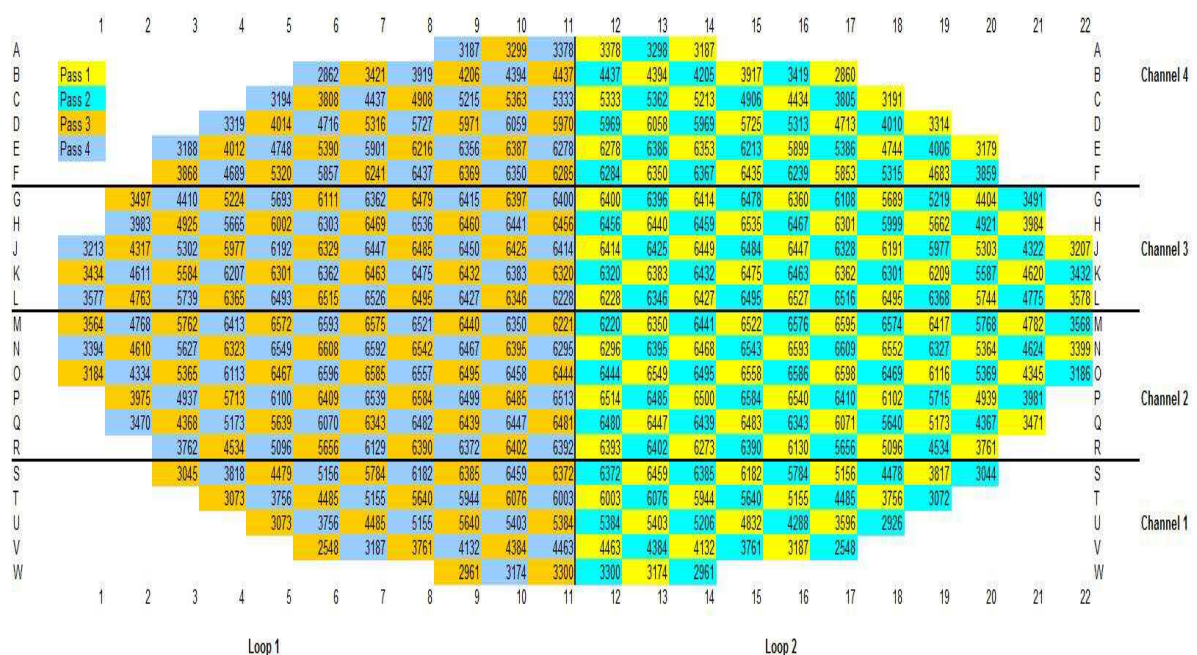


FIG. 3.268. Core power map and the division into representative channels.

### 3.6.2.4. Calandria vessel modelling

Calandria vessel is modelled as two parallel pipe components with three sub-volumes having vertical orientation. Each pipe component simulates half of the calandria volume representing the moderator surrounding fuel channels of one PHTS loop. The analogous volumes of the two parallel pipes are connected through cross flow junctions. The four calandria pressure relief ducts are modelled as pipe components with three sub volumes having vertical orientation. Calandria over pressure rupture disk (OPRD) is modelled as a trip valve and connects CV with containment. Figure 3-269 shows the CV model.

### 3.6.2.5. System modelling after calandria vessel dryout

The SBO analysis is carried out in two steps. In the first step, the entire plant is modelled as described above. The aim of this step of analysis is to study the CANDU plant behaviour until the core collapse occurs. In the second step, once the fuel channels collapse on the bottom of the calandria vessel, the debris and the calandria wall are modelled using the COUPLE module. Improvements in COUPLE module were made which allow properly modelling of a horizontal cylinder (calandria vessel) [34].

The models included with COUPLE in SCDAP are capable of calculating the heat up of the debris and of the surrounding structures. A two-dimensional finite element mesh is generated by COUPLE based on the coordinates input of a selected number of nodes. The COUPLE model for the bottom of the CV is shown in Figure 3-270.

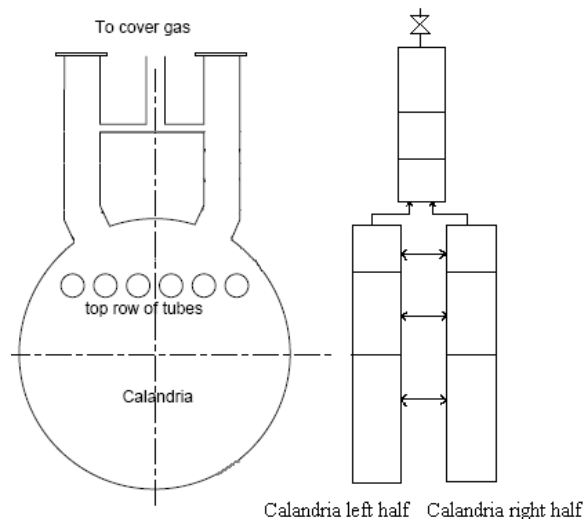


FIG. 3.269. Calandria vessel nodalization.

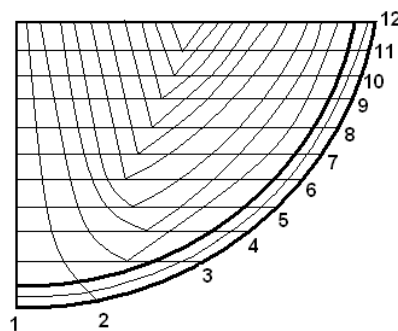


FIG. 3.270. COUPLE meshes (the numbers refer to the CV outside wall nodes).

User-defined slumping of debris was imposed inside the COUPLE mesh at start of this phase, defining the mass, the composition, the porosity and particle diameter of the debris. When using the 'no-slumping' option, the elements of the mesh are filled by the code user with debris and structure material on the desired locations and timing. The rate of heat generation per unit volume has to be defined for the debris material. This imposes the heat load towards the CV wall. Convection and radiation heat transfer take place from the upper boundary of the debris bed towards other connected volumes. Convection heat transfer from the CV wall to surrounding RELAP5 hydrodynamic volumes is considered. As such, it is possible to create a detailed mesh representing the CV filled with debris, connected to volumes at the inside of the mesh that stand for the CV internals and volumes at the outside of the mesh representing the contents of reactor vault (RV).

The RELAP5 hydrodynamic system consists of two independent systems: the first system represents the CV internals and the second system represents the RV. Both CV and RV are connected to the containment.

The following materials are included in the mesh: (1) debris (corium) that consists of  $UO_2$ , oxidized Zircaloy, and Zircaloy, (2) stainless steel for the calandria vessel wall, and (3) null material used to model the debris-to-vessel heat transfer coefficient (or gap heat transfer coefficient). The null material is a virtual material defined to be present in the elements describing the corium-vessel interface. When debris relocates to the lower head, the thermal contact between the debris and the structural material is reduced because of surface roughness and gas trapped between the debris and the surface of the vessel. These interface elements do not possess a 'height' but, by filling them with null material, it is possible to assign a convective heat transfer coefficient to each of these elements and to enable heat transfer between the corium and the vessel wall.

The heat generated in the corium is conducted through the vessel wall, is eventually removed from the CV by the water in the RV surrounding the CV, and is transferred directly to the containment by radiation. A fictitious heat slab on the top of the COUPLE debris-bed is modelled to allow for radiation heat transfer between the debris-bed and the upper calandria wall. The temperature of this fictitious heat slab is the same as the temperature of the top debris bed nodes. The model used for late phase of the severe accident calculation is shown in Figure 3-271.

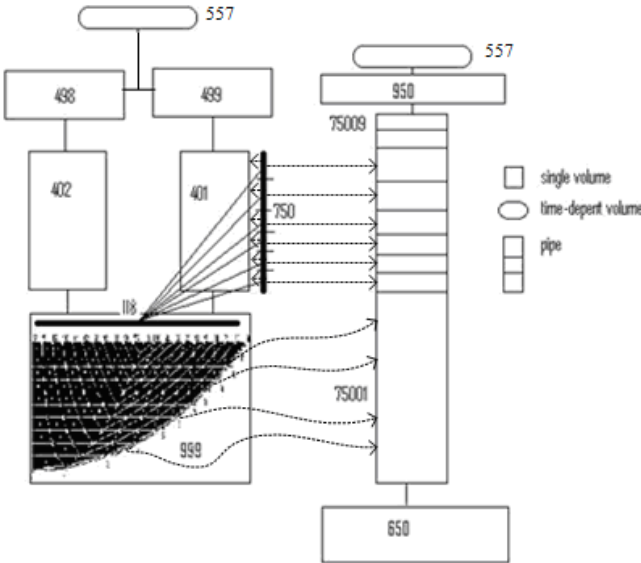


FIG. 3.271. Late phase of the severe accident calculation model.

### 3.6.2.6. Containment model

The containment is modelled using CATHARE 2 code. All fluid discharged from PHTS, CV and RV is considered to occur into boiler room. The volume which represents the environment is also connected to the boiler room to account for the containment leakage and for the containment failure. The nodalization used for the containment modelling is the same as that of AECL.

The transport and deposition of fission product in PHTS is not calculated, hence is assumed that the fission products are released from fuel directly to containment. The behaviour of fission product in containment is also modelled using CATHARE 2 code.

The same containment nodalization was also used to model containment with RELAP5 code. The results presented here are from CATHARE2 simulation as no fission product transport and deposition is calculated in RELAP5.

### 3.6.3. Analysis results

Event timing summary is presented in Table 3-17.

TABLE 3.17. LIST OF SIGNIFICANT TIMING OF EVENTS FOR STATION BLACKOUT SCENARIO

Event	Event timing (h)	Event timing (s)
Class IV and Class III Power loss	0	0
Turbine stop valves closed	0.0056	20
Reactor trips	0	0
First opening of MSSV	0.038	136
Calandria vessel bleed valve opens	1.23	4428
LRVs open for the first time	2.41	8676
SG secondary sides are dry	2.08	7488
Calandria vault rupture disk open	7.68	27 648
Pressurizer empty	3.05	10 980
At least one channel is dry (complete boil-off)	3.22	11 592
First fuel sheath failure	5.38	19 368
Pressure and calandria tubes are ruptured	3.63	13 068
Calandria vessel rupture disks #1-4 open	3.63	13 068
Moderator reaches saturation temperature	3.63	13 068
Beginning of the core disassembly	5.02	18 072
Core collapse to calandria vessel bottom	7.85	28 260
Containment failed	20.14	72 504
Water is depleted inside calandria vessel	11.58	41 688
Water in calandria vault reaches saturation temperature	15.75	56 700
Calandria vessel failed	50.55	181 980
Quenching of debris occurred in calandria vault	50.9	183 240
Water is depleted inside calandria vault	51.5	185 400

### 3.6.3.1. Phase 1

The Phase 1 of the analysis begins with the initiation of Station Black Out (SBO) and ends with the blow of the calandria rupture disk which occurs at  $t=13,068$  s.

The SBO is initiated at time  $t=0.00$  s. The initiation of accident will trip the reactor and close the turbine stop valves with 20 s delay. As PHTS loop isolation valves are not closed, both loops show similar pressure behaviour as depicted in Figure 3-272. Initially the pressure in both loops decreases with time, as the heat extracted initially from the coolant at SGs location is greater than the heat input to the coolant due to the loss of fission power from the reactor core. The heat transfer from the PHTS to the steam generators causes the water boil-off and the increase of the pressure in steam generators secondary side. When the steam generators secondary pressure reaches the set point for the opening of MSSVs, the steam is discharged from the secondary side to the environment outside the containment. First opening of the MSSV occurs at 137 s. The secondary side steam generator pressure then oscillates at the MSSV set point as the MSSVs opens and closes (Fig. 3-273).

Following SBO primary pumps trip and the flow rate through reactor core decreases rapidly to the level of natural circulation. Therefore, the heat transfer through SG is reduced drastically (Fig. 3-274) to the level of core decay heat. Consequently, the primary pressure remains roughly constant during this period.

The SGs mass inventories and therefore the water level in the steam generators continuously decrease as a result of boil-off (Figs 3-275 and 3-276). At  $t=7,488$  s the SG secondary sides are dry. When the SGs secondary side inventories are depleted, the SGs are no longer a heat sink to remove heat from PHTS and the natural circulation in PHTS is ceased. Following this moment, the pressure in the PHTS increases until it reaches the PHTS liquid relief valve set point and then it oscillates at the relief valve set point. LRVs open for the first time at  $t=8,700$  s. At this moment, the liquid relief valve water (LRV) flow is about 83 kg/s (Fig. 3-277).

Although the amount of heat transferred to the moderator from the fuel channels increases after SG dry-out (Fig. 3-278), the loss of SGs as heat sink together with the continuous loss of inventory through the LRVs result in a rapid increase of average PHTS void fraction (Fig. 3-279) and decrease of loops inventory (Fig. 3-280). The decay heat from the core boils off the coolant, eventually leading to fuel channels dry-out at about 11,600 s in Loop 2 and at about 11,900 s in Loop 1.

The boil-off of the coolant inside the fuel channel gives rapid rise to the fuel channel temperatures. When pressure tube wall reaches  $1,000^{\circ}\text{K}$ , the fuel channel ruptures. This happens at 13,068 s for both loops.

The rupture of the pressure tube and calandria tube of fuel channels in each loop generates a rapid blow-down from the PHTS into the CV. When PHTS inventory is discharged into CV, the pressure inside the calandria vessel increases rapidly (Fig. 3-281) and reaches the set point of the rupture disk. The CV rupture disks open at 13,068 s.

During this phase, generally the fuel is well cooled; the temperature of sheath begins to rise at the end of the phase. As the sheath temperature increases and the fuel channel is filled with steam, the Zircaloy oxidation starts at about 12,700 s. However, at the end of the phase only a small amount of Zircaloy is oxidized, which generates about 1.4 kg of hydrogen.

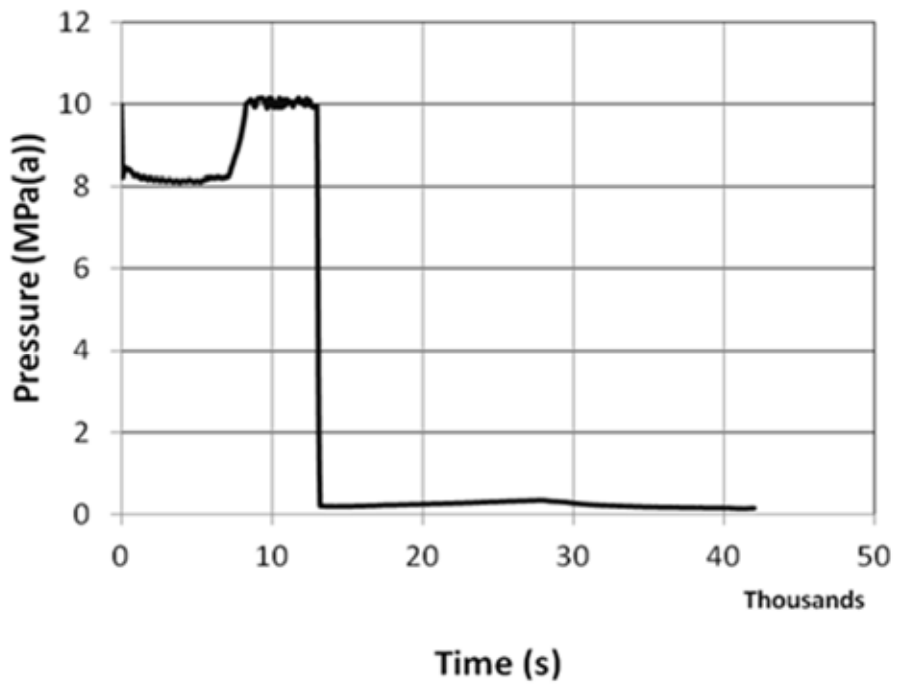


FIG. 3.272. PHTS pressure (outlet header).

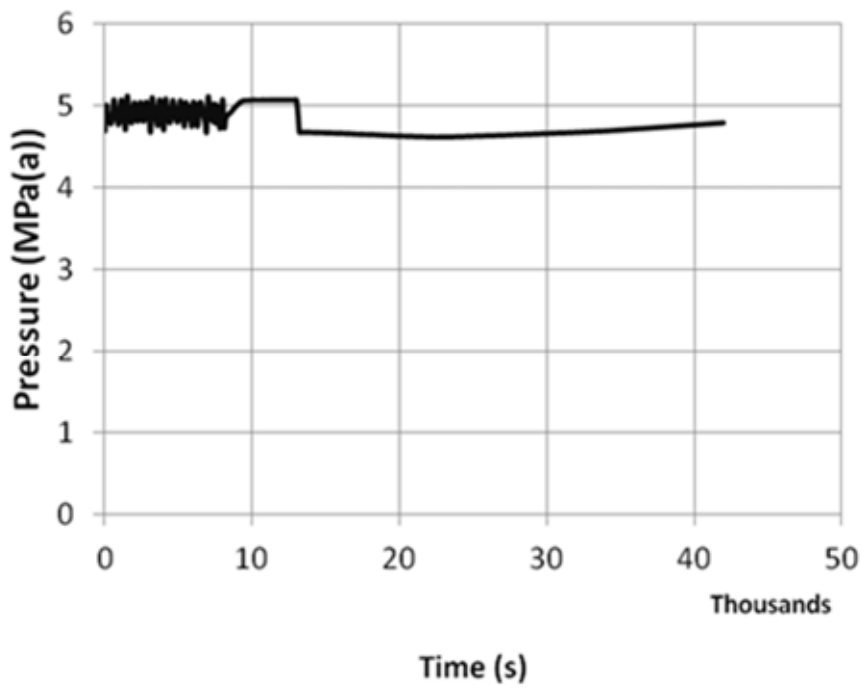


FIG. 3.273. Steam generator pressure.

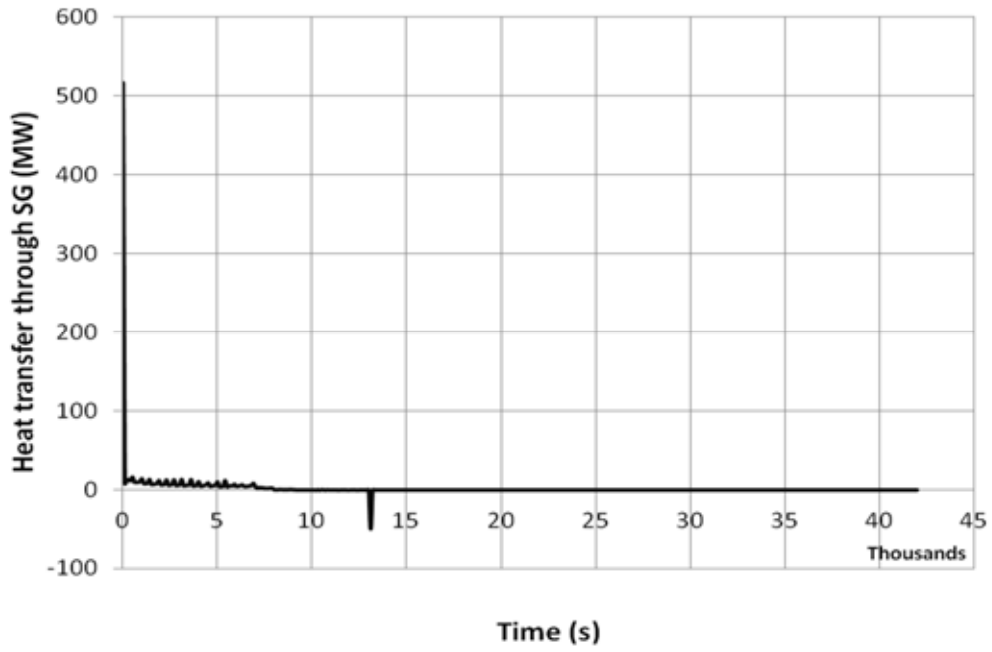


FIG. 3.274. Heat transfer through SG.

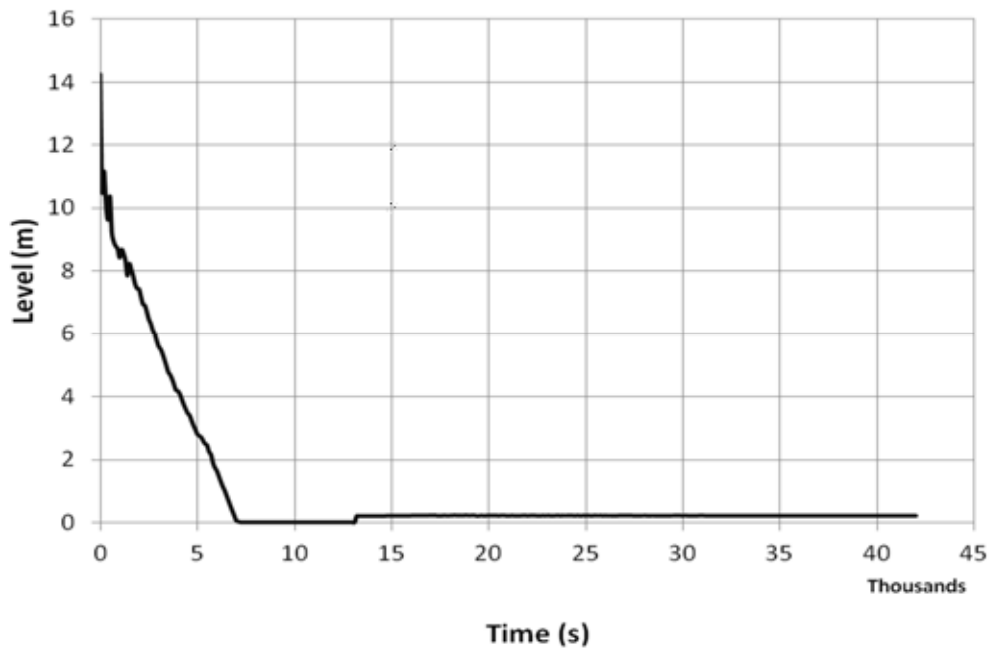


FIG. 3.275. Steam generator level.

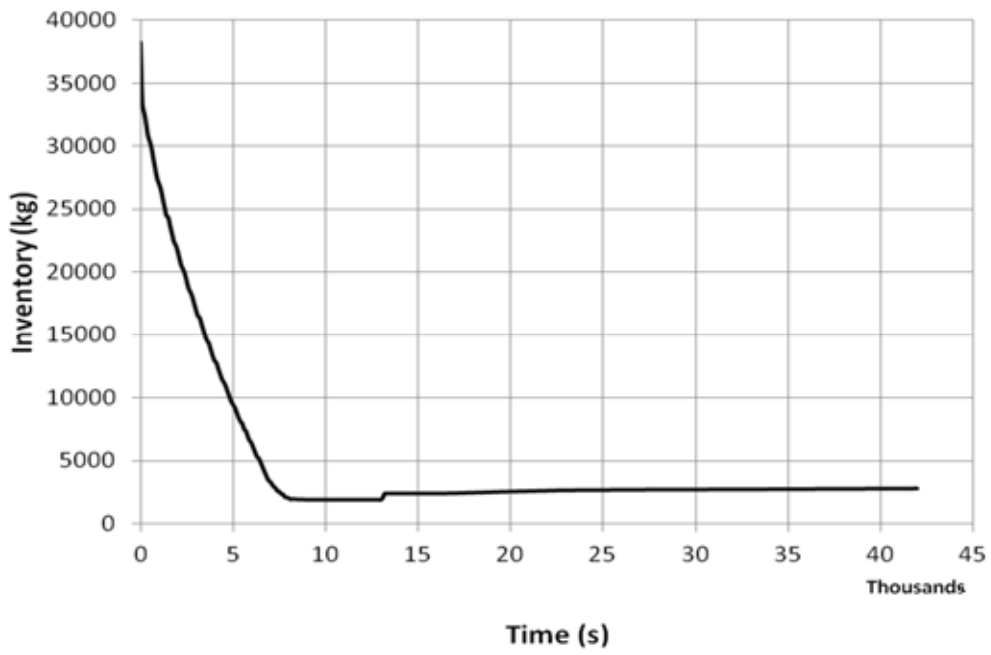


FIG. 3.276. Steam generator mass inventories.

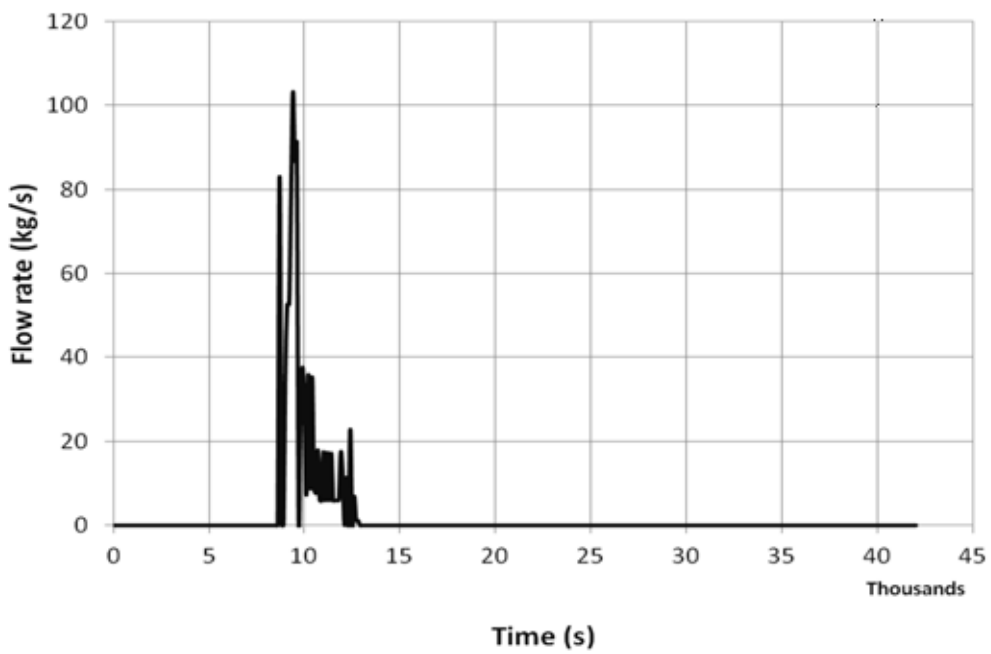


FIG. 3.277. Liquid relief valve total flow rate.

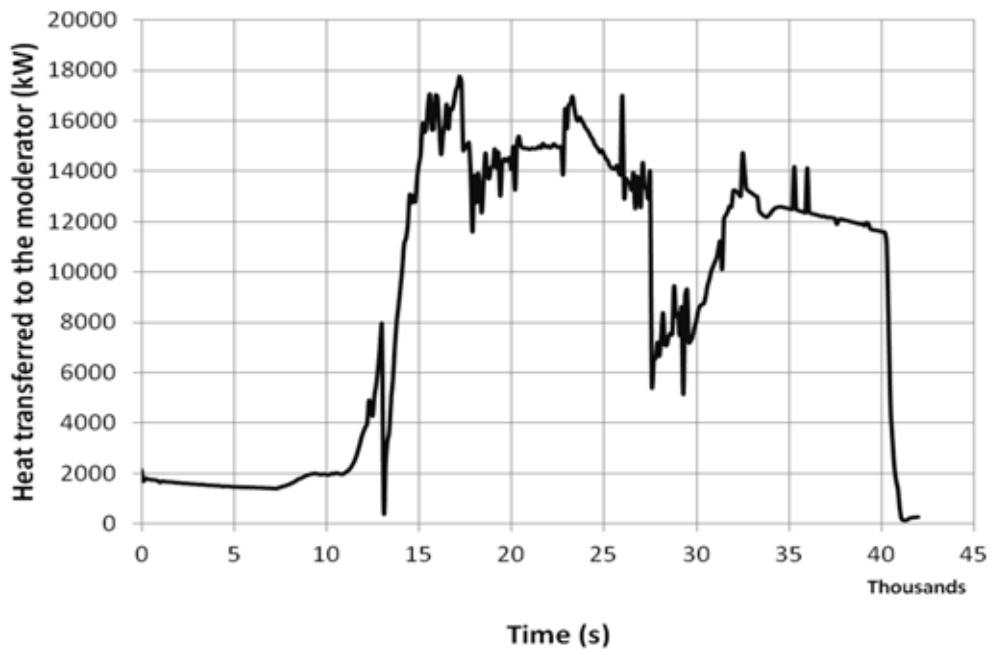


FIG. 3.278. The amount of heat transferred to the moderator from the fuel channels.

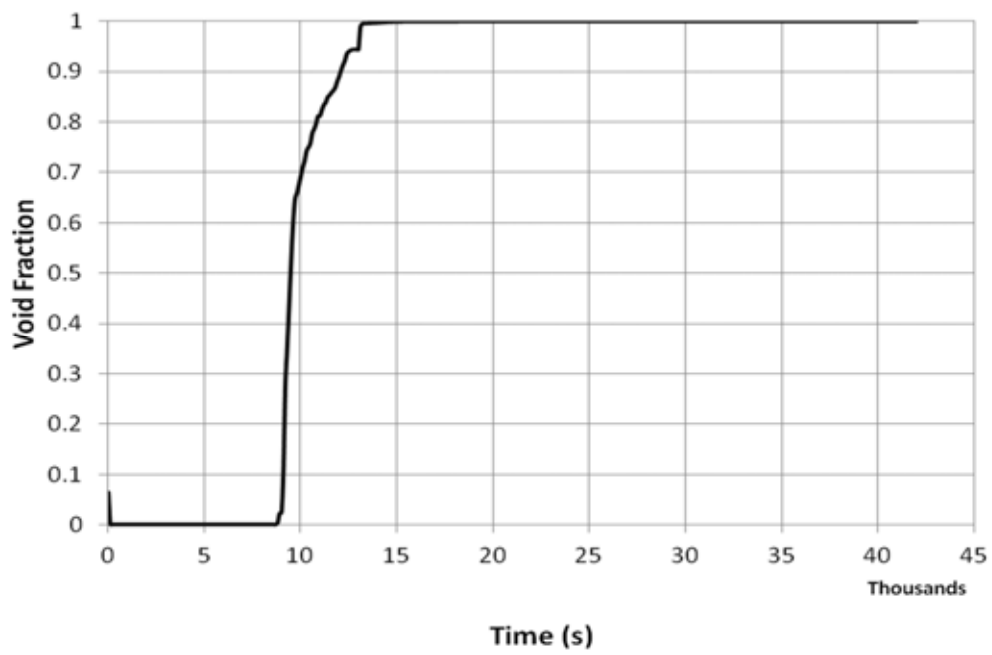


FIG. 3.279. The PHTS Loop 1 void fraction.

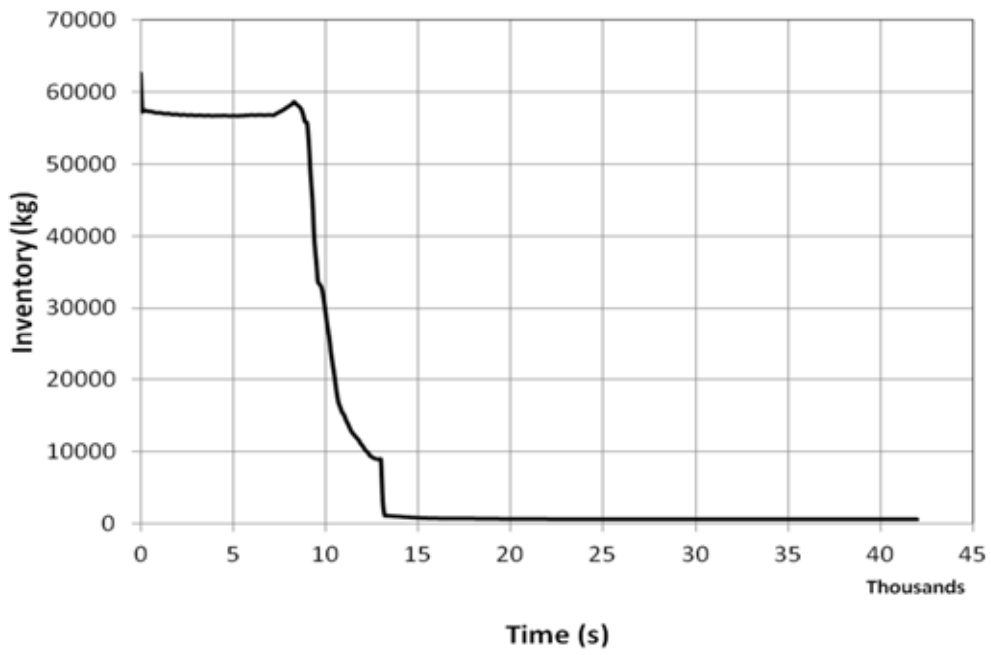


FIG. 3.280. Mass inventories in the primary HTS Loop 1 (including all pressurizer inventories).

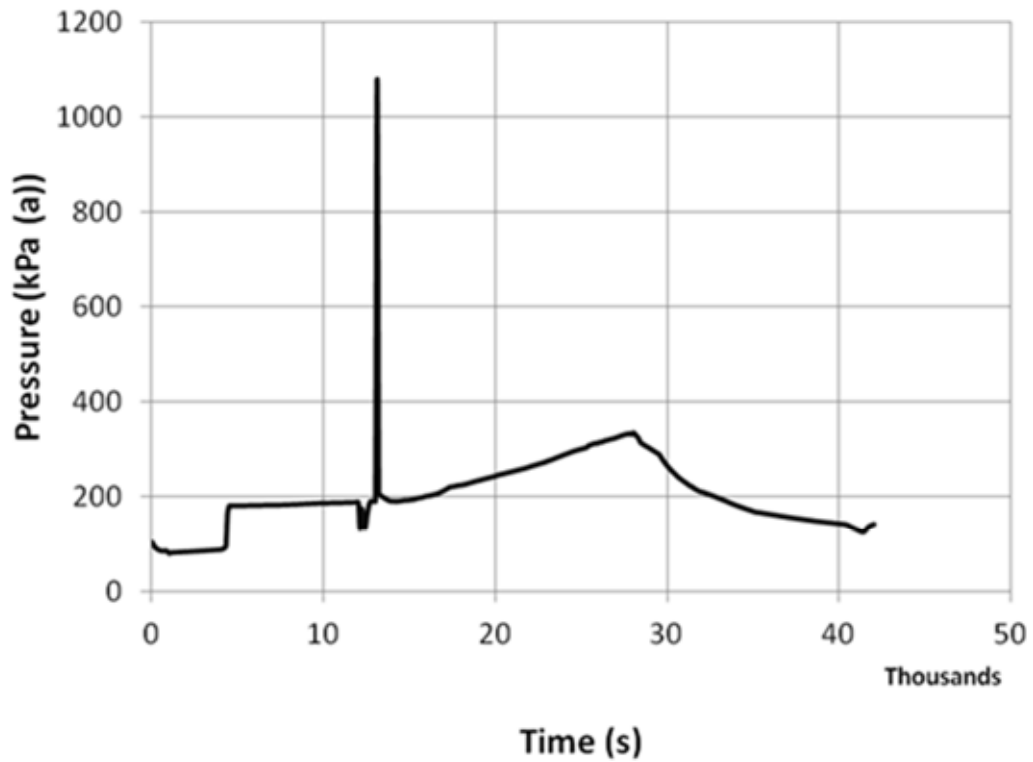


FIG. 3.281. Average calandria vessel pressure.

### 3.6.3.2. Phase 2

The Phase 2 starts when the rupture disk blows i.e. at  $t=13,068$  s and ends with the core collapse that occurs at  $t=28,249$  s.

When the rupture disks open, a rapid decrease in the CV water level occurs (Fig. 3-282). After the initial rapid moderator expulsion, the moderator continues to discharge gradually into the containment as a result of continued moderator boil-off due to the heat transfer from the core (Fig. 3-289).

Following initial rapid moderator expulsion, about half of the fuel channels located on the upper side of CV becomes uncovered. Consequently, fuel, sheath, PT and CT temperatures increase rapidly (Fig. 3-283). First sheath failure is predicted to occur at  $t=19,367$  s from the beginning of the accident. The sheath failure is predicted to occur at bundle 8, channel 3 of pass 4 (see Fig. 3-268). The sheath failure is due to high temperature under compression loading. Sheath temperature is predicted to be  $1,900^{\circ}\text{K}$  at this point. As a result, the fission products from gap inventory start to be released in PHTS (Fig. 3-284).

The temperature of the calandria tube in the uncovered fuel channels increase rapidly as those channels had lost the moderator as heat sink. First time the disassembly criteria is met at bundle 6, channel 4 of pass 3 at  $t=18,067$  s. Since the present version of the SCDAPSIM/RELAP5 code has no specific CANDU model for core disassembly, in our analysis the suspended debris remains in its initial location until either the axial disassembled segment of the fuel channel relocates on the bottom of the calandria vessel or the core collapse criteria is met. A temperature of  $2,500^{\circ}\text{K}$  was considered for debris relocation from suspended debris to the bottom of the calandria vessel.

Once the core disassembly starts, the mass of suspended debris increases rapidly to about 20,000 kg per loop. This is the result of uncover of the fuel channels located in the upper half of the calandria vessel after CV rupture disks opens. Following this increase, for the next approximately 9,000 s the mass of the suspended debris remains roughly constant as the mass added to it from the new disassembled fuel channel segment is compensated by the mass lost due to relocation of debris parts on the bottom of the calandria vessel (Fig. 3-285). When decreased moderator level uncovers the fuel channels located in the lower half of the CV (channels 2 on Fig. 3-268), the rate of added mass becomes higher than the rate of mass removed by relocation. Then again the mass of suspended debris increase rapidly and when the mass of suspended debris bed exceeds 25,000 kg per loop, the core material in the suspended bed and the intact channels relocate to the bottom of the calandria vessel at 28,249 s. The mass of  $\text{UO}_2$  in the undeformed intact channels in core and the mass of terminal debris are shown in Figures 3-286 and 3-287 respectively.

During this phase, almost all Zircaloy oxidation is calculated to occur and thus almost all “in-vessel” hydrogen is generated, i.e. 285 kg (Fig. 3-288).

At the end of this phase, about 30% of the initial fuel inventory fission products are released into PHTS. Only Xe, Kr, I, and Cs were considered in the analysis (Fig. 3-284).

The containment pressure starts to increase by LRV opening at 8,676 s (Fig. 3-290). Steam condensation on containment wall and steel wall initially decreases the pressure; then the pressure increases again at a slower rate as the moderator boils.

A small amount of fission products is released into the environment through containment leakage, Figures 3-293 and 3-294. By the end of phase 2, 0.005 kg of Kr, 0.114 kg of Xe, 0.0055 kg of I, and 0.054 kg of Cs are released into the environment.

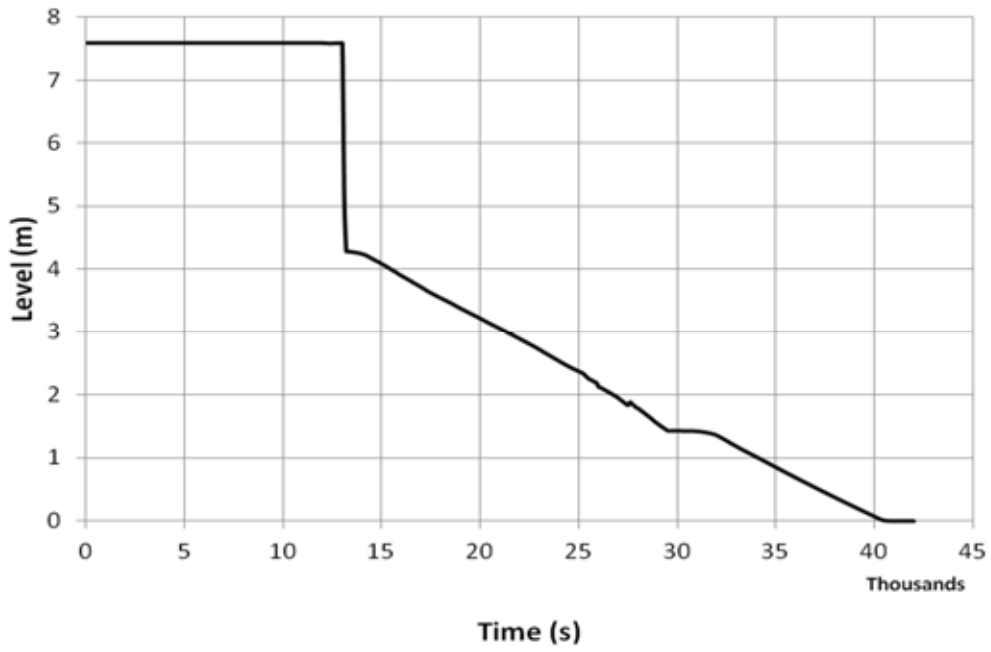


FIG. 3.282. Collapsed water level in the calandria vessel.

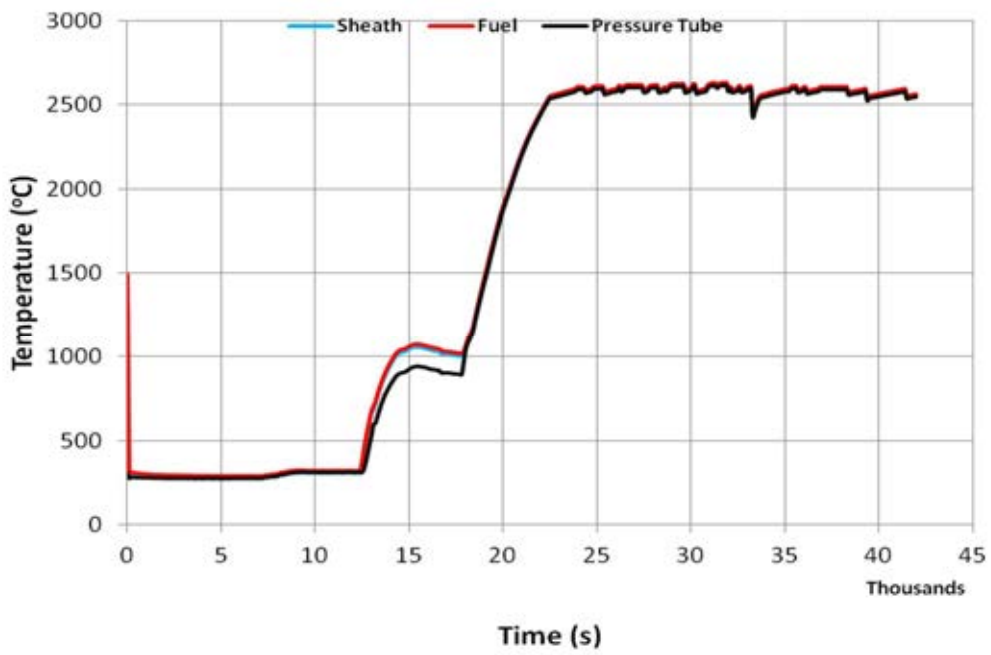


FIG. 3.283. Fuel channel temperatures (axial segment 8, channel 3, core pass 4).

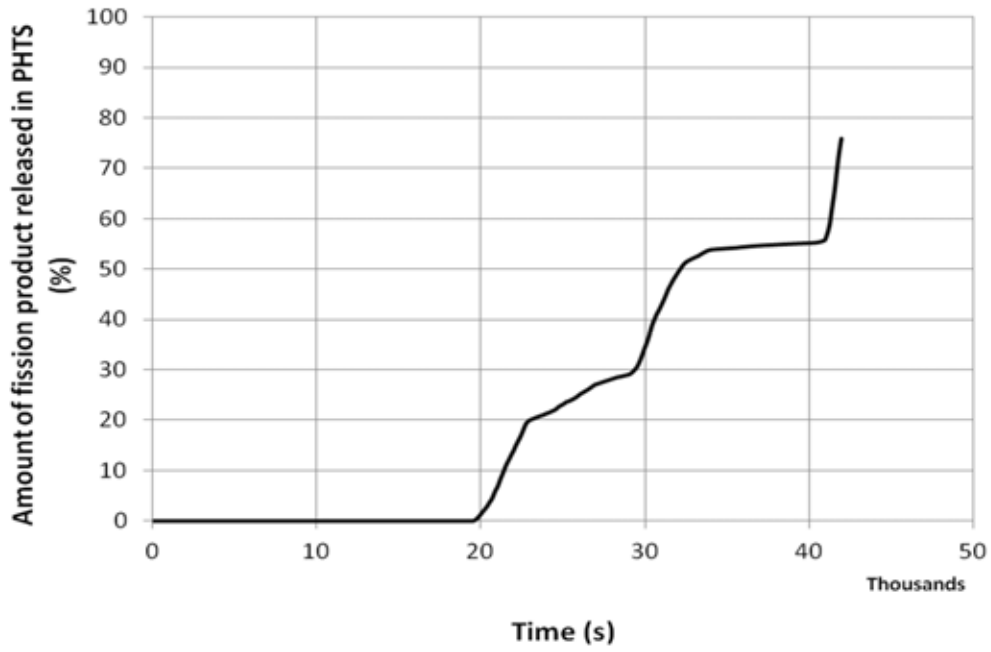


FIG. 3.284. Amount of fission product (Xe, Kr, Cs, I) in PHTS (% of initial fuel inventory).

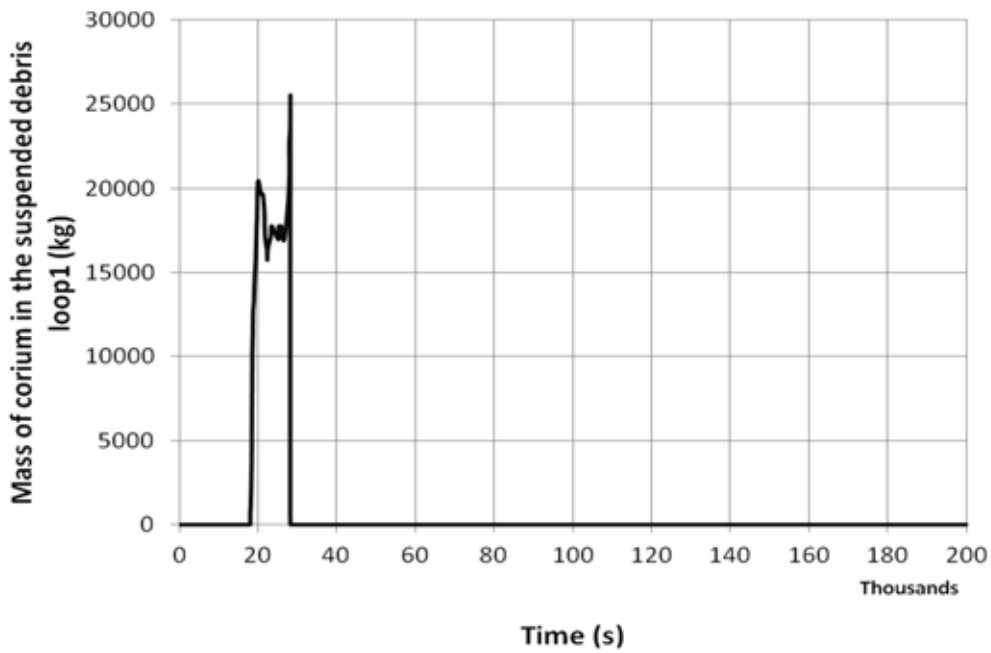


FIG. 3.285. Mass of corium in the suspended debris per loop.

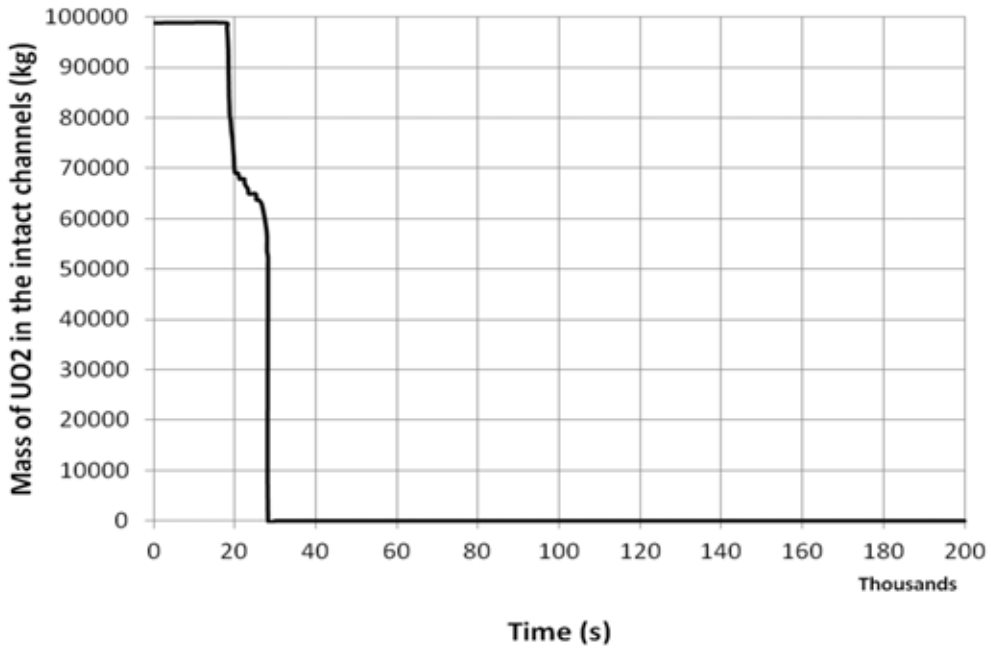


FIG. 3.286. Mass of UO<sub>2</sub> in the undeformed intact channels in core.

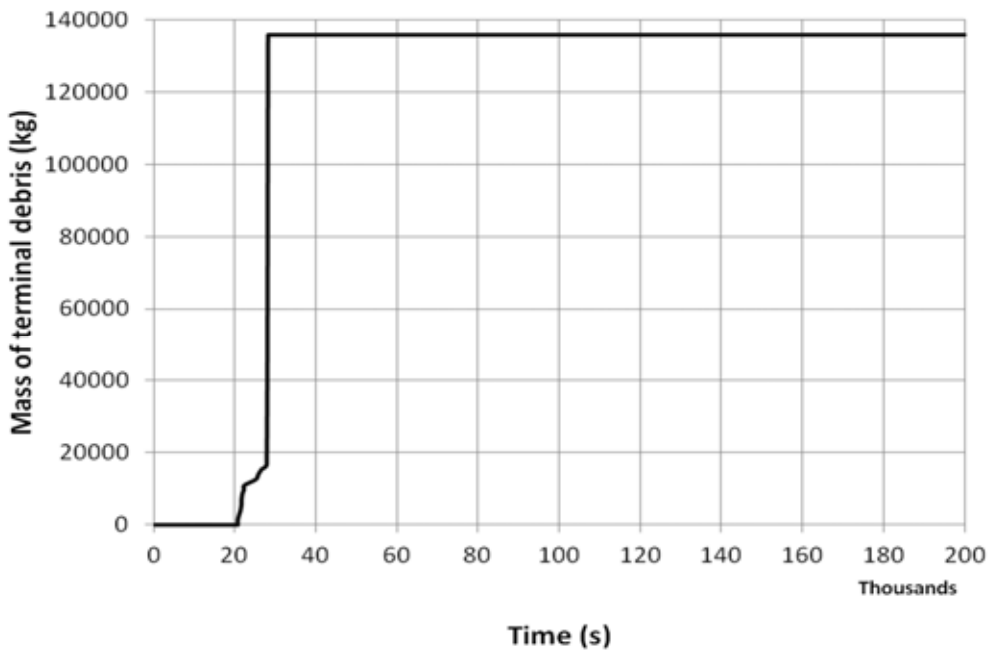


FIG. 3.287. Mass of terminal debris.

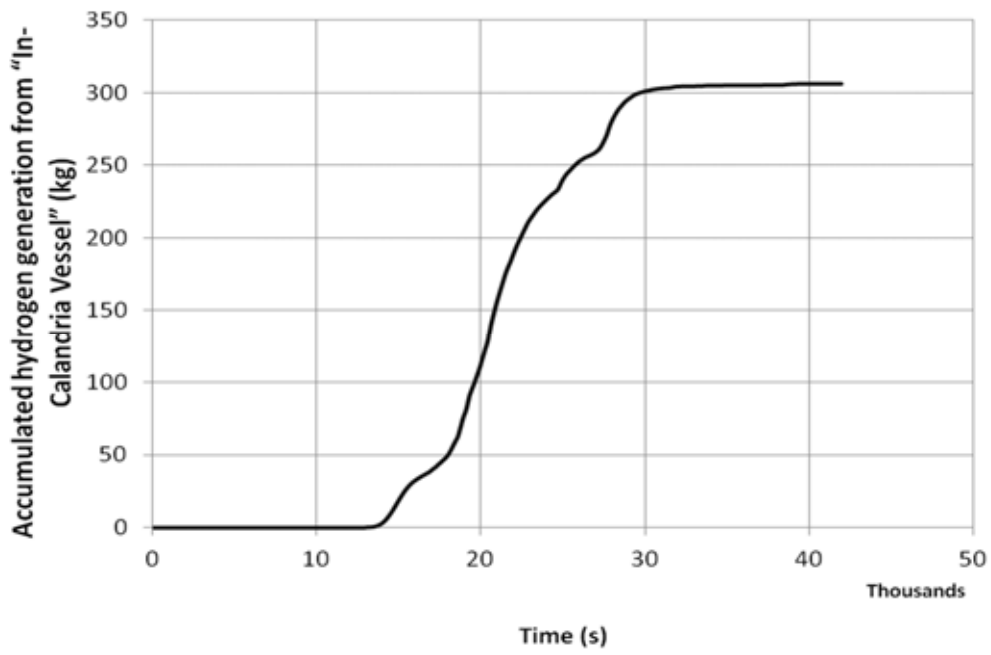


FIG. 3.288. Accumulated hydrogen generation from "In-Calandria Vessel".

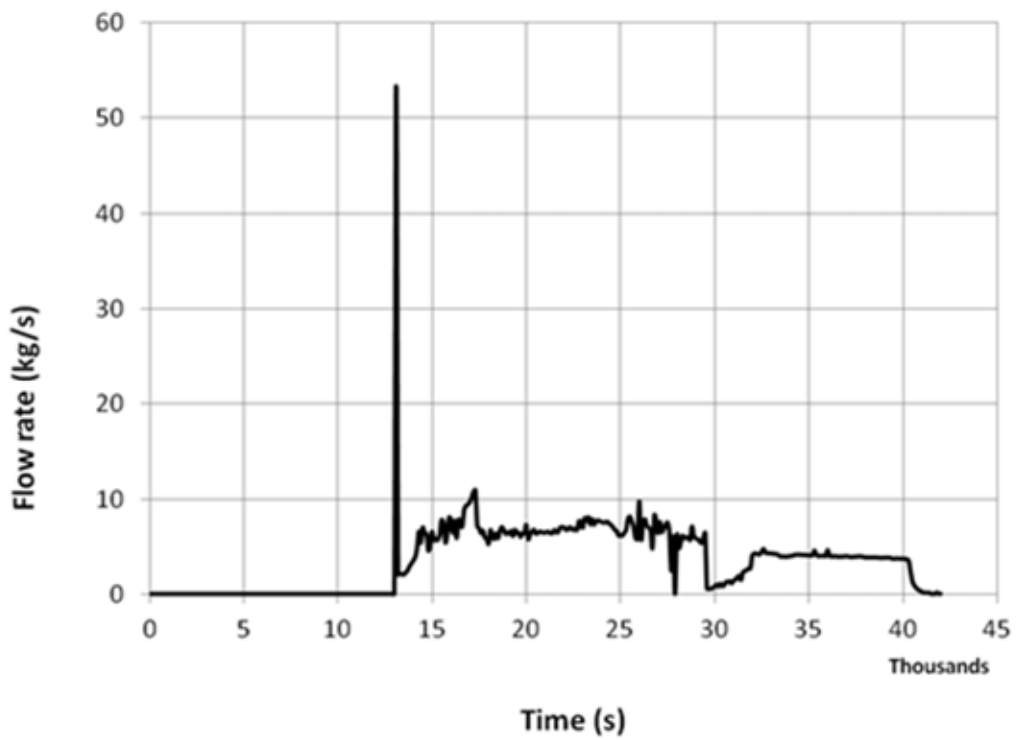


FIG. 3.289. Steam flow rate from the calandria vessel to the containment.

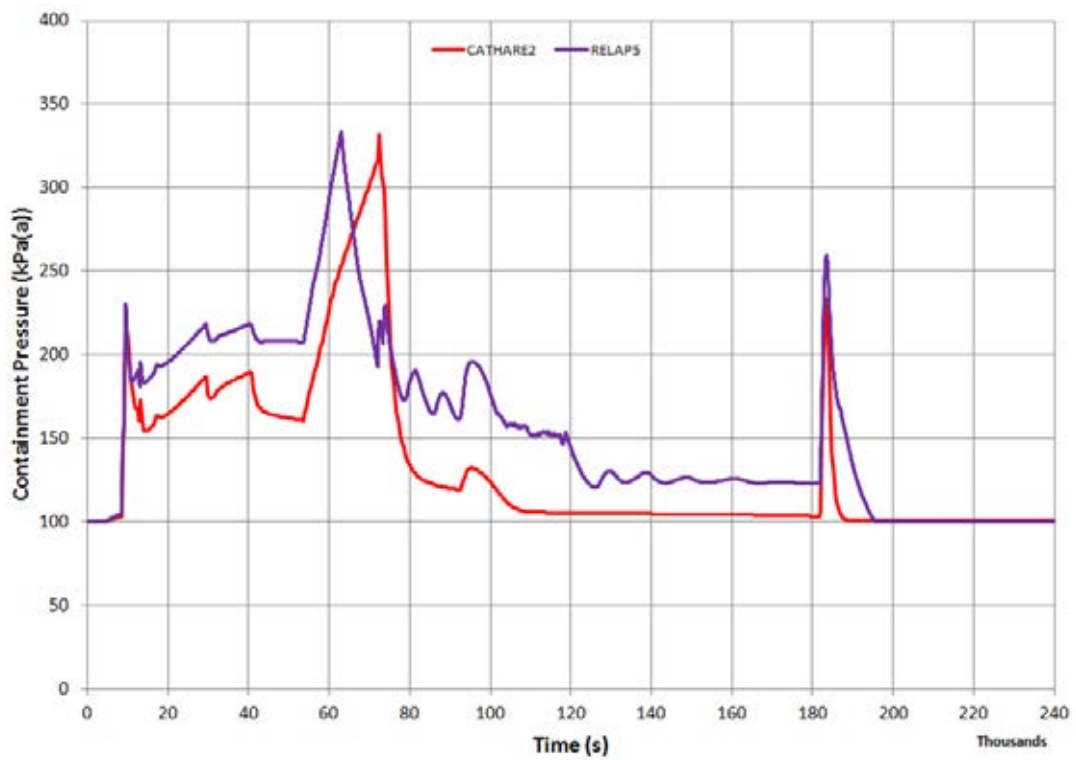


FIG. 3.290. Containment pressure.

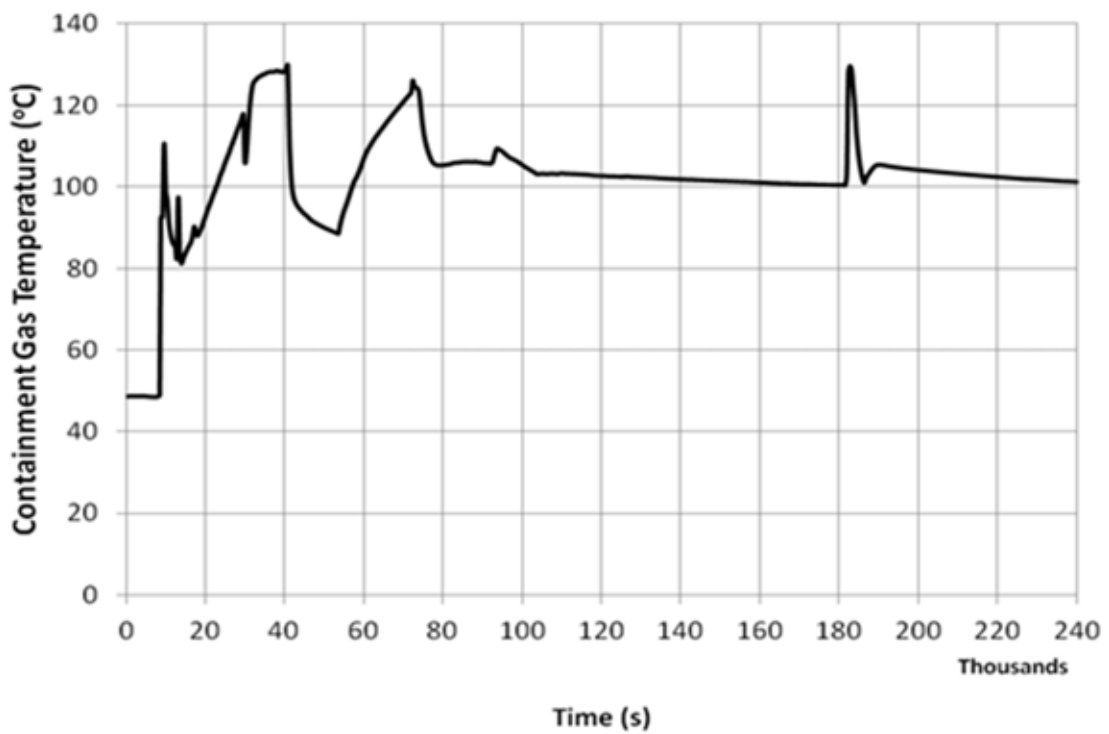


FIG. 3.291. The containment gas temperature (CATHARE2 calculation).

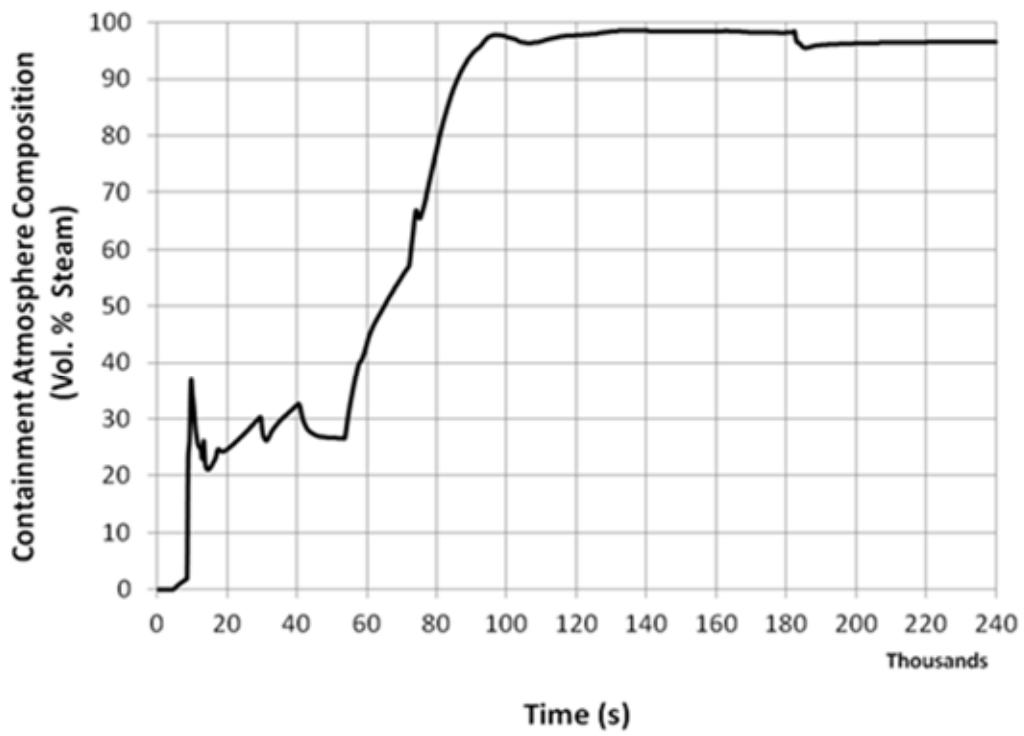


FIG. 3.292. The percent volume of steam in the containment atmosphere (CATHARE2 calculation).

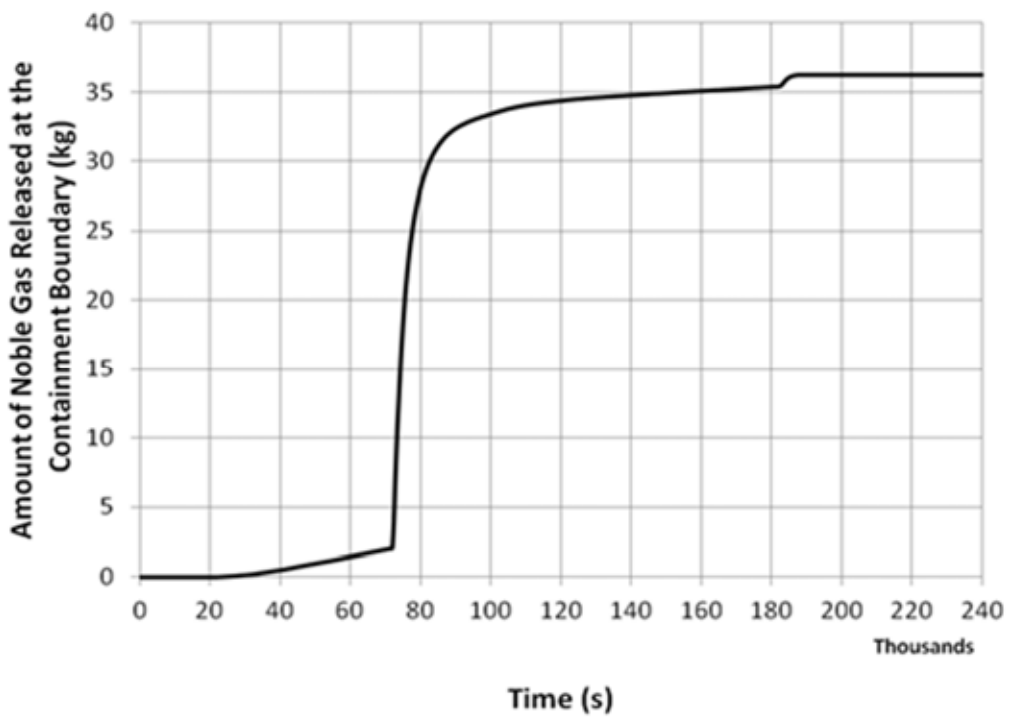


FIG. 3.293. The amount of noble gas released at the containment boundary (CATHARE2 calculation).

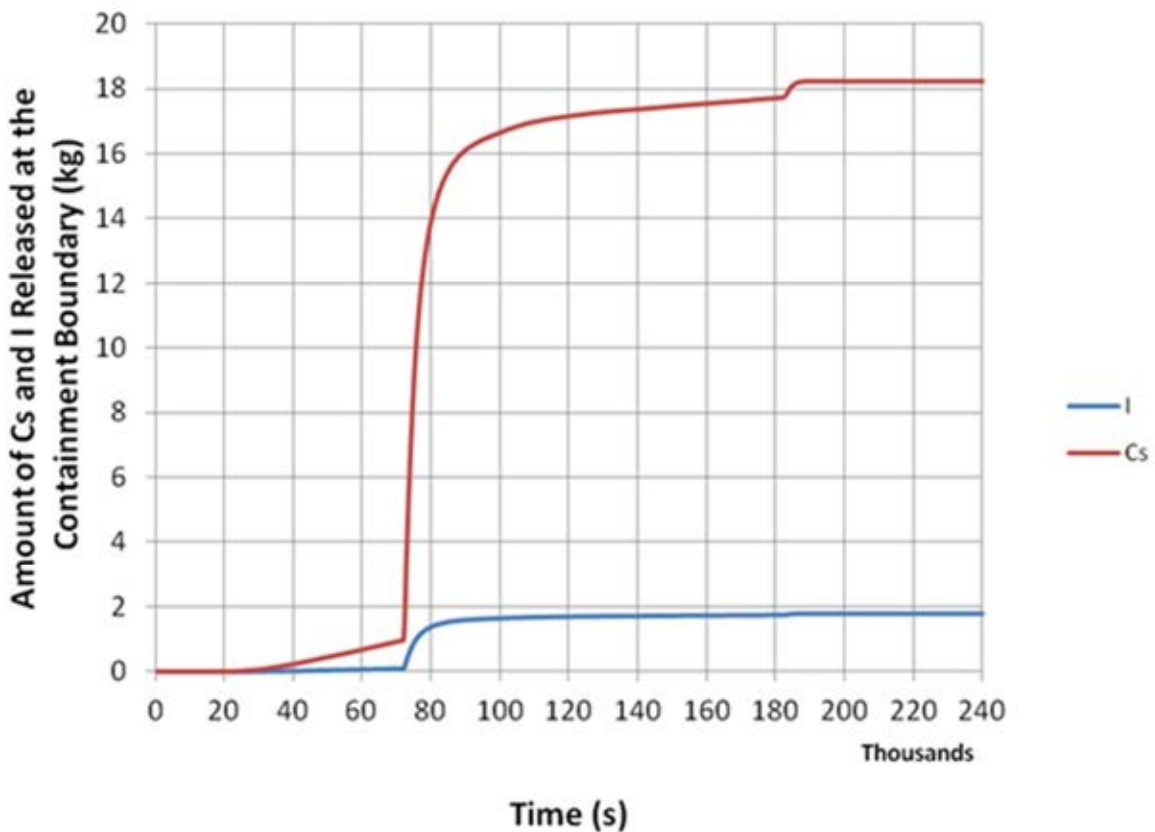


FIG. 3.294. The calculated amount of Cs and I released at the containment boundary (CATHARE2 calculation).

### 3.6.3.3. Phase 3

The Phase 3 starts with core collapse at  $t=28,249$  s and ends with the calandria vessel failure which occurs at  $t=181,987$  s.

At the moment of core collapse the moderator level is 1.72 m (Fig. 3-282). As a result, the debris relocated on the CV bottom is quenched by the water remaining in the CV at this time. Continuously heat transfer from the relocated debris to the remaining water in calandria vessel eventually leads to boiling of remaining water. The calandria vessel water is depleted at about 41,717 s.

Consequently, the debris relocated into the CV bottom heats up rapidly (Fig. 3-295). The debris starts to melt at about 50,700 s and begins to form a molten pool surrounded by a crust. The molten fraction of the debris increases rapidly to about 46%, and then it remains almost constant until depletion of RV water occurs (Fig. 3-296). Then the fraction suddenly increases to 75%. However, the non-melt corium temperature is close to the melting temperature, as it can be seen from the values for maximum and average debris temperature shown in Figure 3-295.

The water in the reactor vault acts as a heat sink and cools the CV wall, maintaining the calandria vessel integrity. After the initiating event the RV pressure increase gradually due to the loss of shield and moderator cooling. At 27,648 s the RV rupture disks burst due to pressure build up resulting from water thermal expansion. The reactor vault inventory reaches the saturation temperature and starts to boil at about 56,700 s. Consequently, the reactor vault water level begins to decrease (Fig. 3-297). Eventually, the water level in the RV falls below

the CV bottom level at about 179,500 s. Subsequent to this moment, the CV bottom heats up rapidly and fails due to creep, at about 181,987 s (Fig. 3-298).

During this phase an amount of about 19.6 kg of hydrogen is generated. After the calandria vessel water depletes, generation of “in-vessel” hydrogen is not considered, as steam is not available.

During phase 3 about 46% of the initial fuel inventory fission products are released into PHTS, thus at the end of this phase about 76% of the initial fuel inventory fission products are released (Fig. 3-284).

At the beginning of the phase, the containment pressure continues to increase as the moderator boils (Fig. 3-290). Then the containment pressure decreases during the period between the moment when the calandria vessel water depletes and the moment when the reactor vault water starts to boil. When RV water starts to boil, the containment pressure gradually increases and at 72,504 s reaches the failure set point of air lock seal (Fig. 3-290). RELAP5 calculation shows a similar trend for the containment pressure. However, the condensation rate calculated by RELAP5 is lower than those calculated by CATHARE2 code, so the containment failure occur at 63,000 s. Also the pressure in the lower SG room calculated by RELAP5 is constantly higher than the pressure calculated by CATHARE2 during the transient by about 30 to 50 kPa.

The containment gas temperature in the lower steam generator room is shown in Figure 3-291 and the volume fraction of steam in the lower steam generator room are shown in Figure 3-292. Soon after the containment failure, almost all amount of noble gas, I and Cs existing in lower SG room are released in the environment, Figures 3-293 and 3-294. By the end of the phase 3, 0.032 kg of Kr, 35.34 kg of Xe, 1.734 kg of I, and 17.73 kg of Cs are released into the environment through containment leakage, Figures 3-293 and 3-294.

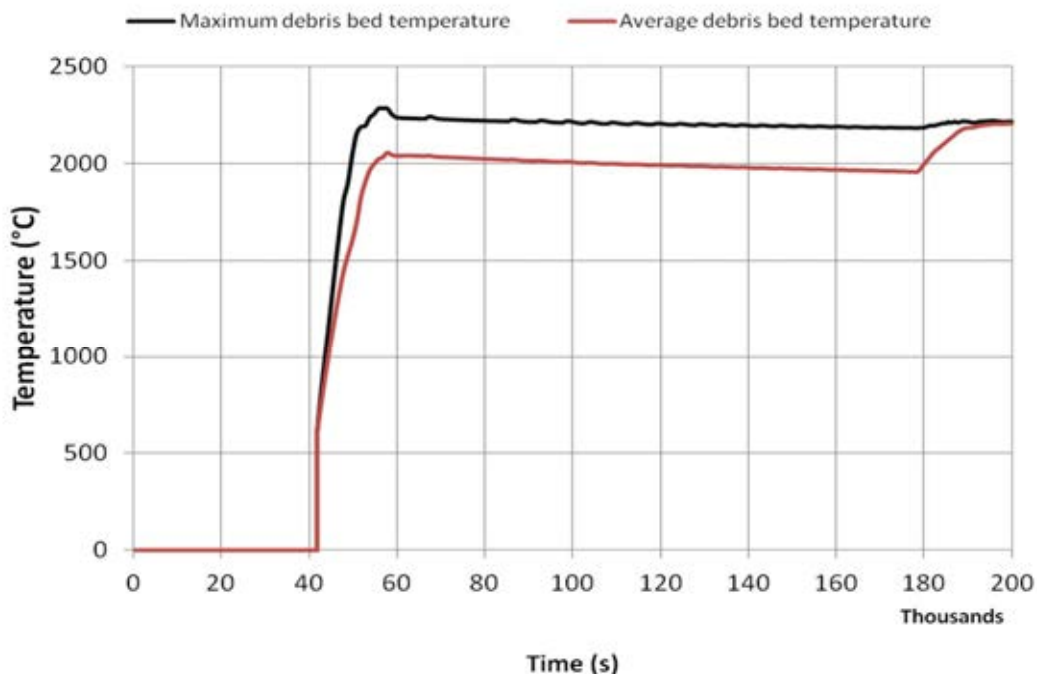


FIG. 3.295. Temperature of the debris bed.

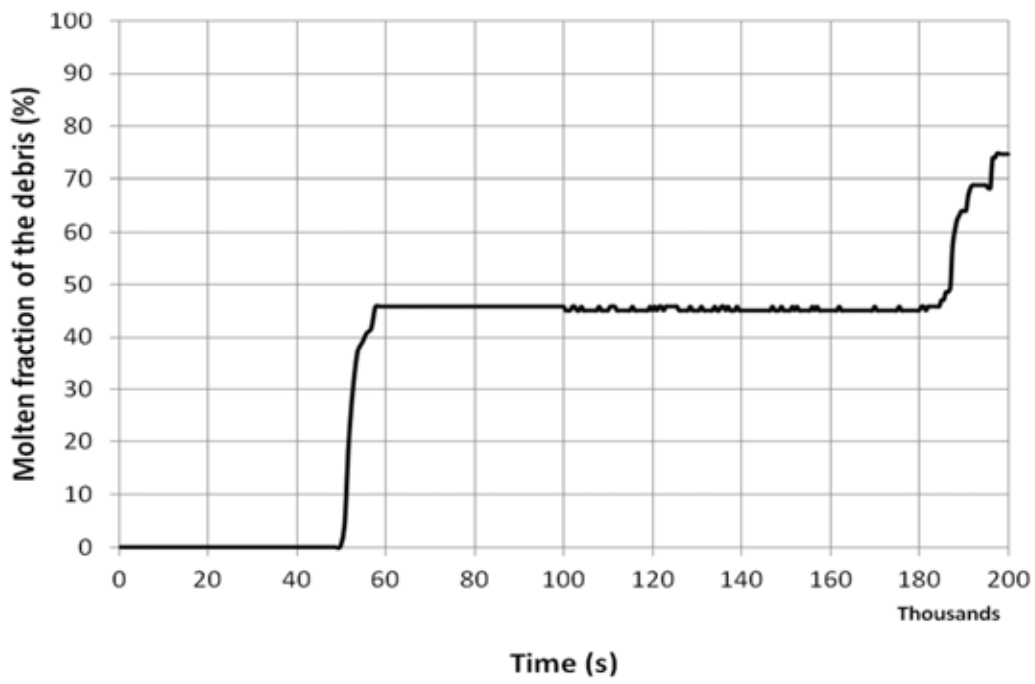


FIG. 3.296. Molten fraction of the debris.

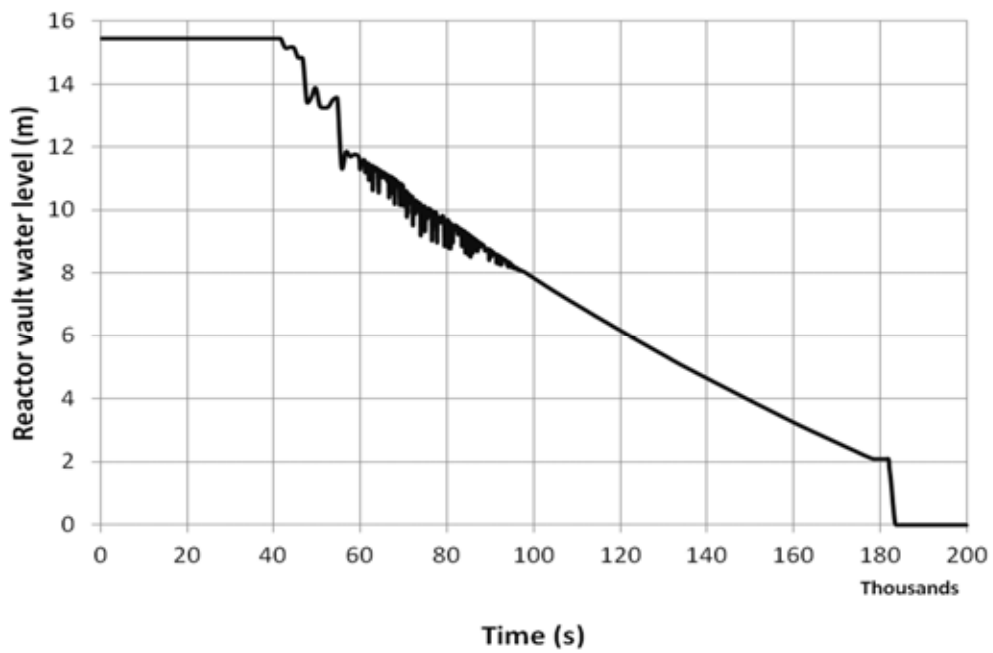


FIG. 3.297. Reactor vault water level.

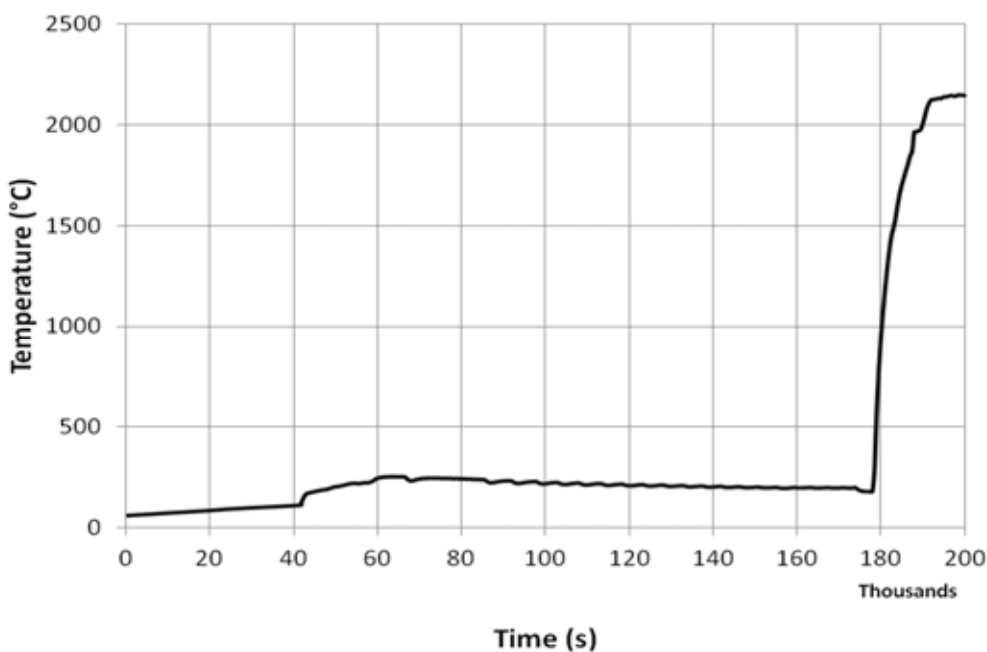


FIG. 3.298. Calandria vessel wall temperature at the bottom.

#### 3.6.3.4. Phase 4

The Phase 4 starts with the calandria vessel failure at  $t=181,987$  s. Subsequent to the CV bottom failure, the corium in the CV relocates onto the reactor vault floor. Rapid steam generation is predicted by the code as a result of debris quenching (Fig. 3-299). Eventually, all the water in the reactor vault dries out at about 185,387 s (Fig. 3-297).

During the quenching of corium, a large quantity of steam is produced causing a rapid increase of containment pressure (Fig. 3-290).

The total amount of fission products released to environment is presented in Table 3-18.

No other parameters were calculated for this phase.

TABLE 3.18. TOTAL AMOUNT OF FISSION PRODUCTS RELEASED TO ENVIRONMENT

Fission product	Amount released (kg)	% of initial core inventory
Xe	36.2	67.3
Kr	0.032	0.8
Cs	18.24	71.9
I	1.78	68.4

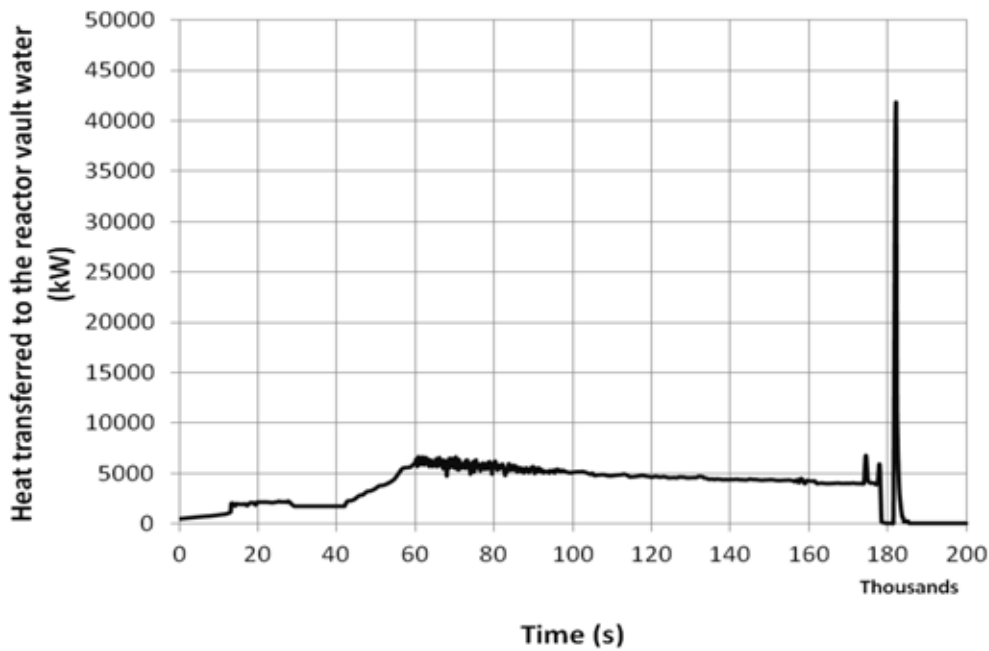


FIG. 3.299. Amount of heat transferred to the reactor vault water.

### 3.7. SJTU

#### 3.7.1. Computer codes

The SCDAP/RELAP5 Mode 3.4 has been used in the CANDU severe accident analysis.

The SCDAP code could be used to model the core behaviors during the severe accidents and includes detailed core components. The core treatment includes the fuel rod heat up, ballooning and rupture, rapid oxidation, Zircaloy melting,  $\text{UO}_2$  dissolution, freezing of molten fuel and cladding, debris formation. The control rods and flow shroud could be also modeled with the code. The COUPLE model in the code could simulate the lower plenum debris and vessel structures.

As the best-estimate transient analysis code used in light water reactor postulated accidents, the RELAP5/MOD3 series codes are based on a non-homogeneous and non-equilibrium model for the two-phase system [14]. The code includes component models that could be used to simulate reactor systems. The component models include pumps, valves, pipes, reactor kinetics, heaters, turbines, separators, accumulators, and control systems. Additionally, special models are also included, such as choked flow, counter-current flow limitation, flow at the abrupt area change, and non-condensable gas transport.

Comparing with the previous versions of the code, the MOD 3.4, which has most advanced models for severe accidents analysis, could runs more reliability than the previous versions of SCDAP/RELAP5 code. The code improves numeric and minimizes “water property” failures. The improved code allow the user to run new classes of thermo-hydraulics problems, such as spent fuel storage and research or pool type reactor transients, and the detailed SCDAP fuel behavior.

#### 3.7.2. Phenomena and system idealization

##### 3.7.2.1. Debris thermal hydraulics [37]

Once the fuel channels collapse to the bottom of the calandria vessel, the debris and the calandria wall were modeled with the COUPLE module. A model based upon the COUPLE code is used to calculate the heat-up of reactor core material that slumps to the lower head of the calandria vessel and is subsequently represented as debris. The debris thermal hydraulics correlations include the heat conduction model, thermal conductivity model and gap conductance model, which have been validated with some specific tests.

#### 3.7.2.2. *Material oxidation model [37]*

The material oxidation model calculates the generation of heat, production of hydrogen, and reduction of steam. This model uses oxidation rate equations with material temperatures defined by the component heat conduction model.

#### 3.7.2.3. *Thermal mechanical deformation model [38]*

The models used in the CANDU 6 severe accident simulation include the fuel rod cladding deformation model and the vessel creep failure model. The former is to calculate the elastic-plastic deformation that can occur in fuel rods, and the latter is to calculate creep damage and rupture time of the vessel material.

#### 3.7.2.4. *Fission product release model [37]*

The models described calculate the rate of fission product release from intact fuel rods and rods that have experienced fuel liquefaction or fragmentation, including the release model for intact fuel and the release during UO<sub>2</sub> Liquefaction and Fragmentation.

The theoretical model is used for predicting the behavior of fission gas in UO<sub>2</sub>-based fuels during steady-state and transient conditions. Fission products released from the fuel are assumed to reach the fuel surface by successively migrating from the grains to grain faces and then to the grain edges, where the fission products are released through a network of interconnected tunnels of fission gas induced and fabricated porosity.

#### 3.7.2.5. *PHTS Model*

The heat transport system model mainly consists of the core, pressurizer, heat transport pumps, steam generators (SGs) and the corresponding pipes (Fig. 3-300).

The CANDU6 core consists of 380 fuel channels arranged in 22 rows and 22 columns. A simplified nodalization represented the numbers of fuel channels and there are four channels considered. Each fuel channel corresponds a reactor inlet header (RIH), heat transport pump and a reactor outlet header (ROH), and two channels flow in inverse direction make up one loop respectively. The shield plug was modeled as pipe component and the end-fitting as annulus component.

The fuel bundles in the CANDU fuel channel were modeled as 12 axial nodes and the 37 fuel elements of the each fuel bundle, the Pressure Tube (PT), the Calandria Tube (CT) and the gas-filled annulus were modeled with the SCDAP core components. The pressure tube, calandria tube and the CO<sub>2</sub> between the PT and the CT were modeled with the shroud component (as shown in Fig. 3-301).

The heat transport pump was modeled with the pump component. The one phase and two phases curves of heat transport pump are generated according to the pump characteristic curves.

The primary section of the SG model consists of inlet plenum, U-tube and outlet plenum, as shown in Figure 3-302. The U-tube is modeled as one U-tube according to the total flow area

and volume. The secondary section of the SG model consists of feeder water inlet, down comer, separator, dryer, and drum.

For pipes of the core cooling system, inlet and outlet feeders, inlet and outlet headers, and other corresponding pipes, were modeled as pipe components.

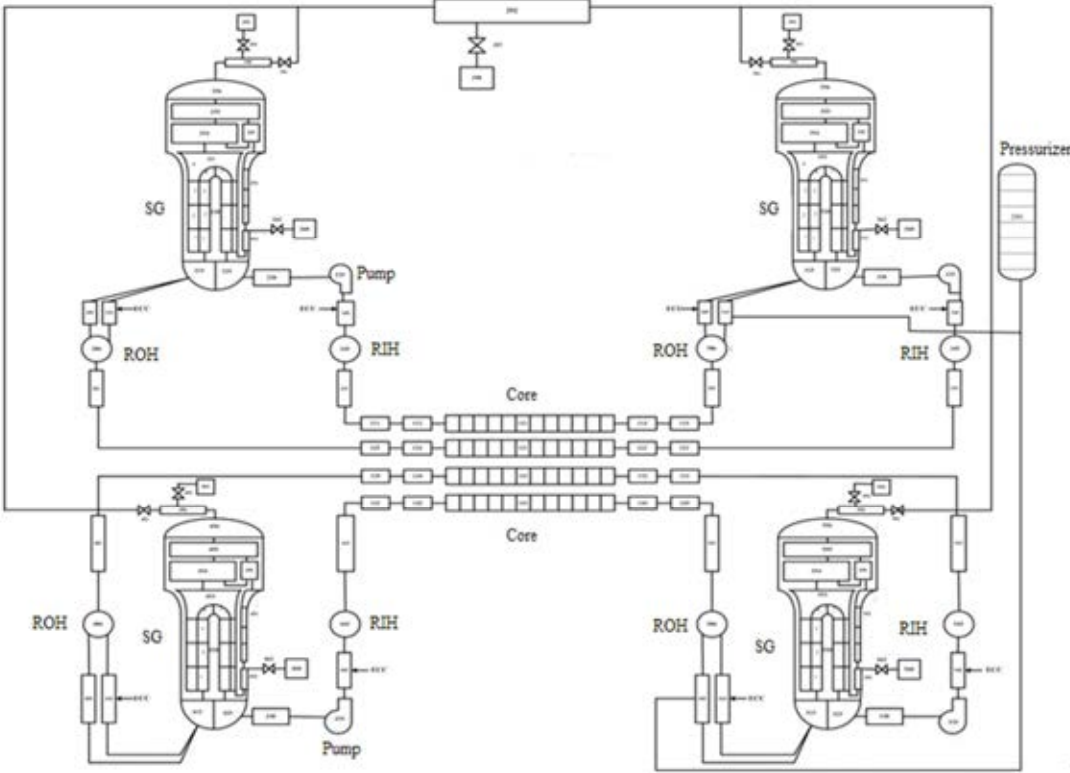


FIG. 3.300. Nodalization of CANDU6 NPP.

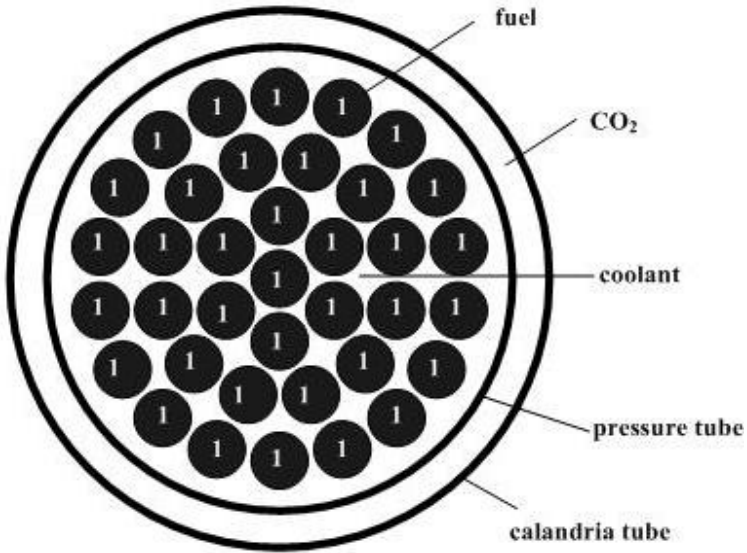


FIG. 3.301. SCDAP model of the fuel channel

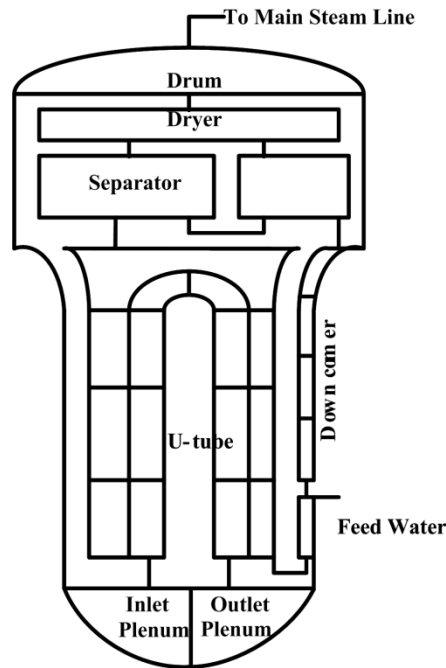


FIG. 3.302 Steam generator model.

### 3.7.2.6. Secondary system model

The secondary system includes the main feed water system and the main steam system. The model of the main feeder water system consists of volume control components and flow rate control valves. The model of the main steam system consists of main steam pipe, main steam insulate valves and safety valves, and the turbine. The feeder water system was modeled as the time-dependent volume and time-dependent junction components. The steam lines and turbine were represented by the time-dependent volumes and the main steam isolation valves and safety valves were modeled with the valve components, as shown in Figure 3-303.

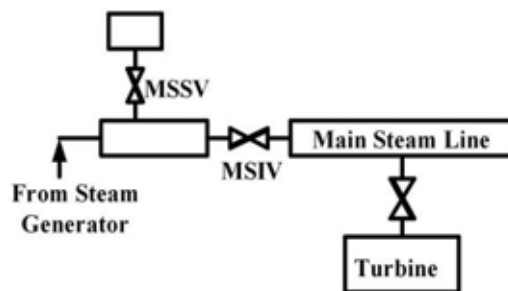


FIG. 3.303 Main steam lines and turbine model.

### 3.7.2.7. Moderator system model

The moderator system mainly consists of the calandria vessel and cover gas. The calandria vessel was modeled with the pipe component and the calandria over pressure rupture disk was modeled with a trip valve connecting the calandria vessel with containment, as shown in Figure 3-304.

Once the fuel channels collapse to the bottom of the calandria vessel, the debris and the calandria wall were modeled with the COUPLE module. A two-dimensional finite element mesh is generated by COUPLE based on the coordinates input of a selected number of nodes,

20 in horizontal directions and 16 in vertical directions. The COUPLE model for the bottom of the calandria vessel is shown in Figure 3-305.

The calandria vault model consists of the body and the corresponding pipes, which were modeled with the pipe component.

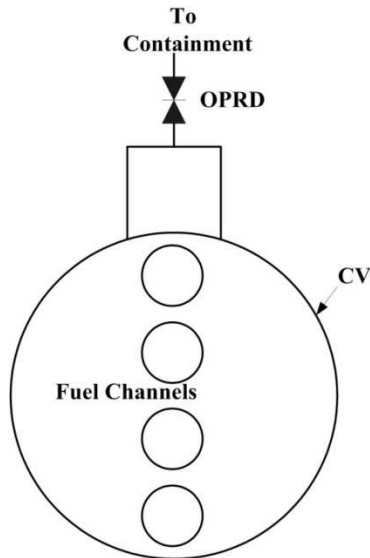


FIG. 3.304. Calandria vessel model.

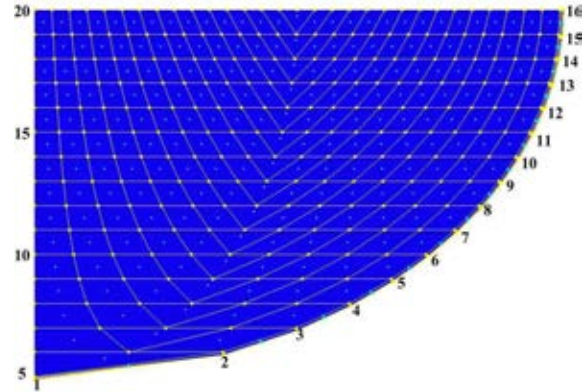


FIG. 3.305. COUPLE meshes (the numbers refer to the CV outside wall nodes).

### 3.7.2.8. Containment model

The containment is modeled as a single volume component. The coolant in the heat transport system, the moderator in the calandria vessel and the water in the calandria vault, are vented into the containment, which is modeled with junctions.

## 3.7.3. Analysis results

### 3.7.3.1. Phase I (0 – 11,750 s)

This phase simulation is about the thermal hydraulics behaviors from the accident initiation to the first channel uncover. The Class III and Class IV Power loses at 0 s. The reactor shuts down and the main feeder water turns off at the same time. Turbine main stop valves are closed after accident initiation. The valve closure time is assumed to be 20 s.

The calculated results are shown in Figures 3-306 to 3-324. Initially, the channel flow rate reduces (Fig. 3-306) after the reactor scram and the SG water inventory decreases (Fig. 3-307) due to feed water close and steam discharge. When steam generator secondary pressure reaches the set point for opening the MSSVs at 5.11 MPa(a) and 25 s after the accident initiation, the steam is discharged from the secondary side of the SGs through the valves, and the steam generators secondary side pressure oscillates at the MSSV set point with the MSSVs opening and closing (Fig. 3-308). The water inventory in the steam generator secondary side decreases as a result of steam discharging from MSSVs (Fig. 3-307) and the steam generator secondary side depletes at about 6,380 s (Loop 1) and 6,400 s (Loop 2).

Before the steam generators lose inventory thoroughly, the maximum fuel sheath keeps in a low level (Fig. 3-309). After the steam generators dry out, the pressure in the HTS increases gradually until it reaches the set point for opening the liquid relief valves (LRVs) in the HTS loop, 10.34 MPa(a) discharging the liquid coolant (Fig. 3-310) and then oscillates at this

opening pressure as shown in Figure 3-311. The coolant in the ROH gets saturated and vapor generated, as shown in Figure 3-312.

The water level decreases (Fig. 3-313) and HTS inventory loses due to discharge of coolant through LRVs (Fig. 3-307). The void fraction in one channel of Loop 2 reaches 0.9 for the entire channel at about 8,700 s (Fig. 3-314). The fuel sheath and the pressure tube is heated up and the fuel channel ruptures when the pressure tube inner surface temperature reaches 1,000°K, and the moderator is heated-up and the pressure of calandria vessel increases causing the rupture disk ruptures (Fig. 3-315), resulting in the moderator gets saturated (Fig. 3-316), the moderator level decreases (Fig. 3-317) and the HTS depressurization (Fig. 3-311). Due to the pressure tube rupture, the fuel sheath temperature decrease, and then the loss of moderator inventory leads to the fuel channel uncovered, therefore the temperature of fuel clad increases (Fig. 3-309).

The hydrogen generates due to the fuel material oxidation, and the mass is about 4.5 kg as shown in Figure 3-318. The containment pressure transient and the heat transfer through the SG are shown in Figures 3-319 and 3-320, respectively. Fuel sheath oxide thicknesses for the four channels are shown from Figures 3-321 to 3-324. The key events time is shown in Table 3-19.

TABLE 3.19. KEY PARAMETERS FOR PHASE 1

Parameters	Unit	Value
Time for first opening of MSSV	s	25
Time for SG secondary side is dry	s	6380, 6400
Time for LRV first opening	s	6420
Time for pressurizer empty	s	7670
Time for at least one channel is dry Loop 1	s	9060
Time for at least one channel is dry Loop 2	s	8700
Time for fuel sheath failed (fuel channel 3, bundle 7)	s	9490
Time for pressure and calandria tubes are ruptured Loop 1	s	9850
Time for pressure and calandria tubes are ruptured Loop 2	s	9850
Time for Calandria vessel rupture disks #1-4 open	s	9850
Time for moderator in calandria vessel reaches saturation temperature	s	10 280
Time when first channel uncoverly occurs (Channel 1)	s	11 750
Hydrogen generation mass	kg	4.5
Moderator level remains	m	6.07
Moderator mass remains	kg	175 717

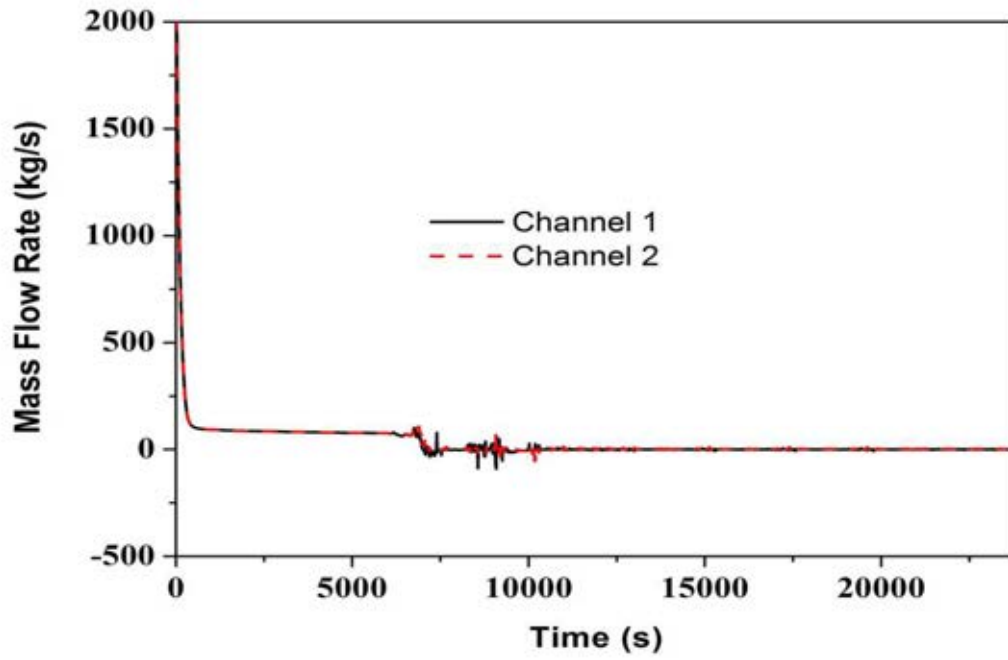


FIG. 3.306. Channel flow rate.

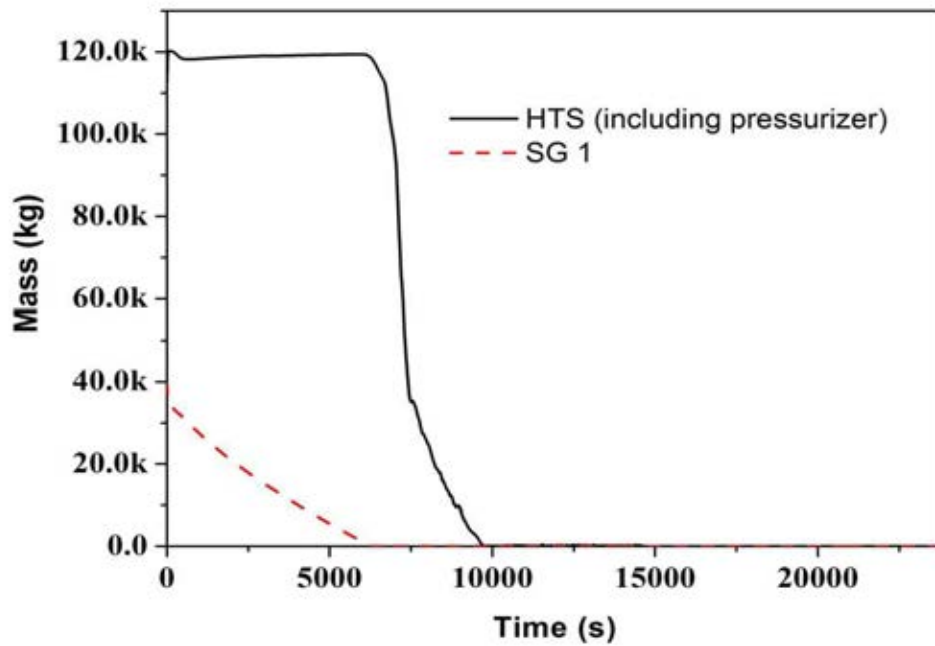


FIG. 3.307. Mass inventory of SG 1 and HTS (including pressurizer).

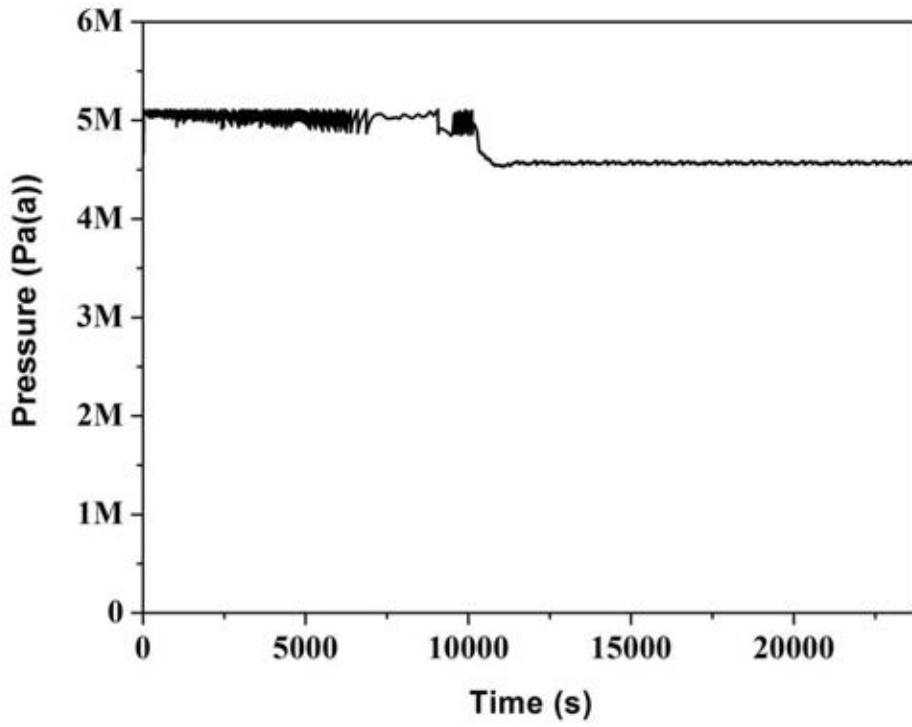


FIG. 3.308. SG secondary pressure.

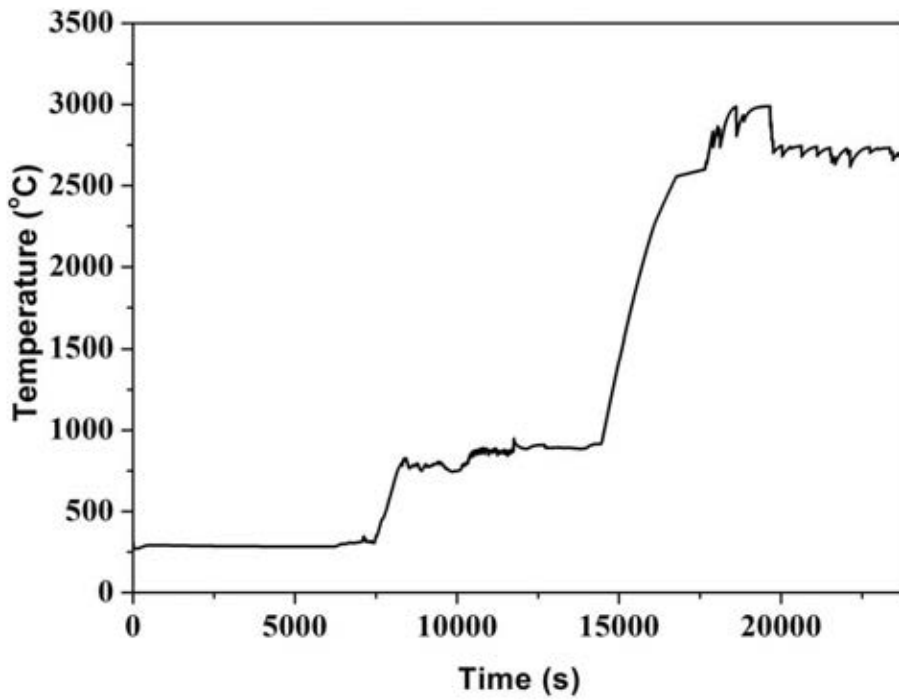


FIG. 3.309. Maximum sheath temperature.

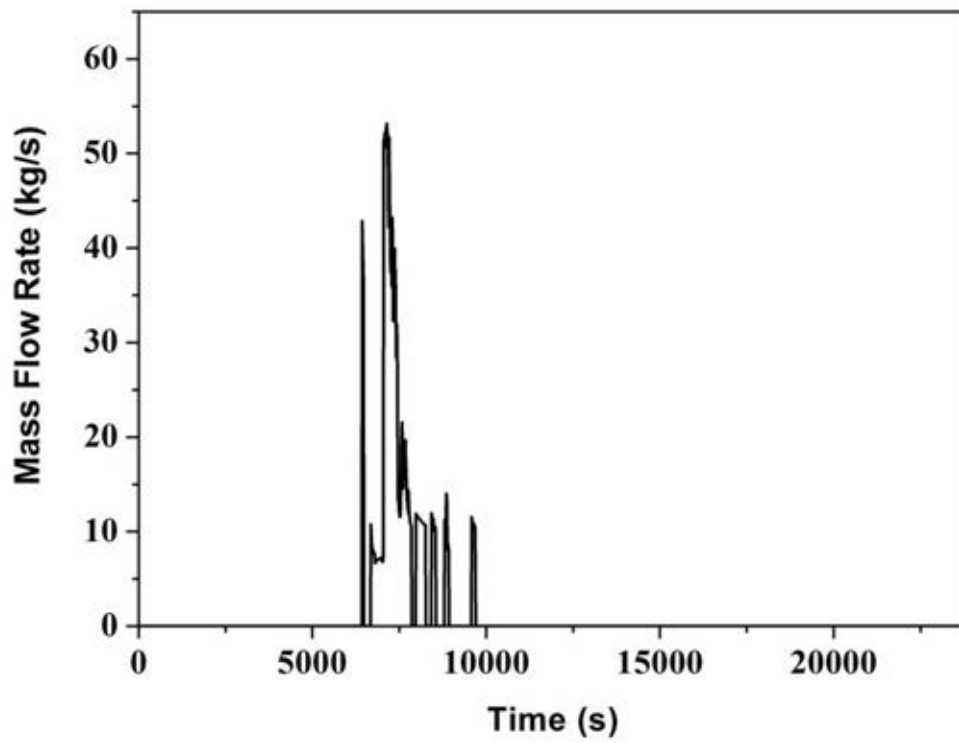


FIG. 3.310. LRV 1 mass flow rate.

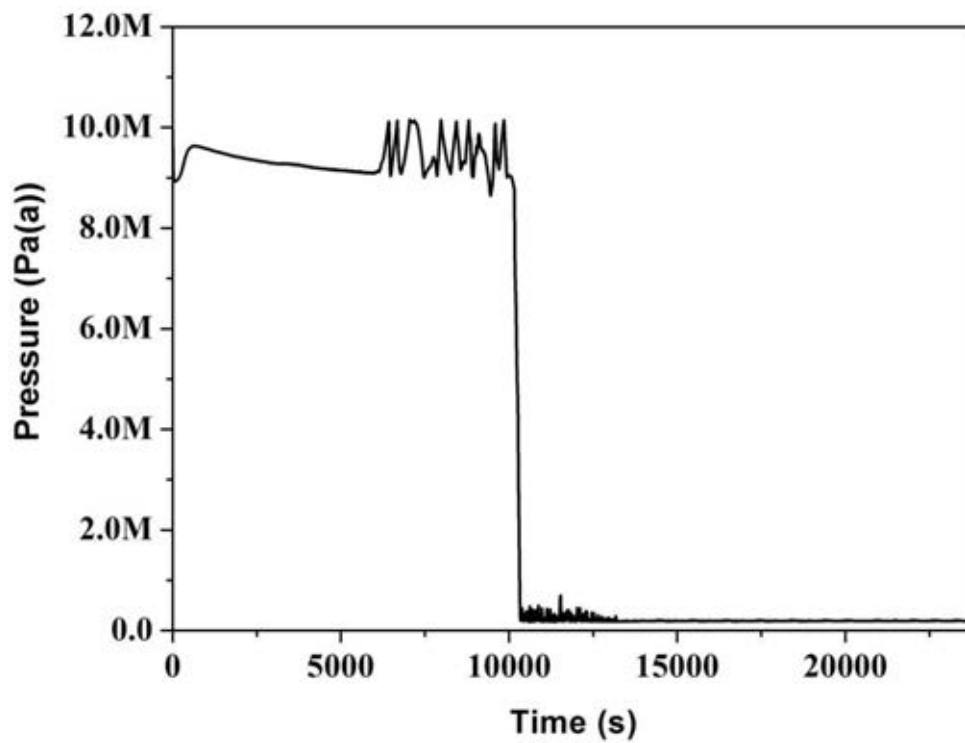


FIG. 3.311. ROH 5 pressure.

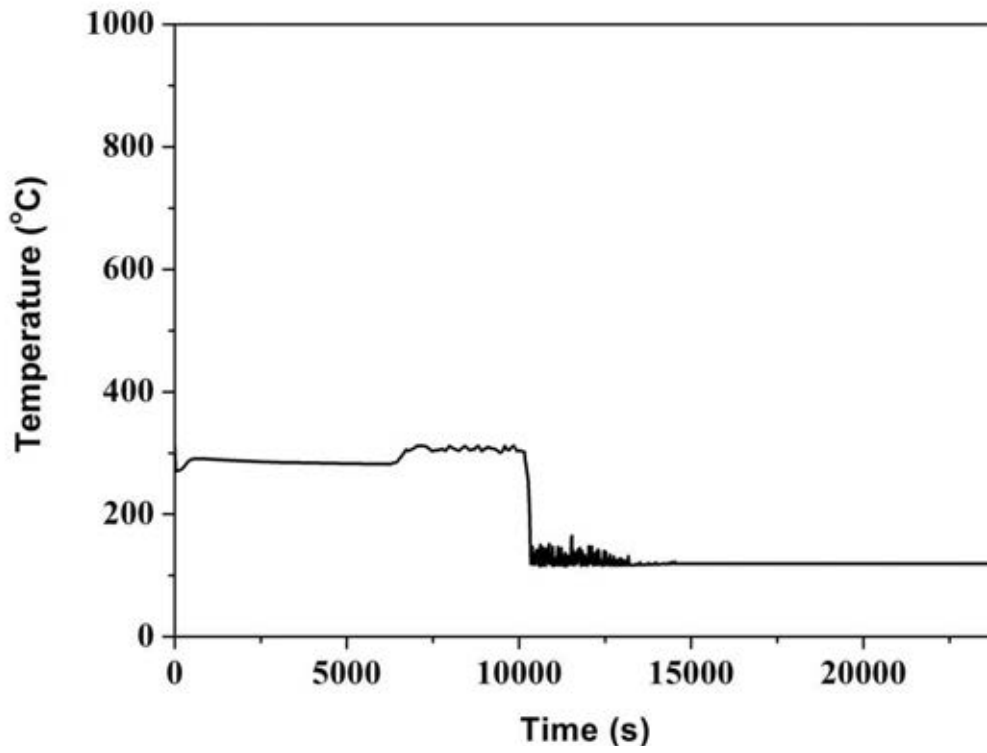


FIG. 3.312. ROH temperature.

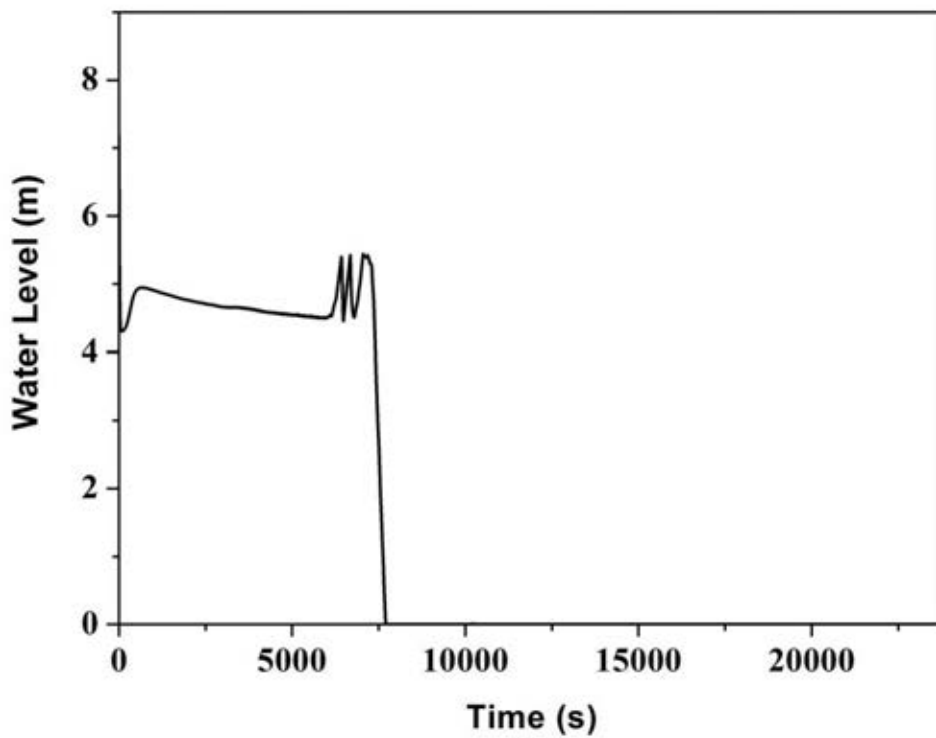


FIG. 3.313. Pressurizer water level

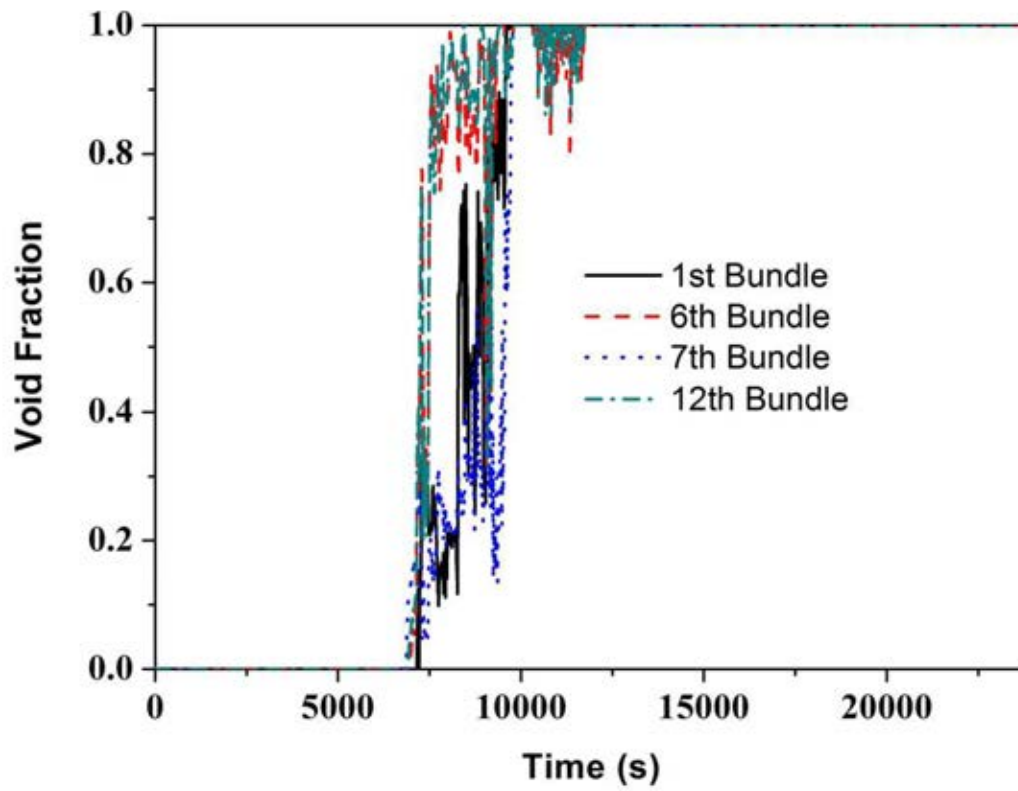


FIG. 3.314. Void fraction in channel one.

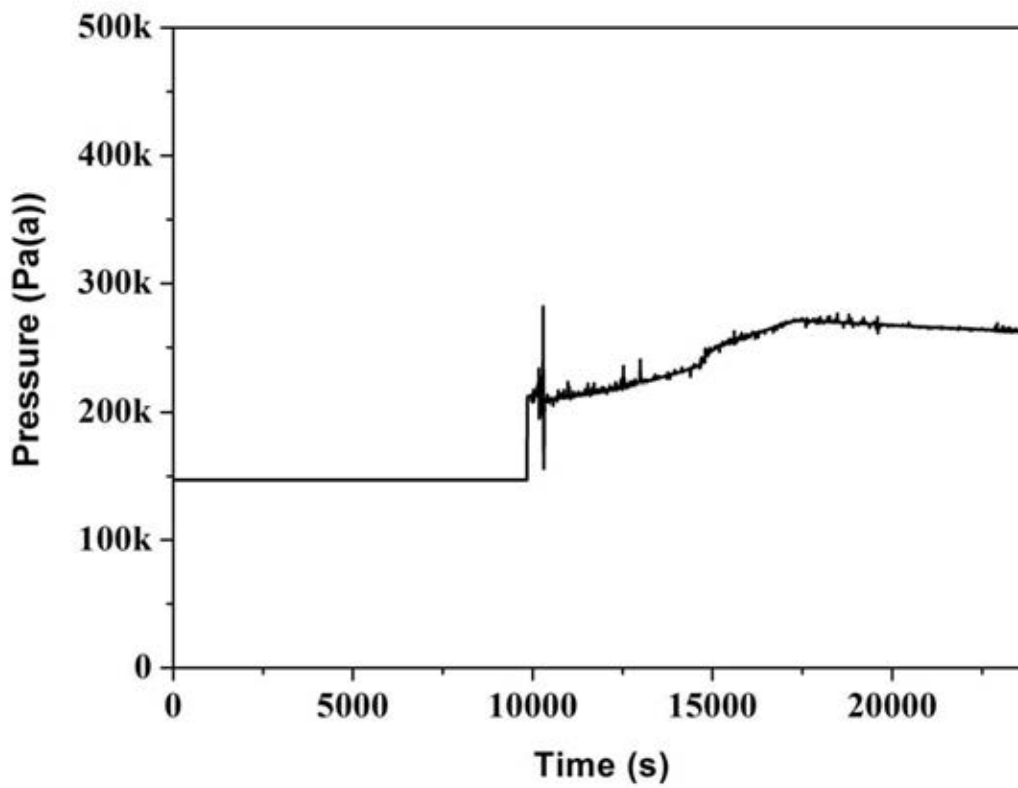


FIG. 3.315. Moderator pressure.

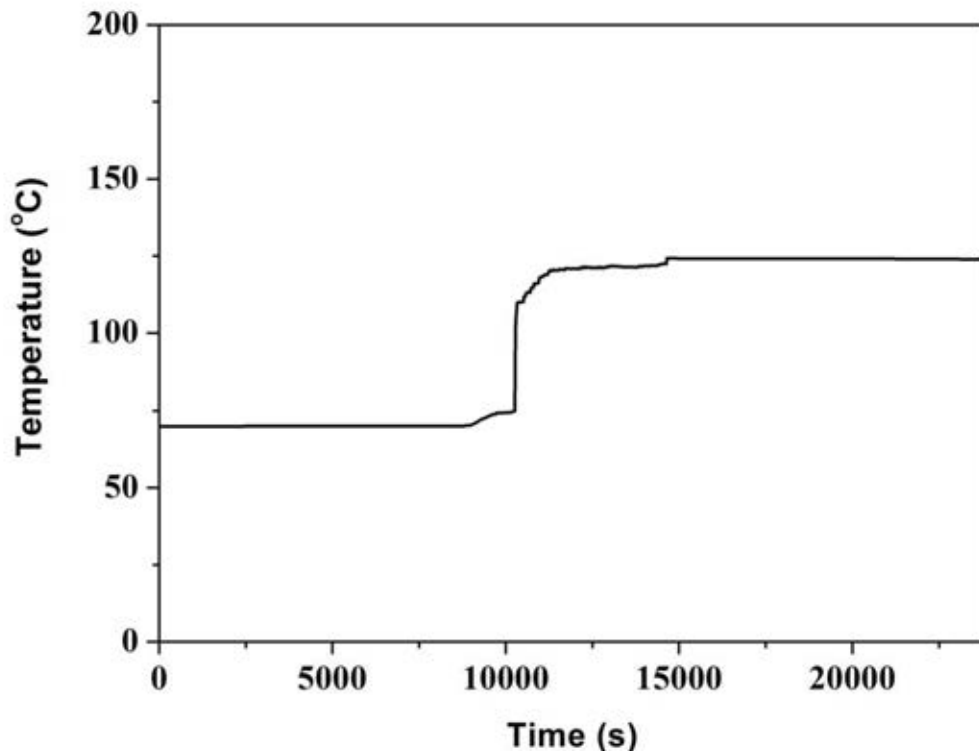


FIG. 3.316. Moderator temperature.

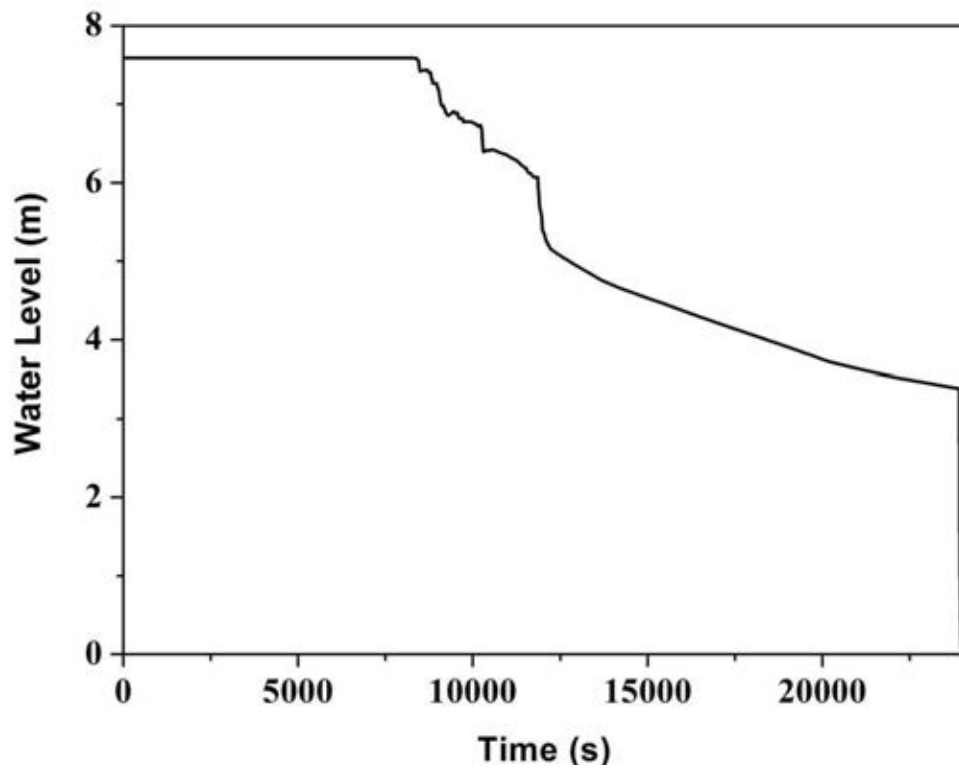


FIG. 3.317. Moderator level.

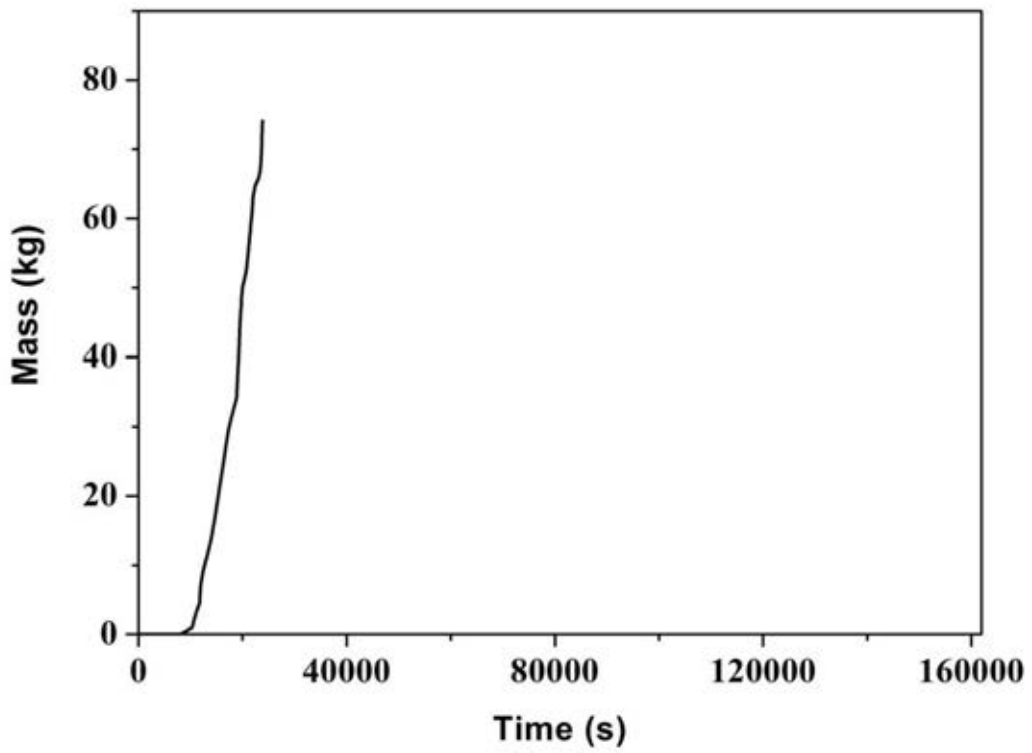


FIG. 3.318. H<sub>2</sub> mass.

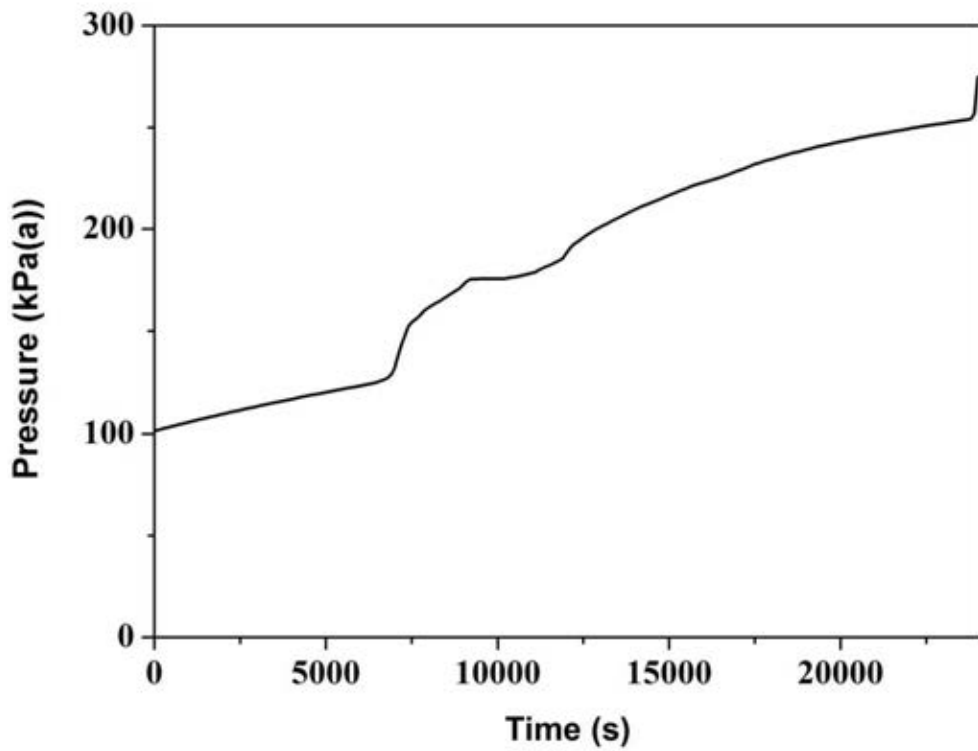


FIG. 3.319. Containment pressure.

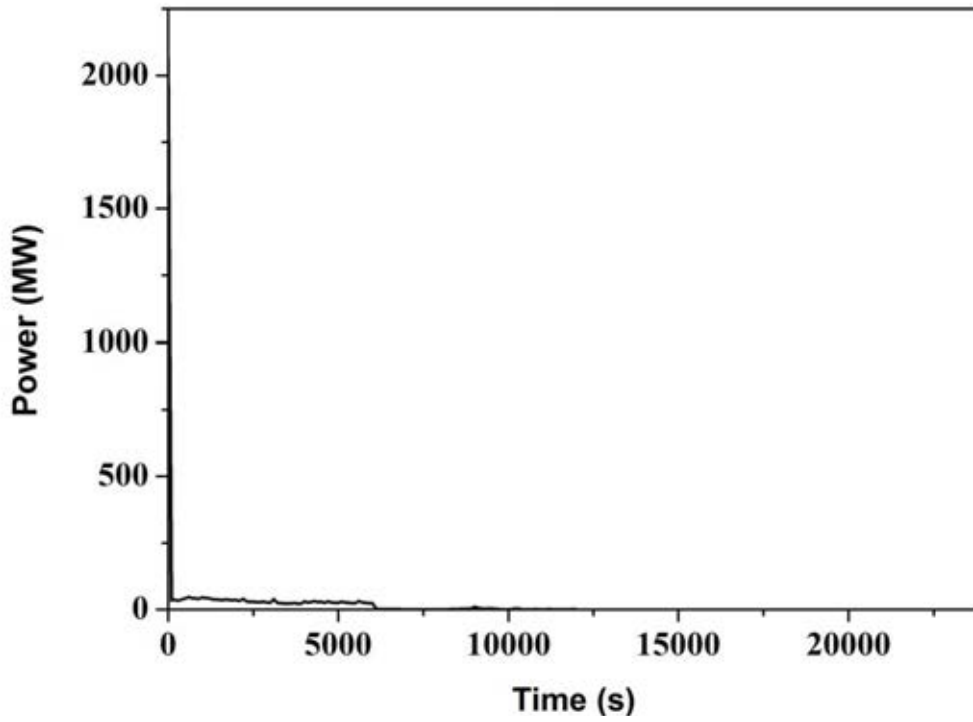


FIG. 3.320. Heat transfer through SG.

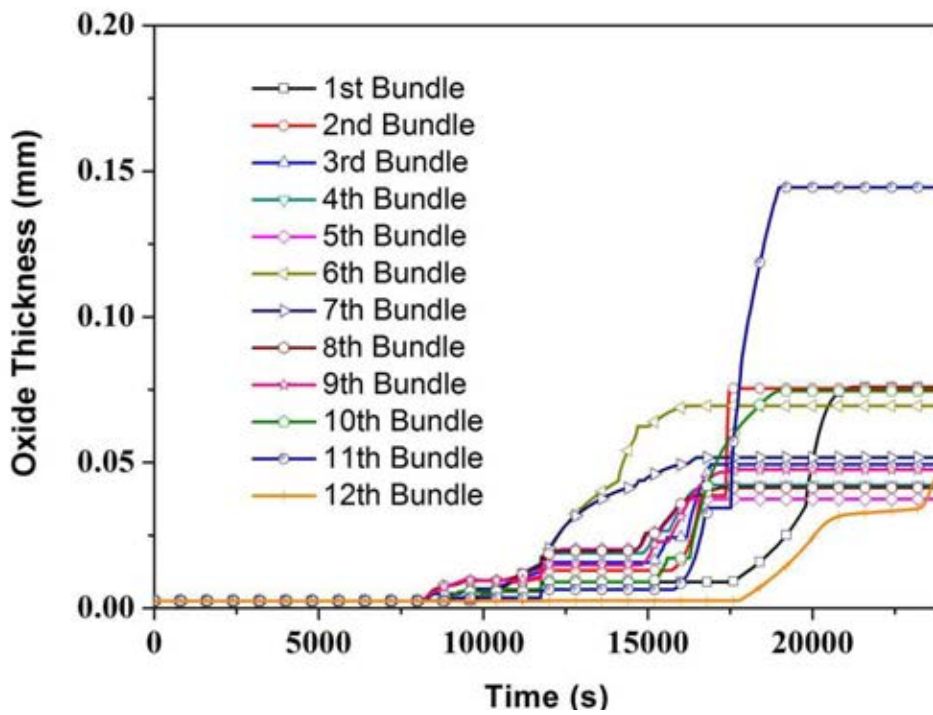


FIG. 3.321. Oxide thickness for sheath in Channel 1.

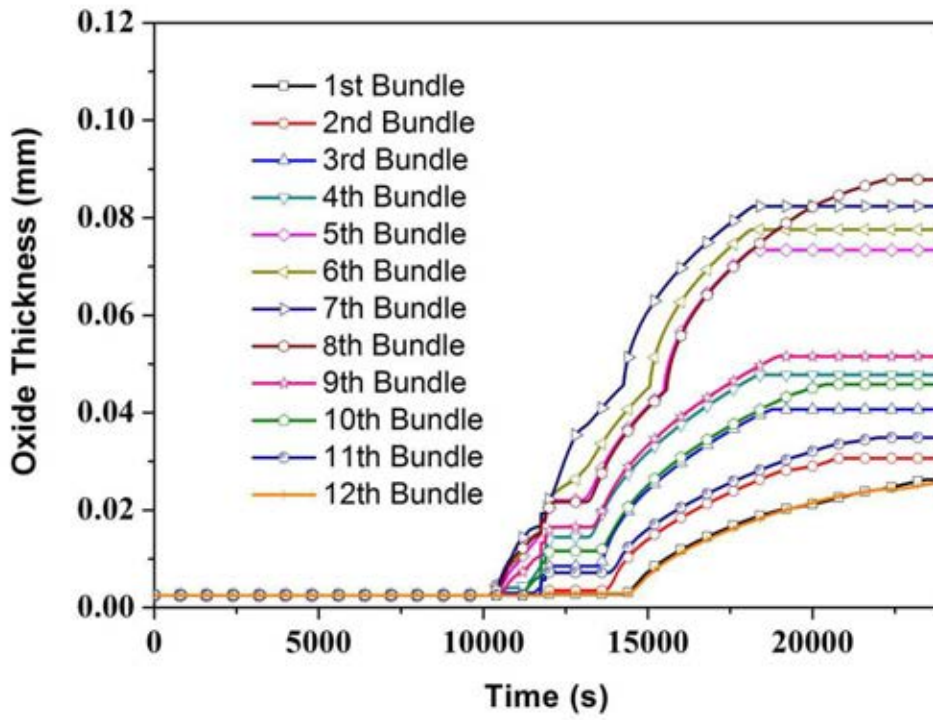


FIG. 3.322. Oxide thickness for sheath in channel 2.

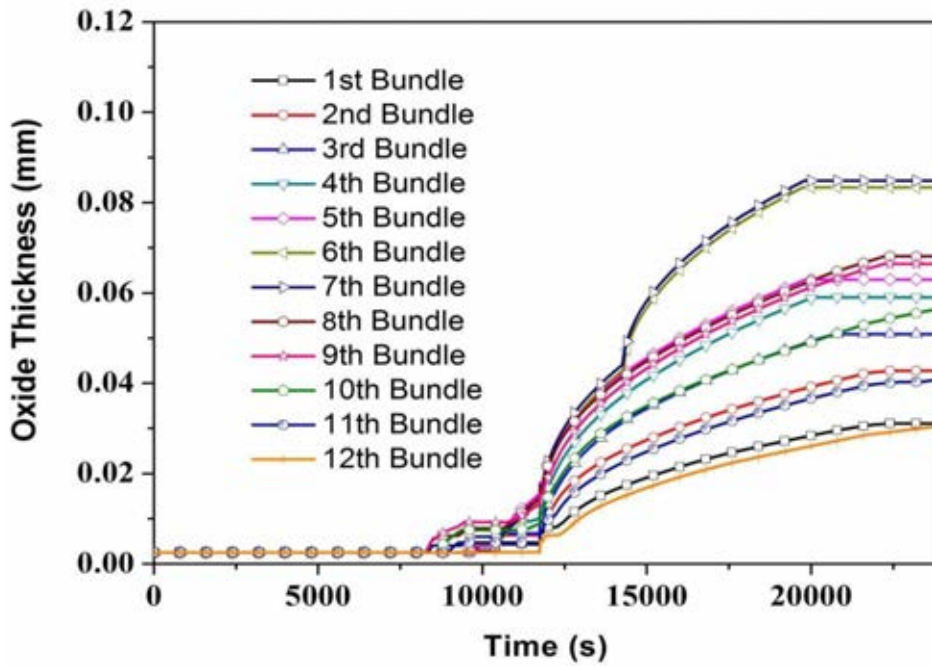


FIG. 3.323. Oxide thickness for sheath in Channel 3.

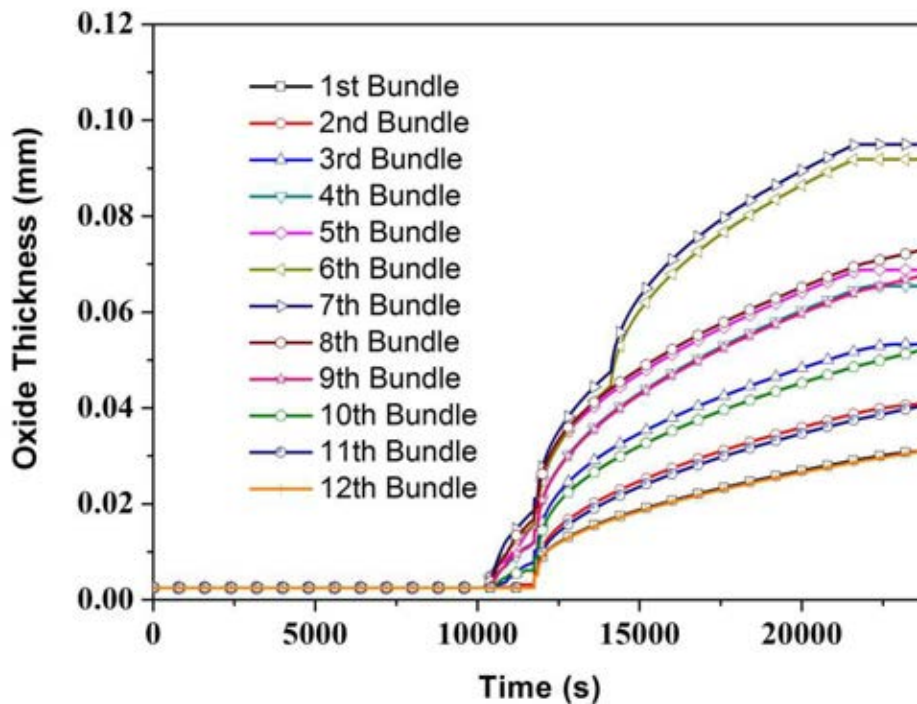


FIG. 3.324. Oxide thickness for sheath in Channel 4.

### 3.7.3.2. Analysis and results-phase 2 (11,750 – 23,850 s)

This phase simulation is about the behaviors of the accident process from the fuel channel uncover to the core collapse.

The moderator evaporates due to heat up by the fuel channel, and the mass and the level of the moderator decreases gradually, shown in Figures 3-325 and 3-317. Sheath temperature transient of the uncovered fuel channel is shown in Figure 3-309, and it shows that the sheath gets to a high level. The molten pool forms with the core temperature increases as shown in Figure 3-326. The core collapse into the calandria vessel bottom at about 23,850 s including about 98,810.0 kg  $\text{UO}_2$  (Fig. 3-327) and 38,645.0 kg Zircaloy (Fig. 3-328), the material down to the vessel causes the rapid moderator evaporation. After the core collapse, the moderator level is about 0.06 m. The hydrogen mass generation in this phase is about 69.6 kg, as shown in Figure 3-318, and the fission products mass released is shown in Figure 3-329. For the non-condensable fission product, about 565.8 kg mass is released and for the soluble fission product, the mass is about 315.6 kg. During the phase process, the calandria vessel wall temperature keeps at 69°C before the core collapse, and after the collapse, the temperature is about 266.6°C, as shown in Figure 3-330. The Figure 3-331 shows the steam flow rate from the calandria vessel, and it shows that the flow rate is low due to the slow moderator evaporation rate until the core collapse which causes a peak flow rate. The moderator evaporation into the containment, increasing the containment pressure, and after the core collapse, the pressure gets to about 275.4 kPa(a), as shown in Figure 3-319.

The key parameters at the end of this phase are in Table 3-20.

TABLE 3.20. KEY PARAMETERS FOR PHASE 2

Parameters	Unit	Value
Time for core collapse	s	23 850
Hydrogen generation mass	kg	69.6
Non-condensable fission product released	kg	565.8
Soluble fission product released	kg	315.6
Maximum sheath temperature	°C	2579.8
Total mass of UO <sub>2</sub> in calandria vessel bottom	kg	98 810.0
Total mass of Zircaloy in calandria vessel bottom	kg	38 645.0

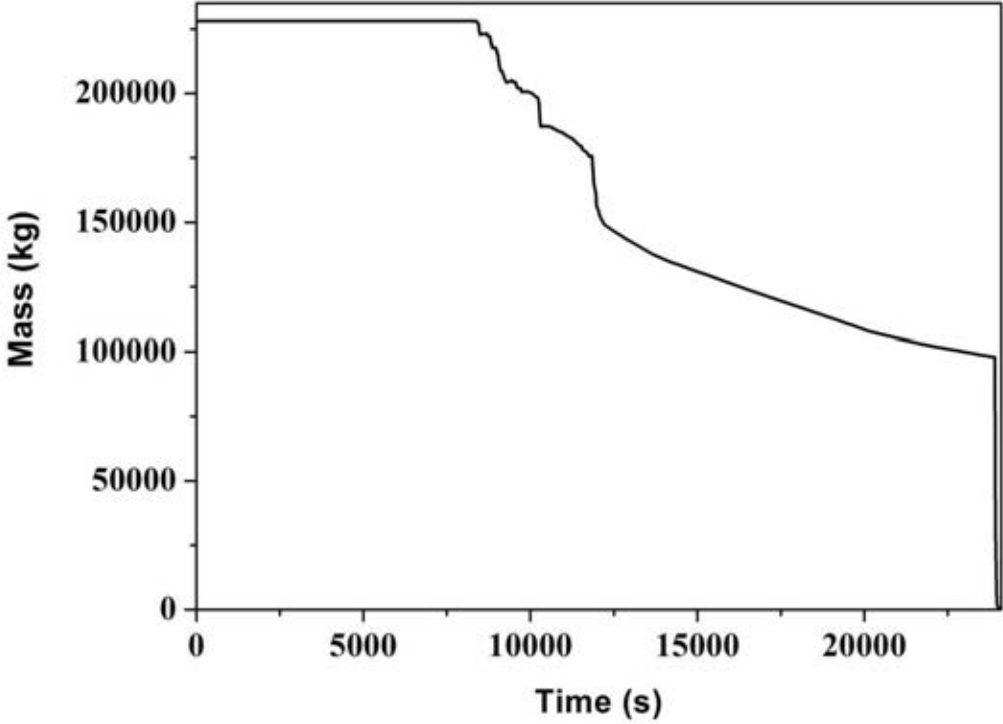


FIG. 3.325. Moderator mass inventory.

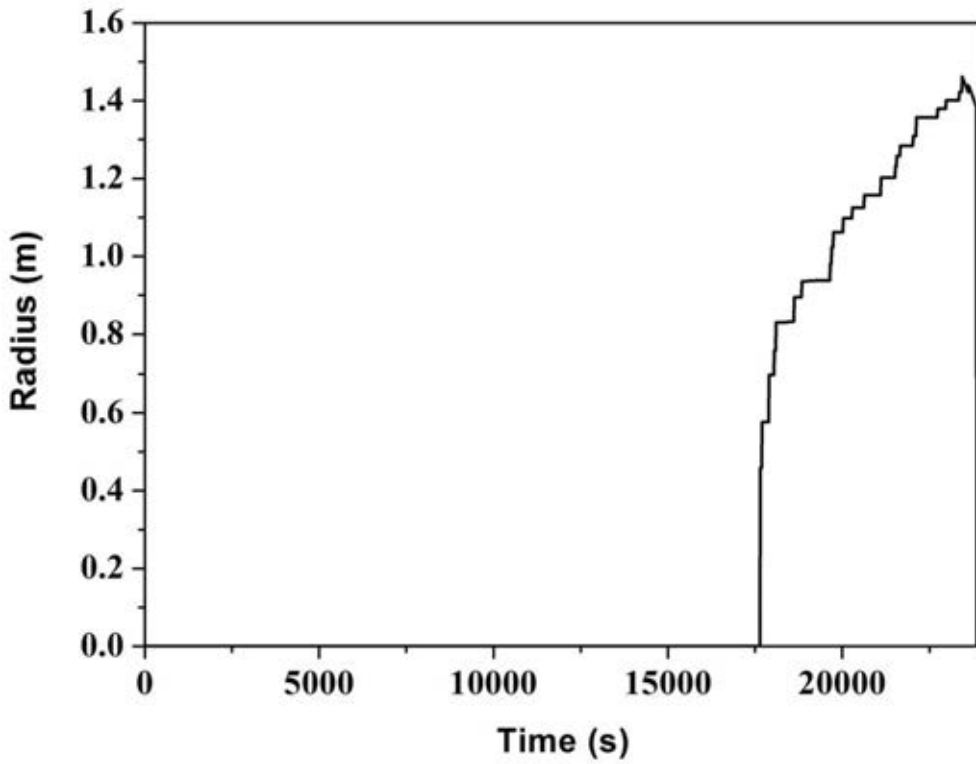


FIG. 3.326. Molten pool equivalent radius of core material.

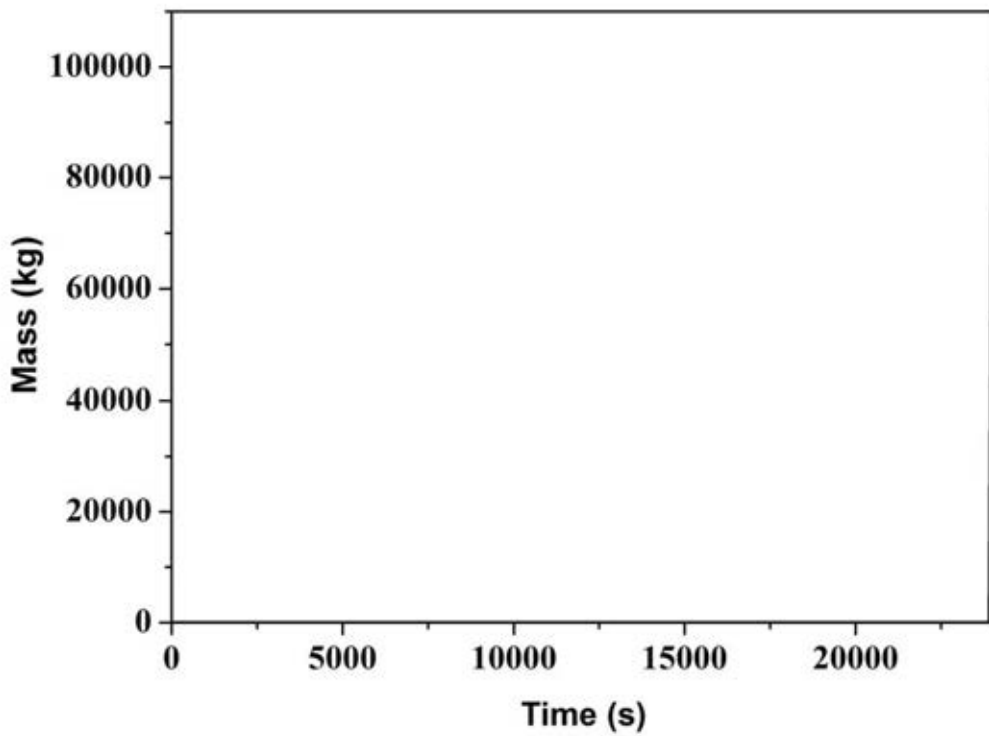


FIG. 3.327.  $UO_2$  mass drops into calandria vessel botton.

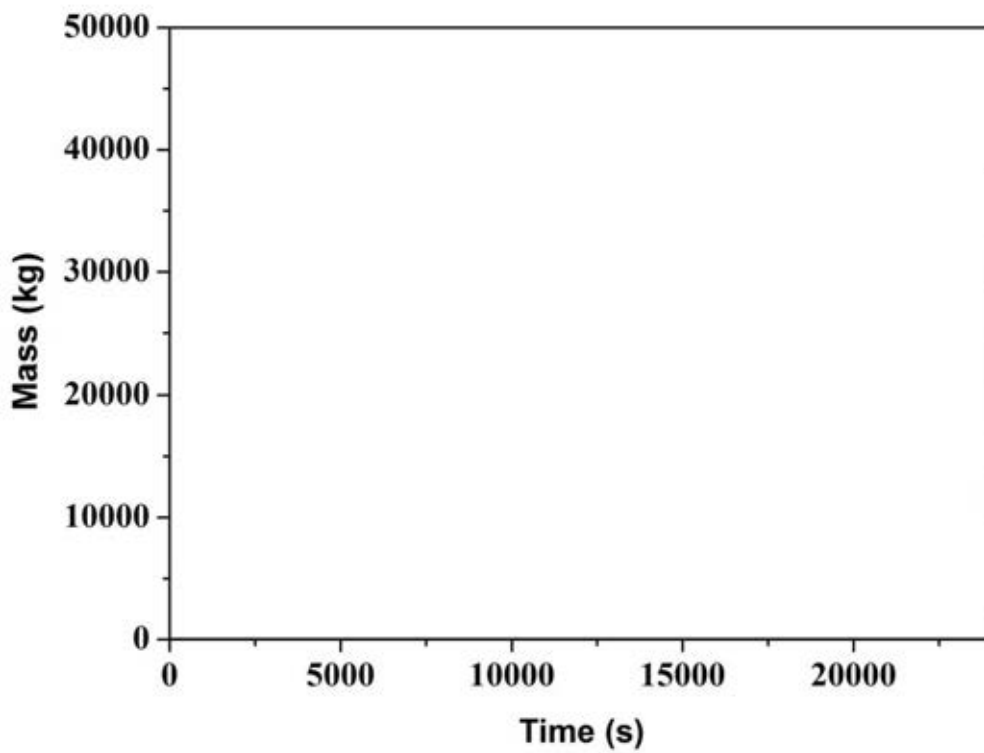


FIG. 3.328. Zircaloy mass drops into calandria vessel bottom.

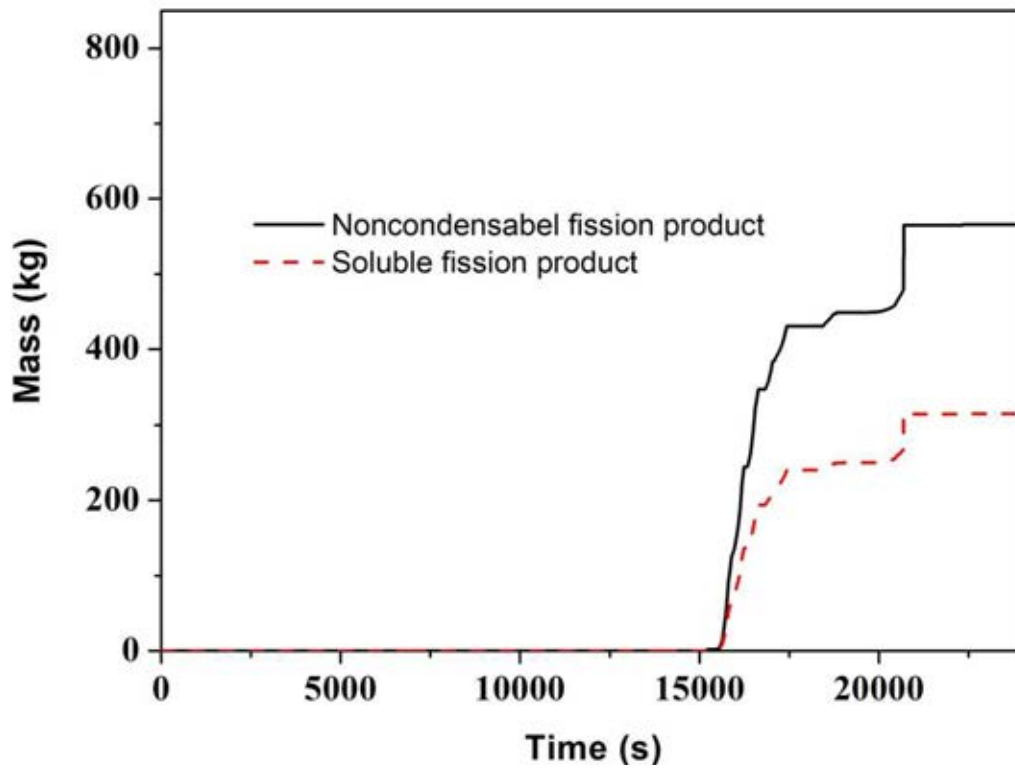


FIG. 3.329. Fission products mass.

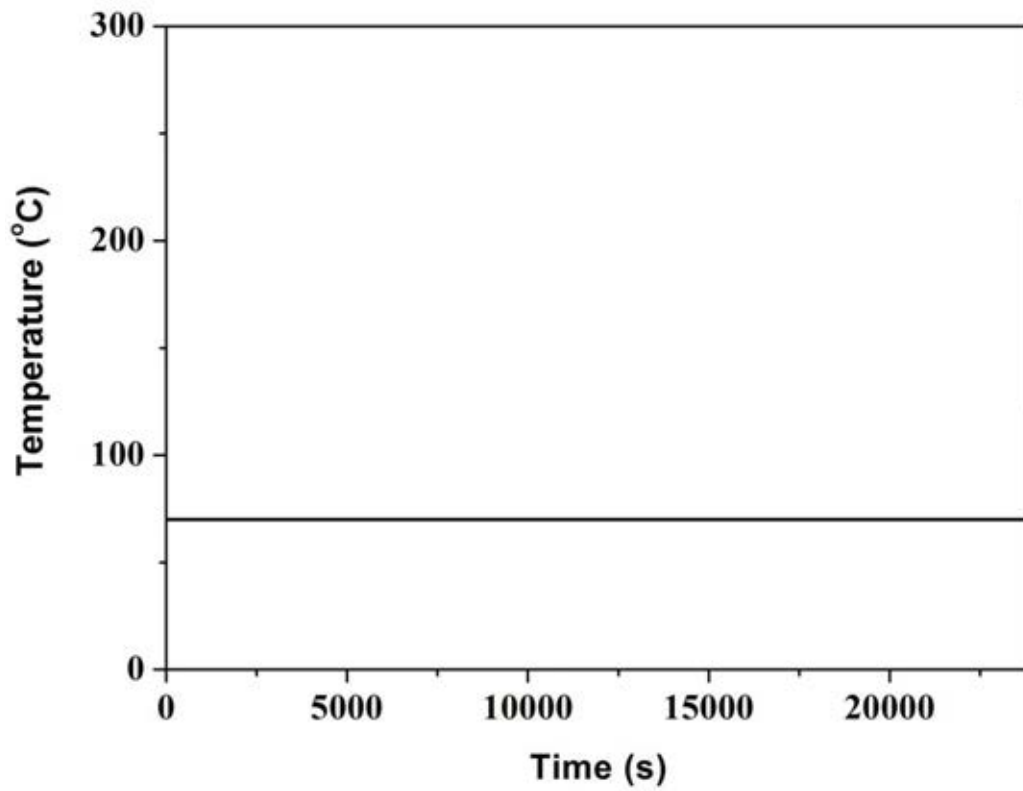


FIG. 3.330. Calandria vessel bottom wall temperature.

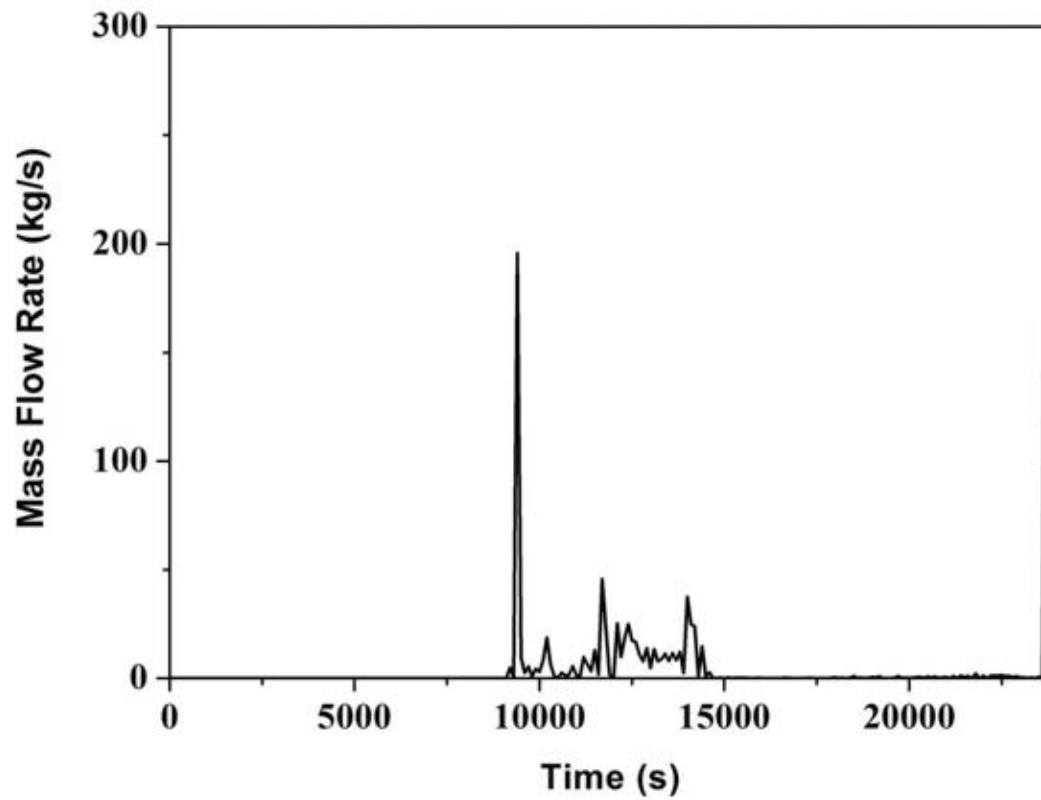


FIG. 3.331. Steam flow rate from calandria vessel.

### 3.7.3.3. Analysis and results-phase 3 (23,850 – 161,960 s)

This phase simulation is about the behaviors from the core collapse to the calandria vessel failure.

During this phase, the relocated core material in the calandria vessel bottom is about 137,455.0 kg from the core collapse, including UO<sub>2</sub> and Zircaloy, as shown in Figures 3-332 and 3-333. The moderator depletes at 30,900 s due to the heat up by the slumping core material in the calandria vessel bottom. After this, water in calandria vault is heated up and the vault RD opens at about 40,280 s. The evaporation in the calandria vault decreases the water level (Fig. 3-334), causing the wall of the calandria vessel heat up gradually (Fig. 3-335). The steam discharge from the calandria vault leads the containment heat up and increases the containment pressure as shown in Figure 3-336. At about 76,310 s, the pressure in containment reaches to the failure set point of the equipment air lock seal and the broke depressurizes the containment gradually, as shown in Figure 3-336. At about 161,960 s, the calandria vessel failed when the wall temperature reaches to 1600°C, as shown in Figure 3-335. During this phase, there is about 5.0 kg hydrogen generated, the released fission products mass of the non-condensable and the soluble are 612.5 kg and 341.7 kg, respectively. The total heat load to the calandria vessel is about 15,734.0 kW. Parameters summary about this phase is shown in Table 3-21.

TABLE 3.21. KEY PARAMETERS FOR PHASE 3

Parameters	Unit	Value
Time for moderator depletion	s	30900
Time for calandria vault RD opens	s	40280
Time for containment equipment airlock seal failure	s	76310
Time for calandria vessel failure	s	161960
Non-condensable fission product released	kg	612.5
Soluble fission product released	kg	341.7
Hydrogen generated	kg	5.0
Total heat load to calandria vessel	kW	15734.0
Total mass of UO <sub>2</sub> in calandria vessel bottom	kg	98810.0
Total mass of Zircaloy in calandria vessel bottom	kg	38645.0
Total mass of relocated core material	kg	137455.0

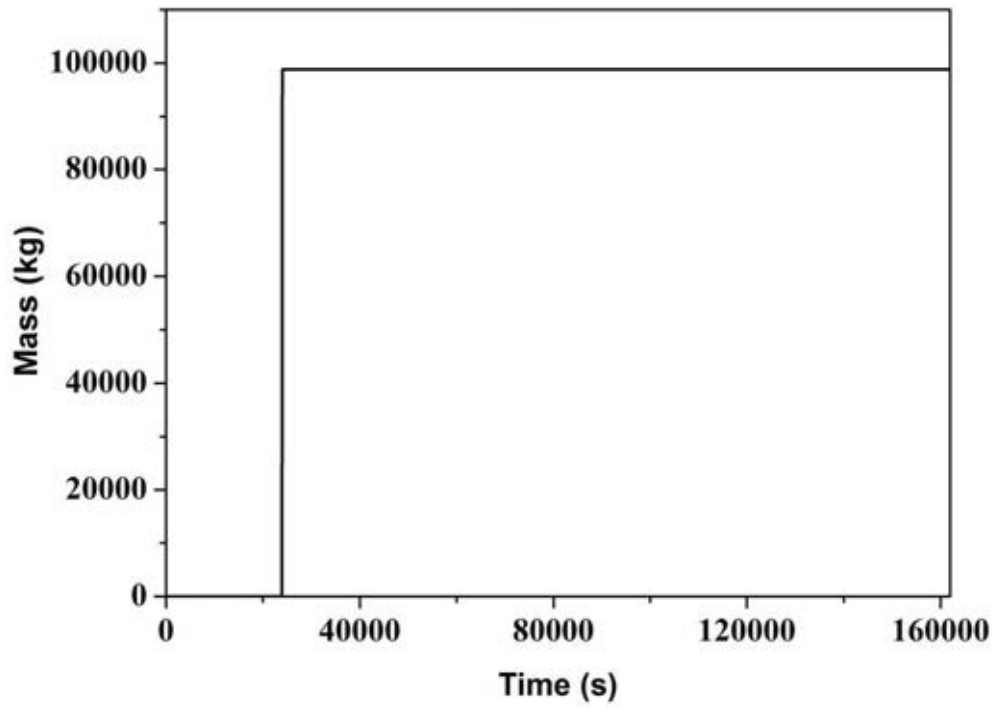


FIG. 3.332. Mass of  $UO_2$  relocated core material.

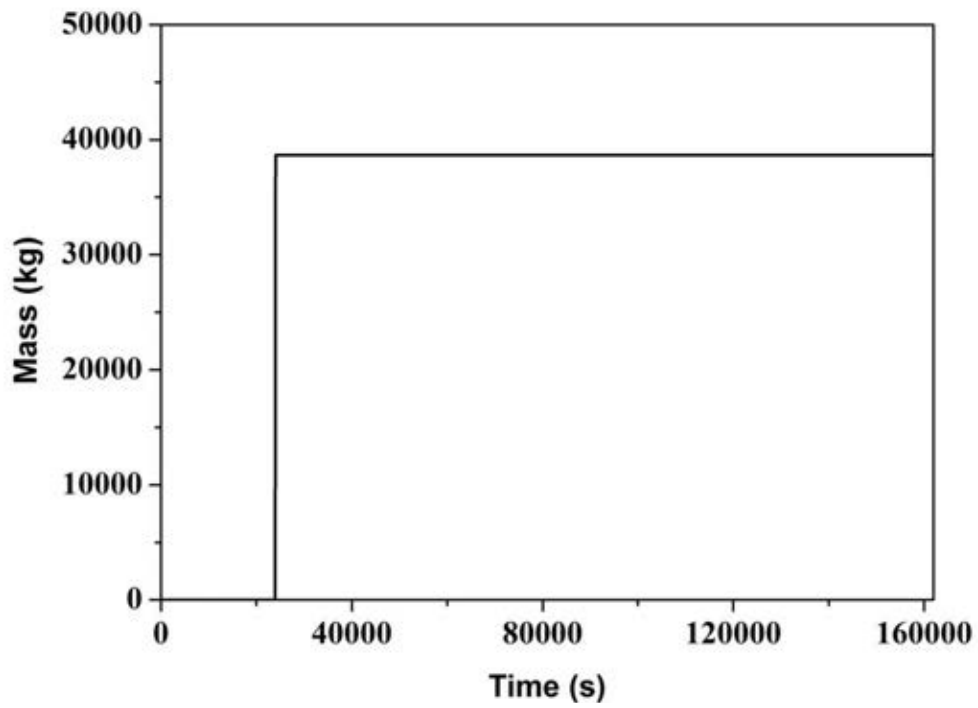


FIG. 3.333. Mass of Zircaloy relocated core material.

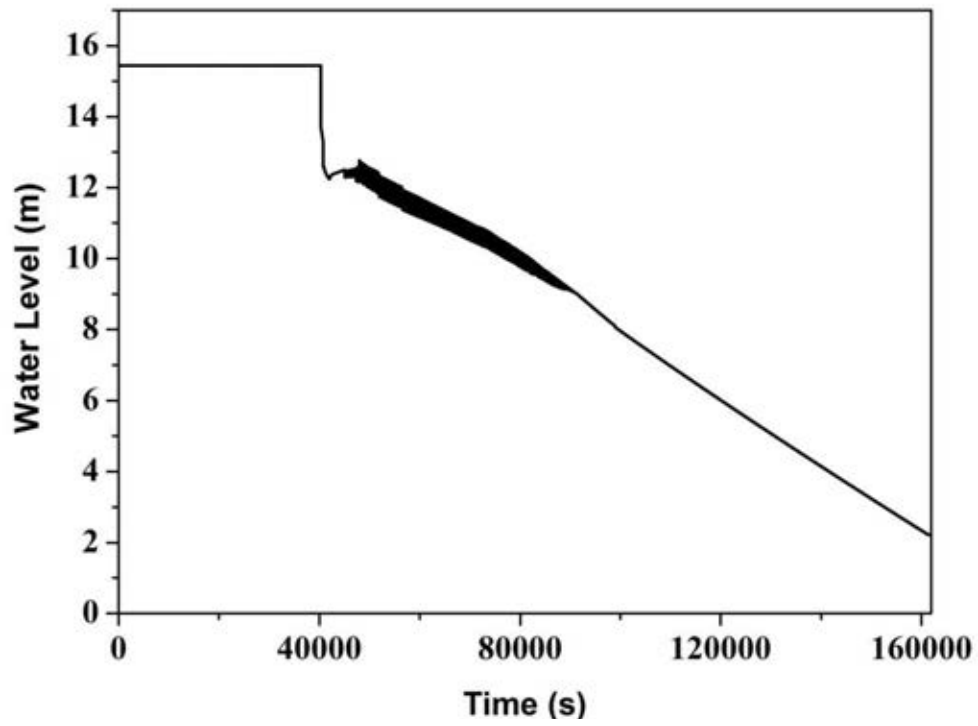


FIG. 3.334. Clandria vault water level.

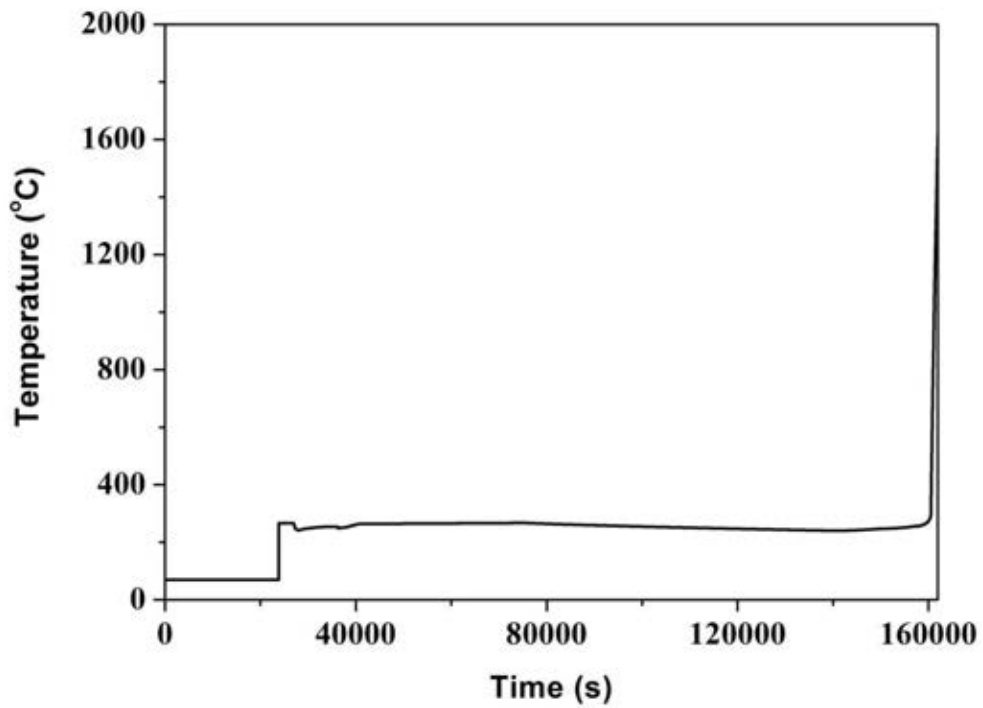


FIG. 3.335. Calandria vessel wall temperature.

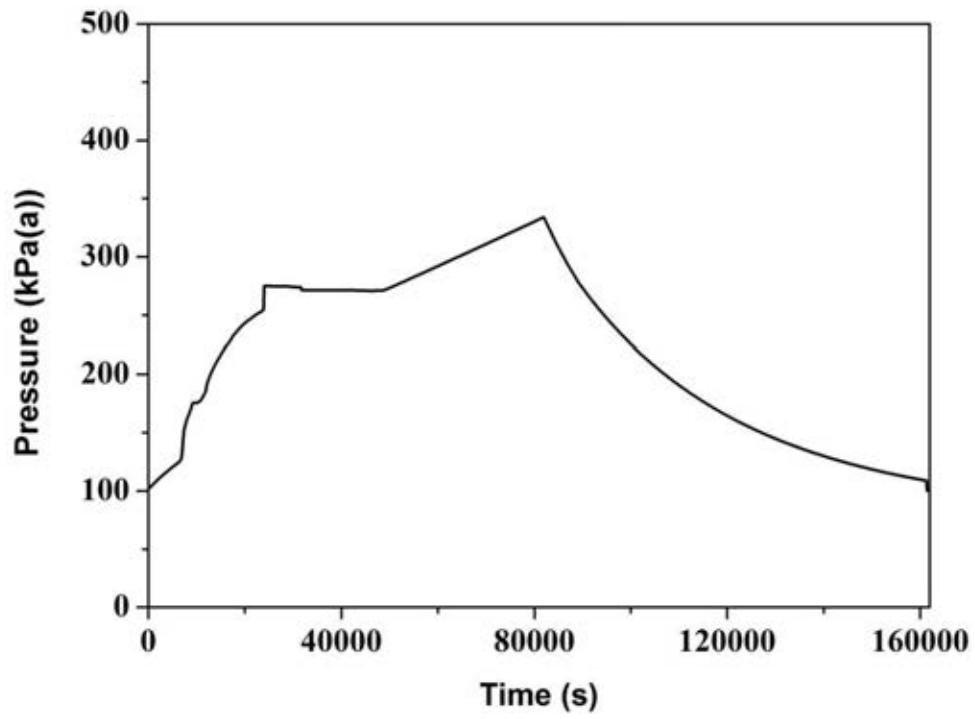


FIG. 3.336. Containment pressure.

#### 4. COMPARISON OF KEY RESULTS

In this section the key results from the CANDU 6 station blackout analysis, performed by the participating organizations, are compared. The comparison of key results is a form of benchmarking and identifying "best practices", mainly the code capabilities and the user effects. The search for "best practices" is to understand and evaluate the current state-of-the-art within the user community and identify areas for improvement.

The following seven organizations took part in the benchmarking study:

- Atomic Energy of Canada Limited (AECL);
- Bhabha Atomic Research Center, Reactor Engineering Division (BARC – RED);
- Bhabha Atomic Research Center, Reactor Safety Division (BARC – RSD);
- Korea Atomic Energy Research Institute (KAERI);
- Nuclear Power Corporation of India Limited (NPCIL);
- Politechnical University of Bucharest (PUB);
- Shanghai Jiao Tong University (SJTU).

A variety of severe accident analysis codes or code combinations were used by the organisations to simulate the station blackout scenario. The codes used by the participating organizations are:

- AECL – MAAP4-CANDU v4.0.6A;
- BARC-RED – RELAP5 Mod 3.2, ANSWER, CAST3M, MELCOOL;
- BARC-RSD – SCADAP/RELAP5 Mod 3.2/ , PHTACT, ASTEC;
- KAERI – ISAAC 4.02;
- NPCIL – ATMIKA.T, CONTACT, SEVAX, PACSR/STAR, ACTREL;
- PUB – SCDAPSIM/RELAP5 Mod 3.4;
- SJTU – SCDAP/ RELAP5 Mod 3.4.

The goal of the severe accident analysis benchmarking, through the Coordinated Research Project, is to increase confidence and assess the validity of consequence analysis tools in member states with HWR nuclear installations. The capabilities of the consequence analysis tools vary significantly because of the complexity of the phenomena, behaviour of the materials at extreme temperatures, and the numerical methods used for the solution of conservation and constitutive equations. The benchmarking of severe accident analysis codes was considered an effective way to get a common understanding and judgment about the codes and user capabilities on an international basis. Comparing computer code calculations of a given severe accident scenario is a convenient way to improve the understanding of code capabilities, user effects and to some degree, the various physical phenomena applicable to the physical problem the code is attempting to solve.

The objectives of the benchmarking exercise are to:

- contribute to a better understanding of the postulated severe accident sequence;
- compare and evaluate the code capabilities;
- suggest improvements to the code developers, and;
- improve the abilities of code users.

In the following sections the consequence analyses completed by the participating organizations is compared to draw insights into the phenomena and code capabilities.

#### 4.1. PRIMARY HEAT TRANSPORT SYSTEM BEHAVIOUR

The station blackout accident cases were simulated with the reactor at full power at time = 0 s, when Class III and IV power was lost. The reactor trips immediately, because the shutdown rods are held out of the core by electromagnetic clutches that de-energize upon loss of Class IV power. The four heat transport system pumps, served by the Class IV buses, also begin to run down. The Primary Heat Transport System (PHTS) is the first available heat sink, not only because it contains a large volume of coolant, but also because it has large mass of pipes that is able to conduct heat from the fuel to the steam generators (SG). After the heat transport system pumps run down, it is assumed that natural circulation of water in the heat transport system transports decay power from the core to the steam generators. In the steam generators the secondary side water boils off the steam, and therefore, heat is discharged to atmosphere via spring-loaded main steam safety valves (MSSVs).

The PHTS pressure transient calculated by all of the analysis codes following reactor trip appears to be consistent, as shown in Figure 4-1, even though the magnitude of the pressure drop varies by as much as 2 MPa within the first 5,000 s. The termination of the fission heat input and the continued heat removal by the secondary side in the steam generators causes the initial pressure drop in the PHTS. The PHTS pressure drop, during the initial period of the transient, demonstrates that the codes have the appropriate models to simulate heat transport phenomena from the fuel to the secondary side. The majority of the codes calculate the PHTS repressurizing to approximately 10 MPa after the initial drop in pressure. The PHTS pressure increases as the steam generator secondary side becomes dry around 2 h after reactor trip (simulated between 1.69 and 2.65 h by all codes). The mean time predicted for steam generator becoming dry is  $2.08 \pm 0.44$  h for all codes and that the calculations are within half an hour of the mean is encouraging.

The primary coolant remained at  $\sim 300^\circ\text{C}$  (i.e., saturation) until about 7,500 s in all of the seven analysis results (Fig. 4-2). In the simulation completed by BARC-RSD, the primary coolant temperature after 7,500 s shown in Figure 4-2 is steam temperature, with thermodynamic quality greater than one, which increases to a maximum of about  $830^\circ\text{C}$ . Figure 4-3 shows that the pressurizer water level either decreases (Figure 4-3) from  $\sim 15$  m (AECL, BARC-RSD, NPCIL, and KAERI) or  $\sim 10$  m (BARC-RED, SJTU, and PUB) as water flowed into the PHTS, while the PHTS inventory cooled and shrank. Although all seven codes calculated the initial rapid drop in pressurizer water level, their quasi steady state after the initial level drop was not consistent. As Figure 4-3 indicates, essentially two different steady-state pressurizer water levels are predicted by the participating organizations. The code calculations from BARC-RSD, AECL, KAERI, and NPCIL indicate the level to drop to approximately 10 m whereas in SJTU, BARC-RED, and PUB calculated the level to drop to approximately 4 m. In both cases the drop in the water level of the pressurizer is approximately 6 m (i.e., from 16 to 10 m or 10 to 4 m); therefore it appears that inconsistent initial conditions may have caused this difference in pressurizer levels. Also, all participating organizations (except NPCIL) predicted pressurizer draining after the pressure-tube calandria-tube rupture. In the NPCIL simulation, the pressure-tube/calandria-tube rupture did not occur until much later in the sequence during fuel channel disassembly. After a pseudo-steady-state period, the sharp drop in pressurizer level (except for NPCIL) indicates water inventory being transferred in to the PHTS. This drop in the water level shown in Figure 4-3 for BARC-RED and SJTU coincides with the time LRVs opened (i.e., when the primary coolant discharged into the degasser condenser or containment). For KAERI, PUB, and BARC-RSD, the drop in pressurizer inventory coincides with the pressure-tube calandria-tube rupture (i.e., when the coolant discharges into the calandria vessel) and the PHTS pressure drops. In the AECL analysis, the inventory transfer from the pressurizer coincides with the phase change in the

PHTS as shown by the rapid increase in void fraction (Figure 4-4). At that time the pressurizer water flowed into the PHTS, to be replaced by steam from the PHTS loop.

At 6,000 s (1.7 h) to ~11,000 s (3.1 h) the PHTS liquid relief valves open for the first time as shown in Figure 4-5. After the steam generators dryout, the PHTS pressure increases, until the LRVs open. The difference in the timing of the LRV opening for the first time among the code calculations is small (i.e., ~1.4 h) and it is indicative of a reasonably comparable heat input/output between the PHTS and the steam generator secondary side for all codes. The pressurizer water level increased along with the LRVs opening (Figs 4-3 and 4-5), to accommodate the primary coolant expansion. The continued rise in the pressurizer water level was due to liquid thermal expansion as the sub-cooled primary coolant inventory heated to the saturation temperature. The rise in PHTS pressure prior to LRV opening for the first time is captured by most of the code calculations as shown in Figure 4-1. Subsequently, the channel inventory is lost and a sudden drop in PHTS pressure occurs due to pressure-tube calandria-tube rupture. This behaviour is generally seen in the results of most participating organizations, as shown in Figure 4-1.

Some salient observations include:

- The timing of the PHTS pressure increase is different in each simulation, which can be attributed to the differences in SG dryout time given in Section 4.2.
- In the KAERI study, a sharp drop in the PHTS pressure occurs at around 6,000 s, which is coincident with the LRVs opening.
- The AECL and KAERI results indicate that the LRVs open before the SGs dryout. In the BARC-RED, BARC-RSD or SJTU results, the difference in timing between LRVs opening and SG dryout events is minimal whereas in the NPCIL and PUB studies the LRVs opens after the SGs dryout. These differences could be explained by the differences in the models used in calculating the heat transfer from PHTS to SGs.
- The sudden fall in PHTS pressure to ~0.1 MPa coincides with the fuel channel failure. The PHTS pressure drop occurs first in KAERI and SJTU simulations and followed by BARC-RSD, PUB, BARC-RED, AECL, and NPCIL. These differences in the timing of fuel channel rupture can be attributed to the differences in the PHTS coolant inventory histories, and the fuel channel failure criteria used. In the NPCIL and BARC-RED calculations no pressure-tube calandria-tube rupture is predicted, despite the continuing high pressure and loss of all primary coolant. The pressure falls when channel disassembly occurs. In the AECL results, the coolant loss and channel voiding are much slower and therefore the pressure-tube calandria-tube rupture occurs later than most of the other codes.

The opening of the LRVs causes PHTS inventory to escape from the PHTS and in turn increases the void fraction of PHTS loop 1 as shown in Figure 4-4. Loop 2 void fraction histories should be almost identical, given the symmetric nature of the two loops and the lack of loop isolation. The rapid rate of increase in void fraction is calculated in the analyses. The AECL simulation shows the void fraction of about 0.5 quite similar to the rates calculated by the other six participating organizations, and a second stage increase slower than the first stage. The 0.5 void fraction is a user-input value at which the PHTS fluid was assumed to change from a homogeneous two-phase fluid to separate liquid and gas phases, in AECL analysis. The channel dryout timings as indicated by the transient void fraction in Figure 4-4 of SJTU, BARC-RED, and BARC-RSD are similar. The oscillations indicate partial void collapse due to water transferring from the pressurizer. The trends of PHTS void fractions are fairly consistent with each other among these three analysis simulations.

Figure 4-5 shows the LRV opening timings and Section 4.2 provides the SG dryout timings (Fig. 4-11). A comparison of the two figures shows that AECL and KAERI predicted the

LRV opening much earlier than the SG dryout. This may be due to heat transfer models from PHTS to SG and the thermal expansion of the liquid, which is dictated by the SG level.

As the PHTS loop void fractions increased, due to boiling and the loss of coolant through the LRVs, the loop water masses decreased rapidly as shown in Figure 4-6. The total mass in the PHTS and pressurizer remained constant until the LRVs first opened (Fig. 4-5). Once the pressurizer was empty, the PHTS void fraction increased because there was no more pressurizer water to take the place of the expelled coolant.

Examining Figure 4-6 reveals the initial PHTS mass inventory used in the analyses by some participating organizations was inconsistent. The PHTS mass inventory used by AECL, SJTU, NPCIL, BARC-RED and BARC-RSD was close to 120,000 kg; whereas the initial inventory used by KAERI and PUB were about 110,000 kg and 105,000 kg, respectively. The difference between the lowest and the highest PHTS mass was ~15,000 kg which is 12.5% of the nominal inventory. This level of variation is likely to have an impact on the timing of the sequence progression.

Figure 4-7 shows the calculated mass flow rates from the liquid relief valves. The liquid relief valves discharge from about 6,000 s to 16,000 s for all simulations. The discharges from AECL, KAERI, BARC-RSD, SJTU and PUB show that the valves remain open for some time before closing whereas in the calculated discharges of BARC-RED and NPCIL show the relief valves opening and closing rapidly. Despite these differences, reasonable agreement is shown, within about 6,000 s, in the first opening of the liquid relief valves.

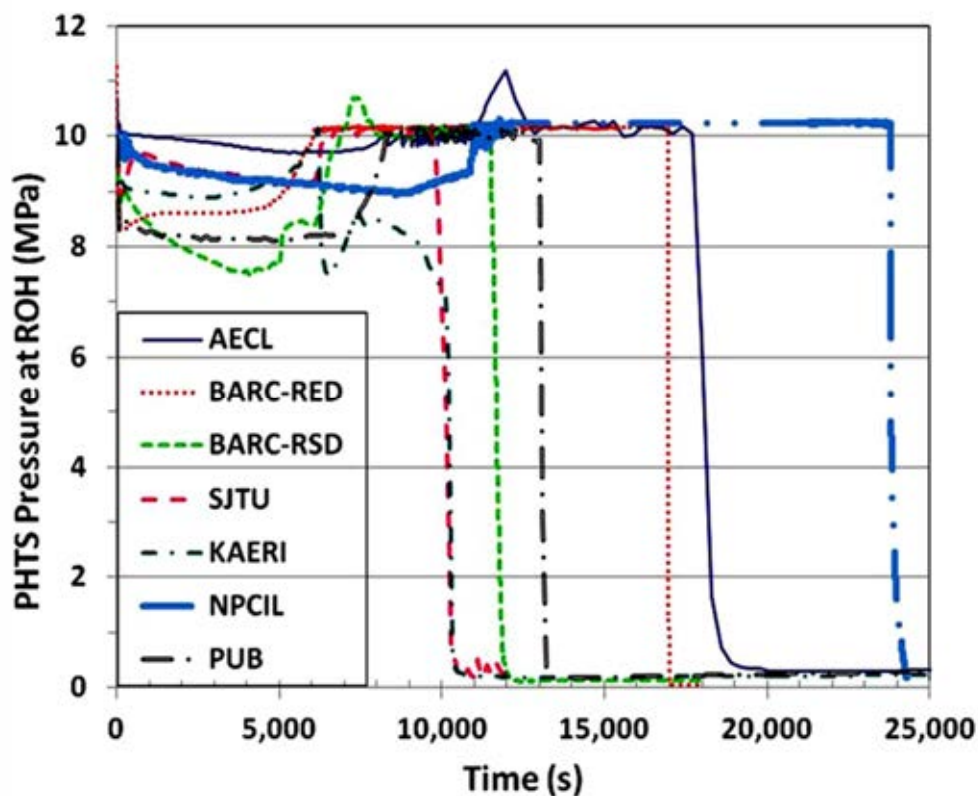


FIG. 4.1. A comparison of calculated PHTS pressure at ROH.

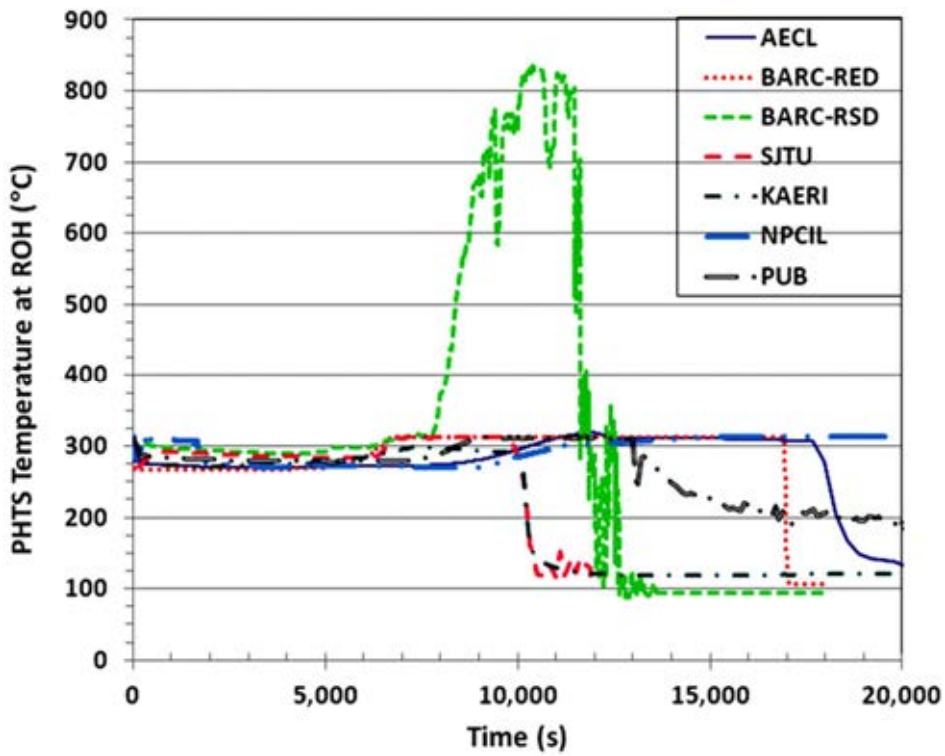


FIG. 4.2. The calculated PHTS temperature at ROH showing consistent results for up to 7,500s among the seven codes.

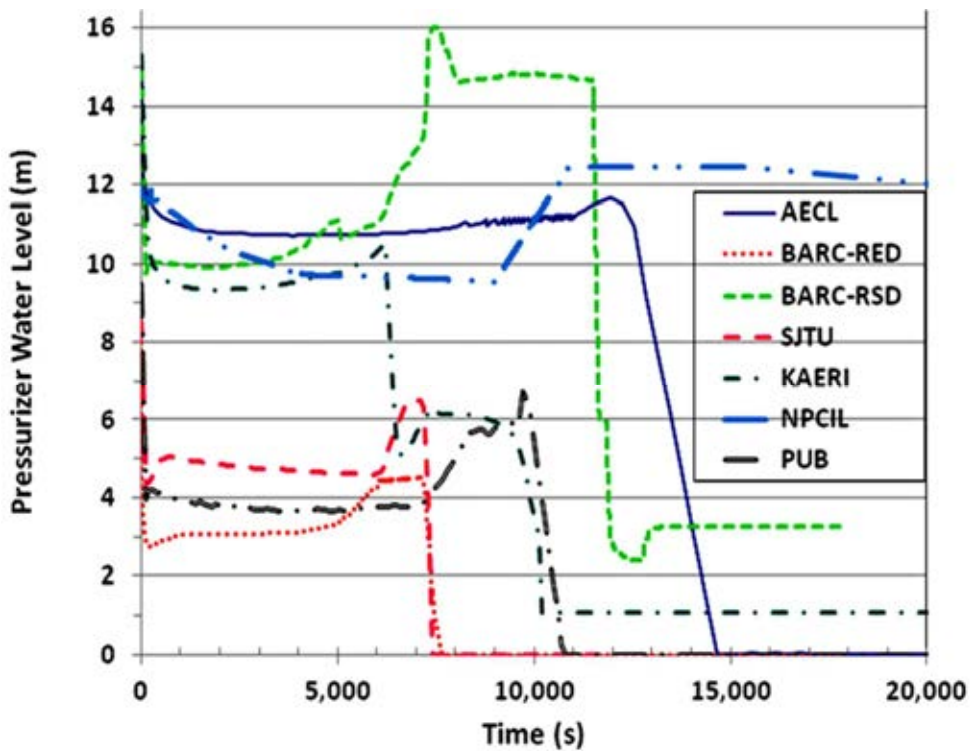


FIG. 4.3. The rapid drop in the Pressurizer water level showing water entering into the PHTS as it cooled down during the initial 200 s in all seven code calculations.

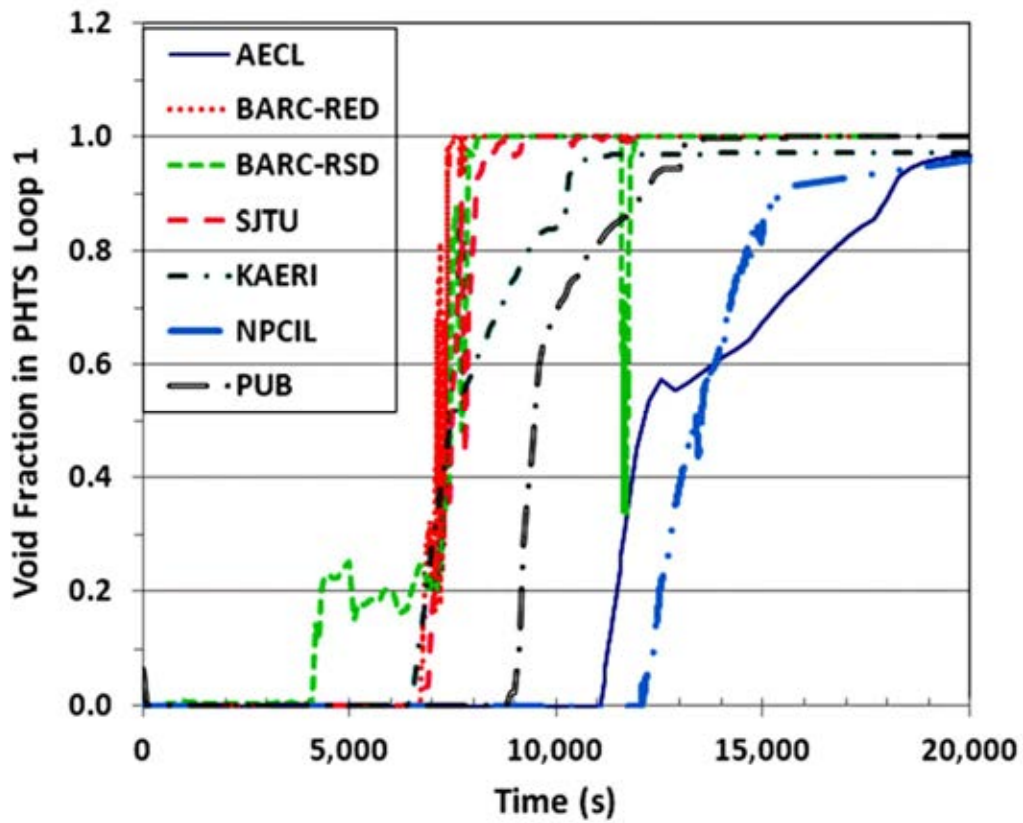


FIG. 4.4. The calculated transient void fraction in the PHTS loop 1.

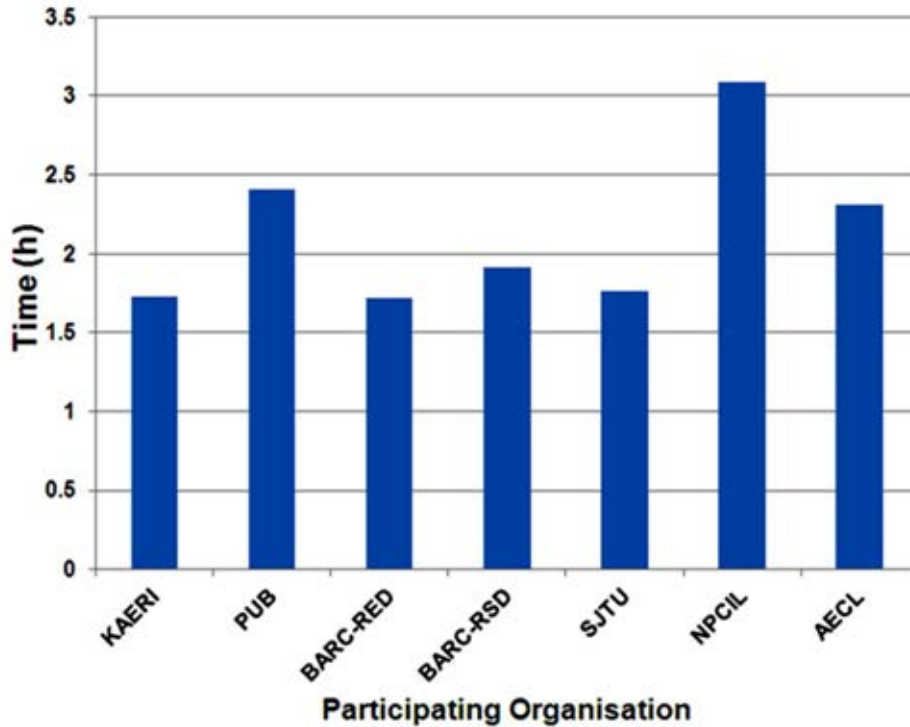


FIG. 4.5. A comparison of the time when liquid relief valves in the PHTS open for the first time in loops 1 and 2.

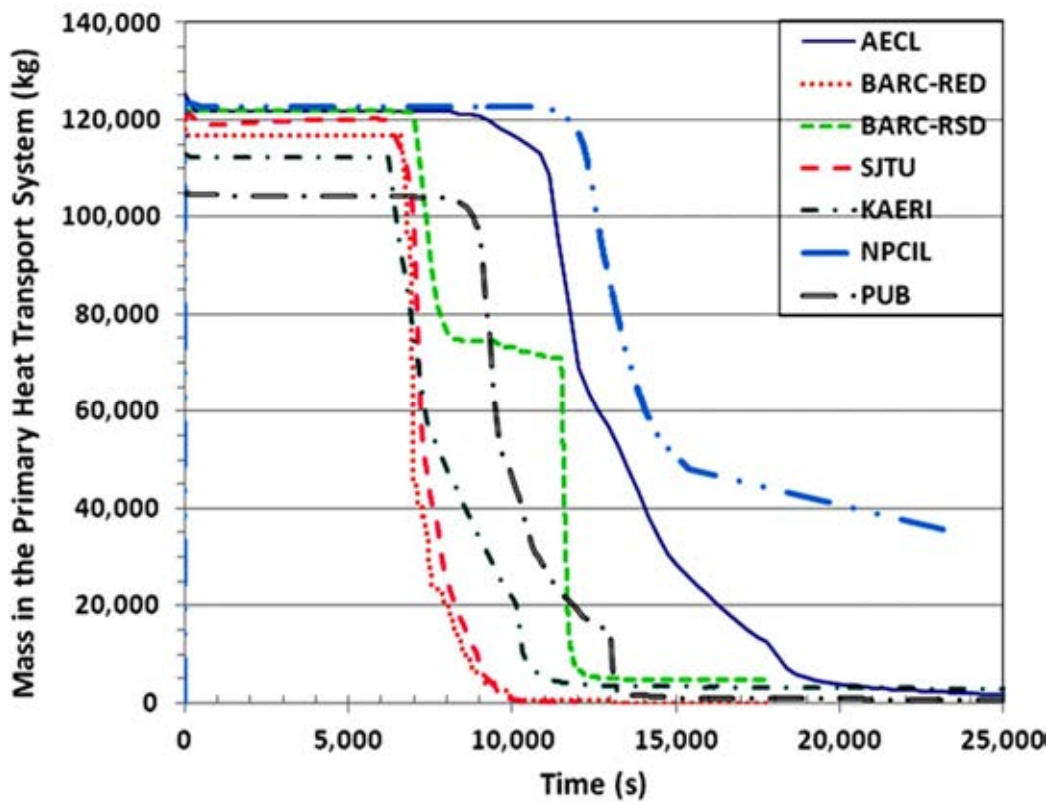


FIG. 4.6. A comparison of total coolant mass in the PHTS and pressurizer.

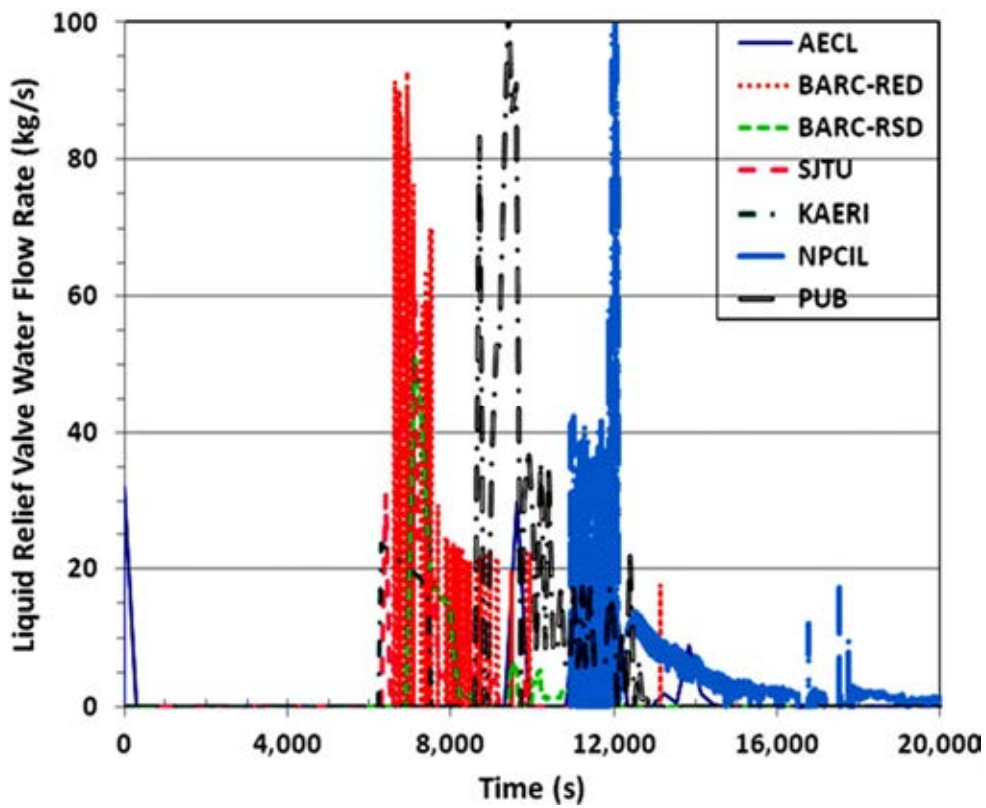


FIG. 4.7. A comparison of calculated water flow rates from the liquid relief valves.

## 4.2. STEAM GENERATOR SECONDARY SIDE BEHAVIOUR

The steam generator secondary side water was not replenished due to the loss of feedwater when the power failed at 0 s. The SGs boiled dry from approximately 7,000 s to 9,000 s (Fig. 4-8) in most of the analyses. The rate of boiloff (i.e., the slope of the curves) is approximately in agreement with each other. The SG pressure (Fig. 4-9) stays approximately constant as the MSSV open and close. After the PHTS emptied (by liquid and vapour discharge through the LRVs, and then through the fuel channel failure), the secondary side of the SGs depressurized slowly because the heat transfer from the PHTS decreased and was insufficient to keep the secondary side (now steam) sufficiently hot. The steam generator dryout ends the heat sink for the PHTS and therefore the PHTS pressure and temperature begin to increase as shown in Figures 4-1 and 4-2, respectively. The agreement between steam generator dryout and the PHTS temperature escalation is reasonably good among all participating organizations. In case of BARC-RED and BARC-RSD, the steam generator secondary side pressure in Figure 4-9 was terminated after approximately 15,000 s because of fuel channel disassembly and therefore the calculation became redundant.

The SG water level histories are shown in Figure 4-10, the trends of SG level and SG mass agree with each other as expected. The rate of SG water level decrease is similar among all participating organizations except the NPCIL simulation. The level variation is a function of the SG cross sectional geometry and therefore it appears the geometrical data used are different amongst the simulations. The time of SG dryout was reasonably close among the participating organizations as shown in Figure 4-11, with NPCIL and AECL lagging. The maximum difference in the dryout timing is about 1 h. This difference can be attributed to the differences in the assumed heat loss from piping which was not an input parameter supplied to the participating organizations. Some differences in the assumed initial conditions and in the models could also influence these results.

The SG level and mass histories dictate the timing of LRV opening because the SG heat sink decreases the pressure in the PHTS. The SG dryout timing (Fig. 4-11) and the LRVs first open time (Fig. 4-5) show reasonable agreement among most of the participating organizations however, in the case of KAERI and AECL the LRVs open before the SGs dryout, whereas the simulations by others show the SGs dryout prior to the LRVs first opening. The differences in the timing between these two events are about half an hour for all participating organizations. Given the complexity of the heat transfer phenomena and the complexity of the system geometry, the agreement within 0.5 h is reasonably good.

An examination of the SG mass inventory in Figure 4-8 shows that the liquid inventory does not completely boiloff in NPCIL, BARC-RSD and PUB analyses. A residual mass of approximately 2,000 kg to 5,000 kg remained in the SG. This residual mass in NPCIL is an artefact of sectors such as down comer and riser in the boiler retaining trapped mass without boiling off. The other contributor is (for PUB, NPCIL, BARC-RSD) steam mass within the steam generator which is added to the mass inventory. The steam generator water level shown in Figure 4-10, however, indicates complete dryout for BARC-RSD and PUB. The NPCIL analysis shows approximately 0.5 m of water remaining in the SG at 15,000 s.

In the steam generators, the secondary side water boils off and the steam is discharged to atmosphere via spring-loaded main steam safety valves (MSSVs). The timings of the MSSV openings are shown in Figure 4-12. The secondary side of the SGs was saturated, at a pressure below the opening set point pressure of the MSSVs. When the power was lost at 0 s, the feedwater flow stopped and the turbine stop valve closed. Thus the SG secondary side pressure increased rapidly so the MSSV begins to open and release the steam. The differences in this timing among most participating organizations were small, in the order of about 100 s. The differences were very small between KAERI, BARC-RED, SJTU, NPCIL, and AECL.

The timing was somewhat late for PUB and BARC-RSD compared to the other five participating organizations. These differences may be due to the heat transfer modelled in the SG and the length of time the secondary side pressure was maintained by the SG inventory, which was slightly different among the participating organizations, as shown in Figure 4-8.

A comparison of heat transferred through the steam generator is shown in Figure 4-13, which is a good indicator of the heat balance within the computer codes; however, the interpretation of the term “heat transfer” may have different definitions in different codes. The heat transfer rate through the steam generator is in reasonable agreement among all participating organizations, however, a much more closer agreement is shown among AECL, BARC-RSD, SJTU, BARC-RED, and KAERI. All codes show a rapid drop in heat transfer within a few seconds of reactor trip and then reach a quasi-steady condition until the steam generator inventory is boiled off.

The initial core heat to the SGs from both loops is expected to be ~2060 MW, which drops to ~1% (i.e., 20 MW) by 5,000 s. The analyses of all participating organizations are in reasonable agreement with this expectation. The agreement is indicative of reasonable heat balance within the codes used in the benchmarking exercise.

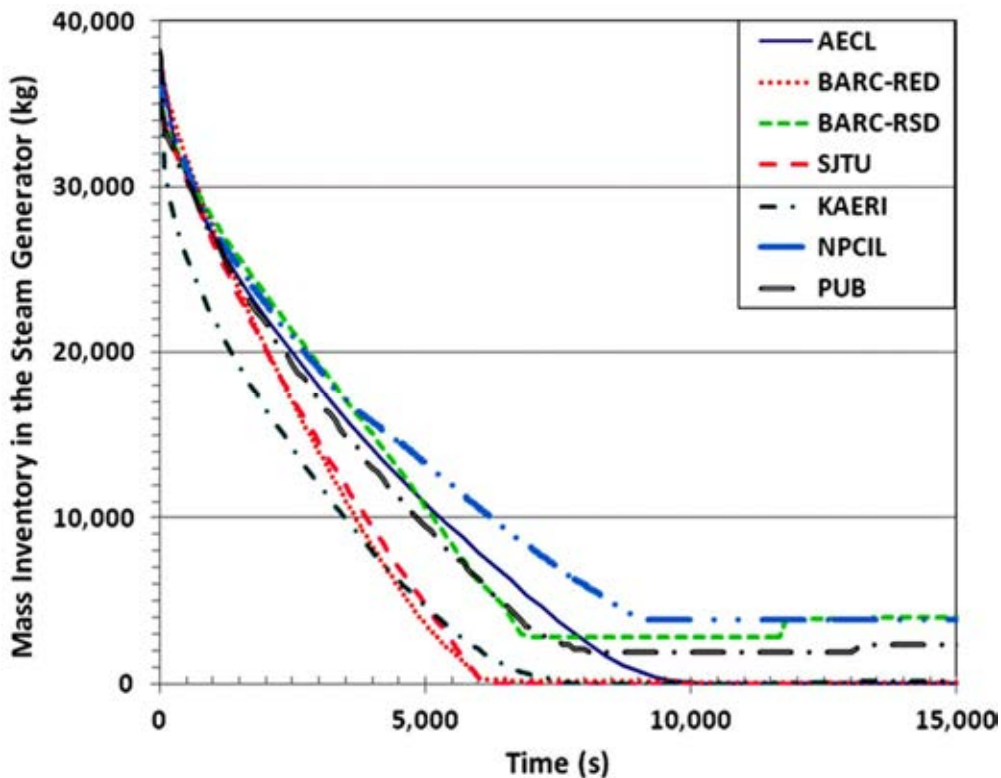


FIG. 4.8. A comparison of mass inventory in the steam generator.

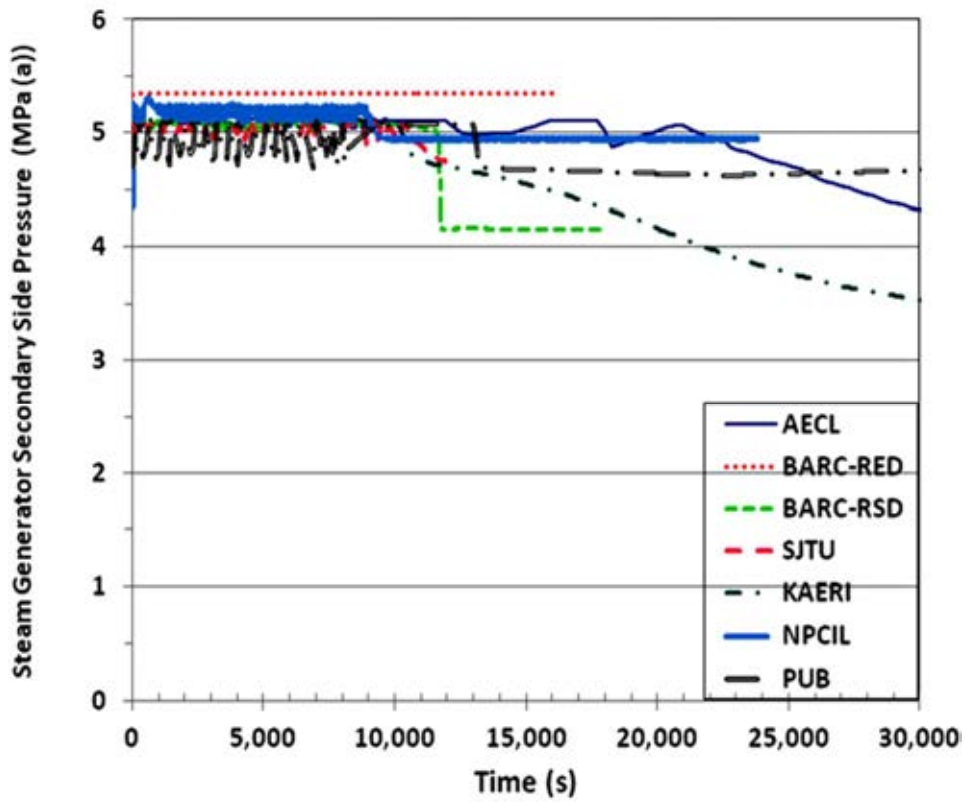


FIG. 4.9. The simulated steam generator pressure.

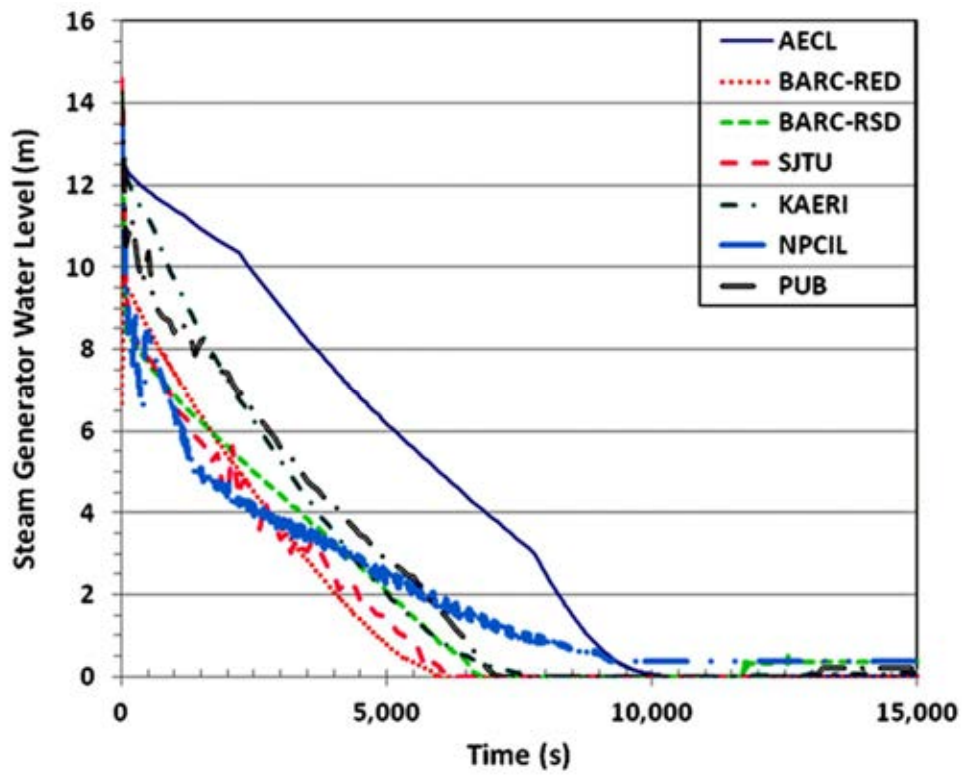


FIG. 4.10. A comparison of the steam generator water level variation.



FIG. 4.11. The time SG dryout calculated by participating organizations.

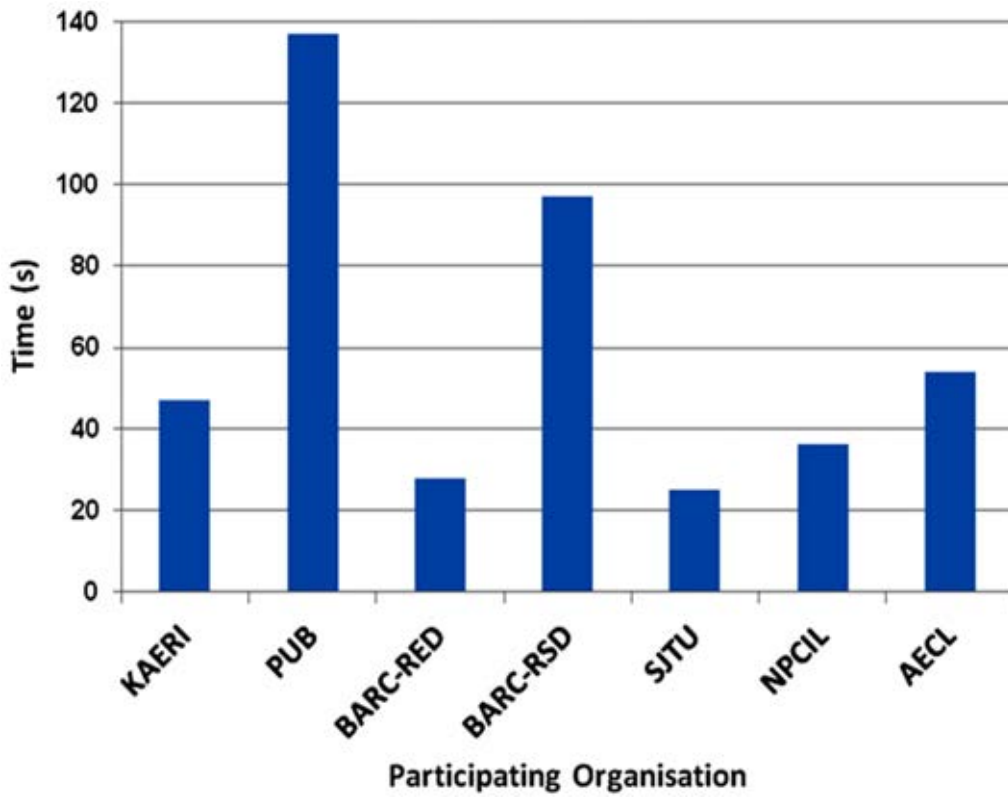


FIG. 4.12. A comparison of when MSSV first opens in the simulation.

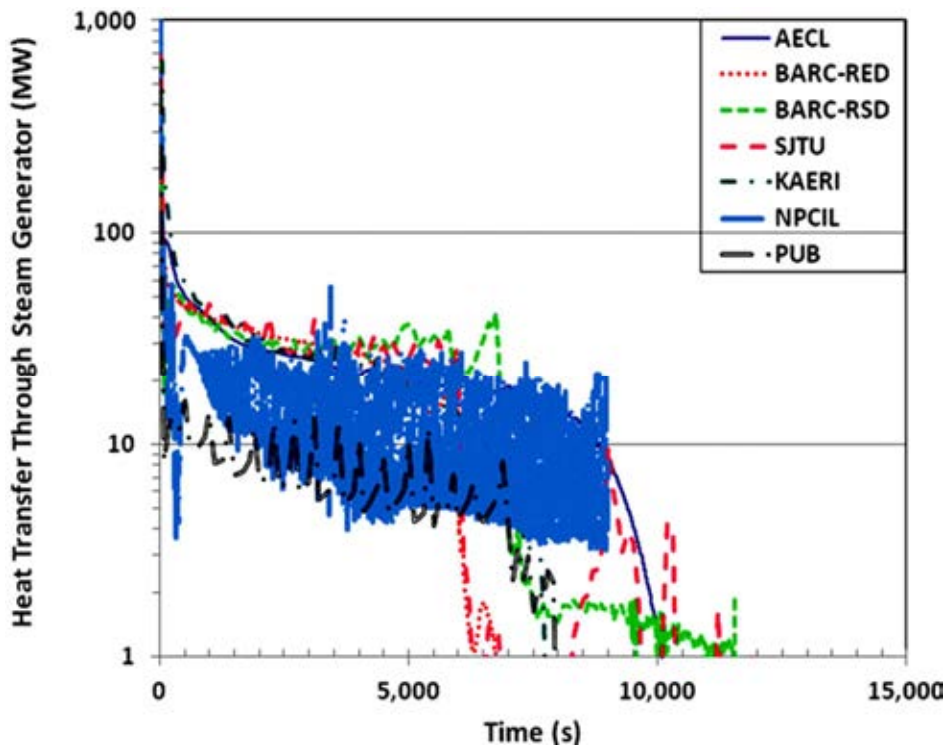


FIG. 4.13. The calculated amount of heat transferred from PHTS to steam generator.

#### 4.3. MODERATOR SYSTEM BEHAVIOUR

During the early stages of the accident progression, the moderator slowly heats up because of the loss of the moderator cooling system and the addition of decay heat from the fuel. Heat is transferred from the PHTS across the fuel channel annuli to the moderator, and is also directly deposited in the moderator by absorbing gamma radiation from the fuel. Figure 4-14 shows the amount of heat transferred from the fuel channels. The calculated heat transfer varies significantly among the simulations until ~23,000 s, however, they converge to 10,000 kW briefly until 29,000 s. The trends predicted by AECL, PUB, NPCIL, and KAERI are in agreement; for example, the heat transfer decreases sharply as soon as the reactor is tripped and then reaches a quasi-steady state from about 10,000 s to about 20,000 s. The heat transfer increases to ~10,000 kW at the end of the quasi-steady-state period. In the NPCIL simulated heat transfer from the fuel channel to the moderator after ~20,000 s shows spiked heat releases. In this simulation, no pressure-tube/calandria-tube rupture was predicted and therefore pressure tubes in various rows ballooned into contact with the calandria tube sequentially, releasing stored heat in the pressure tube. The sudden heat spikes due to pressure tube ballooning contact is reflected as spiked heat release to the moderator.

The time when moderator reaches saturation temperature is shown in Figure 4-15. In the AECL and NPCIL simulations, the moderator reaches saturation temperature at 5 and 5.6 h, respectively, while for the other participating organizations the moderator reaches the saturation temperature an hour earlier between 3 and 4 h. It appears that the heat load from the fuel channels is lower in case of NPCIL and AECL compared with the other participating organizations. The comparison shown in Figure 4-15 also shows that the time moderator reaches its saturation temperature calculated by BARC-RSD, AECL and PUB agree with pressure-tube and calandria-tube rupture. In case of BARC-RED and NPCIL simulations, the moderator reached its saturation temperature when the calandria vessel pressure reached the saturation pressure due to heat flow from pressure-tube to calandria-tube contact. In KAERI

and BARC-RED calculations the moderator reached the saturation temperature with a delay following calandria rupture disks opening.

Figure 4-16 shows the calandria vessel pressure calculated by the severe accident analysis codes. Except for PUB, the calculated pressure transients were consistent until about 10,000 s. In case of PUB, a sudden pressure spike reaching approximately 1100 kPa was calculated at ~13,100 s which is coincident with the rupture of pressure-tube/calandria-tube and the opening of the calandria vessel rupture disk. A similar pressure spike of 360 kPa was calculated by AECL at approximately 17,900 s, which is coincident with pressure-tube/calandria-tube rupture. Similar pressure spikes, but with a lower peak pressures, were also calculated by SJTU, BARC-RED, and BARC-RSD. A pressure spike was not calculated by NPCIL because no pressure-tube/calandria-tube rupture was predicted, however, the calandria vessel pressure decreased to ambient pressure at 20,000 s due to the rupture of Over Pressure Rupture Disc (OPRD). The gradual increase of calandria vessel pressure was calculated by AECL, KAERI and PUB from about 12,000 s. The NPCIL and BARC-RED calculations predicted the rupture disk to open due to thermal expansion of moderator liquid, whereas the others predicted the rupture disk to open when pressure-tube/calandria-tube ruptured.

The level and the inventory of the moderator are compared in Figures 4-17 and 4-18. In AECL's simulation, the moderator bleed valves opened and closed initially to maintain the pressure as the moderator heated and the level swelled due to thermal expansion. In the simulations completed by other participating organizations, as shown in Figure 4-17, the moderator level remained quasi-steady during the initial 10,000 s. Opening of the bleed valves slowed the calandria vessel pressurization and contributed to the rate of pressure increase in the containment; it also released some moderator to the containment, which resulted in a small decrease in the moderator mass (Fig. 4-18). When the pressure inside the calandria vessel reached the set point pressure of the rupture disk, i.e., 238 kPa (a), the calandria vessel rupture disk failed and a rapid decrease in the calandria vessel water level was observed in most calculations. After the initial rapid moderator expulsion, the moderator continued to boiloff gradually into the containment due to the heat transferred from the core. In the boiloff phase of the transient, the moderator level and the moderator mass show somewhat similar rate of depletion in most of the calculations shown in Figures 4-17 and 4-18. In the case of KAERI and NPCIL simulation, the water level in the calandria vessel (Fig. 4-17) does not dryout because the level calculated includes the corium mass at the bottom of the calandria vessel.

As shown in Figure 4-18, the calculations by PUB and AECL estimate an expulsion of approximately 80,000 kg of moderator inventory during the pressure-tube and calandria-tube rupture. SJTU and KAERI estimated relatively small amounts of moderator loss during pressure-tube calandria-tube rupture. The loss of moderator estimated by NPCIL due to swelling and bursting of rupture disk was very small compared with the moderator expulsion estimated by AECL and PUB. The loss of moderator mass calculated by BARC-RSD up to the failure of the calandria vessel was about 60,000 kg.

There are two key opportunities in this benchmarking study to assess the robustness of energy balances among the analyses. The first opportunity for an energy balance was provided in the steam generator secondary side boiloff. The slopes of the curves in Figure 4-8 are directly related to the decay power transferred to the steam generator secondary side water. The rate of boiloff not only captures the decay power but also a large number of associated phenomena involved in transferring the nuclear heat from the fuel to the steam generator secondary side water through a convoluted path involving heat and mass transfer. If the boiloff curves have approximately similar slopes, it would be indicative of a normalised similarity in the energy transfer process from the fuel to SG secondary side steam. In a complex simulation like the

station blackout analyses, expecting perfect agreement in the boiloff rates (i.e., slopes) of Figure 4-8 would be very optimistic, however, the degree of agreement among the seven simulations, shown in the figure, leads to cautious optimism in the benchmarked code capabilities of primary heat transport system and the steam generator secondary side models.

The second opportunity for the energy balance is provided by the rate of moderator boil off. The slope of the curve in Figure 4-18 is also related to the energy transfer from the fuel to the moderator back up heat sink. Although not perfect, the slopes of the seven analyses provide another cautious conclusion on the agreement in the benchmarking of all processes from the fuel to the moderator within the analyses codes.

Figure 4-19 shows a comparison of time taken to boiloff the moderator in the analyses completed by participating organizations. The AECL and NPCIL calculations indicate about 14.5 h to boiloff the moderator whereas KAERI, BARC-RED, BARC-RSD, and PUB show approximately 10 to 12 h to boiloff the moderator. The SJTU calculations show approximately 8 h to boiloff the moderator. Although AECL expelled significant amount of moderator inventory when the rupture disk failed, moderator takes longer to boiloff because of the gradual disassembly of the core. Given the complexity of the channel disassembly and core collapse phenomena, the differences in the moderator boiloff times appear to be reasonable.

The hydrogen generated in-vessel includes the hydrogen produced in the fuel channels and in the suspended debris bed. Major contribution to hydrogen production occurs after the pressure tubes and calandria tubes fail due to excessive heating of the fuel and the channel without cooling. Figure 4-20 shows the variation of in-vessel hydrogen generation during accident progression. In case of PUB and BARC-RED, the curves end at 42,000 s and 50,000 s, respectively, because in-vessel hydrogen generations ended at these times and ex-vessel calculations began for BARC-RED while PUB did not have the models to calculate ex-vessel hydrogen. The maximum in-vessel hydrogen generation calculated by KAERI, BARC-RED and NPCIL, as shown in Figure 4-21, is reasonably close, given the nature of the complexity associated with steam availability for zirconium oxidation. Although the ex-vessel hydrogen generation (to be discussed in Section 4.5) is comparable among the participating organizations, the “in-calandria vessel” hydrogen generation calculated by KAERI, BARC-RSD, and NPCIL is about twice than the amount calculated by AECL and PUB. The BARC-RSD calculated hydrogen generation is the highest among all participating organizations. In the simulation completed by NPCIL, the oxidation of the debris is calculated during channel slumping and in the terminal debris which is one of the reason for the high generation of hydrogen shown in Figure 4-20.

The calculations completed by BARC-RSD indicated that a significant amount of hydrogen generation occurred inside the terminal debris bed (870 kg) within the calandria vessel from the 35 tons of available Zr mass (un-oxidised clad, pressure tube and calandria tube). At this time BARC-RSD estimated 88% of the 40 tons of Zr inventory is un-oxidised. The hydrogen generation capacity for the 35 tons of Zr was estimated to be ~1.5 tons of hydrogen and the steam required was ~15 tons based on stoichiometry. About 108 tons of moderator was available for oxidation. According to BARC-RSD the generation of 870 kg hydrogen in their analysis is well within the available moderator inventory that boils-off in this phase.

The availability of steam does not necessarily ensure accessibility of steam to unoxidized Zr mass. For example, submerged channels cannot oxidize although steam is available above these channels. Major constraints to hydrogen generation occur due to poor accessibility of steam. The accessibility is also poor within the steam exposed channels. For steam to have sufficient accessibility to the Zr mass contained within the intact channels, channel perforation must occur at the inter-bundle junctions as channels sag and form the suspended

debris. The amount of hydrogen generation calculated by BARC-RSD up to the core collapse is about 200 kg. This is generated from the suspended debris and the amount is comparable to the amount of hydrogen generated from the suspended debris by AECL and PUB and (Figure 4-21). Large amount of hydrogen generation predicted by BARC-RSD is attributed to the assumption of full accessibility of steam to Zirconium after core collapse.

The moderator temperatures predicted by the severe accident computer codes are shown in Figure 4-22. The predicted trends are quite similar but the variation from the highest to the lowest prediction is about 40°C. Except for the NPCIL prediction, all other simulations show a sharp rise in the temperature following pressure-tube/calandria-tube rupture. These sharp rises represent the increase in moderator temperature due to primary coolant mixing with the moderator following pressure-tube/calandria-tube rupture.

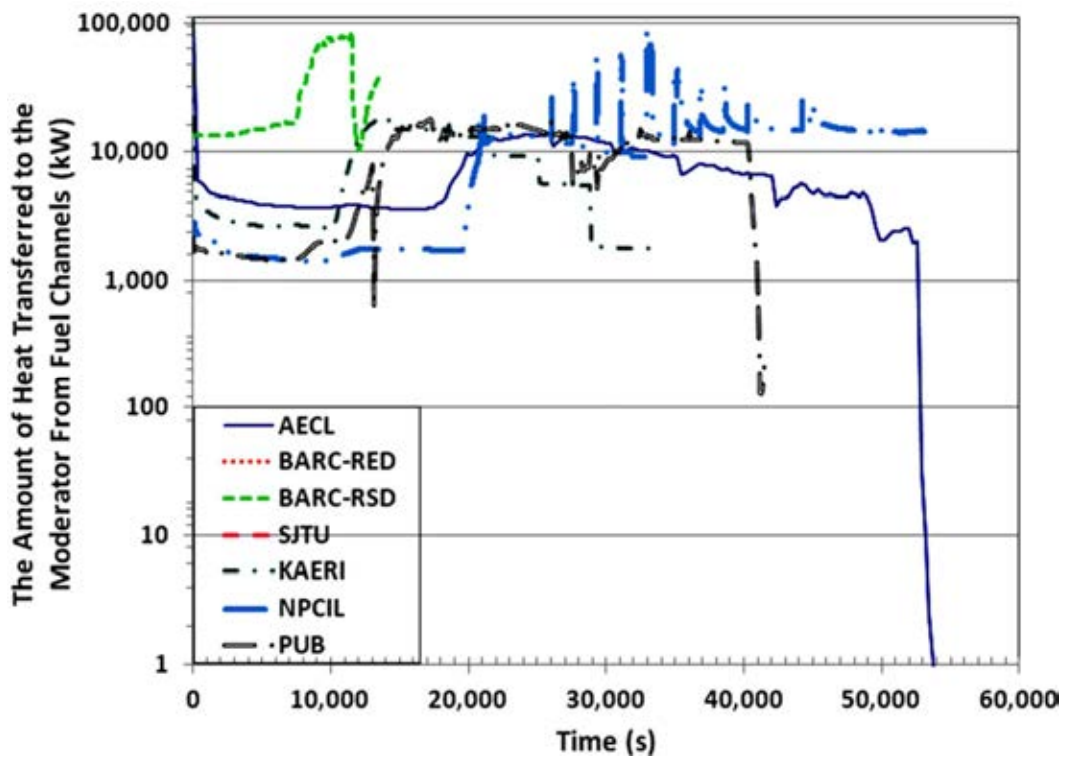


FIG. 4.14. The calculated amount of heat transferred to the moderator from the fuel channels, by conduction across the fuel channel annuli and by gamma heating.

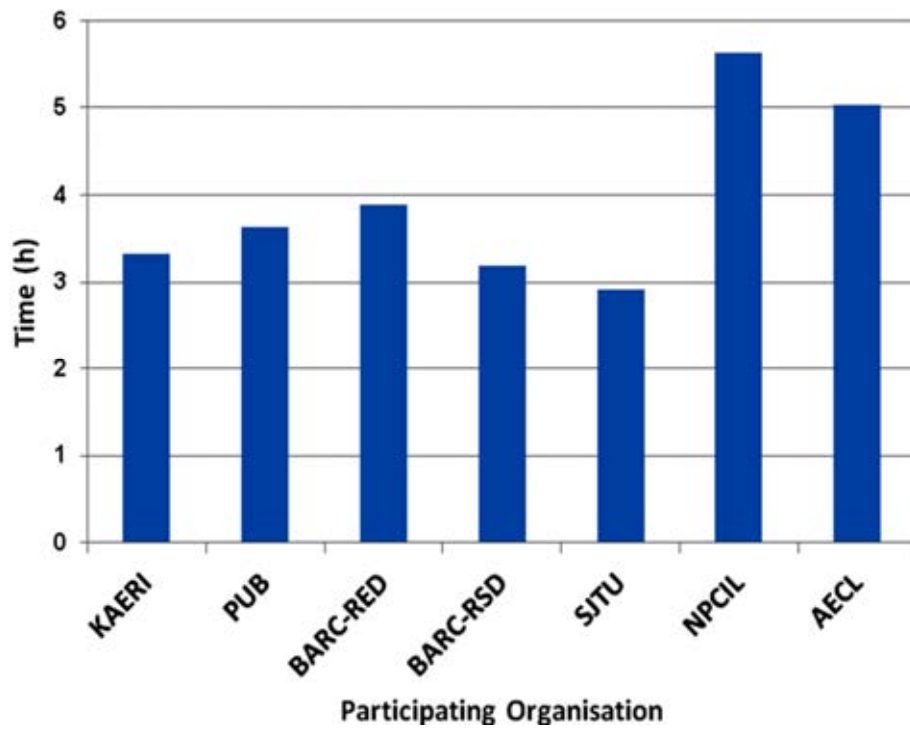


FIG. 4.15. A comparison of the time when the moderator reaches saturation temperature.

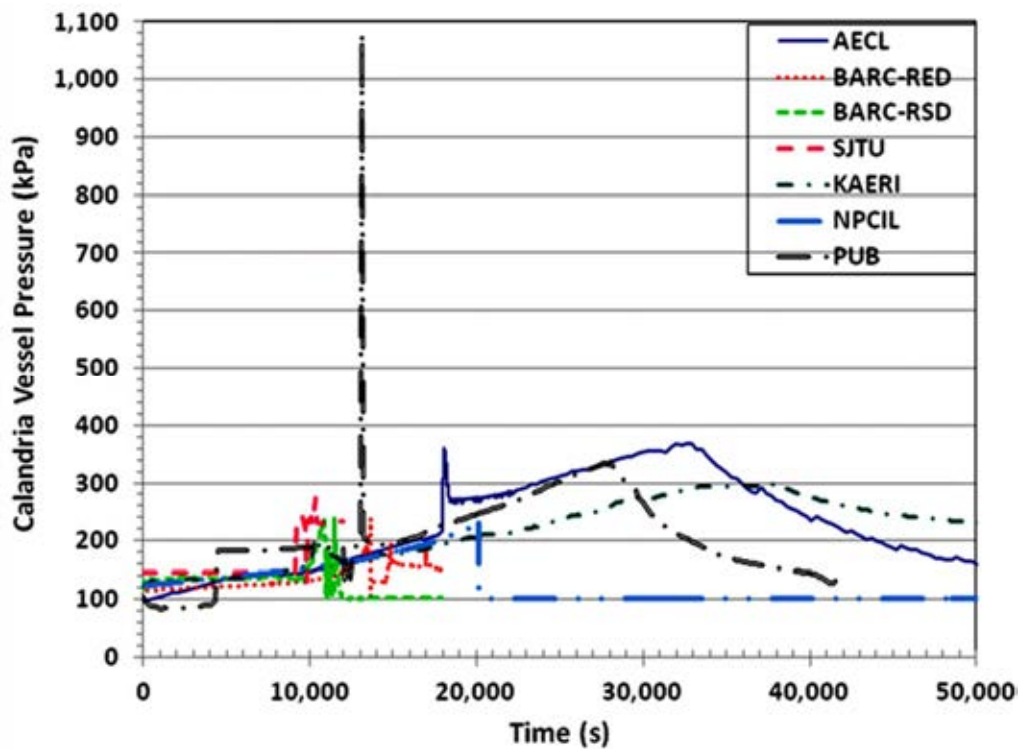


FIG. 4.16. The transient calandria vessel pressure simulated by participating organizations.

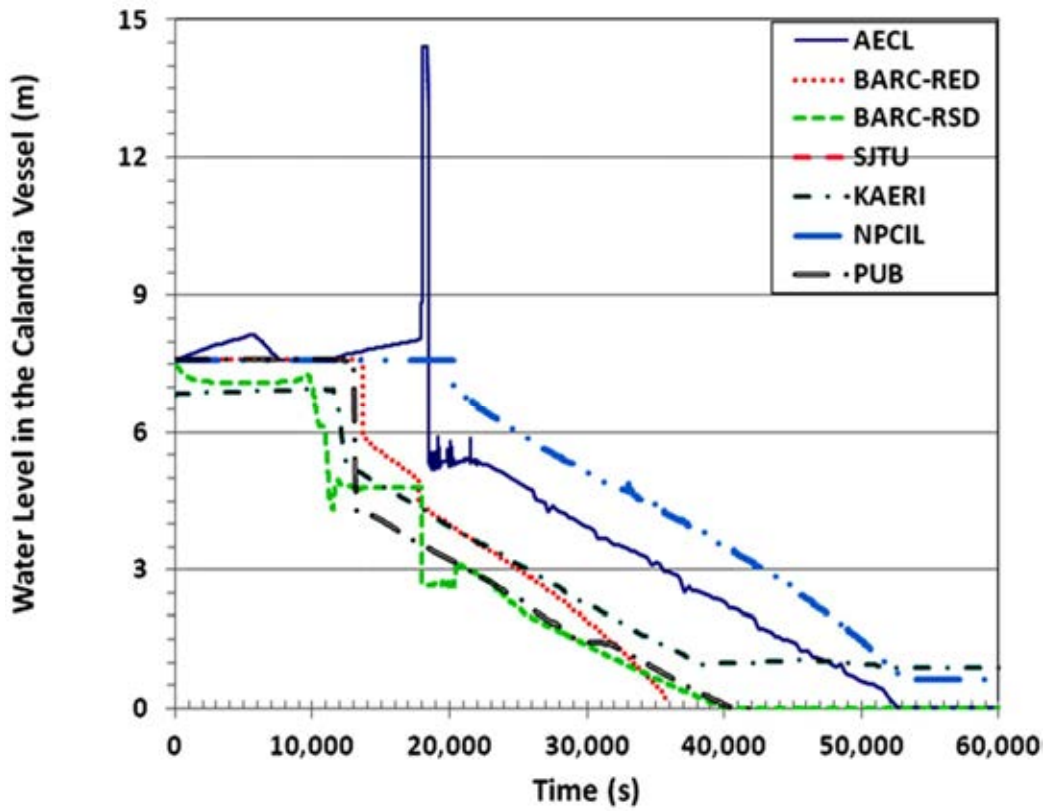


FIG. 4.17. The moderator level predicted by severe accident codes.

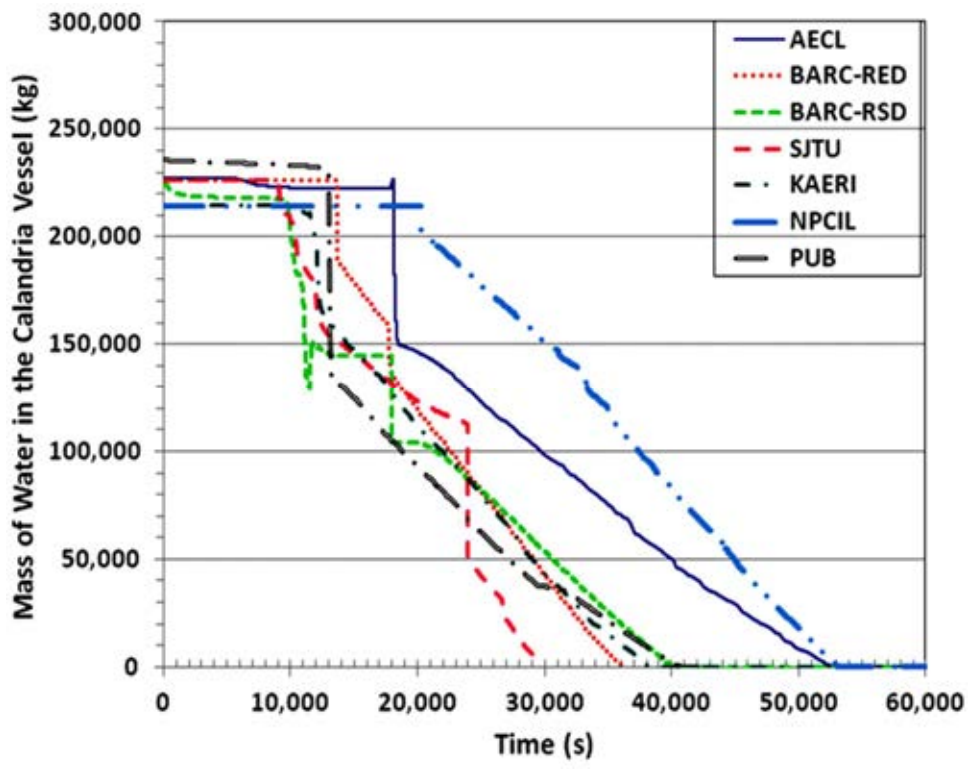


FIG. 4-18. The calculated variation of moderator inventory.

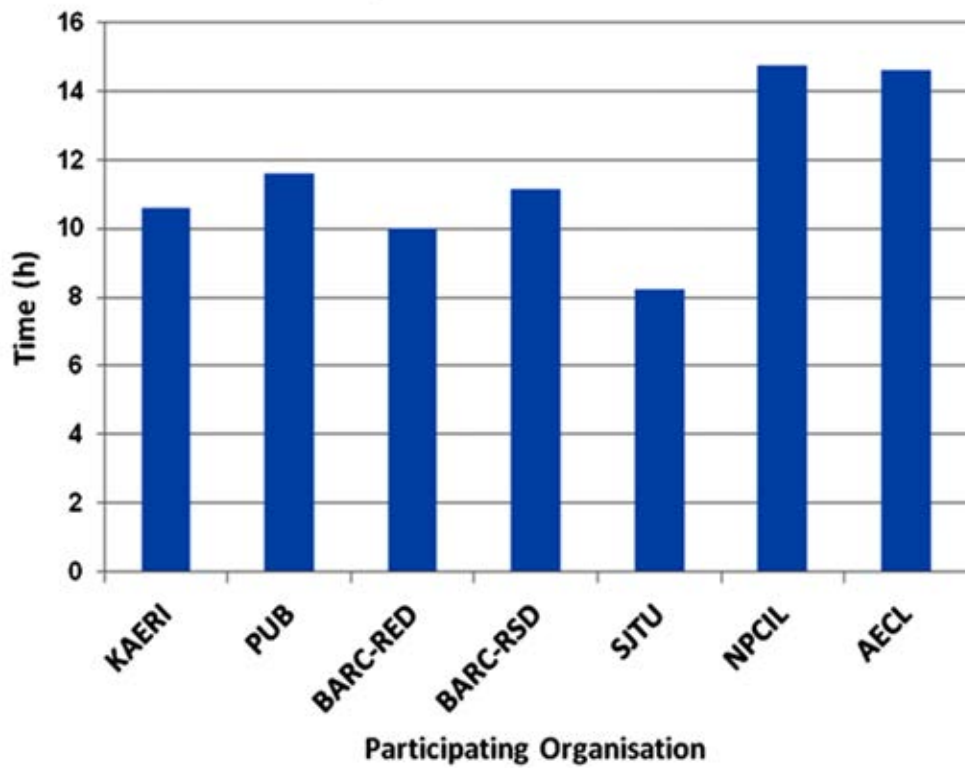


FIG. 4-19. Comparison of time taken to boil off the moderator inventory completely.

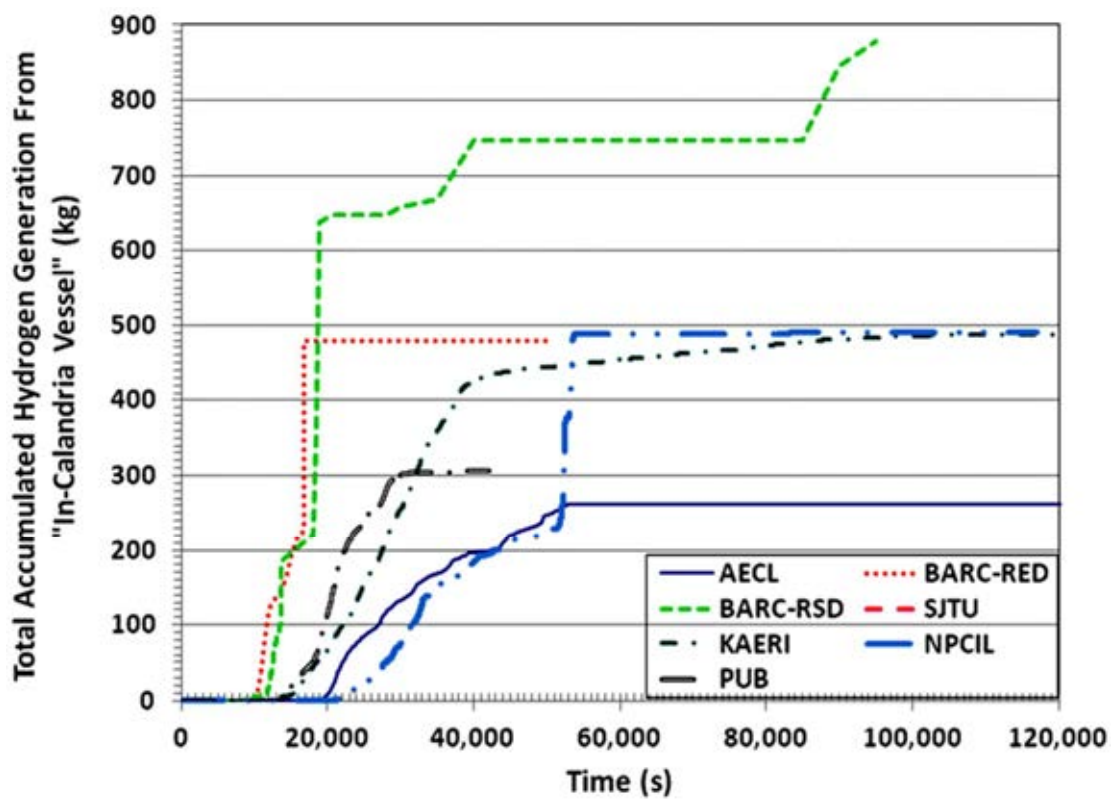


FIG. 4.20. A comparison of hydrogen generated inside the calandria vessel.

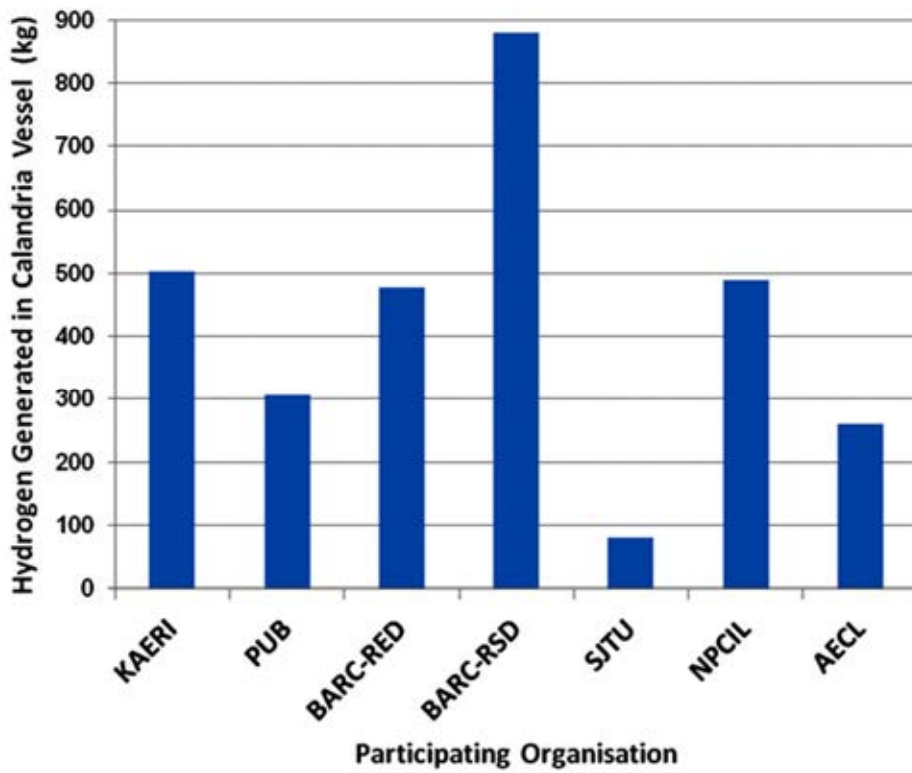


FIG. 4.21. The mass of in-calandria vessel hydrogen calculated by severe accident codes.

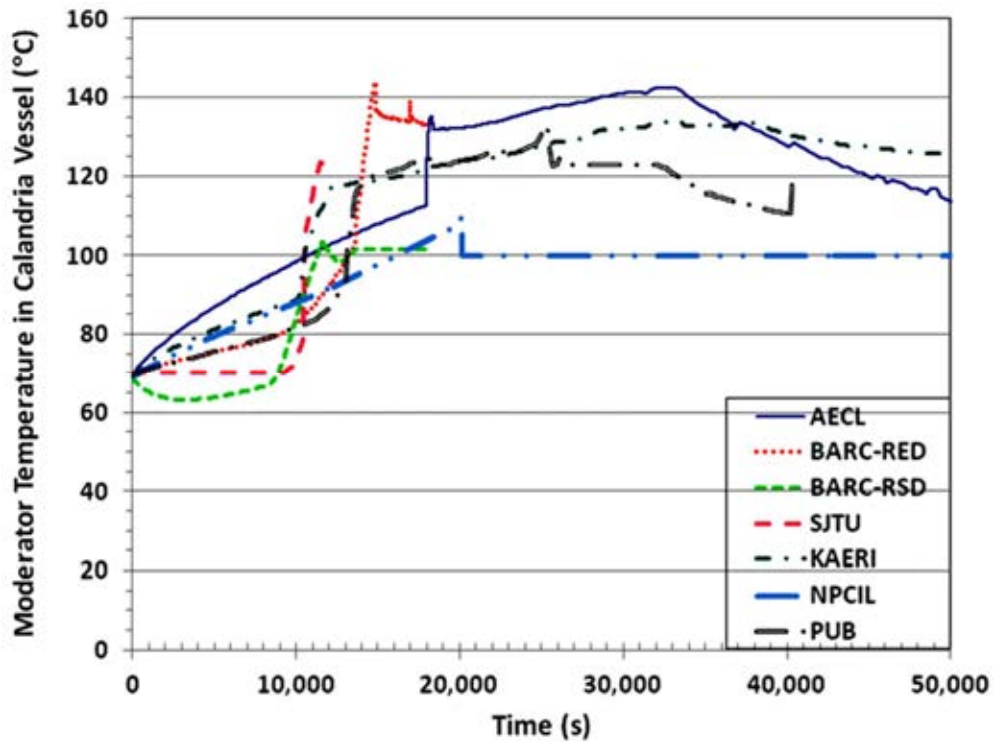


FIG. 4.22. The moderator temperature calculated by the severe accident codes.

#### 4.4. CORE MELT RELOCATION BEHAVIOUR

The mass of UO<sub>2</sub> retained in the intact fuel channels during fuel channel disassembly and the formation of the suspended debris bed is shown in Figure 4-23. As can be seen in the figure, the disassembly begins between 14,000 s and 22,000 s in most of the simulations, except in case of SJTU (not shown in the figure) and NPCIL calculations which indicated a delayed fuel channel disassembly at 33,000 s. The differences in the initiation of core disassembly are due to the fuel channel disassembly and slumping models used in the analyses. The UO<sub>2</sub> mass tended to decrease in steps for AECL and KAERI, small steps representing a few channels and larger steps representing several channels. The simulations completed by other organisations show one, two or three step core disassembly. In KAERI simulation, the mass of UO<sub>2</sub> includes the mass of Zircaloy in the fuel channels and therefore it is 40,000 kg higher than the mass given by the other code users.

The total mass of suspended debris is shown in Figure 4-24. The mass increased as channels disassembled, but some suspended material melted and moved to the terminal debris bed and this relocation is represented by the undulations in the suspended debris bed mass. AECL, BARC-RSD, and PUB calculated the suspended debris bed with a “core collapse”, occurring upon reaching the core collapse criteria, representing a large scale relocation of debris and the underlying channels to the terminal debris bed. This core collapse phenomena is represented by the vertical line showing the disappearance of the mass from the suspended debris. The time core collapse is predicted to occur in PUB and BARC-RSD simulation is about 25,000 s and 40,000 s earlier, respectively, than the core collapse time calculated by AECL simulation. The reason why such a large time difference occurs in the core collapse time requires further investigation. In KAERI calculation, the suspended debris mass changed with time and therefore no core collapse occurred because the accumulated debris mass in each loop was less than the global core collapse criteria. BARC-RED, NPCIL, and SJTU did not provide the suspended debris mass data.

Figure 4-25 compares the temperature of the suspended debris calculated by AECL, BARC-RSD, and KAERI. Although timing of the debris bed appearance was inconsistent among the calculations the peak temperatures between AECL and KAERI are in good agreement. BARC-RED, NPCIL, PUB, and SJTU did not provide suspended debris bed temperature calculations. The core material in the suspended debris bed is expected to heat up due to decay heat and the exothermic Zircaloy/steam reaction until the debris remains suspended. When the suspended debris relocates, the temperature in the suspended debris is expected to decrease to the gas temperature. This behaviour is predicted somewhat by AECL, BARC-RSD, and KAERI calculations. Eventually the molten material relocates from the suspended debris bed to the bottom of the calandria vessel and is quenched in water. A comparison of the time total mass of corium appears in the suspended debris bed as shown in Figure 4-24 for AECL appears to have a mismatch with the time the temperature of the suspended debris bed shown in Figure 4-25. The mass is calculated to be in the suspended debris bed between ~20,000 s and 53,000 s, whereas the suspended debris bed temperature is shown to exist between ~50,000 s and 53,000 s. The mass in the suspended debris bed is calculated for all nodes forming the debris bed, whereas the temperature information was plotted only for the bottom most nodes where the debris appears only at the end of the debris relocation process and therefore appears as a sudden spike lasting only for ~3,000 s between 50,000 s and 53,000 s.

As stated earlier, the mass in the suspended debris bed relocated to the bottom of the calandria vessel when the debris bed mass exceeded a user- specified value. This relocation is captured in Figure 4-26. The material transfer from the suspended bed to the calandria vessel bottom can be verified by comparing Figures 4-24 and 4-26. The terminal debris accumulation starts

at approximately at 20,000 s for AECL, PUB, BARC-RSD, BARC-RED, NPCIL and KAERI. The maximum terminal debris mass is approximately equal (~140,000 kg) for PUB, NPCIL, BARC-RED, BARC-RSD, and KAERI whereas for AECL, the maximum mass in the terminal debris was approximately 5,000 kg higher than the others.

The amount of heat transferred to the calandria vault water was calculated by PUB, BARC-RED, NPCIL, and AECL (Fig. 4-27). Until about 70,000 s, the amount of heat transferred is approximately equal in all calculations, however, the AECL and BARC-RED calculated amounts of heat transfer doubled compared to the amount calculated by PUB after 70,000 s. At approximately 182,000 s, the amount of heat transferred to the calandria vault water increased by about eight times in PUB calculation. Similar increases were also observed with NPCIL and BARC-RSD simulations approximately at 55,000 and 40,000 s. The timing of these increases, coincide with the time calandria vessel failure and debris quenching.

The predicted core collapse in the analyses ranged between 4.98 h (BARC-RSD) and 42 h (KAERI results show that all corium is delivered into the calandria vessel through the normal relocation process. No core collapse occurs). The fuel channel slumping models, oxidation models and other assumed failure criteria dictate the timing of complete core collapse. The range of predicted core collapse time is almost an order of magnitude wide.

The calandria vessel wall temperatures simulated by the participating organizations, excluding SJTU, are compared in Figure 4-28 and the agreement among the calculated wall temperatures is poor. Because of the large variation in the calculated calandria vessel wall temperatures, the simulated calandria vessel failure times ranged between 26.58 h (BARC-RSD) and 55.06 h (AECL). This range of variation is approximately 100,000 s (or ~28 h) and this level of uncertainty in the code predictions requires further investigation to reduce the uncertainty.

Figure 4-29 compares the timings of calandria vault water reaching saturation temperature. The time calculated by BARC-RSD and SJTU is almost 8 h lower than the time calculated by other participating organizations. The time taken for calandria vault water to reach saturation is directly related to the amount of heat transferred to the calandria vault water shown in Figure 4-27. The calandria vault water reaching saturation faster in BARC-RSD and SJTU is indicative of relatively high heat transfer from calandria vessel walls earlier on in the sequence in comparison to other simulations. The high heat transfer from the calandria vessel to the calandria vault water is expected to be accompanied by an early moderator boiloff and core collapse. An examination of Figure 4-15 reveals that BARC-RSD and SJTU predicted the moderator to reach saturation approximately 0.5 to 2.5 h earlier than the time calculated by the other participating organizations. In case of BARC-RSD, the upper region of the moderator reaches saturation from the primary heat transport fluid coming out of channel break. The moderator regions below attain saturation temperature with decay heat from the channels and thermal mixing with upper regions of the moderator. The bottom most regions of the moderator attain saturation about 0.3 h later, which is comparable with the timings of KAERI and PUB. The time taken to boiloff the moderator, shown in Figure 4-19, is approximately 2 to 6 h earlier in SJTU simulation compared with the other simulations.

Figure 4-30 shows the calculated molten fraction of the debris. The time of debris melting, as calculated by NPCIL, KAERI, PUB, and AECL, appears to be consistent. The calculation by BARC-RED shows slightly delayed melting of the debris. After a sharp increase (except BARC-RED), the molten fraction reaches a plateau until it is expelled from the calandria vessel. The calculated peak molten fraction ranged between 0.45 and 0.8.

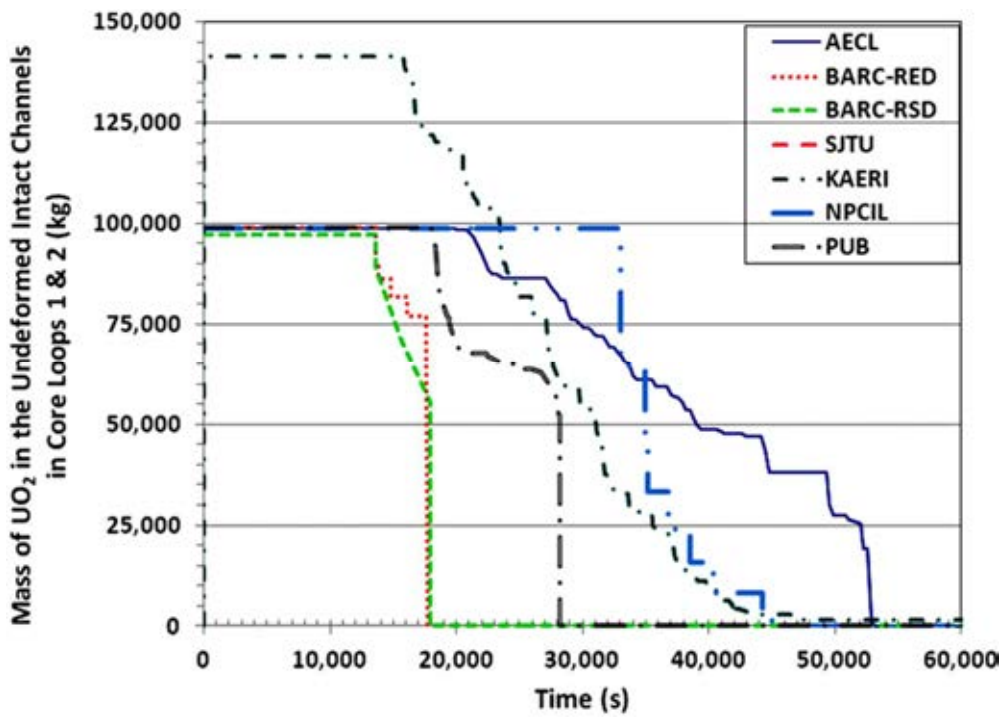


FIG. 4.23. The UO<sub>2</sub> mass in the intact core that shows the variation in the core disassembly process calculated by various severe accident codes.

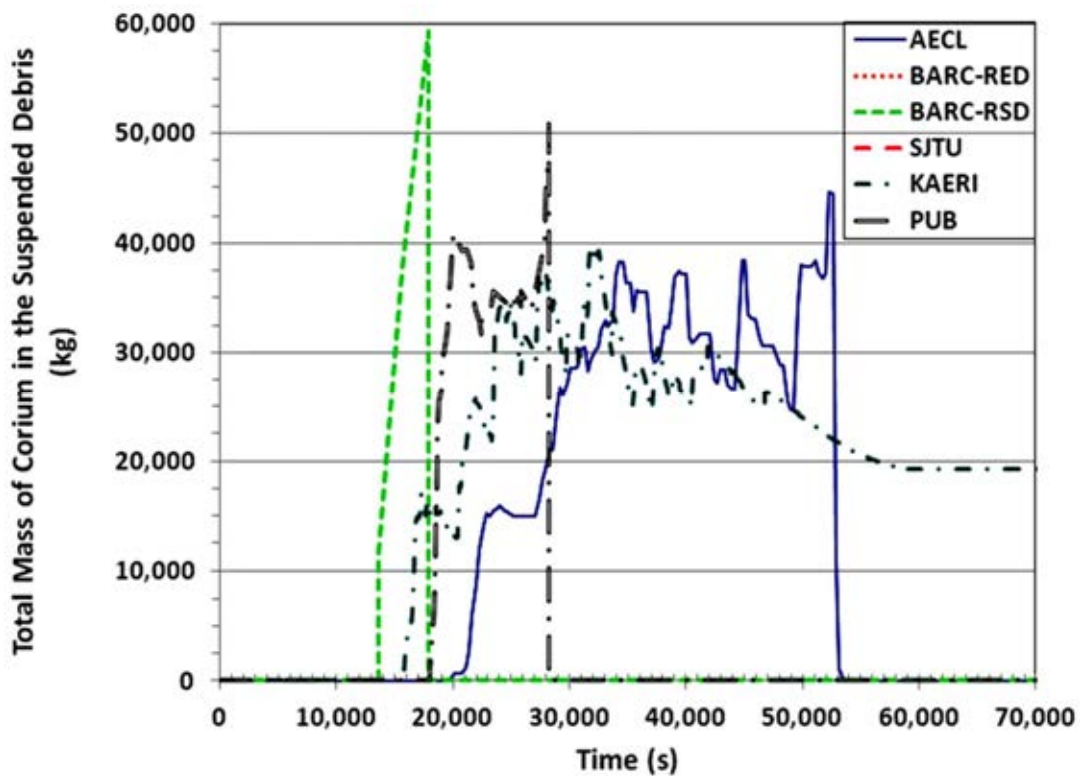


FIG. 4.24. The corium mass in the suspended debris bed showing accumulation and sudden collapse (in KAERI, BARC-RSD, AECL, and PUB calculations only).

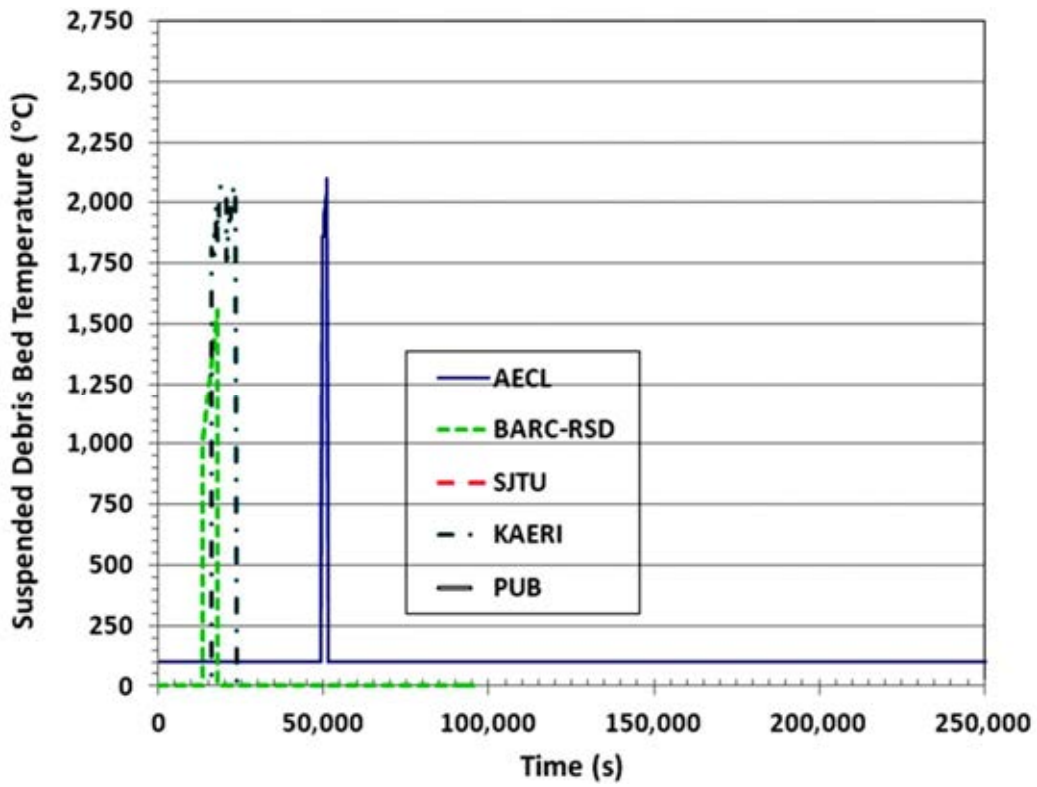


FIG. 4.25. The temperature of the suspended debris bed.

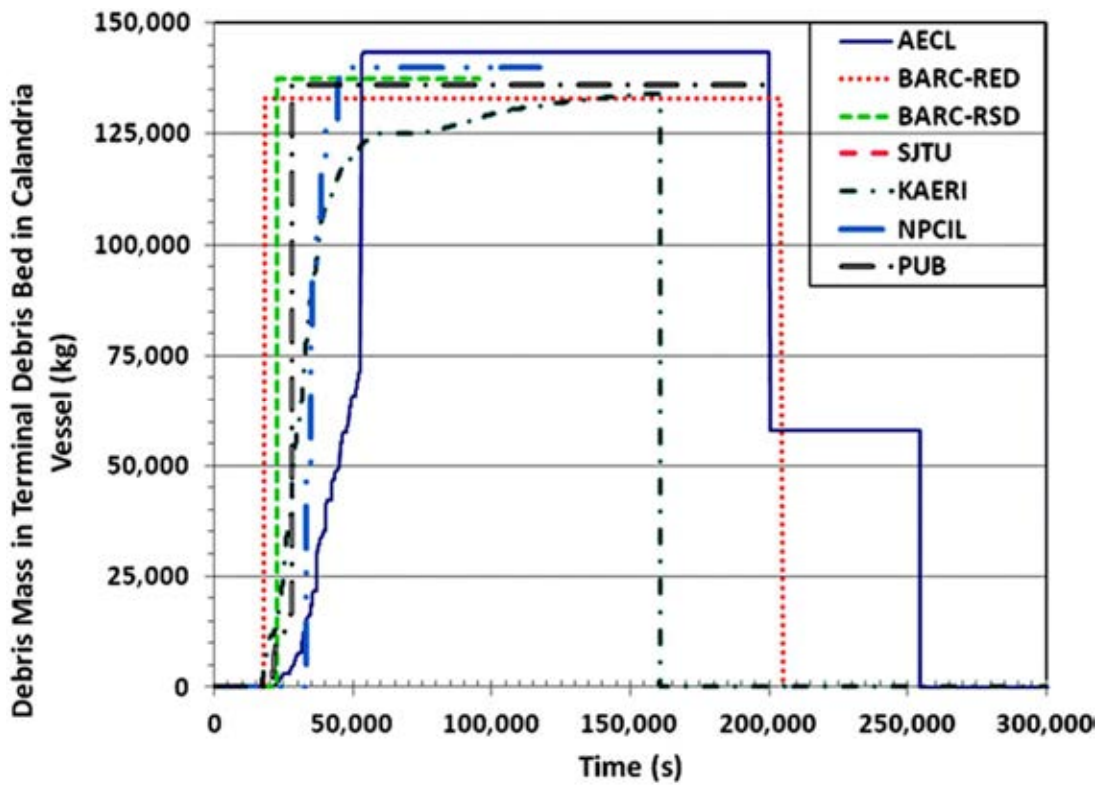


FIG. 4.26. The corium mass in the terminal debris bed.

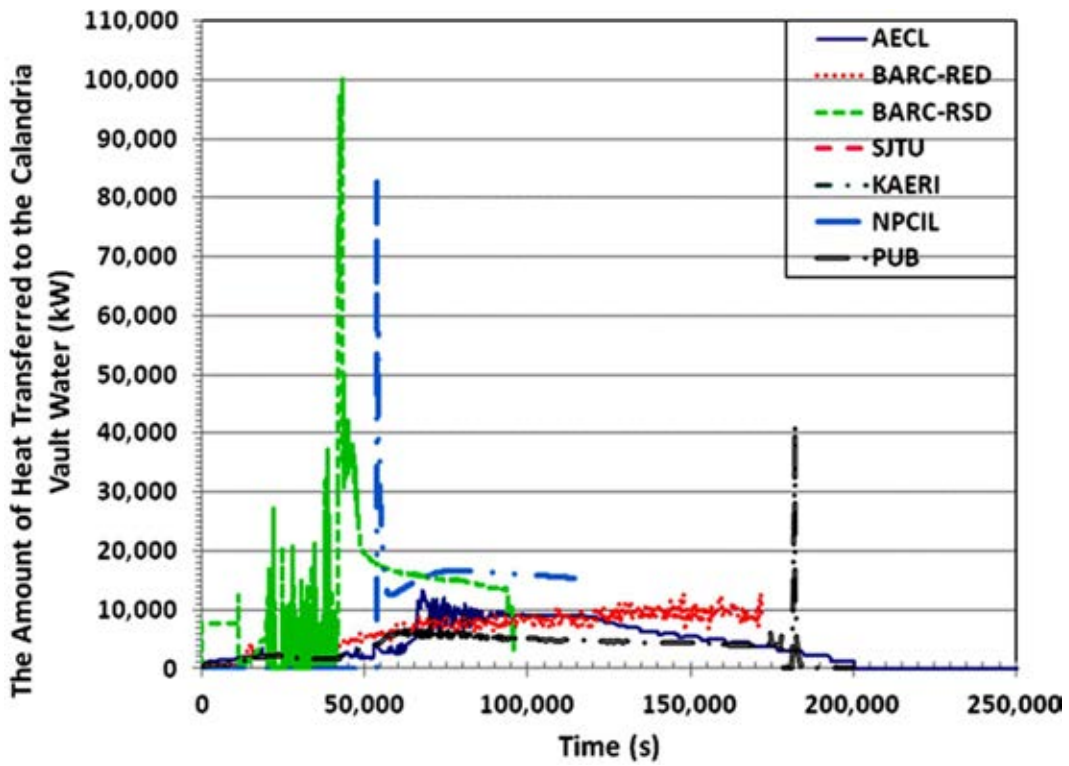


FIG. 4.27. The calculated rate of heat transfer to the calandria vault water.

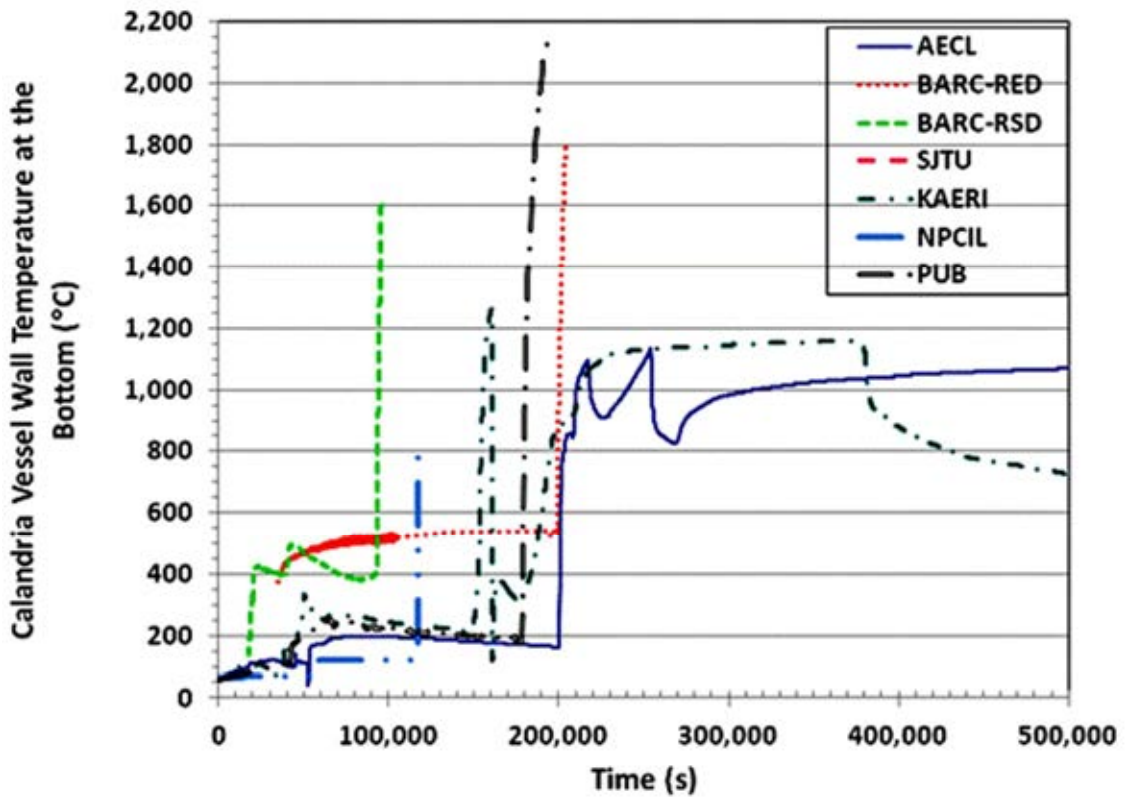


FIG. 4.28. The calculated calandria vessel wall temperature.

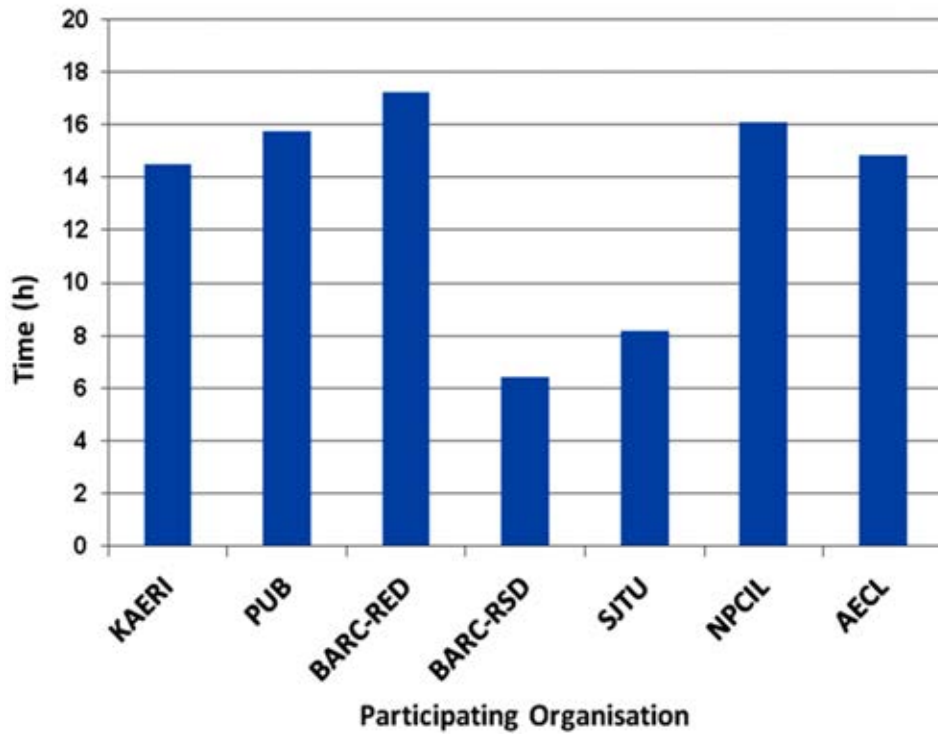


FIG. 4.29. The time when calandria vault water reaches saturation calculated by severe accident codes.

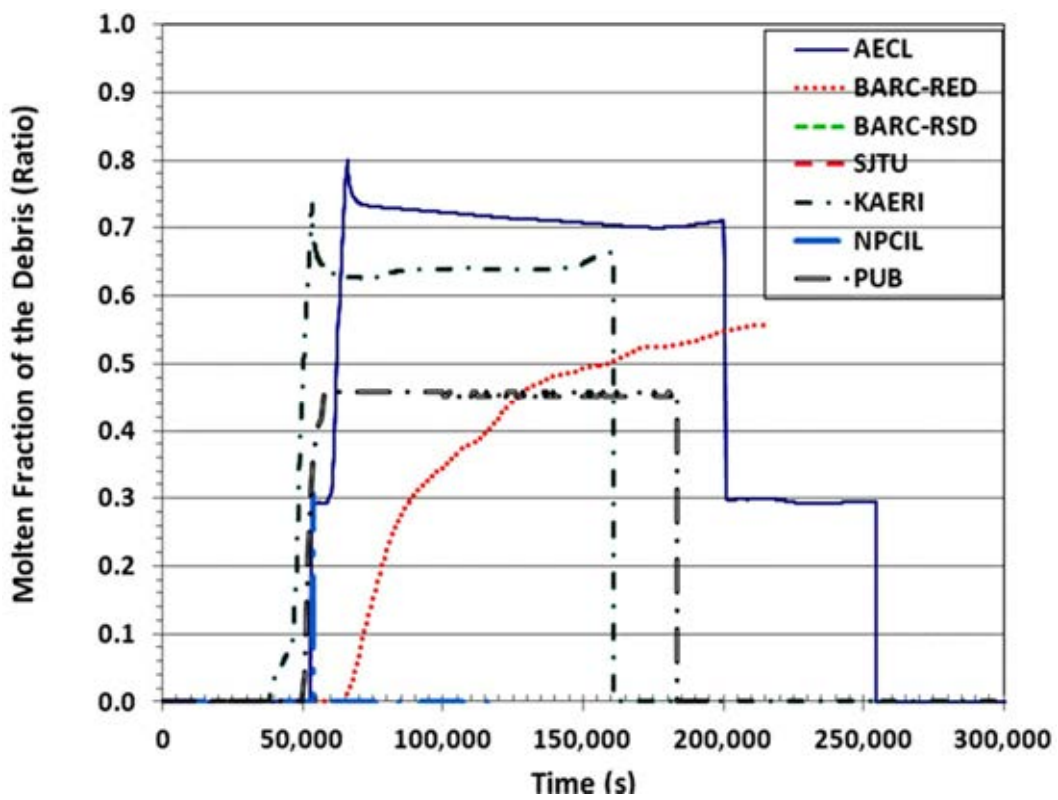


FIG. 4.30. A comparison of the calculated molten fraction of the debris.

#### 4.5. CONTAINMENT SYSTEM BEHAVIOUR

The containment pressure is expected to increase gradually as the water is discharged into the containment through the PHTS liquid relief valves. A rapid increase to containment pressure occurs when pressure tubes and calandria tubes rupture; and the PHTS coolant is released, first to the calandria vessel and then to the containment through the calandria-vessel-rupture disks. The containment pressure decreases following pressurization due to steam condensation on the containment walls and structures such as steel beams, columns, stairs, etc. which are relatively cold during the initial period of the accident. A rapid increase of containment pressure can be expected if corium relocates to the basement after the reactor vault failure.

A comparison of the containment pressure calculated by the participating organizations is shown in Figure 4-31. The variation in the predicted containment response is large. This can be attributed to the variation in the rate of steam discharge into the containment during accident progression. AECL, KAERI and PUB predicted sudden containment pressure increase after the failure of pressure tube and calandria tube. The pressure subsequently decreases due to wall condensation in AECL, BARC-RSD, KAERI, and SJTU calculations. The containment pressure increases to 328 kPa at ~100,000 s in SJTU, NPCIL, KAERI and BARC-RED calculations. The calculation by BARC-RED shows a sharp containment pressure drop to about 180 kPa at approximately 114,000 s. The calculation by PUB, KAERI, and AECL show a secondary pressure increase around 200,000 s due to corium relocation to the reactor vault after calandria vessel failure. The corium relocation time is related to the calandria vault water level shown by Figure 4-32. The rate of water depletion in the calandria vault is consistent among AECL, BARC-RSD, BARC-RED, SJTU, PUB, NPCIL, and KAERI, whereas only the initial depletion rate up to 51,000 s, calculated by BARC-RSD, was in agreement with the other calculations. In KAERI's simulation another pressure spike occurs at ~380,000 s (Fig. 4-31). This spike is due to calandria vault failure which creates a rapid pressure increase.

Figure 4-33 compares the failure times of containment equipment airlock seal among participating organizations. The variation in the predicted failure time is approximately five times among the participating organizations. The containment equipment airlock seal failure predicted by AECL is the lowest among all participating organizations. In NPCIL and PUB simulations, the estimated containment equipment airlock seal failure time coincides with the calandria vessel failure time, whereas in all of the other simulations the containment equipment airlock seal failures were related to steam generation from the reactor vault water.

The concrete ablation during molten core concrete interaction is shown in Figure 4-34. SJTU and PUB did not estimate concrete ablation in their analyses. The slope of the curves representing the ablation rate is approximately equal for BARC-RSD, BARC-RED, KAERI and AECL, although starting times are significantly different. The ablation rate of NPCIL is significantly different from others. The differences are perhaps due to the methods used in defining concrete ablation. For example, AECL and KAERI used the melting temperature of concrete as ablation criteria, whereas BARC-RSD used ASTEC code estimate of concrete ablation. NPCIL used dehydration phenomena as ablation criteria.

The total amount of hydrogen accumulation during in-vessel and ex-calandria vessel is shown in Figure 4-35. The amount of hydrogen generated varied by a significant amount between 79 kg (SJTU) and 2400 kg (KAERI). The total amount of hydrogen differs mainly due to oxidation models used in the fuel channels, core disassembly, slumping, debris cooling and core-concrete interaction stages. The total amount of hydrogen generated is compared in Figure 4-36. The SJTU and PUB did not calculate ex-vessel hydrogen generation as this feature is not available in their codes. The total hydrogen calculated by KAERI, BARC-RSD and AECL are consistent. In NPCIL's calculation, as seen in Figure 4-21, hydrogen

generation is continued in core as well as when the debris are at the bottom of the calandria. NPCIL has predicted calandria vault failure at 191,000 s (53 h) and after that no further hydrogen generation is considered inside the calandria vessel. The amount of hydrogen calculated by BARC-RED is somewhat in between the two extremes described above.

The volume concentration of hydrogen and steam in the containment atmosphere are shown in Figs 4-37 and 4-38. Not all participating organizations provided the transient concentration of hydrogen and steam in the containment for comparison. Among those participating organizations who provided the calculated data, there were significant variation in time and magnitude. Typically the hydrogen concentration remained below 23% for KAERI, BARC-RSD, BARC-RED, NPCIL and AECL. The hydrogen concentration beyond approximately 230,000 s was not provided by NPCIL, BARC-RED and BARC-RSD. The high steam concentration (around 100%) was not coincident with high hydrogen concentrations predicted by AECL and KAERI, leading to the potential for hydrogen detonation. In case of BARC-RSD simulations, the steam concentration decreased from about 90% as the hydrogen concentration increased from approximately 4% to 23%.

The calculated containment gas temperature is shown in Figure 4-39. All of the calculations show a gradual increase to the containment temperature as expected during a station blackout sequence. Both AECL and KAERI predictions show similar trends. The calculations provided by NPCIL, PUB, BARC-RED, and BARC-RSD do not extend to 500,000 s. The peak gas temperature predicted by PUB occurs earlier than KAERI and AECL predictions by about 130,000 s and 170,000 s, respectively. BARC-RED calculations indicate a drop in containment gas temperature at 200,000 s while AECL calculation shows an increase in gas temperature at the same time. The importance of such small differences in timing and magnitude is not understood, however, they can be attributed to the differences in the models used in calculating phenomena that controls gas temperature in the containment.

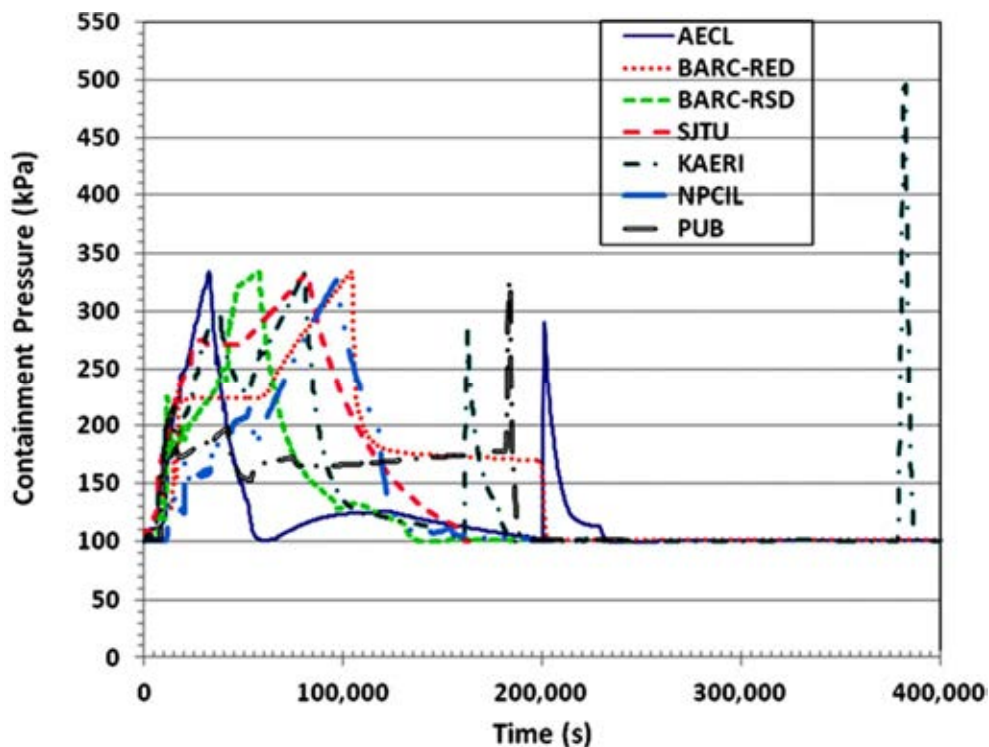


FIG. 4.31. The transient containment pressure calculated by the participating organizations.

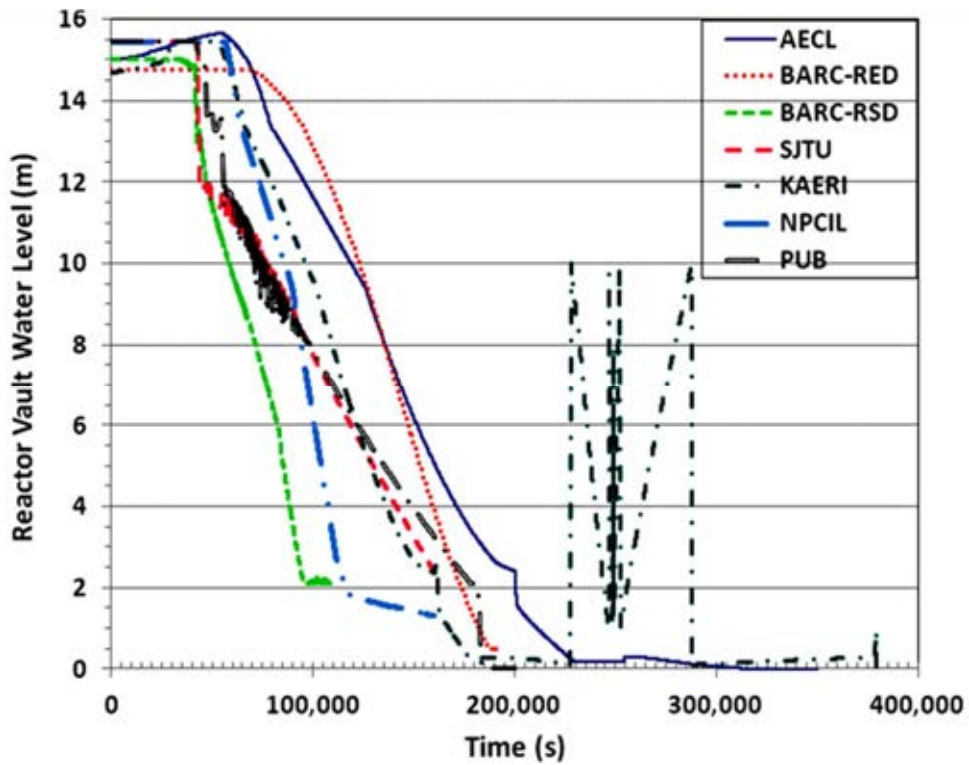


FIG. 4.32. The reactor vault water level calculated in the station blackout simulations.

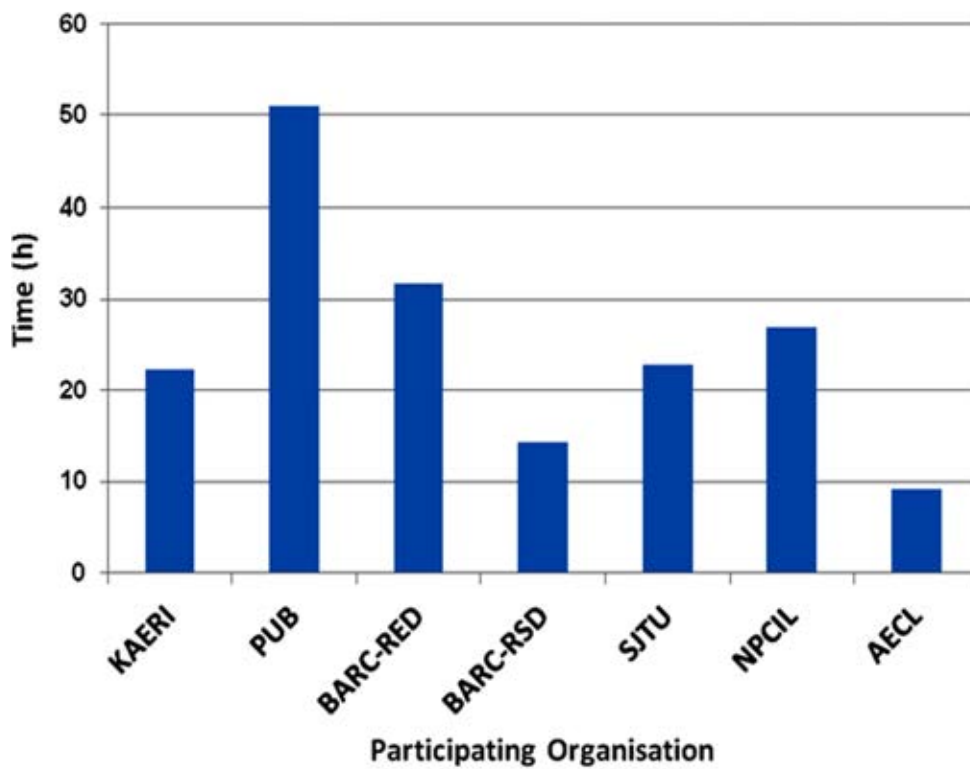


FIG. 4.33. Timing of containment equipment airlock seal failure.

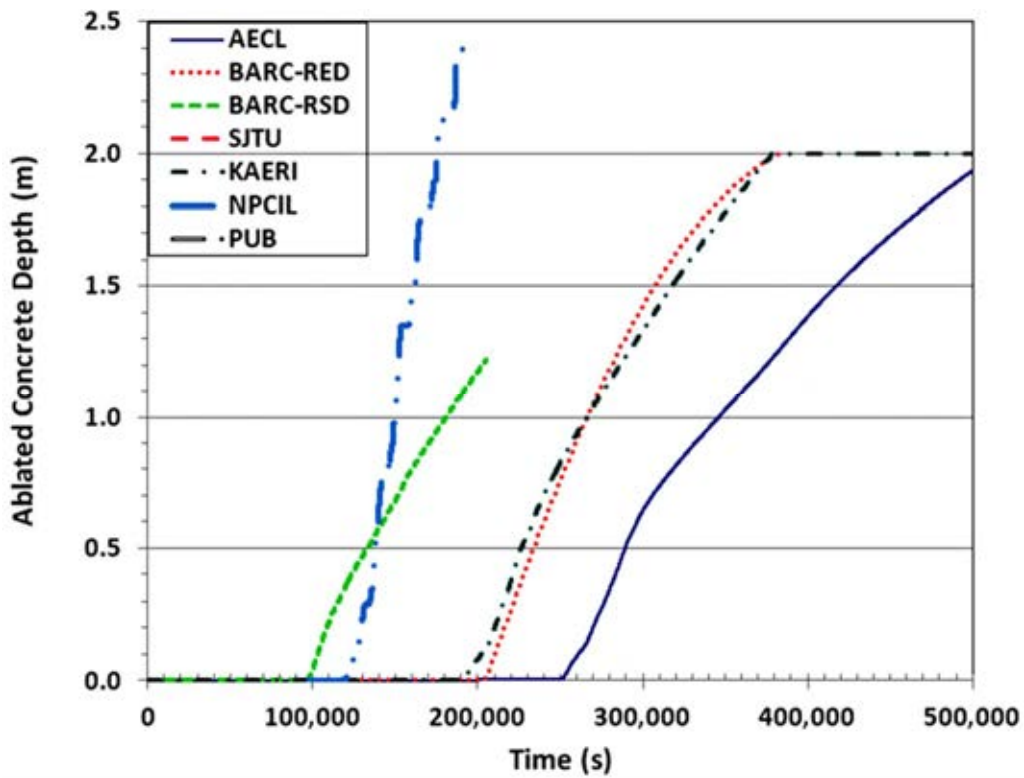


FIG. 4.34. The ablated concrete depth calculated by participating organizations following molten core concrete interaction.

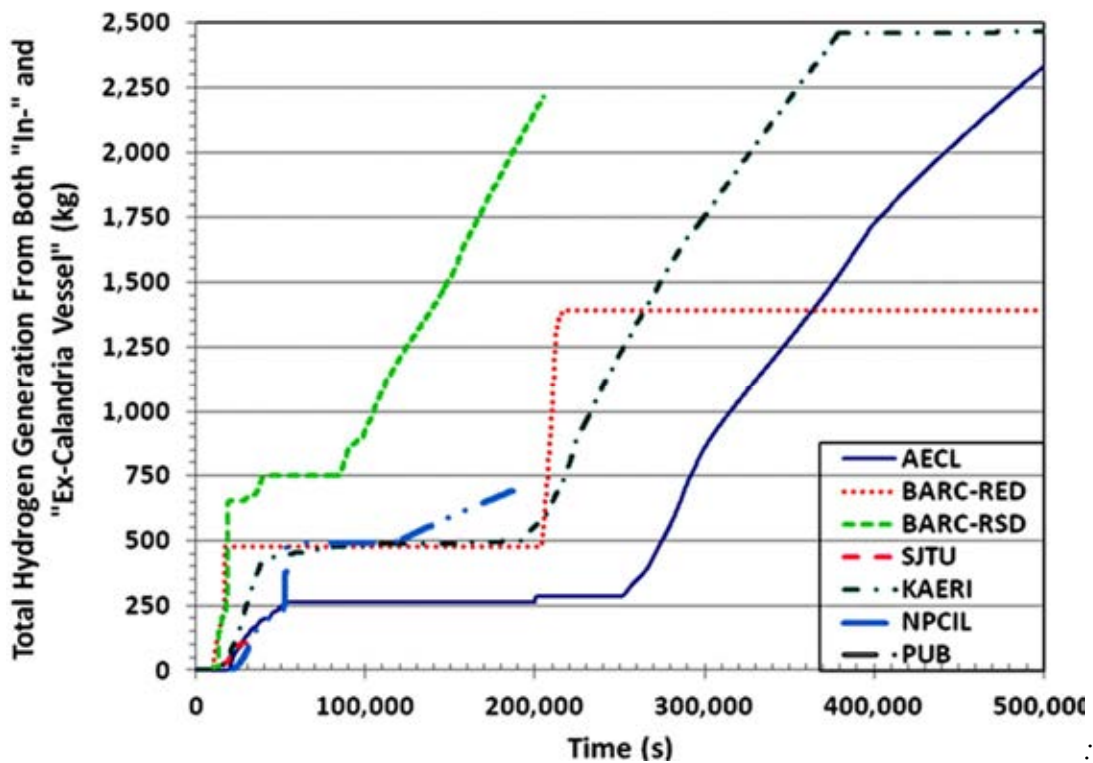


FIG. 4.35. The amount of hydrogen generation both from in- and ex-calandria vessel.

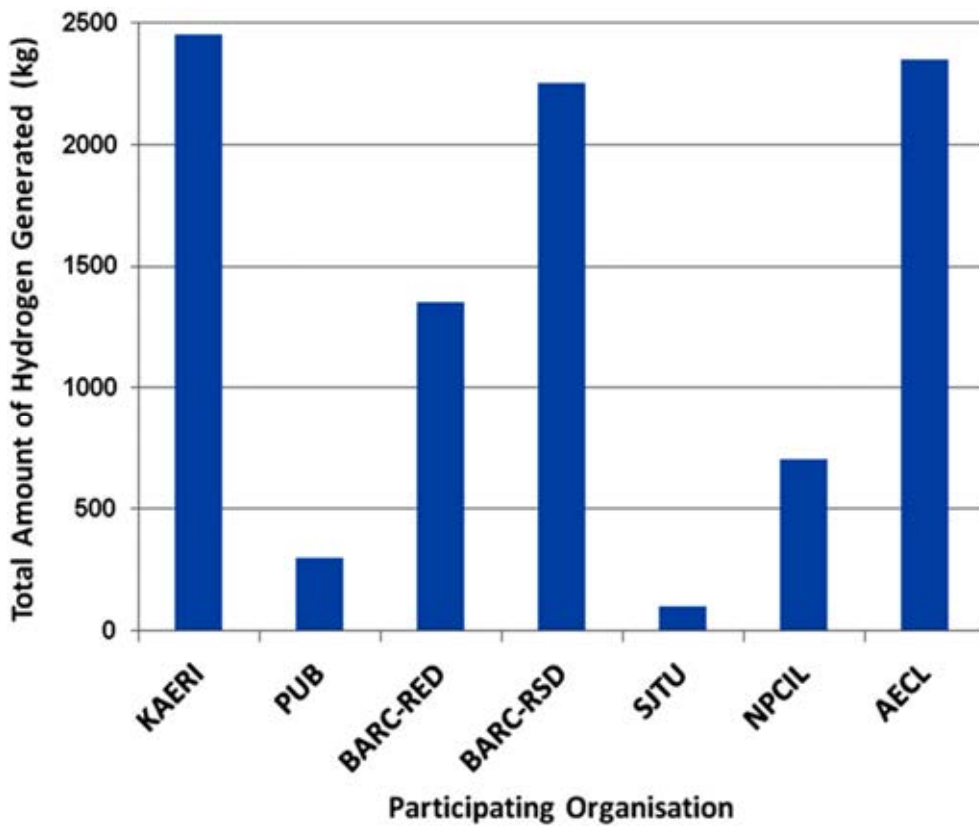


FIG. 4.36. Total amount of hydrogen generated during accident.

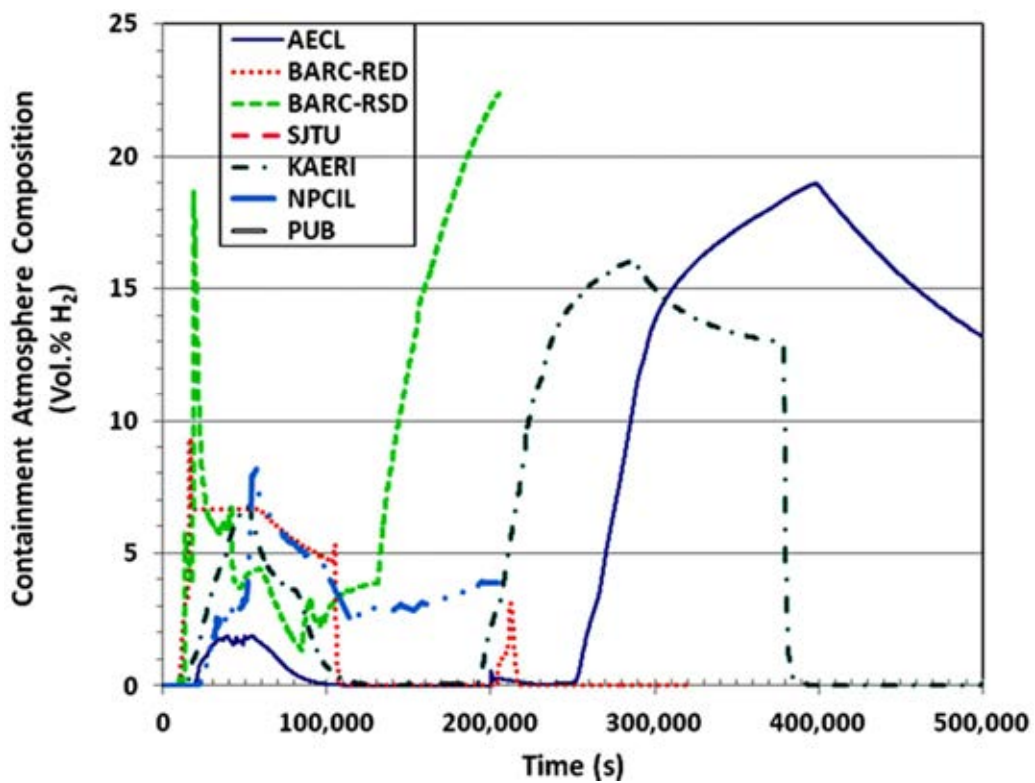


FIG. 4.37. The percent volume of hydrogen in the containment atmosphere calculated by the participating organizations.

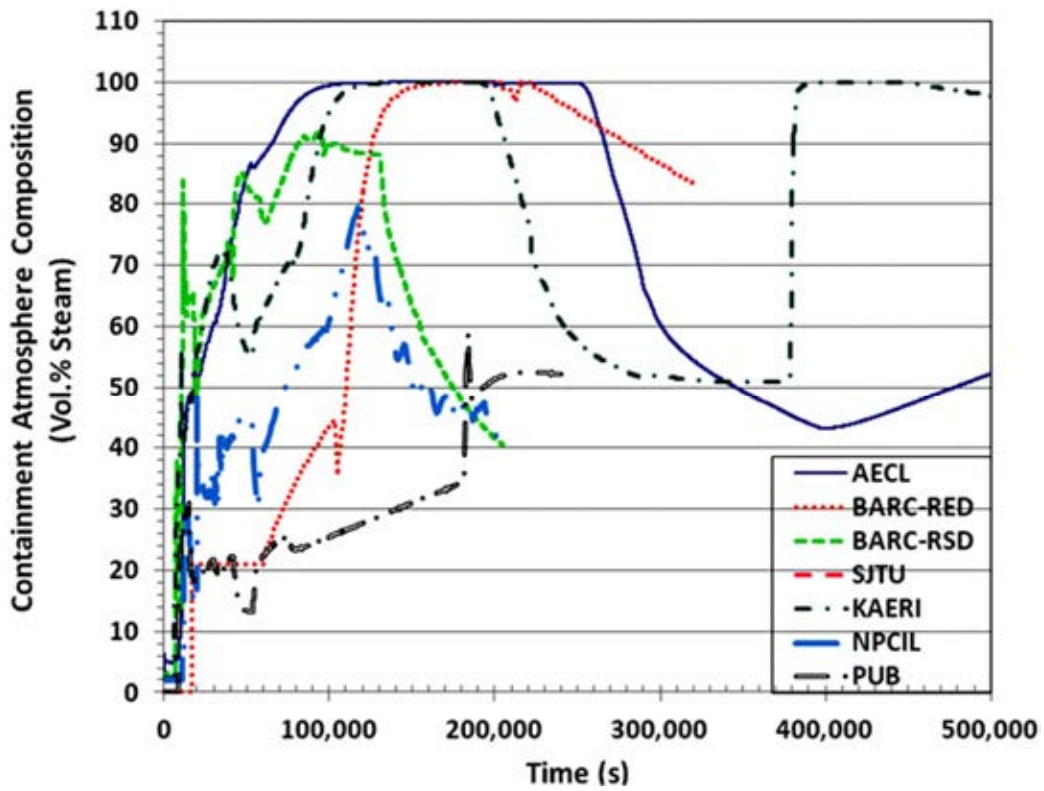


FIG. 4.38. The percent volume of steam in the containment atmosphere.

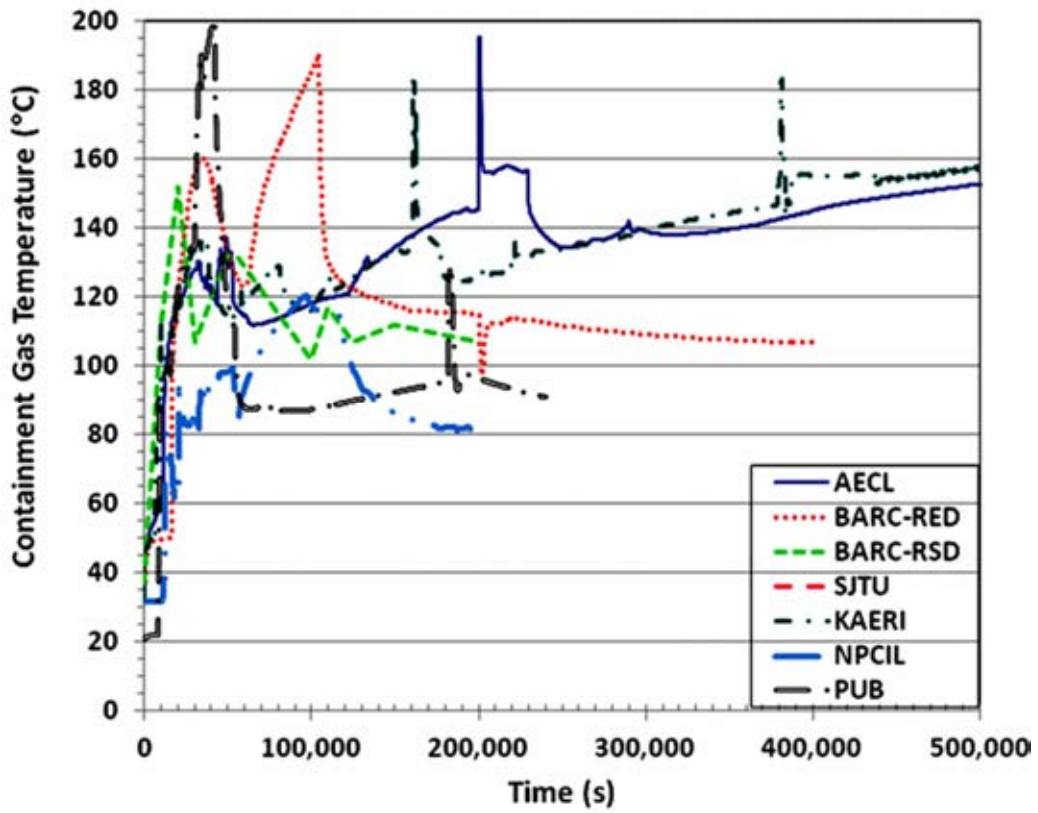


FIG. 4.39. The Containment gas temperature calculated by the participating organizations.

#### 4.6. FISSION PRODUCTS BEHAVIOUR

The escalation of fuel element temperatures would eventually lead to fuel sheath failure and fission product releases to the PHTS. Some of the fission products released would be deposited in the PHTS, depending on a number of factors such as chemical species, agglomeration, adsorption, and deposition, etc. Additional fission product releases occur during core disassembly and heat up of suspended debris. During core collapse, the release of fission products would stop temporarily when the debris is submerged in water. The steam discharged from the calandria vessel usually carries fission products into the containment. The amount of fission products in the primary heat transport system, as a percent of the total fuel inventory, is shown in Figure 4-40. The calculations by AECL and PUB agree reasonably well while the amount calculated by BARC-RSD is slightly lower.

The amount of CsI calculated at the containment boundary by participating organizations is shown in Figure 4-41. The amounts calculated show quite significant variation. The total amount of Cesium Iodide (CsI) released to the environment during the accident is shown in Figure 4-42. The releases to the environment calculated by PUB, BARC-RSD, NPCIL, KAERI, and AECL varied by an order of magnitude. The lowest amount of release was calculated by KAERI and the highest value was calculated by PUB. While KAERI expects very small release of CsI to the environment, the amount calculated by PUB is the sum of Cs and iodine hence it appears as significantly higher than others. The variation of CsI release can be attributed to the use of different retention mechanisms. In this analysis, BARC-RED and SJTU did not provide CsI estimates.

The amount of noble gas released inside the containment is shown in Figure 4-43. The amounts predicted has significant variations, however, AECL, NPCIL, KAERI, and BARC-RSD values are somewhat closer after 200,000 s. These final noble gas released to the environment, calculated by KAERI, BARC-RSD, NPCIL, and AECL, are very close, as shown in Figure 4-44. The amount calculated by PUB is somewhat lower than the others. The low value of noble gas release may have been due to the delayed containment failure. The codes used by PUB, BARC-RED, and SJTU did not calculate ex-vessel fission product release and therefore they did not provide either because there was no noble gases or the values were low, when calculations were performed.

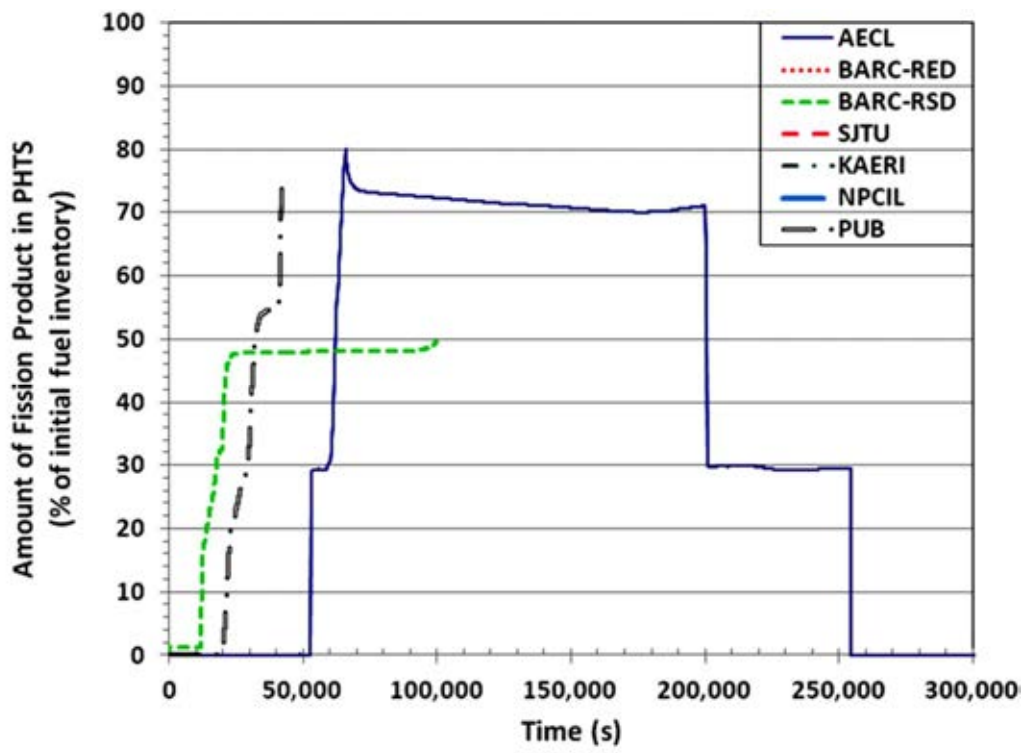


FIG. 4.40. The amount of fission products calculated in the primary heat transport system.

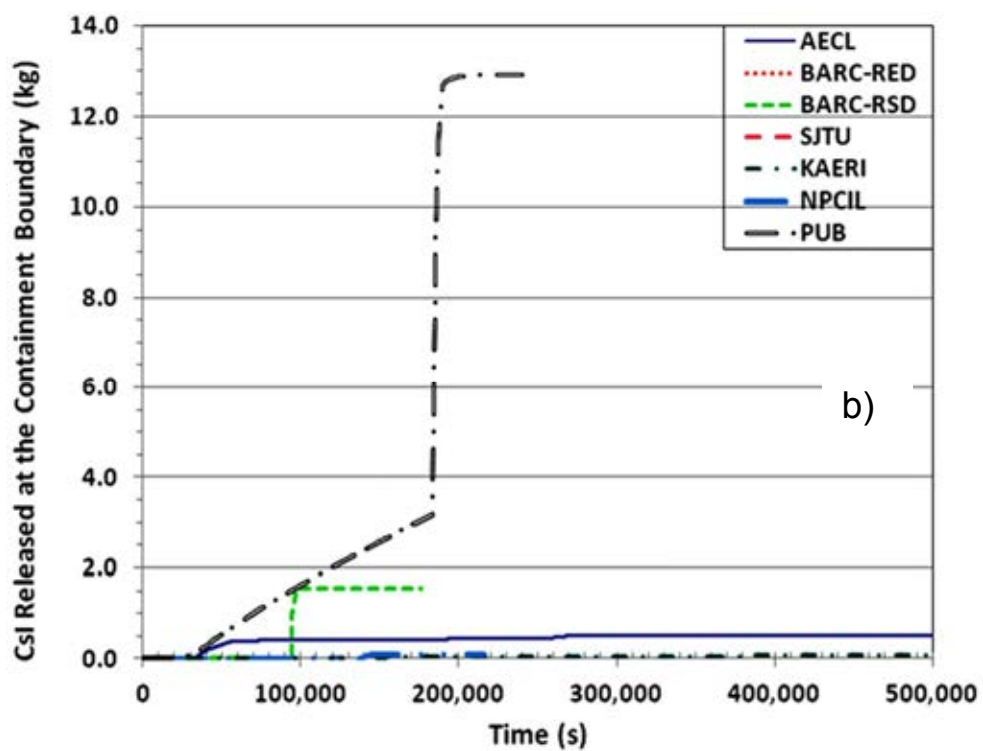
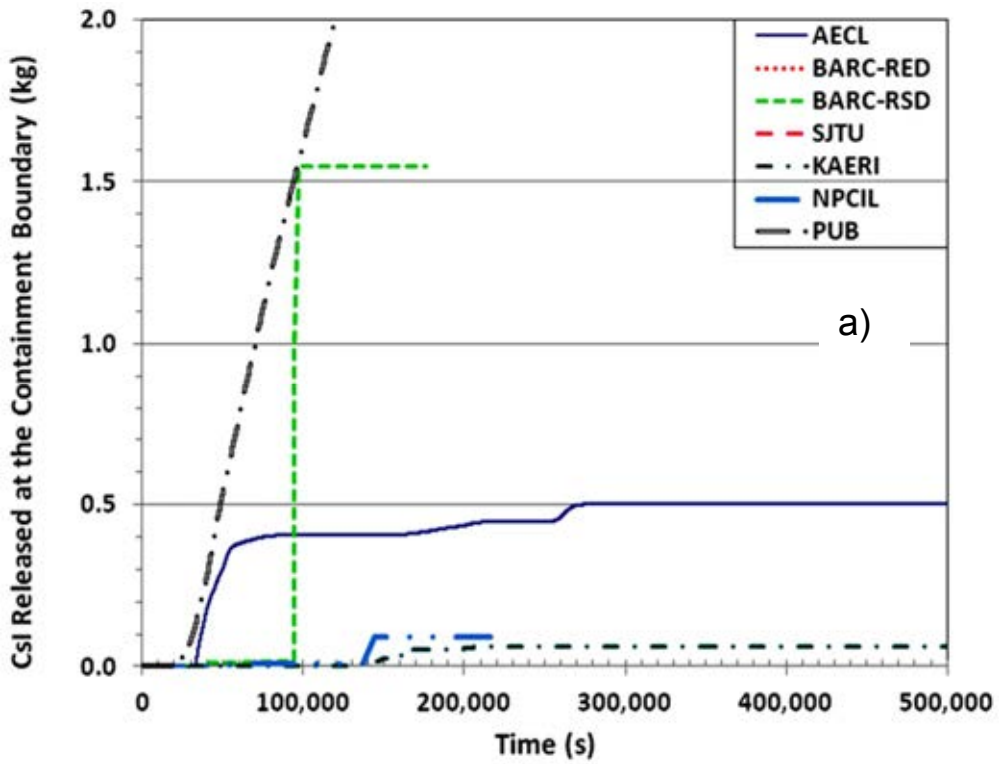


FIG. 4.41. The calculated amount of CsI released at the containment boundary a) low range and b) high range.

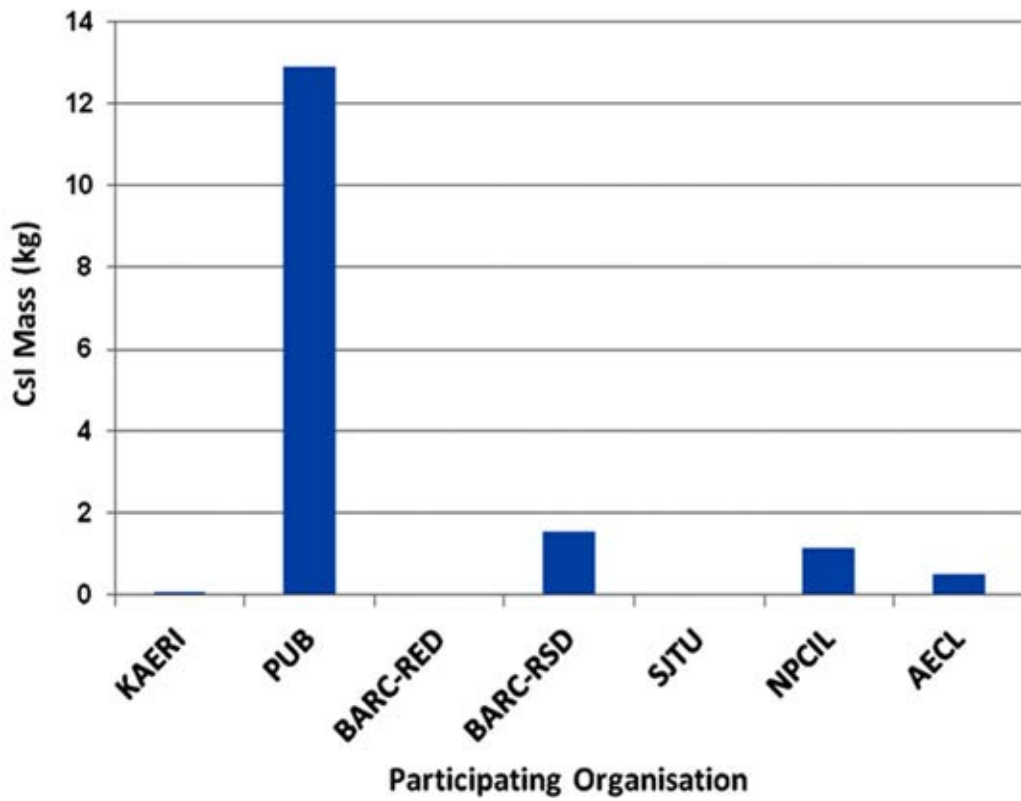


FIG. 4.42. Total amount of CsI released to environment during the accident.

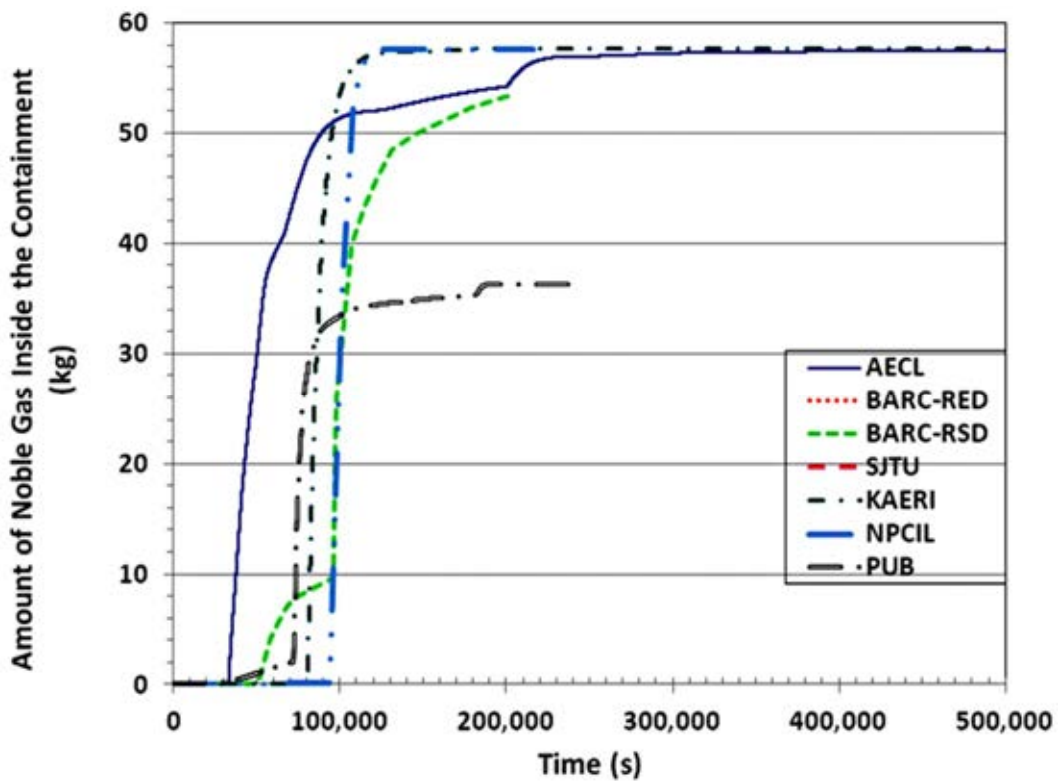


FIG. 4.43. The amount of noble gas released to the containment.



FIG .4.44. Total amount of noble gases release to environment.

## 5. LESSONS LEARNED

In general the Coordinated Research Project on benchmarking severe accident computer codes for pressurized heavy water reactor applications gave an extensive and valuable outlook on status of code performance because:

- Several different codes were compared amongst each other, and;
- Different users using the same code provided a measure of user effects.

There were seven different participating organizations in the benchmarking study who used four different sets of severe accident analysis codes. Three of the codes had single users and one code had three users, which provided some information on user effects. The following code suites were used to perform the consequence analysis of station blackout sequence in a CANDU 6 nuclear power plant:

- AECL – MAAP4-CANDU v4.0.6A;
- BARC-RED – RELAP5 Mod 3.2, ANSWER, CAST3M, MELCOOL;
- BARC-RSD – SCADAP/RELAP5 Mod 3.2, PHTACT, ASTEC;
- NPCIL – ATMICA.T, CONTACT, SEVAX, PACSR/STAR, ACTREL;
- KAERI – ISAAC 4.02;
- PUB – SCDAPSIM/RELAP5 Mod 3.4;
- SJTU – SCADAP/ RELAP5 Mod 3.4.

Most of the participating organizations initialized their codes very well based on the CANDU 6 plant parameters and input data provided, however, there were some rare instances for which not all input conditions were met in their entirety, perhaps due to code limitations that required a work around. The code limitations and the work around used are known to the users alone and therefore the comparisons and the observations provided in this document should be used for self guidance, reflection, and improvement of the codes.

Except for a very limited number of codes (MAAP4-CANDU and ISSAC), the current status of some severe accident analysis codes is far from being able to cover the entire spectrum of the severe accident sequence required to predict the consequences of an accident. The benchmarking exercise therefore focused on carefully selected items to identify gaps.

The role of nodalization remains a major area not covered in this benchmarking study, however, the decisions to choose an appropriate nodalization scheme was left with the code users, to ensure they are sufficiently tested for establishing grid independence with appropriate node density required for the problem. Oscillations in some analyses cases likely points to convergence issues.

The station blackout sequence proceeded thorough distinct stages involving increasingly more complex phenomena and these stages were used for the assessment of the code capabilities. Five distinct stages of the sequence were compared using the average of the timing of an event reported by participating organizations and the standard deviation of the spread for that event. The selected stages in ascending degree of complexity, the average timing of the event ( $\mu$ ) and the standard deviations ( $\sigma$ ) for the event are given below:

- Steam generator secondary side dryout;  $\mu = 2.1$  h,  $\sigma = 0.4$  h;
- Moderator reaching saturation temperature;  $\mu = 3.9$  h,  $\sigma = 1.0$  h;
- Moderator in the calandria vessel becoming dry;  $\mu = 11.4$  h,  $\sigma = 2.2$  h;
- Calandria vault water reaches saturation temperature;  $\mu = 13.3$  h,  $\sigma = 4.2$  h;
- Containment failed  $\mu = 26.9$  h,  $\sigma = 14.2$  h, and;

- Calandria vessel failure;  $\mu = 45.7$  h,  $\sigma = 11.4$  h.

A comparison of the five stages is shown in Figure 5-1 and it is apparent that the calculated timing has less dispersion between participating organizations during the early stages of the sequence when the severe accident phenomena are relatively less complex. The phenomena and the processes related to Phase 1, i.e., accident initiation to start of fuel channel uncover - the rupture disk failure, require no special severe accident models. When complexity increases towards core disassembly and corium vessel interactions, the agreement among the predicted results is poor and more divergent (i.e., increasing standard deviation). This observation is indicative of the need to improve the models, additional experiments to understand phenomena, and validation of the models with experiments.

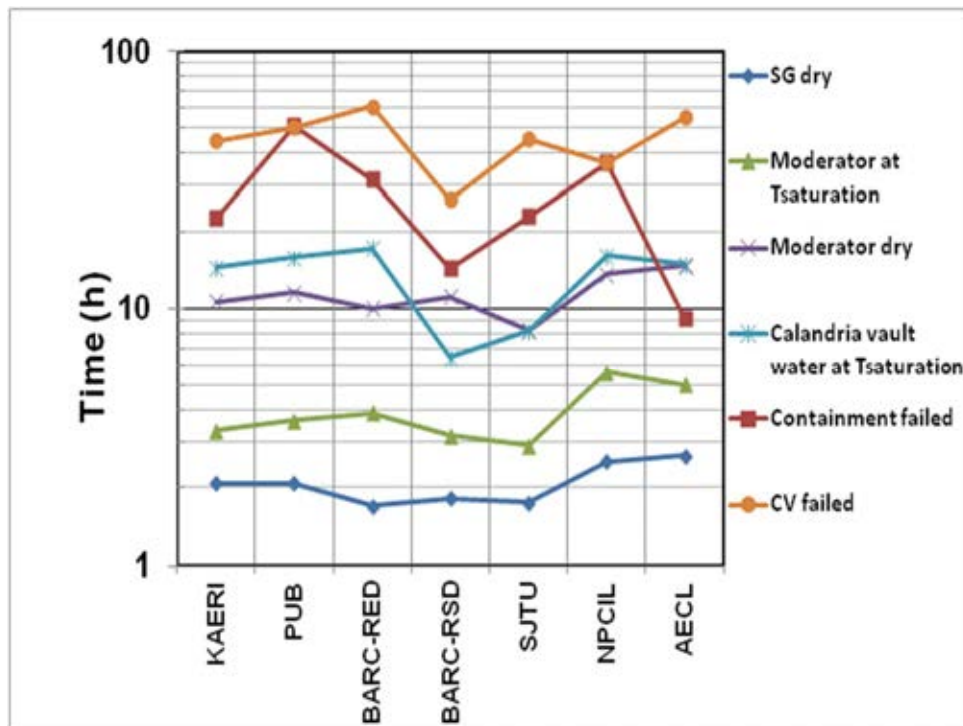


FIG. 5.1. A comparison of different stages of the station blackout sequence with increasing complexity.

The average and the standard deviations provided above is intended only to illustrate the point that the agreement among the codes used in the benchmarking analysis was diverging during the late stages of the sequence where the phenomena are more complex and the temperatures are extreme. The context of the numbers used is to qualitatively illustrate that the divergence of the results requires additional review. These numbers taken alone are misleading and therefore the context of the numbers is important. Without the context the numbers are meaningless.

The failure criteria can alter the predicted behaviour, and they require experimental validation to improve confidence in the simulation. The failure criteria were not consistently used by all participating organizations. In some codes, some of the failure criteria could not be used. The influence of the failure criteria was not studied. An assessment of the failure criteria and their justifications will benefit code users.

In some accident analysis codes not all of the capabilities required to perform an analysis were present. In these cases, a set of multiple codes simulating several complex and dominant phenomena was used in the simulation at various stages of the sequence. An output from one

code was used as input to another code, which is not very conducive to the robustness of the analysis. In some cases, the representation of the average channel in the code was difficult and core disassembly was found to be more difficult to predict with channel disassembly occurring in stages rather than the total mass of the channel slumping in the calandria vessel.

The expulsion of moderator due to OPRD rupture is sensitive to the Cover Gas System parameters. Hence it is preferable to have cover gas system details with connecting line lengths so that an accurate prediction of loss of moderator during OPRD rupture can be made, and subsequent boil-off times can be predicted with better accuracy.

In some codes, significant challenges were encountered in modelling core collapses inside the calandria vessel bottom, terminal debris transformation to molten pool and containment thermohydraulics behaviour. The limitations handicapped these users and may have contributed to the divergence of calculated event timings. Improved core disassembly, core collapse, and containment behaviour models are required in these codes to improve the confidence in the predictions.

The ultimate objective of severe accident consequence analysis is to predict the dose to public from a postulated severe accident. To satisfy this requirement the severe accident codes should have the capability to estimate the hydrogen produced, noble gas release and the airborne CsI content within the containment boundary and the estimated release to the environment, if containment integrity is compromised. As can be seen from Section 4.6 and Figures 4-40 through 4-44 not all participating organizations were able to estimate the fission product release and hydrogen generation in the analyses. From the few that produced the estimates, the variations were quite large. The phenomena leading to fission products release are quite complex, nevertheless a concerted effort is required to improve the understanding of the behaviour and improve modelling capabilities.

During the initial stages of the accident the in-vessel hydrogen generation predicted by the participating organizations ranged between 100 kg and 450 kg with the average being 250 kg, whereas with ex-vessel hydrogen generation, the range was between 860 kg and 2,070 kg with the average being 1,290 kg. The main reason for the variation in the predictions is modelling assumptions such as the surface area exposed to steam in the PHTS, suspended debris bed and terminal debris bed to calculate the exothermic Zircaloy steam reaction. An enhancement of models and improved code capabilities to calculate hydrogen production during severe accidents are required.

## 6. CONCLUSIONS AND RECOMMENDATIONS

A Coordinated Research Project (CRP) was completed to benchmark computer codes used for consequence analysis of severe accidents at HWRs. The purpose of the benchmark was to compare the integrated effects of embedded models in the codes, gain an understanding of their limitations, assess the level of uncertainties, and increase the confidence in severe accident code predictions. The exercise promoted international collaboration among IAEA Member States to improve the phenomenological understanding and analysis capability of severe core damage accidents. The scope included the identification and selection of a severe accident sequence, selection of appropriate geometrical and boundary conditions, and conducting benchmark analyses, comparing the results of all code outputs, evaluating the capabilities of existing computer codes to predict important severe accident phenomena, and suggesting necessary code improvements and/or new experiments to reduce uncertainties.

The severe accident benchmarking provided an opportunity to test the accuracy of energy balances among the analyses. A comparison of the rate of boiloff of steam generator secondary side coolant among the seven simulations revealed consistent amount of heat removal. The agreement in the rate of liquid boiloff captured the decay power generation and a large number of associated phenomena involved in transferring the nuclear heat from the fuel to the steam generator secondary side water through a convoluted path involving heat and mass transfer.

The rate of moderator boil off was predicted by seven participating organizations; however, the reasonable agreement of the slopes of the seven analyses provides another cautious benchmarking of all processes from the decay heat generated by the fuel to moderator boiloff within the analyses codes.

The calculated timing of events was more consistent among the seven analyses during the early stages of the sequence when the severe accident phenomena are relatively less complex. In this respect, the phenomena and the processes related to primary heat transport system and steam generator response required no special severe accident models. When complexity of the phenomena increased towards core disassembly and corium-vessel interactions, the agreement among the predicted results was more divergent from the mean and the standard deviation increased. This observation is indicative of the need to improve the models, to conduct additional experiments to understand phenomena, and validation of the models in the core disassembly phase of the severe accident to molten core concrete interaction leading to severe challenge to containment integrity.

### **Recommendations for future activities**

- The coordinated research project identified that there was good agreement on timing of predicted events among participating organizations at the less complex, early stages of the sequence, whereas the processes involving more complex latter stages of the sequence had poor agreement. More complex phenomena like core disassembly, debris oxidation, and corium-vessel interactions require further research to improve the understanding. As a first step towards initiating such a research program a detailed investigation of why severe accident codes differed in their timing of events is required. The reason why the predicted timings were in poor agreement could be due to the use of inconsistent initial and boundary conditions or internal bugs in the implementation of the models in the code, Although the coordinated research project made every effort to eliminate input differences, the details of how code inputs are handled within the code was not verified. The verification that the variation of the event timings was not due to inconsistent input conditions or bugs in the codes is required;

- Porosity and its distribution in the debris bed (suspended and terminal) were not consistent among the various codes used in the CRP. A collection of the current values used by CRP participating organizations and a survey of the modelling of this phenomenon in LWR analyses is useful to further the understanding. In particular it can affect the overall corium relocation behaviour as well as hydrogen generation rate from the calandria vessel. Following a systematic study of the use and the physical analysis basis of the porosity numbers used by the participating organizations, a sensitivity analysis is required to determine the effect of porosity in the range of 0.2 to 0.5. A rigorous definition of the porosity and why is it used in the analysis is required;
- The mechanism of steam generation after calandria vessel failure requires an improved understanding as this would have an effect on the predicted containment pressure at the latter stages of the accident sequence;
- The core collapse and disassembly modelling requires additional research and improved understanding. The current approaches followed in the various severe accident codes require documentation along with the rationale for the approaches. One of the approaches involve column-wise failure based on the load from seven channels stacked on top of a channel that results in the shearing of the supporting channel. Another approach is using the  $ZrO_2$  melting temperature;
- The oxidation of debris under different configurations (suspended and terminal debris bed) controls the amount of hydrogen generation. The installation of passive autocatalytic recombiners and hydrogen burners are dependent on these assessments and therefore how steam availability to a complex geometry like the suspended debris influences hydrogen generation requires additional research and improved understanding;
- The rupture area of the fuel channel that ruptures first by initial fuel heat-up requires additional experimental verification and assessment. Various assumptions are implemented in the severe accident codes and these assumptions require a systematic sensitivity analysis to determine the implications. The sensitivity analysis may be performed by changing the break area and calculating the dynamic pressure on the calandria vessel wall, PHTS pressure, and inventories of PHTS and calandria vessel. The sensitivity assessment may be completed with 1 to 20 channel ruptures with an increment of 5 channels;
- The behaviour of the calandria vessel while the molten pool is formed requires understanding and experimental data;
- The rate and species of fission product release from the terminal debris bed requires additional understanding as this would have an effect on the decay heat generation in the terminal debris bed;
- The end shield behaviour requires further understanding and experimental investigation.



## REFERENCES

- [1] MATHEW, P.M., NITHEANANDAN, T., and BUSHBY, S.J., Severe Core Damage Accident Progression within a CANDU 6 Calandria Vessel, ERMSAR Seminar, 3rd European Review Meeting on Severe Accident Research, Nesseber, Bulgaria (2008).
- [2] NITHEANANDAN, T., Severe Accident R&D for Enhanced CANDU 6 Reactors, Paper No. FA0050, The 18th Pacific Basin Nuclear Conference (PBNC 2012), BEXCO, Busan, South Korea (2012).
- [3] INTERNATIONAL ATOMIC ENERGY AGENCY, Analysis of Severe Accidents in Pressurized Heavy Water Reactors, IAEA-TECDOC-1594, IAEA, Vienna (2008).
- [4] ATOMIC ENERGY OF CANADA LTD., CANDU 6 Technical Summary, Reactor Development Business Unit, AECL (2005).
- [5] INTERNATIONAL ATOMIC ENERGY AGENCY, Heavy Water Reactors: Status and Projected Development, Technical Reports Series No.407, IAEA, Vienna (2002).
- [6] HILL, R., The Mathematical Theory of Plasticity, Oxford: Clarendon Press 317-325 (1950).
- [7] MENDELSON, A., Plasticity: Theory and Application, New York: MacMillan 100- 104 (1968).
- [8] AWADH, B. and PETOUKHOV, S.M., CANDU 6 Plant Parameters for Severe Accident Codes Comparative Analysis for the Coordinated Research Project (CRP NO. 1451), AECL Report 153-115380-440-006 (2010).
- [9] FAUSKE AND ASSOCIATES INC. AND OPG INC., MAAP4-CANDU - Modular Accident Analysis Program for CANDU Power Plant, Volumes 1-3 (1998).
- [10] ROGERS, J.T., MENELEY, D.A., BLAHNIK, C., SNELL, V.G., and NIJHAWAN, S., Coolability of Severely Degraded CANDU Cores, Heat and Mass Transfer in Severe Nuclear Reactors Accidents, Begell House Inc., New York, Wallingford, UK 317-334 (1996).
- [11] ROGERS, J.T. and LAMARI, M., Transient Melting and Re-Solidification of CANDU Core Debris in Severe Accidents, Proc. Canadian Nuclear Society Nuclear Simulation Symposium, Niagara-on-the-Lake (1997).
- [12] MENELEY, D.A., BLAHNIK, C., ROGERS, J.T, SNELL, V.G., and NIJHAWAN, S., Coolability of Severely Degraded CANDU Cores, AECL Report AECL-11110 (1996).
- [13] AWADH, B. and PETOUKHOV, S.M., CANDU 6 Plant Parameters for Severe Accident Codes Comparative Analysis for the Coordinated Research Project (CRP # 1451), AECL Report, 153-115380-440-006 (2010).
- [14] NUCLEAR REGULATORY COMMISSION, NUREG/CR-5535, INEL-95/0174, RELAP5/Mod3.2 Code Manual, Washington DC (1995).
- [15] SINHA, R., NAYAK, A.K., and SEHGAL, B.R., Modeling the Natural Convection Heat Transfer and Dryout Heat Flux in a Porous Debris Bed, Journal of Heat Transfer 130 ,104503-1 to 104503-4 (2008)
- [16] DUREJA, A.K., SINHA, S.K., SRIVASTAVA, A., SINHA, R.K., CHAKRAVARTTY, J.K., SESHU, P., and PAWASKAR, D.N., Flow behaviour of autoclaved, 20% cold worked, Zr-2.5Nb alloy pressure tube material in the temperature range of room temperature to 800 °C, Journal of Nuclear Materials 412 22-29 (2011)
- [17] CHABOCHE, J.L., Anisotropic Creep Damage in the Framework of Continuum Damage Mechanics, Nuclear Engineering and Design 79 309-319 (1984).
- [18] GERA, B., KUMAR, M., THANGAMANI, I., PRASAD, H., SRIVASTAVA, A., MAJUMDAR, P., ANUDUTTA, V., VERMA, S., GANJU, B., CHATTERJEE, H.G., LELE, V., RAO V.S.S., and GHOSH, A.K., Estimation of source term and

- related consequences for some postulated severe accident scenarios of Indian PHWR, Nuclear Engineering and Design, Volume 240, Issue 3529-3538 (2010)
- [19] NUCLEAR REGULATORY COMMISSION, NUREG/CR-6150, INEL-96/0422, SCDAP/RELAP5/MOD3.2 Code Manual, Volume II: Damage Progression Model Theory (1997).
- [20] INTERNATIONAL ATOMIC ENERGY AGENCY, Inter comparison and validation of computer codes for thermal-hydraulic safety analysis of heavy water reactors, IAEA TECDOC 1395, IAEA Vienna (2004).
- [21] VAN DORSSELAERE, J.P., S., PIGNET, C., SEROPIAN, T., MONTANELLI, P., Giordano, JACQ, F., and SCWHINGES, B., Development and assessment of ASTEC code for severe accident simulation, NURETH-11, Avignon, France, October 2-6 (2005).
- [22] MAJUMDAR, P., CHATTERJEE, B., NANDAN, G., MUKHOPADHYAY D., and LELE, H.G., Assessment of the code “PTCREEP” for IPHWR Pressure Tube Ballooning Study, Journal of Pressure Vessel Technology, Vol.133, 014503-1 to 014503-4 (2011).
- [23] NANDAN, G., MAJUMDAR, P., SAHOO, P.K., KUMAR, R., CHATTERJEE, B., MUKHOPADHYAY, D., and LELE, H.G., Study of Ballooning of a completely voided Pressure Tube of Indian PHWR under heat up conditions, Nuclear Engineering and Design, vol. 243 ,301-310 (2012).
- [24] LELE, H.G., MAJUMDAR, P., MUKHOPADHYAY, D., GUPTA, S.K., and VENKATRAJ, V., A Methodology for Estimation of Release of Fission Products during LOCA with Loss of ECCS, IAEA TCM on Fuel Behavior under Transient and LOCA Conditions, Halden, Norway (2001).
- [25] NUCLEAR SAFETY CENTER, Solidus/Liquidus of UO<sub>2</sub>-ZrO<sub>2</sub> Concrete mixtures. Version 0 for peer review. INSC Material Properties Database (1998).
- [26] KOREA ATOMIC ENERGY RESEARCH INSTITUTE, ISAAC Computer Code User’s Manual, Rep. KAERI/TR-3645/2008, KAERI, Daejeon (2008).
- [27] ELECTRIC POWER RESEARCH INSTITUTE, MAAP4 Modular Accident Analysis Program for LWR Power Plants User’s Manual, Rep. 1015309 and 1015310, EPRI, Palo Alto, CA (1994-2005).
- [28] THOMSON, P.D. and KOHN, E., Fuel and fuel channel behaviour in accident without availability of ECC System, AECL (Special meeting on water reactor fuel Safety in off-normal and accident condition (1983).
- [29] SHEWFELT, R. S. W., LYALL, L. W., and GODIN, D. P., A High- Temperature Creep model for Zr-2.5 wt% Nb Pressure Tubes, Journal of Nuclear Materials 125 (1984).
- [30] SEVÓN, T. and CORE, M., Concrete Interactions in Nuclear Accidents: Theory and Design of an Experimental Facility, Master's thesis, Department of Engineering Physics and Mathematics, Helsinki University of Technology, Finland, October 6 (2005).
- [31] Proceedings of an International Symposium on Thermodynamics of Nuclear Materials, IAEA, Jülich, Germany (1979).
- [32] THOMSON, J.F, WARSI, Z.U.A., and MASTIN, C.W., Numerical Grid Generation, Foundations and Applications, Elsevier Science Publishing Company, New York (1985).
- [33] DUPLEAC, D., PRISECARU, I., MLADIN, M., and NEGUT, G., Investigation on Coolability of Severely Degraded CANDU6 Core – Preliminary Results, Proceedings of ICAPP '08, Anaheim, CA USA, 1095-1101 (2008).

- [34] MLADIN, M., DUPLEAC, D., PRISECARU, I., and MLADIN, D., Adapting and applying SCDAP/RELAP5 to CANDU in-vessel retention studies, *Ann. Nucl. Energy* Volume 37, Issue 6 845-852 (2010).
- [35] FAVARQUE, M., User's manual of Cathare 2 v1.3E, CEA-CENG, STR/LML/EM/91-61 (1991).
- [36] DUPLEAC, D., MLADIN, M., and PRISECARU, I., Effect of CANDU Fuel Bundle Modelling on Severe Accident Analysis, *Proceedings of Top Fuel 2009*, Paris, France (2009).
- [37] NUCLEAR REGULATORY COMMISSION, SCDAP/RELAP5/MOD3.2 Code Manual Assessment of Modeling of Reactor Core Behaviour During Severe Accidents, Vol. 5, Rev. 2, Rep. NUREG/CR-6150, INEL-96/0422, Office of Nuclear Regulatory Research, Washington DC (1997).
- [38] NUCLEAR REGULATORY COMMISSION, SCDAP/RELAP5/MOD3.2 CODE Manual MATROP—A Library of Material Properties for Light-Water-Reactor Accident Analysis, Vol. 4, Rev. 2, Rep. NUREG/CR-6150, INEL-96/0422, Office of Nuclear Regulatory Research, Washington DC (1997).



## GLOSSARY

Beyond design basis accident (BDBA):	Accident conditions more severe than a design basis accident. It may or may not involve core degradation.
Bundle slumping:	A phenomenon likely to appear in both ballooned and sagged pressure tube state and is due to deteriorating end support for the fuel. The elements can slip from their central spacers sideways, allowing the bundle to assume a settled geometry.
Calandria;	Low pressure vessel containing the heavy water moderator, through which the fuel channels run.
Calandria tube:	Zircaloy tube surrounding the pressure tube for each channel, separated by an insulating gas gap.
Channel sagging:	High temperature plastic deformation of the pressure tube which may contact the calandria tube.
Class III power:	Diesel generated emergency electric power. There are two independent and widely separated sets of Class III diesels: Group 1 diesels and Group 2 diesels. The latter are seismically qualified.
Class IV power:	Normal AC electric power from the grid or from the turbine generator via the unit service transformer.
Core collapse:	The collapse of supporting channels when significant amount of debris becomes lodged on top and exceeds their load bearing capacity. Under these conditions the supporting channels are expected to pull out from the rolled joints.
Core damage:	The loss of core geometry with release of radioactive material due to overheating. The core damage affecting more than one channel is known as severe core damage whereas conditions affecting a single channel is called limited core damage.
Core degradation:	A process that leads to core damage.
Core disassembly:	Process leading to core geometry degradation caused by failure of the fuel channels.
Core pass:	Transit of fluid between the inlet and outlet headers. The typical CANDU heat transport system consists of one or more figure-of-eight loops, each of which has two core passes (i.e. fluid goes through the core twice before returning to its starting point). From LOCA point of view, the loop in which a LOCA is assumed to have occurred is called the broken loop; the other loop is called the intact loop.
Corium:	Complex mixtures originating from the melting of the constituents of a nuclear reactor at different stage of a severe accident.

Crash cooldown:	Rapid cooldown of the steam generator secondary side through all main steam safety valves.
Debris:	Degraded core state in which fuel and fuel channel disintegrate due to overheating and oxidation.
Debris bed:	A collection of debris in the suspended (suspended debris bed) or terminal (terminal debris bed) state. The debris bed is characterized by porosity and particle size.
Degasser-condenser relief valves:	Two spring loaded relief valves with pneumatic actuators to provide over pressure protection for the degasser-condenser.
Design basis accident (DBA):	Accident conditions against which a nuclear power plant is designed according to established design criteria and for which the damage to the fuel and the release of radioactive material are kept within authorized limits.
Dousing:	Containment pressure suppression by spraying water under gravity in some CANDU containments.
Emergency operating procedures:	Plant specific procedures containing instructions to operating staff for implementing measures to prevent core degradation, for both DBA and BDBA.
Fuel channel:	Fuel channel consisting of a pressure tube and its surrounding calandria tube.
Fuel channel disassembly:	Disassembly of fuel and channel structural materials separating from the original channel.
Fuel channel failure:	Fuel channel failure is defined as a perforation of pressure tube and calandria tube followed by mass transfer between the fuel channel and the calandria vessel.
Fuel channel perforation:	Crack formation on the fuel channels as result of the strain concentration between the fuel bundle junctions as sagging leads to wall-thinning.
Fuel channel uncover:	Exposure of the fuel channels to steam environment due to the loss of moderator level.
Molten pool:	Corium in a molten state is called molten pool.
Severe accident:	An accident leading to severe core damage.
Sheath ballooning:	Plastic deformation of the fuel sheath during temperature escalation that can lead to sheath rupture.

## ABBREVIATIONS

AECL	Atomic Energy of Canada Limited
ASDV	Air-operated atmospheric Steam Discharge Valve
ASTEC	Accident Source Term Evaluation Code
BARC	Bhabha Atomic Research Center
BARC-RED	BARC Reactor Engineering Division
BARC-RSD	BARC Reactor Safety Division
CANDU	CANada Deuterium Uranium reactor
CAST3M	Code for Analysis Structure
CATHARE	Code for Analysis of THERmalhydraulics during an Accident of Reactor and safety Evaluation
CATHENA	Canadian Algorithm for THERmal hydraulic Network Analysis
CCFL	Counter-Current Flow Limitation
CCI	Core-Concrete Interaction
CRP	Coordinated Research Project
CSDV	Condenser Steam Discharge Valve
CT	Calandria Tube
CV	Calandria Vessel
DCT	Degasser Condenser Tank
ECCS	Emergency Core Cooling System
EDF	Electricite de France
EPRI	Electric Power Research Institute
FEM	Finite Element Method
FRC	Fractional Release Coefficient
HTS	Heat Transport System
HWR	Heavy Water Reactor
ICW	Inner Containment Wall
IRSN	Institut de Radioprotection et de Sûreté Nucléaire
ISAAC	Integrated Severe Accident Analysis code for CANDU plants
KAERI	Korea Atomic Energy Research Institute
LAC	Local Air Cooler
LCDA	Limited Core Damage Accident
LOCA	Loss-Of- Coolant Accident
LRV	Liquid Relief Valve
LWR	Light Water Reactors
MAAP	Modular Accident Analysis Program
MCCI	Molten Core-Concrete Interaction
MSIV	Main Steam Isolation Valves
MSSV	Main Steam Safety Valve
NPCIL	Nuclear Power Corporation of India Limited

NRC	Nuclear Regulatory Commission
OPRD	Over Pressure Rupture Disk
P&IC	Pressure and Inventory Control
PACSR	Post Accident Containment System Response
PAR	Passive Autocatalytic Recombiner
PCP	Primary Circulation Pump
PHTS	Primary Heat Transport System
PSA	Probabilistic Safety Assessment
PT	Pressure Tube
PUB	Politechnical University of Bucharest
RB	Reactor Building
RD	Rupture Disk
RELAP	Reactor Excursion and Leak Analysis Program
RIH	Reactor Inlet Header
ROH	Reactor Outlet Header
SA	Severe Accident
SAMG	Severe Accident Management Guideline
SBO	Station Blackout
SCDA	Severe Core Damage Accident
SCDAP	Severe Core Damage Accident Progression
SG	Steam Generator
SJTU	Shanghai Jiao Tong University
TWG	Technical Working Group
UVET	Unequal Velocity Equal Temperature

## **CONTRIBUTORS TO DRAFTING AND REVIEW**

Cao, X.	Shanghai Jiao Tong University, China
Choi, J.-H.	International Atomic Energy Agency
Dupleac, D.	Politechnica University of Bucharest, Romania
Kim, D.-H.	Korea Atomic Energy Research Institute, Rep. of Korea
Lele, H.G.	Bhabha Atomic Research Center, India
Nayak, A.K.	Bhabha Atomic Research Center, India
Nitheanandan, T.	Atomic Energy of Canada Limited, Canada
Rammohan, H. P.	Nuclear Power Corporation of India Limited, India

## **RESEARCH COORDINATION MEETINGS**

25 - 27 February 2009, IAEA, Vienna, Austria;

4 - 7 May 2010, NPCIL, Mumbai, India;

30 August - 2 September 2011, KAERI, Daejeon, Rep. of Korea;

1 - 4 May 2012, AECL, Ottawa, Canada;





# IAEA

International Atomic Energy Agency

No. 23

## ORDERING LOCALLY

In the following countries, IAEA priced publications may be purchased from the sources listed below, or from major local booksellers.

Orders for unpriced publications should be made directly to the IAEA. The contact details are given at the end of this list.

### AUSTRALIA

#### *DA Information Services*

648 Whitehorse Road, Mitcham, VIC 3132, AUSTRALIA

Telephone: +61 3 9210 7777 • Fax: +61 3 9210 7788

Email: [books@dadirect.com.au](mailto:books@dadirect.com.au) • Web site: <http://www.dadirect.com.au>

### BELGIUM

#### *Jean de Lannoy*

Avenue du Roi 202, 1190 Brussels, BELGIUM

Telephone: +32 2 5384 308 • Fax: +61 2 5380 841

Email: [jean.de.lannoy@euronet.be](mailto:jean.de.lannoy@euronet.be) • Web site: <http://www.jean-de-lannoy.be>

### CANADA

#### *Renouf Publishing Co. Ltd.*

Telephone: +1 613 745 2665 • Fax: +1 643 745 7660

5369 Canotek Road, Ottawa, ON K1J 9J3, CANADA

Email: [order@renoufbooks.com](mailto:order@renoufbooks.com) • Web site: <http://www.renoufbooks.com>

#### *Bernan Associates*

4501 Forbes Blvd., Suite 200, Lanham, MD 20706-4391, USA

Telephone: +1 800 865 3457 • Fax: +1 800 865 3450

Email: [orders@bernan.com](mailto:orders@bernan.com) • Web site: <http://www.bernan.com>

### CZECH REPUBLIC

#### *Suweco CZ, spol. S.r.o.*

Klecakova 347, 180 21 Prague 9, CZECH REPUBLIC

Telephone: +420 242 459 202 • Fax: +420 242 459 203

Email: [nakup@suweco.cz](mailto:nakup@suweco.cz) • Web site: <http://www.suweco.cz>

### FINLAND

#### *Akateeminen Kirjakauppa*

PO Box 128 (Keskuskatu 1), 00101 Helsinki, FINLAND

Telephone: +358 9 121 41 • Fax: +358 9 121 4450

Email: [akatilaus@akateeminen.com](mailto:akatilaus@akateeminen.com) • Web site: <http://www.akateeminen.com>

### FRANCE

#### *Form-Edit*

5, rue Janssen, PO Box 25, 75921 Paris CEDEX, FRANCE

Telephone: +33 1 42 01 49 49 • Fax: +33 1 42 01 90 90

Email: [fabien.boucard@formedit.fr](mailto:fabien.boucard@formedit.fr) • Web site: <http://www.formedit.fr>

#### *Lavoisier SAS*

14, rue de Provigny, 94236 Cachan CEDEX, FRANCE

Telephone: +33 1 47 40 67 00 • Fax: +33 1 47 40 67 02

Email: [livres@lavoisier.fr](mailto:livres@lavoisier.fr) • Web site: <http://www.lavoisier.fr>

#### *L'Appel du livre*

99, rue de Charonne, 75011 Paris, FRANCE

Telephone: +33 1 43 07 50 80 • Fax: +33 1 43 07 50 80

Email: [livres@appeldulivre.fr](mailto:livres@appeldulivre.fr) • Web site: <http://www.appeldulivre.fr>

### GERMANY

#### *Goethe Buchhandlung Teubig GmbH*

Schweitzer Fachinformationen

Willstaetterstrasse 15, 40549 Duesseldorf, GERMANY

Telephone: +49 (0) 211 49 8740 • Fax: +49 (0) 211 49

Email: [s.dehaan@schweitzer-online.de](mailto:s.dehaan@schweitzer-online.de) • Web site: <http://www.goethebuch.de/>

### HUNGARY

#### *Librotade Ltd., Book Import*

PF 126, 1656 Budapest, HUNGARY

Telephone: +36 1 257 7777 • Fax: +36 1 257 7472

Email: [books@librotade.hu](mailto:books@librotade.hu) • Web site: <http://www.librotade.hu>

## INDIA

### **Allied Publishers**

1<sup>st</sup> Floor, Dubash House, 15, J.N. Heredi Marg  
Ballard Estate, Mumbai 400001, INDIA  
Telephone: +91 22 2261 7926/27 • Fax: +91 22 2261 7928  
Email: alliedpl@vsnl.com • Web site: <http://www.alliedpublishers.com>

### **Bookwell**

3/79 Nirankari, Dehli 110009, INDIA  
Tel.: +91 11 2760 1283 • +91 11 27604536  
Email: bkwell@nde.vsnl.net.in • Web site: <http://www.bookwellindia.com/>

## ITALY

### **Libreria Scientifica "AEIOU"**

Via Vincenzo Maria Coronelli 6, 20146 Milan, ITALY  
Tel.: +39 02 48 95 45 52 • Fax: +39 02 48 95 45 48  
Email: info@libreriaaeiou.eu • Web site: <http://www.libreriaaeiou.eu/>

## JAPAN

### **Maruzen Co., Ltd.**

1-9-18 Kaigan, Minato-ku, Tokyo 105-0022, JAPAN  
Tel.: +81 3 6367 6047 • Fax: +81 3 6367 6160  
Email: journal@maruzen.co.jp • Web site: <http://maruzen.co.jp>

## NETHERLANDS

### **Martinus Nijhoff International**

Koraalrood 50, Postbus 1853, 2700 CZ Zoetermeer, NETHERLANDS  
Tel.: +31 793 684 400 • Fax: +31 793 615 698  
Email: info@nijhoff.nl • Web site: <http://www.nijhoff.nl>

### **Swets**

PO Box 26, 2300 AA Leiden  
Dellaertweg 9b, 2316 WZ Leiden, NETHERLANDS  
Telephone: +31 88 4679 263 • Fax: +31 88 4679 388  
Email: tbeysens@nl.swets.com • Web site: [www.swets.com](http://www.swets.com)

## SLOVENIA

### **Cankarjeva Založba dd**

Kopitarjeva 2, 1515 Ljubljana, SLOVENIA  
Tel.: +386 1 432 31 44 • Fax: +386 1 230 14 35  
Email: import.books@cankarjeva-z.si • Web site: [http://www.mladinska.com/cankarjeva\\_zalozba](http://www.mladinska.com/cankarjeva_zalozba)

## SPAIN

### **Díaz de Santos, S.A.**

Librerías Bookshop • Departamento de pedidos  
Calle Albasanz 2, esquina Hermanos García Noblejas 21, 28037 Madrid, SPAIN  
Telephone: +34 917 43 48 90  
Email: compras@diazdesantos.es • Web site: <http://www.diazdesantos.es/>

## UNITED KINGDOM

### **The Stationery Office Ltd. (TSO)**

PO Box 29, Norwich, Norfolk, NR3 1PD, UNITED KINGDOM  
Telephone: +44 870 600 5552  
Email (orders): books.orders@tso.co.uk • (enquiries): book.enquiries@tso.co.uk • Web site: <http://www.tso.co.uk>

On-line orders:

### **DELTA International Ltd.**

39, Alexandra Road, Addlestone, Surrey, KT15 2PQ, UNITED KINGDOM  
Email: info@profbooks.com • Web site: <http://www.profbooks.com>

## United Nations (UN)

300 East 42<sup>nd</sup> Street, IN-919J, New York, NY 1001, USA  
Telephone: +1 212 963 8302 • Fax: 1 212 963 3489  
Email: publications@un.org • Web site: <http://www.unp.un.org>

## UNITED STATES OF AMERICA

### **Bernan Associates**

4501 Forbes Blvd., Suite 200, Lanham, MD 20706-4391, USA  
Tel.: +1 800 865 3457 • Fax: +1 800 865 3450  
Email: orders@bernan.com • Web site: <http://www.bernan.com>

### **Renouf Publishing Co. Ltd.**

812 Proctor Avenue, Ogdensburg, NY 13669, USA  
Tel.: +800 551 7470 (toll free) • +800 568 8546 (toll free)  
Email: orders@renoufbooks.com • Web site: <http://www.renoufbooks.com>

## Orders for both priced and unpriced publications may be addressed directly to:

IAEA Publishing Section, Marketing and Sales Unit, International Atomic Energy Agency  
Vienna International Centre, PO Box 100, 1400 Vienna, Austria  
Telephone: +43 1 2600 22529 or 22488 • Fax: +43 1 2600 29302  
Email: sales.publications@iaea.org • Web site: <http://www.iaea.org/books>





**International Atomic Energy Agency**  
**Vienna**  
ISBN 978-92-0-114413-3  
ISSN 1011-4289